THE JOURNAL OF PHYSICAL CHEMISTRY

VOLUME 67, NUMBER 6 JUNE, 1963

A. Bruce King and Henry Wise: Reaction Kinetics of Hydrogen Atoms with Carbon Films 1163

Manesh J. Shah, Donald C. Thompson, and Cleve M. Hart: Reversal of Electro-Optical Birefringence in Bentonite Suspensions 1170

R. H. Dinius, M. T. Emerson, and G. R. Choppin: Nuclear Magnetic Resonance Study of Ion-Exchange Resins. I. Hydrated Dowex-50 Resins 1178

S. K. Alley, Jr., and R. L. Scott: N.m.r. Studies of Hydrogen Bonding in Hydrofluorocarbon Solutions 1182

B. E. Dawson and T. Henshall: An Investigation of the Reactions between Substituted Benzaldehydes and 5,5-Dimethylcyclohexanedione-1,3 1187

Michael A. Greenbaum, M. Louis Arin, and Milton Farber: The Thermodynamic and Physical Properties of Beryllium Compounds. III. Heat of Formation and Entropy of $BeF_2(g)$ 1191

Sidney W. Benson and Charles S. Copeland: The Partial Molar Volumes of Ions 1194

D. J. C. Yates and P. J. Lucchesi: The Coexistence of Independent Sites on Alumina as Shown by the Infrared Spectra of Chemisorbed Acetylene and Ethylene 1197

Ching-hsien Wu, Merritt M. Birky, and Loren G. Hepler: Thermochemistry of Some Bromine and Iodine Species in Aqueous Solution 1202

W. T. Carnall: The Near-Infrared Transitions of the Trivalent Lanthanides in Solution. II. Tb^{+3}, Dy^{+3}, Ho^{+3}, Er^{+3}, Tm^{+3}, and Yb^{+3} 1206

H. A. Saroff and M. S. Lewis: The Binding of Calcium Ions to Serum Albumin 1211

A. K. R. Unni, L. Elias, and H. I. Schiff: The Conductivities of Some Quaternary Ammonium Chlorides and Bromides in Nitromethane at 25° 1216

S. Blum and H. I. Schiff: Transference Numbers and Ionic Conductances of Some Quaternary Ammonium Chloride and Bromide Ions in Nitromethane at 25° 1220

Robert L. Kay, S. C. Blum, and H. I. Schiff: The Electrophoretic and Relaxation Contribution to the Conductance of Several Quaternary Ammonium Chlorides and Bromides in Nitromethane 1223

Akio Teramoto, Reisuke Okada, and Hiroshi Fujita: Viscosity of Polyalkyl Methacrylate Plasticized with Diethyl Phthalate. I. Poly-*n*-butyl Methacrylate 1228

J. Kivel, F. C. Albers, D. A. Olsen, and R. E. Johnson: Surface Areas by Adsorption of a Quaternary Ammonium Halide from Aqueous Solution 1235

S. Lindenbaum and G. E. Boyd: Spectrophotometric Investigation of the Extraction of Transition Metal Halo-Complex Ions by Amine Extractants 1238

Akira Amano and Masao Uchiyama: Thermal Hydrogenolysis of Propylene 1242

Marcel W. Nathans: The Dehydration of Polyhalite 1248

F. Neil Hodgson, Michel Desjardins, and William L. Baun: A Study of Polynuclear Aromatic Hydrocarbons Using the Vacuum Spark Mass Spectrograph 1250

Daniel Hershey and John W. Prados: Soret Coefficients for $CuSO_4$, $CoSO_4$, and Mixed Salt Aqueous Solutions Using an Improved Design of a Soret Cell 1253

Daniel Hershey and John W. Prados: Thermal Diffusion. A Non-rigorous Set of Equations for Predicting Separations in Gases and Liquids 1255

Eugene E. Schrier and Herbert M. Clark: Interaction in Salt Vapors and Activity Coefficients in the Potassium Chloride–Magnesium Chloride System 1259

D. Verdin: The Radiolysis of the Xylene Isomers and Ethylbenzene 1263

Hajime Hasegawa: Spectroscopic Studies on the Color Reaction of Acid Clay. III. The Coloration with Polyenes and Polyacenes 1268

Joshua Jortner, Michael Ottolenghi, and Gabriel Stein: Solvent Effects on the Photochemistry of the Iodide Ion 1271

Sheldon H. Cohen, Reynold T. Iwamoto, and Jacob Kleinberg: The Effect of $LiClO_4$, LiCl, and LiBr on the Polarographic Behavior and Ultraviolet Spectrum of Praseodymium(III) in Ethanol 1275

S. Levy and M. Folman: Surface Conductivity of High Surface Area Adsorbent Due to the Presence of Adsorbed Molecules 1278

Brice G. Hobrock and Robert W. Kiser: Electron Impact Investigations of Sulfur Compounds. III. 2-Thiapropane, 3-Thiapentane, and 2,3,4-Trithiapentane 1283

Suresh K. Gupta and Richard F. Porter: Infrared Spectra of Solid Boroxine 1286

Gordon Lewis and Clifford E. Myers: Vaporization Properties of Iron Phosphides 1289

H. Morawetz and J. A. Shafer: Characterization of Counterion Distribution in Polyelectrolyte Solutions. II. The Effect of the Distribution of Electrostatic Potential on the Solvolysis of Cationic Esters in Polymeric Acid Solution 1293

Charles P. Poole, Jr.: Adsorption Statistics and the Physical Properties of Transition Metal Catalysts 1297

Marvin Ross and Joel H. Hildebrand: Energy Volume Relations of Octamethylcyclotetrasiloxane and its Mixtures with Carbon Tetrachloride 1301

M. J. Blandamer and M. C. R. Symons: Significance of New Values for Ionic Radii to Solvation Phenomena in Aqueous Solution 1304

W. D. Good, S. S. Todd, J. F. Messerly, J. L. Lacina, J. P. Dawson, D. W. Scott, and J. P. McCullough: Perfluoropiperidine: Entropy, Heat of Formation, and Vapor Pressure; N–F Bond Energy; and Solid-State Transitions 1306

W. D. Good, D. R. Douslin, and J. P. McCullough: 1,2-Bis-difluoroamino-4-methylpentane: Heats of Combustion, Formation, and Vaporization; Vapor Pressure; and N–F Thermochemical Bond Energy 1312

Andrew D. Liehr: The Three Electron (or Hole) Cubic Ligand Field Spectrum 1314

William P. Hauser and W. D. Walters: The Kinetics of the Thermal Isomerization of Cyclobutene 1328

Adi Eisenberg: The Multi-dimensional Glass Transition 1333

Douglas W. McKee: Catalytic Activity and Sintering of Platinum Black. II. Demethanation and Hydrogenolysis of Cyclopropane 1336

A. C. Testa: The Effect of Light Intensity at 313 mμ on the Photochemical Disappearance of Benzophenone in Isopropyl Alcohol 1341

Debbie Fu-Tai Tuan and Raymond M. Fuoss: Electrostriction in Polar Solvents. I 1343

N. C. Deno and Charles H. Spink: The McDevit–Long Equation for Salt Effects on Non-electrolytes 1347

Geoffrey Beeston and Robert H. Essenhigh: Kinetics of Coal Combustion: The Influence of Oxygen Concentration on the Burning-Out Times of Single Particles 1349

NOTES

Louis Watts Clark: The Decarboxylation of Oxalic Acid in Cresols and Glycols 1355

P. Rama Murthy and C. C. Patel: Crystal Structure of Zirconyl Perchlorate Dihydrate by X-Ray Powder Diffraction Method 1357

L. A. Errede and J. P. Cassidy: The Chemistry of

Xylylenes. XIX. The Co-pyrolysis of *p*-Xylene and Hexachloroethane 1358
George A. Miller: On the Calculation of Thermal Transpiration 1359
R. K. Kullnig and F. C. Nachod: The Coupling of Nuclear Spins of Protons in Two Allenes 1361
D. K. Anderson and A. L. Babb: Mutual Diffusion in Non-ideal Liquid Mixtures. IV. Methanol–Carbon Tetrachloride and Dilute Ethanol–Carbon Tetrachloride Solutions 1362
George A. Miller: The Vapor Pressure of Solid Decaborane 1363
E. Lee Purlee and Ernest Grunwald: The Potentiometric Measurement of Ion-Pair Dissociation Constants. The Alkali Chlorides and $(CH_3)_4NCl$ in 70% Dioxane–30% Water 1364
D. E. Woessner: N.m.r. Spin-Echo Self-Diffusion Measurements on Fluids Undergoing Restricted Diffusion 1365
R. Srinivasan: Mercury Photosensitized Isomerization of 1,5-Hexadiene 1367
Robert C. Paule and John L. Margrave: A Langmuir Determination of the Sublimation Pressure of Boron 1368
Robert W. Carr, Jr., and W. D. Walters: The Thermal Decomposition of Cyclobutane 1370
George Van Dyke Tiers: Fluorine N.m.r. Spectroscopy. XIII. Further Coupling Constants for Isotopic C_3F_8 1372
George Van Dyke Tiers: Fluorine N.m.r. Spectroscopy. XIV. Like Signs for the Coupling Constants, $J(C^{13}H)$ and $J(FH)$, in Dichlorofluoromethane 1373
Dilip Kumar Majumdar: A Semi-empirical Formula for Viscosity of a 12:6 Liquid 1374
Stanislaw Ciborowski: Radiation Induced Reaction of Nitric Oxide with Cyclohexane 1375
R. A. Gardner and R. E. Petrucci: Adsorbate–Adsorbent Interactions in the Chemisorption of Carbon Monoxide 1376
James T. Richardson: Magnetic Properties of $Ni_2O_3 \cdot H_2O$ 1377
A. J. Tench and P. Coppens: Free Radicals Formed from *o*-Substituted Nitro Compounds 1378
J. F. Walling: The Third Virial Coefficient of Potassium as Estimated from its Vapor Pressure 1380
Francis J. Wunderlich and R. E. Rebbert: The Reactions of Methyl Radicals with Aromatic Compounds. III. The Fluorotoluenes 1382
R. Kent Murmann and D. R. Foerster: Visible Spectra and Acid Association Constants of $[Re(en)_2O_2]^+$ Type Compounds 1383
Daniel Cubicciotti: Mass Spectrometric Study of the Vapors over Bismuth–Sulfur Melts 1385
M. H. Gianni, E. L. Stogryn, and C. M. Orlando, Jr.: Nuclear Magnetic Resonance Spectral Correlation of Some Symmetrically Substituted Epoxides and Olefins 1385
Joan B. Berkowitz-Mattuck and Alfred Büchler: A Transpiration Study of Lithium Hydroxide 1386
José D. Gómez-Ibáñez and Chia-Tsun Liu: The Excess Volume of Binary Mixtures of Normal Alkanes 1388
Per Beronius: An Electrodeposition Method for Following Moderately Rapid Exchange Reactions 1391
Walter Z. Heldt and Claus D. Weis: The Electrical Conductivities of Some Iron Isonitrile Complexes 1392
Sadhan Basu and John Greist: Resonance Transfer of Excitation Energy between Nucleosides and Acridine Orange 1394

COMMUNICATIONS TO THE EDITOR

H. B. Kostenbauder and Patrick P. DeLuca: Reversible Photobinding of Riboflavin to Macromolecules in Aqueous Solution 1395
J. E. Mark and P. J. Flory: Stress-Temperature Coefficients for Isotactic and Atactic Poly-(butene-1) 1396
James King, Jr.: The Chromatographic Separation of the Hydrogen Isotopes Including Tritium 1397
W. W. Brandt: Dynamic Theory of Polymer Segmental Motion 1397
David Allan Cadenhead: The Neutron Irradiation of a Graphitized Carbon Black 1398

AUTHOR INDEX

Albers, F. C., 1235
Alley, S. K., Jr., 1182
Amano, A., 1242
Anderson, D. K., 1362
Arin, M. L., 1191

Babb, A. L., 1362
Basu, S., 1394
Baun, W. L., 1250
Beeston, G., 1349
Benson, S. W., 1194
Berkowitz-Mattuck, J. B., 1386
Beronius, P., 1391
Birky, M. M., 1202
Blandamer, M. J., 1304
Blum, S., 1220, 1223
Boyd, G. E., 1238
Brandt, W. W., 1397
Büchler, A., 1386

Cadenhead, D. A., 1398
Carnall, W. T., 1206
Carr, R. W., Jr., 1370
Cassidy, J. P., 1358
Choppin, G. R., 1178
Ciborowski, S., 1375
Clark, H. M., 1259
Clark, L. W., 1355
Cohen, S. H., 1275
Copeland, C. S., 1194
Coppens, P., 1378
Cubicciotti, D., 1385

Dawson, B. E., 1187
Dawson, J. P., 1306
DeLuca, P. P., 1395
Deno, N. C., 1347
Desjardins, M., 1250
Dinius, R. H., 1178
Douslin, D. R., 1312

Eisenberg, A., 1333
Elias, L., 1216
Emerson, M. T., 1178
Errede, L. A., 1358
Essenhigh, R. H., 1349

Farber, M., 1191
Flory, P. J., 1396
Foerster, D. R., 1383
Folman, M., 1278
Fujita, H., 1228
Fuoss, R. M., 1343

Gardner, R. A., 1376
Gianni, M. H., 1385
Gómez-Ibáñez, J. D., 1388
Good, W. D., 1306, 1312
Greenbaum, M. A., 1191
Greist, J., 1394
Grunwald, E., 1364
Gupta, S. K., 1286

Hart, C. M., 1170
Hasegawa, H., 1268

Hauser, W. P., 1328
Heldt, W. Z., 1392
Henshall, T., 1187
Hepler, L. G., 1202
Hershey, D., 1253, 1255
Hildebrand, J. H., 1301
Hobrock, B. G., 1283
Hodgson, F. N., 1250

Iwamoto, R. T., 1275

Johnson, R. E., 1235
Jortner, J., 1271

Kay, R. L., 1223
King, A. B., 1163
King, J., Jr., 1397
Kiser, R. W., 1283
Kivel, J., 1235
Kleinberg, J., 1275
Kostenbauder, H. B., 1395
Kullnig, R. K., 1361

Lacina, J. L., 1306
Levy, S., 1278
Lewis, G., 1289
Lewis, M. S., 1211
Liehr, A. D., 1314
Lindenbaum, S., 1238
Liu, C.-T., 1388
Lucchesi, P. J., 1197

Majumdar, D. K., 1374

Margrave, J. L., 1368
Mark, J. E., 1396
McCullough, J. P., 1306, 1312
McKee, D. W., 1336
Messerly, J. F., 1306
Miller, G. A., 1359, 1363
Morawetz, H., 1293
Murmann, R. K., 1383
Murthy, P. R., 1357
Myers, C. E., 1289

Nachod, F. C., 1361
Nathans, M. W., 1248

Okada, R., 1228
Olsen, D. A., 1235
Orlando, C. M., Jr., 1385
Ottolenghi, M., 1271

Patel, C. C., 1357
Paule, R. C., 1368
Petrucci, R. H., 1376
Poole, C. P., Jr., 1297
Porter, R. F., 1286
Prados, J. W., 1253, 1255
Purlee, E. L., 1364

Rebbert, R. E., 1382
Richardson, J. T., 1377
Ross, M., 1301

Saroff, H. A., 1211
Schiff, H. I., 1216, 1220, 1223
Schrier, E. E., 1259
Scott, D. W., 1306
Scott, R. L., 1182
Shafer, J. A., 1293
Shah, M. J., 1170
Spink, C. H., 1347
Srinivasan, R., 1367
Stein, G., 1271
Stogryn, E. L., 1385
Symons, M. C. R., 1304

Tench, A. J., 1378
Teramoto, A., 1228
Testa, A. C., 1341
Thompson, D. C., 1170
Tiers, G. V. D., 1372, 1373
Todd, S. S., 1306
Tuan, D. F., 1343

Uchiyama, M., 1242
Unni, A. K. R., 1216

Verdin, D., 1263

Walling, J. F., 1380
Walters, W. D., 1328, 1370
Weis, C. D., 1392
Wise, H., 1163
Woessner, D. E., 1365
Wu, C., 1202
Wunderlich, F. J., 1382

Yates, D. J. C., 1197

THE JOURNAL OF
PHYSICAL CHEMISTRY

(Registered in U. S. Patent Office)

VOLUME 67, NUMBER 6 JUNE 14, 1963

REACTION KINETICS OF HYDROGEN ATOMS WITH CARBON FILMS[1]

BY A. BRUCE KING AND HENRY WISE

Division of Chemical Physics, Stanford Research Institute, Menlo Park, California

Received April 18, 1962

The reaction kinetics of hydrogen atoms with evaporated carbon films have been studied in the temperature range from 365 to 500°K. and at total gas pressures from 0.02 to 0.10 mm. The removal of carbon by chemical reaction, as detected by the variation of film thickness with time, was found to occur at two distinct rates with activation energies of 9.2 and 7.1 kcal./mole. The kinetics appear to be related to the degree of crystallinity of the film. Simple hydrocarbons such as methane and ethane are the principal reaction products. In addition, formation of hydrogen molecules by atom recombination on the carbon film takes place; this reaction, with an activation energy of 2.3 kcal./mole, predominates over hydrocarbon formation in the temperature range studied.

Introduction

Studies of the recombination of hydrogen atoms on various solid surfaces[2] led to the observation that, in addition to molecular hydrogen, stabile volatile hydrides may be produced as a result of the interaction of hydrogen atoms with some of the group IV elements, such as C, Ge, and Sn. The reaction kinetics of such a heterogeneous system, the reaction of hydrogen atoms with carbon, forms the subject of this paper.

Several studies have been reported on the reactions of hydrogen atoms,[3-5] oxygen atoms,[5-7] and nitrogen atoms,[8] with various forms of solid carbon. Hydrogen atoms have been found to produce principally methane,[4,5] while oxygen atoms form CO_2 with CO suggested as the initial product followed by further oxidation on surface to CO_2.[6] No volatile products were formed from the reaction of pure nitrogen atoms.[8] Although some studies have been made of the effect of the structure of the solid on the reaction rate with oxygen atoms,[5-7] no detailed study of the reaction kinetics of these systems has been reported.

Experimental

The reactions were studied in a Pyrex vacuum system in which residual pressures of less than 10^{-6} mm. were routinely obtained. All mercury and stopcock grease vapors were prevented from entering the reaction section by suitably placed liquid nitrogen traps. Metal bellows valves were used in the reaction section of the system. The hydrogen (prepurified Matheson) was further purified by passage through a Deoxo unit, liquid nitrogen trap, and a heated palladium thimble. The latter was necessary to remove N_2, present as a 0.1 vol. % impurity, which was converted in about 50% yield to ammonia on passage through the electric discharge employed for hydrogen atom production. Hydrogen flow rate was controlled either by the temperature of the palladium or by means of an Edwards Ltd. needle valve placed downstream from the palladium thimble. The pressure was determined with a McLeod gage, located downstream from the main trap, and calibrated empirically for the pressure in the reaction section.

The carbon films in the form of a circular spot (about 16 mm. in diameter) were prepared by evaporation onto circular microscope glass cover slides (18.1 mm. diameter, 0.066 mm. thickness n_D 1.531) located about 3 cm. from an electric arc between graphite rods of spectroscopic grade.[9] The residual gas pressure during evaporation was kept at about 2×10^{-5} mm. Several samples were also deposited onto Vycor disks (12.7 mm. diameter, 1.6 mm. thickness, n_D 1.4607). After some practice, it was possible to obtain deposits with thicknesses of about 1000 to 3500 Å. Electron diffraction studies showed the films contained graphite crystallites with an average particle size of about 50–75 Å.

As shown in Fig. 1 the hydrogen atoms were produced by means of an electrodeless radiofrequency discharge in the main tube (5.0 cm. in diameter). A side arm closed at one end (60 cm. long, 2.5 cm. in diameter) was connected to the main tube, about 20 cm. downstream from the edge of the visible plasma which was prevented from extending by suitably placed bar magnets on the outside of the cylinder. The carbon-coated slide was placed in a glass holder in the side arm (see Fig. 1) 5.0 cm. from the juncture with the main tube. In this region the temperature of the furnace surrounding the side arm was fairly uniform. The temperatures used in the study ranged from 365–500°K. as determined with thermocouples mounted on the outside of the glass cylinder. The slide was positioned perpendicular to the light beam and it nearly filled the cross section of the cylinder. Optical windows sealed onto the system permitted continuous measurement of the optical transmission of the film during the reaction. The light source was a sodium lamp. Suitable apertures and lenses were used to obtain a parallel light beam through the center half of the film area. The transmitted light at 5890–5896 Å. was measured on a photomultiplier tube (RCA 1P21) after passage through an interference filter and a Corning 3482 filter. The relative incident light intensity was determined using a partially silvered mirror which split the incident beam and directed it to a second phototube. The signals of the photomultipliers were fed to a two-channel recorder giving a record of both

(1) The authors gratefully acknowledge support of this work by the Physical Sciences Research Committee, Stanford Research Institute.

(2) B. J. Wood and H. Wise, *J. Phys. Chem.*, **65**, 1976 (1961).

(3) L. E. Avramenko, *Zh. Fiz. Khim.*, **20**, 1299 (1946).

(4) G. M. Harris and A. W. Tickner, *Nature*, **160**, 871 (1947).

(5) J. D. Blackwood and F. K. McTaggart, *Australian J. Chem.*, **12**, 533 (1959).

(6) J. D. Blackwood and F. K. McTaggart, *ibid.*, **12**, 114 (1959).

(7) J. Streznewski and J. Turkevich, "Proceedings of the Third Symposium on Carbon," Pergamon Press, New York, N. Y., 1959, p. 273.

(8) W. G. Zinman, "Proceedings of the Conference on Physical Chemistry in Aerodynamics and Space Flight," Pergamon Press, New York, N. Y., 1961, p. 46.

(9) Similar to that described by Bradley (D. E. Bradley, *Brit. J. Appl. Phys.*, **5**, 65 (1954)).

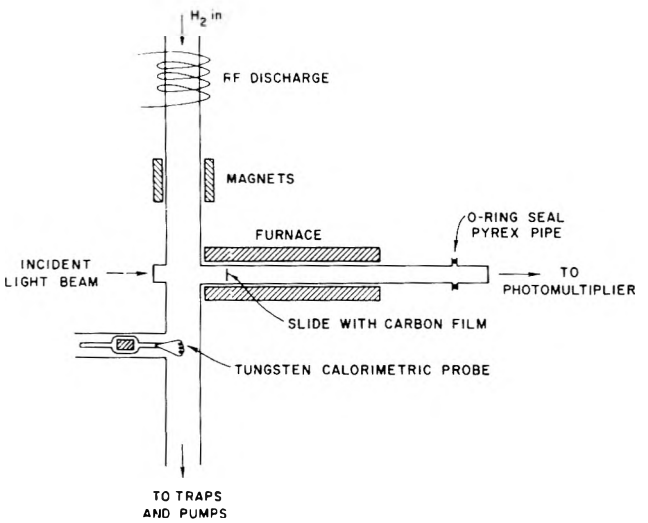

Fig. 1.—Diagram of reaction system.

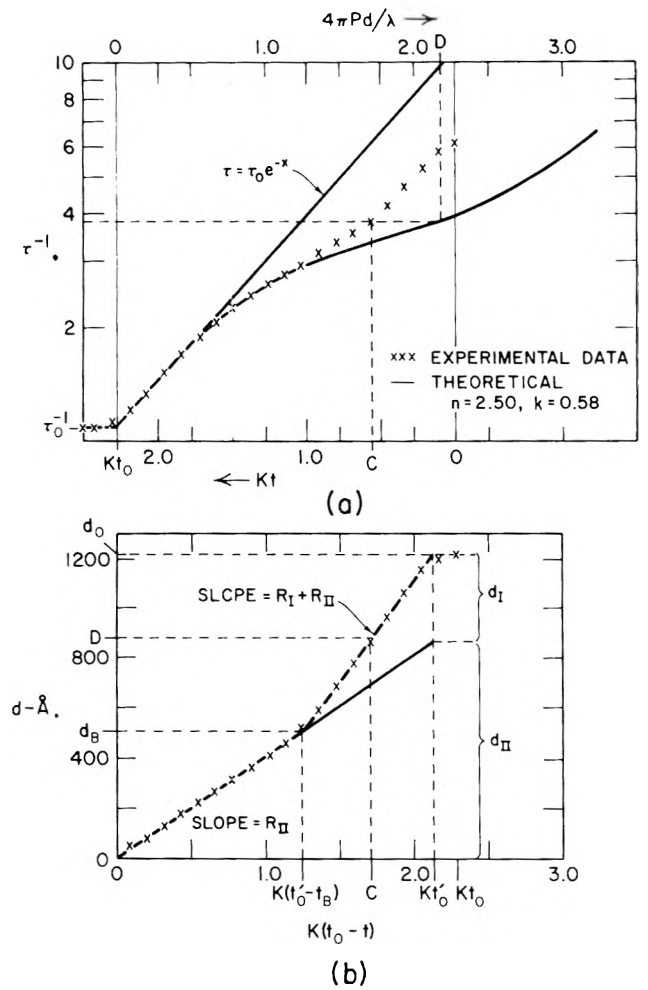

Fig. 2.—(a) Experimental measurement of transmission *vs.* time. (Experimental conditions: T = 498.8°K., [H] = 1.32 × 10^{14} atom cm.$^{-3}$, total pressure = 0.040 mm., $\bar{\lambda}$ = 5893 Å., normalization constants: K = 6.43 × 10^{-4} sec.$^{-1}$, P = 1.179.) (b) Reduced curve of thickness *vs.* time for experimental data shown in Fig. 2a. (Initial thickness (d_0) is 1240 Å; points C and D refer to corresponding points in (a); R_I, R_{II}, d_I, d_{II}, t_B, and d_B are defined as shown in the figure.)

outputs with time. In all of the experiments reported, the progress of the reaction was followed until the film was completely removed. The absolute transmission was determined from the known transmission of the bare glass slide and the ratio of the photomultiplier outputs at the completion of the reaction.

The hydrogen atom concentration could be controlled by means of the power input into the transmitter. The atom density was measured calorimetrically[2] with a tungsten filament (portion of a 150 watt light-bulb filament) located in the main tube, 10 cm. downstream from the juncture of the side arm containing the carbon sample. The filament was generally operated at about 750°K. The atom recombination efficiency of the tungsten probe[2] was found to be 0.053.

The recombination coefficient of carbon for hydrogen atoms was determined from separate measurements of the hydrogen atom concentration profile in a glass cylinder whose inside surface was coated with evaporated carbon and placed in the heated side arm. In these experiments the atom density as a function of distance was probed with a tungsten filament. For a first-order surface reaction an exponential decay in atom density prevails when the probe is located at large distances from the atom source.[10-12] Such a logarithmic decrease in atom concentration was observed at all temperatures studied.

From the relative heat released on the tungsten filament and the measured recombination efficiencies for tungsten, carbon, and glass,[13] the hydrogen atom concentration at the carbon surface located in the side arm may be calculated.[11] On the basis of these calorimetric measurements the hydrogen atom concentrations[14] used in the experimental measurements varied from 2 × 10^{13} to 8 × 10^{14} atom cm.$^{-3}$. The total pressure in the system ranged from 20 to 100 μ. The effect of convective flow on the atom density gradient in the main tube may be neglected.[15]

A liquid nitrogen-cooled trap was located immediately downstream from the tungsten probe to remove any condensable products. In some experiments a second liquid nitrogen trap, containing "Linde 5-Ångstrom Molecular Sieve" ($^1/_{16}$-in. pellets), was located further downstream. For product analysis this trap could be isolated and the products transferred separately to a standard gas-analysis system consisting of a Ward–LeRoy still,[16] Toepler pumps, and gas buret, for determination of the volume of each fraction and isolation of each sample for mass spectrometer analysis. Three fractions of the condensable products were taken from the Ward–LeRoy still at 108, 137, and 173°K.

Results

1. Method of Analysis.—The rate of disappearance of the carbon deposit as a result of the chemical reaction with gaseous atomic hydrogen is obtained by graphical analysis of the variation of the logarithm of the reciprocal of the light transmission of the film (τ) with reaction time (t). In a typical experiment, the complex curve shown in Fig. 2a is obtained. In order to relate the thickness d of the carbon film to the reaction time t, a comparison of the experimental curves with the corresponding theoretical curves is necessary. The details of this analysis are given in Appendix A. The values for the optical constants so derived for all of the films used in this study are plotted in Fig. 3. In general the films obtained from the same carbon-evaporation process were found to have the same optical constants.

From the theoretical curve appropriate to the derived optical constants the film thickness as a function of reaction time may be obtained for each experiment. A typical example is shown in Fig. 2b, derived from the experimental data shown in Fig. 2a. A striking feature of the resulting curve is the pronounced change in slope during the course of the reaction as was observed in practically all experiments. It should be emphasized that this feature is not the result of the curve-fitting procedure used, which does not favor an abrupt change

(10) W. V. Smith, *J. Chem. Phys.*, **11**, 110 (1943).
(11) H. Wise and C. M. Ablow, *ibid.*, **29**, 634 (1958).
(12) B. J. Wood and A. B. King, *ibid.*, **35**, 1530 (1961).
(13) B. J. Wood and H. Wise, *J. Phys. Chem.*, **66**, 1049 (1962).
(14) These data include a correction for the accommodation coefficient for transfer of the energy of atom recombination to the probe, which is 0.5 for tungsten (B. J. Wood and H. Wise, to be published).
(15) H. Wise and C. M. Ablow, *J. Chem. Phys.*, **35**, 10 (1961).
(16) D. J. LeRoy, *Can. J. Res.*, **B28**, 492 (1950).

in rate over a gradual one. The data suggest that the removal of carbon proceeds at two distinct rates during the course of the experiment.[17]

If the production of hydrogen atoms is interrupted for short periods (*e.g.*, 5 min.) without interrupting the flow of molecular hydrogen, the rate of carbon removal will continue without any discontinuity when the atom density is restored to its former level. However, if the system is evacuated for a few hours and then hydrogen is admitted at the same total pressure and atom density, a brief induction period is observed in the rate similar to that noted at the start of the experiment. In several experiments, the reaction was interrupted when only partially completed. The slide containing the partially reacted film was removed from the vacuum and more carbon evaporated on top of the residue. When the redeposited film was now subjected to reaction with hydrogen atoms, a marked decrease in reaction rate was observed at a film thickness corresponding to that of the original partially reacted film before deposition of additional carbon. These observations all point to the presence of surface-adsorbed species and their effect on the reaction rate.

2. Experimental Measurements.—The kinetics of the two reaction regions can be treated by assuming that initially two simultaneous reactions (I and II) occur, while in the latter phase only one reaction (II) prevails. The rate of reaction II, R_{II}, was found to vary with hydrogen atom concentration (Fig. 4), temperature (Fig. 5), and the index of refraction of the carbon film (Fig. 6). It is noted from Fig. 4 that the reaction appears to be of first order at low atom concentrations, but of half order at higher atom concentrations. The point at which the change in order occurs ($[H]_0$) is independent of temperature over the range studied. The rate constant k_{II}, equal to $R_{II}/[H]$ in the first-order region and equal to $R_{II}/([H][H]_0)^{1/2}$ in the half-order region, is shown in Fig. 5 and 6 as a function of temperature and index of refraction. No significant effect of the pressure of molecular hydrogen on the reaction rate R_{II} was observed (see Fig. 4–6). If one expresses the rate of carbon removal in atoms cm.$^{-2}$ sec.$^{-1}$ (assuming a density of evaporated carbon of 2.0 g. cm.$^{-3}$) and the hydrogen atom density in atoms cm.$^{-3}$, the rate of reaction in the first-order region is

$$R_{II} = 9.0 \times 10^4\,[H] \exp\left\{-\frac{9170 \pm 130}{RT} + (1 - n)(0.917 \pm 0.041)\right\} \text{ atoms cm.}^{-2}\text{ sec.}^{-1} \quad (1)$$

and for the half-order region the pre-exponential term in equation 1 is

$$1.4 \times 10^{12}\,[H]^{1/2} \text{ atoms cm.}^{-2}\text{ sec.}^{-1}$$

The variation of the rate of reaction I with atom concentration and temperature is shown in Fig. 7 and 8, respectively. The order of the reaction is approximately 0.5 and the activation energy is slightly less than that for R_{II}. In sharp contrast with R_{II}, R_I shows no significant trend with index of refraction (Fig. 9). Here again, the effect of molecular hydrogen pressure appears

(17) Because of minor variations in rate at the beginning of each experiment (see example in Fig. 2b) presumably due to surface contaminants, an effective origin for the start of the run ($t = t_0 - t_0'$) was obtained by extrapolation of the initial rate to the initial thickness (d_0).

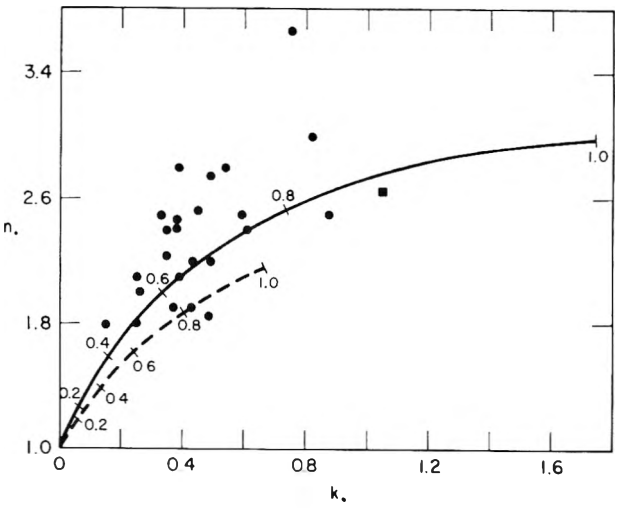

Fig. 3.—Optical constants for evaporated carbon: ●, this work; ■, Thorn and Winslow. Calculated optical constant from eq. 5 as a function of q, using graphite constants given in ref. 20 and 24.

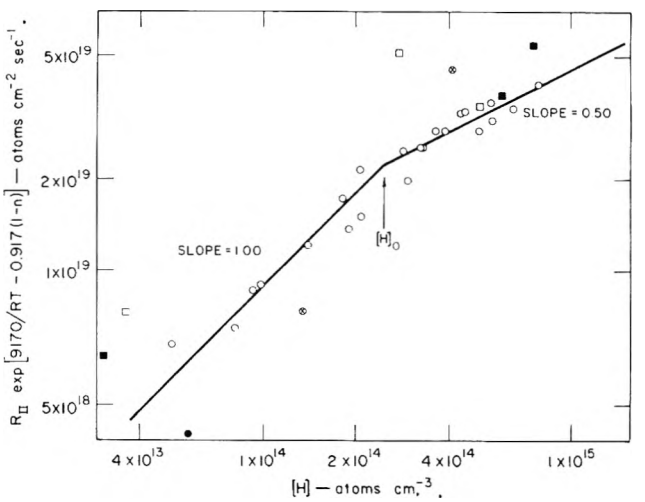

Fig. 4.—Rate of reaction II, corrected for temperature and index of refraction, *vs.* hydrogen atom concentration: ○, 0.040 mm.; ⊗, 0.040 mm.—Vycor substrate; ●, 0.040 mm.—irradiated sample; □, 0.020 mm.; ■, 0.100 mm.

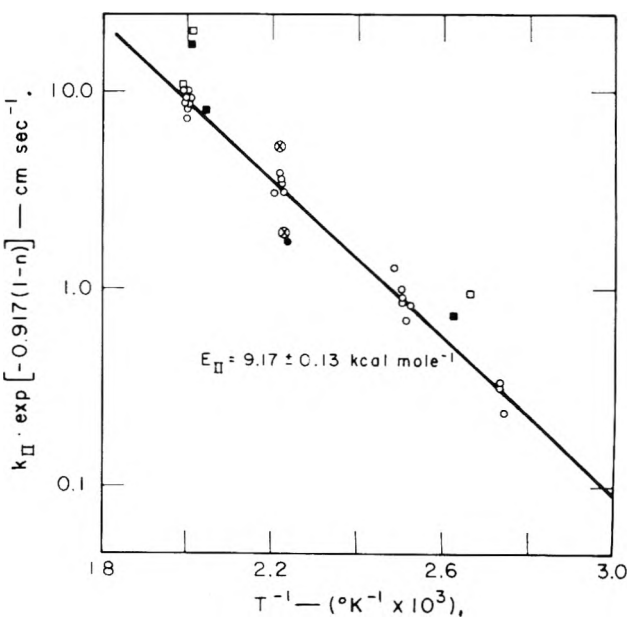

Fig. 5.—Rate constant for reaction II (corrected for index of refraction) *vs.* temperature: ○, 0.040 mm.; ⊗, 0.040 mm.—Vycor substrate; ●, 0.040 mm.—irradiated sample; □, 0.020 mm.; ■, 0.100 mm.

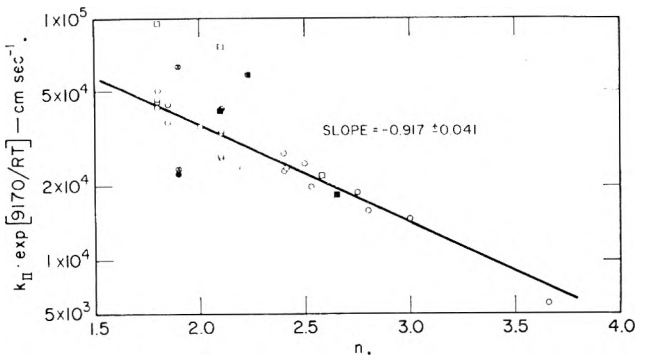

Fig. 6.—Rate constant for reaction II (corrected for temperature) *vs.* index of refraction: O, 0.040 mm.; ⊗, 0.040 mm.—Vycor substrate; ●, 0.040 mm.—irradiated sample; □, 0.020 mm.; ■, 0.100 mm.

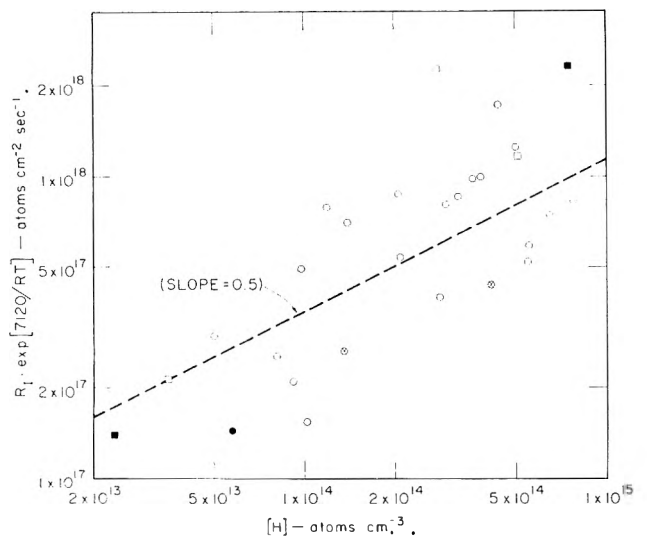

Fig. 7.—Rate of reaction I, corrected for temperature *vs.* hydrogen atom concentration (a line of slope 0.5 is drawn in for reference): O, 0.040 mm.; ⊗, 0.040 mm.—Vycor substrate; ●, 0.040 mm.—irradiated sample; □, 0.020 mm.; ■, 0.100 mm.

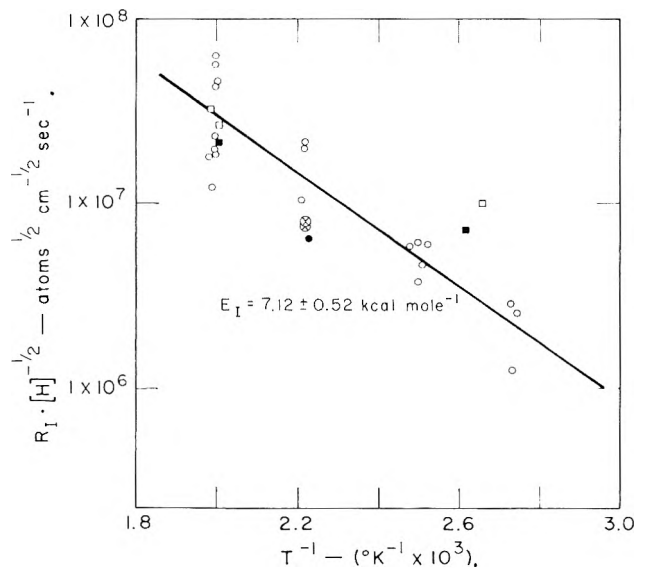

Fig. 8.—Rate of reaction I, corrected for atom concentration *vs.* temperature: O, 0.040 mm.; ⊗, 0.040 mm.—Vycor substrate; ●, 0.040 mm.—irradiated sample, □, 0.020 mm.; ■, 0.100 mm.

to be insignificant. The rate of reaction I can be expressed as

$$R_I = 3.3 \times 10^{10}\,[H]^{1/2} \exp\left(-\frac{7120 \pm 520}{RT}\right)$$

atoms cm.$^{-2}$ sec.$^{-1}$ (2)

The measured values of the hydrogen atom recombination efficiency of evaporated carbon (γ_c) at various temperatures are shown in Fig. 10. These recombination efficiencies represent the total loss of hydrogen atoms by recombination and reaction with the carbon. However, over the temperature range of this study, reaction with the solid accounts for less than 0.5% of the total removal of hydrogen atoms. Therefore the data in Fig. 10 represent essentially the recombination process on the carbon film. From these data one obtains for the rate of hydrogen atom recombination on the carbon surface [defined as $R_H = (\gamma_c \bar{c}/4)[H]$, where $\bar{c}$ is the mean atomic velocity, and $\gamma_c = 0.38 \exp(-2300/RT)$]

$$R_H = 6.1 \times 10^3 [H]\, T^{1/2} e^{-2300/RT}$$

atoms cm.$^{-2}$ sec.$^{-1}$ (3)

It is of interest to note that irrespective of the experimental conditions, such as temperature, atom concentration, and initial film thickness, reaction I ceases at a constant fraction of the total reaction time, $t_B/t_0' = 0.46 \pm 0.05$ (*cf.* Fig. 2b). The constancy of this value with reaction conditions is best seen in Fig. 11, where d_I/d_{II} is plotted against R_I/R_{II} for various reaction temperatures (d_I and d_{II} refer to the thicknesses of film that react by each reaction path, see Fig. 2b). The linearity of this plot is equivalent to a constant value of t_B/t_0', since $d_I = R_I t_B$, and $d_{II} = R_{II} t_0'$, and therefore

$$\frac{d_I}{d_{II}} = \frac{t_B}{t_0'} \times \frac{R_I}{R_{II}} \qquad (4)$$

Several determinations of the reaction rates of carbon films evaporated onto Vycor disks demonstrated no detectable effect of the substrate. Similarly, a carbon film was reacted that had been subjected to gamma radiation (0.55 megarad from a Co^{60}-source in an argon atmosphere). Again such an irradiated film showed no significant variation from the remainder of the data.

In order to see whether the change in reaction rate with time was a feature of the carbon films or the reaction mechanism, several experiments were performed using oxygen atoms instead of hydrogen atoms at 360–380°K. In the curve of film thickness *vs.* time no indication of a break was found similar to that observed for hydrogen atoms. It is concluded therefore that the abrupt change in rate at constant reaction time is a feature of the reaction mechanism involving hydrogen atoms. Also the reaction rate at 365°K. was found to be at least 5 times that observed at room temperature, in contrast to the lack of a temperature effect reported for this reaction.[7]

The product analyses were subject to considerable error because of the small amount of products obtained (about 3–10 μmoles), the array of products observed, and the background sources of products in the system. The principal carbon-containing products observed were methane and ethane, with acetylene becoming important at higher temperatures. Both ratios, C_2H_2/C_2H_6 and C_2H_6/CH_4, increased with increasing temperature and atom concentration. Other products detected

were the alkanes through C_7 (in order of decreasing yield: *n*-butane, propane, isopentane), traces of cyclohexanes, benzene, diacetylene, CS_2, and alkyl sulfides. Also CO, CO_2, H_2O, and traces of oxygenated compounds through C_3 were found. The sulfur products were not observed in the blank runs in the absence of the carbon films, while the CO, CO_2, and H_2O persisted. This indicates that the sulfur compounds arise from an impurity of sulfur in the carbon, while the oxygen presumably comes from adsorbed water on the walls or the glass itself. In addition, after a number of runs a visible deposit of polymeric material was built up in the trap. The yields of some of the minor products observed (principally oxygenated compounds) were found to be significantly reduced when the polymer was removed from the trap.

In order to test the importance of back diffusion on the product distribution methane was bled into the side arm, where the carbon film was normally located, while the discharge was operating. The condensable products observed under these conditions were principally acetylene with smaller amounts of propane. Many of the other higher hydrocarbons were also found in quantities comparable to those observed in the hydrogen atom–carbon reaction. The yield of ethane was significantly less than that observed at comparable yields of acetylene in the hydrogen atom–carbon work. It would seem that the acetylene, and possibly some of the other higher hydrocarbons, arise from back diffusion of the methane into the plasma.[18] The marked effect of increasing temperature and atom concentration (hence increasing rates of carbon removal) on the acetylene yield may result from the higher partial pressure of methane in the plasma and its effect on the decomposition reaction (*e.g.*, favoring processes that are second order in carbon compounds over those that are first order). It is therefore concluded that the primary products from the hydrogen atom–carbon reaction are methane and ethane in a ratio of CH_4/C_2H_6 varying from about 4 to 16 over the range of experimental conditions.

The form of the solid carbon appears to have an effect on the reaction rate. In an experiment performed with a spectroscopic grade graphite rod placed in the position usually occupied by the films, the product distribution was approximately the same as that for the carbon-evaporated films at comparable reaction rates. From the yield of all hydrocarbon products and the geometric surface area of the graphite, the rate of reaction per unit area for graphite was found to be about $^1/_{10}$ of that observed for the films under comparable conditions of temperature and atom concentration.

Discussion

The variation of the reaction rate (principally of R_{II}) with the index of refraction (see Fig. 6) is presumably a result of a variation of the structure of the solid. Within a single batch of evaporated carbon films, the deposits showed little variation of the optical constants, while larger variations were observed for different batches. Thus the evaporation conditions are probably an important parameter in determining the properties of the solid. Since these films have been shown to contain microcrystallites of graphite, the crystallite size or degree of crystallinity may affect the reaction kinetics.

(18) F. Fischer and K. Peters, *Z. physik. Chem.*, **141A**, 180 (1929).

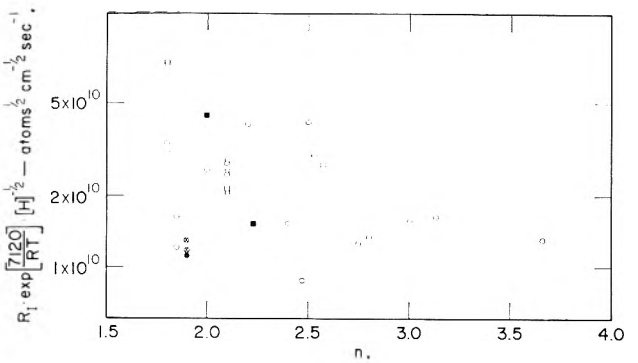

Fig. 9.—Rate of reaction I, corrected for atom concentration and temperature, *vs.* index of refraction: O, 0.040 mm.; ⊗, 0.040 mm.—Vycor substrate; ●, 0.040 mm.—irradiated sample; □, 0.020 mm.; ■, 0.100 mm.

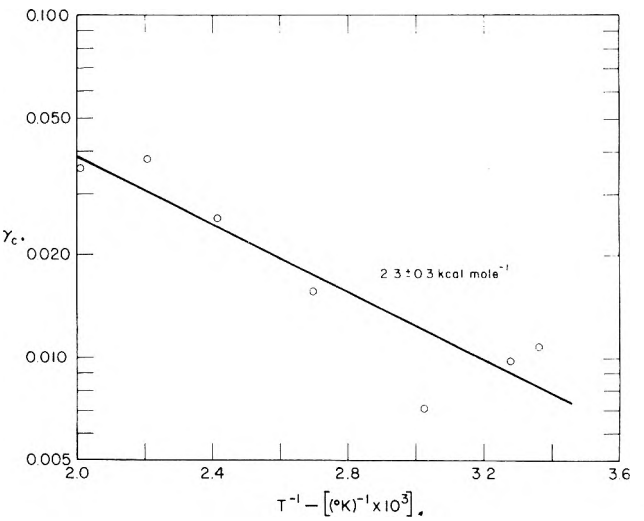

Fig. 10.—Recombination coefficient of carbon for hydrogen atoms.

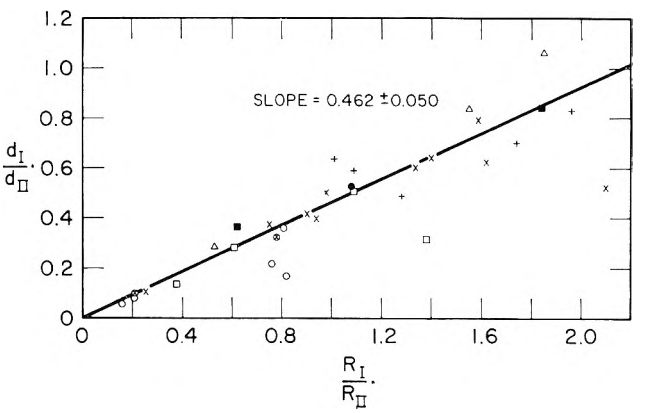

Fig. 11.—Plot of d_I/d_{II} *vs.* R_I/R_{II} (*cf.* eq. 4); 0.040 mm. total pressure: ×, 500°K.; O, 450°K.; ⊗, Vycor substrate; ●, irradiated sample; +, 400°K.; △, 365°K.; □, 0.020 mm. (500 and 375°K.); ■, 0.100 mm. (500 and 375°K.).

A number of theories have been advanced to relate the effective optical constant of a film of microcrystallites to the degree of crystallinity. The simplest model is that proposed by Garnett[19] who derived an effective optical constant ($N \equiv n - ik$) for a film of spherical crystallites of optical constant $N_c (N_c \equiv n_c - ik_c)$, dispersed in an amorphous material with an assumed optical constant of unity (*i.e.*, same as vacuum). The result is

$$\frac{N^2 - 1}{N^2 + 2} = f \frac{N_c^2 - 1}{N_c^2 + 2} \qquad (5)$$

(19) J. C. M. Garnett, *Phil. Trans.*, **203**, 385 (1904); **205**, 237 (1906).

where q is the volume fraction of crystalline material.

Among the published values of the optical constants for bulk graphite, one finds considerable disagreement. These results for Na-D or yellow light are summarized in Table I. These values appear to fall into two distinct groups.

Table I

Optical Constants for Graphite

(Wave length 5893 Å.)

n	k	Ref
2.98	1.74	20
3.04	1.82	21
1.97	0.66	22
$1.93 < n < 2.07$	...	23
2.15	0.66	24

The optical constants of evaporated carbon observed in our work, and by Thorn and Winslow,[25] are compared in Fig. 3 with the calculated effective optical constants as a function of q (eq. 5) using the constants for graphite given in ref. 20 and 24. If the optical constants of the amorphous component of the carbon film differ from unity, the left-hand terminus of the theoretical curves will be shifted without altering the general shape of the curves. Using this crude model of spherical crystallites the only qualitative conclusions that can be made from this comparison are (1) our data tend to favor the higher values of the optical constants for graphite and (2) increasing index of refraction indicates increasing degree of crystallinity (note that the increase of n with q is more nearly linear than the increase of k with q). If these conclusions are correct, the reaction rate R_{II} decreases with increasing crystallinity, while R_I does not change significantly. Such a conclusion is in line with the observation by Blackwood and McTaggart[6] that in the case of oxygen atoms the reaction rate decreases in going from charcoal to graphite to diamond.

The constancy of the position on the relative reaction time scale where the reaction rate changes has been established by eq. 4. Because of the variety of reaction conditions and initial film thicknesses (1000–3500 Å.), the thickness at the break varies markedly (320–1000 Å.). It therefore does not seem possible that the position of the break has any direct relation to the structure of the solid. Similarly, the optical transmission at the break varies markedly from experiment to experiment, and the constancy of t_B/t_0' cannot be attributed to an artifact of the optical analysis. Thus d_I/d_{II} is *not* an *intrinsic* property of the film but is determined solely by the relative rates of R_I and R_{II} by equation 4, where the time of the break on the reaction time scale is the proportionality constant. In effect, the relative quantity of material that reacts by the two reaction paths is proportional to the relative reaction rates involved.

It seems reasonable to suppose that the cessation of reaction I results from the build-up of an intermediate or product on the sites that are active to reaction I, and it should then be possible to relate the total extent of reaction up to the breakpoint to the quantity of carbon remaining at this time, in order to explain the constancy of the breakpoint in time. If one calculates this relationship for reaction I, reaction II, and the sum of reactions I and II, one finds that only reaction II gives a constant ratio of material remaining to material reacted (*i.e.*, $d_B/d_{II} - d_B) = 0.54/0.46 = 1.17$), independent of R_I/R_{II}, and hence independent of the reaction parameters. Thus the constancy of the break on the time scale can be explained by an inhibition of reaction I due to a build-up of products or intermediates of reaction II. Since reaction II occurs preferentially on the less crystalline sites, we are tempted to conclude that reaction I takes place on the crystalline sites.

As mentioned earlier, the predominant heterogeneous reaction of hydrogen atoms on the carbon surface leads to the formation of molecular hydrogen by a reaction that is first order in gaseous atom concentration. This recombination may be represented by a Rideal-type mechanism

$$S_\alpha + H \rightleftarrows S_\alpha - H \qquad (6)$$

$$S_\alpha - H + H \longrightarrow S_\alpha + H_2 \qquad (7)$$

where reaction 6 is fast and the activation energy (*cf.* eq. 3) is associated with reaction 7.

The experimental results do not yield a detailed mechanism for the formation of a hydrocarbon molecule by the reaction of atomic hydrogen with carbon. It is not known whether a radical containing carbon and hydrogen evaporates from the surface or whether the reaction goes to completion entirely on the surface of the solid.

The observed dependence of the carbon removal rate on gaseous hydrogen atom concentration suggests a mechanism involving some additional surface species, which are formed by a first-order reaction of gaseous hydrogen atoms and disappear by a reaction of higher order.

Appendix A

Analysis of Experimental Data.—The experimental and theoretical curves may both be fitted at low film thickness to an equation of the form $\tau = \tau_0 e^{-x}$; x represents $K(t - t_0)$ for the experimental curves, and $4\pi Pd/\lambda$ for the theoretical curves, where K and P are the empirically derived normalization constants, λ is the wave length of the incident light, and t_0 is the effective time for complete film removal based on an extrapolation of the experimental curve to the measured final transmission, τ_0 (*cf.* Fig. 2a). The observed curvature at the end of the run is presumably due to variations of uniformity of thickness of the film over the width of the light beam (the calculated thickness at the start of the curvature is no more than 25–50 Å. and is consistent with the non-uniformity expected from the geometry of the film evaporation).

When the theoretical transmission is plotted against $4\pi Pd/\lambda$, the shape and position of the curves are sensitive to the optical constants of the film, n and k (*cf.* appendix B). This effect is analyzed best in the region of the inflection point which occurs at values of τ^{-1} equal to about 2 to 3. Thus from the shape and position of the inflection region, a crude estimate of the optical constants can be made. On this basis, a preliminary examination of the optical data from various experiments was made and the following generalizations could be concluded: (1) the optical constants vary appreciably from

(20) H. Von Wartenberg, *Ber. physik. Ges.*, **12**, 105 (1910).
(21) C. Zakrzewski, *Bull. intern. acad. Sci. Cracovie, Ser. A*, 116 (1910).
(22) H. Senftleben and E. Benedict, *Ann., Phys.*, **54**, 65 (1917).
(23) P. Gaubert, *Compt. rend.*, **177**, 1123 (1923).
(24) J. T. McCartney and S. Ergun, "Proceedings of the Third Conference on Carbon," Pergamon Press, New York, N. Y., 1959, p. 223.
(25) R. J. Thorn and G. H. Winslow, *J. Chem. Phys.*, **26**, 186 (1957).

sample to sample and (2) at the beginning of the experiment the rate of increase of transmission is greater than predicted on the basis of both the rate constant and the optical constants of the film derived from the experimental data at the latter stages of the reaction (see example in Fig. 2a). It is therefore necessary that the optical data from each experiment be analyzed separately in order to obtain the data of thickness *vs.* reaction time.

This variation in the rate of change of transmissivity with time from the theoretical predictions may be due to two causes: (1) a change in reaction rate without variation of optical constants, or (2) constant reaction rate and change in optical constants. In order to examine the latter hypothesis the rate of change of thickness with time was assumed to be constant and equal to that observed at the later stages. The change of optical constants with time necessary to fit the data in the initial period was then calculated. From such an analysis it was found that: (1) the values of the optical constants have to decrease during the initial stages, (2) the initial values of the optical constant n so derived are all significantly greater than 3.0, the largest value observed for pure graphite (see text), and (3) the change in n during the initial stages is much greater than the change in the extinction coefficient k as affected, for example, by changes in crystallinity. These observations are inconsistent in the light of the known relationship between the degree of crystallinity and the optical constants, and contrary to the expectation of preferential reaction at the non-crystalline sites. Therefore, an interpretation of the results in terms of a change in the reaction rate with time was attempted.

A computer program was written for the Burroughs 220 computer which selected the optical constants for each film by a curve-fitting procedure that best satisfied two test criteria: (1) $4\pi Pd/\lambda \geq 0.95\,K(t_0 = t)$ and (2) the slope between a pair of experimental points $\geq 95\%$ of the slope at the previous pair of points tested at a lower value of $K(t_0 - t)$. (The factors of 0.95 were added to ensure that a good fit would not be rejected because of small fluctuations from the predicted curve.)

Appendix B

Optical Constants.—The equations for light transmission of a thin film deposited on a substrate of different optical constants have been derived by Heavens[26] and used in various forms by several authors.[25,27,28] These equations, however, give the transmission *into* the substrate and do not consider the effect of the third interface (substrate to vacuum) on the transmission. The third interface will reflect a constant fraction of the light and the principal effect of ignoring this will be to change the transmission by a constant factor, independent of thickness. However, for the high values of n observed for carbon, the reflection at the carbon–vacuum interface (first interface) is quite high, and a significant portion of the light reflected at the third interface will be re-reflected at the first interface. This component will have to make two passes through the carbon and hence will be greatly attenuated for large values of film thickness, and the secondary effect of the third interface on the total transmission is therefore only important at low values of film thickness.

Using the equations for transmission of a double layer of films on a transparent substrate[26] one can calculate the total transmission of a thin film deposited on a film, or slab, of transparent substrate suspended *in vacuo*. These equations involve second-order terms in $\cos \omega_2$ and $\sin \omega_2$, where $\omega_2 = 2\pi n_2 d_2/\lambda$, and n_2 and d_2 are the index of refraction and thickness of the substrate. When ω_2 is large (100 for our case), the interference phenomena in the substrate can be neglected, because variations in the absolute thickness of the substrate over the width of the light beam are much greater than $\lambda/4n_2$. If these variations are assumed to be random, then the terms in $(\cos^2 \omega_2 - \sin^2\omega_2)$ and $(\sin \omega_2 \cos \omega_2)$ can be set equal to zero.

Thus, assuming a transparent ($k_2 = 0$) substrate of random thickness, one obtains

$$\tau^{-1} = \frac{p_{12}^2 + q_{12}^2 + g_3^2(r_{12}^2 + s_{12}^2)}{l_{13}^2 + m_{13}^2} \qquad \text{(B-1)}$$

where

$$\begin{aligned}
l_{13} &= (1 + g_1)(1 + g_2)(1 + g_3) \\
m_{13} &= h_1(1 + g_2)(1 + g_3) + h_2(1 + g_3)(1 + g_1) \\
p_{12} &= p_2 + g_1 t_2 - h_1 u_2 \\
q_{12} &= q_2 + h_1 t_2 + g_1 u_2 \\
r_{12} &= r_2 + g_1 v_2 - h_1 w_2 \\
s_{12} &= s_2 + h_1 v_2 + g_1 w_2 \\
p_2 &= e^{\varphi_1} \cos \omega_1 \\
q_2 &= e^{\varphi_1} \sin \omega_1 \\
t_2 &= e^{-\varphi_1}(g_2 \cos \omega_1 + h_2 \sin \omega_1) \\
u_2 &= e^{-\varphi_1}(h_2 \cos \omega_1 - g_2 \sin \omega_1) \\
v_2 &= e^{-\varphi_1} \cos \omega_1 \\
w_2 &= -e^{-\varphi_1} \sin \omega_1 \\
r_2 &= e^{\varphi_1}(g_2 \cos \omega_1 - h_2 \sin \omega_1) \\
s_2 &= e^{\varphi_1}(h_2 \cos \omega_1 + g_2 \sin \omega_1) \\
\varphi_1 &= \frac{2\pi\, kd}{\lambda} \\
\omega_1 &= \frac{2\pi\, nd}{\lambda} \\
g_1 &= \frac{1 - n^2 - k^2}{(1 + n)^2 + k^2} \\
h_1 &= \frac{2k}{(1 + n)^2 + k^2} \\
g_2 &= \frac{n^2 - n_2^2 + k^2}{(n + n_2)^2 + k^2} \\
h_2 &= \frac{-2n_2 k}{(n + n_2)^2 + k^2} \\
g_3 &= \frac{(n_2 - 1)}{(n_2 + 1)}
\end{aligned}$$

On substitution one obtains the transmission of a thin film on a thick transparent substrate suspended *iu vacuo*, which is in the form

$$\tau^{-1} = \frac{1}{D}\left[C_1 e^{4\pi kd/\lambda} + C_2 e^{-4\pi kd/\lambda} + C_3 \cos\left(\frac{4\pi nd}{\lambda}\right) + C_4 \sin\left(\frac{4\pi nd}{\lambda}\right)\right] \qquad \text{(B-2)}$$

where

(26) O. S. Heavens, "Optical Properties of Thin Solid Films," Academic Press, New York, N. Y., 1955, p. 74 ff.
(27) W. H. Brattain and H. B. Briggs, *Phys. Rev.*, **75**, 1705 (1949).
(28) F. Abeles, *Rev. Optique*, **32**, 257 (1953).

$$D = (1 + g_3)^2[(1 + g_1)^2 + h_1^2][(1 + g_2)^2 + h_2^2]$$
$$C_1 = 1 + g_3^2(g_2^2 + h_2^2)$$
$$C_2 = (g_1^2 + h_1^2)(g_2^2 + h_2^2 + g_3^2)$$
$$C_3 = 2[g_1g_2(1 + g_3^2) - h_1h_2(1 - g_3^2)]$$
$$C_4 = 2[g_2h_1(1 + g_3^2) + g_1h_2(1 - g_3^2)] \quad \text{(B-3)}$$

The equations (B-3) are to be contrasted to the case when the third interface is neglected,[25,26] where

$$D = n_2[(1 + g_1)^2 + h_1^2][(1 + g_2)^2 + h_2^2]$$
$$C_1 = 1$$
$$C_2 = (g_1^2 + h_1^2)(g_2^2 + h_2^2)$$
$$C_3 = 2(g_1g_2 - h_1h_2)$$

and

$$C_4 = 2(g_1h_2 + g_2h_1) \quad \text{(B-4)}$$

The calculated results using equations (B-2 and B-3) for $n = 2.5$, $k = 0.4$, and $n_2 = 1.531$, shows a deviation from a logarithmic plot of about 3% as d approaches 0, while equations (B-2 and B-4) predict no such deviation. Thus the differences between the results of equations (B-3) and (B-4) for the optical constants used in this work are all small, but not negligible, except for the direct correction for reflective loss at the third interface.

REVERSAL OF ELECTRO-OPTICAL BIREFRINGENCE IN BENTONITE SUSPENSIONS

BY MANESH J. SHAH, DONALD C. THOMPSON, AND CLEVE M. HART

Development Laboratory, IBM Corporation, San Jose, California

Received May 8, 1962

An investigation in the birefringence behavior of various monodisperse bentonite suspensions containing a threefold range of particle sizes (2500–7800 Å.) is presented. The dimensions of the macromolecules and their degree of dispersion were determined with the aid of an electron microscope. Birefringence measurements were carried out using monochromatic light, applying pulsed d.c. field as well as a.c. and square wave fields to the bentonite dispersions in water-cooled cells with 10- and 40-mm. light path lengths. Suspensions of various concentrations and various particle sizes were employed in this study. It was concluded that the negative birefringence exhibited by bentonite in weak fields is brought about by a permanent dipole along the axis of symmetry of the bentonite disk. The permanent dipole orientation is perpendicular to the strong field orientation, which is predominantly governed by the electrical anisotropy of the macromolecule. Experimental results with square wave and a.c. fields in support of this model are presented.

Introduction

Electro-optical birefringence of colloids has been of considerable value in the characterization of some rigid macromolecules. A number of colloidal systems have been studied by this method[1-11] for determination of the size as well as the electrical properties of tobacco mosaic virus, bentonite, and other colloidal particles. It has been observed that some colloidal suspensions exhibit a reversal in the sign of birefringence[6,7] especially at high concentration of the suspensions. Although this behavior may be explained on the basis of interactions between the particles and their ionic atmospheres at high concentrations,[6] recent investigations in our laboratory[12] in birefringence of dilute bentonite suspensions indicate that the reversal of birefringence could be an inherent property of the macromolecule.

In this article, we present birefringence measurements of essentially monodisperse bentonite suspensions which were obtained by fractional centrifugation with a supercentrifuge. A mean value of semi-major axis of the particle was determined on an electron microscope in each of the four suspensions prepared for the birefringence study. The concentration of the suspensions was varied from 0.05 to 0.6%, whereas the electrical energy was supplied in the form of pulsed d.c. fields, pulsed and steady sinusoidal fields and square wave fields. The purpose of our investigations was to examine the orientation mechanisms contributing to the reversal of birefringence in bentonite suspensions.

In the first part of this paper we have described the preparation of the bentonite suspensions with the help of a supercentrifuge and measurements of particle semi-major axis on the electron microscope. In the second part we present the birefringence measurements under pulsed d.c. fields and discuss the effect of particle dimensions and interactions on birefringence reversal. In the third part, experimental measurements with a.c. and square wave fields are shown, and an analysis of the results are given, to account for the birefringence reversal of bentonite.

Experimental

Optical Assembly.—The optical assembly for birefringence measurements of colloids has been described by several previous investigations.[1,3,6,8,12] In our study Glan Thompson prisms were used as polarizer and analyzer, whereas magnitude and the sign of the optical retardation was determined with a Babinet Soleil compensator and a photomultiplier tube (RCA 6217). A mercury vapor lamp with a low noise power supply was used as the light source. This assembly enabled measurements of optical retardation with an error of less than one degree.

Birefringence Cell.—The majority of the measurements were carried out with the cell shown in Fig. 1. It consisted of a quartz cell enclosed in a plexiglass-sealed water jacket, provided with threaded aluminum tubes for light path. The optical strain in the quartz cell was negligible. The electrode insert assembly consisted of various pieces of carefully machined nylon and the platinum electrodes were assembled and held together by

(1) A. Kahn and D. R. Lewis, *J. Phys. Chem.*, **58**, 10, 801 (1954).
(2) C. T. O'Konski and J. B. Applequist, *Nature*, **178**, 1464 (1956).
(3) C. T. O'Konski and A. J. Haltner, *J. Am. Chem. Soc.*, **79**, 5634 (1957).
(4) S. Krause and C. T. O'Konski, *ibid.*, **81**, 5082 (1959).
(5) R. M. Pytkowicz and C. T. O'Konski, *Biochim. Biophys. Acta*, **35**, 466 (1959).
(6) C. T. O'Konski and B. H. Zimm, *Science*, **111**, 113 (1950).
(7) B. W. Sakmann, *J. Opt. Soc. Am.*, **35**, 66 (1945).
(8) H. Benoit, *Ann. Phys.*, **6**, 561 (1951).
(9) C. T. O'Konski, K. Yoshioka, and W. H. Ortung, *J. Phys. Chem.*, **63**, 1558 (1959).
(10) I. Tinoco, *J. Am. Chem. Soc.*, **77**, 3476 (1955).
(11) I. Tinoco, *ibid.*, **79**, 4336 (1957).
(12) M. J. Shah and C. M. Hart, *IBM J. Res. Develop.*, **7**, 44 (1963).

nylon screws. The electrodes were spaced 3.81 mm. apart, and the light path length in the cell was 12.7 mm.

For measurements at low concentrations and in weak fields, a silica cell with 40-mm. path length was used. The water jacket assembly for this cell was identical to that of the quartz cell, except that the dimensions were larger and that the nylon part for electrode assembly was made in one piece. There was a small strain birefringence in this cell assembly.

Electrical Assembly.—The electrical assembly was arranged to select any of the four types of fields to the birefringence cell; namely, pulsed d.c., pulsed a.c., continuous a.c., and square wave fields, by interconnecting through a switching box.

For pulsed d.c. fields a 300-w. Sorenson variable power supply with a range of 0–600 v. was employed. Pulsing was achieved by means of an electronic pulse generator driving two mercury relays.

The sinusoidal field was generated by a Hewlett-Packard 200 CDR audio oscillator, a Dynakit 70-watt power amplifier and a step up transformer (Thordarson 25s27) to provide a maximum field of 500 v. r.m.s. The field was pulsed by means of a neon relaxation oscillator driving a mercury relay. For fields lower than 200 v., a continuous sinusoidal voltage was utilized, when the heating of the solution was not significant. In this case, the output of the HP-200 CDR oscillator was fed into a wide band power amplifier (Krohn-Hite DCA-50), to extend the frequency range to 5–500,000 c.p.s.

The square wave field was obtained with a Hewlett–Packard 211A square wave generator, and the Krohn–Hite wide band power amplifier. This system had a frequency range of 1 to 100,000 c.p.s. For frequencies lower than 10 c.p.s. the output of the power amplifier was connected through a 150 μf., 440 v. external capacitor in series with the cell.

Fractionation of Particles.—A batch of 12 l. of 1.5% bentonite[13] dispersion was prepared by thoroughly stirring the bentonite powder in demineralized water. The solids in the dispersion were then fractionated by continuously feeding the suspension into the Sharples supercentrifuge. The equivalent spherical diameter of particles settling in a continuous centrifuge with a cylindrical bowl, varies inversely with the speed of rotation ω and is directly proportional to the square root of the linear velocity V of the solution in the bowl,[14] so that the values of V and ω were varied to yield particles with equivalent diameter in the proportions of 1, 1.5, 2, 3, and 4.

To ensure the homogeneity of the suspensions for each set of values of ω and V, the centrifugations were repeated as shown in Fig. 2. The solids were collected on a thin layer of polyvinyl chloride (Delchem X-769) on the wall of the bowl. The film was peeled and removed as a tube, and then cut into three equal portions. The lower portion which contained the larger particles was discarded, whereas the upper portion containing smaller particles was remixed with the main solution stream. The middle portion was redispersed in demineralized water, recentrifuged, and the above division procedure was repeated. These dispersions were then dialyzed for a period of 10 to 30 days. The concentration of the dispersion was determined by evaporating a previously weighed sample at 50° under vacuum. The dispersion was then diluted to the required strength.

Electron Microscope Measurements.—Each of the fractions was analyzed under an electron microscope to determine the average value of the semi-major axis of bentonite particles as well as the degree of uniformity in size distribution. The original samples were first diluted to a concentration of 0.0004% and the particles were deposited on an electrically charged grid, taking advantage of the net negative charge on the particles. A field of about 6 to 10 v. was used on the grids for about 1 to 5 sec. This procedure proved to be successful in depositing a large number of individual bentonite micelles, although stacking could not be eliminated altogether.

Blank grids were prepared with water and photographed to assure the flatness of the formvar coating on the grid. Then, for each bentonite suspension carrying one particle size, several grids were prepared, and micrographs were obtained at different locations on each grid. The length of the semi-major axis of the individual flakes was calculated from the photographs by measuring the largest and the smallest diameters of the flat area of the particles. Independent electron micrographs of bentonite suspensions prepared from the same original sample indicated that the particles were about 100 to 150 Å. thick. The well known shadowing technique was used for this purpose.

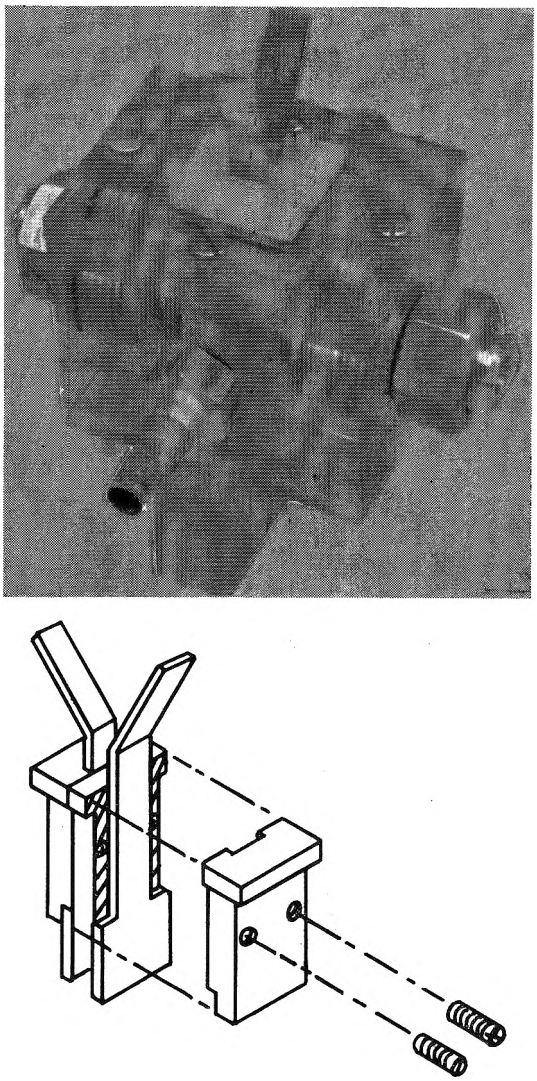

Fig. 1.—The birefringence cell with 12.7-mm. path length and the electrode assembly.

Birefringence Measurements under Pulsed D.c. Fields.[15]—The pulse width for the d.c. field was first adjusted to a time greater than the rise time of birefringence for the solution. At a fixed field strength the compensator was then adjusted until the light output on the photomultiplier tube was minimal at the pulse time when the birefringence reached a steady state level. Figure 3 shows the light output pulse in three positions. The first photograph indicates light pulse before adjusting the compensator, and the second photograph represents the pulse after adjustment. The last photograph shows the trace at correct compensation.

Conductivity of the suspension was evaluated and repeatedly checked during the compensator measurements with an impedance bridge. The duration of the repetitive pulsed field was limited to 2 or 4 sec. at a time to prevent heating of the suspension. When compensator adjustment required longer time, the final reading was taken after letting the suspension cool for a few minutes.

The decay of birefringence was displayed on the oscilloscope screen and photographed on 35 mm. film. The developed film was then mounted on the projector of a Benson–Lehner data reduction machine. On the screen of the projector were two

(13) The Wyoming bentonite used in this study was obtained from Baroid Division of the National Lead Company, and unlike the work of Kahn[1] was not converted to the sodium form. A portion of the suspension was run through a cation-exchange resin and the resin was then leached with HCl to determine the cations on the bentonite surface. The analysis indicated the presence of Ca, Mg, and Na on the surface of the bentonite in the ratio of 6.4:3.2:1.

(14) J. H. Perry, "Chemical Engineers Handbook," Third Edition, McGraw–Hill Book Co., New York, N. Y., 1950, p. 995.

(15) For a comprehensive description of experimental methods, see references 1, 3, 6, and 8.

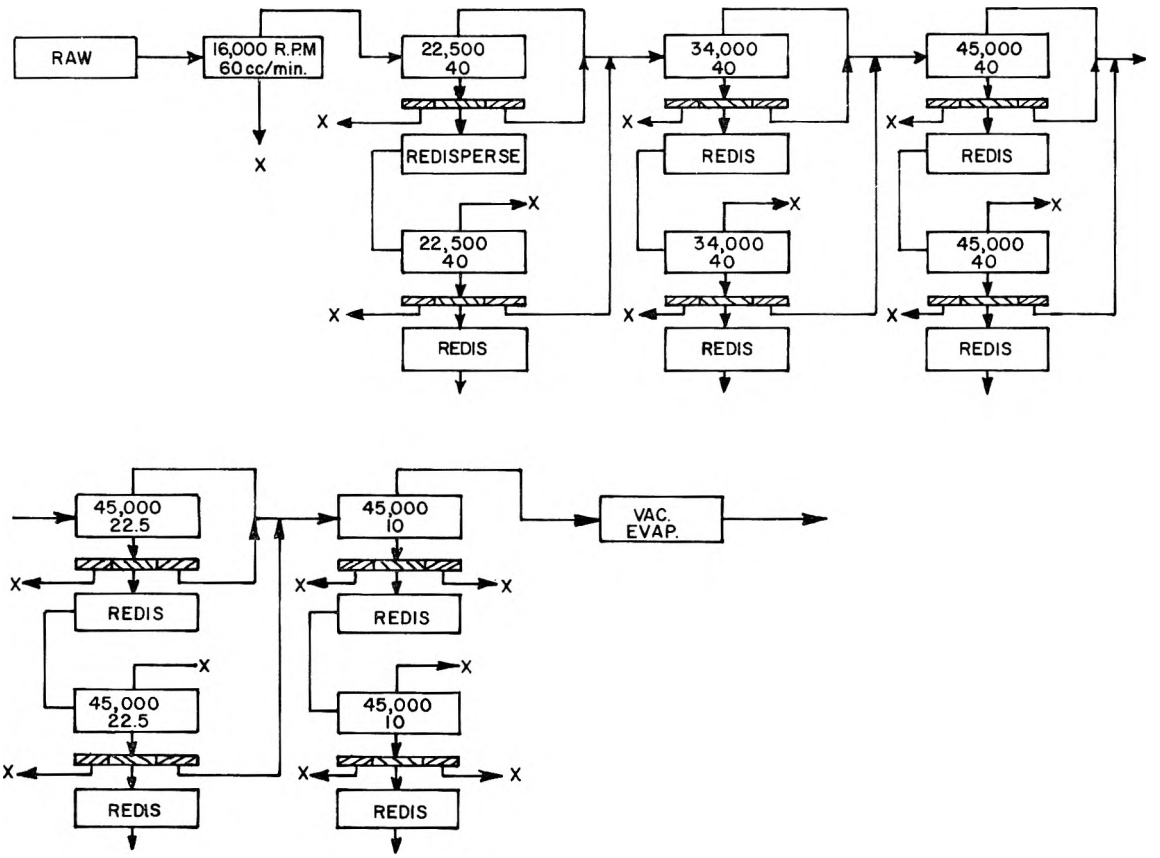

Fig. 2.—Fractionation procedure for bentonite suspensions in the supercentrifuge.

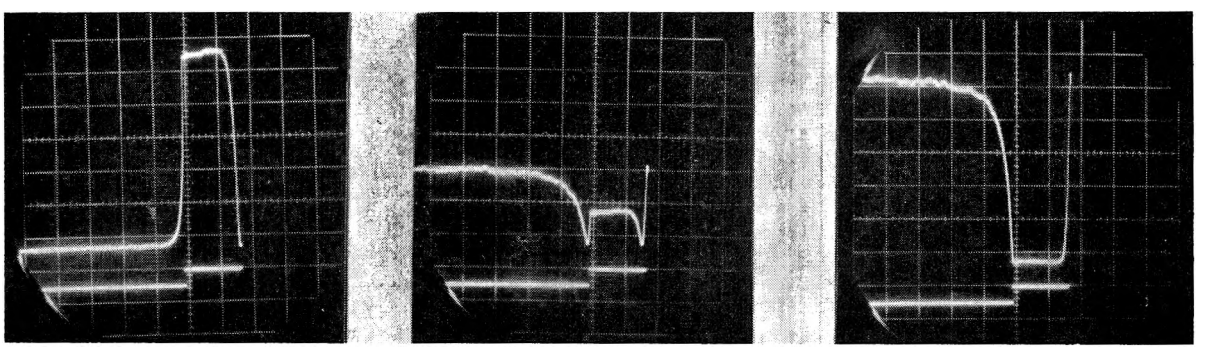

Compensation $\delta = 0$. Compensation $\delta > 0$. Exact compensation.

Fig. 3.—Photographs of light pulse under d.c. fields before and after adjustment of Babinet–Soleil compensator.

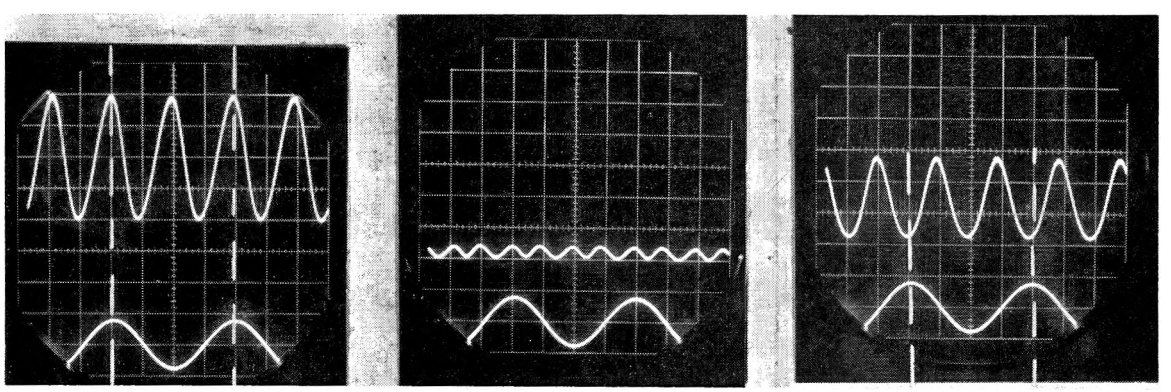

Compensation smaller than exact δ. Compensation of exact value of δ. Compensation larger than exact δ.

Fig. 4.—Photographs of light output under a.c. fields, showing steady and alternating value of δ at various positions of the compensator.

movable cross wires which located points on the curve. The x and y coördinates of the points were then transferred to punched cards with the help of a reader connected to the Benson–Lehner machine. The y values represented the light intensity related to the optical retardation δ by

$$\delta(t) = 2 \arcsin(\sqrt{I/I_m} \cdot \sin \delta_m/2)$$

where I_m is the value of maximum light intensity attained before the field is cut off and δ_m is the corresponding value of optical retardation determined by the compensator. With the aid of a computer program on an IBM 704, the results were then transformed to plots of the optical retardation δ *vs.* time.

Birefringence Measurements under A.c. Fields.—The light output under a.c. fields is generally composed of a steady as well

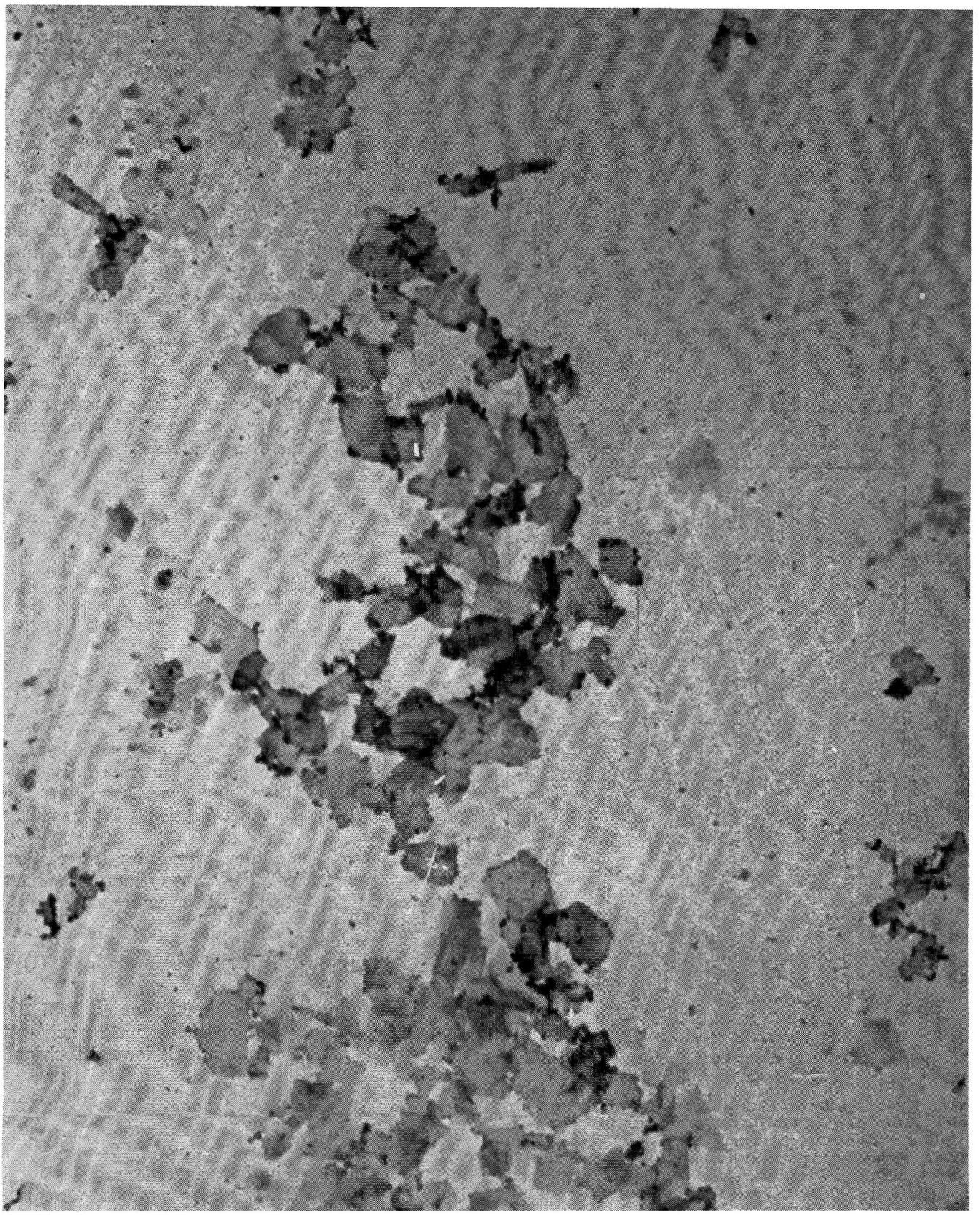

Fig. 5.—Electron micrograph of bentonite prepared by the supercentrifuge: fraction 2 (22,500 ×).

as alternating components due to the various birefringence orientation mechanisms. Sakmann[7] assumed that all the orientation mechanisms follow Kerr's law, an assumption valid only for weak fields. Furthermore, Sakmann's method of determining the alternating component from the oscilloscope trace curve does not yield sufficiently accurate results. The Babinet–Soleil compensator in our apparatus, on the other hand, enables a direct measurement of both the steady and alternating component of the optical retardation.

Initially, for low voltage (below 100 v.) continuous low frequency (10–50 c.p.s.) a.c. fields, the photomultiplier response showed the birefringence to follow the field completely with no steady component. At slightly higher frequencies the birefringence response was in the form of repeating wave motion containing various magnitudes and signs of optical retardation. In both these cases, the value of δ could be measured directly with the compensator for each maximum of the periodic light output. These measurements were then repeated at higher voltages.

At still higher frequencies, and at higher voltages for all fre-

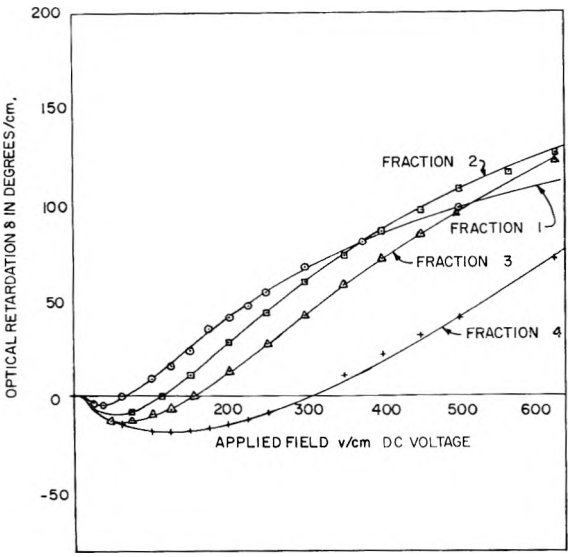

Fig. 6.—Optical retardation of 0.2% bentonite suspensions containing various particle sizes, under d.c. fields.

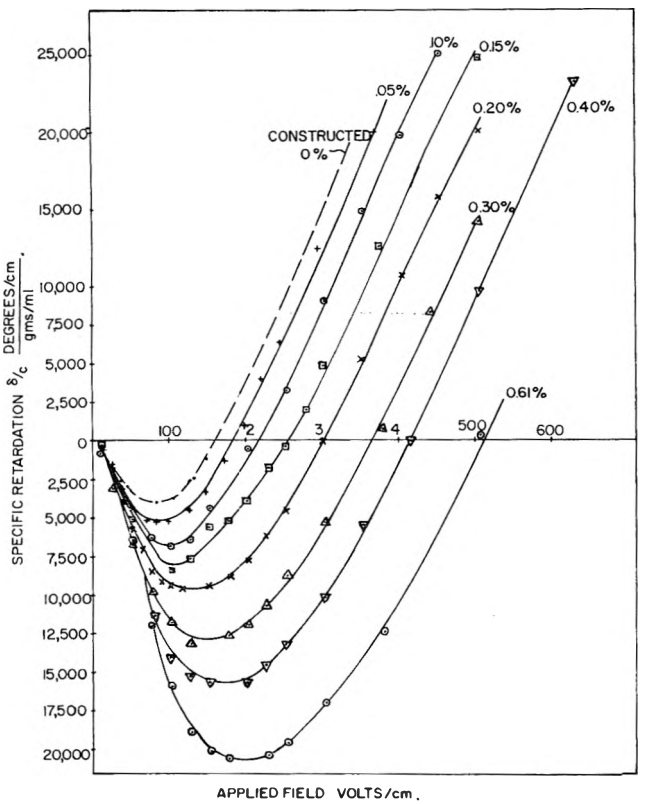

Fig. 7.—Specific retardation for the suspension of fraction 4 at various concentrations, weak field region.

quencies, the magnitude of the steady component increased. In this case, the value of δ for the steady component was determined by bringing the mean steady level of the photomultiplier output wave corresponding to the mean d.c. level to a minimum with the compensator adjustment. In Fig. 4 the light output at the minimum and at higher and lower positions on the compensator is shown. It is seen that at the adjusted position of the compensator the alternating components for the values of δ for overcompensation and for undercompensation are equalized.

At some (characteristic) frequency for a particular particle size, the alternating component became negligible. For these conditions, δ was measured in the same manner as under pulsed d.c. fields. At fields above 200 v./cm., the electrodes were switched to pulsed a.c. to prevent heating effects. The birefringence decay curves under high frequency a.c. fields were also photographed for comparison with measurements under d.c. fields.

Birefringence Measurements under Square Wave Fields.—Measurements of optical retardation under square wave fields were carried out in the same manner as under d.c. and a.c. fields. The oscilloscope trace of the photomultiplier output was photographed, and the sign as well as the magnitude of phase retardation at the trace peaks was determined by the compensator.

Discussion and Results

Electron Microscope Measurements and Size Determination.—In Fig. 5 we have shown a typical electron micrograph of bentonite present in the fractionated suspensions. The particles have the shape of flakes, and the method of deposition on the microscope grid leads to some unavoidable piling and chain formation as well as rolling over of flakes. The small dark spots seen around the flakes are impurities. The dimensions on the semi-major axes of individual particles were measured for a number of particles on the grids.

Table I lists the average dimensions in various samples together with the root mean square deviation, σ, which suggests to some extent the degree of uniformity. The columns a and b represent the longer and shorter semi-major axes of the oval disk, respectively.

TABLE I

MEASUREMENTS OF PARTICLE SIZE FROM ELECTRON MICROGRAPHS

Sample	Mean semimajor axis dimensions, Å. a	b	$r = \sqrt{ab}$	Root mean square dev.	r calcd. from relaxation curves F_1	F_2
1	7813	4707	6064	0.14	5700	2610
2	6150	4333	5162	.138		
3	5157	3275	4110	.178		
4	3760	2346	2970	.196	2730	1450
5	3167	1898	2452	.222		

It seems that an additional step of centrifuging and redispersing could have possibly improved the uniformity of size distribution, but unfortunately, the quantity of the solids in the suspensions was too small to permit it.

The values of the semimajor axes for two particle sizes were also calculated from the relaxation curves. The measurements were fitted to an expression

$$\frac{\Delta n}{\Delta n_0} = F_1 e^{-6D_1 t} + F_2 e^{-6D_2 t} \qquad (1)$$

using Prony's interpolation formula[16] on an IBM 704 computer. The mean geometric semimajor axis was then obtained with Perrin's formula for a disk-shaped particle[17]

$$r^3 = \frac{3}{32}\frac{kT}{\eta D} \qquad (2)$$

Values of r calculated in this manner for samples 1 and 4 are also listed in Table I. One can see that the calculated values of r, for the larger fraction of the particles F_1 (eq. 1), are in good agreement with the measured values. The magnitude of F_1 indicates that the samples were about 70% monodisperse. The electron micrographs reveal that the bentonite suspensions prepared by fractionation on the supercentrifuge are fairly monodisperse and contain particles with a range of 2500–6000 Å. mean semi-major axis.

(16) F. B. Hildebrand, "Introduction to Numerical Analysis," McGraw-Hill Book Co., New York, N. Y., 1956.

(17) F. Perrin, *J. phys.*, 497 (1934); 1 (1937).

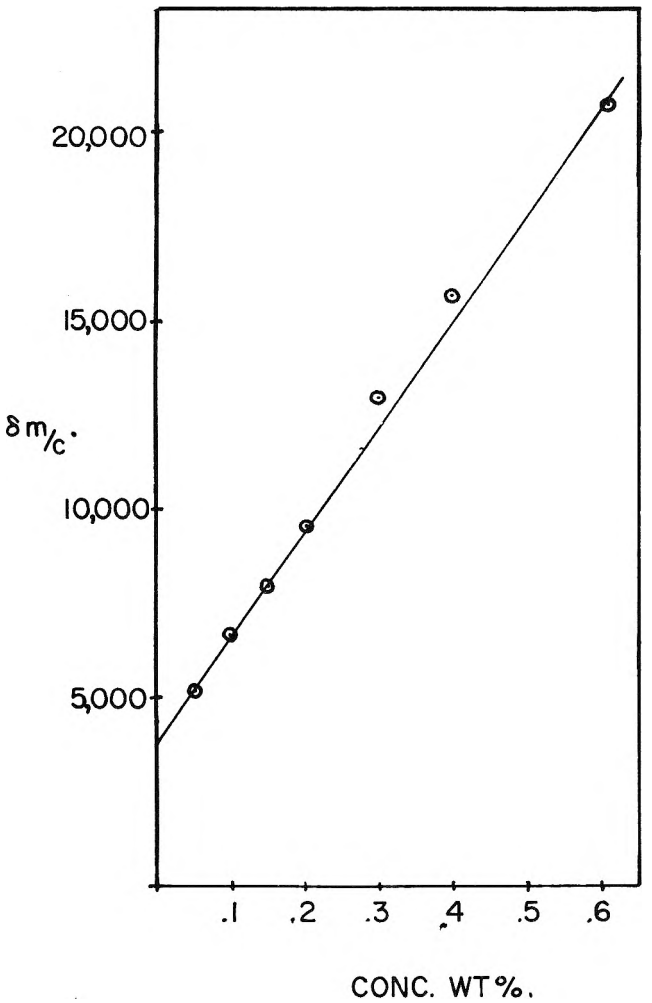

Fig. 8.—Minimum value of specific retardation as a function of concentration for suspensions of fraction 4.

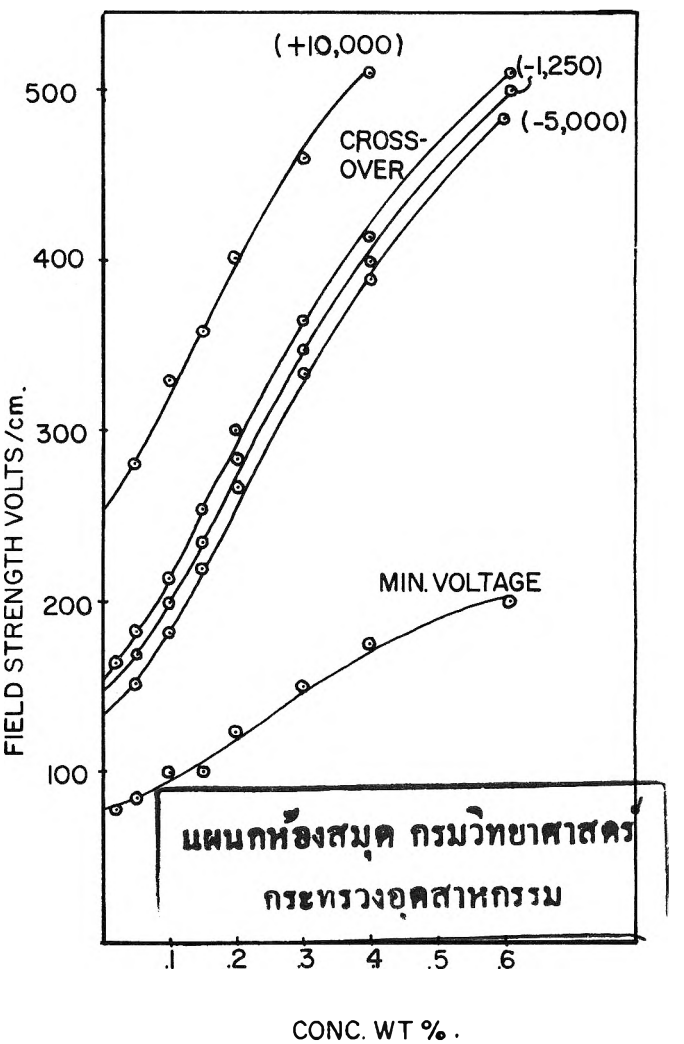

Fig. 9.—Field strength as a function of concentration at various specific retardation values (fraction 4).

Birefringence Measurements.—In Fig. 6 the optical retardation of 0.2% suspensions containing various sized particles under d.c. fields is presented. The plot shows that bentonite particles of all sizes exhibit reversal of birefringence. The magnitude of the negative δ and the value of birefringence reversal field E_R decrease with increasing value of r. If one were to assume the thickness of all particles to be the same, the results suggest that a decrease in the ratio of the particle thickness to the semi-major axis, brings about a reduction in negative birefringence and E_R. The larger particles saturate at lower field strengths in the positive region, and the magnitude of their saturation birefringence is smaller in comparison to smaller particles.

Fractions 2 and 4 (see Table I) were selected for a study of the effect of interactions on the negative birefringence. In Fig. 7 we have presented results of specific optical retardation (defined as δ per unit concentration with units of deg. ml./cm. g.) of progressively diluted suspensions of fraction 4 as a function of field strength. The measurements covered a concentration range of 0.61 to 0.05%. As seen in the figure, the value of the negative specific retardation as well as the birefringence reversal voltage decreases steadily as concentration is reduced. Interestingly enough, the slopes of curves in the vicinity of the reversal voltage are nearly the same for all concentrations.

Using the results of Fig. 7, we have plotted δ_m/c, the minimum value of specific optical retardation (negative maximum) *vs.* concentration in Fig. 8. The curve shows a linear relationship between δ_m/c and c and has an intercept of 4000 deg. ml./cm. g. at zero concentration. Similarly, in Fig. 9 the field strength is shown as a function of concentration for various values of negative and positive δ. Although these curves do not show a linear dependence, the intercepts on the ordinate for zero concentration appear to be finite, so that with the aid of Fig. 8 and 9, extrapolated values of δ/c for various voltages for an infinitely dilute suspension are shown in Fig. 7 as a dotted curve. These results suggest, then, that even in very dilute solutions the birefringence reversal persists. To confirm this statement, values of field strengths for minimum birefringence, zero birefringence, and a positive value of birefringence were determined for a 0.02% suspension. Although the magnitude of δ below reversal voltage could not be ascertained with sufficient accuracy at this dilution, the sign of birefringence was indeed identified as negative, and the data fell on the curves shown in Fig. 8 and 9.

A study of variation in decay times with increasing concentration was also made to determine the concentration at which the interactions become significant. It was found that for the fraction 4 the decay time rose sharply above 0.3%, but below this concentration dilution had little effect on the relaxation time.

It appears, then, that although the particle–particle interactions play a significant role in enhancing the

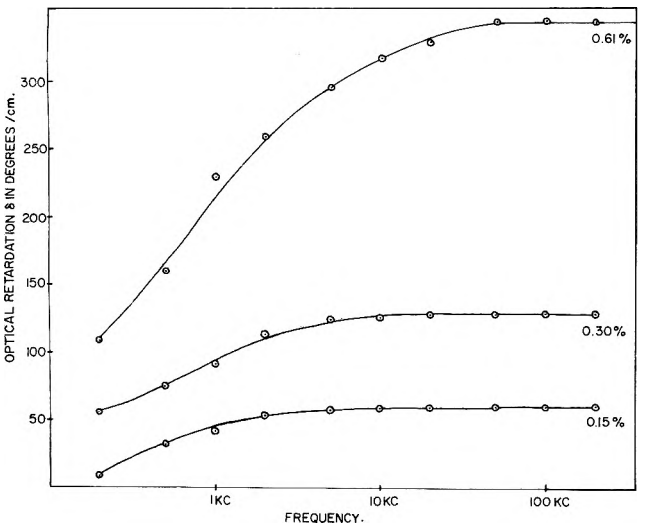

Fig. 10.—Optical retardation of the suspensions of fraction 4 under a.c. fields, as a function of frequency.

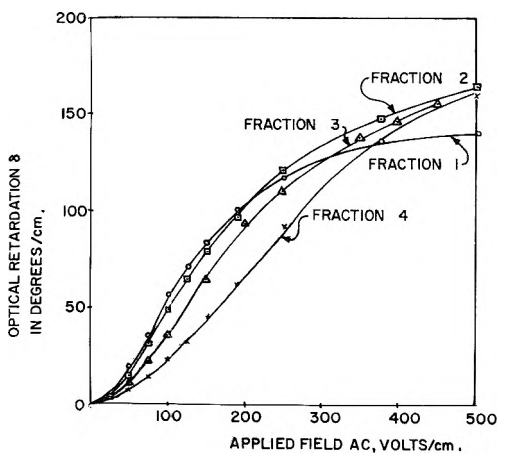

Fig. 11.—Birefringence of 0.2% bentonite suspensions containing various particle sizes under a.c. fields. Frequency: above "characteristic" frequency for each suspension.

negative birefringence, the bentonite particles exhibit negative birefringence even in the absence of interactions, and therefore the birefringence reversal is due to an intrinsic property of the particles. It remains, then, to determine the orientation mechanisms contributing to this property of bentonite.

It is known[3] that sinusoidal fields may bring into play various orientation mechanisms, depending upon the field frequency. It was observed for fraction 5 that for frequencies of 20 to 40 c.p.s. the birefringence was negative and that the particles followed the field completely. At frequencies of 80 to 160 c.p.s., the birefringence consisted of a mixture of positive and negative wave forms, and the particle still followed the field. At 250 c.p.s. the negative form was eliminated, whereas at 500 c.p.s. there was a direct as well as an alternating component of birefringence, with the total birefringence being positive. As the frequency of the field was further increased, the alternating components completely vanished, indicating that the orientation ceased to follow the field.

These results indicate that in low fields and at low frequencies the particles orient under the influence of at least two different mechanisms, one of which predominates at very low frequencies, whereas the other is important at high frequencies. For intermediate frequencies, a mixed orientation brings about negative as well as positive birefringence. In the absence of interactions the only orientation mechanism responsible for birefringence under high frequency a.c. fields is the induced polarization, which gives rise to the direct component of birefringence.

In Fig. 10 the direct component of the optical retardation is plotted against frequency for the fraction 4 suspensions of various concentrations. The results show that the induced polarization orientation contribution increases with increasing frequency, and as the concentration of the suspension is increased, this dependence extends to higher frequencies. In all cases, however, δ reaches a steady value at a characteristic frequency which depends not only on the particle size but also on the concentration.

The induced dipole birefringence of 0.2% suspensions containing the first four fractions of Table I under a.c. fields with frequencies above the characteristic values is presented in Fig. 11. The figure shows that the optical retardation shows a quadratic dependence on voltage in weak fields. The Kerr constant, K, increases with increasing particle size, and the larger particles saturate earlier, as indeed one would expect from the theory.

Also, in Fig. 12 specific optical retardation under sinusoidal fields is plotted *vs.* r.m.s. voltage for various concentrations of the fraction 4 suspensions. The results of Fig. 13 indicate that for the smaller particles the specific retardation is essentially the same for 0.05 and 0.15% suspensions, whereas slight gain is noticeable at 0.3%. The birefringence response of the 0.61% suspension, however, shows a rather large interaction effect, which, as described earlier, was also noticed in the decay time measurements.

In summary, we may state that under low frequency a.c. fields the bentonite particles follow the field, with at least two orientation mechanisms contributing to birefringence. At a high frequency, the alternating component of birefringence becomes negligible as a result of the predominance of the induced polarization, and the suspensions obey Kerr's law in weak fields with saturation at higher fields. The interaction of particles under a.c. fields is small below about 0.2% concentration for particles of 3000 Å. semimajor axis.

It was observed that our bentonite suspensions undergo a reorientation in square wave fields indicating the presence of a permanent dipole on the particle. The low frequency a.c. data as stated earlier also suggested the possibility of two orientation mechanisms, one of which gives rise to negative birefringence. Professor O'Konski, during a discussion in our laboratory, suggested that the saturation effects in a system involving both permanent and induced polarization mechanisms may be able to account for the birefringence reversal on the basis that the two orientation torques are perpendicular to each other. Since the birefringence saturation theory[11] does not deal with this special case, the proposed model was examined from the point of view of Benoits[8] approximate equation for the birefringence of a colloidal suspension. It was observed that if the absolute magnitude of the term in Benoit's equation due to the permanent dipole were larger than the magnitude of the term due to the electrical anisotropy term, the expression predicted negative birefringence in low fields and positive birefringence at high fields. However, the ratio of the birefringence reversal voltage to the

voltage for minimum birefringence indicated by Benoit's equation was much lower than the ratio observed for our suspensions.

In what follows we present birefringence measurements under square wave field in the vicinity of the reversal voltage to support the model of opposing permanent and induced orientation torques. First, we assume that the permanent polarization is along the axis of symmetry of bentonite, whereas the induced polarization is along the semi-major axis. The permanent dipole orientation predominates at low fields and saturates rapidly with increasing voltage. At high fields the stronger induced polarization orientation torque gives rise to positive birefringence. At the reversal voltage the orientation torques are equal, and the particles are oriented with their axes of symmetry at some angle θ_R to the field. At this voltage, zero steady-state birefringence occurs due to equal probability of orientation of the particles in plus and minus directions.

The birefringence of the fraction 4 suspension under square wave fields is shown in Fig. 13, where drawings of the oscilloscope traces of the photomultiplier output, as well as the applied field, are shown for four different frequencies. Four voltage values characteristic for birefringence response under d.c. fields were selected; *viz.*, voltages for (1) the negative region below minimum δ, (2) minimum value of δ, (3) zero value of δ, and (4) a positive value of δ. The traces in the figures move from right to left, and the time scale, as well as the scale on the photomultiplier output trace, is different for each photograph. The magnitude and the sign of the optical retardation at the peak value in the trace are noted below the traces.

At a field of 50 v./cm., the particle undergoes a complete reorientation at 10 c.p.s. frequency and, furthermore, exhibits only negative birefringence, suggesting a predominant permanent dipole orientation. At 126 v./cm. and at the same field frequency, a small positive birefringence appears, and the positive component rises to a sharp spike at the birefringence reversal voltage (3). As the field is further increased to 500 v./cm., the alternating component of birefringence vanishes.

At low frequencies the particles undergo reorientation, so that the reversal of sign in square wave field causes the particles to undergo rotation at the reversal voltage. During this rotation, momentary particle alignment along the semimajor axis occurs, which explains the sharp positive spike at the instant the field direction is reversed. At higher fields the net birefringence is positive, but the spikes are retained due to the particle rotations, although they are less than the rotation angle of the reversal voltage. The reorientation spikes disappear when field frequency is increased beyond the relaxation frequency of the particles, as shown by the oscilloscopic traces at 1000 c.p.s. At intermediate frequencies and at voltages higher than the birefringence reversal point, particle rotations occur, although the orientation angle between the field direction and the semimajor axis of the particle is other than θ_R. These particle rotations, therefore, produce a positive spike at the instant the field direction is reversed.

It is concluded then that the square wave measurements support the hypothesis that the negative birefringence in weak fields is produced by a predominant

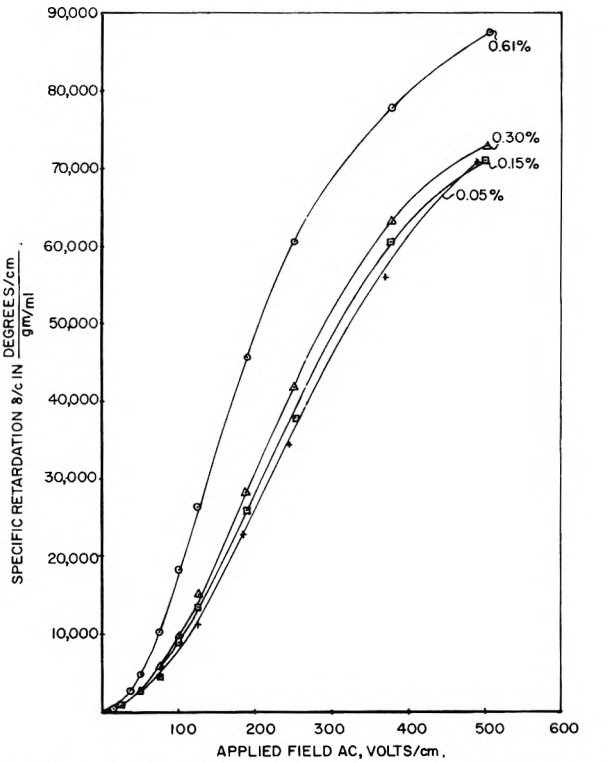

Fig. 12.—Specific optical retardation under a.c. fields (frequency 100 kc.) for fraction 4 suspensions of various concentrations.

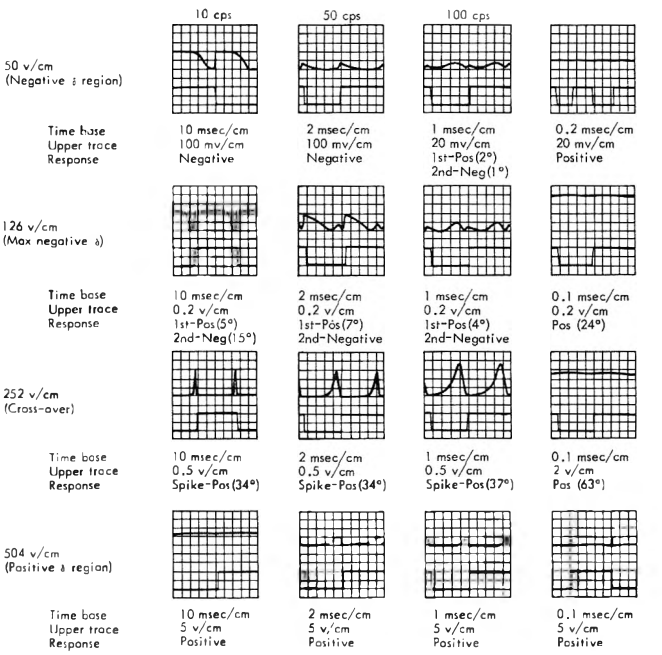

Fig. 13.—Birefringence of a 0.2% fraction 4 under square wave fields of various frequencies (all time bases: right to left; all zero light outputs center line).

permanent dipole orientation, whereas at higher field strengths the stronger induced dipole orientation gives rise to a net positive birefringence. The permanent dipole orientation vanishes when the frequency of the square wave field becomes higher than the relaxation frequency of the particles, a result compatible with a.c. measurements.

Finally, under saturating fields, measurements of δ in high frequency a.c. fields, as well as in d.c. fields, reached the same saturation value, thus confirming the predominance of induced polarization orientation in strong fields. Furthermore, in weak d.c. fields, the suspen-

sions were found to obey Kerr's law after the field value was corrected for the electrode potential. This was done by measuring the value of the current at the end of the current trace on the oscilloscope and multiplying it by the resistance determined independently with an impedance bridge. The predominance of permanent dipole orientation in weak fields was also confirmed in this manner.

Summary and Conclusions

Birefringence measurements of monodisperse bentonite suspensions prepared by careful centrifugation and redispersion on a supercentrifuge were carried out utilizing monochromatic light and a Babinet–Soleil compensator. It was observed that in the range of particle sizes 2500 to 7000 Å. all bentonite micelles exhibit negative birefringence in weak d.c. fields and birefringence reversal with increasing field strength. The magnitude of negative birefringence, as well as the value of birefringence reversal voltage, decreases as the ratio of the length of semimajor axis to the thickness of the particles increases. An examination of specific birefringence $\Delta n/c$ at various concentrations of the suspensions showed that although the negative birefringence of bentonite increases with increasing concentration, suspensions exhibit birefringence reversal at infinite dilution. It appears, therefore, that an intrinsic property of the bentonite macromolecules is responsible for their abnormal behavior.

Measurements with sinusoidal and square wave fields of various frequencies indicate that the particles have a permanent dipole along their symmetry axis. This dipole brings about an orientation of the disk-shaped particles in a direction perpendicular to the alignment at higher voltages, thereby giving rise to negative birefringence in weak fields. In stronger fields the particles orient under opposing torques due to permanent and induced dipoles. At some particular field value characteristic for a particle size, the two orientation torques are equalized, and zero net birefringence is obtained. In saturating fields the induced polarization orientation is predominant. Interactions in suspensions of higher concentrations give rise to an augmentation of orientation along the symmetry axis, although the interaction effect is relatively smaller on induced orientation. Finally, the positive birefringence in weak d.c. fields shows obedience to Kerr's law, and saturation data under a.c. as well as d.c. fields confirm predominance of induced polarization orientation in strong fields.

Acknowledgments.—The authors take pleasure in acknowledging the helpful suggestions of Professor C. T. O'Konski of the University of California during this investigation. The authors are also grateful to a number of colleagues in Advanced Technology (Development Laboratory, IBM Corp., San Jose, Calif.) for their cooperation in this project, to Mr. R. K. Van Valkenberg for preparing the electron micrographs, and to Mr. Terrance Kelly for assistance with numerical computations.

NUCLEAR MAGNETIC RESONANCE STUDY OF ION-EXCHANGE RESINS. I. HYDRATED DOWEX-50 RESINS

By R. H. Dinius, M. T. Emerson,[1] and G. R. Choppin

Department of Chemistry, Florida State University, Tallahassee, Florida

Received July 2, 1962

The proton magnetic resonance spectra for hydrated ion-exchange resin samples have been measured. The effect on the chemical shift and line width was observed as a function of resin phase hydration, resin cross linkage, and temperature for Dowex-50. The effects are interpreted in terms of changes in water structure and rapid proton exchange in the resin phase.

Introduction

Bauman and Eichhorn[2] first suggested that ion-exchange resins could be considered as concentrated solutions of strong electrolytes. In this model, a Donnan membrane equilibrium is established between the resin phase and the external solution phase. Solvent and mobile ions are free to exchange between the phases, but the fixed resinate ions are restrained in the resin phase. When this model was modified to take into account the strain energy ("swelling pressure") resulting from the volume expansion of the cross-linked resin on sorption of solvent, reasonable success was achieved in accounting for many properties of ion-exchange resins.[3–5]

This thermodynamic model has been criticized by Rice and Harris[6] as not being an accurate physical representation of the ion-exchange resins. These authors offer a model of a resin as a cross-linked polyelectrolyte gel in which ion pair formation accounts for the specific interaction between the fixed exhange groups and the exchangeable ions. A comparison of the heats, free energies, and entropies of exchange for resins and for concentrated chloride solutions showed no detailed agreement, although the free energies were of the same order in the two systems.[7] These data were interpreted as indicating that ion pair formation is responsible for the specific interactions of the resin. It was further postulated that the majority of cations (for polystyrenesulfonic acid resin) not in ion pairs are distributed in a charged layer around the resin chains. The formations of ion pairs is further supported by the work of Kotin and Nagasawa.[8]

(1) Department of Chemistry, Wayne State University, Detroit, Michigan.

(2) W. C. Bauman and J. Eichhorn, *J. Am. Chem. Soc.*, **69**, 2832 (1947).

(3) (a) H. P. Gregor, *ibid.*, **73**, 3537 (1951); (b) E. Glueckauf and G. P. Kitt, *Proc. Roy. Soc.* (London), **A228**, 322 (1955).

(4) J. F. Duncan, *Australian J. Chem.*, **8**, 293 (1955).

(5) G. E. Myers and G. E. Boyd, *J. Phys. Chem.*, **60**, 521 (1956).

(6) S. A. Rice and F. E. Harris, *Z. Physik. Chem.* (Frankfurt), **8**, 207 (1956).

(7) E. H. Cruickshank and P. Meares, *Trans. Faraday Soc.*, **53**, 1299 (1957).

(8) L. Kotin and M. Nagasawa, *J. Chem. Phys.*, **36**, 873 (1962).

Glueckauf[9] has recently postulated that the ion-exchange resin is a gel-like structure within which there is a large variation in the degree of cross linking. He also postulates fissures inside the gel with widths up to 2000 Å., these fissures being connected by many small channels through which solvent and electrolyte may diffuse. Using this model he has been able to explain the deviations from Donnan equilibrium which was found earlier.[10]

An investigation of the proton magnetic resonance spectra of hydrated ion-exchange resins was undertaken in an attempt to obtain further information on the physical state of the internal resin phase. Data on the chemical shifts and line widths for H_2O in the resin phase could provide a basis for accepting or rejecting the ion pair formation model as a correct physical picture.

Furthermore, it is possible in principle to obtain rates of exchange and rates of diffusion as well as equilibrium constants for processes in the resin. Previously, we have made a preliminary report[11] on the chemical shift as a function of water content. In an independent note and paper, Gordon[12] has reported somewhat similar studies on resins immersed in water and other solvents.

Experimental

The hydrogen form of the cation-exchange resin, Dowex-50, used in this work, was obtained from Bio-Rad Laboratories Co. as 200–300 mesh spherical beads. Special care was taken to remove contaminating metal ions by carrying each resin sample through a washing process described previously.[13] Spark spectroscopic analysis indicated that the metal ion concentrations in the purified resin were less than 15 parts per million. The washed resin was stored wet. Prior to use, the resin was dried (for about 2 hr.) to constant weight at 80° under a pressure of 0.3 mm. Initially, the water content of the dried resin was determined by a Karl Fischer titration in methanol. After a number of such determinations had indicated the absence of water, constancy of weight on drying was assumed a sufficient criterion for complete removal of the water. Samples of resin having a definite water content were made by equilibrating the samples with water vapor and measuring the increase in weight due to the added water. The resin samples were sealed in 5 mm. n.m.r. sample tubes to ensure against gain or loss of water. Samples used to study the transition from a one- to a two-phase system were prepared by weighing increments of water into weighed samples of dried resin.

The nuclear magnetic resonance spectra were taken on a Varian HR 60 spectrometer. An external reference of cyclohexane was sealed in a 1 mm. capillary and inserted inside the resin sample tube. All chemical shifts were measured with respect to cyclohexane and converted to water as a reference by subtracting the water–cyclohexane shift. Negative shifts mean shifts to lower field. The bracketing side-band technique was used in calibrating the spectra. The audio side-bands were produced by audio modulation of the static magnetic field using a Hewlett–Packard 200 CD audio oscillator, the audiofrequency being measured by a Hewlett–Packard 523 B frequency meter.

The effect of temperature was studied rather qualitatively, since a thermostated probe was not available at the time, by warming or cooling the samples before running the spectrum. The spectrum was then run as rapidly as possible while the temperature drifted back to room temperature. For this work starting temperatures of 2–3° and 90° were used. All other spectra were taken at 25 ± 1°.

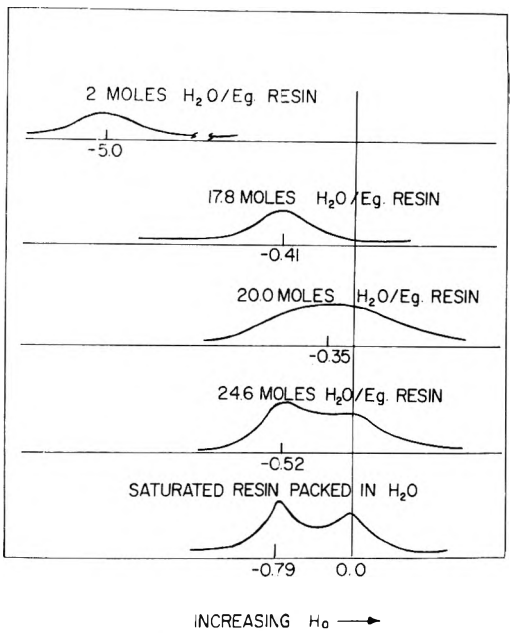

Fig. 1.—N.m.r. spectra for Dowex-50 (4% DVB) resin samples of varying degrees of hydration.

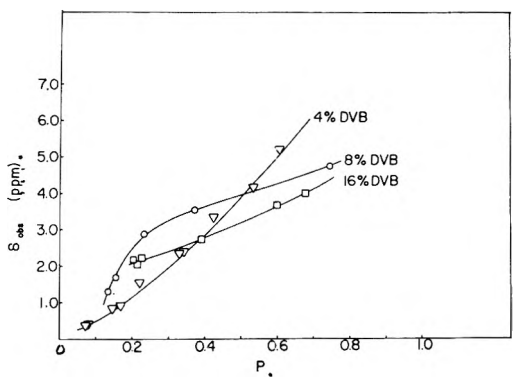

Fig. 2.—Observed chemical shift for hydrated Dowex-50 resin as a function of hydration, where P is the mole fraction of protons on hydronium ions.

Results and Discussion

The n.m.r. spectra of three forms of Dowex-50 ion-exchange resin having 4, 8, and 16% divinylbenzene (DVB) content were measured at different degrees of hydration. A single rather broad line due to the water protons is observed at low water content. A second line appears as soon as the water begins to form a layer on the outside of resin bands. Typical spectra for the 4% DVB resin are shown in Fig. 1. It is noted that the width of the single resonance line at low water content increases as the water content decreases.

The position of the line shifts markedly to lower field with decreased water content. Plots of the observed shift of the internal water line as a function of the amount of hydration are shown in Fig. 2 for the three forms of resin. These chemical shifts are not corrected for magnetic susceptibility differences. The samples are composed of a collection of nearly perfect spheres. The magnetic field inside a spherical sample is independent of the bulk susceptibilities.[12] The observed chemical shift variations can be explained if there is a rapid exchange of protons between the acid sites of the resin and the water protons. The resulting shift would be given by the weighted average of the chemical shifts of the acid, water, and hydronium ion protons

(9) E. Glueckauf, *Proc. Roy. Soc.* (London), **A268**, 350 (1962).
(10) E. Glueckauf and R. E. Watts, *ibid.*, **A268**, 339 (1962).
(11) R. H. Dinius and G. R. Choppin, *J. Phys. Chem.*, **66**, 268 (1962).
(12) J. E. Gordon, *Chem. Ind.* (London), 267 (1962); *J. Phys. Chem.*, **66**, 1150 (1962).
(13) G. R. Choppin and R. H. Dinius, *Inorg. Chem.*, **1**, 140 (1962).

which are in equilibrium. Hood and Reilly[14] have shown that the chemical shift can be used to obtain acid dissociation constants of strong acids. We have reported similar work on *p*-toluenesulfonic acid.[11]

It was originally hoped that a similar treatment could be used to obtain acid dissociation constants for the ion-exchange resins. This was not possible since one cannot sufficiently saturate the resins with water to obtain the needed dilute solution shifts. However, it can be shown that in concentrated solutions of strong acids[11]

$$\delta_{obsd} \approx \delta_1 \alpha P$$

where δ_1 is the intrinsic hydronium ion shift, α the degree of acid dissociation, and P the mole fraction of protons of hydronium ions. Since δ_1 is assumed constant, by comparing the slopes of the plots of δ_{obsd} *vs.* P of several acids, a crude estimate of the magnitude of α can be obtained. This, then, provides a measure of the relative acid strength.

Approximate acid strengths were obtained by comparing the slopes in Fig. 2 with similar data for strong acids.[11,14,15] The indications are that the 4% DVB resin is a stronger acid than HCl or *p*-toluenesulfonic acid and probably similar in strength to $HClO_4$. The 16% resin seems to be weaker and more on the order of nitric acid. The 8% falls somewhere in between. It is reasonable to postulate that the order of acid strengths results from the increase in the more extensive organic cross linking for the higher DVB resins, which causes a decrease in the effective dielectric constant in the vicinity of the sulfonate group.[11] The lower dielectric constant in higher DVB resins would promote ion pair association, and it seems likely that this is the explanation of the different apparent acidities rather than any difference in the intrinsic acid dissociation constants.

The proton shift of the water inside the resin may very well be dependent upon factors not present in the solutions for which the above treatment was worked out. For instance, in the derivation of the chemical shift, the shift for the water protons is assumed constant and set equal to zero (using pure water as the reference). However, it is known that the shift of pure water is dependent on the degree of hydrogen bonding, as has been shown by the variation of its shift with temperature.[16] Any interactions which would change the degree of hydrogen bonding inside the resin from that in pure water would give rise to a variation in the observed shifts not attributable to the acid dissociation process. The non-polar and, hence, hydrophobic character of the resin matrix would be expected to discourage a uniform distribution of water throughout the resin. Instead, for unsaturated resins, we would expect the water molecules to cluster around the highly polar acid sites forming domains of water. The size and shape of these domains would be limited by the geometry of the surrounding resin matrix; the more highly cross-linked the resin, the smaller the size.

It is reasonable to expect that the presence of highly polar sites in the resin will affect the structure of the water by changing the degree of hydrogen bonding. The extent of the disruption of structure is dependent on the amount of water present. The greater change in the water structure would be expected to occur at low water concentrations. If there is only one water molecule at a site, it could bond only with the site itself. One would expect that the protons of this molecule would have a different chemical shift than pure liquid water. It is known that the resonance line moves upfield as hydrogen bonds in water are broken,[16] and hence it is reasonable to expect that at lower water concentrations there would be an upfield shift contribution to the water line position for the resin. This would cause a decrease in slope at higher P in Fig. 2.

From a measurement of the swelling of the resin as water is added, we know the resin matrix expands up to a point near saturation, at which point it can expand no farther. It is known that large osmotic pressures are present near the point of saturation.[2,17] It is reasonable to expect that the large forces produced would affect the internal water structure by attempting to crowd the molecules closer together, thereby enhancing the hydrogen bonding and producing an increase in the negative chemical shift at high P.

The presence of aromatic rings in the form of divinylbenzene units might also affect the observed shift through possible π-bonding. Also, the aromatic ring currents would tend to shift the resonance to higher fields[18] and thus tend to decrease the slopes. The magnitude of the shifts would be dependent on the number of benzene rings present and hence should increase in going from the 4% to the 16% DVB resin. The upfield shift should also increase with decrease in distance from the benzene ring to the water protons. Thus the shift should increase somewhat with water content. This last effect would be progressively smaller for the 8 and 16% DVB resins.

The effect of the resin on the water structure is apparent in Fig. 2 by causing non-linear variations in the plots. The water in the 8% DVB resin is not able to assume a normal water structure until a fairly high degree of hydration is reached and never becomes as complete as the 4% DVB resin. The water in the 16% DVB resin never reaches a high degree of structure before the matrix forces take over and causes a decrease in slope. The conclusions regarding the resin effect on the water structure do not, however, invalidate the previously proposed acid strengths, since association between the sulfonate site and the proton would increase with acid strength and polarity.

The width of the internal water line is much larger (20 to 100 c.p.s.) than that of pure water (0.5 c.p.s.) but much less than in ice, indicating that the water molecules are in rapid, though probably somewhat restricted, motion. The results of the line width measurements on 16% DVB resin are shown in Fig. 3. Although extensive data on the 4 and 8% resins were not taken, the indication was that the same trends are present except for a shift of the minimum to progressively lower P from 4 to 16% DVB. The peak in the plot occurs as a layer of water begins to form on the exterior of the bead. At this point the exchange of protons with the external phase causes the line to

(14) G. C. Hood and C. A. Reilly, *J. Chem. Phys.*, **27**, 1126 (1957).

(15) J. A. Pople, W. G. Schneider, and H. J. Bernstein, "High Resolution Nuclear Magnetic Resonance," McGraw-Hill Book Co., New York, N. Y., 1960, p. 443.

(16) W. G. Schneider, H. J. Bernstein, and J. A. Pople, *J. Chem. Phys.*, **28**, 601 (1958).

(17) E. Glueckauf, *Proc. Roy. Soc.* (London), **A214**, 207 (1952).

(18) J. S. Waugh and R. W. Fessenden, *J. Am. Chem. Soc.*, **79**, 846 (1957).

broaden and the spectrum appears as shown in Fig. 1. The shift in the peak position to lower water content with increased resin cross linking reflects the decrease in water capacity of the more highly cross-linked resins. For resin samples with less than 2 moles of water per equivalent of resin the lines become too broad to observe by high resolution techniques. The matrix resinate proton n.m.r. line-width of 8 gauss has been reported[19] and therefore is not observable by high resolution techniques.

It is postulated that a large part of the increase in line width of the water inside the resin bead as compared to that in a concentrated electrolyte solution is caused by magnetic field inhomogeneity inside the resin. Above, we have pictured the hydrated resin beads as containing domains of water surrounded by the resin matrix. This structure can be approximated on a semimicro scale by a sample of organic resin beads with water filling the interstitial space. Since a collection of beads does not form a solid mass the water is free to diffuse between interstitial domains. To determine the broadening of this model system, we filled a sample tube with 50 to 100 mesh beads and water. The measured line width was about 10 c.p.s. and was practically independent of the amount of water present. Similar findings have been made by Gordon.[12]

A second experiment which shows the dependence of the line width on the size of the water domains for domain sizes approaching microscopic dimensions was performed with flowers of sulfur in water. A freshly shaken sample of sulfur dispersed uniformly through the water phase exhibited a water line comparable in width to pure water. However, as the sulfur settled, the line width increased to a width of approximately 100 c.p.s. This increase is obviously related to the decrease in interstitial space between sulfur particles as the sulfur settles, *i.e.*, domain size. This parallels the decrease in water domain size which would accompany the shrinkage of a hydrated resin as the water of hydration is removed, and therefore we would expect an increase in line width as the amount of water in the resin decreases.

Other mechanisms of broadening such as restriction of motion of the water molecules and exchange with the acid protons are also probably responsible for some of the observed line broadening. One would expect that as the water content is reduced the remaining water molecules would become more tightly bound to the resin and thus cause a decrease in transverse and longitudinal relaxation times T_2 and T_1. Proton exchange in acid–water systems is known to be much too fast to measure by n.m.r. We would, therefore, expect this exchange to be very rapid even in the resin phase since they are strong and easily ionizable acids. The change in line position also shows we are looking at a fast exchange process and this mode would not contribute to the line broadening.

A crude measurement of T_1 by the progressive saturation[20] method indicated that the T_1 for water in the saturated resin was the same as that of pure water and decreased by about an order of magnitude at the lowest water content. These results should only be taken as an order of magnitude indication. They do indicate that the restriction of motion of the water molecules is not very great.

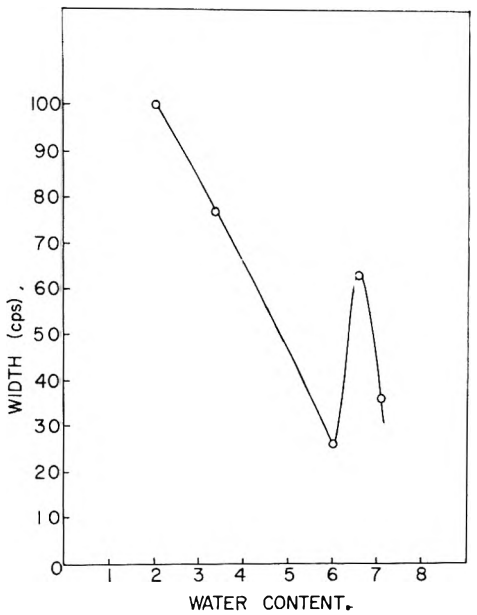

Fig. 3.—The variation of the full width at half maximum for hydrated Dowex-50 (16% DVB) resin as a function of water content in moles of water per equivalent of resin.

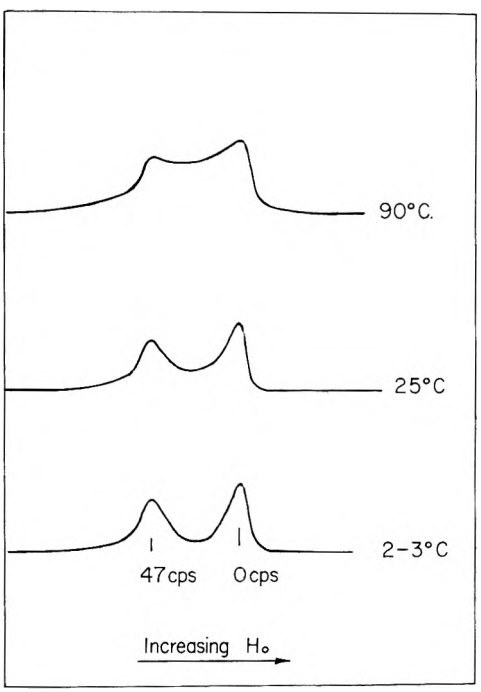

Fig. 4.—N.m.r. spectra for hydrated Dowex-50 (4% DVB) resin at different temperatures.

Another possible cause of the increase in line widths is that the line may be composed of a number of close lines arising from water protons in different parts of the resin which are not exchanging with each other. At lower degrees of hydration one would expect to find that some acid sites were more highly hydrated than others, and thus, as discussed above, the protons at the different sites need not have the same chemical shift. The experimental spectrum, in this case, would be a statistical distribution of lines forming, apparently, a single broader resonance line. A critical evaluation of these possibilities awaits the measurements of T_1 and T_2 by a more accurate method.

On adding excess water to the resin, a second line

(19) L. V. Holroyd, R. S. Codrington, B. A. Mrowca, and E. Guth, *J. Appl. Phys.*, **22**, 696 (1951).

(20) E. L. Hahn and D. E. Maxwell, *Phys. Rev.*, **84**, 1246 (1951).

appears. This line corresponds to the water external to the resin and, for the 4% DVB resin, appears at about 0.79 p.p.m. upfield from the internal water peak (see Fig. 1, d and e). As the external water is reduced, the two lines coalesce into a single very broad peak. This behavior is indicative of exchange of resin phase water protons with the external water. The effect of temperature was studied to confirm this hypothesis. The resulting spectra at three temperatures are shown in Fig. 4. At approximately 0° the two lines are sharpened, and the minimum between the peaks is greatly reduced. At approximately 90° the valley is much shallower, with the height of the minimum being about 90% of that of the peak (see Fig. 4a). As the samples return to room temperature the spectra return to their original shape at 25°, indicating complete reversibility of this process. The merging of the two lines as the temperature is raised is consistent with an increase in the rate of exchange with increase in temperature.

The measurement of the diffusion rate of water from the external phase into the resin phase has been made, using D_2O. A sample of the 4% DVB resin (100 mesh) was saturated with H_2O and centrifuged to remove excess water. To measure the diffusion rate, the H_2O hydrated resin was immersed in D_2O and the time dependent spectrum recorded for the transformation of the single resin water line into the double peak spectrum of the two phase resin–external water system. The reverse process of adding deuterium-form resin saturated with D_2O to external H_2O also was studied. In a third experiment, the water-saturated resin was added to D_2O with stirring in a thermostated container. Samples of liquid were withdrawn at 3 to 5 sec. intervals and assayed for proton content by n.m.r. This latter experiment was similar to that of Boyd and Soldano, who used O^{18}-labeled water.[21] The data of all three experiments were treated in the manner of Boyd and Soldano,[22] and the value of the diffusion coefficient of the 4% DVB resin was 800×10^{-6} cm.^{2} sec.$^{-1}$ corresponding to an exchange lifetime of 13 sec., which is within the experimental error of the earlier measurements.[20]

(21) G. E. Boyd and B. A. Soldano, *J. Am. Chem. Soc.*, **75**, 6105 (1953).

(22) We wish to thank Dr. G. E. Boyd for supplying the theoretical curves necessary to make these calculations.

Conclusions

Our observations on the variation of the n.m.r. spectra of the hydrated Dowex-50 resins are consistent with the polyelectrolyte gel model of the ion-exchange resin proposed by Glueckauf. The change in line position and line width with the decrease in degree of hydration indicate the internal water protons are exchanging rapidly enough to average out the internal field inhomogeneities and the chemical shifts of any individual species present. The behavior of the chemical shift of the resin phase water protons is explainable by the strong acid character of the Dowex-50 resin. The shift and line width data lead to a picture of the hydrated resin in which the water molecules form domains of water around the polar acid sites. The physical structure of the water is changed by the polar sites and the organic matrix. The chemical shift data can be interpreted to indicate that the apparent acid strength increases with decrease in resin cross linking. However, other interactions can also affect the measured line position. One such interaction is that of ion pair formation. In this study we are not able to determine the contributions of these other possibilities.

In the presence of excess water the internal and external water protons are easily distinguishable by n.m.r. The temperature dependence of the spectra of this system indicates a rather slow rate of proton transfer between the resin and liquid phases. This result is consistent with the Donnan membrane model. A quantitative measurement of the rate of proton exchange was carried out using D_2O. The rate of proton exchange was found to be very nearly the same as the rate of O^{18} exchange measured earlier by Boyd.

Acknowledgment.—This research was supported by contracts with the U. S. Atomic Energy Commission and the Office of Naval Research. We also wish to thank Dr. Ernest Grunwald for his interest and encouragement and both Dr. Grunwald and Dr. Robert Kromhout for helpful discussions.

N.M.R. STUDIES OF HYDROGEN BONDING IN HYDROFLUOROCARBON SOLUTIONS

By S. K. Alley, Jr., and R. L. Scott

Department of Chemistry, University of California, Los Angeles 24, California

Received October 16, 1962

Nuclear magnetic resonance spectroscopy has been used as a tool for obtaining information regarding the strengths of hydrogen bonds formed between $C_7F_{15}H$ and electron donor solvents such as ketones and amines. Concentration and temperature dependences of chemical shifts of the involved data were used to obtain free energies and enthalpies of hydrogen bonding. The strengths of the hydrogen bonds between $C_7F_{15}H$ and ketones or amines were found to be in the range of 2–5 kcal./mole. These specific interactions substantially change the solubility of $C_7F_{15}H$ in electron donor solvents as compared with that of C_7F_{16}.

Introduction

Fluorinated carbon compounds containing terminal protons show considerably different solubility behavior than do those which are fully fluorinated or fully protonated. These terminal protons are quite electrophilic and are capable of forming hydrogen bonds with appropriate Lewis bases such as ketones and amines. The magnitude of these interactions is difficult to measure because of overlapping effects such as differences in intermolecular attractions between fluorine–hydrogen

and fluorine–fluorine or hydrogen–hydrogen atoms. Calorimetric heats of mixing of the materials yield values which are composites of these non-specific repulsion effects and specific hydrogen-bonding effects. Nuclear magnetic resonance spectroscopy (n.m.r.) offers a possible means of separating these two energy effects, since only the hydrogen bonding perturbs the system in a manner detectable by n.m.r. Therefore in a system such as $C_nF_{2n+1}H$, the behavior of the single proton resonance with concentration and temperature changes should yield valuable information concerning these interactions.

It has long been recognized that n.m.r. is a useful tool for studying hydrogen-bonding effects[1] and it has been utilized by various workers[2-4] for studying hydrogen bonding systems in a qualitative manner. The n.m.r. method can be extended to relatively weak hydrogen bonds where infrared frequency shifts are sometimes not detectable. This latter difficulty prompted Huggins, Pimentel, and Shoolery[5] to make quantitative n.m.r. studies as well as infrared studies on chloroform-base systems. For strong hydrogen-bonding systems, the information obtained from these two methods is essentially complementary.

The significant feature of n.m.r. pertinent to hydrogen bonding studies is the decrease in diamagnetic shielding of the participating proton. This change is associated with a decrease in the average electron density near the proton upon formation of a hydrogen bond. A hydrogen bonding system in solution represents a dynamic equilibrium of bonded and non-bonded states of the proton. N.m.r. cannot resolve these two states, but observes a time average signal which can be correlated with concentration and temperature changes in the system. In the present work these changes were measured and used to derive interaction energies between $C_7F_{15}H$ and various electron donor solvents.

Experimental

A. Materials. 1.—1-Hydropentadecafluoroheptane ($C_7F_{15}H$) was prepared from the perfluorocarboxylic acid, $C_7F_{15}COOH$ (Matheson, Coleman and Bell, K 7996) according to the method of LaZerte, *et al.*[6] This method consists of decarboxylation of the sodium salt in ethylene glycol. The boiling point of the purified *n*-$C_7F_{15}H$ was 94–94.2° at 760 mm. This product contains a small amount of a branched isomer of $C_7H_{15}H$; however, it apparently had little or no effect on the n.m.r. behavior of the single proton.

2. Cyclohexane.—Eastman Kodak Spectro Grade No. S702 cyclohexane was used without further purification as an internal standard.

3. Acetone.—Baker reagent grade No. 9006 acetone was distilled and a cut boiling at 56 ± 0.1° was used in the n.m.r. work. Some samples were run initially using acetone as received and no detectable differences were noted in the resulting chemical shifts, as compared with those obtained using the distilled acetone.

4. Triethylamine.—Eastman Kodak triethylamine No. 616 was used without further purification.

5. Diethyl Ketone.—Eastman Kodak diethyl ketone No. 1330 was distilled and a cut boiling at 101.9–102.1° was used.

6. Diethyl Ether.—Mallinckrodt anhydrous diethyl ether No. 0848 was used without further purification.

B. N.m.r. Samples.—In order to carry out the resonance measurements at three temperatures it was necessary to prepare permanent samples of the mixtures. The mole fraction range from zero to one was covered by 10 to 12 samples consisting of 4.95-mm. o.d. Pyrex tubes 19.5 cm. in length. Components were degassed and added to the tubes by means of hypodermic syringes. A trace of cyclohexane was added to each constituent before addition to the tubes. The amount of cyclohexane was approximately 0.25% of the total and was not considered in the mole fraction calculations. The samples were then sealed off under vacuum at liquid nitrogen temperature.

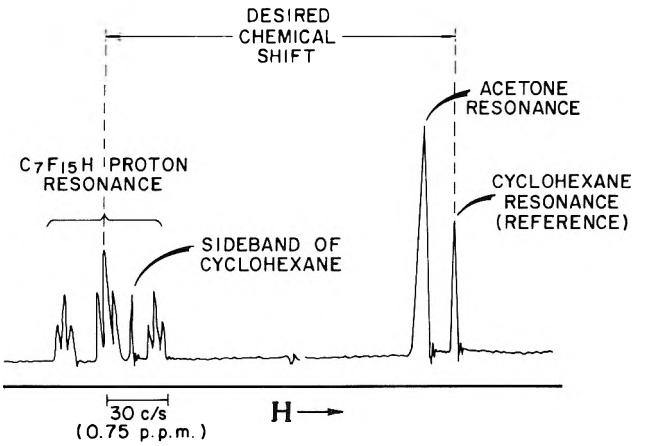

Fig. 1.—N.m.r. studies of hydrogen bonding in hydrofluorocarbon solutions.

C. Apparatus.—The apparatus used for measuring chemical shifts in these experiments was a Varian Associates V-4300-B high resolution n.m.r. spectrometer with super stabilizer and associated V-4012-A 12-in. electromagnet system. The magnetic field used for proton measurements was approximately 9400 gauss, corresponding to a precession frequency of 40.0 Mc./sec.

In runs conducted at other than room temperature, a Varian Associates Model V-4331-THR dewar probe insert was used. The temperature of the probe was measured by a Rubicon precision portable potentiometer using a copper–constantan thermocouple.

For chemical shift measurements, a Hewlett-Packard 200-D variable audio oscillator was used to modulate the magnetic field impressed upon the sample and thus to calibrate the sweep axis.

Results

Proton n.m.r. spectra of the mixtures showed a low field multiplet which could be attributed to the single terminal proton of $C_7F_{15}H$. This multiplet could be described as a tripletized triplet resulting from the spin–spin coupling of the proton with two adjacent CF_2 groups. A typical spectrum is shown in Fig. 1.

This multiplet absorption was found to move to lower field with increase in dilution or decrease in temperature. This decrease was followed by measuring the separation (in c.p.s.) from a cyclohexane standard using the well known sideband technique.[7] The separation (chemical shift) at 100% $C_7H_{15}H$ was treated as the zero point, this value being subtracted from all subsequent measurements as dilution increased. Values of chemical shifts at various compositions for $C_7F_{15}H$ with four solvents are shown in Table I. Each chemical shift value is a result of at least three measurements. The estimated probable error is ±1.0 cycle.

The behavior found is that expected of systems with protons in rapid equilibrium between two molecular species. This supports the supposition that one is dealing with a hydrogen-bonded system involving the proton on $C_7F_{15}H$ and the solvent, as illustrated for acetone

(1) J. T. Arnold and M. E. Packard, *J. Chem. Phys.*, **19**, 1608 (1951).
(2) R. A. Ogg, *ibid.*, **22**, 560 (1954).
(3) W. Drinkard and D. Kivelson, *J. Phys. Chem.*, **62**, 1494 (1958).
(4) E. C. Becker, *J. Chem. Phys.*, **31**, 269 (1959).
(5) C. M. Huggins, G. C. Pimentel, and J. N. Shoolery, *ibid.*, **23**, 1244 (1955).
(6) J. D. LaZerte, L. J. Hals, T. S. Reid, and G. H. Smith, *J. Am. Chem. Soc.*, **75**, 4525 (1953).
(7) J. T. Arnold and M. E. Packard, *J. Chem. Phys.*, **19**, 1608 (1951).

Table I

Chemical Shift Data for $C_7F_{15}H$ in Various Solvents

A. Acetone

Mole fraction acetone	Chemical shifts at temp. of 80°	30°	−20°
0.00	0.00	0.00	0.00
.180	4.9	6.5	8.5
.258	7.8	10.9	14.3
.343	11.5	15.7	21.0
.457	16.3	22.3	29.9
.530	19.4	26.5	36.2
.623	23.3	31.7	39.9
.713	25.1	33.7	44.2
.800	28.2	36.7	46.3
.891	30.1	38.6	48.0
1.000	(32.0)	(40.2)	(49.0)

B. Triethylamine

Mole fraction triethylamine	Chemical shifts at temp. of 80°	30°	−20°
0.000	0.0	0.0	0.0
.140	1.9	3.9	5.8
.248	3.7	7.4	11.0
.333	5.1	10.6	18.2
.427	6.8	14.8	25.9
.545	8.9	19.6	35.2
.618	10.1	22.1	37.1
.702	11.5	23.9	39.7
.774	12.5	26.1	41.3
.889	13.7	27.7	42.3
.926	14.3	28.5	42.6
1.000	(5.1)	(29.5)	(43.1)

C. Diethyl ether

Mole fraction diethyl ether	Chemical shift at temp. of 80°	30°	−20°
0.000	0.00	0.0	0.0
.205	3.3	4.3	6.1
.329	5.8	7.6	11.0
.525	9.7	12.7	19.5
.589	11.4	14.8	21.3
.696	12.9	16.9	24.7
.779	14.6	18.9	27.5
.852	15.5	20.3	28.4
.899	16.3	20.9	29.7
.936	16.8	21.6	30.5
1.000	(17.6)	(22.5)	(31.4)

D. Diethyl ketone

Mole fraction diethyl ketone	Chemical shift at temp. of 80°	30°	−20°
0.000	0.0	0.0	0.0
.136	4.6	5.4	6.3
.480	19.9	24.3	30.2
.521	22.4	27.1	33.2
.641	26.5	32.1	39.8
.725	29.9	35.8	42.6
.769	30.7	36.8	43.5
.800	31.4	37.7	43.8
.850	33.1	38.4	45.4
.884	33.7	39.3	45.6
.917	33.9	39.8	46.0
.944	34.7	40.2	46.6
1.000	(35.6)	(40.9)	(47.0)

$$(CH_3)_2C{=}O + n\text{-}C_7F_{15}H = C_7F_{15}H\cdots O{=}C(CH_3)_2$$

If a simple one-to-one complex is assumed the mole fraction equilibrium constant may be defined as

$$K_x = \frac{(C)(A + B - C)}{(A - C)(B - C)} \qquad (1)$$

where C = moles complex present; A = moles $C_7F_{15}H$ originally present (formal); and B = moles solvent originally present.

Equation 1 is of course an approximation since it assumes that K_x is a constant independent of composition, *i.e.*, that the activity coefficient product $\gamma_C/\gamma_A\gamma_B$ is unity for all values A and B. There is no way to assess the magnitude of the error introduced by this approximation since the activity coefficient γ_C is inaccessible. Reasonable theoretical estimates and the reasonableness of the results deduced from eq. 1 suggest however that this error is not very large.

A related problem is the choice between a mole fraction constant K_x and a molar concentration constant K_c; the assumption that the activity coefficient product is unity cannot be valid for both,[8] so they are nonequivalent. An alternative volume fraction approach leading to a K_ϕ, essentially equivalent to K_c except for a constant of proportionality, is presented in the Appendix. For systems like the ones presented in this paper, values for the heat of formation of the hydrogen bond and for its contribution to the heat of mixing, obtained from K_ϕ, do not differ by more than 20% from those deduced from K_x.

If one assumes that the free and complexed forms of $C_7F_{15}H$ protons each have a distinct precessional frequency and that the observed frequency is a weighted average of the two

$$\nu_{obsd} = x_f\nu_f + x_b\nu_b \qquad (2)$$

where ν_f = distinct frequency of free proton; ν_b = distinct frequency of bound proton; x_f, x_b = mole fractions in respective states, it becomes possible to develop a relationship between observed frequencies and equilibrium constants. Expression 2 is valid[9] as long as the lifetime of each state is longer than one Larmor precession but short compared to the reciprocal of $(\nu_f - \nu_b)$ in sec.

Utilizing (1) for K_x and defining some new relationships for limiting cases, it becomes possible to arrive at an equation relating observed values to calculated values. The following relationships are useful in this procedure

$$a = K/(K + 1)$$

$$x = B/(A + B),\ (1 - x) = A/(A + B)$$

$$z = C/A,\ y = (z)/(z)_{x=1}$$

Then, from (1)

$$K_x = \frac{a}{1 - a} = \frac{z[1 - z(1 - x)]}{(1 - z)[x - z(1 - x)]} \qquad (3)$$

$$\text{at } x = 1,\ K_x = \frac{a}{1 - a} = \frac{z}{1 - z}$$

and since

$$(z)_{x=1} = a,\ y = \frac{z}{a}$$

Thus

$$\frac{1}{1 - a} = \frac{y(1 - ay + ayx)}{(1 - ay)(x - ay + ayx)} \qquad (4)$$

(8) R. L. Scott, *Rec. trav. chim.*, **75**, 787 (1956).

(9) H. S. Gutowsky and A. Saika, *J. Chem. Phys.*, **21**, 1688 (1953).

or solving for y

$$y = \frac{1 - \sqrt{1 - 4a(1 - x)x}}{2a(1 - x)} \qquad (5)$$

where $y = (\Delta\nu_x - \Delta\nu_0)/(\Delta\nu_1 - \Delta\nu_0)$; $\Delta\nu_x$ = chemical shift [10] in frequency units at composition x (related to z); $\Delta\nu_0$ = chemical shift[10] in frequency units at x solvent = 0; and $\Delta\nu_1$ = chemical shift[10] in frequency units at x solvent = 1.0 (related to $(z)_{x=1}$) (not the same as the frequency of the bound proton).

Equation 5 for y as a function of x and a is a sort of reduced equation relating the observed frequency to functions of an equilibrium constant (a). By assigning values to a (and thus fixing K_x), the expected behavior of y with variation in x can be calculated and graphed for comparison with determined curves. All observed chemical shifts at intermediate mole fractions of solvent are divided by the extrapolated chemical shift in cycles at $x_{\text{solvent}} = 1$. Thus y varies from zero to one as x varies from zero to one, making all reduced experimental curves directly comparable with a single set of calculated curves, regardless of the magnitude of experimental values.

Figure 2 shows the experimental reduced curve for $C_7F_{15}H$ and acetone at 30° along with calculated curves for K values of 2.6 and 1.4. It can be seen that the best fit for an experimental K value is 2 ± 0.6. In actual practice, a set of calculated curves were drawn on transparent paper and placed over the reduced experimental curves for comparison.

$C_7F_{15}H$ was examined by n.m.r. in the four solvents, acetone, diethyl ketone, triethylamine, and diethyl ether, over a temperature range of 100° and a composition range of zero to unity. From the temperature dependence of the equilibrium constants (log K_x *vs.* $1/T$) enthalpies of hydrogen bonding were calculated for these four systems. These results have been listed in Table II.

TABLE II

EQUILIBRIUM CONSTANTS AND ENTHALPIES OF HYDROGEN BONDING

Solvent	Equilibrium constants at temp. of 80°	30°	−20°	ΔH_f, kcal./mole
Acetone	1.0 ± 0.4	2.0 ± 0.6	4.0 ± 1.0	−2.5 ± 0.5
Triethylamine	0.45 ± .15	1.5 ± .5	7.0 ± 2.0	−4.9 ± .9
Diethyl ether	0.4 ± .2	0.6 ± .2	1.0 ± 0.4	−1.7 ± .4
Diethyl ketone	1.4 ± .4	2.2 ± .6	3.8 ± 0.8	−1.8 ± .4

Discussion

The results obtained here indicate that it is possible to obtain approximate values for hydrogen bond energies for $C_7F_{15}H$ with various electron donor solvents using n.m.r. spectroscopy. The described procedure of fitting experimental curves to calculated curves seems to work reasonably well except in the low base region. In no case could an experimental chemical shift curve be fitted throughout the entire mole fraction range by a single theoretical K value. In all cases however, as the mole fraction of base increased above 0.3 or 0.4, the experimental behavior falls more and more into line with some calculated curve. The reason for this behavior in the low solvent region is not understood. There are conceivably other equilibria in these solutions

(10) The use of $\Delta\nu$ is introduced here to indicate that all the quantities involved are differences between two frequency values, and that the zero reference itself represents a chemical shift.

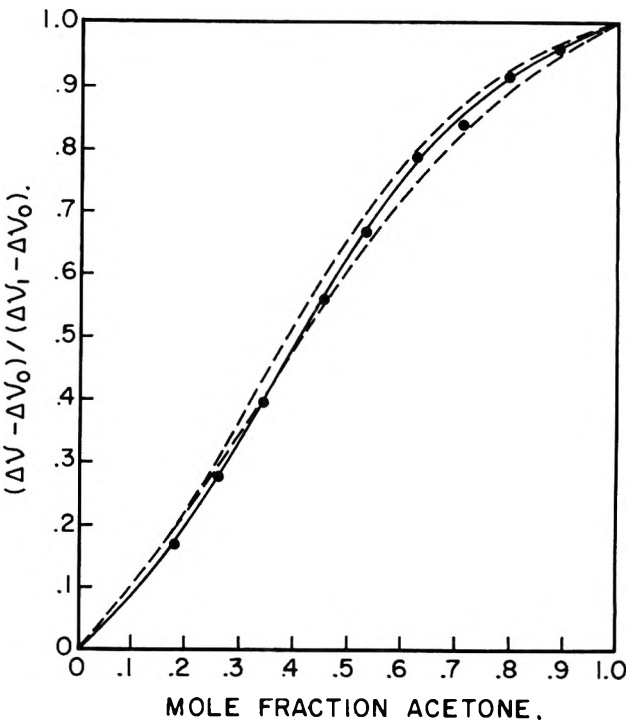

Fig. 2.—N.m.r. studies of hydrogen bonding in hydrofluorocarbon solutions ($C_7F_{15}H$ + acetone at 30°).

and the activity coefficients of the constituents may deviate significantly from unity. The treatment here assumes that the only species in solution, besides the two components A and B, is the simple one-to-one complex. Formation of any higher complexes would cause the simple treatment to fail. The nature of any such complexes in these systems is difficult to visualize because of the weakness of the forces involved. Use of a volume fraction equilibrium constant (see Appendix) will account for part of this effect.

Plots of ln K *vs.* $1/T$ for the equilibrium constants determined in the high base region give fairly straight lines and what would seem to be reasonable values of ΔH_f for the hydrogen bonds involved. These factors are not proofs of the reliabilities of the determined equilibrium constants, but there are no serious inconsistencies to be explained.

A check on the consistency of results for a given system can be made by taking advantage of the relation between the limiting chemical shifts at each temperature. Unless the equilibrium constant were infinity, the limiting chemical shift does not represent the frequency of the bound proton in $C_7F_{15}H$ but is related to this frequency by the equation

$$\left(\frac{K+1}{K}\right) \cdot \Delta\nu_{x\text{base}=1} = \Delta\nu_{\substack{x=1 \\ K=\infty}} = \Delta\nu_b$$

Thus with a K value at one temperature and the limiting chemical shift at the other two temperatures, one can calculate the expected K values at these other temperatures without resorting to comparison with theoretical curves. This was done for all the systems presented here, and the agreement between calculated K values by this method and those determined by comparison with theoretical curves was fairly good. (See Table III.) In no case was the agreement completely inadequate.

No direct comparisons for these systems are avail-

able from the literature; however, some comments can be made concerning the consistency of the results obtained here. It is interesting to note that the $C_7F_{15}H$ proton has a higher limiting frequency at 80° in diethyl ketone than in acetone. Additionally, this results in slightly larger K values at higher temperatures for the diethyl ketone system than for the acetone system. However, the temperature dependence of the equilibrium constant is less in the case of diethyl ketone than in the case of acetone, and it is this factor which results in a lower value of ΔH_f for the $C_7F_{15}H$–diethyl

Table III

Comparison of Predicted Limiting Chemical Shifts for $C_7F_{15}H$ with Various Bases

Compound	Temp., °C.	K determined	$\Delta\nu_{K=\infty}^{x=1}$ calcd., c.p.s.
Acetone	80	1	64
Acetone	30	2	60.3
Acetone	−20	4	65
Triethylamine	80	0.45	48.7
Triethylamine	30	1.5	49.2
Triethylamine	−20	7.0	49.3
Diethyl ether	80	0.4	61.6
Diethyl ether	30	0.6	60.0
Diethyl ether	−20	1.0	62.8
Diethyl ketone	80	1.4	61.0
Diethyl ketone	30	2.2	59.5
Diethyl ketone	−20	3.8	59.4

ketone system. This indicates that the limiting chemical shift of $C_7F_{15}H$ in different bases cannot be directly correlated, although it might be assumed that the stronger the hydrogen bond formed, the greater would be the chemical shift. This limiting shift can be due to a combination of factors and is not necessarily a function of the strength of the hydrogen bond formed.

As previously pointed out, formation of a hydrogen bond results in a decrease in the diamagnetic shielding of the proton involved, and thus to a lower resonance frequency. This means that the proton experiences less electron density after the formation of the bond than before, a view which might be unexpected from simple electrostatic considerations. However, acknowledging the experimental findings, one can speculate that, as the hydrogen bond interaction becomes quite strong and the two atoms involved approach one another more closely, the simple decrease in diamagnetic shielding may no longer occur. Indeed, Coulson and Danielsson[11,12] have made calculations which indicate that as the two atoms involved in hydrogen bonding approach each other, covalency contributions may become appreciable. Any covalency terms should result in an increase in the average electron density around the proton and thus to less of a decrease in resonance frequency upon hydrogen bond formation. Such considerations may account for the behavior of the limiting chemical shifts of the systems studied here, but do not invalidate the process used for determining energies of formation.

Calorimetric studies by our research group[13] of heats of mixing in the $C_7F_{15}H$ + acetone system are consistent with the ΔH_f obtained from these n.m.r. data. The contribution of hydrogen bond formation to the total heat of mixing will be $\Delta H_f C/(A + B)$, or in terms of the quantities previously defined, $\Delta H_f ay(1 - x)$. At $x = 1/2$ this yields a contribution of −530 cal. at 30°. The calorimetric heat of mixing at 35° is −124 cal., leaving a difference of +400 cal., the right order of magnitude for the "physical" interaction of acetone with a fluorocarbon. A variant method of calculation based upon a volume fraction equilibrium constant K_ϕ is given in the Appendix.

Self-association in $C_7F_{15}H$.—Consideration was given to the possibility that the observed behavior of the $C_7F_{15}H$ systems in the low base region was due to self-association in the hydrofluorocarbon. If this were occurring, the observed chemical shift would only be a measure of the difference between self-associated $C_7F_{15}H$ and the complex with the base. As a check on this possibility, pure $C_7F_{15}H$ (plus cyclohexane as a reference) was diluted with n-C_7F_{16} and secondly with n-C_7H_{16}. Over a large concentration range, a variation of only 0.4 cycle was observed for C_7F_{16} as the diluent and 0.9 cycle for C_7H_{16}. These chemical shift variations were within the normal instrument variation and indicate that self-association in $C_7F_{15}H$ is not responsible for the behavior in the low base region.

Appendix

Volume Fraction Equilibrium Constants.—It is by no means obvious that a mole fraction formulation of the equilibrium constant yields the number which is most nearly constant over the whole composition range. The following argument, somewhat more closely applicable to high polymeric systems than to these, leads to a volume fraction constant: For the activities a_A, a_B, and a_C, we write

$$\ln a_A = \ln \phi_A + 1 - r_A/\bar{r} + r_A[(\beta_{AB}\phi_B + \beta_{AC}\phi_C)(\phi_B + \phi_C) - \beta_{BC}\phi_B\phi_C] \quad (A.1a)$$

$$\ln a_B = \ln \phi_B + 1 - r_B/\bar{r} + r_B[(\beta_{AB}\phi_A + \beta_{BC}\phi_C)(\phi_A + \phi_C) - \beta_{AC}\phi_A\phi_C] \quad (A.1b)$$

$$\ln a_C = \ln \phi_C + 1 - r_C/\bar{r} + r_C[(\beta_{AC}\phi_A + \beta_{BC}\phi_B)(\phi_A + \phi_B) - \beta_{AB}\phi_A\phi_B] \quad (A.1c)$$

where the parameters r_A, r_B, and r_C are proportional to the molar volumes (in lattice theory the number of sites occupied by each molecule), $\bar{r} = x_A r_A + x_B r_B + x_C r_C$, and the volume fraction $\phi_A = x_A r_A/\bar{r}$, etc. For convenience we assume the r's independent of temperature, or equivalently define the volume fraction with respect to molar volumes at a particular reference temperature; in either case the volume fractions are temperature invariant.

Equations A.1 come directly from simple polymer solution theory; they are a combination of the simple Flory entropy of mixing with a volume fraction dependent interaction energy.[14,15]

For complexes like these, it is reasonable to assume approximate additivity of molar volumes ($r_C = r_A + r_B$). With this assumption and equations A.1,

(11) C. A. Coulson and V. Danielsson, *Arkiv Fysik*, **8**, 239, 245 (1954).
(12) C. A. Coulson, *Research* (London), **10**, 149 (1957).
(13) D. L. Andersen, R. A. Smith, D. B. Myers, S. K. Alley, A. G. Williamson, and R. L. Scott, *J. Phys. Chem.*, **66**, 621 (1962).
(14) J. H. Hildebrand and R. L. Scott, "Solubility of Non-electrolytes," 3rd Ed., Reinhold Publ. Corp., New York, N. Y., 1950, Chapters VI, VII, XII, and XX.
(15) J. H. Hildebrand and R. L. Scott, "Regular Solutions," Prentice-Hall, New York, N. Y., 1962, Chapters 3 and 7.

we obtain for the activity product for the reaction A + B = C, the equation

$$\ln(a_C/a_A a_B) = \ln(\phi_C/\phi_A\phi_B) - 1 - \beta_{AB}[r_A\phi_B + r_B\phi_A] + \beta_{AC}[r_A(\phi_A - \phi_C) + r_B\phi_A] + \beta_{BC}[r_A\phi_B + r_B(\phi_B - \phi_C)] = \text{constant} \quad (A.2)$$

If we assume the geometric mean for the interaction energies of unlike pairs, we can express the β's in terms of the "solubility parameters" δ: $\beta_{AC} = (\delta_A - \delta_C)^2$, $\beta_{BC} = (\delta_B - \delta_C)^2$, $\beta_{AB} = (\delta_A - \delta_B)^2$. Moreover, the solubility parameter of the complex should approximate the volume average of its constituents: $\delta_C = (r_A\delta_A + r_B\delta_B)/(r_A + r_B)$. If we make these substitutions into eq. A.2, we obtain

$$\ln(a_C/a_A a_B) = \ln(\phi_C/\phi_A\phi_B) - 1 + (\delta_A - \delta_B)^2 r_A r_B/(r_A + r_B) = \text{constant}$$

$$\text{or } \phi_C/\phi_A\phi_B = \text{constant} \quad (A.3)$$

From this argument one would conclude that it is the volume fraction equilibrium constant $K\phi$ or the virtually equivalent molar concentration constant K_c which should be more or less independent of concentration and not the mole fraction constant K_x. This argument is by no means conclusive for small molecules; the Flory entropy certainly over-corrects (even in the case of high polymers) for the effect of differences in size, and there is considerable uncertainty about the validity of the solubility parameter assumptions. Nonetheless it is not unreasonable to assume that the actual situation lies somewhere between a constant K_x (assumed in the body of the paper) and a constant K_ϕ; consequently we examine here the modifications involved in assuming K_ϕ constant instead of K_x.

The equation equivalent to eq. 3 can be written as

$$K_\phi = \frac{(r_A + r_B)(C)(r_A A + r_B B)}{r_A(A - C)r_B(B - C)} = \frac{(r_A + r_B)}{r_A r_B^2}\frac{b}{1 - b} \text{ or } \frac{(C)(\alpha A + B)}{(A - C)(B - C)} = \frac{b}{1 - b} \quad (A.4)$$

With the substitutions $z = C/A$, $x = B/(A + B)$, $(z)_{x=1} = b$, and $y = z/b$, we obtain the equation corresponding to (4)

$$\frac{1}{1 - b} = \frac{y[1 + (\alpha - 1)(1 - x)]}{(1 - by)(x - by + byx)} \quad (A.5)$$

or

$$(1 - x)b^2y^2 - (1 + \eta)y + x = 0 \quad (A.6)$$

where $\alpha = r_A/r_B$ and $\eta = (\alpha - 1)(1 - b)(1 - x)$.

When $\alpha = 1$, the solution of eq. A.6 is given by eq. 5 with $a = b^2$. For our systems however $\alpha \neq 1$; indeed for $C_7F_{15}H$ + acetone, $\alpha = 2.9$. It is interesting to note that for eq. A.6, the initial slope of the curve of y *vs.* x $(dy/dx)_{x=0} = 1/(1 + \eta)$; since for an α greater than 1, η is necessarily positive, this may help to explain the fact that in Fig. 2, the initial slope is less than unity (the value predicted from eq. 5).

If we apply eq. A.6 to the data for $C_7F_{15}H$ + acetone, we obtain for the quantity $b/(1 - b)$, which is proportional to K, the values 21, 12, and 8 for the temperatures −20, +30, and +80°, respectively. From these one deduces a heat of formation of the complex $\Delta H_f = -2.0$ kcal. mole^{-1}, lower than the value obtained from the mole fraction K_x, but within the uncertainty of that number. The actual contribution of the hydrogen bonding to the observed heat of mixing is equal to $\Delta H_f C/(A + B)$; at $x = 1/2$, this is equal to $\Delta H_f by/2$ or to about −570 cal. mole^{-1}, as compared with the figure of −510 from K_x, for $C_7F_{15}H$ + acetone at 30°. This difference of 10% is certainly within the experimental error of the measurement and uncertainty of the theory, so it does not seem worthwhile to pursue the more complicated volume fraction theory any further at this time.

AN INVESTIGATION OF THE REACTIONS BETWEEN SUBSTITUTED BENZALDEHYDES AND 5,5-DIMETHYLCYCLOHEXANEDIONE-1,3

By B. E. Dawson[1] and T. Henshall[2]

Department of Chemistry, Sir John Cass College, London, England

Received October 16, 1962

The reaction between 5,5-dimethylcyclohexanedione-1,3, dimedone, and a substituted benzaldehyde has an over-all order of two, the reaction rate depending strongly on the pH of the solution. The pH–rate curve shows a sharp maximum at pH 4.6, and the free energies of activation, ΔF^*, of substituted benzaldehydes toward dimedone fall roughly into the same sequence as their half-wave potentials in polarographic reduction in acid buffer solutions. The variability of the Arrhenius A factors shows that the over-all reaction is complex. A reaction mechanism is proposed to account for these observations.

Introduction

The use of 5,5-dimethylcyclohexanedione-1,3, dimedone, as a reagent for the identification of aldehydes[3] and for the estimation of formaldehyde and acetaldehyde[4] is well known. A modification in the gravimetric procedure for formaldehyde has been suggested[5] as a result of a kinetic study of the reaction.[6] This showed

(1) The Coopers' Company's School, London, E.3.

(2) The Royal College of Advanced Technology, Salford, 5.

(3) D. Vorländer, *et al.*, *Z. anal. Chem.*, **77**, 241 (1929); D. Vorländer, *Z. angew. Chem.*, **42**, 46 (1929); W. Weinberger, *Ind. Eng. Chem., Anal. Ed.*, **3**, 365 (1931); E. C. Horning and M. G. Horning, *J. Org. Chem.*, **11**, 95 (1946).

(4) D. Vorländer, C. Ible, and H. Volkholz, *Z. anal. Chem.*, **77**, 321 (1929); M. V. Ionescu and C. Bodea, *Bull. soc. chim.*, **47**, 1408 (1930); J. G. Yoe and L. C. Reid, *Ind. Eng. Chem., Anal. Ed.*, **13**, 238 (1941).

(5) D. Spencer and T. Henshall, *Anal. Chim. Acta*, **11**, 428 (1954).

(6) D. Spencer and T. Henshall, *J. Am. Chem. Soc.*, **77**, 1943 (1955).

that the reaction rate is strongly dependent on the pH of the solution and reaches a maximum at pH 8.5 which corresponds to the complete ionization of dimedone. A satisfactory interpretation of the observed kinetics of this reaction involves an ion–polar molecule mechanism.

The influence on the reaction of the change in structure of the aldehyde is demonstrated in this investigation. The over-all reaction order remains unchanged at two; the activation energies are much lower; and the reaction rates slower, than for the formaldehyde–dimedone reaction. Also, the maximum rate of reaction between a substituted benzaldehyde and dimedone occurs at a lower pH as shown in the figure.

Experimental

Materials.—Dimedone was recrystallized from aqueous alcohol to constant melting point (147°); colorless needles.

The aldehydes used were purified either by recrystallization to constant melting point or by fractional distillation under a conveniently diminished pressure.

All other reagents used were of analytical reagent grade quality.

Kinetic Studies.—The reactions were shown to be of first order in each reactant, and over-all second-order kinetics were also established experimentally by the application of the integrated rate equation and the over-all stoichiometry.

Determination of the Order of Reaction with Respect to Dimedone.—Convenient quantities of dimedone and aldehyde in 50% v./v. aqueous alcohol were equilibrated at 25.00 ± 0.01°. The solutions were mixed and aliquots were withdrawn at fixed time intervals, the reaction being quenched in an excess of formaldehyde. After 20 minutes, the precipitate of formaldehyde–dimedone condensation product was transferred to a sintered-glass crucible of known weight, washed with 3% aqueous alcohol to remove the yellow color from the precipitate, and washed twice with water before being dried at 110° to constant weight. Each precipitate was identified by melting point and mixed melting point with a standard sample of formaldehyde–dimedone condensation product (190 ± 1°).

The results for the salicylaldehyde–dimedone reaction are given in Table I from which it follows that the order of reaction with respect to dimedone is one.

TABLE I

Initial concn. of dimedone, 0.02062 *M*; initial concn. of salicylaldehyde, 0.3051 *M*; extent of reaction followed, 77.9%

Time of reaction *t*, sec.	Wt. of ppt., g.	10^5k, sec.$^{-1}$
0	0.0752	...
3240	.0395	7.6
8040	.0424	(7.1)
11340	.0396	8.4
17400	.0176	8.3
18780	.0166	8.0
	Mean	7.9

Spectrophotometric Method.—In the reactions of dimedone with *o*- and *m*-hydroxybenzaldehyde, the ultraviolet absorption spectrum of the aldehyde had a characteristic absorption maximum not found in the spectra of the other constituents of these systems (Table II) if the solvent used was sufficiently alkaline. These measurements were made with a Unicam SP500 spectrophotometer and the property was used to determine the aldehyde concentration in these cases.

TABLE II

Solute in 0.10 *N* NaOH	λ_{max}, mμ, max.	log ε	λ_{max}, mμ, max.	log ε
Dimedone	282	4.41		
Salicylaldehyde	265	3.92	376	3.79
Anhydride derivative of salicylaldehyde	227	4.17	289	4.36
m-Hydroxybenzaldehyde	235	4.31	358	3.41
Methone derivative of *m*-hydroxybenzaldehyde	235	4.00	285	4.43

Polarographic Method.—Benzaldehyde and substituted benzaldehydes behave similarly at the dropping mercury cathode, the reduction being strongly dependent on the pH of the supporting electrolyte.[7] When the reduction is carried out in fairly strong acid buffer solution, the reduction process is reversible,[8] and well defined waves result. In the case of *p*-hydroxybenzaldehyde–dimedone reaction, it was more convenient to use a buffer solution of pH 7.10.

Under the experimental conditions used, neither dimedone nor the various condensation products gave polarograms.

A Cambridge polarograph was used in making these measurements after calibrating it against a standard 0–15 μa. meter. The characteristics of the dropping mercury cathode used were: (a) dropping time in 0.10 *N* KCl: 7.61 sec. (mean value from 50 drops); (b) Hg flow: 0.58 mg./sec. (mean value from 50 drops); (c) Hg head used: 59.0 cm. Data used in the polarographic estimation of aldehydes are given in Table III.

TABLE III

POLAROGRAPHIC REDUCTION OF SUBSTITUTED BENZALDEHYDES IN BUFFER SOLUTIONS CONTAINING 0.01% W./V. GELATIN AND 50% W./W. ALCOHOL AT 25.00 ± 0.05°

Aldehyde substituent	pH	i_d/c, ma. mole^{-1}	Measurement made at $-E$, v. (Hg pool)
H	1.40	1.22	1.0
o-MeO	1.50	1.50	1.0
p-MeO	1.55	1.43	1.1
p-Cl	1.55	1.28	1.1
p-HO	7.10[a]	3.39	1.8
p-Me	1.35	1.27	1.0
o-Cl	1.44	1.15	1.0

[a] Buffer solution used in this case was H_3BO_3–KCl–NaOH and contained 1% alcohol. In all other cases, the buffer mixture used was NaOAc–HCl. In all cases, the concentration range tested was 0–0.0010 *M*.

Determination of the Order of Reaction with Respect to Benzaldehyde.—Solutions of dimedone and benzaldehyde were allowed to attain thermal equilibrium in a suitable thermostat before being mixed. Filtered aliquots were withdrawn at known intervals and analyzed polarographically in a sodium acetate–hydrochloric acid buffer solution containing 50% v./v. alcohol and 0.01% w./v. gelatin. Hydrogen was bubbled through the solution before analysis (20 minutes) and over the solution during analysis. The results shown in Table IV demonstrate that the order of reaction with respect to the aldehyde is unity.

TABLE IV

Initial concn. of dimedone, 0.150 *M*; initial concn. of benzaldehyde, 0.0098 *M*; extent of reaction followed, 82.8%; temp., 50.00 ± 0.05°.

Time of reaction *t*, sec.	10^3[benzaldehyde], moles l.$^{-1}$	10^4k, sec.$^{-1}$
0	9.80	...
1800	7.09	1.8
3660	5.06	1.8
4860	4.22	1.7
6060	3.71	1.6
7440	2.71	1.7
9240	1.87	1.8
10800	1.68	1.6
	Mean	1.7

Variation of the Second-order Rate Constant with Hydrogen Ion Concentration. Salicylaldehyde–Dimedone Reaction.—A buffered solution of dimedone (25 ml.) was equilibrated in a thermostat regulated to ±0.02°. An ethanolic solution of salicylaldehyde (0.53 ml.) was added, and filtered 1-ml. aliquots were removed and quenched in sodium hydroxide. The concentration of the aldehyde in 0.10 *N* sodium hydroxide was estimated spec-

(7) M. Tokuoka, *Coll. Czech. Chem. Comm.*, **7**, 392 (1935); R. Pasternak, *Helv. Chim. Acta*, **31**, 753 (1948); I. A. Korshunov and L. N. Sazanova, *Zh. Fiz. Khim.*, **23**, 202 (1949); F. Santavy *Coll. Czech. Chem. Comm.*, **14**, 145 (1949); E. Gergely and T. Iredale, *J. Chem. Soc.*, 3226 (1953); L. Hollick and H. Marsen, *Z. Elektrochem.*, **53**, 944 (1953); R. A. Day and R. M. Powers, *J. Am. Chem. Soc.*, **76**, 3085 (1954).

(8) R. Pasternak, ref. 7.

trophotometrically. Sample results are recorded in Table V for a run carried out at pH 0.72. A summary of the principal data for this reaction is given in Table VI.

TABLE V

Initial concn. of salicylaldehyde, 0.010 *M*; initial concn. of dimedone, 0.020 *M*; ionic strength of reaction mixture, 0.70; alcohol concn., 5% v./v.; temp., 50.00 ± 0.02°.

Time of reaction *t*, sec.	Optical density at 376 mμ (mean value of 4 readings)	[Salicylaldehyde] × 10^3, moles/l.$^{-1}$	10^2k, mole^{-1} l. sec.$^{-1}$
0	...	10.0	..
1800	0.425	6.86	1.27
3600	.336	5.42	1.17
5460	.278	4.49	1.13
7440	.226	3.65	1.17
9000	.192	3.10	1.24
10800	.168	2.71	1.24
		Mean	1.2

TABLE VI

Initial concn. of salicylaldehyde, 0.01 *M*; initial concn. of dimedone, 0.020 *M*; other conditions as for Table V.

pH	10^2k, mole^{-1} l. sec.$^{-1}$	10^2k_{calc}, mole^{-1} l. sec.$^{-1}$	pH	10^2k, mole^{-1} l. sec.$^{-1}$	10^2k_{calc}, mole^{-1} l. sec.$^{-1}$
0.72[a]	1.2	0.003[d]	4.55[a]	17.0	17.9[d] 17.8[e]
0.94[a]	1.0	.005[d]	5.19[a]	11.7	10.8[e]
1.59[a]	1.0	.024[d]	5.25[a]	8.0	10.0[e]
2.01[a]	1.3	.064[d]	6.13[b]	2.0	2.2[e]
3.00[a]	3.0	.63[d]	6.24[b]	1.6	1.7[e]
3.56[a]	7.5	2.2[d]	7.30[b]	0.2	0.2[e]
4.06[a]	10.6	6.7[d]	7.55[b]	.003	0.1[e]
4.40[a]	15.0	13.4[d] 18.8[e]	8.68[c]	.0006	.007[e]

[a] Buffer containing NaOAc + HCl + KCl; ionic strength = 0.70. [b] Buffer containing KH_2PO_4 + NaOH + KCl; ionic strength = 0.70. [c] Buffer containing H_3BO_3 + NaOH + KCl; ionic strength = 0.70. [d] Calculation based on $k_{calc} = 0.92/[(H^+)/K_a + 1]$ (*cf.* 7). [e] Calculation based on $k_{calc} = 32500(H^+)/[(H^+)/K_a + 1]$ (*cf.* 9).

Benzaldehyde–Dimedone Reaction.—The procedure used was that described earlier for the determination of the order of reaction with respect to benzaldehyde. The results of a typical run at pH 3.20 are reported in Table VII. A summary of the principal data for this reaction is given in Table VIII.

TABLE VII

Initial concn. of benzaldehyde, 0.01 *M*; initial concn. of dimedone, 0.020 *M*; ionic strength of reaction mixture, 0.70; alcohol concn., 8% v./v.; temp., 50.00 ± 0.02°.

Time of reaction *t*, sec.	Cor. wave height at −1.0 v. (Hg pool) and unit sensitivity	[Benzaldehyde] × 10^3, moles l.$^{-1}$	10^2k, mole^{-1} l. sec.$^{-1}$
0	310	10.0	..
1200	250	8.06	(1.00)
2640	160	5.16	1.80
3570	125	4.19	1.95
4800	102.5	3.31	2.10
6000	95	3.06	1.90
7200	75	2.42	2.20
8340	67.5	2.18	2.15
9600	60	1.94	2.10
10800	50	1.61	2.40
		Mean	2.1

Activation Energy.—In view of the shapes of the curves shown in the figure, it was decided to measure the energy of activation for the salicylaldehyde–dimedone reaction at or near pH 4.6 and in the region of pH 1.0. Measurements of activation energy for the other systems studied were made at pH near 4.6.

Buffer mixtures of the types used were compared with potassium hydrogen phthalate[9] at various temperatures. From the results obtained, it appeared reasonable to assume that the change in pH over the temperature range 18 to 50° was within 0.08 unit of pH.

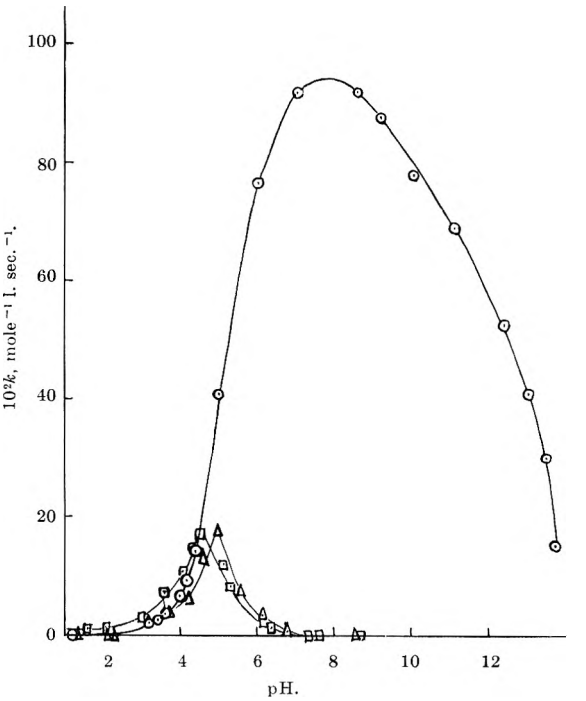

Fig. 1.—Variation of second-order rate constant with pH: ⊙—⊙, formaldehyde–dimedone reaction at 25°[6]; △—△, benzaldehyde–dimedone reaction at 50°, μ = 0.70; ⊡—⊡, salicylaldehyde–dimedone reaction at 50°, μ = 0.70.

TABLE VIII

Initial concn. of benzaldehyde, 0.010 *M*; initial concn. of dimedone, 0.020 *M*; other conditions as for Table VII.

pH	10^2k, mole^{-1} l. sec.$^{-1}$	10^2k_{calc}, mole^{-1} l. sec.$^{-1}$	pH	10^2k, mole^{-1} l. sec.$^{-1}$	10^2k_{calc}, mole^{-1} l. sec.$^{-1}$
1.33[a]	0.4	0.01[d]	4.55[a]	12.8	17.9[d] 21.6[e]
2.10[a]	.4	.09[d]	5.00[a]	17.5	16.0[e]
2.24[a]	.4	.10[d]	5.60[a]	7.8	7.2[e]
3.20[a]	2.1	1.0[d]	6.12[b]	3.4	2.7[e]
3.70[a]	3.4	3.0[d]	6.80[b]	0.8	0.6[e]
4.24[a]	5.9	9.7[d]	8.50[c]	Little reaction occurs	0.01[e]

[a,b,c] Compositions of buffers *a*, *b*, and c are given in Table VI. [d] Calculation based on $k_{calc} = 0.92/[(H^+)/K_a + 1]$ (*cf.* 7). [e] Calculation based on $k_{calc} = 39400(H^+)/[(H^+)/K_a + 1]$ (*cf.* 9).

Only minor modifications to the experimental procedures given were necessary for the other systems studied, except in the reactions using *o*-, and *p*-nitrobenzaldehydes when the alcohol content of the reaction mixtures had to be raised to 40% v./v. This made any comparison of a quantitative nature difficult, and only preliminary experiments were carried out in these cases.

The principal data for all the systems studied are shown in Table IX.

Investigation of General Acid Catalysis.—The data recorded in Table X supports the view that the reaction between an aromatic aldehyde is catalyzed by hydrogen ions over the pH range investigated and is not subject to general acid catalysis.

Discussion

Reaction Mechanism.—For the cases shown in the figure, the reaction rate at first increases with increase of pH; this suggests that one of the active species in the rate determining step is the negatively charged dimedone ion. Thus, the possible slow stage for the

(9) British Standard 1647 (1950); R. G. Bates, *Chem. Rev.*, **42**, 1 (1948)

Table IX

Aldehyde substituent	10^3k, mole^{-1} l. sec.$^{-1}$ 25°	30°	35°	40°	45°	50°	pH	Energy of activation, kcal.	A at 35°
H	41.0	61.0	74.0[a]	83.0[b]	97.0[c]	128.0	4.55	7.9	2.77×10^7
o-Cl		123.7	163.8	206.6			4.55	9.7	1.27×10^9
p-Cl	46.7	63.8	75.3	90.7	106.9		4.55	6.5	3.08×10^6
o-HO			3.8	5.7	7.4	9.7	0.94	13.7	1.95×10^{10}
o-HO		44.5	61.6	80.4	120.1	170.0	4.55	13.0	1.02×10^{11}
m-HO	35.2	47.0	56.4	74.5			4.58	9.2	2.13×10^8
p-HO			2.6	3.6	4.4	5.8	4.58	10.2	4.46×10^7
o-MeO	77.0	93.0	125.0	147.0	169.0	205.0	4.55	7.5	2.44×10^7
p-MeO	4.1	5.8	9.5	12.1	15.3	18.0	4.55	11.9	2.60×10^9
p-Me			19.0	22.6	30.3	37.0	4.58	8.9	3.64×10^7

[a] 34.4°. [b] 39.0°. [c] 44.0°.

Table X

Initial concn. of benzaldehyde, 0.010 *M*; initial concn. of dimedone, 0.020 *M*; ionic strength, μ 0.091; alcohol concn., 8.2% v./v.; temp., 50.00 ± 0.05°.

[Acid], molar	[Salt], molar	[Sodium chloride], molar	pH	10^2k, mole^{-1} l. sec.$^{-1}$	Extent of reaction followed, %
Acetic acid–sodium acetate					
0.0909	0.0909	....	4.90	10.1	88
.0682	.0682	0.0227	4.90	10.2	90
.0455	.0455	.0455	4.90	10.1	90
.0227	.0277	.0682	4.85	10.3	89
.1363	.0909	....	4.34	11.3	80
.0818	.0546	.0364	4.34	11.3	90
.0546	.0364	.0546	4.34	11.0	86
Phosphoric acid–sodium dihydrogen phosphate					
0.0909	0.0909	....	2.70	1.2	51
0.0455	0.0455	0.0455	2.65	1.2	44
Potasisum dihydrogen phosphate–potassium hydrogen phosphate					
0.0227	0.0227	....	6.04	4.2	80
.0170	.0170	0.0227	6.00	4.2	71
.0114	.0114	.0455	5.97	4.2	66

reaction depends on the availability of the dimedone ion, and as the pH of the medium increases so the concentration of this ion increases and with it the over-all rate of the reaction.

The formation of a kinetic maximum in acid solution in the pH–rate curve is unusual but is not unique. The reaction of carbonyl compounds with hydroxylamine,[10] and with semicarbazide,[11] give a similar effect. Jencks[12] has demonstrated that the over-all rate of reaction of a carbonyl compound with a nitrogen base at neutral pH is dependent on the equilibrium concentration of an intermediate addition compound and on the rate of its acid catalyzed dehydration. The appearance of a maximum in the pH–rate curve in these instances is interpreted to be the result of a transition to a rate limiting attack of free base on the carbonyl compound at acid pH. Further, the maximum in the pH–rate curve is not dependent on general acid catalysis.

The features of the pH–rate curves for aromatic aldehyde–dimedone reactions shown in the figure can be accounted for in terms of the mechanism put forward to interpret the formaldehyde–dimedone reaction[6] if one includes the possibility of a change in the rate-determining step from that of an ion-polar molecule to that of the dehydration of the addition compound in the presence of hydrogen ions for a part of the pH–rate curve.

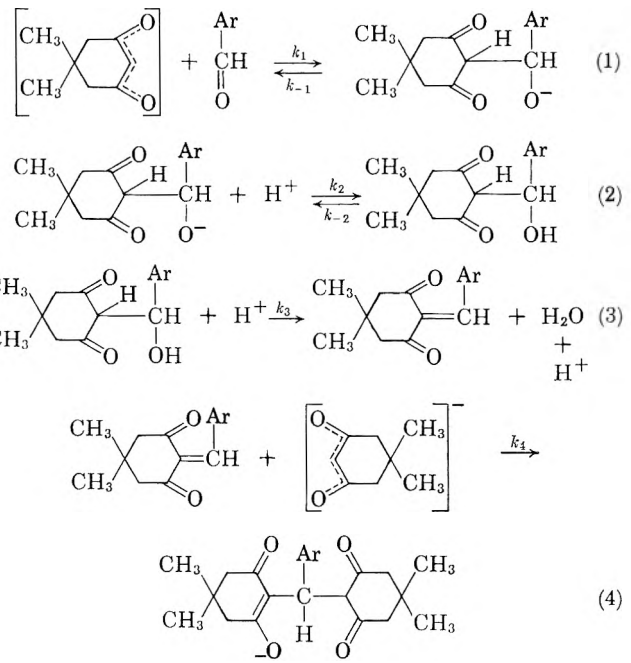

Following Spencer and Henshall,[6] let (1) be the rate-determining stage at low pH (*i.e.*, at pH less than about 4.0). Then, when k_{-1} is insignificant or zero, the over-all rate of reaction may be expressed by (5)

$$v = k_1(\mathrm{D}^-)(\mathrm{A}) \qquad (5)$$

The experimental data reported in the previous section are calculated on the basis of (6)

$$v = k_{obs}(\mathrm{A})\{(\mathrm{HD}) + (\mathrm{D}^-)\} \qquad (6)$$

since dimedone is a weak acid.[13] From (5) and (6)

$$k_{obs} = \frac{k_1}{(\mathrm{H}^+)/K_a + 1} \qquad (7)$$

where K_a is the dissociation constant of dimedone and has the value 6.8×10^{-6}.

At somewhat higher values of pH (*i.e.*, at pH between 4.5 and 6.2), let (2) be the rate-determining stage. Then, when k_{-2} is insignificant or zero, the over-all rate of reaction may be expressed by (8)

$$v = K_1k_2(\mathrm{D}^-)(\mathrm{A})(\mathrm{H}^+) \qquad (8)$$

(10) S. F. Acree and J. M. Johnson, *Am. Chem. J.*, **38**, 308 (1907); E. Barrett and A. Lapworth, *J. Chem. Soc.*, **93**, 85 (1908); A. Olander, *Z. physik. Chem.*, **129**, 1 (1927); D. G. Knorre and N. M. Emanuel, *Dokl. Akad. Sci. SSSR.*, **91**, 1163 (1953).

(11) J. B. Conant and P. D. Bartlett, *J. Am. Chem. Soc.*, **54**, 2881 (1932); F. H. Westheimer, *ibid.*, **56**, 1962 (1934); F. P. Price and L. P. Hammett, *ibid.*, **63**, 2387 (1941).

(12) W. P. Jencks, *ibid.*, **81**, 475 (1959).

(13) R. von Schilling and D. Vorländer, *Ann.*, **308**, 193 (1899); G. Scharzenbach and K. Lutz, *Helv. Chim. Acta*, **23**, 1147, 1162 (1949).

where K_1 is the equilibrium constant for reaction 1. The form of (8) will be unchanged should one consider that reactions 2 and 3 occur in a single step as was suggested with the formaldehyde–dimedone reaction.[6]

From (6) and (8)

$$k_{obs} = \frac{K_1 k_2 (H^+)}{(H^+)/K_a + 1} \qquad (9)$$

The constant term in (9) will depend on the reaction system and a best value can be obtained using experimental values for the second-order rate constant at a known hydrogen ion concentration (as shown in Tables VI and VIII).

If the value of k_1 in (7) is 0.92, then at pH less than about 4.0, the agreement between observed and calculated values of the second-order rate constant is approximate (Tables VI and VIII). Above pH 4.0, the rate of increase in the calculated value of the second-order rate constant with increase in pH is greater than that found experimentally, as might be expected from the postulated change in the rate-determining step. It is noteworthy that similar relationships were obtained by Jencks in accounting for the rates of reaction of hydroxylamine with acetone and with furfural as a function of pH.[12]

The vertical displacement of the experimental rate curves above the theoretical curve at pH less than about 4.0 suggests that some reaction occurs between dimedone and aromatic aldehydes in this region. Further, such reaction is catalyzed by hydrogen ions (Table X). The increased reactivity of aromatic aldehydes compared with formaldehyde in this region of low pH may be due to the formation of ions of the type $Ar{\cdot}\overset{+}{C}HOH$ which participate in the rate-determining step. However, all attempts to detect the existence of such ions under these conditions were unsuccessful. Such ions are commonly proposed to account *inter alia* for the polarographic reduction of aldehydes, which is strongly dependent on the pH of the supporting electrolyte.[7]

Arrhenius Parameters.—The value of the A-factor of the Arrhenius equation has been found not to be constant for this sequence of reactions. In the majority of cases, as the value of the Arrhenius energy of activation increases, the value of A increases thereby showing that the over-all reaction mechanism is complex.

The electronic influence of the substituent group on the reactivity of the aldehyde may be shown by comparing the free energy of activation for these reactions with the ease of reduction of the aldehyde at the dropping mercury cathode in acid buffer solutions. Relevant data are recorded in Table XI.

TABLE XI

Aldehyde substituent	ΔF^*, kcal. at 25°	$-E_{1/2}$, v. at 25°
p-HO	17.21	1.116
p-MeO	16.61	1.07[a]
p-Me	16.01	1.020
o-HO	15.46	1.050
m-HO	15.34	1.008
H	15.14	1.000
p-Cl	15.10	0.952
o-MeO	14.88	.960
o-Cl	14.76	.868

[a] With the exception of the reduction of *p*-methoxybenzaldehyde which was carried out in aqueous buffer at pH 1.81,[14] all reductions were carried out in 60% alcoholic buffers at pH 1.73.[15]

Acknowledgments.—Grateful acknowledgment is made to the Central Research Fund of the University of London for a grant toward the cost of apparatus, and to Imperial Chemical Industries Ltd., for a grant toward the cost of materials.

(14) F. Santavy, ref. 7.
(15) E. Gergely and T. Iredale, ref. 7.

THE THERMODYNAMIC AND PHYSICAL PROPERTIES OF BERYLLIUM COMPOUNDS. III. HEAT OF FORMATION AND ENTROPY OF $BeF_2(g)$[1]

BY MICHAEL A. GREENBAUM, M. LOUIS ARIN, AND MILTON FARBER

Thermodynamics Section, Rocket Power, Inc., Pasadena, Calif.

Received October 22, 1962

The reaction $BeO(s) + 2HF(g) \rightarrow BeF_2(g) + H_2O(g)$ has been employed to yield values for ΔHf_{298} and S^0_{298} of $BeF_2(g)$. The experimentally determined values for ΔH_r and ΔS_r for the above reactions over the temperature range 943–1243°K. are 20.5 ± 1.7 kcal. and 6.0 ± 0.3 cal./deg./mole, respectively. From these values and available thermodynamic data on all the species of interest, the second-law values for ΔHf_{298} and S^0_{298} of $BeF_2(g)$ were found to be −191.3 ± 2.0 kcal./mole and 52.4 ± 0.3 cal./deg./mole, respectively. The third-law ΔHf_{298} for $BeF_2(g)$ was determined to be −191.2 ± 0.4 kcal./mole.

I. Introduction

A direct experimental determination of the heat of formation and entropy of $BeF_2(g)$ has not been previously reported. A value of −184.5 kcal./mole for ΔHf_{298} has been reported,[2] however, based upon an experimental determination of the heat of formation of $BeF_2(s)$ by means of solution thermochemistry of BeO in aqueous HF and a measured heat of vaporization of BeF_2.[3] The entropy of $BeF_2(g)$ has been calculated by Stull, *et al.*,[2] using the spectroscopic data (first two vibrational levels, symmetric stretching mode and bending mode) of Buchler and Klemperer[4] and the bond length data of Akishin and Spiridonov.[5]

Because of the uncertainty in all the data involved in

(1) This research was supported by the Air Research and Development Command of the United States Air Force.

(2) JANAF Thermochemical Tables, USAF Contract No. AF 33(616)-6149, Advanced Research Projects Agency, Washington 25, D. C., Sept. 1961.

(3) (a) V. P. Kolesov, M. M. Popov, and S. M. Skuratov, *Zh. Neorg. Khim.*, **4**, 1233 (1959); (b) K. A. Sense and R. W. Stone, *J. Phys. Chem.*, **62**, 453 (1958).

(4) A. Buchler and W. Klemperer, *J. Chem. Phys.*, **29**, 121 (1958).

(5) P. A. Akishin and V. P. Spiridonov, *Kristallografiya*, **2**, 475 (1957).

the derivations of the available thermodynamic data for $BeF_2(g)$ (a new experimental value for the heat of vaporization of BeF_2 has recently been reported[6]), new determinations of the heat of formation and entropy of $BeF_2(g)$ were carried out by measuring the equilibrium constants of the reaction

$$BeO(s) + 2HF(g) \longrightarrow BeF_2(g) + H_2O(g) \quad (1)$$

Based on the available thermodynamic data on all the species involved, it appeared that good equilibrium measurements could be carried out in the range of 1200–1700°K. It was found, however, that good equilibrium data could be obtained at considerably lower temperatures. The measurements were carried out in the 943–1243°K. range.

II. Experimental

The procedure used to determine the heat and entropy of formation of $BeF_2(g)$ was to pass gaseous HF through an effusion cell made of high purity BeO, the entire apparatus being under vacuum. Measurements of the weight loss of the BeO tube coupled with the measurement of the amount of HF used provides a ready method of calculating the requisite equilibrium constants. This procedure was employed recently by Farber[7] for the measurements of thermodynamic properties of BOF.[8] To ensure molecular flow conditions, reactions were carried out under a good vacuum with pressures in the range of 10^{-5} to 10^{-6} atm.

Hydrogen fluoride was generated by heating sodium bifluoride under vacuum at temperatures between 100 and 200°. The $NaHF_2$ generator and 0.25 in. tubing leading into the furnace which held the BeO cell were constructed of copper. Since the HF and copper in this part of the apparatus were never heated above 150°, there was no problem of HF attack on the copper. The part of the apparatus which connected the BeO effusion cell to the copper tubing of the HF generator was constructed of either graphite (a 1-in. inside diameter tube with graphite reducing fittings at each end) or high purity nickel (0.25-in. tubing soldered to the copper tubing at one end and holding a nickel adapter at the other). Runs were made using both materials at most temperatures to ensure that HF was not reacting with either material and that the products of the HF–BeO reaction (BeF_2, H_2O) likewise did not react with either material.

The BeO effusion cell employed was a 0.5-in. o.d. tube, 2 in. in length with a 1-mm. effusion orifice located about 0.5 in. from the closed end of the tube. The tube of 99+% purity BeO was obtained from the Brush Beryllium Company.

It was necessary to ensure that the entire apparatus from HF generator to BeO cell was gas tight. Any leakage of HF along the system would result in erroneously low equilibrium constants. Any reaction of the HF with any of the materials, other than the BeO would, again, result in low K values. Further, any reaction of either the BeF_2 or H_2O produced from the BeO–HF reaction, with materials of the cell before escaping through the effusion orifice would result in high K values. With these considerations in mind, it was necessary to use two different methods of attaching the BeO cell to the carbon and nickel tubes.

When a graphite tube was used to connect the copper tubing of the HF generator to the BeO cell, a graphite adapter was used for the latter. This adapter held the BeO cell around the outside, *i.e.*, the BeO cell fitted into a graphite holder rather than having the graphite fit inside the BeO cell. When the reverse procedure was tried, it was found that the H_2O formed during the HF–BeO reactions very rapidly reacted with the graphite to yield high equilibrium constants. It was necessary to replace the graphite adapter frequently because of gradual loosening of the BeO cell from continued removal and insertion in the adapter. This would result in a combination of HF leakage and reaction of the outside surface of the BeO cell with leaking HF, coupled with reaction of the formed H_2O with the adjacent carbon. However, when the graphite adapters were replaced after 5–6 runs, no such problems were encountered.

With the nickel connecting tube it was necessary to insert the nickel adapter inside the BeO cell rather than the reverse procedure, because of differences in the coefficients of expansion of BeO and Ni. By making the Ni finger slightly smaller than the inside diameter of the BeO cell, allowance for the differential thermal expansions could be made. It was not necessary to ensure a gas-tight fit in this case as any HF vapors which might tend to escape from around the Ni finger would, of necessity, be forced to escape back along more than half the length of the BeO cell and would thus still have an opportunity to react.

It should be pointed out that the necessity for a connecting tube between the copper tubing of the HF generator and the BeO cell existed because of the nature of the furnace used to heat the BeO cell. The furnace was a standard automatically controlled Leco tube furnace. The length of the tubes in this furnace are 18 in. with a significant temperature gradient along this length. It thus was necessary to place the BeO tube in the center section of the furnace to ensure maximum temperature. Insertions of copper tubing into the hot reaction of the furnace would have resulted in reaction with the HF.

The experimental procedure consisted of weighing the BeO effusion cell, attaching it to the adapter, connecting tube and HF generator, and inserting the BeO cell, adapter and connecting tube into the large Ni tube in the furnace. A weighed sample of $NaHF_2$ contained in a graphite cell was placed in the copper cell and the bottom sealed with a copper, flanged gasket. The system was evacuated through two copper traps cooled in liquid nitrogen until the requisite 10^{-5} to 10^{-6} atm. pressure had been reached. The $NaHF_2$ cell was then heated to the desired temperature by means of a heating tape wound around the outside and connected to a powerstat. After an experiment the $NaHF_2$ cell was cooled in water and the apparatus disassembled. Weighing of the $NaHF_2$ cell and beryllia tube resulted in the necessary weight loss information from which the equilibrium constants were calculated.

Runs were made at six different temperatures over the range 943–1243°K. Temperatures were checked frequently during the actual runs by means of a thermocouple inserted in a well in the cell. At least three runs were made at each temperature, a total of 27 being made in all. The actual temperature inside the BeO cell was determined for each setting on the furnace control by inserting a calibrated chromel–alumel thermocouple inside the cell and obtaining a graph of the temperature *vs.* time curve by means of a Leeds and Northrup automatic recorder–controller. Calibrations were made at frequent intervals to ensure no fluctuations in the furnace.

To ensure that no NaF was being lost under the conditions employed to generate HF from $NaHF_2$, a sample of pure NaF was heated under vacuum in the HF generator to a temperature 100° higher than was used in any of the actual runs. After two hours time, the longest ever employed for a run, no loss in weight of the NaF was detected. In addition, heating sample of $NaHF_2$ to a high temperature for a prolonged period of time under vacuum resulted in the loss of the theoretical amount of HF and never any more, also indicating no loss of NaF under the experimental conditions.

III. Discussion of Results

The experimentally determined quantities in the investigation of the heat of formation of $BeF_2(g)$ were weight loss of HF (from a sample of $NaHF_2$) and weight loss of BeO. From these values it was necessary to determine the equilibrium constant, K, which in turn would lead to values of ΔHf_{298} and S^0.

The equilibrium expression for the reaction

$$BeO(s) + 2HF(g) = BeF_2(g) + H_2O(g) \quad (1)$$

is

$$K = \frac{p_{H_2O}\, p_{BeF_2}}{p^2_{HF}} \quad (2)$$

In the molecular flow regime, the pressures of the various components are given by the Knudsen equation. Thus the pressures of interest are defined as

$$p_{H_2O} = \frac{n_{H_2O}\sqrt{2\pi kNTM_{H_2O}}}{At} \quad (3)$$

(6) M. A. Greenbaum, J. N. Foster, M. L. Arin, and M. Farber, *J. Phys. Chem.*, **67**, 36 (1963).

(7) M. Farber, *J. Chem. Phys.*, **36**, 1101 (1962).

(8) M. Farber and J. Blauer, *Trans. Faraday Soc.*, **58**, 2090 (1962).

$$p_{BeF_2} = \frac{n_{BeF_2}\sqrt{2\pi kNTM_{BeF_2}}}{At} \quad (4)$$

$$p_{HF} = \frac{n_{HF}\sqrt{2\pi kNTM_{HF}}}{At} \quad (5)$$

where n = moles; k = Boltzmann constant; T = temperature; M = molecular weight; A = area of effusion orifice; t = time; and N = Avogadro's number.

Rewriting eq. 3, 4, and 5 and equating moles of $H_2O(g)$ and $BeF_2(g)$ formed to moles of BeO(s) lost leads to

$$n_{H_2O} = \frac{p_{H_2O}At}{\sqrt{2\pi kNTM_{H_2O}}} = n_{BeO} \quad (6)$$

$$n_{BeF_2} = \frac{p_{BeF_2}At}{\sqrt{2\pi kNTM_{BeF_2}}} = n_{BeO} \quad (7)$$

$$n_{HF} = \frac{p_{HF}A}{\sqrt{2\pi kNTM_{HF}}} = n_{HF}^* - 2n_{BeO} \quad (8)$$

where n_{HF}^* is the number of moles of HF lost from the $NaHF_2$. Substituting eq. 6, 7, and 8 into the equilibrium expression, equation 2, leads to

$$K = \frac{\left(\frac{n_{BeO}\sqrt{2\pi kNTM_{BeF_2}}}{At}\right)\left(\frac{n_{BeO}\sqrt{2\pi kNTM_{H_2O}}}{At}\right)}{(n_{HF} - 2n_{BeO})^2\left(\frac{2\pi kNTM_{HF}}{(At)^2}\right)} \quad (9)$$

which reduces to eq. 10

$$K = \left(\frac{(n_{BeO})^2}{(n_{HF} - 2n_{BeO})^2}\right)\left(\frac{\sqrt{M_{H_2O}\,M_{BeF_2}}}{M_{HF}}\right) \quad (10)$$

The reaction of BeO(s) with HF(g) was studied over the temperature range 943–1243°K. At these temperatures it was assumed that (a) the BeF_2 formed from the reaction was all gaseous, and (b) that the H_2O formed in the reaction did not react with the BeO effusion cell. Previous work[6] on the heat of vaporization of BeF_2 demonstrated that at the temperatures and pressures employed in the present investigation any BeF_2 formed would be gaseous and exist only as a monomer. Physical inspection of the apparatus after all runs never gave any indication of condensed BeF_2 in or around the BeO cell. As a further check on the formation of $BeF_2(g)$ from the BeO–HF reaction, as opposed to formation of a condensed phase of BeF_2, the effect of HF partial pressure on the equilibrium constant was studied in detail at 1073°K. The reaction as shown in equation I is pressure independent. If any significant amount of $BeF_2(s,l)$ is formed the K values should show a marked pressure dependence. A series of 7 runs was made at 1073°K., where the HF partial pressure was varied by a factor of more than 10. The calculated K values were found to be independent of pressure within experimental error. A sixfold variation in HF pressure at 1003°K. likewise showed no effect on the calculated K values and a 2.5-fold variation in HF pressure at the lowest temperatures studied, 943°K., also failed to demonstrate any pressure dependence of K.

The possibility of reaction of the H_2O formed during the reaction with the BeO was considered because of reported reactions of H_2O and BeO in the literature.[9-10] These reports stated that significant weight losses occurred from the passage of $H_2O(g)$ over BeO(s) at temperatures as low as 1473°K. Although this temperature was 230° higher than any used in the present studies, it was considered necessary to eliminate the possibility of any such reaction occurring at the highest temperatures used. Using the identical experimental apparatus employed in the BeO–HF runs, 2 g. of gaseous H_2O was passed through the BeO effusion cell at 1243°K. Weighing of the BeO cell after reaction indicated that within the experimental error (±0.5 mg.) no reaction occurs between $H_2O(g)$ and BeO(s) at the highest temperatures employed in the current investigation.

To ensure that none of the materials of the experimental apparatus were reacting with either the HF or with the H_2O and BeF_2 produced from the reaction, two entirely different set-ups were used, one made of graphite and the other of nickel. If reactions were occurring between the gaseous species and the tube materials, then the calculated K values would be different when carbon and nickel were used at the same temperature. The formation of NiF_2 and NiO by reaction of Ni with BeF_2, HF, and H_2O was considered in the temperature range of the investigation. The reaction of H_2O and Ni at temperatures up to 1100° has been reported not to occur.[11] Theoretically, employing data in the literature,[2] the reaction of HF and Ni at temperatures as high as 1250°K. is unlikely. Weighings of the nickel holder prior to and after each determination indicated a negligible reaction with the HF gas at the experimental temperatures. This is in agreement with the results of Farber, Darnell, and Ehrenberg[12] and Myers and Delong.[13] The reaction of $BeF_2(g)$ with Ni was previously found not to occur.[6] (These same studies indicated that graphite did not react with gaseous BeF_2 in this temperature range.)

However, both experimentally and theoretically the reaction of water vapor and graphite does take place in this temperature range. Therefore, as explained in the Experimental section, it was necessary to minimize the possible reaction of H_2O with C. A gas-tight fit of the BeO cell in the graphite holder was necessary to prevent any HF escaping along the outside of the BeO cell. If this occurred, the reaction of H_2O formed with the carbon would take place yielding high values for the equilibrium constant. When reactions were carried out using both the Ni and C systems, the resulting K values were the same within experimental error at both the highest and lowest temperatures. Weight of the Ni holder before and after several runs indicated no significant reaction was occurring between the Ni and any of the species present. To ascertain whether NaF was evaporating from the $NaHF_2$ a sample of reagent grade NaF was heated to the highest temperature to which the sodium bifluoride was subjected with no apparent weight

(9) L. I. Grossweiner and R. L. Seifert, *J. Am. Chem. Soc.*, **74**, 2701 (1952).

(10) W. A. Yound, U. S. Atomic Energy Commission Report No. NAA-SR-4446, March 15, 1960.

(11) M. Farber, *J. Electrochem. Soc.*, **106**, 751 (1959).

(12) M. Farber, A. J. Darnell, and D. Ehrenberg, *ibid.*, **102**, 446 (1955).

(13) W. R. Myers and W. B. Delong, *Chem. Eng. Progr.*, **44**, 5, 359 (1948).

loss. Under the conditions of these experiments NaF will react with beryllium oxide.

The values for K as calculated from the experimental data are listed in Table I. A plot of log K *vs.* $1/T$ yields a least squares slope of 20.5 ± 1.7 kcal., corresponding to the ΔH_r over the temperature range.

TABLE I

Temp., °K.	Wt. of HF lost, mg.	Wt. of BeO lost, mg.	$K \times 10^3$	ΔF Reaction, kcal./mole	$\Delta Hf/BeF_2$
943	308.8	7.9	0.61	13.9	−192.6
943	399.3	10.9	0.69	13.6	−192.9
943	164.7	4.3	0.63	13.8	−192.7
1003	534.5	16.2	0.99	13.8	−192.5
1003	86.9	2.8	0.97	13.8	−192.5
1003	251.2	7.7	0.87	14.0	−192.3
1073	1368.3	61.9	1.90	13.4	−192.6
1073	465.7	22.7	2.21	13.0	−193.0
1073	842.5	36.0	1.71	13.6	−192.4
1073	130.6	5.1	1.42	14.0	−192.0
1073	561.6	28.7	2.41	12.9	−193.1
1073	146.5	7.0	2.12	13.1	−192.9
1073	855.3	43.4	2.41	12.9	−193.2
1133	464.6	33.8	4.87	12.0	−193.7
1133	267.7	17.7	4.07	12.4	−193.3
1133	124.5	6.7	2.69	13.3	−192.4
1133	277.2	16.6	3.31	12.9	−192.8
1133	114.6	6.8	3.28	12.9	−192.8
1188	91.6	8.2	7.47	11.6	−193.8
1188	87.2	6.8	5.65	12.2	−193.2
1188	200.4	14.0	4.56	12.7	−192.7
1188	164.2	12.9	5.74	12.2	−193.2
1243	134.7	12.0	7.37	12.1	−193.1
1243	59.6	5.6	8.21	11.9	−193.3
1243	194.4	16.9	6.68	12.4	−192.8
1243	274.7	25.2	7.89	12.0	−193.2
1243	114.4	10.2	7.38	12.1	−193.1

Using the available thermodynamic data for all species involved[2] and extrapolating to 298°K., a value for the ΔHf_{298} of $BeF_2(g)$ of −191.3 ± 2.0 kcal./mole is obtained. The corresponding third law value is −191.2 ± 0.4 kcal./mole. From a plot of ΔF_r *vs.* T the ΔS_r of 6.0 ± 0.3 cal./deg./mole is obtained over the reaction temperature range by means of a least squares analysis. Using the available entropy data[2] for BeO(s), HF(g), and $H_2O(g)$, a value of 52.4 ± 0.3 cal./deg./mole is obtained for the S^0_{298} of $BeF_2(g)$. This compares with a theoretical value of 52.3 cal./deg./mole calculated from spectroscopic data.[4,5] A calculation of the S^0 for $BeF_2(g)$ at 1100°K., using the experimental ΔS_r and the thermodynamic values for the other species at this temperature, leads to a value of 67.5 cal./deg./mole compared to 66.9 reported in the JANAF Tables.[2] The ΔH_{298} and S^0_{298} of $BeF_2(g)$ reported here represent the first experimentally determined values of these thermodynamic properties. Since the thermodynamic values of $H_2O(g)$, HF(g), and BeO(s) are considered to be of a high order of reliability at this time, the thermodynamic values for $BeF_2(g)$ reported here based on experimental measurements of a reaction involving only these species should be considered established.

Employing the latest value for the heat of sublimation[6] the data of Kolesov, *et al.*,[3a] lead to a value of approximately −188 kcal./mole for ΔHf of $BeF_2(g)$. The remaining discrepancy between this work and that of Kolesov may be due in part to the extensive polymerization of HF(g) at room temperature, since Kolesov's work[3a] did not take this polymerization into account in employing a value of the heat of solution of gaseous HF monomer to form HF(aq).

THE PARTIAL MOLAR VOLUMES OF IONS[1]

BY SIDNEY W. BENSON AND CHARLES S. COPELAND

Chemistry Department, University of Southern California, Los Angeles 7, California

Received October 31, 1962

It is shown that the recent successes of Mukerjee in correlating partial molar volumes of ions with the continuum model of Born can be understood in terms of an isomorphic replacement of water molecules in a simple cubic lattice by ions whose sizes range from smaller to not too much larger than H_2O. The anomalously large values of the intrinsic volumes are then shown to be accounted for very closely by the void volume of the ion in such a lattice. This lends strong support to Mukerjee's suggestion that ion volumes should be monotonic functions of crystal radius, independent of the sign of the charge. A simple free volume model is used to show that the radius of an ion in either a solid or a solution should be the same to within 0.02 Å. of its "hard sphere" radius. The effects of temperature on partial molar volume are discussed briefly. Finally it is pointed out that the dipole–dipole repulsions between solvation shell molecules prevent the large ions such as Cs^+, Cl^-, Br^-, I^-, etc., from having very large coördination numbers.

Introduction

The partial molar volumes of salts at infinite dilution can be obtained from precise density measurements on salt solutions and must be additive in the individual partial molar volumes of the ions, $\bar{V}_i^0$. However, as with all such ionic quantities there is no direct experimental method of making a separation of the sum of the $\bar{V}_i^0$ into the separate $\bar{V}_i^0$ and one is forced to other criteria if such separations are to be made. Any theory of the $\bar{V}_i^0$ should of course predict the individual values and should be tested by direct comparison with experimental values, an apparently circular dilemma.

Recently Mukerjee[2] has argued that for spherically symmetrical ions such as the alkali metal cations and the halide anions, the partial molar volume should be a smooth monotonic function of the ionic radius quite independent of the sign of the ionic charge. This would seem to be an inescapable argument if the solvent molecule, H_2O, were also spherically symmetrical. Unfortunately, such is not the case and in fact a number of authors have made quite strong arguments[3] in favor of

(1) This work has been supported by a grant from the Office of Naval Research.

(2) P. Mukerjee, *J. Phys. Chem.*, **65**, 740, 744 (1961).

an appreciable difference in interaction of positive and negative ions with solvent H_2O molecules. These arguments have been based on empirical correlations of entropies and free energies of solvation with ionic radii. However, there is good reason for believing that the latter thermodynamic quantities are much more sensitive functions[4] than the partial molar ionic volumes and hence might not provide a sound basis for extrapolation.

It is the purpose of the present paper to show that Mukerjee's hypothesis is not only a fairly reasonable one but that in addition it provides an empirical correlation which can be readily justified in a quantitative basis by means of the Born electrostatic model for ion solvation.

The Born Model for Electrostriction.—$\bar{V}_i^0$, the partial molar volume of an ion i at infinite dilution, can be considered as the difference of two terms. The first is the intrinsic ion volume V_i or the physical volume occupied by the ion considered as an impenetrable solid. The second is V_e, the diminution in volume of the solvent caused by the enormous electrical field of the ion tending to compress it. Thus

$$\bar{V}_i^0 = V_i - V_e \qquad (1)$$

Considering the ion to be a hard sphere of radius r_i, most authors have set $V_i = 4/3\pi r_i^3$. If we treat the solvent as a structureless dielectric, the electrostriction volume can be calculated from the electrostatic pressure and the compressibility of the solvent. Again using the spherical model of the ion, the free energy of charging it in the solvent of constant dielectric D is given by[5]

$$\Delta F_s = -\frac{\epsilon^2 Z^2}{2r_i}\left(1 - \frac{1}{D}\right) \qquad (2)$$

where ϵ = the electronic charge and Z = valence. Minus the volume change accompanying this charging is the electrostriction volume. From thermodynamics

$$V_e = -\Delta V_s = -\left[\frac{\partial(\Delta F_s)}{\partial P}\right]_T = \frac{\epsilon^2 Z^2}{2r_i D}\left(\frac{\partial \ln D}{\partial P}\right)_T = \frac{\beta\epsilon^2 Z^2}{2r_i D}\left(\frac{\partial \ln D}{\partial \ln \rho}\right)_T \qquad (3)$$

where $\beta = (\partial \ln \rho/\partial P)_T$ = the compressibility of the solvent and ρ = density.

A slightly different result but in our opinion more accurate may be obtained from the work of Frank.[6] It has the approximate form

$$V_e \sim \left\langle \frac{\beta\rho}{D\rho_0}\left(\frac{\partial \ln D}{\partial \ln \rho}\right)_T \right\rangle \frac{\epsilon^2 Z^2}{2r_i} \qquad (4)$$

where the average is to be taken over all the solvent extending from the surface of the ion.[7] In both cases the variation of r_i with P has been ignored.

(3) (a) R. H. Moelwyn-Hughes, *Proc. Cambridge Phil. Soc.*, **45**, 477 (1948); (b) R. E. Powell and W. M. Latimer, *J. Chem. Phys.*, **19**, 1139 (1951).

(4) In addition, it is not obvious how we would go about separating van der Waals interactions from coulombic interaction. These could produce significant effects on ΔF_s and ΔS_s without changing $\bar{V}_i^0$ appreciably. From crystal structures of hydrates it appears that the radius of contact of the water molecule is the same for positive and negative ions.

(5) M. Born, *Z. Physik.*, **1**, 45 (1920).

(6) H. S. Frank, *J. Chem. Phys.*, **23**, 2023 (1955), has shown that the dielectric constant D is not a constant but must vary with electric field intensity due to compression of the solvent.

(7) Similar calculations, not as accurate, have been made by T. J. Webb, *J. Am. Chem. Soc.*, **48**, 2589 (1926), and by H. M. Evjen and F. Zwicky, *Phys. Rev.*, **33**, 860 (1929).

Using the experimental values, $(\beta\rho/\rho_0) \sim 5 \times 10^{-5}$ atm.$^{-1}$; $(\partial \ln D/\partial \ln\rho)_T = 1.4$; $D = 85$ we find that $V_e = 6Z^2/r_i$ cc. Å./mole with r_i in units of Ångstroms. This yields 6 cc. as the electrostriction for a univalent ion of 1 Å. radius which is of the proper order of magnitude.

Combining these results we may write for the limiting partial molar ionic volume

$$\bar{V}_i^0 = Ar_i^3 - \frac{BZ^2}{r_i} \qquad (5)$$

with $A = 4/3\pi N_{av} = 2.51$ cc./mole Å.^{3} and $B \sim 6$ cc. Å./mole for $Z = 1$, 24 cc. Å./mole for $Z = 2$, and 54 cc. Å./mole for $Z = 3$.

Hepler[8] using Goldschmidt's crystal radii for ions and Fajans and Johnson's[9] assignment of individual $\bar{V}_i^0$, found that all of the positive ions fit an equation of the form of eq. 5 with $A = 5.3$ cc./mole Å.^{3} and $B = 4.7$ cc. Å./mole. The maximum deviation was 5 cc. while the average was about 2 cc. For the halide anions and OH^-, the data fell on a nearly parallel line with $A = 4.6$ cc./mole Å.^{3} and $B = 19$ cc. Å./mole. This very large electrostriction for anions seems to us completely indefensible.

Mukerjee[2] assigned the individual $\bar{V}_i^0$ so that all univalent ions ($Z = 1$) fell on the same smooth curve when the assigned $\bar{V}_i^0$ were plotted against Pauling's calculated crystal radii.[10] He found that these $\bar{V}_i^0$ fit an equation of the form of 5 with $A = 4.50$ cc./mole Å.^{3} and $B = 8.0$ cc./Å. mole. Both positive and negative ions now fit on the same curve with no deviations larger than ±2 cc./mole.

For the univalent ions, Hepler's value for B of 4.7 cc. Å./mole and Murkerjee's value of 8.0 cc. Å./mole can both be considered in reasonable agreement with the value of 6 cc. Å./mole calculated from equation 4. In addition for the divalent and trivalent cations Murkerjee found that V_e is about 32 ± 4 and 58 ± 4 cc./mole, respectively, apparently independent of the ionic radius. Aside from the radius dependence these values are in good quantitative agreement with the values of 24 and 54 cc./mole predicted, respectively, for 1 Å. radius ions.

The coefficient A in eq. 5 is equal to $4\pi N_{av}/3 = 2.51$ cc./Å.^{3} mole. However, both Hepler and Mukerjee find values almost double this.[11] To account for this apparently abnormal size of ions in solution a number of arguments have been advanced. These arguments all appeal to the molecular structure of the solution. A macroscopic model is clearly inadequate. We shall examine this problem in detail in the following section.

The Intrinsic Volumes of Ions.—A number of authors have assumed that the reason for the apparently large intrinsic volumes of ions in solution lies in the fact that ions in crystals are under greater compressive forces than they are in solution. The order of magnitude of these effects on the ion sizes can be estimated from a simple free volume model. If we assume that the ions can be represented by hard spheres of radius r_i

(8) L. G. Hepler, *J. Phys. Chem.*, **61**, 1426 (1957).

(9) K. Fajans and O. Johnson, *J. Am. Chem. Soc.*, **64**, 668 (1942), used as their basis for assigning $\bar{V}_i^0$ that $\bar{V}_i^0(NH_4^+) = \bar{V}_i^0(Cl^-) = 18.0$ cc./mole.

(10) His choice led to $\bar{V}_i^0(Cl^-) = 22.3$ cc./mole; $\bar{V}_i^0(NH_4^+) = 13.5$ cc./mole.

(11) An earlier paper of A. M. Couture and K. J. Laidler, *Can. J. Chem.*, **34**, 1107, 1209 (1956), had shown that $\bar{V}_i^0$ of the spherical ions could be fitted to a simple curve $\bar{V}_\pm^0 = 16 + 4.9r_s^3 - 26|Z\pm|$, where again the A term is roughly twice the intrinsic ion volumes.

imbedded in a cavity of radius $r_c > r_i$, the chemical potential of an ion in a solution (or a crystal) can be written as

$$\mu_i = F_i + \frac{3}{2}kT - kT \ln v_{fi} \qquad (6)$$

where v_{fi} is the appropriate free volume of the ion and F_i (neglecting van der Waal's forces) is the electrostatic work of charging the ion. For an ion in a crystal F_i can be written as

$$F_{ic} = \frac{-AZ^2\epsilon^2}{2r_n} + \frac{\epsilon^2Z^2}{2r_i} \qquad (7)$$

where A is the Madelung constant for the lattice and r_n is the near-neighbor distance.[12] The second term $\epsilon^2Z^2/2r_i$ is the self-energy of the ion and will disappear from the subsequent calculations.

In a solution F_i becomes

$$F_{is} = \frac{Z^2\epsilon^2}{2r_cD} - \frac{Z^2\epsilon^2}{2}\left(\frac{1}{r_c} - \frac{1}{r_i}\right) \qquad (8)$$

This term is somewhat different from the Born term since it includes the extra term of carrying charge across the cavity to the ion surface. It yields however the same expression for the energy of solvation of the gas ion.[13]

In the crystal we can take $v_f = r_f^3 = (r_n - r_{i+} - r_{i-})^3$ while for the solution $v_f = 4/3\pi(r_c - r_i)^3$. If we now minimize the chemical potentials for the crystal and solution with respect to r_n and r_c, respectively, we can solve for r_n and r_c. We find for the crystal

$$1 - \frac{(r_{i+} + r_{i-})}{r_n} = \frac{6kTr_n}{AZ^2\epsilon^2} \qquad (9)$$

$$= 0.0062r_n \text{ (at 300°K., } r_n \text{ in Å.)}$$

and for the solution

$$1 - \frac{r_i}{r_c} = \frac{6kTr_c}{Z^2\epsilon^2}\left(\frac{D-1}{D}\right) \qquad (10)$$

$$= 0.011r_c \text{ (at 300°K., } r_c \text{ in Å.)}$$

In the case of solutions we see that the cavity radius is at best a few hundredths Ångstrom greater than the hard sphere radius while the same is true for the near neighbor distance r_n. If $r_{i+} = r_{i-}$ then the expressions for crystal and solution give almost identical results.

We may thus conclude that there is no basis for believing that ions in a solution are under less electrostatic pressure than are the ions in a crystal and we may expect to find that ion–water distances in crystal hydrates should be the same as the ion–water distances in solutions.[14]

The free volume model which we have employed gives qualitatively correct values for the coefficient of thermal expansion and compressibility of crystal lattices so that it is a reasonable first approximation for ionic solids.

If the large intrinsic volumes in solution cannot be accounted for by expansion of the ions, we are forced to look to other models. A very reasonable explanation is given by consideration of the discrete structure of both crystals and solutions. In a simple crystal of the NaCl type, the lattice volume is only partially filled by the ions. There is a considerable amount of void space between ions. This has been entirely neglected in the macroscopic models used for ionic volumes in solution.

We can calculate a void space correction to be applied to the ions in such a crystal, as the ratio of the crystal volume to the volume of the ions taken as spheres

$$f = \frac{V_{cryst}}{V_+ + V_-} = \frac{2r_n^3}{4/3\pi(r_+^3 + r_-^3)} = \frac{1.5}{\pi}\frac{(r_+ + r_-)^3}{(r_+^3 + r_-^3)} \qquad (11)$$

When $r_+ = r_-$, f has its maximum value of $6/\pi = 1.91$ which is very close to Hepler's value for the intrinsic volume correction and only 6% larger than Mukerjee's. For $r_+ = r_-/2$, $f = 1.43$ while for $r_+ = 0.414r_-$ which leads to anion–anion contact, f has its minimum value of 1.26.

For CsCl type lattices the values of f range from 1.47 to 1.37 and for hexagonal close-packing ($r_+ = r_-$) f is 1.41. At the other extreme, a diamond lattice gives an f value of 2.94.

In order to apply such corrections to ionic solutions we must thus consider the geometry of the coördination shell and the geometry of packing of normal water molecules. If for example we consider H_2O molecules to be packed normally in a simple cubic lattice (coordination 6) and further consider that an ion simply replaces a H_2O molecule in a lattice site,[15] then the intrinsic ion volume is just 1.91 times its spherical volume. If on the other hand we assume the ice lattice for H_2O (coördination 4) and a similar isomorphic replacement, the f factor becomes 2.94.

For ions with radius not too different from the 1.55 Å. value applicable to the van der Waal's radius for water the hypothesis of isomorphic replacement seems quite reasonable and yields the proper packing factor. Of the univalent ions only Li^+ with $r_c = 0.6$ Å. appears to have an anomalously high intrinsic volume. It is in fact too high to attribute simply to a high packing factor ($f = 6$ would be required) and it appears as though Li^+ (aq) is just structurally different from the other ions.

For the divalent ions and the trivalent ions, Mukerjee has shown that the volumes are nearly the same in each class and are almost independent of radius implying that one has reached a saturation effect relative to the first solvent shell of water molecules for +2 and +3 ions. This is quite reasonable on the isomorphic replacement model. An octahedral water shell around a central ion could accommodate central ions with a radius of from 0.8 to 1.2 Å. with very little change in external dimensions. What little expansion does occur is very well compensated by the increased space be-

(12) Note that $r_n = r_{i+} + r_{i-} + r_f$ where r_f is the "free" distance between ions.

(13) The interpretation of the resulting expression $Z^2\epsilon^2/2r_c\left(\frac{D-1}{D}\right)$ is however different.

(14) We could reach the same result intuitively by noting that the enthalpies of solution of most salts are very small if not zero. This then implies that the lattice energies and solvation energies must be nearly equal. Since both depend on the inverse first powers of the ionic radii, we can thus conclude that the electrostatic compressions must be also nearly the same in the two phases.

(15) By this we mean that without disturbing the packing geometry, there will of course be rotations of the adjacent water molecules to electrostatically more favorable orientations.

tween the water molecules and thus a lesser void space in terms of the 2nd shell packing.

Temperature Effects.—The effect of temperature on $\bar{V}_i^0$, if we assume that the intrinsic volume is not affected must be attributed to the electrostriction term $\bar{V}_e$. If we differentiate $\bar{V}_e$ (eq. 3) we find

$$\left(\frac{\partial \bar{V}_i^0}{\partial T}\right)_P \sim -\left(\frac{\partial \bar{V}_e}{\partial T}\right)_P = -\frac{\bar{V}_e}{T}\left\{\left(\frac{\partial \ln \beta}{\partial \ln T}\right)_P - \left(\frac{\partial \ln D}{\partial \ln T}\right) + \frac{\left(\frac{\partial^2 \ln D}{\partial \ln \rho\, \partial \ln T}\right)}{(\partial \ln D/\partial \ln \rho)_T}\right\} \quad (12)$$

For water, one finds that the third term in brackets is negative and generally small, the second term is negative and of order of magnitude of -1.4 for water at 25° while the first term is positive for water at pressures below 1000 atm. and negative above. The first term also changes sign at 40° being positive above and negative below. From the observation that $(\partial \bar{V}_i^0/\partial T)_P$ is positive for most salts at 25°,[7] tending to decrease with increasing temperature we conclude that the bracketed expression must be negative so that either the effect of dielectric saturation is to reduce considerably the effect of temperature on the effective dielectric constant of the first solvent shell or else the first term must have a value of the order of -2 for the first solvent shell. This is about three times the value that it has at 3000 atm. (*e.g.*, -0.6) and is not an unreasonable result.[16] The values of $(\partial \bar{V}_i^0/\partial T)_P$ reported at 25°[7] vary from 0.07 cc./°C. for the alkali chlorides to 0.14 cc./°C. for NaI. Qualitatively they can be said to be of the order of V_e/T.

(16) The electrostatic pressure in the first solvent shell is of the order of 10^4 to 10^5 atm. so such high values are in an expected range.

The effects of pressure have been discussed in detail elsewhere[17] and will not be repeated here.

Coördination Number of Ions in Solution.—The assumption of isomorphic replacement which seems to account reasonably well for the intrinsic volume of ions raises some interesting questions regarding the solvation shell. From the point of view of the central ion, the simple Born model would lead one to think that an ion will tend to pack as many solvent molecules into its first solvation shell as possible. However, very simple calculations on the large cations and anions such as Cs^+ (1.69 Å.) and I^- (2.16 Å.) immediately show that if such were the case (14 and 18 near neighbors possible for each), the electrostriction volume would be much greater than it is and the V_i^0 for these ions anomalously small.

The reason that these large coördinations do not occur[18] is that in placing water molecules in the hydration shell one loses a considerable fraction of the energy of vaporization by breaking the previously favorable H-bonding. In addition one creates a dipole–dipole repulsion arising from the unfavorable disposition of the water dipoles in the solvent shell. This repulsion is weak compared to the ion–dipole attraction but it is multiplied by the number of H_2O–H_2O interactions or roughly $Z^2/2$ (Z = coördination number) whereas the ion–dipole attraction goes as Z.

If we set up a crude model with rigid point dipoles and calculate the optimum value of Z, it turns out to be between 6 and 8 for ions of radius between 1 and 2 Å.

Acknowledgment.—S. W. B. wishes to acknowledge his appreciation to Prof. P. Mukerjee and Dr. H. L. Friedman for many stimulating discussions on the above topics.

(17) H. S. Harned and B. B. Owen, "Physical Chemistry of Electrolyte Solutions," Third Edition, Reinhold Publ. Corp., New York, N. Y., 1958.

(18) See discussion in J. D. Bernal and R. H. Fowler, *J. Chem. Phys.*, **1**, 515 (1933).

THE COEXISTENCE OF INDEPENDENT SITES ON ALUMINA AS SHOWN BY THE INFRARED SPECTRA OF CHEMISORBED ACETYLENE AND ETHYLENE

By D. J. C. Yates and P. J. Lucchesi

Esso Research and Engineering Company, Linden, New Jersey

Received October 31, 1962

On alumina infrared studies have shown that acetylene is rapidly chemisorbed and have established an end-on configuration for the adsorbed molecule. Separate studies have shown that ethylene is slowly chemisorbed in a complex reaction involving only ethylene and forming adsorbed ethyl groups by self-hydrogenation. In the present work, two types of experiments have been performed to determine whether the sites responsible for these processes are independent or not. The first experiments involved a study of exchange reactions using OD surfaces and the various normal and deuterated acetylenes and ethylene. Secondly, competitive coverage experiments also have been carried out. It is shown that the sites responsible for ethylene self-hydrogenation are only slightly affected by the presence of pre-adsorbed acetylene. Conversely, the end-on coverage of acetylene is unaffected to within 5% by the preformation of surface ethyl groups *via* self-hydrogenation of C_2H_4. In the presence of pre-adsorbed deuterioacetylene, C_2H_4 undergoes self-hydrogenation to ethyl groups that are undeuterated. The present studies therefore provide strong evidence that on aluminum oxide the sites responsible for acetylene chemisorption and for ethylene self-hydrogenation are independent. Evidence is also presented to show that the sites are physically remote.

I. Introduction

Recent work in this Laboratory has shown by means of infrared spectroscopy that acetylene[1] and ethylene[2] are chemisorbed on alumina. The acetylene retains its triple bond character on adsorption and was found to be adsorbed in two configurations. The strongly held acetylene was held normal to the surface, while the weakly adsorbed acetylene was held parallel to the surface. The sites responsible for the acetylene adsorption

(1) D. J. C. Yates and P. J. Lucchesi, *J. Chem. Phys.*, **35**, 243 (1961).

(2) P. J. Lucchesi, J. L. Carter, and D. J. C. Yates, *J. Phys. Chem.*, **66**, 1451 (1962).

have not been identified precisely, but are probably adjacent to certain types of the OH groups on the surface. This is shown by the fact that OD groups are formed on adding C_2D_2 to a surface initially containing only OH groups.[1]

In contrast, ethylene loses its double bond character on adsorption. The chemisorbed species has no CH stretching frequencies characteristic of olefinic species, only bands due to paraffinic CH species being present. In this case, species of differing CH_3/CH_2 ratios were found on two different aluminas.[2] On the alumina which formed ethyl groups, it was found that the hydrogen for this process came from ethylene, as no alkyl C–D bonds were formed on adding C_2H_4 to an alumina covered with OD groups.[2] This would indicate that the sites active in self-hydrogenation of ethylene are probably physically remote from the surface hydroxyl groups.

As chemisorbed acetylene exchanges with surface hydroxyl groups, while chemisorbed ethylene does not, it seems very likely that the sites which adsorb the two molecules are different. Experiments have been performed to examine this idea.

Two methods have been used. To an alumina containing only OD groups, deuterioacetylene was added. After removing the excess C_2D_2, ethylene then was added. The adsorption of ethylene in this experiment was slow, and the inverse experiment was tried. Normal ethylene was added to an OD covered alumina, the excess removed, and deuterioacetylene added. By determining the nature of H–D exchange in the adsorbed species, the nature of the sites can be deduced.

Coverage experiments have also been performed to determine whether pre-adsorbed ethylene blocks the acetylene sites. To a deuterated sample of known thickness, deuterioethylene was added, and left until $-C_2D_5$ groups were present. After evacuating the excess ethylene, acetylene was added. After removing the excess C_2H_2, the intensity of an absorption band in the end-on adsorbed acetylene was measured. Acetylene was added to another deuterated sample and the intensity of the same band was measured under identical conditions.

Both the exchange and the coverage experiments show that the sites for ethylene and acetylene, on the alumina used, are independent.

II. Experimental

(a) **Materials and Apparatus.**—The η-alumina used was prepared by heating a β-trihydrate for four hours at 600°, and had a surface area of 295 m.²/g. The trihydrate was prepared from aluminum alcoholate. Details of the impurities have been given in reference 2; the alumina used in this work is identical with that designated (A) Al_2O_3 in the earlier paper.

The acetylene, deuterioacetylene, and deuterium suppliers and purities are described elsewhere,[1] and the corresponding data for ethylene and deuterioethylene are given in reference 2.

The cell, vacuum system, and spectrometer used are described in detail in an earlier paper.[2] The slit width and resolution used are the same as these used for alumina in the ethylene work.

(b) **Procedure.**—After inserting the samples in the cell, they were heated and evacuated simultaneously. After reaching 600°, evacuation was continued at this temperature until the vacuum was 5×10^{-6} mm. Deuterium then was added, at pressures between 14 and 20 cm., and left for times between 3 and 10 hr. The deuterium was then evacuated at 600° for 15 min., the final vacuum being about 5×10^{-6} mm. The sample was then cooled down *in vacuo*, the adsorbate admitted, and spectra run. In one case, the sample was not deuterated, and it was evacuated only for the time necessary to reach 5×10^{-6} mm. at 600°, and then cooled down *in vacuo*. No hydrogen treatment was given to this sample.

In some cases deuterioacetylene was added first, and then C_2H_4; in other cases, C_2H_4 and then deuterioacetylene. Experiments were also carried out with deuterioethylene initially added and then C_2H_2. The details of the procedure used in each case are given in the following section. The acetylene and ethylene were added in all cases at room temperature.

III. Results and Interpretation

(a) **Exchange Experiments. (i) Ethylene on Preadsorbed Deuterioacetylene.**—The first method that has been used to determine the presence of independent sites is to see whether any exchange takes place between the adsorbed species. In the first series of experiments C_2D_2 was added initially, then C_2H_4. In another series, C_2H_4 was added first, then C_2D_2. The purpose of these experiments was to use the frequencies and intensities of infrared bands of adsorbed molecules to detect the presence or absence of isotopic exchange in the adsorbed phase. If no exchange is found, this would make it very probable that the adsorption sites are independent. Table I gives a summary of the frequency assignments of surface species discussed in this work.

TABLE I

SUMMARY OF BANDS OBSERVED (IN CM.$^{-1}$) IN SURFACE SPECIES

OD groups 2790, 2755, and 2730 (OD str.)
C_2D_2 (strongly held) 2570 (CD str.) 1890 (C≡C str.)
C_2D_2 (weakly held) 2410 (CD str.) 1740 (C≡C str.)
C_2H_2 (strongly held) 3300 (CH str.) 2007 (C≡C str.)
CD (saturated species) 2230 (CD str.)
C_2H_5 groups 2965 (CH_3 a. s. str.) 2925 (CH_2 a. s. str.)
C_2H_5 groups 2880 (CH_3 s. str.) 2850 (CH_2 s. str.)
C_2H_5 groups 1382 (CH_3 bend) 1465 (CH_3 and CH_2 bend)

With the alumina used here, the OD groups had similar stretching frequencies to those found on the alumina used for the acetylene work.[1] The bands are at 2790, 2755, and 2730 cm.$^{-1}$, and have similar relative intensities to those observed earlier. On adding 68 cm. of C_2D_2 to such a sample, the 2790 cm.$^{-1}$ OD band disappeared, and the other two OD bands became much weaker. A broad band also was seen at lower frequencies. This was caused by hydrogen bonding between the two low frequency OD groups and the weakly held C_2D_2. This is very similar to that observed in earlier work; the high frequency OD groups interact mainly with the strongly held acetylene, and the two lower frequency groups with the weakly held acetylene. Bands of the strongly held C_2D_2 were observed at 2570 cm.$^{-1}$ (CD stretching) and at 1890 cm.$^{-1}$ (C≡C stretching). Corresponding bands of the weakly held C_2D_2 were observed at 2410 and 1740 cm.$^{-1}$. All these frequencies are the same as those reported earlier[1] for C_2D_2 adsorbed on alumina, and the conclusions about the nature and orientation of adsorbed acetylene deduced there apply to the alumina used in this work.

To make the experiment unambiguous, it is necessary to remove all the gaseous C_2D_2 from the system before adding ethylene. On doing so, in addition to the bands of the strongly held C_2D_2, a band at 2230 cm.$^{-1}$ was observed. This shows that the species producing this band is strongly held to the surface. Its frequency is that expected for a saturated CD group. No assignment can be given to this species, as there is very little data on the spectra of either adsorbed deuteriohydro-

carbons, or of deuterioethyl compounds. The spectrum is, however, quite different from that found on adding C_2D_4 to alumina.[2] Only one band is found in the 2200 cm.$^{-1}$ region here, instead of two, and also the band formed on adding C_2D_2 has a much greater half-width than the bands formed from C_2D_4. This band at 2230 cm.$^{-1}$ had not been observed in earlier work. However, it has always been found with this alumina, even when the C_2D_2 is added after pre-adsorbed C_2H_4 (see next section).

After the evacuation of the C_2D_2 had been completed, C_2H_4 was added, at a pressure of 66 cm. Figure 1, curve a, shows the peak optical density of the CH_3 group in the adsorbed species, measured at 2965 cm.$^{-1}$. The rate of formation of ethyl groups, although much slower than usual, is linear with time. In order to obtain accurate optical densities of the adsorbed phase, the gaseous ethylene was taken out of the cell each time a spectrum was run. After this, fresh ethylene, at the same pressure, was put in the cell again. No exchange took place between either gaseous or adsorbed C_2H_4 and the adsorbed species containing saturated CD groups. The band due to the latter, at 2230 cm.$^{-1}$, remained at a constant optical density of 0.18 ($\pm$0.02) during the whole experiment (Fig. 1, line b). This indicates that no deuterated ethyl groups were being formed, while quite large quantities of C_2H_5 groups were being formed by self-hydrogenation.

With the adsorbed C_2D_2, in contrast, some exchange did take place. The rate of decrease of the 1890 cm.$^{-1}$ band was quite rapid at first (Fig. 1, curve c) and slowed down later on. At the same time, a small amount of adsorbed end-on C_2H_2 was formed as shown by the growth of a band at 2007 cm.$^{-1}$ (curve d). Spectra obtained in this work show that the extinction coefficient of a C$\equiv$C vibration in adsorbed C_2H_2 is the same (to within $\pm$5%) as that of the corresponding vibration in adsorbed C_2D_2. The band due to the C$\equiv$C vibration in adsorbed C_2H_2 had a density of 0.019 after 140 hours, while the corresponding band in C_2D_2 had decreased in optical density by 0.10 in the same time. Thus, as the C$\equiv$C band in C_2H_2 has such a similar intensity to the C$\equiv$C band in C_2D_2, there has been a greater decrease in coverage of C_2D_2 than increase in coverage of C_2H_2.

At the time when the most rapid decrease in intensity of the 1890 cm.$^{-1}$ band was occurring (0–40 hr.) very few adsorbed ethyl groups were present. The band at 2965 cm.$^{-1}$ had an optical density of 0.04 at 40 hr. Furthermore, the number of CH_3 groups increases linearly with time, while the rate of decrease of C_2D_2 species falls off at longer times. These facts can both be explained by assuming that the exchange between the two forms of acetylene takes place *via* gaseous or physically adsorbed C_2H_4, not *via* chemisorbed C_2H_5, or from any products formed from C_2H_4 while C_2H_5 is being made. Since only small quantities of C_2H_3D would be produced in the gas phase by this exchange, no significant formation of deuterated ethyl groups would be expected. The pressure of gaseous C_2H_4 is essentially constant during the experiment, and the decrease in rate of formation of C_2H_2 with time is probably a reflection of the heterogeneity of the surface. This could make some of the chemisorbed C_2D_2 molecules more difficult to exchange than others.

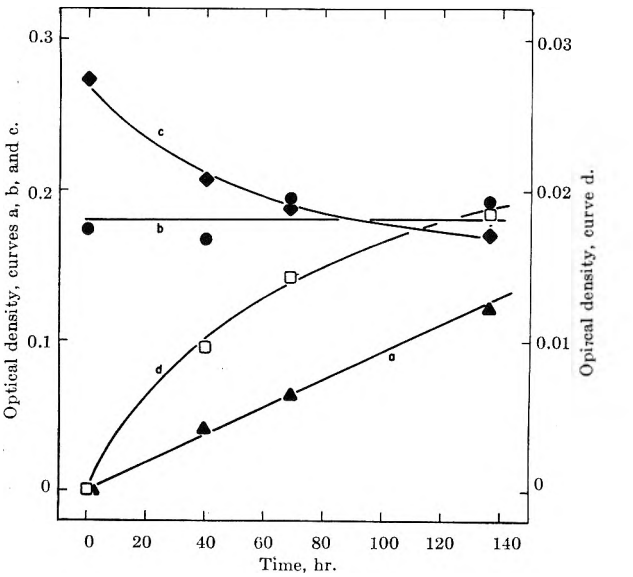

Fig. 1.—Changes in peak optical density of adsorbed species as a function of time after adding C_2H_4 to an alumina covered with pre-adsorbed C_2D_2. Curve (a), 2965 cm.$^{-1}$ band of the CH_3 groups in the $-C_2H_5$ groups; curve (b), band at 2230 cm.$^{-1}$ of the saturated CD species; curve (c), the C$\equiv$C stretching band at 1890 cm.$^{-1}$ in C_2D_2; curve (d), the corresponding band at 2007 cm.$^{-1}$ in C_2H_2.

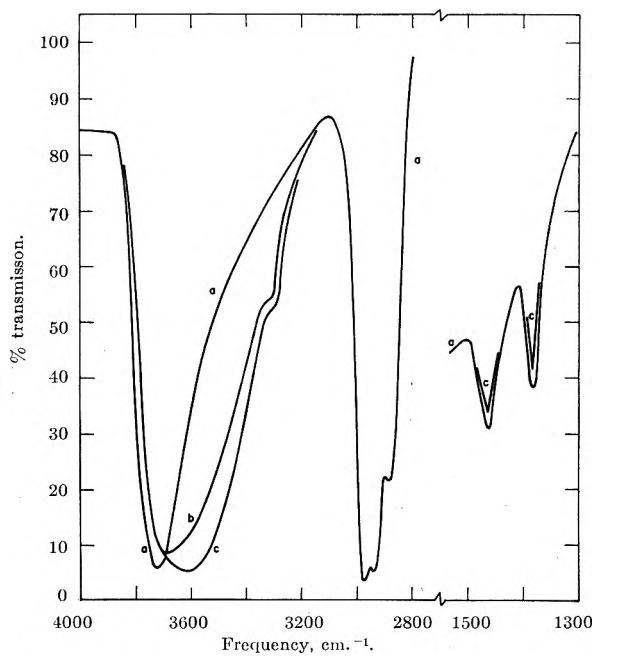

Fig. 2a.—Curve (a), spectrum obtained after adding C_2H_4 (24.5 cm.) for 70 hr. and then evacuating the sample; curve (b), after adding C_2D_2 at a pressure of 4.0 cm.; curve (c), C_2D_2 pressure 44.0 cm.

(ii) Deuterioacetylene on Pre-adsorbed Ethylene. —To another deuterated alumina sample, 13.5 cm. of C_2H_4 was added, and left for 18 hr. In agreement with earlier work on this alumina, no CD or OH groups were formed by exchange, and $-C_2H_5$ groups were formed by self-hydrogenation. The gaseous C_2H_4 was then removed, and 4 cm. of C_2D_2 added. Bands due to strongly and weakly held C_2D_2 were seen, and the high frequency OD band decreased in intensity as usual. A very small amount of end-on C_2H_2 was formed as shown by the presence of a weak band at 3300 cm.$^{-1}$. While no C$\equiv$C stretching band at 2007 cm.$^{-1}$ was detected, this band is normally much weaker than the 3300 cm.$^{-1}$ band (see Fig. 1b and 2b in ref. 1). A small

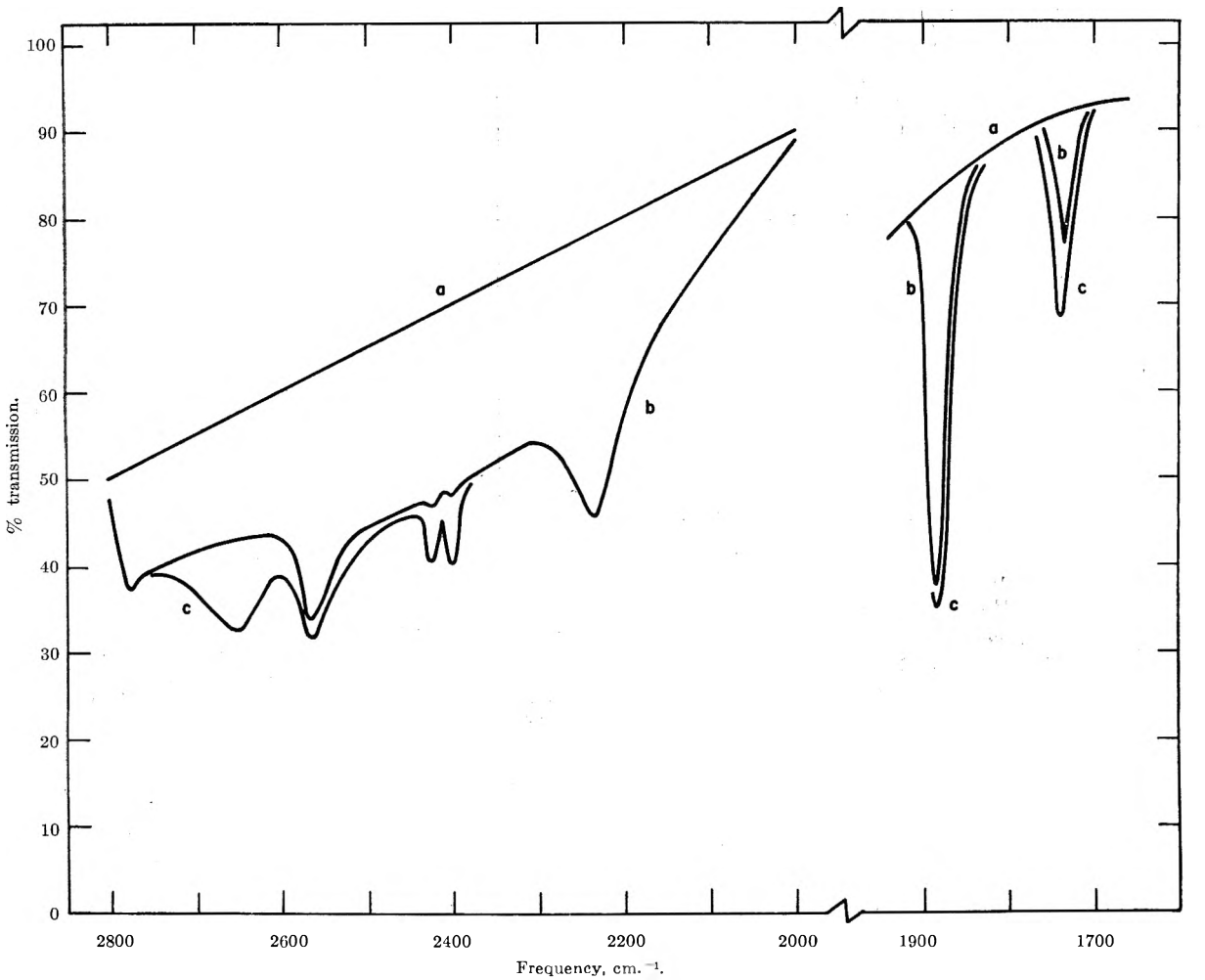

Fig. 2b.—Curve (a), spectrum obtained after adding C_2H_4 (24.5 cm.) for 70 hr. and then evacuating the sample; curve (b), after adding C_2D_2 at a pressure of 4.0 cm.; curve (c), C_2D_2 pressure 44.0 cm.

number of adsorbed species containing CD groups were found at 2240 cm.$^{-1}$, but no decrease in the bands due to the pre-adsorbed C_2H_5 groups could be detected. This point is considered further in the following discussion.

Experiments were then conducted at higher pressures. To a sample of alumina containing only OH groups, 24.5 cm. of C_2H_4 was added, and left for 70 hr. The C_2H_4 then was evacuated and 4 cm. of C_2D_2 added. Figure 2 shows the spectrum obtained after evacuating the C_2H_4 and the changes after adding the C_2D_2. To check the effects of pressure, a second dose of C_2D_2 was then added, the final pressure then being 44 cm.

In agreement with the experiment on the OD surface, little exchange took place between the pre-adsorbed C_2H_5 groups and the C_2D_2, as shown by the fact that no decrease in intensity of the 2970, 2930, and 2880 cm.$^{-1}$ bands took place (Fig. 2a). These CH stretching bands in the $-C_2H_5$ groups were intense, and hence not well suited to detecting small decreases in intensity. The CH_2 and CH_3 bending bands at 1383 and 1465 cm.$^{-1}$ also were recorded prior to the adsorption of the C_2D_2. These bands both had optical densities of 0.230 before adding C_2D_2. After the 44 cm. of C_2D_2 was added, these optical densities decreased to 0.191 and 0.203, respectively. An estimate of how many of the pre-adsorbed $-C_2H_5$ groups had been either exchanged into $-C_2D_5$ groups or desorbed from the surface can be obtained from these figures. The values after adsorption are 17.1 and 12.0% smaller, and the average will be taken as 15%. Although the band due to CH bending in CH_3 groups (1382 cm.$^{-1}$) decreased more than that due to both CH_3 and CH_2 groups[3] (1465 cm.$^{-1}$), this difference is not much larger than the experimental error and will be neglected. Thus, in the presence of an excess of gaseous C_2D_2, a maximum of 15% of the $-C_2H_5$ groups had been replaced with $-C_2D_5$ groups. In these circumstances, it is concluded that the exchange between C_2D_2 (both gaseous and adsorbed) and adsorbed $-C_2H_5$ groups can be considered to be very small, which indicates that the sites are independent.

Figure 2b shows that quite a strong band is observed at 2230 cm.$^{-1}$, caused by the presence of saturated CD groups. It is possible that some of these groups have been formed by deuterium exchange, from C_2D_2, with the pre-adsorbed $-C_2H_5$. However, the intensity of the band at 2230 cm.$^{-1}$ is larger than one would expect from the 15% decrease in the intensity of the CH bending bands. The other possibility is that some of the C_2D_2 goes directly into a saturated adsorbed species, which would give a band at about 2230 cm.$^{-1}$. While this had not been observed in earlier work with a different alumina,[1] other experiments discussed earlier showed a band at 2230 cm.$^{-1}$ after adding C_2D_2 to an OD surface having no pre-adsorbed ethylene.

Figure 2a shows that hydrogen bonding between the weakly adsorbed C_2D_2 and the surface OH groups takes place. Figure 2b shows the CD stretching vibrations in strongly and weakly held C_2D_2 (2570 and 2410 cm.$^{-1}$),

(3) L. J. Bellamy, "The Infrared Spectra of Complex Molecules," Second Edition, Methuen & Co., Ltd., London, 1958.

and the corresponding C≡C vibrations (1890 and 1740 cm.$^{-1}$). Again, a very small amount of end-on adsorbed C_2H_2 was formed, as shown by the weak band at 3300 cm.$^{-1}$. As the alumina was covered with OH groups, it is possible that C_2H_2 was formed by exchange between C_2D_2 and surface OH groups. Figure 2b shows that OD groups are formed after adding C_2D_2, by exchange with the OH groups.

(b) **Coverage Experiments.**—Although the previous experiment showed that very little exchange took place between pre-adsorbed C_2H_4 and C_2D_4, it was considered that coverage experiments to determine whether pre-adsorbed ethylene blocked the acetylene sites would give additional information.

To a deuterated alumina sample, of thickness 0.0174 g./cm.^{2}, C_2D_4 was added at 4 cm., and left for 4 days at room temperature. Figure 3a shows the OD stretching region, and the CD bands due to the chemisorbed deuterioethylene. After evacuating the C_2D_4, 4.7 cm. of C_2H_2 was admitted (Fig. 3b) and left in the cell for 24 hr. As the coverage of sideways held acetylene is quite pressure dependent, it was decided to use only the strongly held end-on acetylene as a measure of coverage. After increasing the C_2H_2 pressure to 46 cm. for 30 min. to ensure maximum coverage, the acetylene was evacuated, and the C≡C stretching band at 2007 cm.$^{-1}$ measured. This had an optical density of 0.0864. The 3300 cm.$^{-1}$ band could also have been measured, but the steeply sloping background spectrum in this region caused difficulty in measuring optical densities.

To another deuterated sample (thickness 0.0190 g./cm.^{2}) C_2H_2 was added directly at a pressure of 30 cm. After evacuating, the 2007 cm.$^{-1}$ band had an optical density of 0.0934.

In the first case, if the sample had had a "thickness" of 0.020 g./cm.^{2}, the optical density would have been 0.0993. In the second case the corresponding figure is 0.0983. Hence, to within the experimental error, the amount of acetylene adsorbed on the ethylene sample is the same as on the sample without ethylene. In this work, the errors in the optical density are such that the average density, if the samples had been 0.020 g./cm.^{2} thick, is 0.0988 to within ±0.004. This can be expressed as showing that the coverage of acetylene is the same with or without the pre-adsorbed deuterioethylene to within ±5%. It is clear that very few of the sites active in the end-on adsorption of acetylene are occupied by pre-adsorbed deuterioethylene.

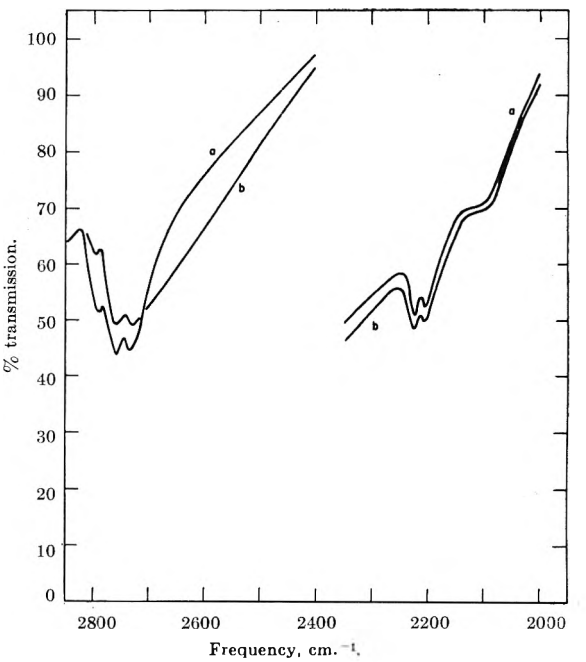

Fig. 3a.—Curve (a), spectrum after adding 4.0 cm. of C_2D_4 to a deuterated alumina, leaving for 4 days, and evacuating the sample; curve (b), spectrum soon after adding C_2H_2 at a pressure of 4.7 cm.

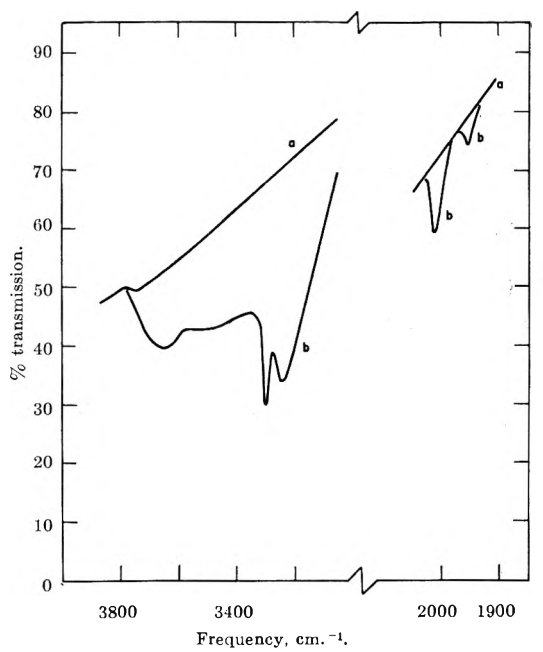

Fig. 3b.—Curve (a), spectrum after adding 4.0 cm. of C_2D_4 to a deuterated alumina, leaving for 4 days, and evacuating the sample; curve (b), spectrum soon after adding C_2H_2 at a pressure of 4.7 cm.

IV. Discussion

For the "end-on" strong chemisorption of acetylene, the following is known about the nature of the adsorption sites:

(a) Previous work has established that acetylene is held to the surface by a hydrogen atom. Since acetylene can behave as an acid in the Brönsted sense, *i.e.*, a proton donor, the site on the Al_2O_3 may be said to have basic properties, relative to acetylenic hydrogen.

(b) These sites must be close to one type of OH groups on the alumina. Exchange takes place very quickly between the highest frequency OH groups and C_2D_2, giving high frequency OD groups. The two lower frequency OH groups do not exchange at all with C_2D_2, either with the strongly or weakly chemisorbed C_2D_2. Another explanation may be that the adsorbed end-on acetylene is quite mobile over the surface. This seems very unlikely in view of the fact that evacuation at 300° is necessary to remove the adsorbed acetylene. A further point is that, if the adsorbed species were mobile, it would be expected that all of the OH groups would exchange with C_2D_2, rather than very selectively changing only with the high frequency OH group.

(c) The sites do not, however, depend on the presence of a high frequency OH group. If they did, removal of the OH groups by evacuation at 900° would be expected to prevent or inhibit the end-on adsorption. This was not found to be the case, as the adsorption of acetylene was affected very little by such high temperature treatment.

(d) The site can be of atomic dimension, as it only

needs to be large enough to interact with one acetylenic hydrogen atom.

In the self-hydrogenation of ethylene to form chemisorbed ethyl groups, the following is known about the nature of the adsorption sites:

(a) The ethyl group is probably held "end-on" to the surface by a carbon atom. This is confirmed by the fact that the ratio of the optical densities of the bands due to CH_3 and CH_2 is similar to that in molecules such as ethyl bromide. Since ethylene is much less acidic than acetylene and can behave as a weak base, *i.e.*, a proton acceptor, the sites on the alumina which are holding the ethyl groups can be said to have some acidic character.

(b) The sites active in the formation of $-C_2H_5$ groups appear to be remote from the surface OH groups, as only $-C_2D_5$ groups were found on adding C_2D_4 to a surface containing only OH groups. This also implies that the adsorbed species are not mobile, as discussed in (d) below. This is particularly interesting since the self-hydrogenation of ethylene in these surfaces must be at least a bimolecular process in which extensive bond formation and bond breakage occur.

(c) In agreement with the above, removal of all the OH groups from an alumina by evacuation at 1000° did not change the species formed after admitting ethylene.

(d) There must be at least two pairs of adjacent sites available, to act simultaneously, for the self-hydrogenation of ethylene to take place. Conceptually, we can envisage two ethylene molecules adsorbing side by side. Both open up their double bonds, and one donates hydrogen to the other. This would leave a stable $-C_2H_5$ group held strongly on one side to the surface, and a residue of nominal composition $-C_2H_3$. Possibly, a second ethylene molecule would then adsorb adjacent to the (presumably) reactive $-C_2H_3$ group, giving $-C_2H_5$ and a residual group of low hydrogen to carbon ratio. If the latter process takes place, one has to invoke three adjacent pairs of sites, if all the adsorbed species are immobile. Little direct information is available on the last point, except that it seems very likely that any reactive hydrogen-containing mobile adsorbed species would exchange with surface OD groups. No exchange has been observed between C_2H_4 and OD groups, and between C_2D_4 and OH groups in any experiment.

Finally, we are led to the conclusion that the sites for ethylene self-hydrogenation seem to be slightly affected by pre-adsorbed acetylene, and, conversely, that the end-on adsorption of acetylene is unaffected (to within ±5%) by the pre-adsorption of ethyl groups. In view of the fact that acetylene exchanges with one type of OD group, and ethylene does not exchange at all with OD groups, even while undergoing self-hydrogenation, it is to be expected that the sites are independent, and displaced physically from each other on the surface. An even more striking example of the physical separation between the sites is provided by the experiment using pre-adsorbed deuterioacetylene. Even though subsequently added ethylene formed $-C_2H_5$, no evidence was found for the existence of $-C_2D_5$ or $-C_2H_4D$ species in the adsorbed phase formed from C_2H_4.

This evidence suggests that all of the adsorbed species are immobile, and that the end-on acetylene is adsorbed near to one type of OH group. While some donation of hydrogen must take place during the formation of ethyl groups by self-hydrogenation, neither of the (at least two) molecules involved in this rearrangement is in a reactive condition while close to an OH group. Relatively large patches of the surface must be involved in self-hydrogenation of ethylene, while if an acetylene molecule impinges on its potential site with the correct orientation, the formation of end-on held acetylene can take place immediately. Both these ideas are consistent with the fact that acetylene adsorption is very fast, in most cases within 10 min., while the formation of $-C_2H_5$ is a process usually taking over 12 hr. to form significant amounts of adsorbed material. Also of interest is the fact that on a given sample there seem to be a definite number of sites which rapidly form end-on acetylene. Increasing the pressure of the acetylene, and waiting for several days gave no increase in the number of end-on species. With ethylene, in marked contrast, the rate of formation of ethyl groups is slow, and at constant C_2H_4 pressure the alumina continues to form $-C_2H_5$ groups for the longest times which have been used (8 days).

THERMOCHEMISTRY OF SOME BROMINE AND IODINE SPECIES IN AQUEOUS SOLUTION

By Ching-hsien Wu, Merritt M. Birky, and Loren G. Hepler

Departments of Chemistry, University of Virginia, Charlottesville, Virginia, and Carnegie Institute of Technology, Pittsburgh, Pennsylvania

Received November 5, 1962

Calorimetric determinations of the following have been made: (a) ΔH of solution of Br_2(liq) in water, (b) ΔH of reaction of Br_2(liq) with OH^-(aq), (c) ΔH of reaction of Br_2(liq) with excess I^-(aq), (d) ΔH of solution of I_2(c) in excess I^-(aq), and (e) ΔH of reaction of KIO_3(c) with excess I^-(aq). Results of these experiments have been used with data from the literature for calculation of thermodynamic properties of Br_2(aq), I_2(aq), OBr^-(aq), HOBr(aq), IO_3^-(aq), and KIO_3(c).

Introduction

Most of the enthalpy data for bromine and iodine species in aqueous solution are based on calorimetric experiments done more than fifty years ago, or on temperature variations of equilibrium constants. Results of different investigators are in poor agreement for several species. We have, therefore, undertaken calorimetric measurements of the following: (a) ΔH of solution of Br_2(liq) in water, (b) ΔH of reaction of Br_2(liq) with OH^-(aq), (c) ΔH of reaction of Br_2(liq) with excess

I^-(aq), (d) ΔH of solution of I_2(c) in excess I^-(aq), and (e) ΔH of reaction of KIO_3(c) with excess I^-(aq). Results of these measurements have been used with data from the literature for thermochemical calculations.

Experimental

Most of the measurements reported here were made with a calorimeter similar to that described by O'Hara, Wu, and Hepler.[1] The calorimeter used for some of our measurements differs from that described earlier in that the calorimeter heater and thermometer were enclosed in a glass coil rather than between concentric silver and copper cylinders as in the earlier calorimeter. A few of the measurements reported here were made in another calorimeter that has been described.[2,3] All calorimetric measurements were made at 25.0 ± 0.3° with 950 ml. of water or solution in the calorimeter. Bromine was handled as previously described.[4] None of the reactions took longer than five minutes to reach completion.

Reagent grade bromine from Baker and Adamson and also from Mallinckrodt (containing *less* than 0.3% Cl_2 as principal impurity) was used without further purification. Reagent grade iodine was sublimed twice and stored in a desiccator over phosphorus pentoxide. Analytical grade KIO_3 was recrystallized and then dried at 120°. Other chemicals were of C.P. grade and were used without further purification except for drying. Stock solutions were made and standardized by common methods.

Results and Calculations

Results of measurements of the heat of solution of liquid bromine in 0.1 *M* perchloric acid are given in Table I. These measurements were carried out in dilute acid to prevent hydrolysis of Br_2 to HOBr and Br^-. The standard heat of formation of Br_2(aq) given in NBS Circular 500[5] corresponds to a value of 1.1 kcal./mole for ΔH^0 of solution, based upon old work of Berthelot, Pickering, and Thomsen.

TABLE I

HEATS OF SOLUTION OF BROMINE IN DILUTE AQUEOUS ACID

Moles Br_2/ 950 ml. soln.	ΔH (kcal./mole)
0.00601	−0.15
.03185	− .19
.03519	− .23
.04619	− .15
.04840	− .27

ΔH (av.) = − 0.20 kcal./mole Av. dev. = 0.04 kcal./mole

Because there is no significant dependence of ΔH of solution of Br_2(liq) on the concentration of the final solution, we take the standard heat of solution of Br_2(liq) to be the average of the values reported in Table I with estimated maximum uncertainty of ±0.08 kcal./mole. Therefore, $\Delta H_f^0 = -0.20$ kcal./mole for Br_2(aq).

It is also possible to estimate ΔH^0 for solution of Br_2(liq) from solubility data for bromine in water.[6] Following earlier calculations[7,8] we have taken the activity coefficient γ to depend on concentration m as in

$$\ln \gamma = km \qquad (1)$$

The activity of bromine in saturated solution varies with temperature according to the integrated van't Hoff equation

$$\ln m_s\gamma_s = -\frac{\Delta H^0}{RT} + C \qquad (2)$$

where m_s and γ_s represent the molality and the activity coefficient of bromine in saturated solution. Substituting (1) in (2) gives

$$\ln m_s + km_s = -\frac{\Delta H^0}{RT} + C \qquad (3)$$

We also write the general equation 3 with m_s^* and T^* and designate this specific equation 3′. Then subtraction of (3′) from (3) and rearrangement gives

$$\frac{\log \dfrac{m_s}{m_s^*}}{m_s - m_s^*} = \frac{\Delta H^0}{2.303R}\left[\frac{T - T^*}{(m_s - m_s^*)(TT^*)}\right] - \frac{k}{2.303} \qquad (4)$$

Equation 4 has been applied by letting m_s^* be the solubility at 273° and setting $T^* = 273°$. The slope and intercept of a graph of $(\log m_s/m_s^*)/(m_s - m_s^*)$ against $(T - T^*)/(m_s - m_s^*)(TT^*)$ lead to $\Delta H^0 = -0.17$ kcal./mole and $k = -3.59$. The concentration of the saturated solution at 25° is 0.219 molal, so $\gamma_s = 0.46$.

Rearrangement of equation 3 gives

$$\log m_s + \frac{\Delta H^0}{2.303RT} = -\frac{km_s}{2.303} + \frac{C}{2.303} \qquad (5)$$

A graph of the left side of (5), taking $\Delta H^0 = -200$ cal./mole, against m_s has slope 1.50, leading to $k = -3.46$ and $\gamma_s = 0.42$.

Use of equation 1 with the same k at different temperatures implies that ΔH of dilution of aqueous bromine is small. Interpretation of the solubility of bromine in water in terms of the equilibrium

$$Br_2(liq) = Br_2(aq)$$

implies that the solubility of water in bromine is negligible.

Taking γ_s and m_s to be 0.44 and 0.219, we calculate for the standard free energy of solution and formation of Br_2(aq) in water at 298°

$$\Delta F^0 = -RT \ln m_s\gamma_s = 1.38 \text{ kcal./mole}$$

Combining ΔF^0 with ΔH^0 gives $\Delta S^0 = -5.3$ cal./deg. mole for solution of bromine in water. Since the standard entropy of Br_2(liq) is 36.38 cal./deg. mole,[9] we calculate that the standard partial molal entropy of Br_2(aq) is 31.1 cal./deg. mole.

We have measured the heat of solution of Br_2(liq) in aqueous sodium hydroxide (0.25–1.3 *M*) where the principal reaction is

$$Br_2(liq) + 2OH^-(aq) = Br^-(aq) + OBr^-(aq) + H_2O \qquad (6)$$

Data are given in Table II.

The average ΔH reported in Table II cannot be attributed entirely to reaction 6 because of the side reaction

(1) W. F. O'Hara, C. H. Wu, and L. G. Hepler, *J. Chem. Educ.*, **38**, 512 (1961).
(2) R. L. Graham and L. G. Hepler, *J. Am. Chem. Soc.*, **78**, 4846 (1956).
(3) C. N. Muldrow and L. G. Hepler, *ibid.*, **79**, 4045 (1957).
(4) L. G. Hepler, J. S. Sweet, and R. A. Jesser, *ibid.*, **82**, 304 (1960).
(5) "Selected Values of Chemical Thermodynamic Properties," Circular 500, National Bureau of Standards (1952).
(6) A. Seidell, "Solubilities of Inorganic and Metal Organic Compounds," Vol. I, D. Van Nostrand, New York, N. Y., 1940.
(7) M. A. Paul, *J. Am. Chem. Soc.*, **75**, 2513 (1953).
(8) L. P. Fernandez and L. G. Hepler, *J. Phys. Chem.*, **63**, 110 (1959).
(9) D. L. Hildebrand, W. R. Kramer, R. A. McDonald, and D. R. Stull, *J. Am. Chem. Soc.*, **80**, 4129 (1958).

$$Br_2(liq) + 2OH^-(aq) = \frac{5}{3}Br^-(aq) + \frac{1}{3}BrO_3^-(aq) + H_2O \quad (7)$$

Table II

Heats of Solution of Br_2(liq) in Aqueous NaOH

Moles Br_2/ 950 ml. soln.	ΔH (kcal./mole Br_2)
0.00758	−9.81
.00940	−9.97
.01021	−9.85
.01069	−9.90
.01131	−10.02
.01480	−9.97
.01483	−9.98
.02341	−9.83

ΔH (av.) = −9.92 kcal./mole Av. dev. = 0.07 kcal./mole

Using NBS[5] heats of formation of OH^-(aq), Br^-(aq), and H_2O and −18.3 kcal./mole for ΔH_f^0 of bromate ion,[10] we calculate $\Delta H^0 = -12.7$ kcal./mole of Br_2 for reaction 7. Representing the measured heat given in Table II by ΔH_m, we write

$$\Delta H_m = (1 - f)\Delta H_6 - 12.7f \quad (8)$$

where f designates the fraction of the Br_2 that reacts according to equation 7. Following McDonald and Cobble,[11] we find that f is small and approximately 0.01 for all of our experiments. Taking $\Delta H_m = -9.92$ kcal./mole and $f \cong 0.01$, we calculate from (8) that $\Delta H_6 = -9.89$ kcal./mole. Since reaction 6 involves equal numbers of ions in dilute solution with −1 charges among reactants and products, we assume that heats of dilution cancel and take $\Delta H_6^0 = -9.9 \pm 0.4$ kcal./mole. Combining this value of ΔH_6^0 with NBS[5] data for the species in reaction 6 leads to $\Delta H_f^0 = -22.6$ kcal./mole for the standard heat of formation of OBr^-(aq). McDonald and Cobble[11] found −23.0 kcal./mole for this heat of formation.

Kelley and Tartar[12] have reported $\Delta F'^0_9 = 11.7$ kcal./mole, $\Delta H_9^0 = 6.8$ kcal./mole, and $\Delta S_9^0 = -16.6$ cal./deg. mole for the ionization of hypobromous acid at 298°K.

$$HOBr(aq) = H^+(aq) + OBr^-(aq) \quad (9)$$

It is possible that considerable uncertainty should be attached to these values because the data obtained by Kelley and Tartar also lead to $\Delta C_p^0 = -215$ cal./deg. mole for ionization of aqueous hypobromous acid, as compared to a usual value of about −40 cal./deg. mole, for such reactions.

Liebhafsky[13] has measured K at several temperatures for the reaction

$$Br_2(aq) + H_2O = HOBr(aq) + H^+(aq) + Br^-(aq) \quad (10)$$

His equation for log K as a function of temperature leads to $\Delta F_{10}^0 = 11.23$ kcal./mole, $\Delta H_{10}^0 = 13.1$ kcal./mole, and $\Delta S_{10}^0 = 6.3$ cal./deg. mole at 298°K.

Combining reactions 9 and 10 with

$$2H^+(aq) + 2OH^-(aq) = 2H_2O \quad (11)$$

gives

$$Br_2(aq) + 2OH^-(aq) = Br^-(aq) + OBr^-(aq) + H_2O \quad (12)$$

Similar combination of the thermodynamic data above for reactions 9, 10, and 11 gives $\Delta F_{12}^0 = -15.3$ kcal./mole, $\Delta H_{12}^0 = -6.8$ kcal./mole, and $\Delta S_{12}^0 = 28.2$ cal./deg. mole. Combining our calorimetric ΔH_6^0 and ΔH^0 of solution of liquid bromine in water gives $\Delta H_{12}^0 = -9.7$ kcal./mole. Since all errors in our calorimetric results are less than one kcal./mole and our ΔH_6^0 differs by less than 0.5 kcal./mole from that of McDonald and Cobble,[11] we conclude that the calorimetric $\Delta H_{12}^0 = -9.7$ kcal./mole is the more reliable value.

Since we have no calorimetric value for ΔH_9^0, we use the value given by Kelley and Tartar[12] with the above heat of formation of OBr^-(aq) to calculate $\Delta H_f^0 = -29.4$ kcal./mole for HOBr(aq).

Combining $\Delta F_{12}^0 = -15.3$ kcal./mole with our data for Br_2(aq) with NBS[5] data for the other species in reaction 12 leads to $\Delta F_f^0 = -7.8$ kcal./mole for the standard free energy of formation of OBr^-(aq). Using this free energy with the free energy of ionization of HOBr(aq) given by Kelley and Tartar[12] leads to $\Delta F_f^0 = -19.5$ kcal./mole for HOBr(aq).

For further calculations we obtain $\Delta S_{12}^0 = 18.8$ cal./deg. mole by combining $\Delta F_{12}^0 = -15.3$ kcal./mole with our calorimetric $\Delta H_{12}^0 = -9.7$ kcal./mole. Using this ΔS_{12}^0 with our entropy of Br_2(aq) and NBS[5] entropies of the other species in reaction 12 leads to 8.8 cal./deg. mole for the standard partial molal entropy of OBr^-(aq). Since we have no calorimetric value for ΔH^0 of ionization of HOBr(aq), we use the results of Kelley and Tartar[12] with values reported above for OBr^-(aq) to calculate 25.4 cal./deg. mole for the standard partial molal entropy of HOBr(aq).

We have determined the heat of reaction of bromine with excess aqueous iodide. Most of the iodine in the final solutions was in the form of I_3^-(aq) so the principal reaction was

$$Br_2(liq) + 3I^-(aq) = I_3^-(aq) + 2Br^-(aq) \quad (13)$$

To obtain ΔH_{13}^0 from measured heats, corrections must be made for the small amounts of I_2(aq) present in the final solutions.

Davies and Gwynne[14] determined K at several temperatures, leading to $\Delta H^0 = -3.8$ kcal./mole for

$$I_2(aq) + I^-(aq) = I_3^-(aq) \quad (14)$$

Our calorimetric results are summarized in Table III where the actual measured heats are listed under Q (all heats were exothermic). Corrections for reaction 14 are listed under Q_{14} and are almost negligible. Thus, the particular value of ΔH_{14}^0 is not important for evaluation of ΔH_{13}^0.

Since reaction 13 involves the same number of equally charged ions on each side and all solutions were quite dilute, we assume that heats of dilution cancel and take ΔH_{13}^0 to be the average of the values listed in Table III. Combining $\Delta H_{13}^0 = -29.36 \pm 0.3$ kcal./mole with NBS[5] data for Br^-(aq) and I^-(aq) gives $\Delta H_f^0 = -11.7$ kcal./mole for I_3^-(aq).

(10) H. C. Mel, W. L. Jolly, and W. M. Latimer, *J. Am. Chem. Soc.*, **75**, 3827 (1953).
(11) J. E. McDonald and J. W. Cobble, *J. Phys. Chem.*, **65**, 2014 (1961).
(12) C. M. Kelley and H. V. Tartar, *J. Am. Chem. Soc.*, **78**, 5752 (1956).
(13) H. A. Liebhafsky, *ibid.*, **56**, 1500 (1934).
(14) M. Davies and E. Gwynne, *ibid.*, **74**, 2748 (1952).

TABLE III

HEATS OF REACTION OF Br_2(liq) WITH AQUEOUS KI

G. Br_2(liq)/ 950 ml. soln.	Moles KI/ 950 ml. soln.	HCl (M)	Q (cal.)	Q_{14} (cal.)	ΔH_{13} (kcal./ mole)
0.7423	0.2302	0.0239	135.76	0.10	−29.26
1.2022	.3778	.0191	221.11	.10	−29.41
1.4197	.3464	.0239	259.79	.13	−29.26
1.4970	.1832	.0095	275.93	.27	−29.49

We also have measured the heat of solution of I_2(c) in excess I^-(aq) where the principal reaction is

$$I_2(c) + I^-(aq) = I_3^-(aq) \qquad (15)$$

Corrections similar to those discussed above for presence of I_2(aq) are summarized with our data in Table IV.

TABLE IV

REACTION OF I_2(c) WITH AQUEOUS IODIDE ION

G. I_2(c)/ 950 ml. soln.	Moles KI/ 950 ml. soln.	HCl (M)	Q (cal.)	Q_{14} (cal.)	ΔH_{15} (kcal./ mole)
0.9896	0.1777	0.0192	−5.68	0.11	1.43
1.2924	.0917	.0239	−6.67	.29	1.24
0.6438	.1149	.0239	−3.44	.11	1.31
0.8466	.1603	.0239	−4.44	.10	1.30
0.4958	.1521	.0965	−2.83	.07	1.41

Assuming that heats of dilution cancel for the charged species in dilute solution on each side of reaction 15, we take $\Delta H_{15}^0 = 1.34 \pm 0.2$ kcal./mole. Combining our ΔH_{15}^0 with ΔH_f^0 of I^-(aq) from the NBS[5] gives $\Delta H_f^0 = -12.0$ kcal./mole for I_3^-(aq). We take $\Delta H_f^0 = -11.9$ kcal./mole of I_3^-(aq) to be the best value based on all of our data.

Stern and Passchier[15] have measured the heat of solution of I_2(c) in 2 M KI and reported $\Delta H = 0.89$ kcal./mole. On the basis of this ΔH and estimated heat of dilution corrections they calculated $\Delta H_f^0 = -12.7$ kcal./mole for I_3^-(aq). Since reaction 15 involves the same number of ionic charges on each side, we have assumed that heats of dilution cancel and have calculated $\Delta H_f^0 = -12.5$ kcal./mole for I_3^-(aq) from their ΔH. Because heats of dilution for our dilute solutions introduce less uncertainty than for the concentrated iodide solutions used by Stern and Passchier,[15] we believe our *standard* $\Delta H_f^0 = -11.9$ kcal./mole for I_3^-(aq) is more reliable.

From the solubility of iodine[6,16] in water at 25°, we calculate the standard free energy of solution of I_2(c) to be 3.93 kcal./mole. Therefore, $\Delta F_f^0 = 3.93$ kcal./mole for I_2(aq). From the temperature coefficient of the solubility we calculate $\Delta H_{16}^0 = 5.2$ kcal./mole and $\Delta S_{16}^0 = 4.4$ cal./deg. mole for

$$I_2(c) = I_2(aq) \qquad (16)$$

Combining this ΔS_{16}^0 with NBS[5] entropy of I_2(c) leads to 32.3 cal./deg. mole for the standard partial molal entropy of I_2(aq).

Combining our calorimetric $\Delta H_{15}^0 = 1.3$ kcal./mole with the above ΔH_{16}^0 gives $\Delta H_{14}^0 = -3.9$ kcal./mole, in good agreement with the heat calculated from the determination by Davies and Gwynne[14] of the temperature coefficient for reaction 14. Using Davies and Gwynne's[14] value of $K_{14} = 768$ with our free energy of formation of I_2(aq) and the NBS[5] free energy of formation of I^-(aq), we calculate $\Delta F_f^0 = -12.35$ kcal./mole for I_3^-(aq). Similarly, we calculate 58.5 cal./deg. mole for the standard partial molal entropy of I_3^-(aq).

We have also investigated the heat of reaction of KIO_3 with HI. Table V presents both experimental and calculated data for these experiments. In each experiment two reactions took place in the calorimeter

$$KIO_3(c) + 6H^+(aq) + 8I^-(aq) = 3I_3^-(aq) + 3H_2O + K^+(aq) \qquad (17)$$

and reaction 14.

In Table V, Q represents the heat measured in the calorimeter, Q_{14} has the meaning given before, and ΔH_{17} is the heat of reaction 17. Assuming that heats of dilution of triiodides do not differ from those of the corresponding iodides in dilute solutions and combining heats of dilution of KI and HI with our values for ΔH_{17}, we obtain $\Delta H_{17}^0 = -73.4 \pm 0.8$ kcal./mole of KIO_3.

TABLE V

REACTION OF KIO_3(c) WITH AQUEOUS HI

G. KIO_3(c)/ 950 ml. soln.	Moles HI/ 950 ml. soln.	Q (cal.)	Q_{14} (cal.)	ΔH_{17} (kcal./ mole)
0.9696	0.05577	331.52	3.45	−73.94
.5930	.11153	202.08	0.46	−73.10
.4684	.05577	159.23	.85	−73.14
.2547	.05577	85.91	.38	−72.50
.2179	.16730	75.78	.95	−74.52

Combination of the above ΔH_{17}^0 with our ΔH_f^0 of I_3^-(aq) and NBS[5] data for I^-(aq), H_2O, and K^+(aq) leads to $\Delta H_f^0 = -120.3$ kcal./mole for KIO_3(c). Then the previously determined heat of solution of KIO_3(c)[17] leads to $\Delta H_f^0 = -53.7$ kcal./mole for IO_3^-(aq), compared to earlier values of −54.6 kcal./mole[15] and −55.0 kcal./mole.[5]

Our values of standard free energies and heats of formation and partial molal entropies are summarized in Table VI.

TABLE VI

SUMMARY OF THERMODYNAMIC PROPERTIES (298°K.)

Species	ΔH_f^0 (kcal./mole)	ΔF_f^0 (kcal./mole)	S_2^0 (cal./deg./ mole)
Br_2(aq)	−0.20	1.38	31.1
OBr^-(aq)	−22.6	−7.8	8.8
HOBr(aq)	−29.4	−19.5	25.4
I_2(aq)	5.2	3.93	32.3
I_3^-(aq)	−11.9	−12.35	58.5
IO_3^-(aq)	−53.7	−31.5	28.4[17]
KIO_3(c)	−120.3	−100.5	36.2[5]

Acknowledgment.—This work was supported by the National Science Foundation. We thank J. G. Spencer for making available the data in Table V and Professor Henry Frank for his helpful comments.

(15) J. H. Stern and A. A. Passchier, *J. Phys. Chem.*, **66**, 752 (1962).
(16) L. I. Katzin and E. Gebert, *J. Am. Chem. Soc.*, **77**, 5814 (1955).
(17) J. G. Spencer and L. G. Hepler, *J. Phys. Chem.*, **64**, 499 (1960).

THE NEAR-INFRARED TRANSITIONS OF THE TRIVALENT LANTHANIDES IN SOLUTION. II. Tb^{+3}, Dy^{+3}, Ho^{+3}, Er^{+3}, Tm^{+3}, AND Yb^{+3} [1]

BY W. T. CARNALL[2]

Argonne National Laboratory, Argonne, Illinois

Received November 7, 1962

The solution absorption spectra of Tb^{+3}, Dy^{+3}, Ho^{+3}, Er^{+3}, Tm^{+3}, and Yb^{+3} were measured in molten $LiNO_3$–KNO_3 eutectic at 150° in the 0.35–2.6 μ range and in $DClO_4$ at 23° in the 0.35–1.8 μ range. New observations of a number of absorption bands in solution in the region 1.40–2.6 μ (7140–3850 cm.$^{-1}$) were made by taking advantage of the optical transparency of the $LiNO_3$–KNO_3 eutectic in this portion of the spectrum. Theoretical interpretations of the solution spectra are offered based on recent experimental and theoretical analyses of crystalline salts of the lanthanide ions.

Introduction

In the first communication of this series,[3] it was shown that the use of molten $LiNO_3$–KNO_3 eutectic as a solvent makes possible the observation of lanthanide spectra in solution in the 0.35–2.6 μ range. The light lanthanides were shown to exhibit a number of solution absorption bands in the near infrared just beyond 1.4 μ, the usual infrared cut-off for aqueous solutions.

In the present communication, the investigation of lanthanide absorption bands in the near infrared is extended to the second (or heavy) half of the lanthanide series. The results of recent theoretical and experimental studies of crystal spectra are applied to an interpretation of the numerous absorption bands found. These near infrared bands are of particular theoretical interest since they represent transitions to excited multiplet levels in the 4f configuration which are, in most instances, identifiable. The corresponding bands in the visible–ultraviolet range are much more complex due to overlapping of components of different multiplet levels; theoretical interpretation of the solution spectra in this range is possible in relatively few instances.

The theory of lanthanide spectra has undergone considerable development in the past few years along with the publication of a number of experimental studies of the spectra of crystalline salts of the lanthanides. Consequently, some of the earlier interpretations of solution spectra in the 0.35–1.4 μ range must be revised. It is clear that more experimental work is needed to guide the further development of theory. In some instances the location and structure of solution absorption bands may be of value in testing the first-order theory when the results with crystal spectra are difficult to obtain.

Study of the light lanthanides revealed that the absorption spectra in dilute $DClO_4$ solution and in the molten nitrate medium are in general quite similar; however, certain distinct differences were noted. Since the effects of different solvent media on the intra 4f electron transitions are of interest, experimental results are also given here for the heavy lanthanides in D_2O (dilute $DClO_4$). Use of this solvent enables observation of absorption spectra in a larger portion of the near infrared region than is possible with normal aqueous solutions.

Experimental

The spectral measurements were made using a Cary Model 14 recording spectrophotometer. The aqueous solutions were run at room temperature, 23 ± 2°. The molten salt samples were maintained at 150 ± 3° in a furnace unit that has been described previously.[3] The molten salt matrix used was a eutectic mixture of $LiNO_3$ and KNO_3, containing ~43 mole % $LiNO_3$ and melting at ~132°. Concentrations of the lanthanides up to ~1 *M* in the molten nitrate eutectic were prepared, and the major peaks appeared to follow Beers law. The concentration of $DClO_4$ was in each case ~0.3 *M*. Reagent grade chemicals were used without further purification. The lanthanides were obtained commercially in the oxide form with <1% impurities. The experimental techniques were identical with those described previously.[3,4] Spectrophotometer cells were fabricated from square borosilicate glass tubing. A comparison of the absorption characteristics of H_2O, D_2O, and molten $LiNO_3$–KNO_3 in the 0.35–2.6 μ range already has been published.[3]

Results and Discussion

For each of the trivalent lanthanides considered here, the absorption bands observed in the near infrared region result from transitions either within the ground state multiplet or between the ground level and components of the first excited multiplet. Reference to Fig. 1 shows that only three excited multiplet levels in the heavy half of the lanthanide series lie at wave lengths >2.6 μ, the experimental limit in the present study. Actually, all the excited J-levels of the ground term multiplets of Er^{+3}, Tm^{+3}, and Yb^{+3} also can be observed in the $DClO_4$ medium.

The basic theoretical treatment of the intra 4f transitions for the heavy lanthanides is the same as that for the light half of the series. The energy levels are a function primarily of the Coulomb interaction between electrons, and secondarily of the electronic spin–orbit interaction. When the Coulomb interaction energy is expressed in terms of Slater integrals, F_2, the same energy levels are calculated for f^{14-n} as for f^n. As a first approximation one can also use the same spin–orbit splitting factor for f^{14-n} as is calculated for f^n with pure Russell–Saunders (R–S) coupling. Values for both the energy levels (in terms of F_2) and the spin–orbit splitting factors are summarized in reference 5.

Finally, the effect of the medium on the energy levels of the ion must be considered. The crystal or ligand field gives rise to a splitting of the multiplet levels, so that instead of well defined single transitions, each multiplet level has a structure. The magnitude of the crystal field splitting varies from one solvent medium to another, and theory can be extended to the calculation of this structure in an ordered matrix such as a crystal of known symmetry. However, for many crystalline matrices used experimentally, the detailed

(1) Based on work performed under the auspices of the U. S. Atomic Energy Commission.

(2) Presently at the University of Munich, Munich, Germany.

(3) W. T. Carnall, D. M. Gruen, and R. L. McBeth, *J. Phys. Chem.*, **66**, 2159 (1962).

(4) W. T. Carnall, *Anal. Chem.*, **34**, 786 (1962).

(5) J. P. Elliot, B. R. Judd, and W. A. Runciman, *Proc. Roy. Soc.* (London), **A240**, 509 (1957).

calculation of the crystal field splitting has not yet been reported in the literature.

In solution, the individual crystal field components are usually not resolved. The observed absorption smooths over these components, frequently giving rise to single well defined absorption maxima, particularly in the near infrared region. The energy at which these maxima occur can then be compared to the calculated or experimentally determined centers of gravity of the multiplet levels for purposes of identifying the bands.

The assumption of weak spin–orbit interaction, which is implicit in the use of the R–S coupling scheme, is relatively a much poorer assumption for the heavy than for the light lanthanides. The designation of the multiplet levels in terms of this scheme is, nevertheless, commonly employed for the sake of convenience. This procedure is followed in the present investigation. In most cases, intermediate coupling calculations must be used to obtain satisfactory agreement between theory and experiment.

The effect of different solvents on the 4f electron transitions is usually deduced by comparison; the absorption spectrum in dilute aqueous solution is normally taken as the standard. This is, however, not to be interpreted as an assumption that the water dipoles, which are responsible for the field seen by the lanthanide ion in dilute aqueous solution, give rise to a weak field. The environment in the nitrate melt, nevertheless, is different from that in aqueous solutions. Various lines of evidence indicate that the melt is essentially completely ionic, and thus more akin to an ionic crystal. The short range ionic forces characteristic of the crystal remain, but the long range order is disrupted. Recent X-ray diffraction studies made in molten salts indicate that the average coördination number may be lower in the melt than in the corresponding solid.[6]

Terbium—The highest component of the ground term multiplet in Tb^{+3} is separated by more than 16000 cm.$^{-1}$ from the lowest component of the first excited multiplet; in this respect, the spectra of Eu^{+3} and Tb^{+3} are similar. However, the first excited level of the ground multiplet in Tb^{+3}, $^7F_5$, lies 2080 cm.$^{-1}$ over the $^4F_6$ ground state,[7] so that, in distinction to the situation with Eu^{+3}, *only* the ground state of Tb^{+3} is populated at the temperatures involved in the present investigation. The results of studies of Tb^{+3} spectra in crystalline salts, as shown in Fig. 1, indicate that all but two excited levels of the ground term multiplet of Tb^{+3} occur within the near-infrared transparency range of molten $LiNO_3$–KNO_3.

The absorption bands found in the molten nitrate solution at 2.275 μ (4396 cm.$^{-1}$) and 1.988 μ (5031 cm.$^{-1}$), Fig. 2, agree well with the centers of gravity of the multiplet levels $^7F_3$ (4325 cm.$^{-1}$) and $^7F_2$ (4975 cm.$^{-1}$) as observed by Geisler and Hellwege.[7] These authors also place $^7F_1$ and $^7F_0$ near 5430 and 5660 cm.$^{-1}$, respectively, while in the molten nitrate solution a single band is observed with maximum at 1.838 μ (5441 cm.$^{-1}$). This latter undoubtedly is to be identified with the $^7F_6$ to $^7F_1$ transition, while the $^7F_6$–$^7F_0$ transition can be interpreted as giving rise to a weak absorption lost in the tailing of the 5441 cm.$^{-1}$ band.

(6) G. E. Blomgren and E. R. Van Artsdalen, *Annual Rev. Phys. Chem.*, **11**, 273 (1960).

(7) H. F Geisler and K. H. Hellwege, *Z. Physik*, **136**, 293 (1953).

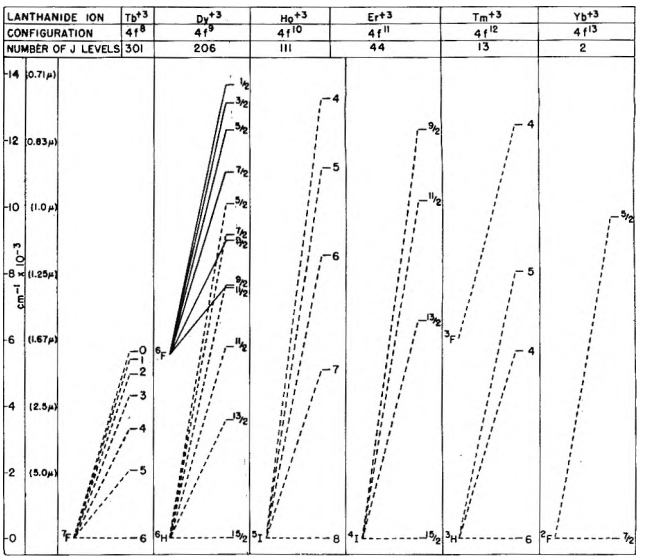

Fig. 1.—Energy levels of the lanthanides in the 0–14,000 cm.$^{-1}$ range. References: Tb^{+3},[7] Dy^{+3},[9,12,14,16] Ho^{+3},[17] Er^{+3},[24a,b] Tm^{+3},[26] and Yb^{+3}.[28]

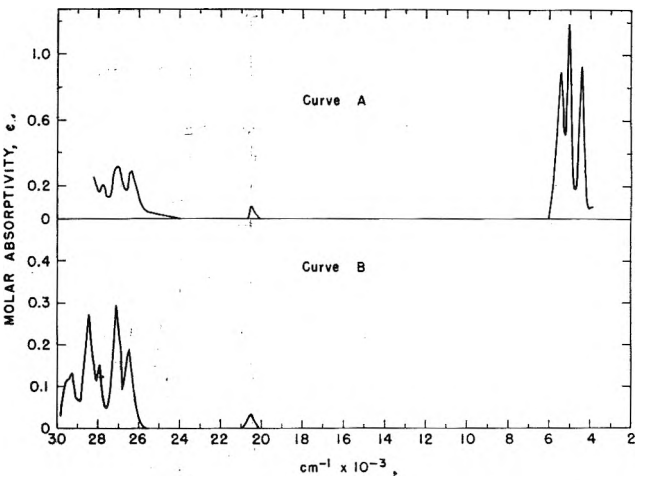

Fig. 2.—The absorption spectrum of Tb^{+3} in (A) molten $LiNO_3$–KNO_3 eutectic at 150° and (B) in $DClO_4$ at 23°.

In the visible region in solution, a weak band, apparently without structure, is found at 0.488 μ (20,490 cm.$^{-1}$). It is well separated from the other visible bands which are grouped at lower wave lengths. Reference to the energy level diagram for Eu^{+3},[3] which has the same ground and first excited terms as Tb^{+3} except that the levels are inverted, would lead one to predict that the first excited multiplet level in Tb^{+3} should be $^5D_4$. This designation has now been confirmed by experiment.[8] The remaining levels in the visible region result from an intermixing of ^5D and ^5L components.[8]

The solution absorption bands of Tb^{+3} in the visible region are not particularly useful for chemical investigations due to their very low intensity. This characteristic increases the importance of the near infrared bands, particularly with respect to spectrophotometric analysis. As was shown earlier, D_2O has an absorption minimum that gives rise to a partial "window" in the 2.12–2.37 μ region.[4] Thus the 2.275 μ band of Tb^{+3} was observed in the dilute $DClO_4$ solution, but quantitative data under such circumstances are difficult to obtain and were not in this case of sufficient interest to warrant further study.

(8) H. G. Kahle and H. Kalbfleish, *ibid.*, **166**, 184 (1962).

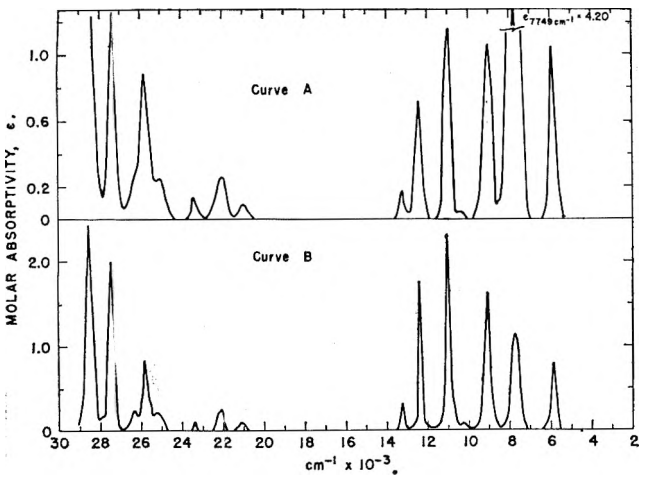

Fig. 3.—The absorption spectrum of Dy^{+3} in (A) molten $LiNO_3$–KNO_3 eutectic at 150° and (B) in $DClO_4$ at 23°.

Dysprosium.—While the results of a number of experimental studies with various crystalline salts of Dy^{+3} have been published, there is still disagreement respecting the assignment of certain levels in the infrared. The structure in the visible region is so complex that interpretation of experimental results must await detailed theoretical calculations.[9]

Jørgensen pointed out some years ago that from the theoretical standpoint, the infrared spectrum of Dy^{+3} must be interpreted as an overlapping of the levels of the ^6H ground state and the ^6F first excited multiplet.[10] The most recent studies with crystals now confirm this interpretation. Judd has calculated the levels of the ground term multiplet, and has shown that the assumption of pure R–S coupling gives poor agreement with experiment.[11] Intermediate coupling calculations do, however, make possible a good fit of experimental results.

Experimental studies of crystal spectra place the centers of gravity of the first two excited components of the ground term multiplet, $^6H_{13/2}$ and $^6H_{11/2}$, at 3574 and 5812 cm.$^{-1}$, respectively.[12] The $^6H_{13/2}$ level lies beyond the range of the present investigation; however, the isolated band found in the nitrate melt at 1.691 μ (5914 cm.$^{-1}$) and in $DClO_4$ at 1.710 μ (5848 cm.$^{-1}$) is clearly identifiable as resulting from the $^6H_{15/2}$ to $^6H_{11/2}$ transition. Gramberg[13] reported the crystal field splitting of the $^6H_{15/2}$ ground term in several crystalline media at 58°K., but not all of the components were observed. In $Dy(NO_3)_3$, the splitting is >95 cm.$^{-1}$, but no corresponding structure is observed in the $^6H_{11/2}$ level in solution.

The center of gravity of the next higher level is reported by Dieke and co-workers[9,12] to lie near 7600 cm.$^{-1}$, while Gobrecht[14] and Rosenthal[15] quote 7800 and 8032 cm.$^{-1}$, respectively. Judd's calculation places $^6H_{9/2}$ at 8010 cm.$^{-1}$ using intermediate coupling.[11] Theory also predicts that the $^6F_{11/2}$ level should lie in this region; its center of gravity has been variously placed at 6500,[10] 7300,[16] and 7900 cm.$^{-1}$.[9] Crosswhite and Dieke found evidence of more crystal levels than could arise from $^6H_{9/2}$ alone near 7600 cm.$^{-1}$ and thus proposed that $^6H_{9/2}$ and $^6F_{11/2}$ are essentially superimposed.[9]

In the nitrate melt, the most intense band found in the spectrum of Dy^{+3} occurs with a maximum at 1.290 μ (7752 cm.$^{-1}$). As indicated in Fig. 3, this band does not appear to have any structure. The same band in $DClO_4$ solution is also intense and without structure; its maximum is at 1.293 μ (7734 cm.$^{-1}$). These results are consistent with the assumption that $^6H_{9/2}$ and $^6F_{11/2}$ are superimposed with the center of gravity of the system near 7730 cm.$^{-1}$.

As shown in Fig. 1, a situation similar to the above arises at ~9000 cm.$^{-1}$. Hellwege and co-workers[16] present evidence for a 9/2 level centered at 9024 cm.$^{-1}$, while Dieke and Singh found four crystal field components with center at 9043 cm.$^{-1}$ which indicated a 7/2 state.[12] A later communication from Dieke and co-workers reported enough crystal field levels to account for both the $^6F_{9/2}$ and $^6H_{7/2}$ levels in the 8900–9000 cm.$^{-1}$ region,[9] although the experimental data cannot establish which level lies lower. As shown in Fig. 3, there is a single band centered at 1.108 μ (9030 cm.$^{-1}$) both in the nitrate melt and in $DClO_4$ solution; this again is consistent with the assumption that the $^6H_{7/2}$ and $^6F_{9/2}$ levels are essentially superimposed.

Reference to Fig. 1 shows that the centers of gravity of the remaining terms in the near infrared as reported from crystal studies are found at 10170, 11100, 12382, and 13177 cm.$^{-1}$.[16] Corresponding bands are observed in the nitrate melt at 10420, 10980, 12400, and 13220 cm.$^{-1}$. These are characterized as transitions from the ground state $^6H_{15/2}$ to multiplet levels designated as $^6H_{5/2}$, $^6F_{7/2}$, $^6F_{5/2}$, and $^6F_{3/2}$, respectively. Experimental confirmation of the $^6F_{1/2}$ level at 13729 cm.$^{-1}$ was reported for the first time quite recently by Hellwege and co-workers.[16] It was not observed by Crosswhite and Dieke.[9] Since this transition was reported to be very weak in crystalline salts of Dy^{+3}, it is perhaps understandable that it was not observed in solution. Although in this case it should be emphasized that no absorption was indicated in the predicted region at the highest concentrations of Dy^{+3} employed (1.02 *M* Dy^{+3} in 0.3 *M* $DClO_4$). This was not a matter of overlap in this region by other more intense bands.

It is seen that the principal bands of Dy^{+3} occur at essentially the same wave length in the nitrate melt and in $DClO_4$.

Holmium.—The infrared spectrum of crystalline salts of Ho^{+3} has been investigated both by Gobrecht[14] and Rosenthal[15]; Judd[11] has compared their results to those calculated for the R–S case and for the intermediate coupling approximation. Crozier and Runciman have extended the theoretical analysis to the excited multiplet levels.[17]

As seen in Fig. 1, the components of the ^5I ground term multiplet are relatively well separated in energy, and there is no overlap with components of the first excited state. Of particular interest with respect to the present investigation is the fact that all the excited J-levels of the ^5I multiplet occur within the range of transparency of the $LiNO_3$–KNO_3 eutectic (Fig. 4).

(9) H. M. Crosswhite and G. H. Dieke, *J. Chem. Phys.*, **35**, 1535 (1961).
(10) C. K. Jørgensen, *Dan. Mat-Fyz. Medd.*, **29**, No. 11 (1955).
(11) B. R. Judd, *Proc. Phys. Soc.* (London), **69A**, 157 (1956).
(12) G. H. Dieke and S. Singh, *J. Opt. Soc. Am.*, **46**, 495 (1956).
(13) G. Gramberg, *Z. Physik*, **159**, 125 (1960).
(14) H. Gobrecht, *Ann. Physik*, **31**, 755 (1938).
(15) G. Rosenthal, *Phys. Z.*, **40**, 508 (1938).
(16) K. H. Hellwege, G. Horstik, S. Hüfner, and H. Lämmermann, *Z. Physik*, **165**, 253 (1961).
(17) M. H. Crozier and W. A. Runciman, *J. Chem. Phys.*, **35**, 1392 (1961).

The center of gravity of the $^5I_4$ level was found from crystal studies to lie near 0.752 μ (13300 cm.$^{-1}$),[18] but this transition has not been reported previously in solution. Using high concentrations of Ho^{+3}, an extremely weak band was found in the nitrate melt at 13370 cm.$^{-1}$. Additional evidence was provided by a a study of Ho^{+3} in dilute $DClO_4$ solution where the band was slightly more intense. It was found to have a structure similar to that observed for the other solution absorption bands ascribed to the ground term multiplet.

A recent study of the absorption spectrum of $Ho(C_2H_5SO_4)_3 \cdot 9H_2O$ revealed that six crystal levels of the $^5I_8$ ground state are populated at 58°K.; the total splitting of the six levels was found to be 117.6 cm.$^{-1}$.[19] Hufner subsequently assumed a center of gravity of ~120 cm.$^{-1}$ for $^5I_8$ for the purpose of comparing experiment and theory.[18] In the present investigation, each absorption band attributed to the ^5I multiplet was observed to be complex and resolvable into two gaussians. The higher energy component of each band agreed well with the energy corresponding to the center of gravity of the ^5I component as observed in crystal studies at low temperatures (Table I).

TABLE I

COMPARISON OF OBSERVED ABSORPTION MAXIMA FOR THE ^5I MULTIPLET OF Ho^{+3} IN DIFFERENT MEDIA

Level	Obsd. in crystals,[17] cm.$^{-1}$	$LiNO_3$–KNO_3 melt, cm.$^{-1}$	$DClO_4$, cm.$^{-1}$	Δ cm.$^{-1}$ Melt	Δ cm.$^{-1}$ $DClO_4$
$^5I_8$	0				
$^5I_7$	5120	4938		260	
		5203			
$^5I_6$	8590	8439	8419	280	250
		8718	8673		
$^5I_5$	11218	11030	10980	270	250
		11300	11230		
$^5I_4$	13319	...	13123	...	260
		13370	13386		

The splitting of the ^5I multiplet levels is nearly the same in aqueous solution at 25° as in the molten nitrate eutectic at 150° and is roughly constant throughout the ^5I levels. If it is assumed that the splitting occurs as a result of transitions from the lowest and highest crystal components of the $^5I_8$ ground state, then the total splitting of this state is of the order of 260 cm.$^{-1}$. This value is in reasonable agreement with the assumption made by Hufner.[18]

The first excited multiplet component was verified by Grohmann and co-workers[19] as $^5F_5$ (15,550 cm.$^{-1}$) in good agreement with the band found in the nitrate melt at 0.6431 μ (15,550 cm.$^{-1}$); this identification had earlier been proposed by Jørgensen.[20]

The sensitivity of the 0.452 μ band of Ho^{+3} to nitrate concentration, Fig. 4, was also reported when the aqueous nitrate solution spectrum was compared to that obtained with nitrate crystals.[21] The intensity of this band and also that of the band at 0.361 μ is, similarly, much greater in molten LiCl–KCl[22] and in acetyl-

(18) S. Hufner, *Z. Physik*, **164**, 257 (1961).
(19) I. Grohmann, K. H. Hellwege, and H. G. Kahle, *ibid.*, **164**, 243 (1961).
(20) C. K. Jørgensen, *Acta Chem. Scand.*, **11**, 981 (1957).
(21) P. W. Selwood, *J. Am. Chem. Soc.*, **52**, 4308 (1930).
(22) C. V. Banks, M. R. Heusinkveld, and J. W. O'Laughlin, *Anal. Chem.*, **33**, 1235 (1961).

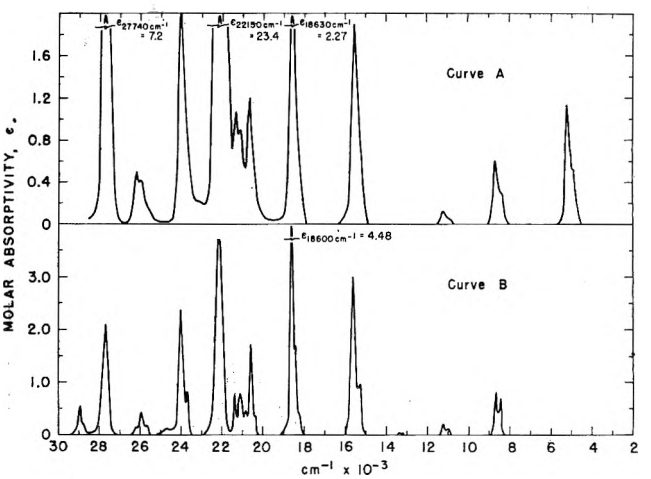

Fig. 4.—The absorption spectrum of Ho^{+3} in (A) molten $LiNO_3$–KNO_3 eutectic at 150° and (B) in $DClO_4$ at 23°.

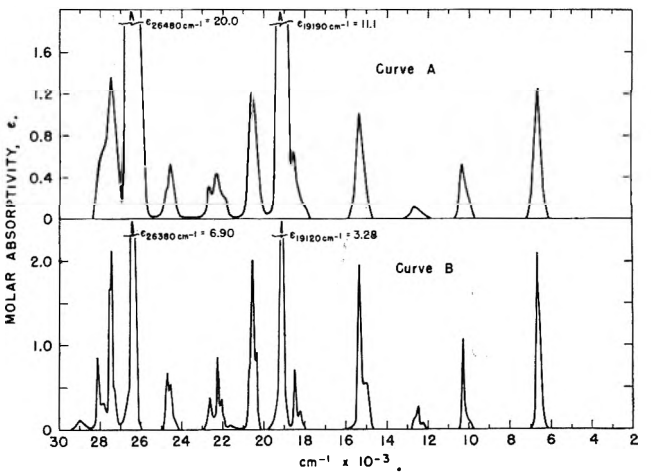

Fig. 5.—The absorption spectrum of Er^{+3} in (A) molten $LiNO_3$–KNO_3 eutectic at 150° and (B) in $DClO_4$ at 23°.

acetone chelates[23] than in dilute aqueous solutions. Selwood found a general shift of the Ho^{+3} bands in solution toward shorter wave lengths in contrast to his results with lighter lanthanides.[21] The present study revealed no apparent systematic shift in band position in either the infrared or visible regions in comparing the spectra of Ho^{+3} in $DClO_4$ and in the nitrate melt.

Erbium.—There have been several recent studies of Er^{+3} spectra in crystals,[24] and the theoretical treatment has been extended to the calculation of the crystal field splitting of the multiplet levels.[24a] Reference to Fig. 1 indicates that the near infrared region of the Er^{+3} spectrum should allow rather simple interpretation in solution. The centers of gravity of the $^4I_{13/2}$, $^4I_{11/2}$, $^4I_{9/2}$, and $^4F_{9/2}$ levels are placed near 6590, 10,200, 12,500, and 15,400 cm.$^{-1}$, respectively.[24b,24c] Corresponding bands were found in the nitrate melt at 1.5 μ (6622 cm.$^{-1}$), 0.968 μ (10,330 cm.$^{-1}$), 0.787 μ (12,706 cm.$^{-1}$), and 0.6505 μ (15,373 cm.$^{-1}$), as shown in Fig. 5. Thus, as was the case with Ho^{+3}, all of the J-levels arising from transitions between the ground term, $^4I_{15/2}$, and excited levels in the ^4I-multiplet are observed in the near infrared in the nitrate melt. In Er^{+3} all of the excited components of the ground multiplet also are observed in $DClO_4$.

(23) T. Moeller and W. F. Ullrich, *J. Inorg. Nucl. Chem.*, **2**, 164 (1956).
(24) (a) E. H. Erath, *J. Chem. Phys.*, **34**, 1985 (1961); (b) G. H. Dieke and S. Singh, *ibid.*, **35**, 555 (1961); (c) H. G. Kahle, *Z. Physik*, **161**, 486 (1961).

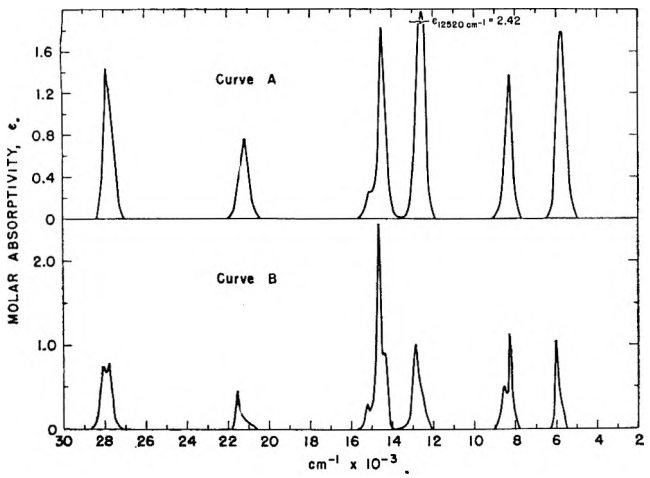

Fig. 6.—The absorption spectrum of Tm^{+3} in (A) molten $LiNO_3$–KNO_3 eutectic at 150° and (B) in $DClO_4$ at 23°.

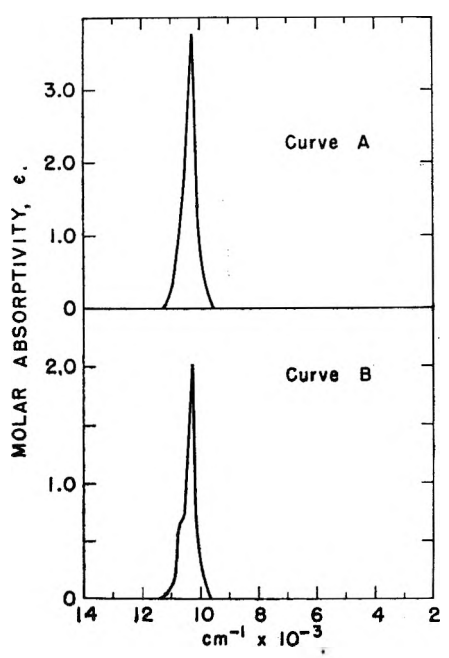

Fig. 7.—The absorption spectrum of Yb^{+3} in (A) molten $LiNO_3$–KNO_3 eutectic at 150° and (B) in $DClO_4$ at 23°.

At present there exists in the literature some confusion with respect to the L–S symbol applied to the multiplet components centered near 12,500 and 15,400 cm.$^{-1}$. The 12500 cm.$^{-1}$ level has been designated both as $^4I_{9/2}$[24b,c] and $^4F_{9/2}$.[24a,25] Varsanyi and Dieke have pointed out that the apparent difference in assignment in this case is actually a difference in nomenclature.[26] This problem may arise when L–S symbols are used to designate levels for intermediate coupling. The conventions adopted in references 24c and 26 are used here. Calculations assuming pure R–S coupling are not sufficiently sensitive to distinguish between the two states.[10]

As was the case with Nd^{+3} and Ho^{+3}, the wave lengths of the maxima of most of the solution absorption bands of Er^{+3} were found to be rather insensitive to a shift in medium from dilute $DClO_4$ to the molten nitrate solvent. However, as Selwood has pointed out, there is a predominant small shift toward the ultraviolet with increasing NO_3^- concentration.[21] The intensity of the absorption bands located at 0.378 and 0.521 μ proved to be particularly sensitive to medium effects. The significant increase in intensity of these bands in the nitrate melt as compared to the $DClO_4$ solution finds a parallel in the effect of molten LiCl–KCl solutions[22] and in acetylacetonate chelate formation.[23]

Thulium.—Considerable theoretical and experimental interest has been manifest in the absorption spectrum of crystalline salts of Tm^{+3}, since the theoretical treatment of 12 f-electrons is relatively simple; the calculation of terms arising from electrostatic interaction is the same as for $Pr^{+3}(f^2)$. The experimental results, summarized in Fig. 1, show that in the near-infrared region, multiplet levels characterized as $^3H_4$, $^3H_5$, and $^3F_4$ occur with centers of gravity near 5647, 8061, and 12,491 cm.$^{-1}$, respectively.[27] In the molten nitrate melt (Fig. 6) the corresponding bands are found at 1.740 μ (5747 cm.$^{-1}$), 1.212 μ (8254 cm.$^{-1}$), and 0.799 μ (12,516 cm.$^{-1}$). The calculated centers of gravity of these same bands are in much better agreement with the molten nitrate results than with those obtained in a study of $Tm(C_2H_5SO_4)_3 \cdot 9H_2O$.[27] As was the case with Pr^{+3}, the relative simplicity of the Tm^{+3} spectrum in solution makes possible the interpretation of the absorption bands in the visible region as well as those in the near-infrared. The calculations of Wong and Richman place the centers of gravity of the $^3F_3$, $^3F_2$, $^1G_4$, and $^1D_2$ levels at 14,478, 14,982, 21,187, and 27,778 cm.$^{-1}$, respectively. The bands in the nitrate melt with maxima at 0.689 μ (14,515 cm.$^{-1}$), 0.665 μ (15,040 cm.$^{-1}$), 0.472 μ (21,186 cm.$^{-1}$), and 0.359 μ (27,855 cm.$^{-1}$) thus are to be characterized as resulting from transitions between the ground state $^3H_6$ and the aforecited excited states, respectively. Seven of the 12 excited J-levels in Tm^{+3} are therefore observed in the nitrate melt. Gruber and Conway have previously identified the $^3H_4$ state in D_2O solution.[28]

There appears to be a slight shift of band maxima toward the infrared associated with changing the solvent from $DClO_4$ to the molten nitrate eutectic; however, none of the visible or near infrared bands exhibits a significant change in intensity under these circumstances.

Yb^{+3}.—Trivalent ytterbium (f^{13}) has only one excited J-level in the f-configuration. The transition between the ground state $^2F_{7/2}$ and this excited state, $^2F_{5/2}$, is observed in crystalline salts near 10,292 cm.$^{-1}$.[29] The corresponding absorption band in solution is well known, and is centered at 0.975 μ (10,256 cm.$^{-1}$) in the nitrate melt as shown in Fig. 7. In the case of Ce^{+3} (f^1) the ^2F doublet is erect; the ground state is $^2F_{5/2}$ and the excited level $^2F_{7/2}$ lies in the infrared beyond the experimental limits of the present investigation. Jørgensen[30] has discussed the theoretical interpretation of the fact that many of the lanthanide absorption bands show a shift toward smaller wave number when the spectrum of a lanthanide ion in an anhydrous crystalline chloride, bromide, or oxide lattice is compared to that of the aquo ion in solution. This effect was noted a number of years ago by Ephraim and coworkers,[30] and the part of their explanation involving

(25) B. G. Wybourne, *J. Chem. Phys.*, **32**, 639 (1960).
(26) F. Varsanyi and G. H. Dieke, *ibid.*, **36**, 2951 (1962).
(27) E. Y. Wong and I. Richman, *ibid.*, **34**, 1182 (1961).
(28) J. B. Gruber and J. G. Conway, *ibid.*, **32**, 1178 (1960).
(29) G. H. Dieke and H. M. Crosswhite, *J. Opt. Soc. Am.*, **46**, 885 (1956).
(30) C. K. Jørgensen, Rept. CERI-TIC-P 10, Cyanamid European Research Inst., Geneva, Switzerland, 1961.

the expansion of the radial function of the partly filled 4f-shell by covalent bonding retains its validity. In general, a similar effect was observed in the present investigation, particularly with the light lanthanides. In the heavy half of the series, a comparison of the spectra of the aquo ion with that in the anhydrous molten nitrate frequently revealed little or no definite change in the energy of the band maxima. In this connection the spectrum of Er^{+3} proved to be an exception, exhibiting in general a small shift toward higher energies. This is in the same direction as the shift observed for many solid anhydrous lanthanide fluorides.

Acknowledgment.—The author wishes to acknowledge numerous helpful discussions with D. M. Gruen and P. R. Fields during the course of this work. The assistance of R. L. McBeth in obtaining the experimental data is also gratefully acknowledged.

THE BINDING OF CALCIUM IONS TO SERUM ALBUMIN

BY H. A. SAROFF AND M. S. LEWIS

National Institute of Arthritis and Metabolic Diseases, National Institutes of Health, Public Health Service, U. S. Department of Health, Education, and Welfare, Bethesda, Maryland, and National Institute of Dental Research, National Institutes of Health

Received November 9, 1962

The binding of Ca^{++}, OH^-, and Cl^- to deionized serum albumin was studied in the pH region of 5 to 10.5. Known constants and simple electrostatic contribution of the charge of the albumin molecule predicted binding in excess by a factor of four over that found experimentally. The interpretation of the data offered in this communication is one involving a carboxylate ion–amino or imidazole chelate as the principal binding site for calcium ions.

A number of studies have been reported on calcium binding to serum albumin.[1-7] The increase in binding with increased pH has generally been attributed to electrostatic effects.[3,4] In order to examine more carefully the binding of calcium ion, simultaneous measurements were made on (1) the binding of Ca^{++}, (2) the binding of OH^-, and (3) the binding of Cl^- in solutions of deionized human serum albumin containing only added calcium hydroxide and calcium chloride. The results of these measurements and their interpretation in light of existing theory are reported in this communication.

Materials and Methods

Human serum albumin was a sample of Fraction V, lot number 752, obtained from the American Red Cross. This sample of albumin, on analysis by velocity ultracentrifugation, was found to be as homogeneous as crystalline preparations used in this Laboratory and was considered adequate for this study. A molecular weight of 68,000 g. was employed in the calculations. The albumin was deionized on a mixed bed resin column according to the procedure of Dintzis.[8]

The water used in preparing solutions for binding measurements was boiled to remove dissolved CO_2. Protein solutions were adjusted to the required pH with calcium hydroxide and the remainder of the required total calcium was added as calcium chloride. All solutions were measured within a period of 24 hours of their preparation and were prepared and kept under nitrogen. Measurements were made at 25 ± 1°. pH measurements were made on a Beckman model G pH meter.

Calcium and chloride ion concentrations were measured by the method previously described[9,10] in a cell equipped with both negative (sulfonic acid resin) and positive (quaternary amine resin) permselective membranes. The membranes were supplied by the National Aluminate Corporation, Chicago, Illinois. The cell consisted of three lucite blocks drilled and clamped together to form three compartments with connecting holes to the sample and solution reservoirs and to the stopcocks in which liquid junctions were made to calomel electrodes. The middle compartment was separated from the compartment on one side by a negative permselective membrane and from the compartment on the other side by a positive permselective membrane. Protein solutions were placed in the center compartment and calcium chloride solutions of known concentrations were placed in the two side compartments allowing for measurement of potentials to determine both Ca^{++} and Cl^- activities.

Results

The experimental results are summarized in Table I and the experimental points of Fig. 1. Although little drift occurred in the measurements of both the calcium and chloride ions the chloride ion measurements became unreliable above pH 9. The cause of this unreliability was probably the biionic potential[11] resulting from the presence of the hydroxyl ion. The value of $\bar{r}_{Cl}$ was taken as zero at pH values above 9. When the hydroxyl, chloride, and calcium binding data are summed to calculate the net charge on the protein molecule it becomes obvious that electrostatic factors in the binding are not of primary importance for the pH dependence of the binding. Thus, from pH 5.3 to 7 the net charge on the albumin increases from −4 to −13 and the binding of calcium ion increases from 0 to 2 ions per mole of albumin, while in the pH region from 7 to 10, the net charge increases from −13 to −20 and the binding increases from 2 to 10 calcium ions per mole.

The electrostatic effect may be evaluated by defining an apparent intrinsic constant, k'_{Ca}, for the binding of calcium ion to serum albumin as

$$k'_{Ca} = k_{Ca}e^{-2z_p w z_{Ca}} \qquad (1)$$

where k_{Ca} is the intrinsic association constant and $e^{-2z_p w z_{Ca}}$ is the electrostatic factor.[12] The symbols z_p and z_{Ca} represent the charge on the protein molecule and the calcium ion, respectively, and w has its usual meaning in the Debye-Hückel theory. For application of the simple electrostatic theory, the following

(1) F. C. McLean and A. B. Hastings, *J. Biol. Chem.*, **108**, 285 (1935).
(2) E. G. Weir and A. B. Hastings, *ibid.*, **114**, 397 (1936).
(3) J. C. Abels, *J. Am. Chem. Soc.*, **58**, 260 (1936).
(4) J. T. Edsall, H. Edelhoch, R. Lontie, and P. R. Morrison, *ibid.*, **72**, 4641 (1950).
(5) C. W. Carr, *Arch. Biochem. Biophys.*, **43**, 147 (1953).
(6) S. Katz and I. M. Klotz, *ibid.*, **44**, 351 (1953).
(7) L. I. Irons and D. J. Perkins, *Biochem. J.*, **84**, 152 (1962).
(8) H. Dintzis, Ph.D. Thesis, Harvard University, 1952.
(9) M. S. Lewis and H. A. Saroff, *J. Am. Chem. Soc.*, **79**, 2112 (1957).
(10) H. A. Saroff and J. W. Healy, *J. Phys. Chem.*, **63**, 1178 (1959).
(11) S. Dray and K. Sollner, *Biochim. Biophys. Acta*, **22**, 213 (1956).
(12) G. Scatchard and E. S. Black, *J. Phys. Colloid Chem.*, **53**, 88 (1949).

Table I

Summary of Binding of Ca^{++}, OH^-, and Cl^- to Deionized Human Serum Albumin

pH	Alb. concn., $M \times 10^4$	Total Ca^{++}, $M \times 10^3$	Total OH^-, $M \times 10^3$	Total Cl, $M \times 10^3$	$c_{Ca^{++}}$, $M \times 10^3$	c_{Cl^-}, $M \times 10^3$	$\bar{\nu}_{Ca}$	$\bar{\nu}_{OH}$	$\bar{\nu}_{Cl}$	z_p
5.34	8.12	10.00	0.00	20.00	10.56	16.60	0.00	0.0	4.19	− 4.19
6.10	5.07	11.76	3.52	20.00	11.74	17.79	0.04	6.94	4.36	−11.2
6.11	8.14	10.29	5.50	15.09	10.33	12.45	0.00	6.76	3.24	−10.0
6.13	8.14	10.31	5.53	15.09	10.33	12.48	0.00	6.79	3.21	−10.0
7.03	8.16	11.05	10.98	11.14	9.77	9.24	1.57	13.4	2.33	−12.5
7.13	8.15	11.42	10.91	11.93	10.38	9.91	1.28	13.4	2.48	−13.4
7.30	6.74	13.03	14.46	13.60	10.85	12.81	3.24	21.5	1.19	−16.2
7.55	6.74	13.17	12.74	13.60	11.90	10.59	3.13	19.0	0.60	−13.3
7.92	8.16	12.87	16.20	9.55	10.09	8.21	3.42	19.8	1.64	−14.6
8.20	5.07	14.00	11.20	16.80	12.00	16.80	3.94	22.1	2.50	−16.7
8.55	8.17	12.91	17.85	7.97	9.53	6.98	4.14	21.9	1.21	−14.8
9.07	5.07	15.99	13.12	18.87	13.18	17.80	5.56	25.9	2.11	−14.8
9.11	8.15	16.94	21.95	11.93	12.54	11.17	5.40	26.9	0.93	−16.1
9.75	8.12	22.79	25.78	19.80	18.11	19.56	5.76	31.7	0.30	−20.2
9.89	6.76	18.26	27.44	9.08	11.24	9.96	10.4	40.5	(−1.30)	−19.7
10.12	6.76	19.27	29.34	9.20	11.87	9.39	11.0	43.2	(−0.28)	−21.2
10.13	6.76	19.09	29.10	9.08	11.78	10.59	10.8	41.5	(−2.23)	−19.9
10.16	8.16	20.38	31.21	9.55	12.13	8.53	10.1	38.1	1.25	−17.9
10.55	6.76	20.92	32.76	9.08	11.90	10.47	13.3	48.0	(−2.06)	−21.4

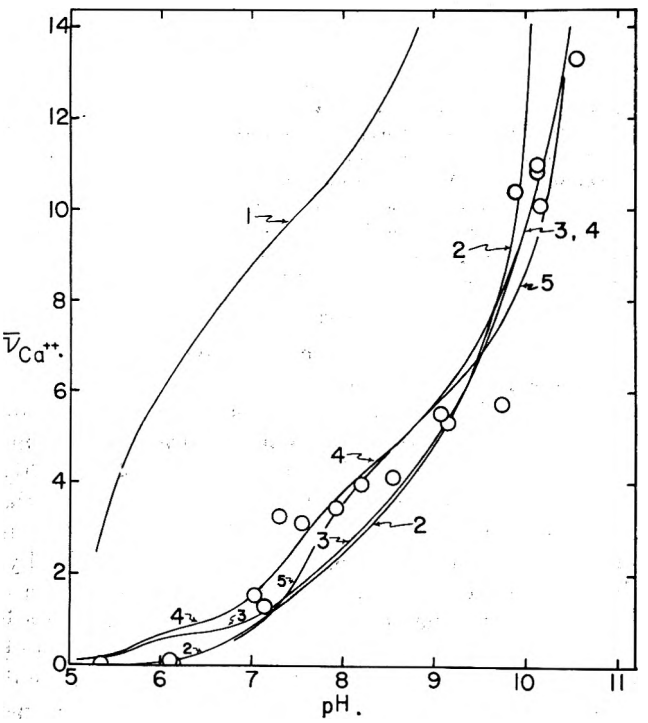

Fig. 1.—pH dependence of the binding of calcium ions to serum albumin. Curve 1, predicted binding of calcium ions to the carboxylate ions of serum albumin calculated with equation 4 and $k_H = 10^5$, $k_{Ca} = 1$, $n = 100$, and $w = 0.045$. Curve 2, predicted binding of calcium ions to the imidazole and amino groups of serum albumin calculated with equation 4 and $k_H = 10^7$, $k_{Ca} = 2.0$, $n = 16$, and $w = 0.045$ for the imidazole groups and $k_H = 10^{9.5}$, $k_{Ca} = 0.6$, $n = 56$, and $w = 0.045$ for the amino groups. Curve 3, predicted binding of calcium ions to serum albumin calculated with equation 10, and the values of Table IV. Electrostatic effects were applied using expressions similar to equation 1 with $w = 0.015$. Curve 4, same as curve 3 except k_{H_2} changed from 10^7 to $10^{6.5}$. Curve 5, predicted binding of calcium ions to serum albumin calculated with equation 15 and the same values as those for curve 4 except $(k_{Ca})_{ch} = 20$.

expression for the average number of calcium ions bound, $\bar{\nu}_{Ca}$, per mole of albumin may be written

$$\bar{\nu}_{Ca} = \frac{k'_{Ca} c_{Ca} n'}{1 + k_{Ca}' c_{Ca}} \qquad (2)$$

where c_{Ca} is the concentration of free calcium ions in solution and n' is the apparent maximum number of sites to which the calcium ions are bound.

If it is assumed that n' is constant between pH 7 and 10 or that binding of calcium ion is to the carboxylate ion of serum albumin and that all of the carboxyl groups are ionized at pH 7 and above, then the following expression follows from equations 1 and 2.

$$\frac{(\bar{\nu}_{Ca})_{pH\ 10}}{(\bar{\nu}_{Ca})_{pH\ 7}} = e^{-4(-7)w} \frac{1 + 0.011 k_{Ca} e^{-4(-13)w}}{1 + 0.011 k_{Ca} e^{-4(-20)w}} \qquad (3)$$

where the values of z_p at pH 10 and pH 7 are −20 and −13, respectively, and the concentration, c_{Ca}, is 0.011 M. The experimental value of the ratio $(\bar{\nu}_{Ca})_{pH\ 10}/(\bar{\nu}_{Ca})_{pH\ 7}$ was found to be about 6. Calculated values for the ratio $(\bar{\nu}_{Ca})_{pH\ 10}/(\bar{\nu}_{Ca})_{pH\ 7}$ are given in Table II for values of $w = 0.065$, 0.045, and 0.015 with values of k_{Ca} varying from 0.1 to 10. The value of $w = 0.045$ is consistent with that employed by Scatchard[13] in applying electrostatic theory to anion binding to serum albumin. The value of 0.015 is consistent with that employed by Saroff[14] in analyzing proton and anion binding to serum albumin. The value $w = 0.065$ is simply that value of w required to give the ratio 5.2. These calculations demonstrate that in order to explain calcium ion binding to serum albumin with the electrostatic theory explaining the primary effect of pH, a value of w of about 0.065 must be coupled with an intrinsic constant of about 0.1 for the binding of calcium ions to serum albumin. Both of these values are inconsistent with existing data and interpretations of protein interactions.

Some reported values for the complexation constants for Ca^{++} and various ligands are collected in Table III. The sites available[15] for the binding of Ca^{++} to serum albumin include 16 imidazole groups (complexation constant, 2) and 56 amino groups (complexation constant, 0.6) as well as approximately one hundred carboxylate ions (complexation constant, 1 to 6).

(13) G. Scatchard, J. S. Coleman, and A. L. Shen, *J. Am. Chem. Soc.*, **79**, 12 (1957).

(14) H. A. Saroff, *J. Phys. Chem.*, **61**, 1364 (1957).

(15) E. Brand, *Ann. N. Y. Acad. Sci.*, **47**, 187 (1946); W. H. Stein and S. Moore, *J. Biol. Chem.*, **178**, 79 (1949).

TABLE II

VALUES OF THE RATIO $(\bar{\nu}_{Ca})_{pH\ 10}/(\bar{\nu}_{Ca})_{pH\ 7}$ CALCULATED FROM EQUATION 3 FOR DIFFERENT VALUES OF k_{Ca}' AND w

k'_{Ca}	w	$(\bar{\nu}_{Ca})_{pH\ 10}/(\bar{\nu}_{Ca})_{pH\ 7}$
	0.065	5.2
0.1	0.045	3.4
	0.015	1.5
	0.065	2.7
1.0	0.045	2.8
	0.015	1.5
	0.065	1.2
10	0.045	1.6
	0.015	1.4

TABLE III

COMPLEXATION CONSTANTS REPORTED FOR Ca^{++} AND VARIOUS UNI- AND BIDENTATE LIGANDS[a]

The value of K_1 is that for the ligand in the unprotonated form.

Ligand	K_1
Ammonia	0.6
Imidazole	2.0[b]
Formic acid	
Acetic acid	1.0 to 6.3
Propionic acid	
n-Valeric acid	
Hippuric acid	2.7
Succinic acid	10 to 100
Glycollic acid	13 to 39
Glycine	22 to 27
Maleic acid	12 to 270
Oxalic acid	1000

[a] J. Bjerrum, G. Schwarzenbach, and L. G. Sillén, "Stability Constants," The Chemical Society, London, 1957. [b] Corrected for the pK of imidazole.

Interpretation of the Binding Data

Imidazole and Amino Groups.—It is obvious that the pK of the imidazole and amino groups control the binding of Ca^{++} to serum albumin.[6] It is also clear from the data presented above that the control of calcium binding by the imidazole and amino groups is not a direct function of the change in charge of these groups. It is possible to explain the experimental data in Table I on the basis of binding to imidazole and amino groups with the constants of Table III. (The guanidino groups of arginine may be ignored since no measurements above pH 10.5 were made.) For calculating the binding of Ca^{++} to the imidazole and amino groups of serum albumin the following expression for competitive binding is applicable[9]

$$\bar{\nu}_{Ca} = \frac{k'_{Ca}c_{Ca}n}{1 + k'_{Ca}c_{Ca} + k'_{H}c_{H}} \qquad (4)$$

where k'_{Ca} is defined in equation 1 and k'_{H} is similarly defined as

$$k'_{H} = k_{H}e^{-2z_{p}wz_{H}} \qquad (5)$$

In equation 4 k_{H} refers to the intrinsic association constant for the binding of hydrogen ion to the same site for which the constant for the binding of calcium ion is k_{Ca}. In this and the following calculations the activity coefficients of hydrogen and calcium ions are assumed to be unity. Equation 4 was used to calculate curve 2 in Fig. 1 with the constants $k_{H} = 10^{7}$, $k_{Ca} = 2.0$, and $n = 16$ for the imidazole group, and the constants $k_{H} = 10^{9.5}$, $k_{Ca} = 0.6$, and $n = 56$ for the amino group. The value of w was taken as 0.045. Curve 2 demonstrates a satisfactory fit with the data for the binding of calcium ions to serum albumin. Although the calculated curve is satisfactory, the imidazole and amino groups cannot be designated as the sole sites of binding without postulating some restrictive behavior for the carboxylate ions.

Carboxyl Groups.—A partial treatment of the binding of calcium ions to the carboxyl groups of serum albumin was presented above with the comparison of the ratio of equation 3 with that of the experimental data. Since reasonable binding constants for the imidazole and amino groups can explain the binding of calcium ions to serum albumin it is of interest to apply an equivalent set of constants to the 100 carboxyl groups. Equation 4 with the constants $k_{H} = 10^{5}$, $k_{Ca} = 1$, $n = 100$, and $w = 0.045$ was employed to calculate curve 1 of Fig. 1. Examination of curve 1 and its comparison with curve 2 demonstrates clearly that neither the imidazole and amino groups nor the carboxylate ions can be designated as the *sole* sites for the binding of calcium ions to serum albumin because of the unusual restrictions required in either case.

Carboxylate Ion–Imidazole or Amino Chelate.—A combination of (1) pH control by the imidazole and amino groups, (2) the unrestricted binding of Ca^{++} to carboxylate ions, imidazole, and amino groups, and (3) the restriction on the activity of both the carboxylate ion and nitrogen groups may be achieved by a structural pairing[14] of the hundred carboxyl groups of serum albumin with the hundred nitrogen centers of serum albumin. When this is done the reaction of a carboxylate ion with its paired imidazolium, ammonium, or guanidinium ion results in a hydrogen bond or "salt linkage." This same structural pairing will also allow the reaction of a calcium ion with the carboxylate ion and the uncharged nitrogen center to form a bidentate chelate with the binding site. To the reactions previously applied in the case of the carboxyl, imidazole, and amino groups

$$\int\!\!-COOH + Ca^{++} = \int\!\!-COOCa^{+} + H^{+} \qquad (6)$$

$$\int\!\!\equiv NH^{+} + Ca^{++} = \int\!\!\equiv NCa^{++} + H^{+} \qquad (7)$$

is now added the reaction

$$\int\!\!-COO^{-}\ldots H^{+}\ldots N\!\equiv\!\int + Ca^{++} = \int\!\!-COO^{-}\ldots Ca^{++}\ldots N\!\equiv\!\int + H^{+} \qquad (8)$$

The symbols, $\int\!\!-COO^{-}\ldots H^{+}\ldots N\!\equiv\!\int$ and $\int\!\!-COO^{-}\ldots Ca^{++}\ldots N\!\equiv\!\int$, represent a single pair of carboxyl and nitrogenous groups in the hydrogen bonded form and calcium chelated form, respectively. When reaction 8 is added to reactions 6 and 7, binding of Ca^{++} to all of the carboxyl, imidazole, and amino groups does not become excessive because of the competition imposed by the hydrogen bond and the restriction imposed on *both* the carboxylate ion and the nitrogen center by the formation of the bidentate chelate. To derive the expressions representing reactions 6, 7, and 8 consider the following competitive reactions in which each carboxyl group is paired with one basic nitrogen group.

(A) $\int\!-COO^- \; N\!\equiv\!\int + H^+ = \int\!-COOH \; N\!\equiv\!\int \cdot k_{H_1} = \dfrac{P_{(COOH,N)}}{P_{(COO^-,N)}c_H}$

(B) $\int\!-COO^- \; H^+N\!\equiv\!\int + H^+ = \int\!-COOH \; H^+N\!\equiv\!\int \cdot k_{H_1} = \dfrac{P_{(COOH,\,H^+N)}}{P_{(COO^-,\,H^+N)}c_H}$

(C) $\int\!-COO^- \; AHN\!\equiv\!\int + H^+ = \int\!-COOH \; AHN\!\equiv\!\int \cdot k_{H_1} = \dfrac{P_{(COOH,\,AHN)}}{P_{(COO^-,\,AHN)}c_H}$

(D) $\int\!-COO^- \; Ca^{++}N\!\equiv\!\int + H^+ = \int\!-COOH \; Ca^{++}N\!\equiv\!\int \cdot k_{H_1} = \dfrac{P_{(COOH,\,Ca^{++}N)}}{P_{(COO^-,\,Ca^{++}N)}c_H}$

(E) $\int\!-COOH \; N\!\equiv\!\int + H^+ = \int\!-COOH \; H^+N\!\equiv\!\int \cdot k_{H_2} = \dfrac{P_{(COOH,\,H^+N)}}{P_{(COOH,\,N)}c_H}$

(F) $\int\!-COO^- \; N\!\equiv\!\int + H^+ = \int\!-COO^- \; H^+N\!\equiv\!\int \cdot k_{H_2} = \dfrac{P_{(COO^-,\,H^+N)}}{P_{(COO^-,\,N)}c_H}$

(G) $\int\!-COOCa^+ \; N\!\equiv\!\int + H^+ = \int\!-COOCa^+ \; H^+N\!\equiv\!\int \cdot k_{H_2} = \dfrac{P_{(COOCa^+,\,H^+N)}}{P_{(COOCa^+,\,N)}c_H}$

(H) $\int\!-COOH \; H^+N\!\equiv\!\int + A^- = \int\!-COOH \; AHN\!\equiv\!\int \cdot k_{A_2} = \dfrac{P_{(COOH,\,AHN)}}{P_{(COOH,\,H^+N)}c_A}$

(I) $\int\!-COO^- \; H^+N\!\equiv\!\int + A^- = \int\!-COO^- \; AHN\!\equiv\!\int \cdot k_{A_2} = \dfrac{P_{(COO^-,\,AHN)}}{P_{(COO^-,\,H^+N)}c_A}$

(J) $\int\!-COOCa^+ \; H^+N\!\equiv\!\int + A^- = \int\!-COOCa^+ \; AHN\!\equiv\!\int \cdot k_{A_2} = \dfrac{P_{(COOCa^+,\,AHN)}}{P_{(COOCa^+,\,H^+N)}c_A}$

(K) $\int\!-COO^- \; N\!\equiv\!\int + Ca^{++} = \int\!-COOCa^+ \; N\!\equiv\!\int \cdot k_{Ca_1} = \dfrac{P_{(COOCa^+,\,N)}}{P_{(COO^-,\,N)}c_{Ca}}$

(L) $\int\!-COO^- \; H^+N\!\equiv\!\int + Ca^{++} = \int\!-COOCa^+ \; H^+N\!\equiv\!\int \cdot k_{Ca_1} = \dfrac{P_{(COOCa^+,\,H^+N)}}{P_{(COO^-,\,H+N)}c_{Ca}}$

(M) $\int\!-COO^- \; AHN\!\equiv\!\int + Ca^{++} = \int\!-COOCa^+ \; AHN\!\equiv\!\int \cdot k_{Ca_1} = \dfrac{P_{(COOCa^+,\,AHN)}}{P_{(COO^-,\,AHN)}c_{Ca}}$

(N) $\int\!-COO^- \; Ca^{++}N\!\equiv\!\int + Ca^{++} = \int\!-COOCa^+ \; Ca^{++}N\!\equiv\!\int \cdot k_{Ca_1} = \dfrac{P_{(COOCa^+,\,Ca^{++}N)}}{P_{(COO^-,\,Ca^{++}N)}c_{Ca}}$

(O) $\int\!-COOH \; N\!\equiv\!\int + Ca^{++} = \int\!-COOH \; Ca^{++}N\!\equiv\!\int \cdot k_{Ca_2} = \dfrac{P_{(COOH,\,Ca^{++}N)}}{P_{(COOH,\,N)}c_{Ca}}$

(P) $\int\!-COO^- \; N\!\equiv\!\int + Ca^{++} = \int\!-COO^- \; Ca^{++}N\!\equiv\!\int \cdot k_{Ca_2} = \dfrac{P_{(COO^-,\,Ca^{++}N)}}{P_{(COO^-,\,N)}c_{Ca}}$

(Q) $\int\!-COOCa^+ \; N\!\equiv\!\int + Ca^{++} = \int\!-COOCa^+ \; Ca^{++}N\!\equiv\!\int \cdot k_{Ca_2} = \dfrac{P_{(COOCa^+,\,Ca^{++}N)}}{P_{(COOCa^+,\,N)}c_{Ca}}$

(R) $\int\!-COO^- \; N\!\equiv\!\int + Ca^{++} = \int\!-COO^-\ldots Ca^{++}\ldots N\!\equiv\!\int \cdot (k_{Ca})_{ch} = \dfrac{P_{(COO^-\ldots Ca^{++}\ldots N)}}{P_{(COO^-,\,N)}c_{Ca}}$

(S) $\int COO^- \; H^+N\!\equiv\!\int = \int\!-COO^-\ldots H^+\ldots N\!\equiv\!\int \cdot k_{D_2} = \dfrac{P_{(COO^-\ldots H^+\ldots N)}}{P_{(COO^-,\,H^+N)}}$

In the above reactions, for a single carboxyl group matched to a single basic nitrogenous group, the symbol $P_{(COO^-,\,N)}$ represents the fraction of that single site of the protein molecule in the form represented by the species described in the parentheses. The symbol COO^- represents a carboxylate ion and N is taken to mean an uncharged, imidazole, amino, or guanidino group. The symbols, k_{H_1}, k_{Ca_1}, k_{H_2}, k_{Ca_2}, and k_{A_2} represent the intrinsic association constants for the binding of H^+ to the carboxylate ion, Ca^{++} to the carboxylate ion, H^+ nitrogen-containing group, Ca^{++} to the nitrogen-containing group, and anion to the positively charged nitrogen group, respectively. The symbol k_{D_2} refers to the association constant for the hydrogen bonding reaction between the carboxylate ion and the positively charged nitrogen ion with the constant k_{H_2}. The symbol $(k_{Ca})_{ch}$ refers to the association constant for the formation of the bidentate chelate from a carboxylate ion and its paired, uncharged nitrogen group.

The symbols c_H, c_A, and c_{Ca} refer to the concentrations of the free hydrogen ions, anions, and calcium ions, respectively.

The quantity $\bar{\nu}_{Ca}$ is defined by the equation

$$\bar{\nu}_{Ca} = n[P_{(COOCa^+,\,N)} + P_{(COOCa^+,\,H^+N)} + P_{(COOCa^+,\,AHN)} + P_{(COO^-,\,Ca^{++}N)} + P_{(COOH,\,Ca^{++}N)} + 2P_{(COOCa^+,\,Ca^{++}N)} + P_{(COO^-\ldots Ca^{++}\ldots N)}] \quad (9)$$

and the following expression for $\bar{\nu}_{Ca}$ may be derived.

$$\bar{\nu}_{Ca} = \frac{nk_{Ca_1}c_{Ca}[1 + k_{Ca_2}c_{Ca} + k_{H_2}c_H(1 + k_{A_2}c_A)] + nk_{Ca_2}c_{Ca}[1 + k_{H_1}c_H + k_{Ca_1}c_{Ca}] + n(k_{Ca})_{ch}c_{Ca}}{1 + (k_{Ca})_{ch}c_{Ca} + k_{H_1}c_H + k_{Ca_1}c_{Ca}[1 + k_{H_2}c_H(1 + k_{A_2}c_A)] + k_{Ca_2}c_{Ca}[1 + k_{H_1}c_H + k_{Ca_1}c_{Ca}] + k_{H_2}c_H[(1 + k_{A_2}c_A)(1 + k_{H_1}c_H) + k_{D_2}]} \quad (10)$$

Electrostatic Effects.—Equation 10 contains no electrostatic correction factors. To add an approximation of the electrostatic effect which is a function of the net charge of the protein molecule each k is replaced by its appropriate k' as defined in equation 1.

Pairing of the carboxylate and ammonium ions introduces an additional, localized electrostatic effect of the charge of a grouping within a given pair. Thus, the same k_{H_1} was applied to reactions (A), (B), (C), and (D).

From the standpoint of the effect of the charge of the paired nitrogen group, the observed value of k_{H_1} for reactions (A) and (C) would be the same but the observed value of k_{H_1} for reactions (B) and (D) would be smaller than that of (A) and (C) because of the electrostatic repulsion of H^+ by the charged nitrogen of the pair. The relationships between the constants for reactions (A), (B), (C), and (D) may be formulated as

$$(k_{H_1})_{\text{reaction (A)}} = (k_{H_1})_{\text{reaction (C)}} = e_H(k_{H_1})_{\text{reaction (B)}} = e_H^2(k_{H_1})_{\text{reaction (D)}} \quad (11)$$

where k_{H_1} is the unperturbed intrinsic association constant and e_H represents the localized electrostatic correction factor resulting from a single positive charge of the nitrogen of a given pair. Similarly

$$(k_{H_2})_{\text{reaction (E)}} = \frac{1}{e_H}(k_{H_2})_{\text{reaction (F)}} = e_H(k_{H_2})_{\text{reaction (G)}} \quad (12)$$

and

$$(k_{A_2})_{\text{reaction (H)}} = e_A(k_{A_2})_{\text{reaction (I)}} = \frac{1}{e_A}(k_{A_2})_{\text{reaction (J)}} \quad (13)$$

where e_A represents the localized electrostatic correction factor for the association constant of the anion.

Curve 3 of Fig. 1 was calculated from equation 10. Electrostatic effects of the net charge were applied by equations similar to equation 1 with $w = 0.015$. The localized electrostatic effect of the pairing was held to a minimum and applied only to the value of k_{D_2}. Table IV summarizes the values used in applying equation 10. These values are consistent with both the chloride binding in the acid region and observed constants for the binding of Ca^{++}.

The value of $k_{D_2}' = 8$ was taken from the chloride ion binding treatment[14] and includes the localized electrostatic effect ($k_{D_2}' = k_{D_2}e_H = 8$).[16]

Equation 10 allows for a distribution of the bound calcium between carboxylate ion–calcium complexes, nitrogen–calcium complexes, and the carboxylate–calcium–nitrogen chelate. The calculated distribution is given in Table V and the total calcium bound is illustrated by curve 3 in Fig. 1. Curve 4 was calculated with the same constants as those used for curve 3 except that the value of k_{H_2} was changed from 10^7 to $10^{6.5}$.

TABLE IV

CONSTANTS FOR THE BINDING OF CALCIUM ION TO HUMAN SERUM ALBUMIN

	Carboxyl–imidazole pair		Carboxyl–amino pair[a]
k_{Ca_1}		2	2
k_{Ca_2}		2	0.6
k_{H_1}		10^5	10^5
k_{H_2}		10^7	$10^{9.5}$
$k_{D_2}e_H$[b]		8	8
$(k_{Ca})_{ch}$		10	10
n	4	12	56
k_{A_2}	2500	50	1

[a] The contribution of the carboxyl–guanidino pair varies from 0.1 for the value of $\bar{\nu}_{Ca}$ at pH 5.5 to 0.2 for the value of $\bar{\nu}_{Ca}$ at pH 10.5 and may be ignored. [b] The values of $k_{D_2} = 0.8$ and $e_H = 10$ such that $k_{D_2}e_H = 8$ to be consistent with chloride ion binding data in the acid region.[16]

TABLE V

DISTRIBUTION OF THE SPECIFIC SITES OF BINDING OF CALCIUM IONS TO SERUM ALBUMIN, CALCULATED WITH EQUATION 10 AND CONSTANTS OF TABLE IV

The value of w was taken as 0.015 and z_i at each pH from Table I.

	Number of Ca^{++} bound to sites on one mole of albumin			
pH	Carboxylate ion	Imidazole and amino groups	Carboxylate ion–imidazole and amino chelate	Total ($\bar{\nu}_{Ca}$)
5.5	0.23	<0.01	< 0.01	0.23
6.0	0.55	<0.01	0.02	0.57
7.0	0.71	0.05	0.22	0.98
8.0	0.93	0.30	1.4	2.6
9.0	1.2	0.64	3.2	5.0
10.0	2.0	0.96	6.8	9.8
10.5	2.7	1.3	10.7	14.7

To maximize the local electrostatic effect for comparison with the calculated curves 3 and 4, where this effect was held to a minimum, reactions (D), (G), (K), (N), (P), and (Q) may be ignored in favor of forming the calcium ion chelate, and reaction (L) may be ignored because of the electrostatic repulsion and competition

(16) The equation for chloride binding written to include the localized electrostatic effect is

$$\bar{\nu}_A = \frac{k_{A_2}c_A n}{\frac{e_H + k_{H_1}c_H}{1 + k_{H_1}c_H} + \frac{1}{k_{H_2}c_H} + k_{A_2}c_A + \frac{k_{D_2}e_H}{1 + k_{H_1}c_H}} \quad (14)$$

Equation 14 with the constants of Table I, reference 14, with $e_H = 10$ and with $k_{D_2}e_H = 8$ results in a calculated curve for $\bar{\nu}_A$ equivalent to that of Fig. 2, reference 14. (The differences between the values of $\bar{\nu}_A$ of equation 14 and those of equation 6, reference 14, are 1.6 at pH 5 and 2.7 at pH 3.).

with the hydrogen bond of reaction (S). Calculations indicate that the contribution of the species ∫—CO-OCa$^+$, AHN≡∫ varies from approximately 0.2 per mole of albumin at pH 7 to approximately 0.003 at pH 10 for $k_{Ca_1} = 4$ and may be ignored. Similarly, the species ∫—COOH, Ca^{++}N≡∫ and ∫—COOH, N≡∫ are present in concentrations small enough to be ignored above pH 6.5. With these restrictions, $\bar{\nu}_{Ca}$ becomes $n.^{D}_{(COO^- \ldots Ca^{++} \ldots N)}$ and, with the assumption that $e_H = e_A$

$$\bar{\nu}_{Ca} = \frac{n(k_{Ca})_{ch}c_{Ca}}{1 + (k_{Ca})_{ch} + k_{H_2}c_H(e_H + k_{A_2}c_A + k_{D_2}e_H)} \quad (15)$$

Equation 15, with the values for k_{H_2}, k_{D_2}, e_H, n, and k_{A_2} the same as those used for curve 4, and with $(k_{Ca})_{ch} = 20$, yields curve 5. As e_H is allowed to increase $(k_{Ca})_{ch}$ must also be increased until the curve calculated from equation 15 moves out of a fit with the experimental data as e_H approaches 100 and $(k_{Ca})_{ch}$ approaches 70. Equations 10 and 15 represent two extremes in treating the uncertain localized electrostatic effect of the pair. Yet in both cases the chelate is the important binding site for calcium ion with the value for the association constant varying between those found from studies on model compounds.

Discussion

The peculiar behavior of serum albumin rests as much in its failure to bind ions as predicted as in its generalized affinity for ions. In the acid region serum albumin binds fewer anions than are calculated.[13] In the alkaline region serum albumin binds fewer calcium ions than are predicted. The anion in serum albumin available for competition with other anions in solution is the carboxylate ion. The cation in serum albumin available for competition with calcium in solution is the ammonium ion. The specific pairing and hydrogen bond formation proposed for calcium and chloride binding represents a consistent treatment for the binding of anions and cations to serum albumin in the pH range from 2 to 10.5.

THE CONDUCTIVITIES OF SOME QUATERNARY AMMONIUM CHLORIDES AND BROMIDES IN NITROMETHANE AT 25°

BY A. K. R. UNNI, L. ELIAS, AND H. I. SCHIFF

Department of Chemistry, McGill University, Montreal, Canada

Received November 9, 1962

The conductance of Me_4NCl, Me_4NBr, Et_4NCl, Et_4NBr, Pr_4NCl, Pr_4NBr, Bu_4NCl, and Bu_4NBr in nitromethane has been determined over the concentration range 0.0001 to 0.01 N. Considerable attention has been given to the purity of the solvent and salts. Limiting conductances were determined by extrapolation of Λ–$\sqrt{c}$ plots. Although this method usually yields values which are slightly high, other methods were found not to be suitable to these electrolytes. The values obtained for Λ_0 were consistent with the Kohlrausch rule of independent ionic mobilities within experimental error. The deviations from the Onsager equation increased in the order $Bu_4NX < Pr_4NX < Et_4NX < Me_4NX$ in accordance with the decrease in ionic size, as indicated by the Λ_0 values. However, the chlorides appeared to be more associated than the bromides even though the Λ_0 values indicated Cl^- to be slightly larger than Br^- in solution. The Robinson–Stokes equation was found not to be applicable to these electrolytes.

Introduction

Conductance data precise to within a few parts in 10,000 have been recorded for aqueous and alcoholic solutions.[1-6] Such data have been important both in the testing and, indirectly, in the development of conductance theory. There are at present, however, virtually no conductance data of comparable caliber available for non-hydroxylic media. In the best work reported to date for these solvents, the great care taken with the electrical measurements has not, in general, been matched with similar care in the preparation and testing of the solvent and solute. The present investigation was undertaken to provide accurate data for nitromethane solutions of some quaternary ammonium halides over the concentration range 0.01 to 0.0001 N, at 25°. The following paper reports ionic conductances for these solutions.

Nitromethane was chosen as the solvent, since it has a dielectric constant in the "intermediate" range where other than the simple coulombic forces of the Debye–Hückel treatment should become important but where a good deal of dissociation will still be expected. Also, comparison of ionic behavior in nitromethane with that in methanol should be instructive, since the solvents have similar dielectric constants but differ chemically. The quaternary ammonium halides were chosen as solutes for reasons of solubility and because they form a homologous series useful for comparison purposes. The salts studied were tetramethyl-, tetraethyl-, tetrapropyl-, and tetrabutylammonium chlorides and bromides.

Experimental

The conductance measurements were made by the d.c. method using a modification[7] of the cell described by Gordon and coworkers.[8] Briefly, the method consists of passing a known current through the solution and measuring the potential drop across a portion of the solution by means of two probe electrodes; the conductance is then calculated from Ohm's law. In the present work, the probes were silver–silver chloride (or bromide) electrodes immersed in aqueous chloride (or bromide) solution. Contact with the nitromethane solution was made through the liquid junction formed between the water–nitromethane solutions in a Type A probe chamber.[7] The electrodes could not be im-

(1) T. Shedlovsky, *J. Am. Chem. Soc.*, **54**, 1411 (1932).
(2) B. B. Owen and H. Zeldes, *J. Chem. Phys.*, **18**, 1083 (1950).
(3) G. C. Benson and A. R. Gordon, *ibid.*, **13**, 470 (1945).
(4) J. P. Butler, H. I. Schiff, and A. R. Gordon, *ibid.*, **19**, 752 (1951).
(5) R. E. Jervis, D. R. Muir, and A. R. Gordon, *J. Am. Chem. Soc.*, **75**, 2855 (1953).
(6) J. R. Graham, G. S. Kell, and A. R. Gordon, *ibid.*, **79**, 2352 (1957).
(7) L. Elias and H. I. Schiff, *J. Phys. Chem.*, **60**, 595 (1956).
(8) H. E. Gunning and A. R. Gordon, *J. Chem. Phys.*, **10**, 126 (1942).

mersed directly in the more concentrated nitromethane solutions of halides owing to a fairly rapid dissolution of the silver halide coating. However, below concentrations of about 5×10^{-4} N the rate of dissolution was sufficiently low that the original Gordon cell could be used. In these cases, comparative tests further verified the previous finding that the conductivities measured by the liquid-junction-probe method were identical with those measured with the Gordon cell.

The Jones and Bradshaw 0.01 demal standard[9] was used to obtain the cell constant. The mean of six determinations yielded a value of 0.16461 ± 0.000006 cm.$^{-1}$ for the cell with liquid junction probes; the same cell with Gordon probes had a cell factor 0.02% lower. The capacity of the cell was about 150 cc. Solvent conductances were measured with a small a.c. cell and bridge circuit to within 3%.

The d.c. measurements were made in the manner described by Gunning and Gordon,[8] with the constant-current circuit modified to accommodate a 6SJ7 rather than 1B4 pentode. Difficulty encountered with the electrical measurements in hot, humid weather was effectively overcome by packing silical gel in the glass tubes surrounding the probe leads. The measurements were made after allowing the cell to stand one hour in an oil bath set at $25.000 \pm 0.005°$. The bath thermometer was periodically calibrated at the Thermometry Division of the National Research Council in Ottawa. Two calibrations taken one year apart showed a variation of 0.003°.

All solutions were prepared gravimetrically, the more dilute ones being prepared by dilution of different stock solutions. Sufficient amounts of materials were used to ensure an accuracy of better than 0.01% in the weighings. In the preparation and transferring of the solutions, precautions were taken to ensure a minimum exposure of the materials to air. These precautions included the use of a drybox for handling the more hygroscopic salts and the use of purified nitrogen under pressure for drying some of the glassware as well as transferring of solvents and solutions. Complete details of the handling technique may be found elsewhere.[10,11]

The nitromethane densities were determined with a pycnometer of the type described by Shedlovsky and Brown.[12] Salt densities used in correcting weights to vacuum were determined in a 25-cc. specific gravity bottle by displacement of ligroin. The pycnometers were thermostated in a water bath held at $25.00 \pm 0.01°$.

Nitromethane.—The method of purification was essentially that devised in this Laboratory by Tink[13] and Bulani[14]: distillation at reduced pressure followed by fractional crystallization.

Nitromethane was obtained from Commercial Solvents Ltd. as a clear, pale yellow liquid. A batch of 5 l. was distilled in a column 3.6 cm. in diameter and 300 cm. in height packed with glass helices. The distillation was carried out at 4–6 cm. pressure, which was regulated with a Cartesian manostat. The reflux ratio was adjusted to 10:1 using a conventional magnetic take off at the head of the column. First and last fractions of about 1.5 l. were rejected, a middle cut of 2 liters being retained. This distillate was fractionally crystallized by fitting the receiver flask with a smaller side-flask and placing the assembly in a wooden box packed with Dry Ice. The nitromethane was allowed to freeze while the box and its contents were agitated on a mechanical shaker. When all but about 200 cc. of the nitromethane was frozen, which required 4–6 hours, the crystallization was stopped and the unfrozen liquid containing the impurities was poured over into the side-flask. After the nitromethane came to room temperature, the side-flask was removed and the receiver flask stoppered. To obtain a clear, solid mass of frozen nitromethane, it was usually necessary to seed the liquid with a small crystal from a preliminary freezing. Once the solvent had been purified as above and used for conductance measurements, it could be recovered in a sufficiently pure state for further use by distillation alone.

Nitromethane contains higher-boiling and lower-boiling impurities, both of which lower the density. The densities of three successive 500-cc. fractions taken at the top of the still were 1.124, 1.130, and 1.131 g./cc. at 25°, while successive fractions taken at the bottom were 1.120, 1.119, and 1.116 g./cc. One crystallization of a rather impure sample raised the density from 1.129 to 1.130, the density of the discarded portion being 1.128 g./cc. The conductance of samples taken at the top or bottom of the still was the same, and is therefore no criterion for purity. After repeated distillations and crystallizations, the density of the solvent was 1.13124 ± 0.00004 g./cc. at 25°, and its specific conductance $0.5–1 \times 10^{-8}$ ohm^{-1} cm.$^{-1}$. The density found here compares favorably with that reported by Hartley,[15] although his conductance value is higher by a factor of 10, undoubtedly due to his distillation procedure at atmospheric pressure and consequent decomposition.

The purity of the nitromethane was determined absolutely by the freezing-curve method of Rossini.[16] About 100 cc. of nitromethane was placed in a vacuum-jacketed test-tube immersed in an acetone–Dry Ice slurry. The liquid was agitated by a vertically operated mechanical stirrer at 150 strokes/min. while dry nitrogen was blown in to exclude air moisture. The cooling rate was less than 2°/min. Temperatures were read off a Beckmann thermometer at recorded time intervals until about $^1/_3$ of the nitromethane was frozen. From a geometrical analysis of a time–temperature plot, the molar purity was found to be 99.96%. The particular sample of solvent used in the purity determination had a density of 1.13120 g./cc. and was certainly not the best product used for the conductance work. Nevertheless, conductivity data obtained with it were indistinguishable from data obtained using nitromethane of higher density. On the other hand, use of water-free solvent of density less than 1.130 g./cc. gave erroneous data. It is interesting to note that Dreisbach and Martin[17] found the purity of a nitromethane sample of density 1.12346 g./cc. to be 99.45%.

Titration of the purified solvent with Karl Fischer reagent[18] showed the water content to be less than 0.001% by weight. The titration procedure was standardized with sodium acetate trihydrate in methanol and checked against nitromethane samples to which small amounts of water had been added.

Corrections were made for the small water content of the solvent by measuring the effect of water on the conductivities of nitromethane solutions. Conductance measurements were made on 0.0005, 0.002, and 0.007 N Pr_4NBr solutions to which known amounts of water up to 0.04% by weight were added, the additions being checked by Fischer titration. After allowing for the slight change in Λ due to the small change in concentration, it was found that the increase in Λ for a given electrolyte concentration was linear in the amount of water added. One per cent by weight of water caused an increase of 7.3, 9.6, and 15.0%, respectively, in the conductances of 0.007, 0.002, and 0.0005 N solutions. A correction, amounting at most to a few hundredths of a Λ unit, was accordingly applied to the results.

The water content of a nitromethane solution left standing for three hours in the cell with liquid junction probes increased by less than 20%, indicating no serious contamination of the cell solution by the probe solution.

Quaternary Ammonium Halides.—The purity of the salts was estimated on the basis of the halide content as determined by gravimetric analysis. The analytical procedure was checked against "conductivity grade" KCl and KBr; the accuracy of the analysis is believed to be better than 0.03%.

After recrystallization from solution, the salts were dried *in vacuo* in an "Abderhalden" type of drying pistol, with a trap immersed in Dry Ice–acetone serving as the desiccant. The part of the drying tube holding the salt was heated by the vapors of a boiling liquid, the drying temperature being determined by the choice of liquid used. The effect of drying temperature on salt purity was the same for all the salts studied: at lower temperatures the purity improved as the temperature was increased, remained constant within a temperature range at higher temperatures, then finally deteriorated at still higher temperatures. Temperatures below 110° were not high enough for drying Pr_4NCl. In this low temperature region the length of drying time had only a slight effect on improving the purity; for example, a sample of Et_4NBr dried at 80° for 12 and 60 hours, respectively, analyzed as 99.55 and 99.57%, which are identical within the limits of analytical precision. Dried at 160° for 12 hours, the salt analyzed 99.97%. At higher tem-

(9) G. Jones and B. B. Bradshaw, *J. Am. Chem. Soc.*, **55**, 1780 (1933).
(10) L. Elias, Ph.D. Thesis, McGill University, 1956.
(11) A. K. R. Unni, Ph.D. Thesis, McGill University, 1958.
(12) T. Shedlovsky and A. S. Brown, *J. Am. Chem. Soc.*, **56**, 1066 (1934).
(13) R. R. Tink, Ph.D. Thesis, McGill University, 1953.
(14) W. Bulani, Ph.D. Thesis, McGill University, 1954.
(15) C. P. Wright, D. M. Murray-Rust, and H. Hartley, *J. Chem. Soc.*, 199 (1931).
(16) F. Rossini, *J. Res. Natl. Bur. Std.*, **35**, 355 (1945).
(17) R. R. Dreisbach and R. A. Martin, *Ind. Eng. Chem.*, **41**, 2875 (1949).
(18) K. Fischer, *Z. angew. Chem.*, **48**, 394 (1935).

peratures, 160° in the case of Pr_4NCl and 180° in the case of Et_4NBr, the salts underwent some decomposition, as indicated by a strong amine smell and decrease in purity; at these temperatures the length of drying time had a marked effect on the purity. The range of drying temperature best suited for each salt was determined by such trials. Salts prepared by alternate procedures and dried at the suitable temperature gave identical conductance results. All were used within a week or two after purification.

The densities of nitromethane solutions of the salts could be adequately expressed by

$$\rho = 1.13124 + b\bar{m}$$

where $\bar{m}$ is the concentration in moles/1000 g. of solution and b is a constant for each salt given below.

Me_4NCl and Me_4NBr were Eastman Kodak products recrystallized from methanol and twice precipitated from methanol by addition of ether. They were dried at 140° for 24 hours, and each analyzed as 99.98% halide. For Me_4NCl, salt density = 1.16 g./cc. and $b = 0.017$; for Me_4NBr, density = 1.58 g./cc. and $b = 0.057$.

Et_4NCl, Pr_4NCl, and Bu_4NCl were prepared by the metathesis of the corresponding iodides by AgCl in methanol, the conversion being checked by the starch test for iodide. After filtration through a sintered-glass funnel, the solutions were evaporated to dryness under vacuum. The ethyl salt was recrystallized from chloroform and precipitated from chloroform with ether, three times; it was dried at 140° for 24 hours; analysis 99.97%, density 1.37 g./cc., $b = 0$. The propyl salt was thrice precipitated from acetone with ether and dried at 132°; analysis 99.96%, density 1.10 g./cc., $b = -0.019$. The butyl salt, which was extremely hygroscopic, was given a preliminary drying at room temperature for 12 hours, then thrice precipitated from acetone with ether and dried at 56°; analysis 99.98%, m.p. 75°, density 1.1 g./cc., $b = -0.053$. The quaternary ammonium iodides used in the methateses were prepared by refluxing the alkyl iodide with the trialkyl amine in methanol for about 24 hours. The unreacted reagents were removed by extracting the solution with ligroin, after which the salts were recovered by evaporating the methanol layer to dryness under vacuum. The iodides so obtained were recrystallized in acetone and precipitated from acetone with ligroin.

Et_4NBr was an Eastman Kodak product precipitated from chloroform with ether and from methanol with ether. It was dried at 160°; analysis 99.97%, density 1.37 g./cc., $b = 0.010$. Pr_4NBr was prepared and purified in a similar manner to that described for the iodides, using *n*-propyl bromide in place of the iodide; it was dried at 132°, analysis 99.97%, density 1.19 g./cc., $b = 0$.

Bu_4NBr was prepared as suggested by Sadek.[19] Tri-*n*-butylamine and *n*-butyl bromide were refluxed in methanol for 30 hours. Water was added and the unreacted reagents extracted with ligroin. The water layer was cooled to a slush and dried *in vacuo* over P_2O_5. One batch of the crude product was recrystallized six times from benzene-ligroin mixtures, a second batch was precipitated three times from acetone with ether. The salt was dried at 80–100°; analysis 99.98%, m.p. 118.5°, density 1.13 g./cc., $b = -0.010$. An alternative preparation in which Bu_4NOH was neutralized with anhydrous HBr in methanol yielded a product of the same purity; the conductance data obtained using this sample agreed with the data derived using the first preparation within experimental precision.

Results and Discussion

Values of the equivalent conductance at round concentrations and limiting conductances are given in Table I. These were obtained from a large scale plot of the Shedlovsky function Λ_0' in a manner similar to that described by Benson and Gordon.[3] Such a plot was made from conductance measurements of at least 24 different solutions with concentrations spanning the concentration range given. The precision of the data over the concentration range 0.01 to 0.001 N was better than 0.02%, but decreased to 0.03% at the highest dilution. The Shedlovsky plots all exhibited pronounced minima except in the case of the methyl salts, where the curves lay entirely below Λ_0.[20]

Λ–$\sqrt{c}$ plots of the data were in all cases linear in the range 0.001 to 0.0005 N within experimental precision.

With the values $D = 36.67$[21] and $\eta = 0.627$ centipoise[15] for nitromethane at 25°, the Onsager equation becomes

$$\Lambda = \Lambda_0 - (0.708\Lambda_0 + 125.1)\sqrt{c}$$

The per cent deviations of these linear portions from the theoretical slopes are: Me_4NCl, 72; Me_4NBr, 55; Et_4NCl, 13; Et_4NBr, 10; Pr_4NCl, 10; Pr_4NBr, 5; Bu_4NCl, 8; Bu_4NBr, 4.

Except for the methyl salts, the quaternary ammonium halides in nitromethane are all reasonably strong electrolytes. The order of increasing ionic strength is $Me_4NX < Et_4NX < Pr_4NX < Bu_4NX$; this is also the order of increasing size of the cation in solution, if one attributes differences in Λ_0 to changes in ionic diameters. The behavior is therefore consistent with the smaller ion having the greater tendency to associate.

On the other hand, the chlorides appear to be more associated than the corresponding bromides, while, if Λ_0 is again taken as a measure of ionic size, the chloride ion is slightly larger than the bromide ion. This behavior is *not* consistent with the smaller ion having a greater tendency toward association. The inconsistency may be resolved by assuming that the radius of the migrating Cl^- is larger than that involved in the distance of closest approach with the cation. This assumption implies that the solvent molecules are loosely held by Cl^- and that the cation is able to penetrate the solvent sheath. Since nitromethane is aprotic and solvation of the anion probably occurs through weak ion–dipole interactions, this interpretation is not unreasonable. It is interesting to note the different behavior of these salts in methanol, for which Hartley has reported conductance data of the tetramethyl- and tetraethylammonium chlorides and bromides.[22] In methanol, where anion–solvent effects should be much stronger, Cl^- is also larger than Br^- but the chlorides are less associated than the bromides, in conformance with the more usual type of behavior.

The Λ_0 values listed in Table I were obtained by a least-squares analysis of the linear portion of the Λ–$\sqrt{c}$ plots. Although this extrapolation yielded Λ_0's for which the difference between bromides and chlorides was 0.22 for each cation within 0.01 Λ unit, the procedure is objectionable on theoretical grounds and leads to Λ_0's which are too high. It was adopted because none of the other available extrapolation methods proved superior. Extrapolation of the Λ_0'–c plots was uncertain because of the steep curvature at the dilute end, except for Pr_4NBr and Bu_4NBr; for these salts, Λ_0's derived from the Shedlovsky curves were 0.05 unit lower than those obtained from the Λ–$\sqrt{c}$ plots. Attempts to fit the data to the form[12] $\Lambda_0' = \Lambda_0 + Bc + Ec \log c$ were for the most part unsuccessful.

(19) H. Sadek and R. M. Fuoss, *J. Am. Chem. Soc.*, **72**, 301 (1950)

(20) The Shedlovsky plot for Bu_4NBr shown in the previous publication to illustrate the conductance method lies above Λ_0 over the entire concentration range. Further work in the dilute range revealed that the curve actually goes through a minimum near $c = 0.0005$ *n* and approaches Λ_0 from below.

(21) A. A. Maryott and E. R. Smith, Natl. Bur. Standards, Circ. 514 (1951).

(22) G. Unmack, R. Bullock, D. M. Murray-Rust, and H. Hartley, *Proc. Roy. Soc.* (London), **A132**, 427 (1931).

TABLE I

EQUIVALENT CONDUCTANCE AT ROUND CONCENTRATIONS

10^4c (g.-equiv./l.)	Equivalent conductance Λ							
	Me_4NCl	Me_4NBr	Et_4NCl	Et_4NBr	Pr_4NCl	Pr_4NBr	Bu_4NCl	Bu_4NBr
100	82.18	86.34	90.24	90.53	83.76	83.95	79.96	79.97
70	87.21	90.91	93.00	93.29	86.18	86.44	82.18	82.23
50	91.51	94.77	95.29	95.64	88.21	88.49	84.04	84.14
20	101.06	103.14	100.39	100.75	92.70	93.10	88.14	88.39
10	106.08	107.49	103.15	103.54	95.17	95.66	90.42	90.75
5	109.56	110.61	105.20	105.58	97.04	97.53	92.18	92.48
2	112.63	113.27	107.07	107.41	98.76	99.21	93.86	94.14
1	114.22	114.62	108.07	108.36	99.70	100.03	94.72	94.98
Λ_0	117.62	117.83	110.37	110.60	101.88	102.10	96.83	97.04

Similarly, a Fuoss–Shedlovsky treatment[23] of the data was also of limited use in determining Λ_0. In the case of the methyl salts, a straight-line relation between ΛS and $c(\Lambda Sf)^2$ existed at higher concentrations but deviated from linearity at lower concentrations. The propyl and butyl salts and Et_4NBr were amenable to the treatment only at concentrations below 5×10^{-4} N, although even here there was a tendency of the plots to curve upward. The Λ_0's obtained by this method were consistently lower by about a tenth of a Λ-unit than the values in Table I. An analysis of the data by the revised Fuoss–Onsager equation[24] is discussed in a subsequent paper.[25]

While some uncertainty exists in the extrapolations, it could by no means account for the discrepancy between Λ_0 for Bu_4NBr found here and that reported by Miller and Fuoss.[26] These workers give a value of 86.80 for this salt in nitromethane at 25°, which differs by more than 10 Λ-units from the present value. At least part of this discrepancy can be attributed to the low purity of their solvent, as indicated by its low density of 1.1251 g./cc. It may also have been contaminated by P_2O_5 from the distillation procedure used, as found in the investigation of Hartley[15] and Walden.[27]

A comparison of the Walden product $\Lambda_0\eta$ for the data of this research with work in other solvents is shown in Table II. The agreement between solvents is not too surprising, since all three have similar dielectric constants and are electron donors.

TABLE II

COMPARISON OF $\Lambda_0\eta$

	$\Lambda_0\eta$		
	Nitromethane (η = 0.627 cp.)	Nitrobenzene[28] (η = 1.1811 cp.)	Dimethylformamide[29] (η = 0.796 cp.)
Me_4NBr	0.738		0.738
Et_4NCl	.694	0.700	
Et_4NBr	.693		0.710
Pr_4NBr	.640		0.659
Bu_4NBr	.608	0.607	

The conductance equation of Robinson and Stokes[30] combined with the law of mass action was not applicable to the data of this research. No reasonable value of $\mathring{a}$ could be found for which the dissociation constant was invariant with concentration.

Acknowledgments.—The authors wish to thank the National Research Council for a grant-in-aid and for the award of Fellowships to L. E. They are also grateful for the award of a Columbo Plan Fellowship to A. K. R. U.

(23) R. M. Fuoss, *J. Am. Chem. Soc.*, **57**, 488 (1935). T. Shedlovsky, *J. Franklin Inst.*, **225**, 739 (1938).

(24) R. M. Fuoss, *J. Am. Chem. Soc.*, **81**, 2659 (1959).

(25) R. L. Kay, S. Blum, and H. I. Schiff, *J. Phys. Chem.*, **67**, 1223 (1963).

(26) R. C. Miller and R. M. Fuoss, *J. Am. Chem. Soc.*, **75**, 3076 (1953).

(27) P. Walden and E. J. Birr, *Z. physik. Chem.*, **A163**, 263 (1933).

(28) C. R. Witschonke and C. A. Kraus, *J. Am. Chem. Soc.*, **69**, 2472 (1947).

(29) P. G. Sears, E. D. Wilhoit, and L. R. Dawson, *J. Phys. Chem.*, **59**, 373 (1955).

(30) R. A. Robinson and R. H. Stokes, "Electrolyte Solutions," 2nd Edition, Butterworths Scientific Publications, London, 1959.

TRANSFERENCE NUMBERS AND IONIC CONDUCTANCES OF SOME QUATERNARY AMMONIUM CHLORIDE AND BROMIDE IONS IN NITROMETHANE AT 25°

By S. Blum and H. I. Schiff

Department of Chemistry, McGill University, Montreal, Canada

Received November 9, 1962

The transference numbers of Me_4N^+, Et_4N^+, Pr_4N^+, Bu_4N^+, Cl^-, and Br^- ions in nitromethane have been determined over the concentration range 0.0002 to 0.01 *N*. A combination of existing experimental techniques has been used which makes the moving boundary method applicable to most electrolytes. Limiting ionic conductances, calculated from these results and the equivalent conductances of the preceding paper, show these electrolytes to be fairly strong, with increasing strength in the order $Me_4NX < Et_4NX < Pr_4NX < Bu_4NX$. The chlorides are more associated than the corresponding bromide, although bromide appears to be the smaller ion. Comparisons of the Walden product and the ratios of ionic conductances for these ions in a number of solvents are discussed in terms of solvation effects.

Introduction

Development of new theories of electrolytes must be accompanied by accurate data on individual ion behavior in a variety of solvents. Although accurate equivalent conductance measurements have been reported for a number of non-aqueous solutions, experimental difficulties have, with few exceptions, restricted measurements of transference numbers to aqueous solutions.

The experimental difficulties stem mainly from the need to extend the measurements to highly dilute solutions in solvents of low dielectric constant. The normal optical methods for following a moving boundary cannot be used because of the vanishingly small differences in refractive indices between leading and indicator solutions. Recently, however, Lorimer, Graham, and Gordon[1] have developed a conductometric method for following such boundaries, which has been applied to solutions of alkali halides in ethanol.[2] This method has been used in the present work along with the liquid-junction technique described by Elias and Schiff.[3] This modification makes the conductometric method applicable to any electrolyte.

The present paper reports measurements of the transference numbers of tetramethyl-, tetraethyl-, tetrapropyl-, and tetrabutylammonium chlorides and bromides in nitromethane at 25°. The data have also been combined with the conductance data of the preceding paper[4] to obtain limiting ionic conductances.

Experimental

The transference cells were similar to those described by Kay and Gordon.[5] A falling boundary cell equipped with their type VIII shearing stopcock was used to obtain cation transference numbers of Me_4N- and Et_4N-halide solutions, with the corresponding Bu_4N-halide solutions serving as indicators.

A rising boundary cell equipped with a type III shearing stopcock was used to obtain anion transference numbers of Pr_4N- and Bu_4N-halide solutions, with the corresponding quaternary ammonium picrates serving as indicators. Measurements were restricted to these ions, since no other indicators could be found which had sufficiently high solubilities and large enough differences in ionic mobilities.

The volumes between microelectrodes were calibrated from the known transference numbers of aqueous KCl solutions.[6] Aqueous NaCl and LiCl solutions were used as indicators for the falling boundary cell and KIO_3 solutions for the rising boundary cell. These cell constants were obtained with an accuracy of better than one part in 3000 and were found to be independent of current, concentration of leading solution, or small deviations of indicator concentration from those required by the Kohlrausch ratio. Ratios of leading solution to indicator solution conductances determined from the recorder traces differed from those calculated from known conductance data for these solutions by about 5%. This is an improvement over the 10% deviations reported by Lorimer, *et al.*,[1] which can probably be attributed to an improvement in the rectifier circuit. The experimental ratios were found to be the same for all pairs of microelectrodes within experimental error.

As mentioned in the preceding paper,[4] nitromethane solutions of halides were found to dissolve silver halides. For this reason the type "A" liquid junction chambers of Elias and Schiff[3] were used in the cathode compartment of each cell. The cathodes consisted of 0.5 cm. × 1 cm. × 0.007 cm. strips of platinum which were silver-plated and dipped in fused silver halides. A sufficiently thick silver halide coating was obtained in this way to prevent stripping and ensuing gas evolution during electrolysis. Tests showed that no contamination of the nitromethane solutions resulted from the use of the probe chambers. The anodes consisted of bars of cadmium which showed no attack by the nitromethane solutions.

Purification of the solvents and the quaternary ammonium halides has been described in the preceding paper,[4] as have been the methods for preparing and handling the solutions. The quaternary ammonium picrates were prepared and purified by the method of Hirsch and Fuoss[7] and, before use, were dried under vacuum for 24 hours at 56°. Partial molal volumes of the picrate solutions were required for the volume corrections of the transference data. The densities of these solutions could be represented over the concentration range of interest by the equation $d = 1.13124 + bm$, where b is 0.0133 for Pr_4NPic and 0.0103 for Bu_4NPic.

For the falling boundary cell, the cathode side was closed and the volume correction was

$$\Delta V = T_{A^+}\bar{V}_{AX} + V_{Ag} - V_{AgX}$$

where T_{A^+} is the transference number of Bu_4N^+ and X is Cl or Br, and V_{AX} is the partial molal volume of the solute.

For the rising boundary cell, the anode side was closed and the volume correction was

$$\Delta V = T_{Pic^-}\bar{V}_{APic} + {}^1/_2\bar{V}_{CdX_2} - {}^1/_2V_{Cd} - \bar{V}_{AX}$$

where T_{Pic^-} is the transference number of picrate ion and A is either Pr_4N^- or Bu_4N.

The cell was immersed in a constant temperature bath regulated at 25.000 ± 0.005°. To minimize current leakage, the tubes surrounding the electrodes were filled with silica gel and the laboratory was air-conditioned.

The a.c. detection circuit was essentially identical with that described by Graham and Gordon[2] except for the rectifier section preceding the strip-chart recorder. An R.C.A. Type 2N-109

(1) J. W. Lorimer, J. R. Graham, and A. R. Gordon, *J. Am. Chem. Soc.*, **79**, 2347 (1957).
(2) J. R. Graham and A. R. Gordon, *ibid.*, **79**, 2350 (1957).
(3) L. Elias and H. I. Schiff, *J. Phys. Chem.*, **60**, 595 (1956).
(4) A. K. R. Unni, L. Elias, and H. I. Schiff, *ibid.*, **67**, 1216 (1963).
(5) R. L. Kay and A. R. Gordon, *J. Chem. Phys.*, **21**, 131 (1953).
(6) R. W. Allgood, D. J. Le Roy, and A. R. Gordon, *ibid.*, **8**, 418 (1940).
(7) E. Hirsch and R. M. Fuoss, *J. Am. Chem. Soc.*, **82**, 1018 (1960).

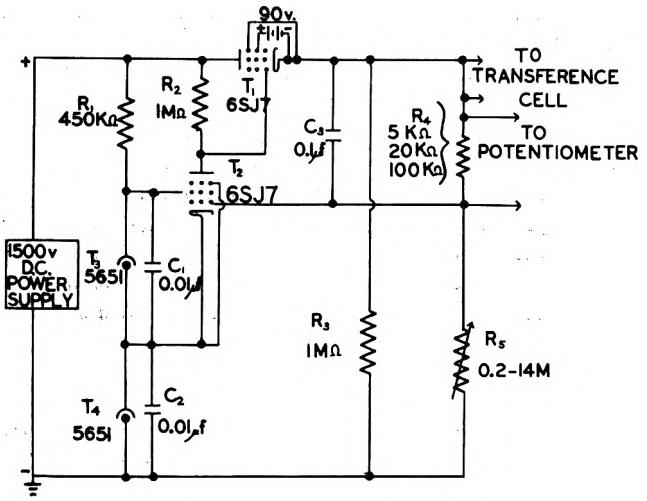

Fig. 1.—Constant current circuit.

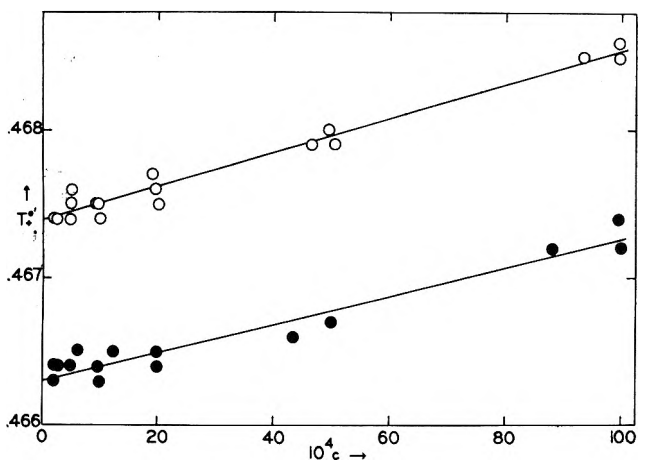

Fig. 2.—Longsworth function *vs.* concentration: ○, Me_4NCl; ●, Me_4NBr.

transistor was chosen because it provided a high degenerative bias on the incoming signal and produced very linear rectification.

Low currents were passed through the cell to prevent resistance heating from causing boundary instability; for dilute solutions in particular the energy generated in the boundary tube should be less than 0.1 watt.[8] The "feed-back" circuit shown in Fig. 1 provided currents from 5 to 500 microamperes which remained constant within 0.3% for a change in cell resistance of a factor of 2 and over a period of several hours. The current was determined from the voltage drop, measured potentiometrically, across a standard resistance in series with the cell. Current readings were taken every 200 seconds and averaged over the time required for the boundary to pass 2 sets of microelectrodes. The maximum possible error in the current measurements was 0.01%.

Time was measured with the combination of a pendulum clock (frequently checked against station WWV), an electric counter, and a chronograph pen on the recorder.

Results and Discussion

The transference number of each ion was measured for more than 20 different concentrations over the range 2×10^{-4} to 1×10^{-2} N. At each concentration at least two experiments were performed with different boundary currents. For experiments with the falling boundary cell, volume corrections were negative and amounted to 7 or 8 units in the last decimal place for the most concentrated solutions and became insignificant below 1×10^{-3} N. The volume corrections for the rising boundary cell were positive and about one-half as large as those for the falling boundary cell. Solvent corrections were necessary only for concentrations below 1×10^{-3} N and never amounted to more than 2 or 3 units in the last decimal place.

(8) A. R. Gordon, private communication.

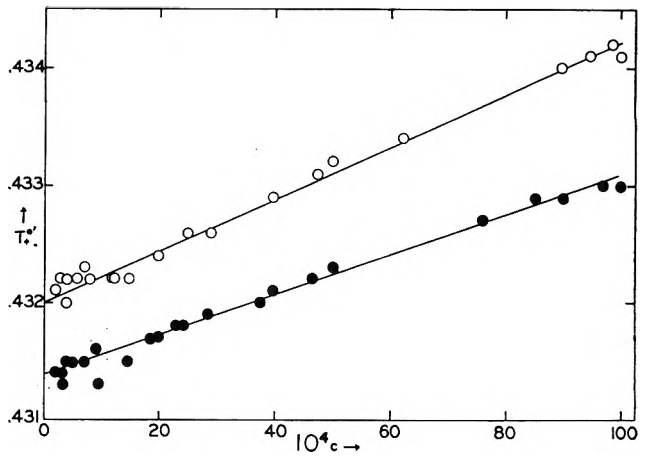

Fig. 3.—Longsworth function *vs.* concentration: ○, Et_4NCl; ●, Et_4NBr.

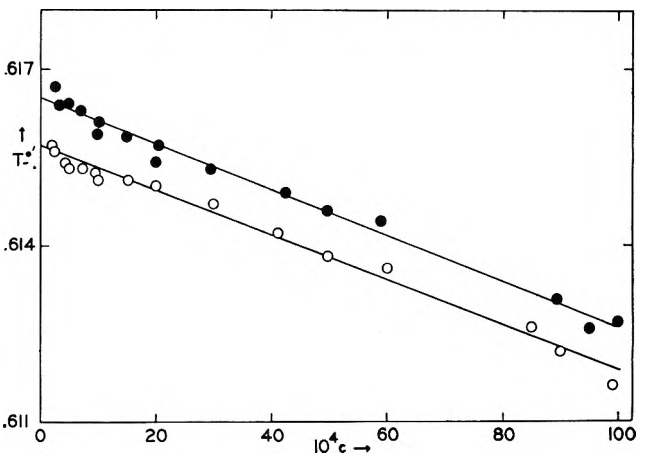

Fig. 4.—Longsworth function *vs.* concentration: ○, Pr_4NCl; ●, Pr_4NBr.

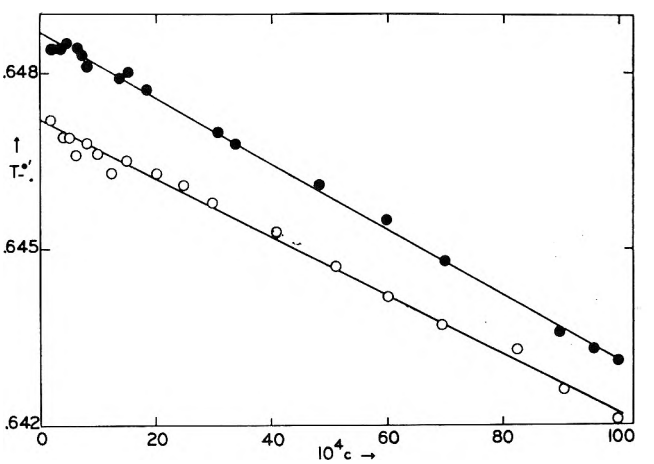

Fig. 5.—Longsworth function *vs.* concentration: ○, Bu_4NCl; ●, Bu_4NBr.

Figures 2–5 show that plots of the Longsworth[9] function $T^{0\prime}$ *vs.* C are linear in this concentration range and therefore permit accurate extrapolations to limiting values of the transference numbers. Such plots essentially represent deviations from theoretical behavior and can be used to show that the precision of the data is 0.04% at concentrations above 1×10^{-3} N and about 0.06% at lower concentrations. Transference numbers at rounded concentrations obtained from large scale plots of this type are shown in Table I.

(9) L. G. Longsworth, *J. Am. Chem. Soc.*, **54**, 2741 (1932).

TABLE I

TRANSFERENCE NUMBERS AT ROUND CONCENTRATIONS

$10^4 \cdot C$	Me_4NCl T^+	Me_4NBr T^+	Et_4NCl T^+	Et_4NBr T^+	Pr_4NCl T^-	Pr_4NBr T^-	Bu_4NCl T^-	Bu_4NBr T^-
100	0.4645	0.4631	0.4252	0.4240	0.6287	0.6298	0.6651	0.6661
50	.4652	.4639	.4271	.4261	.6252	.6261	.6601	.6614
20	.4659	.4648	.4287	.4280	.6218	.6227	.6555	.6569
10	.4663	.4653	.4297	.4290	.6201	.6209	.6531	.6547
5	.4667	.4656	.4304	.4297	.6188	.6197	.6515	.6529
2	.4669	.4658	.4310	.4303	.6177	.6187	.6499	.6514
0	.4674	.4663	.4320	.4314	.6157	.6165	.6474	.6487

The slopes of the T *vs.* $\sqrt{C}$ plots are negative and approach their limiting values from above when the transference number is less than 0.5 and *vice-versa* when the transference number is greater than 0.5. This behavior is similar to that reported by Longsworth[10] for strong aqueous solutions.

The Longsworth function can be modified for incompletely dissociated electrolytes to the form

$$T_j^{0\prime} = \frac{T_j\Lambda_e' + (B/2)\sqrt{\alpha C}}{\Lambda_e' + B\sqrt{\alpha C}}$$

where

$$\Lambda_e' = \Lambda^0 - (A\Lambda^0 + B)\sqrt{\alpha C}$$

The degree of dissociation α was calculated by the Fuoss–Shedlovsky method[11] and suggested the order of electrolytic strength to be $Bu_4N^+ > Pr_4N^+ > Et_4N^+ > Me_4N^+$ and $Br^- > Cl^-$. Straight lines could be drawn through plots of this modified Longsworth function *vs.* αC which were identical with the straight lines shown in Fig. 2–5. However, the experimental points fell closer to the lines when incomplete dissociation was assumed. Nevertheless, the high degree of dissociation calculated by the Fuoss–Shedlovsky method and the linearity of the Longsworth function do not support considering these to be weak electrolytes.

Limiting Ionic Conductances.—Table II presents limiting values of transference numbers and ionic conductances. The numbers in brackets were calculated from the Λ^0 values of the preceding paper and the experimental T^0 values, assuming $T_0^+ + T_0^- = 1$. Agreement of the limiting ionic conductances for a given ion, calculated from different salts, is within experimental error. The assumption that the sum of the limiting transference numbers is unity is justified by the agreement of the calculated λ_0 values with those determined experimentally for the same ion.

TABLE II

LIMITING IONIC CONDUCTANCES

Salt	Λ^0	T_+^0	T_-^0	λ_+^0	λ_-^0
Me_4NCl	117.62	0.4674	(0.5326)	54.97	(62.65)
Me_4NBr	117.83	.4663	(.5337)	54.94	(62.89)
Et_4NCl	110.37	.4320	(.5680)	47.68	(62.69)
Et_4NBr	110.60	.4314	(.5686)	47.71	(62.89)
Pr_4NCl	101.88	(.3843)	.6157	(39.15)	62.73
Pr_4NBr	102.10	(.3835)	.6165	(39.16)	62.94
Bu_4NCl	96.83	(.3526)	.6474	(34.14)	62.69
Bu_4NBr	97.04	(.3513)	.6487	(34.09)	62.95

Limiting ionic conductances provide a more satisfactory test of Walden's rule than do equivalent conductances. Values of the Walden product, $\lambda_0\eta$, are compared in Table III for five solvents. The ionic conductances in nitrobenzene were derived from the values quoted by Witschonke and Kraus[12] for Bu_4N^+. These authors found the value of Λ^0 for tetrabutylammonium triphenylborofluoride to be 23.8 ohm^{-1} cm.^{2} and assumed that, since the two ions were very large, they had identical ionic conductances. The ionic conductances in the other solvents were calculated from reported limiting equivalent conductances and transference numbers of the anions. It should be pointed out that some of the equivalent conductance values are from earlier literature and somewhat unreliable.

TABLE III

ION CONDUCTANCE–VISCOSITY PRODUCES IN VARIOUS SOLVENTS

Ion		CH_3NO_2	$C_6H_5NO_2$	CH_3OH	C_2H_5OH	H_2O
$1000\ \eta$		6.27	18.3	4.45	10.8	8.95
D		36.67	34.8	32.6	24.3	78.5
	λ_0	54.96	17.3	69.1	30.8[14]	44.92[17]
Me_4N^+	$\lambda_0\eta$	0.345	0.317	0.376	0.333	0.402
	$100\lambda_0\eta/D$	0.941	0.911	1.153	1.370	0.512
	λ_0	47.70	16.4	54.0	27.3[15]	32.66[17]
Et_4N^+	$\lambda_0\eta$	0.299	0.300	0.294	0.295	0.292
	$100\lambda_0\eta/D$	0.815	0.862	0.902	1.214	0.372
	λ_0	39.15	13.5	43.9	...	23.45[17]
Pr_4N^+	$\lambda_0\eta$	0.245	0.247	0.252	...	0.210
	$100\lambda_0\eta/D$	0.662	0.709	0.773	...	0.267
	λ_0	34.12	11.9	39.2[12]	...	19.13[17]
Bu_4N^+	$\lambda_0\eta$	0.214	0.218	0.214	...	0.171
	$100\lambda_0\eta/D$	0.584	0.626	0.656	...	0.218
	λ_0	62.70	22.2	52.38[13]	21.85[16]	76.36[18]
Cl^-	$\lambda_0\eta$	0.393	0.406	0.285	0.236	0.683
	$100\lambda_0\eta/D$	1.072	1.167	0.905	0.971	0.870
	λ_0	62.94	21.6	56.55[13]	23.51[16]	78.24[19]
Br^-	$\lambda_0\eta$	0.395	0.395	0.308	0.254	0.700
	$100\lambda_0\eta/D$	1.077	1.135	0.978	1.045	0.892

Reasonable agreement of the Walden product is obtained for the cations but not for the anions. This is not surprising since one of the tacit assumptions in Walden's use of Stoke's law is that the ions retain their radii as the solvent is changed, and one would expect a greater degree of solvation for the smaller anions than for the larger cations. The Walden product is, however, approximately constant for the anions in the 2 nitro-solvents which have almost the same dielectric constants. The product is not constant for the 2 alcohols which have different dielectric constants nor for methanol and nitromethane which have similar dielectric constants but are chemically different.

Account is taken of the dielectric constant in the function $\lambda_0\eta/D$, suggested by Van Rysselberghe and Fristrom[20] and shown for these solvents in Table III. This function improves the agreement between solvents for the anions but not for the cations.

The close agreement for all the ions in the 2 nitro-solvents may, perhaps, be taken as evidence in support of the assumption made by Witschonke and Kraus.

The relative solvation effects can be seen more clearly when limiting ionic conductance ratios are considered. Viscosity effects will tend to cancel and, if Stoke's

(10) L. G. Longsworth, *J. Am. Chem. Soc.*, **57**, 1185 (1935).

(11) R. M. Fuoss and T. Shedlovsky, *ibid.*, **71**, 1496 (1949).

(12) C. R. Witschonke and C. A. Kraus, *ibid.*, **69**, 2472 (1947).

(13) J. P. Butler, H. I. Schiff, and A. R. Gordon, *J. Chem. Phys.*, **19**, 752 (1951).

(14) T. H. Mead, O. H. Hughes, and H. Hartley, *J. Chem. Soc.*, 1207 (1933).

(15) H. Ulich and E. J. Birr, *Z. angew. Chem.*, **41**, 443 (1928).

(16) R. J. Graham, G. S. Kell, and A. R. Gordon, *J. Am. Chem. Soc.*, **79**, 2352 (1957).

(17) H. M. Daggett, E. J. Bair, and C. A. Kraus, *ibid.*, **73**, 789 (1951).

(18) H. E. Gunning and A. R. Gordon, *J. Chem. Phys.*, **10**, 126 (1942).

(19) H. E. Gunning and A. R. Gordon, *ibid.*, **11**, 18 (1943).

(20) P. Van Rysselberghe and R. M. Fristrom, *J. Am. Chem. Soc.*, **67**, 680 (1945).

law is assumed to apply to ions, the change in the ratio from one solvent to another should give information about the effective radii of the ions under consideration.[2] Table IV shows a number of these ratios. For the hydroxyl solvents the cation/anion ratios increase with decreasing dielectric constant and are much higher in the alcohols than in the nitro-solvents. This suggests a higher degree of solvation of anions in the alcohols and/or of cations in the nitro-solvents in agreement with the expected behavior of these solvents. Appreciable anion solvation in the alcohols has been suggested.[2] The ratios in nitromethane are somewhat larger than might have been expected from the aprotoic nature of thiss olvent. Althoughr ather unreliable, calculations of solvation numbers[21] indicate a small degree of solvation for the Me_4N^+ ion in nitromethane and little, if any, for the larger ions.

The anion/anion ratios show chloride to be the slower ion in all the solvents but nitrobenzene. Chloride would therefore appear to be the larger ion as a result of solvation and would be expected to be less associated. This is, however, contrary to the evidence obtained from the dependence on concentration of the transference numbers and equivalent conductances. This point has been discussed in the preceding paper.[4]

(21) R. A. Robinson and R. H. Stokes, "Electrolytic Solutions," 2nd Edition, Butterworth, 1959.

TABLE IV

LIMITING IONIC CONDUCTANCE RATIOS IN VARIOUS SOLVENTS

λ_j^0 – Ratio	CH_3NO_2	$C_6H_5NO_2$	CH_3OH	C_2H_5OH	H_2O
$\lambda^0_{Me_4N^+}/\lambda^0_{Cl^-}$	0.877	0.779	1.319	1.409	0.588
$\lambda^0_{Me_4N^+}/\lambda^0_{Br^-}$	.873	.801	1.222	1.311	.574
$\lambda^0_{Et_4N^+}/\lambda^0_{Cl^-}$	.761	.739	1.031	1.249	.427
$\lambda^0_{Et_4N^+}/\lambda^0_{Br^-}$	.758	.759	0.955	1.161	.417
$\lambda^0_{Pr_4N^+}/\lambda_{Cl^-}$	.624	...	...	...	.307
$\lambda^0_{Pr_4N^+}/\lambda^0_{Br^-}$	.622	...	...	...	.300
$\lambda^0_{Bu_4N^+}/\lambda^0_{Cl^-}$	.544	.536	0.765	...	.251
$\lambda^0_{Bu_4N^+}/\lambda^0_{Br^-}$	.542	.551	0.709	...	.245
$\lambda^0_{Cl^-}/\lambda^0_{Br^-}$	.996	1.028	0.926	0.930	.978
$\lambda^0_{Me_4N^+}/\lambda^0_{Et_4N^+}$	1.150	1.055	1.280	1.128	1.365
$\lambda^0_{Me_4N^+}/\lambda^0_{Pr_4N^+}$	1.404	...	...	...	1.916
$\lambda^0_{Me_4N^+}/\lambda^0_{Bu_4N^+}$	1.611	1.454	1.723	...	2.347

Cation/cation ratios decrease with increasing molecular weight and indicate the same order of ionic size. This can be taken as evidence against a large degree of solvation of the Me_4N^+ ion.

Acknowledgment.—The authors are indebted to the National Research Council of Canada for a Grant-in-Aid and for the award of several fellowships to S. B.

THE ELECTROPHORETIC AND RELAXATION CONTRIBUTION TO THE CONDUCTANCE OF SEVERAL QUATERNARY AMMONIUM CHLORIDES AND BROMIDES IN NITROMETHANE

BY ROBERT L. KAY,

Metcalf Research Laboratory, Brown University, Providence 12, R. I.

S. C. BLUM, AND H. I. SCHIFF

Department of Chemistry, McGill University, Montreal, Quebec

Received November 9, 1962

The conductance of tetramethyl-, tetraethyl-, tetrapropyl-, and tetrabutylammonium chlorides and bromides in nitromethane is analyzed by the Fuoss–Onsager conductance theory. Only the methyl salts are associated to any extent. The $\mathring{a}$ values range from 3.3 to 4.1 and are considerably lower than expected for the rather large ions involved. The values of the limiting ionic conductances obtained from Λ_0 and the limiting transference numbers are in fair agreement except for the tetramethyl salts. The electrophoretic contribution to the conductance has been calculated from the concentration dependence of the transference numbers and shown to agree with that predicted by the Fuoss–Onsager theory in most cases. Using the measured electrophoretic effect and the measured conductances, the relaxation contribution was determined and compared to that obtained from the Fuoss–Onsager equation using the same $\mathring{a}$ as was used to fit the conductance data alone. The slightly higher values of $\mathring{a}$ required are accounted for by a $C^{3/2}$ term eliminated from the electrophoretic effect in the conductance equation. The measured electrophoretic effect is the same for all the salts with possibly two exceptions whereas the extended terms in the relaxation effect are shown to be negative and to increase in magnitude with decreasing size of the cation. It would appear that the rather low $\mathring{a}$ values for these salts cannot be explained by a solution viscosity correction.

Introduction

In the two preceding papers, conductances[1] and transference numbers[2] for Me_4N-, Et_4N-, Pr_4N-, and Bu_4N- chlorides and bromides in nitromethane at 25° have been reported. These yield the first precise ion conductances in dilute solution for ions of considerable size variation and therefore permit a more thorough test of existing electrolyte theories than has been possible in the past. It is the purpose of this paper to report the results of an analysis of the data by the Fuoss–Onsager theory[3,4] and the Kay–Dye experimental method of evaluating the electrophoretic and relaxation contribution to conductance.[5]

A considerable number of investigations have been made as to the validity of the Fuoss–Onsager conductance equation.[6] It has been found to reproduce the measured conductances of the alkali halides in aqueous and methanol solutions but an assumption of association is required for solvents of lower dielectric constant.[7]

(1) A. K. R. Unni, L. Elias, and H. I. Schiff, *J. Phys. Chem.*, **67**, 1216 (1963).

(2) S. Blum and H. I. Schiff, *ibid.*, **67**, 1220 (1963).

(3) L. Onsager and R. M. Fuoss, *ibid.*, **36**, 2689 (1932).

(4) R. M. Fuoss and L. Onsager, *ibid.*, **61**, 668 (1957); **62**, 1339 (1958).

(5) R. L. Kay and J. L. Dye, *Proc. Natl. Acad. Sci.*, **49**, 5 (1963).

(6) E. C. Evers and R. L. Kay, *Ann. Rev. Phys. Chem.*, **11**, 21 (1960).

(7) R. L. Kay, *J. Am. Chem. Soc.*, **82**, 2099 (1960).

Atkinson and Hallada[8] have investigated the validity of the theory for a number of higher valence electrolytes in several solvents. Due to the fact that the ion size parameter was found to increase rapidly at very low dielectric constant, Lind and Fuoss[9] have concluded that significant higher order terms are missing in the theory. Direct evidence that the theory was inadequate at lower dielectric constant was obtained by Kay and Dye,[5] who showed that the association required by the Fuoss–Onsager theory for the alkali halides in ethanol was due entirely to an incorrect evaluation of the electrophoretic effect by the theory.

Theory and Method of Calculation

In its general form the Fuoss–Onsager conductance equation[4] can be expressed as

$$\Lambda = (\Lambda_0 - \Lambda_e)(1 + \Delta X/X) \qquad (1)$$

where Λ_e and $\Delta X/X$ are the contributions to the equivalent conductance from the electrophoretic and relaxation effect, respectively. The factor $1 + FC$, which takes into account the effect of bulk viscosity on the ion mobility, has been eliminated from the denominator of equation 1 since it can be evaluated only if solution viscosity data are available.[10]

In the limiting Onsager equation the electrophoretic terms is given by

$$\Lambda_e = \beta C^{1/2} \qquad (2)$$

and the relaxation term by

$$\Delta X/X = \alpha C^{1/2} \qquad (3)$$

whereas in the Fuoss–Onsager theory[3] Λ_e is given by

$$\Lambda_e = \frac{\beta}{1 + \kappa\mathring{a}} C^{1/2} \qquad (4)$$

where the symbols have their usual significance.[10] Using a dielectric constant of 36.67 and a viscosity of 0.627 centipoise for nitromethane at 25°,[2] α, β, and κ become 0.7176, 125.7, and $0.4810C^{1/2}$, respectively. The extended relaxation effect is a complicated function of solvent properties and of Λ_0 and $\mathring{a}$, the distance of closest approach of two ions. In order to be consistent in the elimination of terms of order $C^{3/2}$ or greater in the final conductance equation, equation 4 was expanded and used in the form

$$\Lambda_e = \beta C^{1/2} - \left(\frac{\beta\kappa\mathring{a}}{C^{1/2}}\right)C \qquad (5)$$

In its most convenient form the Fuoss–Onsager conductance equation for completely dissociated electrolytes can be written as

$$\Lambda = \Lambda_0 - SC^{1/2} + EC \log C + JC \qquad (6)$$

and as

$$\Lambda = \Lambda_0 - S(C\gamma)^{1/2} + EC\gamma \log C\gamma + JC\gamma - K_A C\gamma\Lambda f^2 \qquad (7)$$

for associated electrolytes. Again, the symbols in these equations have been explained in detail by Fuoss[10] and it is sufficient here to state that equation 6 contains the two parameters Λ_0 and J whereas equation 7 contains the added parameter K_A from which the degree of dissociation, γ, can be calculated. A value of $\mathring{a}$ can be calculated from J and it has been demonstrated[11] that if the viscosity correction $1 + FC$ is not included the only parameter affected is J and low values for $\mathring{a}$ result.

The unknowns in equation 6 and 7 were obtained from a least squares fit of the conductance data using an IBM 7070 computer and a Fortran program identical in all essentials with that used previously for the IBM 650 computer.[7] The experimental conductances[12,13] and transference numbers[14] were employed in the calculations in place of the interpolated values at rounded concentrations. All conductance data in the concentration range from 4 to 55 $\times 10^{-4}$ N were included except for 4 points out of a total of 115 points for the 8 salts. At appreciably higher concentrations ($\kappa\mathring{a} = 0.2$ at 64×10^{-4} N for $\mathring{a} = 5.0$) it was noted that the difference between observed and calculated conductances became large as predicted by the theory. No significant difference was obtained if the data were weighted by C or unweighted.

An essential feature of the ion atmosphere model as applied to electrolytic conductance is the fact that the relaxation terms $\Delta X/X$ in equation 1 are the same for both ions in any symmetrical electrolyte. As far as the individual ions are concerned these terms depend only on the distance of closest approach of the two ions and, therefore, could be different for any one ion depending on its partner but for any one symmetrical electrolyte must be the same for both anion and cation. Since a transference number is a ratio of the ion to the salt conductance, the relaxation terms cancel in the ratio.[15] The same is true for the viscosity term $1 + FC$. Since the variation of transference numbers with concentration depends only on the electrophoretic effect, the electrophoretic contribution to conductance can be determined directly from transference measurements.

Kay and Dye[5] have made use of the above fact to determine both the electrophoretic and relaxation effects for a number of systems. They express the transference number in terms of equation 1 and after cancellation of the relaxation terms obtained

$$T^+ = (\lambda_0^+ - \lambda_e^+)/(\Lambda_0 - \Lambda_e) \qquad (8)$$

Since for a 1:1 electrolyte $\lambda_e^+ = 0.5\Lambda_e$, rearrangement of equation 8 gave

$$\Lambda_e = \Lambda_0(T_0^+ - T^+)/(0.5 - T^+) \qquad (9)$$

from which an experimental Λ_e can be calculated provided the limiting conductance and transference number are known. Although conductance data are often difficult to extrapolate owing to association and to exponential terms in $\Delta X/X$, Λ_e is relatively insensitive to Λ_0. However, Λ_e is very sensitive to T_0^+ but, fortunately, transference numbers are insensitive to association and almost any theory produces the same extrapolated value of T_0. Transference numbers can best be extrapolated by rearranging equation 9 to give

(8) G. Atkinson and C. J. Hallada, *J. Am. Chem. Soc.*, **84**, 721 (1962).
(9) J. E. Lind, Jr., and R. M. Fuoss, *J. Phys. Chem.*, **65**, 999 (1961).
(10) R. M. Fuoss, *J. Am. Chem. Soc.*, **81**, 2659 (1959).
(11) R. M. Fuoss and C. A. Kraus, *ibid.*, **79**, 3304 (1957).
(12) L. Elias, Ph.D. Thesis, McGill University, 1956.
(13) A. K. R. Unni, Ph.D. Thesis, McGill University, 1958.
(14) S. Blum, Ph.D. Thesis, McGill University, 1961.
(15) R. H. Stokes, *J. Am. Chem. Soc.*, **76**, 1988 (1954).

TABLE I

CONDUCTANCE PARAMETERS AND CONSTANTS FOR EQUATIONS 6 AND 7

Salt	Λ_0	$\mathring{a}$	K_A	$\sigma\Lambda$	S	E	J	$\partial J/\partial \mathring{a}$
Me_4NCl	116.44 (0.03)	4.0 (0.2)	45 (1)	0.03	209.3	470.4	1283	254
Me_4NBr	116.89 (.03)	4.1 (.2)	31 (1)	.03	209.6	472.7	1295	255
Et_4NCl	110.06 (.02)	3.4 (.1)	2.0 (0.5)	.01	204.7	437.5	1063	256
Et_4NBr	110.45 (.01)	3.3 (.1)	1.7 (0.4)	.01	205.0	439.6	1041	260
Pr_4NCl	101.61 (.01)	3.64 (.02)	.....	.03	198.7	393.6	1044	233
Pr_4NBr	102.13 (.02)	3.44 (.03)	.....	.03	199.0	396.3	1003	238
Bu_4NCl	96.58 (.01)	4.12 (.03)	.....	.03	195.0	367.3	1104	214
Bu_4NBr	96.97 (.02)	3.19 (.03)	.....	.04	195.3	369.6	1061	218

$$T_0^+ = T^+ + \left(\frac{0.5 - T^+}{\Lambda_0}\right)\Lambda_e \qquad (10)$$

and using some theoretical value for Λ_e.

A good check of course can be made on Λ_0 and T_0 by appealing to Kohlrausch's law of independent ion mobilities. Equation 9 is valid even in the presence of considerable association and would give Λ_e at some salt instead of ion concentration.

Kay and Dye also derived the following expression for the relaxation terms for an unassociated 1:1 electrolyte by combining equations 1 and 9.

$$1 + \frac{\Delta X}{X} = \frac{\Lambda}{\Lambda_0}\left(\frac{T^+ - T^-}{T_0^+ - T_0^-}\right) \qquad (11)$$

For associated electrolytes $(1 + \Delta X/X)\gamma$ is obtained from equation 11. In the representation of the relaxation effect graphically it is convenient to define the quantity

$$\Delta\Lambda_r \equiv \Lambda - (\Lambda_0 - \Lambda_e)(1 - \alpha C^{1/2}) \qquad (12)$$

In this way the experimental electrophoretic effect and the limiting relaxation effect are removed from the measured conductances leaving only the extended terms in the relaxation effect and association terms in $\Delta\Lambda_r$.

In the Fuoss–Onsager[10] theory $\Delta\Lambda_r$ for an unassociated electrolyte is given by

$$\Delta\Lambda_r = EC \log C + J'C \qquad (13)$$

where

$$J' = J - \left(\alpha\beta + \frac{\beta\kappa\mathring{a}}{C^{1/2}}\right) \qquad (14)$$

If the electrolyte is associated, equation 13 becomes

$$\Delta\Lambda_r = EC\gamma \log C\gamma + J'C\gamma - K_AC\gamma\Lambda f^2 \qquad (15)$$

Results

The results of an analysis of the data by the Fuoss–Onsager conductance equation are given in Table I where the first four salts were treated by equation 7 and the last four by equation 6. The measured conductances could be reproduced within the precision given by $\sigma\Lambda$, the standard deviation, and the standard deviation for each unknown is given in parentheses. The magnitude of each term in the conductance equation for the chlorides can be seen in Table II.

The methyl salts appear to be associated to the extent of about 10% at 5×10^{-3} N, whereas the ethyl salts are slightly associated if at all and the propyl and butyl salts are completely dissociated. When the ethyl salts were treated as unassociated electroyltes (equation 6) Λ_0 was essentially unchanged and $\mathring{a}$ in each case decreased by only 0.3. Consequently, it would be unwise to claim association for the ethyl salts on the basis of these results, particularly when it is taken into account that the association term in equation 7 is linear in $C\gamma$ in the first approximation and difficult to separate from the $JC\gamma$ term.

TABLE II

COMPARISON OF THE MAGNITUDE OF THE TERMS IN EQUATION 6 AND 7 AT $C = 0.005$ N

Salt	$S(C\gamma)^{1/2}$	$EC\gamma \log C\gamma$	$JC\gamma$	$K_AC\Lambda\gamma f^2$
Me_4NCl	13.92	−4.90	5.68	11.74
Et_4NCl	14.43	−5.01	5.28	0.80
Pr_4NCl	14.05	−4.53	5.22	...
Bu_4NCl	13.79	−4.23	5.52	...

Two significant features of the $\mathring{a}$ values should be noted: much larger values and larger increases as the cation size increases are to be expected for these salts. Both of these observations could possibly be accounted for by the $1 + FC$ viscosity term that was not included in the Fuoss–Onsager equation but, as will be shown below, this explanation is unlikely.

With the exception of the methyl salts, the limiting conductances agree favorably with those obtained by a straight line extrapolation on a $C^{1/2}$ plot.[1] The differences which do exist could possibly be explained by the effect of the log term in the conductance equation.[4] The Λ_0 values for the methyl salts are approximately 1% higher than those obtained from a $C^{1/2}$ plot. The best check on the validity of the Λ_0 values can be obtained from a comparison of the limiting ionic conductances shown in Table III. There is good agreement in the limiting anion conductances for all the salts with the exception again of the methyl salts which are low by a considerable amount indicating that the Λ_0 reported here for these salts are inconsistent with the Λ_0 for the other salts. It is possible that equation 7 has converged to an incorrect value of Λ_0 in order to obtain the best fit of the data. However, if Λ_0 for Me_4NCl is set equal to 117.62, a value consistent with the Λ_0 for the other salts, a $K_A = 86$, and $\mathring{a} = 13$ were obtained from equation 7. The standard deviation of 0.5 showed that the fit was poor and the high $\mathring{a}$ indicated that the results were unreasonable. The same behavior was found for Me_4NBr. Thus the data for the methyl salts cannot be reproduced by equation 7 with a reasonable $\mathring{a}$ and a value of Λ_0 consistent with the data for the other chlorides.

In Fig. 1 the chloride ion conductances are shown for the concentration range over which the theories are applicable. Such plots should converge to the same intercept at infinite dilution. Data such as are shown in Fig. 1 have been used to obtain association constants[16] by assuming Kohlrausch's law of independent ion

(16) M. Spiro, *Trans. Faraday Soc.*, **55**, 1746 (1959).

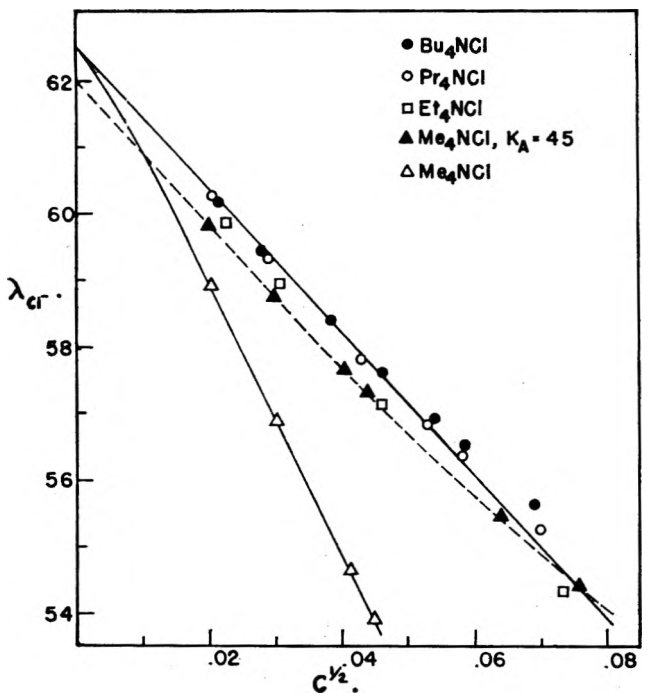

Fig. 1.—A plot of the chloride ion conductances over the concentration range investigated by the Fuoss–Onsager theory. The top solid line gives the Onsager limiting slope. The broken line passes through the results for Me_4NCl after correction for an association constant of 45.

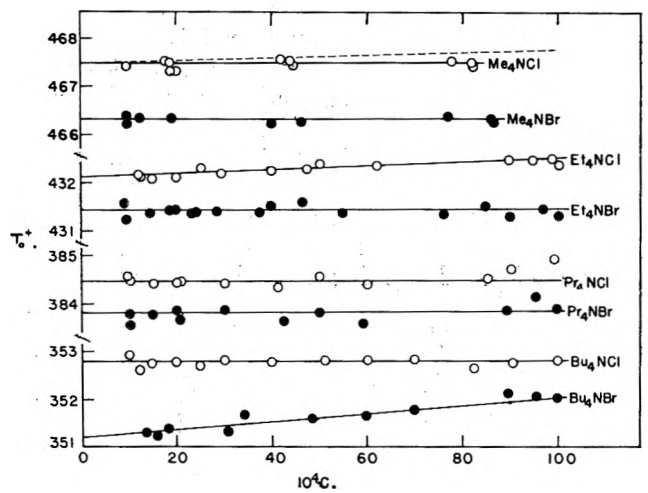

Fig. 2.—A plot of T_0^+ calculated from equations 4 and 10 using the same $\mathring{a}$ as was used in the equation to fit the conductance data. The association constants in Table I were used to calculate the results for the methyl salts. The broken line at the top gives the results for Me_4NCl when no association is assumed.

mobilities holds at finite concentrations and then attributing any difference to ion association. However, this method assumes the same contribution from the electrophoretic and relaxation effects for the common ion of the various salts, but theory predicts this will not be the case unless the distance of closest approach is the same for all the salts. It will be shown below that the differences in the chloride ion conductances for the ethyl, propyl, and butyl salts at finite concentrations can be explained by differences in the relaxation effect alone.

The much larger decrease in λ^- for the methyl salt is typical of an associated electrolyte but when corrected for an association constant of 45 the agreement is still poor at the dilute end and the intercept agrees with the λ_0^- in Table III. It can be seen in Fig. 1 that, with the exception of the methyl salt, the conductances all approach infinite dilution with small negative deviations from the limiting Onsager slope. This is typical behavior for salts in solvents with dielectric constants in the intermediate range. A similar plot for the bromide ion is identical in all essential features with that shown here for λ_{Cl^-}.

TABLE III

LIMITING IONIC CONDUCTANCES

Salt	T_0^+	λ_0^+	$\lambda^0_{Cl^-}$	$\lambda^0_{Br^-}$
Me_4NCl	0.4674	54.52	62.02	
Me_4NBr	.4663	54.51		62.38
Et_4NCl	.4321	47.56	62.50	
Et_4NBr	.4314	47.65		62.80
Pr_4NCl	.3845	39.07	62.54	
Pr_4NCl	.3838	39.20		62.93
Bu_4NCl	.3528	34.07	62.51	
Bu_4NBr	.3512	34.06		62.91

The limiting transference numbers in Table III were obtained by extrapolation of equation 10 to infinite dilution using the Fuoss–Onsager values of Λ_e (equation 4) and the $\mathring{a}$ from Table I. The resulting plots are shown in Fig. 2. The points for the methyl salts were calculated with the ion rather than salt concentration. If no association was assumed the broken line is obtained for Me_4NCl. The small difference illustrates how little transference numbers are affected by considerable association. The same intercept was obtained when the Onsager limiting values of Λ_e were used but the lines had large positive slopes[2] indicating that the Λ_e obtained from equation 2 are too high.

The important feature of these plots is the fact that T_0^+ values, calculated from the Fuoss–Onsager Λ_e using the same $\mathring{a}$ as is needed to fit conductance data, are independent of concentration up to 0.01 N with the exception of Et_4NCl and Bu_4NBr. The values of the experimental Λ_e calculated from equation 9 are shown in Table IV along with values of $\mathring{a}$ obtained in different ways. The numbers in parentheses in the last line are the estimates of the uncertainty in Λ_e due to an assumed uncertainty in T^+ of $\pm 2 \times 10^{-4}$. The first point to note is that up to a concentration of 5×10^{-3} N, the experimental Λ_e is the same for all the salts within experimental error. If the results for Et_4NCl and Br_4NBr are ignored the Λ_e is the same up to 0.01 N. The second point is that the limiting Onsager Λ_e is about one conductance unit higher than the experimental values at 5×10^{-3} N. Consequently, these results are an experimental demonstration of the fact that the success of the Onsager limiting slope in fitting conductance data (see Fig. 1) is due to a cancellation of errors in the limiting electrophoretic and relaxation terms.

The data in Table IV can be used to calculate $\Delta\Lambda_r$ (equation 12), the contribution to conductance from extended terms in the relaxation effect. The results are plotted in Fig. 3 and 4 for the chlorides and bromides, respectively. The points give the experimental $\Delta\Lambda_r$ values obtained from equation 12 using the measured conductances and smoothed values of Λ_e from equation 9. It can be seen that $\Delta\Lambda_r$ is negative indicating that the limiting Onsager electrophoretic effect is too small. Another interesting fact is that $\Delta\Lambda_r$ for the butyl and propyl salts is small in magnitude and linear in concentration except at the very dilute end. It can be seen that the relaxation effect becomes more negative as

TABLE IV

ELECTROPHORETIC CONTRIBUTION TO THE CONDUCTANCE COMPUTED FROM TRANSFERENCE DATA

	Et_4NCl	Et_4NBr	Pr_4NCl	Pr_4NBr	Bu_4NCl	Bu_4NBr
$\mathring{a}(J)$	3.0	3.0	3.6	3.4	4.1	3.9
$\mathring{a}(\Lambda_e)$	4.6	3.3	3.6	3.6	4.2	5.0
$\mathring{a}(\Lambda_r)$	2.7	3.0	3.9	3.6	4.3	3.9
10^4C			Λ_e			
5	2.8	2.8	2.7	2.7	2.6	2.6
10	3.7	3.8	3.7	3.7	3.7	3.7
25	5.7	5.8	5.8	5.8	5.7	5.7
50	7.6	8.1	8.0	8.0	7.8	7.7
75	9.0	9.6	9.5	9.5	9.3	9.1
100	10.0(0.25)	10.8(0.25)	10.7(0.15)	10.7(0.15)	10.5(0.1)	10.1(0.1)

the size of the cation decreases. This change is in the direction predicted by equation 13 on the basis of the distance of closest approach. However, association would also give the same effect as indicated by equation 15. One disturbing feature is the fact that the ethyl salts are the salts most likely to be associated but the $\Delta\Lambda_r$ for these salts show the best agreement with the theoretical values up to concentrations as high as 0.01 N. This illustrates the fact that association constants much lower than 5 can be considerably in error when determined from conductance measurements. Kay and Dye[5] have shown that association constants as high as 40 in ethanol solutions result from defects in the theoretical evaluation of the electrophoretic effect.

When the anions are considered it can be seen that $\Delta\Lambda_r$ for the bromides are more negative than those for the corresponding chlorides. The opposite behavior would be predicted from equation 13 since the bromides should have a larger $\mathring{a}$ than the chlorides. Association would also give the opposite behavior since, on the basis of size, the chlorides should be more associated than the bromides. Possibly the different behavior for the ethyl salts could be explained by assuming more association for the chlorides than the bromide but the excellent agreement with theory makes this assumption undesirable. At 0.01 N $\Delta\Lambda_r$ for the methyl salts is lower than -20 and, since the minimum value from equation 13 is -7, there is no doubt that the methyl salts are considerably associated.

The broken curves in Fig. 3 and 4 give the values of $\Delta\Lambda_r$ from equation 13 for various values of $\mathring{a}$. The Fuoss-Onsager theory predicts the correct form for the extended terms in the relaxation effect and gives the correct magnitude with reasonable values of $\mathring{a}$. It should be noted, however, that the $\mathring{a}$ (Λ_r) required to fit $\Delta\Lambda_r$ up to 5×10^{-3} N differ somewhat from the $\mathring{a}(J)$ required to fit the conductance data. This difference can be accounted for by noting that the electrophoretic contribution (equation 5) used in the conductance equation eliminates the next higher term and cross term

$$\left[\beta\left(\frac{\kappa\mathring{a}}{C^{1/2}}\right)^2 + \alpha\beta\frac{\kappa\mathring{a}}{C^{1/2}}\right]C^{3/2} \qquad (16)$$

which is contained in equation 4 which in turn agrees well with the experimental Λ_e from transference numbers. Owing to the low dielectric constant and viscosity of nitromethane, this term amounts to about 0.2 conductance unit at 0.05 N and accounts for the difference between $\mathring{a}(J)$ and $\mathring{a}(\Lambda_r)$ for the butyl and propyl salts. The agreement between theory and measurements in the case of the butyl salts is not as good as for the propyl salts and explains why the value of $\mathring{a}(J)$ depended on the highest concentration used in the analysis of conductance data by equation 6.

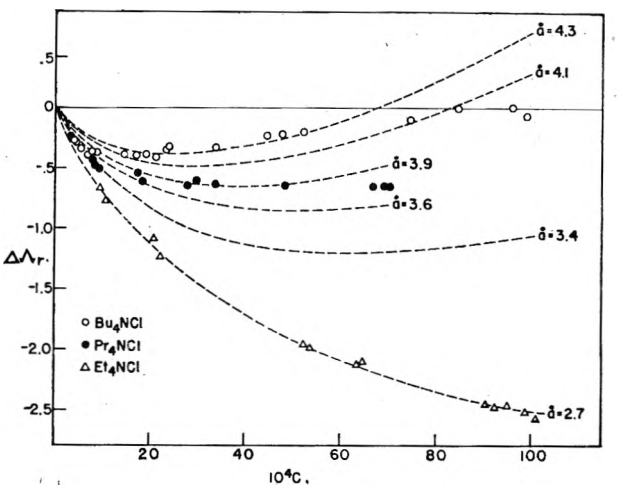

Fig. 3.—The points give the values of $\Delta\Lambda_r$ obtained from transference and conductance data for the chlorides (equation 12) while the broken curves give $\Delta\Lambda_r$ obtained from equation 13 for the indicated values of $\mathring{a}$.

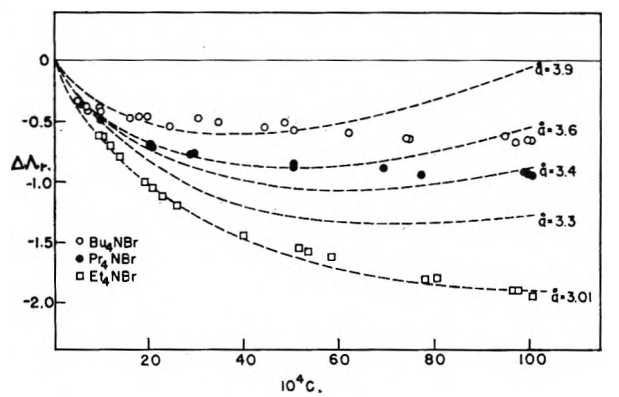

Fig. 4.—The points give the values of $\Delta\Lambda_r$ obtained from transference and conductance data for the bromides (equation 12) while the broken curves give $\Delta\Lambda_r$ obtained from equation 13 for the indicated values of $\mathring{a}$.

The various $\mathring{a}$ values obtained are listed in Table IV. The differences between $\mathring{a}(\Lambda_r)$ and $\mathring{a}(J)$ have been explained above. The differences between $\mathring{a}(\Lambda_r)$ and $\mathring{a}(\Lambda_e)$ are readily explained by the fact that a large change in $\mathring{a}$ produces a small change in Λ_e whereas $\Delta\Lambda_r$ is about 3.5 times as sensitive to changes in $\mathring{a}$.

The results obtained here show that the Fuoss–Onsager theory gives the correct evaluation of the electrophoretic and relaxation effects to within about 0.1 conductance unit since the same $\mathring{a}$ fits both conductance and transference data. Also, the results

indicate that equation 4 instead of equation 5 should be used to evaluate the electrophoretic effect. Kay and Dye[5] reached the same conclusion in their analysis of data for the alkali halides. These results also indicate that the inclusion of the $(1 + FC)$ term cannot be used to explain the rather low $\mathring{a}$ values obtained for the relatively large ions involved. For example, if $\mathring{a}(J)$ for Bu_4NCl is increased by 1 Å. due to the inclusion of this term, Λ_e as calculated from equation 4 would be 0.25 lower than the experimental value obtained from transference numbers. This is a significant difference and indicates that the same values of $\mathring{a}$ would not fit both conductance and transference data. This result will cast considerable doubt on the validity of the $1 + FC$ term for nitromethane solutions if it is shown from viscosity measurements to be large. Since equation 4 rather than equation 5 appears to give the better evaluation of the electrophoretic effect, possibly a better method of handling equation 6 would be to plot Λ^* given by

$$\Lambda^* \equiv \frac{\Lambda - EC \log C}{1 - \alpha C^{1/2}} + \Lambda_e = \Lambda_0 + \frac{J'C}{1 - \alpha C^{1/2}} \quad (17)$$

against $C/(1 - \alpha C^{1/2})$ using an initial value of $\mathring{a}$ to calculate Λ_e if transference data are not available. From the slope J' a better value of $\mathring{a}$ could be obtained and convergence should be rapid since Λ_e is insensitive to $\mathring{a}$.

Acknowledgment.—This work was supported by contract AT(30-1)2727 with the U. S. Atomic Energy Commission (R. L. K.) and by a grant from the National Research Council of Canada.

VISCOSITY OF POLYALKYL METHACRYLATE PLASTICIZED WITH DIETHYL PHTHALATE. I. POLY-*n*-BUTYL METHACRYLATE

BY AKIO TERAMOTO, REISUKE OKADA, AND HIROSHI FUJITA

Department of Polymer Science, Osaka University, Osaka, Japan

Received November 9, 1962

Thev iscosity of a sample of poly-*n*-butyl methacrylate (PBMA) in diethyl phthalate (DEP) was measured, using six different kinds of viscometer, over the complete range of composition (*i.e.*, 0 to 100% in polymer weight fraction) and over the temperature range from 0 to 120°. Plots for the logarithm of viscosity *vs.* weight fraction of polymer at temperatures above 60° showed a curvature convex downward in the region approaching pure solid. This type of viscosity–concentration relation had not been observed in previous studies on other typical amorphous polymers, but is similar to that found very recently for polyethylene mixed with low molecular weight paraffin. The free volume theory of Fujita and Kishimoto for the viscosity of very concentrated solutions of an amorphous polymer has been modified so that effects of the density of chain entanglements may be taken into account. The assumption that the free volumes of polymer and plasticizer are additive has also been discarded. Instead, it has been assumed that the free volume of a given polymer–plasticizer mixture increases linearly with temperature. The free volume theory so modified was found to account well for experimental data in the region where the volume fraction of DEP is smaller than about 0.2. Beyond this limit the analysis in terms of the modified theory led to an anomalous conclusion that the dilution of the density of chain entanglements produces an *increase* of the viscosity of this polymer–plasticizer system. This appears to indicate that the range of concentration in which the free volume theory may be applied may not be as wide as so far supposed.

Introduction

The series of polyalkyl methacrylates offers an excellent opportunity for studying effects of side chain length on physical properties of long chain molecules. Thus various authors have concerned themselves with subjects such as intrinsic viscosity and light scattering in dilute solution[1-3] and viscoelastic[4-6] and dielectric[7-9] dispersions in pure solid and in concentrated solution. The glass transition temperature for this series of polymers has been studied by Rogers and Mandelkern[10] and by Willbourn.[11] Literature survey indicates, however, that no systematic study has yet been performed for the viscosity of solutions of polymethacrylate polymers over the complete range of composition.[12] The present series of study purports to provide such experimental data, in the hope of obtaining information which may aid in understanding how the viscous behavior of a linear polymer molecule in bulk and in concentrated solution is affected by the length of its side chain. Also we are interested in examining, with these new data, the scope of the free volume theory developed by Fujita and Kishimoto[14] for the viscosity of very concentrated polymer solutions.

This paper reports data for poly-*n*-butyl methacrylate in diethyl phthalate. The data cover measurements over the complete range of composition at a number of temperatures between 0 and 120°. To make comparison as definitive as possible all the subsequent studies in this series, which deal with other members

(1) S. N. Chinai and co-workers, *J. Polymer Sci.*, **17**, 391 (1955); **19**, 463 (1956); **21**, 417 (1956); **22**, 555 (1956); **25**, 413 (1957); **33**, 471 (1958); **39**, 363 (1959); **41**, 475 (1959).

(2) H. T. Lee and D. W. Levi, *ibid.*, **47**, 449 (1960).

(3) C. Jen-yuan and S. Liang-ho, *Z. physik. Chem.*, **207**, 60 (1957).

(4) J. D. Ferry and co-workers, *J. Colloid Sci.*, **12**, 53, 327, 389 (1957); **13**, 103 (1958); **14**, 135, 222, 239 (1959); **17**, 10, 409 (1962).

(5) E. A. W. Hoff, D. W. Robinson, and A. H. Willbourn, *J. Polymer Sci.*, **18**, 161 (1955); see also ref. 11.

(6) S. Iwayanagi and T. Hideshima, *J. Phys. Soc. Japan*, **8**, 368 (1953).

(7) G. Offergeld, *Nature*, **178**, 1460 (1956).

(8) L. de Brouckere and G. Offergeld, *J. Polymer Sci.*, **30**, 105 (1958).

(9) S. Strella and co-workers, *ibid.*, **25**, 97 (1957); **25**, 105 (1958); **31**, 45 (1958); *J. Colloid Sci.*, **13**, 459 (1958).

(10) S. S. Rogers and L. Mandelkern, *J. Phys. Chem.*, **61**, 985 (1957).

(11) A. H. Willbourn, *Trans. Faraday Soc.*, **54**, 717 (1958).

(12) The only published viscosity data covering the complete range of polymethacrylate concentration are those of Bueche[13] for polymethyl methacrylate in diethyl phthalate.

(13) F. Bueche, *J. Appl. Phys.*, **26**, 738 (1955).

(14) H. Fujita and A. Kishimoto, *J. Chem. Phys.*, **34**, 393 (1961).

of this series of polymers, will be made with this same organic liquid as diluent.

Experimental

Materials.—The polymer, poly-*n*-butyl methacrylate (hereafter abbreviated PBMA), was prepared according to the procedure which follows. A commercial *n*-butyl methacrylate was washed with water, treated with aqueous Na_2CO_3 to remove hydroquinone and again washed with water. After it had been dried over anhydrous magnesium sulfate, the monomer was fractionally distilled under nitrogen atmosphere of about 8 mm.; 200 g. of the purified monomer, 700 g. of acetone, and 2 g. of azobisisobutyronitrile were mixed and then refluxed for 25 hours. The polymer formed was precipitated in a large bulk of methanol, dried under reduced pressure, and again precipitated from an acetone solution. Finally, it was freeze dried from a benzene solution. The yield of polymer was 160 g. PBMA comes to the theta condition in isopropyl alcohol at 23.7°.[15] The limiting viscosity number of our PBMA under this condition was 0.122 dl./g., which gives a viscosity-average molecular weight of 1.11×10^5 when use is made of the relation given in reference 15. No fractionation of the sample was effected.

The diethyl phthalate (hereafter abbreviated DEP) used as plasticizer was of technical grade. It was put in actual use after drying over anhydrous sodium sulfate and distilled under a pressure of 2.0–2.5 mm. Its refractive index n^{14}_D was 1.50484 and its density at 20° was 1.1190 g./cm.^{3}. These data stand in good agreement with literature values.[16]

Preparation of Solutions.—Solutions below 60 wt.% in PBMA were made up by sealing weighed amounts of PBMA and DEP in a bottle and allowing it to stand at 60–70° for a few days. Since no uniform mixture was obtained with this simple method for higher polymer concentrations, known amounts of polymer and plasticizer were first dissolved in acetone and the acetone was removed by evaporation initially at room temperature and finally at 80°. Complete removal of the solvent was checked by successive weighing of the container. The pure polymer was studied in the coaxial falling cylinder viscometer and in the tensile creep apparatus, details of which are described below. When use was made of the former apparatus, the sample was melted, cooled down to room temperature, and then placed in the working section of the viscometer. Creep measurement was made with a thin film of the sample cut into a narrow strip. An acetone solution of the sample (about 10 wt. %) was cast onto the surface of clean mercury, and the solvent was allowed to evaporate slowly overnight at room temperature. The film formed was peeled off the mercury surface by dipping the whole assembly in water, and was dried *in vacuo* at 50°.

Apparent Specific Volume.—The apparent specific volume of DEP, V_s, measured pycnometrically over the range 20–60°, fitted accurately the relation

$$V_s = 0.893_6 + 7.4_6 \times 10^{-4}(\theta - 20) \qquad (1)$$

where θ is the temperature (centigrade). This relation slightly differs, in the thermal coefficient, from that reported by Fujita and Maekawa,[17] but we believe that the new equation would be more accurate. Density measurements made for the 20 wt. % solution over the range 15–30° yielded for the apparent specific volume V the relation

$$V = 0.903_1 + 7.2_5 \times 10^{-4}(\theta - 20) \qquad (2)$$

Rogers and Mandelkern[10] have given the apparent specific volume of pure PBMA, V_p, over a wide range of temperature. The values of V calculated for $w_2 = 0.2$ (w_2 is the weight fraction of polymer) from their V_p data and relation 1 for V_s, with the assumption that no volume change occurs on mixing PBMA and DEP, agree well with those calculated from equation 2. In view of this result, and partly because density measurements for highly viscous solutions such as those treated in this study are quite difficult, we were content with knowing V values for other concentrations by substituting equation 1 for V_s and the data of Rogers and Mandelkern for V_p into the equation

$$V = (1 - w_2)V_s + w_2V_p \qquad (3)$$

(15) S. N. Chinai and R. J. Valles, *J. Polymer Sci.*, **39**, 363 (1959).
(16) "The Merck Index," Merck & Co., Inc., Rahway, N. J., 1952, p. 417.
(17) H. Fujita and E. Maekawa, *J. Phys. Chem.*, **66**, 1053 (1962).

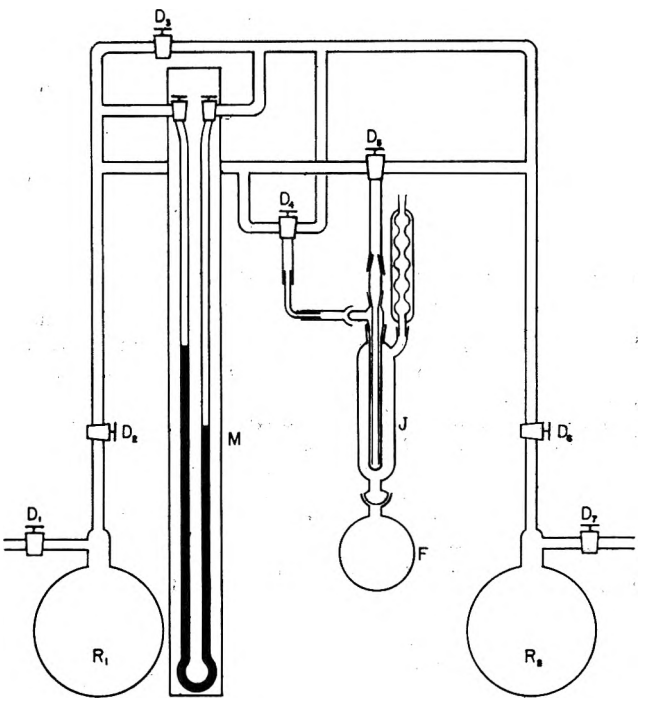

Fig. 1.—Schematic diagram of pressure controlling system for operation of pipet type viscometer and uniform bore viscometer.

which represents the additivity of the volumes of polymer and plasticizer.

Apparatus and Procedure.—We employed six viscometers of different design, depending on the magnitude of viscosity to be measured; Ostwald viscometer (10^{-2}–10^1), pipet type viscometer (10^{-2}–10^2), uniform bore capillary viscometer (10^2–10^6), falling ball viscometer (10^0–10^6), coaxial falling cylinder viscometer (10^4–10^{11}), and tensile creep apparatus (10^{11}–10^{13}). The numbers in parentheses indicate the range of viscosity in poises measured with each instrument.

Figure 1 shows the pressure controlling system constructed for operation of viscometers of the pipet type and the uniform bore type. In designing this system, reference was made to the description given by Takayanagi.[18] Argon was used to apply external pressure to the sample liquid in the capillary tube. In the temperature range below 90° water from a Haake thermostat was circulated through jacket J, with flask F removed and the lower end of the jacket connected to the thermostat with a rubber tubing. The temperature at the working section was then regulated to within ±0.1°. Above 90° jacket J was thermostated by filling it with constant boiling vapor; the accuracy of temperature control was ±0.5°. *n*-Heptane, water, toluene, and 1-butanol were used to obtain vapor of desired temperatures above 90°.

For the determination of viscosity η with the pipet type viscometer, use was made of the relation

$$1/t = (k/\eta)(p_0 + p_1) \qquad (4)$$

which follows immediately from Poiseuille's law for the viscous flow of a newtonian liquid through a straight pipe.[18] Here t is the efflux time for a fixed volume of liquid, p_1 is an externally applied pressure, p_0 is a mean pressure head of the liquid column itself, and k is a constant characteristic of the instrument. We used two capillary tubes whose k values were 7.82×10^{-4} and 2.19×10^{-2} (poise cm.$^{-1}$ sec.$^{-1}$). These k values were determined by calibrating the respective capillaries with 10 and 30 wt. % solutions of the present polymer–plasticizer system, after we had determined the absolute viscosities of these solutions from measurements with the Ostwald viscometer and the falling ball viscometer, respectively. In the actual use of equation 4, t was measured for a series of different p_1 with a fixed value of p_0, and the value of η was obtained from the slope of the resulting plot for $1/t$ *vs.* p_1. In all cases studied with this type of viscometer, this plot was accurately linear.

(18) M. Takayanagi, in "Kobunshi Zikkengaku Koza," Kyoritsu Publ. Co., Tokyo, 1958, Vol. III.

The basic equation for the uniform bore capillary viscometer may be written

$$d(P - B \ln P)/dt = \rho^2 r^2 g/8\eta \qquad (5)$$

where

$$P = B \mp \rho h \qquad (6)$$

$$B = p_1 \pm \rho h_0 \qquad (7)$$

In these equations, t is the time, ρ is the density of the sample liquid, r is the radius of the capillary, g is the acceleration of gravity, h is the length of the liquid column from the lower end of the capillary, h_0 is the length of the portion of capillary that is immersed in the sample liquid, and p_1 is an externally applied pressure. The minus and plus signs in equation 6, and the plus and minus signs in equation 7, correspond, respectively, to the ascending and descending of the liquid through the capillary tube. According to equation 5, if the liquid is newtonian, its viscosity may be determined from the slope of a plot for $P - B \ln P$ *vs.* t. For a given p_1 this plot can be obtained by measuring h as a function of time; h_0 should vary with time as the liquid is pressed up or down through the capillary, but it is possible to design the experiment so that such a variation of h_0 may be ignored.[18]

Equation 5 is inconvenient for use with liquids of very high viscosity, because the slope of $P - B \ln P$ against t becomes too small to be determined with precision. In this case, if the liquid is assumed to be newtonian, use may be made of the equation[18]

$$\eta = \frac{r^2 g\{p_1 \mp \rho[(h_1 + h_2)/2 - \lambda]\}}{4(h_2^2 - h_1^2)} \Delta t \qquad (8)$$

where Δt is the time in which the liquid meniscus in the capillary descends (plus sign) or ascends (minus sign) the distance $\Delta h = h_2 - h_1$. For this equation to be valid the experiment has to be made under such a condition that the pressure P defined by equation 6 is maintained sensibly constant during Δt. This condition is well satisfied if Δh is chosen sufficiently small in comparison to $(1/2)(h_1 + h_2)$ and p_1 is not too small.[18]

In actual evaluation of η with the uniform bore capillary viscometer we made use of the above two methods, depending on the magnitude of η to be determined. It should be noted that this type of viscometer permits absolute determination of viscosity, whereas either the Ostwald type or the pipet type viscometer needs calibration with a liquid of known viscosity. The movement of the liquid meniscus was followed by a traveling microscope reading to 0.01 mm.

Measurements by the falling ball method were performed using steel bearing balls of six different sizes[19] and three glass tubes (about 20 cm. long and about 2 cm. in diameter). The ball's density was obtained by weighing an appropriate number of balls of different sizes and calculating their total volume from the measured diameter values. Thus the value 7.765 g./cm.^{3} was obtained for 12°; this is nearly equal to the density of steel containing 1% carbon. The ball's densities at other temperatures were calculated from this value assuming a value of 3.6×10^{-5} deg.$^{-1}$ for the thermal expansion coefficient. As mentioned before, the density of a given solution at a given temperature was calculated by substituting equation 1 for V_s and the Rogers–Mandelkern data for V_p into equation 3. When fairly large, the velocity of a falling ball was determined from the time in which a given ball moves down for a fixed distance. In practice, the mean of several determinations was taken as the required value. When the liquid was so viscous that the ball fell too slowly, the position of the ball was measured, by means of a traveling microscope, as a function of time and the velocity was obtained from the slope of the resulting plot. The velocities measured in these ways ranged from 1.566×10^{-5} to 1.75 cm./sec. For the calculation of η use was made of Stokes law with the Faxén correction for wall effect.[18] It was found that above 10^4 poises the viscosity values thus obtained depended slightly on the size of the ball used. This is a manifestation of non-newtonian behavior; the effective rate of shear on the surface of a falling ball decreases with decreasing ball diameter. In this case, apparent viscosities were plotted against falling velocity and the desired viscosity was taken as the limit of such a plot at zero velocity.

The coaxial falling cylinder viscometer was a loan from Dr. A. Kishimoto of the Department of Fisheries, Kyoto University, Maizuru. It had originally been constructed in accordance with the design of Fox and Flory,[20] but the steel rod in the original instrument was replaced by an aluminum rod. Before they were put together, the two stainless steel blocks, on which a given polymer–plasticizer mixture or a premolten pure polymer had been loaded, were heated to 60–120° for an appropriate period of time so that air bubbles contained in the sample might be removed. The temperature of the sample was regulated by a small heater inserted in one of the two blocks or by crushed ice packed in plastic bags that were placed in a metal box enclosing the instrument. In this way, any temperature between 1 and 120° was obtained with a fluctuation less than ±0.5°. The velocity of the rod required for the calculation of viscosity was determined from the steady-state portion of a plot of Δh against time, where Δh is the distance fallen by the rod. Above 10^8 poises the viscosity measured in this instrument varied more or less with the total force acting on the rod, *i.e.*, the weight of the rod itself and the externally applied load. In this case, the required viscosity was estimated by graphical extrapolation of measured viscosities to zero total load.

Tensile creep measurements were made by suspending the sample strip (1 cm. wide, 6–10 cm. long, and 0.15 mm. thick) in a glass tube (6 cm. in diameter and 30 cm. tall) sealed at one end. The bottom of the tube was filled with P_2O_5 to prevent the sample from plasticization due to water vapor. The upper end of the strip was fixed relative to the top of the tube, and the desired load was applied to the sample by hanging an appropriately chosen weight from the clamp attached to the lower end of the strip. A simple screw system was devised so that the weight could be suspended without taking off the top of the tube. The glass tube was immersed, nearly up to its upper edge, in a constant temperature water-bath. Elongation of the sample was followed by a traveling microscope reading to 0.01 mm. The viscosity was evaluated by making use of the method proposed by Ninomiya,[21] in which values of $[J(t)/t][d \log J(t)/d \log t]$ are plotted against $1/t$ and the resulting plot is extrapolated graphically to $1/t = 0$; the intercept equals the inverse of the viscosity required. Here $J(t)$ is the creep compliance and t is the time from the start of experiment. In calculating $J(t)$ from elongation measurements we applied the usual correction for the change in sample cross section accompanying the increase in elongation. The viscosity value determined from the above experiment refers to the viscosity in tension, and cannot be compared directly to the viscosity in shear obtained from any one of the other viscometers used in this study. Due to the lack of data for the Poisson ratio of the present polymer–plasticizer system, we have simply assumed that one third of the measured viscosity in tension is equal to the viscosity in shear. Furthermore, we have assumed that within the range of applied load used here the creep data were independent of rate of elongation.

Results

Viscosity as a Function of Temperature and Concentration.[22]—Figure 2 plots the logarithm of viscosity (in poises) against temperature with the weight fraction of polymer, w_2, as parameter. Data determined by different viscometers are shown by different symbols. One can see that in the temperature range where data were taken by more than one method, the results from different instruments agree well with each other; also one observes that for a given w_2 sets of data covering different temperature ranges fall on a single smooth curve.

The trend of the system of curves shown in Fig. 2 is similar to that found previously for other polymer

(19) Several balls were randomly chosen from each group of specified size and their diameters were measured to an accuracy of 0.001 mm. in a "Universal Contour Projector" (Nihon Kogaku Co.). For each ball the measurement was made for two perpendicular diameters and the mean was taken as the desired value. The values so obtained were 0.500, 0.800, 1.191, 1.500, and 2.000 mm., all at 12°. These are in good agreement with the values specified by the manufacturer (Tsubakimoto Kokyu Mfg. Co.).

(20) T. G Fox, Jr., and P. J. Flory, *J. Am. Chem. Soc.*, **70**, 2384 (1948).

(21) K. Ninomiya, Ph.D. Thesis, Kyoto University, 1961.

(22) A table of complete numerical data may be obtained by writing to H. Fujita.

(amorphous) and diluent systems, such as polymethyl acrylate in DEP,[17] polystyrene in diethylbenzene,[23] and polystyrene in dibenzyl ether.[24] Recent data of Kishimoto[25] on polyvinyl acetate in DEP also exhibit a quite similar behavior. Sometimes it is reported that the plot for ln η *vs.* temperature for pure polymer showed inflection at a temperature near the glass transition point of the polymer. The data of Fig. 2 do not show this type of behavior; the glass transition point of pure PBMA is reported by Rogers and Mandelkern[10] to be at 20°, and a little higher value (27°) has been quoted by Child and Ferry.[26] In this connection, however, we must mention that we are not very convinced of the accuracy of our measurements for pure polymer at temperatures below 40°. In this region, the viscosity was so enormous that it was quite doubtful whether we were able to approach the steady-state creep in the interval of time of our measurement.

Figure 3 shows log η as a function of w_2 with temperature as parameter. The points plotted are not directly measured values but have been taken from the smooth curves drawn in Fig. 2. At first glance this system of curves looks quite similar to those of the the polymer–diluent systems quoted above. However, close inspection reveals a feature which distinguishes this polymer–plasticizer system from others referred to above. This is the curvature of the plot in the region near pure polymer. In the other systems mentioned, the data in this region follow, at all temperatures examined, a curve that is convex *downward;* that is, the slope of log η *vs.* w_2 increases as the pure solid is approached. In Fig. 3 one can see this type of behavior in the plots for temperatures below 60°. However, the plot for 80° is almost linear over a range down to about 80 wt. % in polymer, and above 80° the plot becomes convex *upward* in the concentration region in question. Thus one can see that the curves at temperatures above 80° have two inflection points, one at $w_2 \approx 0.5$ and the other at $w_2 \approx 0.8$.

Non-Newtonian Behavior.—For viscosities below 10^3 poises no shear-rate dependence was detectable. Above $10^{3.5}$–10^4 poises the viscosity determined by the uniform bore capillary viscometer decreased more or less with total pressure head (approximately in a linear fashion). Figure 4 shows an example of such data. The desired viscosity was obtained by extrapolating this type of plot to zero pressure head. Data from the falling ball viscometer decreased slightly with increasing the size of ball when they were above 10^4 poises, and the desired viscosity free of size effects was estimated in the manner described in the Experimental section. In the coaxial falling cylinder viscometer the shear-rate dependence appeared when measured values of η were larger than 10^8 poises. The zero shear-rate viscosity was determined by the extrapolation procedure as illustrated in Fig. 5.

In these ways, when necessary, we corrected all data for non-newtonian effects, except for those from creep measurements. This point may be stressed, because non-newtonian effects are generally so appreciable in concentrated solutions of a long chain molecule that

(23) F. Bueche, *J. Appl. Phys.*, **24**, 423 (1953).
(24) T. G. Fox, S. Gratch, and S. Loshaek, in "Rheology," edited by F. R. Eirich, Academic Press, Inc., New York, N. Y., 1956, Vol. I, Chap. 12.
(25) A. Kishimoto, *J. Polymer Sci.*, in preparation.
(26) W. C. Child and J. D. Ferry, *J. Colloid Sci.*, **12**, 327 (1957).

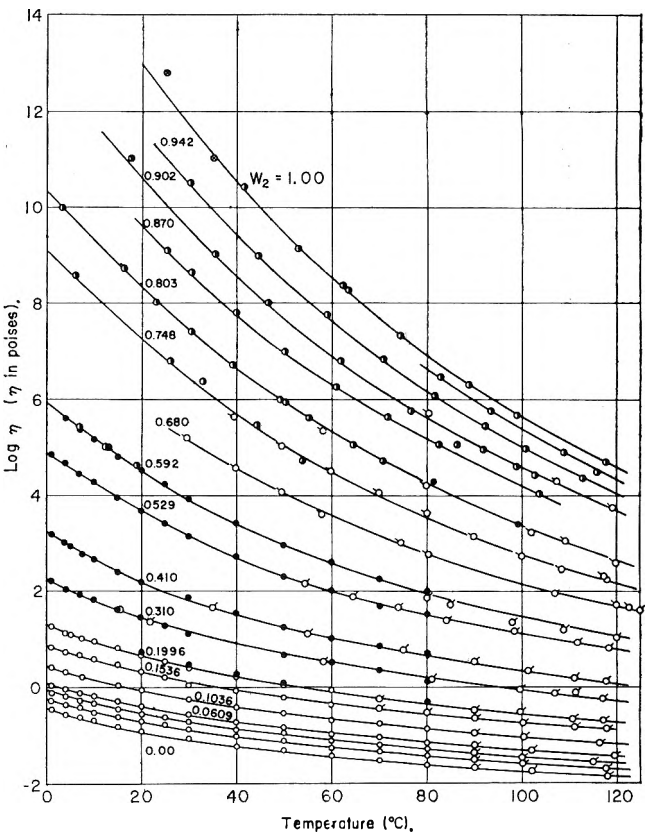

Fig. 2.—Plots of log η *vs.* temperature as a function of weight fraction of PBMA (w_2): O, by Ostwald viscometer; ⊙, by pipet type viscometer; ◔, by uniform bore viscometer; ●, by falling ball viscometer; ◑, by falling cylinder viscometer; ⊗, by creep apparatus.

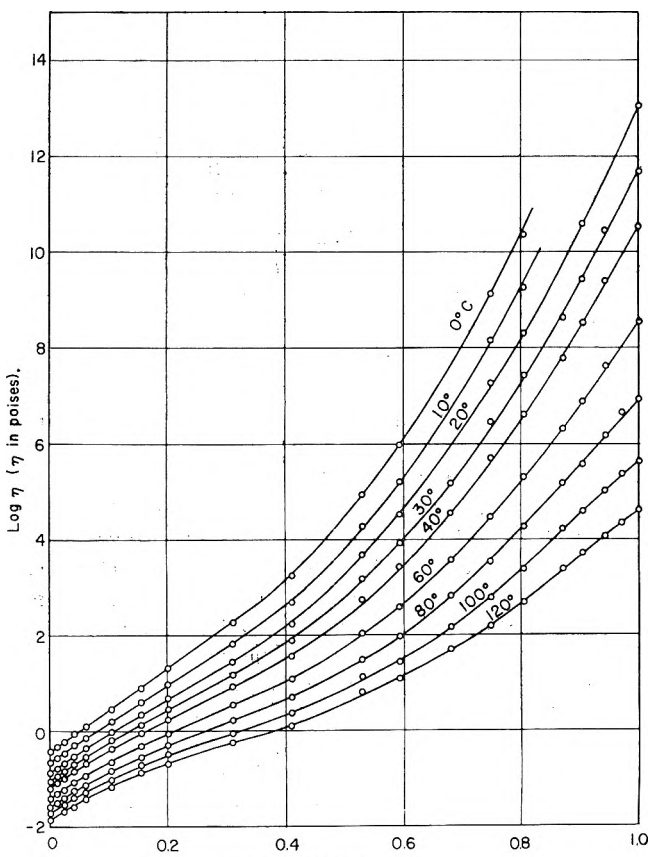

Fig. 3.—Plots of log η *vs.* weight fraction of PBMA as a function of temperature.

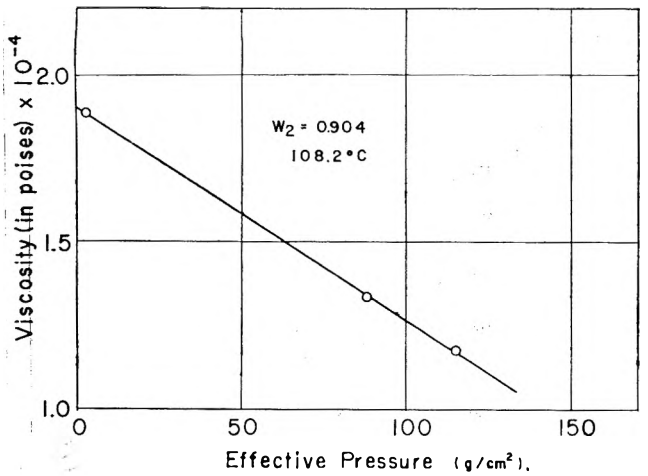

Fig. 4.—Example of pressure dependence of viscosity in uniform bore viscometer.

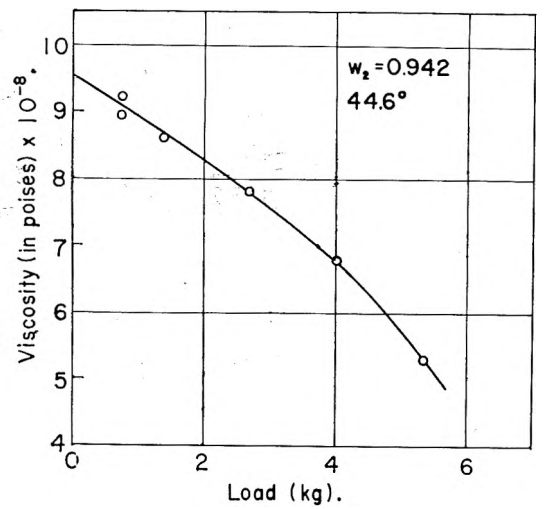

Fig. 5.—Example of load dependence of viscosity in coaxial falling cylinder viscometer.

unless such effects are eliminated, experimental data obtained may be of less value for quantitative discussion of viscosity behavior of such a system.

Discussion

Free Volume Theory.—Fujita and co-workers[14,17,27] have shown that the free volume theory developed by Fujita and Kishimoto[14] for the viscosity of very concentrated polymer solutions accounted well for experimental data on typical amorphous polymers, such as polystyrene, polymethyl methacrylate, polymethyl acrylate, and polyvinyl acetate. In an unpublished study with polyvinyl acetate in DEP Kishimoto[25] has given an additional evidence for the validity of the Fujita–Kishimoto theory. This theory, hereafter referred to as the F–K theory, predicts that at a fixed temperature ln η increases with w_2 following a curve which is convex downward.[28] All the systems so far chosen for the test of the F–K theory showed this type of behavior in the region near pure polymer in which it is expected that the F–K theory is most reliably applicable. The data shown in Fig. 3 reveal that this behavior is not a common feature of amorphous polymer–diluent systems; plots for ln η *vs.* w_2 of the present polymer–diluent system at temperatures above about 80° are either linear or convex *upward* in the concentration region approaching the pure polymer. Incidentally, with polyisobutylene in cetane at temperatures far above the glass transition point of the polymer Ninomiya and Ferry (personal communication) have found plots for ln η *vs.* w_2 which were convex upward down to a polymer concentration of about 60 wt. %. Unpublished data of Kishimoto (personal communication) for polyisobutylene in decalin at similar temperatures demonstrate an analogous curvature even over the complete range of concentration. When converted in the form of ln η *vs.* w_2 the recent data of Busse, *et al.*,[29] for polyethylene mixed with various paraffin waxes give curves having a similar curvature over the complete range of concentration. It is not clear to us what factor is mainly responsible for this new type of dependence of viscosity on concentration. In this connection, it may be worth noticing that these polyisobutylene and polyethylene systems have been studied in the region far above the glass transition temperature of each polymer.

It appears too early to conclude, with these new findings, that any attempt to account for the viscosity behavior in concentrated polymer solutions in terms of the free volume concept is little promising. Close examination of the F–K theory tells that, besides the assumption of the Doolittle type of equation[30] for the monomeric friction coefficient, it contains several approximations which are either to be more clarified or to be preferably taken out. In what follows, an attempt is described that has been made to improve the F–K theory with respect to these points.

If we assume the Doolittle type of equation for the monomeric friction coefficient, the viscosity of a solution in which the volume fraction of diluent is v_1 may be represented by the equation[14]

$$\eta(v_1,T) = KM^{3.4}(1 - v_1) \exp[1/f(v_1,T)] \quad (9)$$

where T is the temperature of the solution, M is the molecular weight of the dissolved polymer (assumed to be monodisperse), f is the fractional free volume in the solution, and K is a factor which has been supposed by Fujita and Kishimoto[14] to depend on the density of interchain entanglements in solution. Equation 9 is concerned with a solution so concentrated in polymer that M is above the critical molecular weight M_c corresponding to the concentration and temperature of the given solution. The exponent 3.4 to M is the empirically accepted value for such a value of M, but it is immaterial for the subsequent discussion. Based on the reason that no definite information is yet available for K, Fujita and Kishimoto have assumed this factor as being independent of concentration and temperature, at least in the region near pure polymer. However, if, as they supposed, K is related in a way to chain entanglements in solution, it is unlikely that this assumption would be legitimate. In the treatment which follows, this factor is left as a parameter which may depend on concentration, but not on temperature. This neglect of the temperature dependence of K appears reasonable, because, as can be estimated from the data for V_s and

(27) (a) H. Fujita and A. Kishimoto, *J. Polymer Sci.*, **28**, 547 (1958); (b) H. Fujita, A. Kishimoto, and K. Matsumoto, *Trans. Faraday Soc.*, **56**, 424 (1960).

(28) Correctly, we must state this in terms of the plot for ln $(\eta/1 - v_1)$ *vs.* v_2, where v_1 and v_2 are the volume fractions of diluent and polymer.[14] For solutions very concentrated in polymer, however, the difference in general trend between ln η *vs.* w_2 and ln $(\eta/1 - v_1)$ *vs.* v_2 is immaterial.

(29) W. F. Busse and R. Longworth, *J. Polymer Sci.*, **58**, 49 (1962).

(30) A. K. Doolittle, *J. Appl. Phys.*, **22**, 1471 (1951); **23**, 236 (1952).

V_p mentioned before, the present polymer–plasticizer mixture at any concentration expands thermally to such a negligible extent that no significant change with temperature may occur in the density of chain entanglements. The notation $K(v_1)$ will be used for K to indicate its dependence on concentration only. Based on the assumption that the free volume produced in a given system by the addition of a diluent is in proportion to the volume of diluent added, Fujita and Kishimoto[14] have deduced the expression

$$f(v_1,T) = f(0,T) + \beta(T)v_1 \qquad (10)$$

where $\beta(T) = \gamma(T) - f(0,T)$, and $\gamma(T)$ is a function of temperature only which may be related, but not necessarily be equal, to the free volume of the diluent. Equation 10 would be reasonable at least for sufficiently small values of v_1, but in the present treatment this equation will not be assumed.

Instead of assuming equation 10 we make use of the assumption that for a fixed value of v_1 the fractional free volume $f(v_1,T)$ increases linearly with temperature. This may be written

$$f(v_1,T) = f(v_1,T_0) + \alpha_f(v_1)(T - T_0) \qquad (11)$$

where T_0 is a reference temperature chosen in accordance with the indication given below and $\alpha_f(v_1)$ is a function of v_1 only which may be regarded as the thermal expansion coefficient of f. With the amazing success of the WLF equation[31,32] demonstrated for a variety of polymer systems, equation 11 is now widely accepted to give a good representation of the temperature dependence of f, provided T is not close to T_g, the glass transition temperature of the given system, nor greatly above T_g. Thus, for equation 11 to be valid the reference temperature T_0 must be chosen in the corresponding region, generally 40–50° above T_g.

We substitute equation 11 into equation 9, with K replaced by $K(v_1)$, and define a quantity a_T by

$$a_T = \eta(v_1,T)/(v_1,T_0) \qquad (12)$$

Then, after some rearrangement, we obtain

$$-\frac{T - T_0}{\ln a_T} = \frac{[f(v_1,T_0)]^2}{\alpha_f(v_1)} + f(v_1,T_0)(T - T_0) \qquad (13)$$

This relation predicts a linear variation of $-(T-T_0)/\ln a_T$ with $T - T_0$; $f(v_1,T_0)$ and $\alpha_f(v_1)$ may be evaluated from the slope and the intercept at $T - T_0 = 0$ of the straight line. Substitution of these values into equation 11 allows calculation of f for other temperatures at the given value of v_1. Of course, it is meaningless to extend this calculation to a temperature at which equation 13 is not obeyed. The above procedure may be repeated for other values of v_1 to determine f as a function of v_1 and T.

The values of $f(v_1,T)$ so obtained and the experimentally measured values of $\eta(v_1,T)$ are now introduced into equation 9 to calculate $KM^{3.4}$ as a function of v_1 and T. The results summarize effects other than those predicted from the free volume theory of Fujita and Kishimoto.

Analysis of Data.—Viscosity data for use in the above calculation for a_T and K must refer to fixed values of v_1. In the polymer–plasticizer system studied in this work the value of v_1 at any fixed w_1 changes by negligible amount with temperature in the entire temperature range treated. For this reason we made a test of equation 13 with the data given in Fig. 2, where ln η at various fixed values of w_2 are shown as a function of temperature. Figure 6 shows $-(T - T_0)/\ln a_T$ plotted against T for several values of w_2; the points indicated have been derived from the smooth curves drawn in Fig. 2. The value of T_0 for each concentration was chosen in such a way that it is nearly 50° above the glass transition temperature T_g of the polymer–plasticizer mixture considered. For the concentration dependence of T_g in this system we referred to the data summarized by Ferry.[32] It is seen that our a_T data follow the expected linear relation in the region above a certain critical temperature which becomes lower as the polymer is more plasticized. Below the critical temperature the plots deviate upward from the straight line, in all the cases examined. The values of $f(v_1,T_0)$ calculated from the slopes of the linear portions of the curves in Fig. 6 have been converted to $f(v_1,60°)$ using the values of $\alpha_f(v_1)$ also determined from these linear portions, and are shown in the lower part of Fig. 7. In the upper section of this figure are shown the values of α_f as a function of v_1.

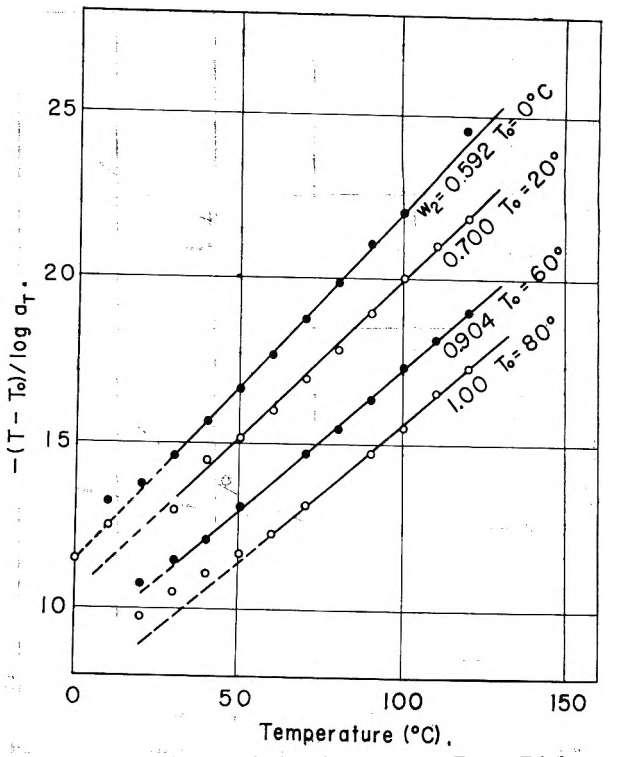

Fig. 6.—Test of linear relation between $-(T - T_0)/\log a_T$ and temperature T.

One can see from Fig. 7 that in the region of v_1 smaller than about 0.2 both $f(v_1,60°)$ and $\alpha_f(v_1)$ increase linearly with v_1, and may be represented by

$$f(v_1,60°) = 0.0325 + 0.0447v_1 \qquad (14)$$

$$\alpha_f(v_1) = 2.26 \times 10^{-4} + 6 \times 10^{-6}v_1 \qquad (15)$$

Combination of equations 11, 14, and 15 yields an expression for $f(v_1,T)$ which agrees in form with equation 10. This implies that the linear variation of f with v_1 assumed in the F–K theory is valid at least in the region

(31) M. L. Williams, R. F. Landel, and J. D. Ferry, *J. Am. Chem. Soc.*, **77**, 3701 (1955).

(32) J. D. Ferry, "Viscoelastic Properties of Polymers," John Wiley and Sons, Inc., New York and London, 1961.

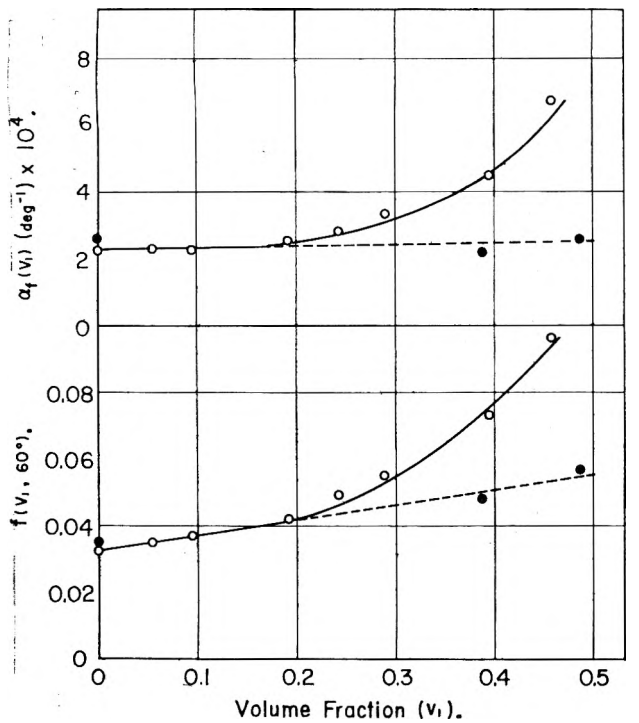

Fig. 7.—Variations of $f(v_1,60°)$ and $\alpha_f(v_1)$ with volume fraction of DEP (v_1): ○, values from present viscosity data; ●, values from dynamic mechanical data of Saunders, *et al.*

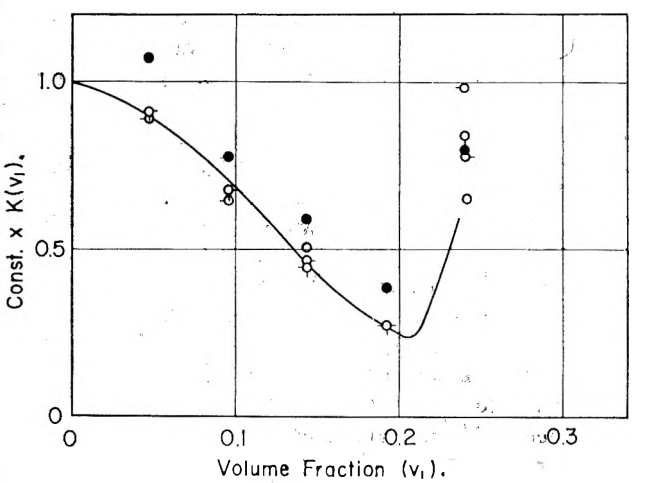

Fig. 8.—Variation of K with volume fraction of DEP (v_1): ●, 40°; ○, 60°; ○, 80°; ♀, 100°; ○120°.

of concentration sufficiently close to pure polymer solid. Comparison yields

$$f(0,T) = 0.0325 + 2.26 \times 10^{-4}(T - 60) \quad (16)$$

$$\beta(T) = 0.0447 + 6 \times 10^{-6}(T - 60) \quad (17)$$

where T is the centigrade temperture. Taking the glass transitior temperature T_g^0 for pure PBMA to be 27° (Child and Ferry[26]), we obtain $f(0,T_g^0) = 0.025$ from equation 16. This is in perfect agreement with the value deduced for $f(0,T_g^0)$ from the WLF equation.[31] The value for $\alpha_f(0)$ obtained from equation 15 is 2.26×10^{-4}, which is lower than one-half of the value predicted from the WLF equation,[31] but well consistent with 2.6×10^{-4} reported by Child and Ferry.[26] It has been inferred[17] that when comparison is made at T_g^0 of each polymer, the value of $\beta(T)$ is roughly independent of polymer species and characteristic of the kind of diluent used. By analyzing dynamic mechanical data of Saunders, *et al.*,[33] for PBMA in DEP Fujita and Kishimoto[34] have deduced a value 0.050 for $\beta(T_g^0)$. A value 0.065 was derived for this quantity from steady-flow viscosity data of Fujita and Maekawa[17] for polymethyl acrylate in DEP. These values of $\beta(T_g^0)$ are higher than 0.045 deduced from equation 17. Thus it seems more adequate to consider that the parameter $\beta(T_g^0)$ depends not only on polymer species but also on what type of data are used to determine it.

Figure 7 shows that in the region of v_1 greater than about 0.2 both $f(v_1,60°)$ and $\alpha_f(v_1)$ increase with v_1 more sharply than in linear fashion. The closed circles in this figure indicate values of $f(v_1,60°)$ and $\alpha_f(v_1)$ calculated from the article of Saunders, *et al.*,[33] who applied equation 13 to their dynamic mechanical data encompassing glass to rubber transition, with T_0 chosen as 0° for all the concentrations they studied. These points do not agree with our results but incidentally come close to the straight lines defined by our f and α_f for small values of v_1. The reason for this discrepancy is not clear to us. It is readily shown that in the region of v_1 where this discrepancy occurs, η calculated with Saunders' f and α_f depends more strongly on temperature than does η actually measured in this work.

Values of $K(v_1)$ have been calculated for 40, 60, 80, 100, and 120° by using the procedure described in foregoing lines, and are shown in Fig. 8. Except for the values at 40°, the data at other temperatures fall approximately on a single curve in the region of v_1 smaller than about 0.2. This fact is in gratifying agreement with the starting assumption made for this quantity. Initially $K(v_1)$ decreases with increasing v_1, but beyond v_1 of about 0.2 it increases abruptly and exceeds its value at $v_1 = 0$. If, as has been supposed, K is related in a way to the density of interchain entanglements its initial decrease with v_1 is in conformity to what we might expect intuitionally; as the polymer is more diluted, the density of entanglements is lowered, and as a result individual polymer molecules are allowed to move more easily relative to others and will give less resistance to external shearing force. The upswing of K at larger v_1 apparently does not conform to this picture. It is hardly acceptable that as the polymer is plasticized beyond a certain limit, the relative movement of polymer molecules becomes less free than in the undiluted state. This peculiar consequence of our analysis stems from the fact that, as illustrated in Fig. 8, the values of $f(v_1,T)$ we derived swing up markedly as the volume fraction of DEP exceeds about 0.2. It is shown that if $f(v_1,T)$ for use in equation 9 is taken from the straight line which defines our $f(v_1,T)$ at small v_1, one obtains a plot for $K(v_1)$ which no longer exhibits such a peculiarity as found here.

Summarizing, we may conclude that for the system poly-*n*-butyl methacrylate and diethyl phthalate the F–K theory modified in the way presented above accounts adequately for the dependence of steady-flow viscosity on temperature and concentration, provided that the volume fraction of plasticizer is sufficiently small (<0.2) and the temperature is not too close to the glass transition temperature of pure PBMA. For

(33) P. R. Saunders, D. M. Stern, S. K. Kurath, C. Sakoonkim, and J. D. Ferry, *J. Colloid Sci.*, **14**, 222 (1959).

(34) H. Fujita and A. Kishimoto, *Bull. Chem. Soc. Japan*, **33**, 274 (1960).

higher plasticizer concentrations the present modification ceases to be effective, leading to a very peculiar result.

Acknowledgments.—Thanks are due to Dr. K. Ninomiya, Japan Synthetic Rubber Co., Dr. A. Kishimoto, Department of Fisheries, Kyoto University, and Dr. M. Kurata, Institute for Chemical Research, Kyoto University, for their interest in this study. Support in part came from the Ministry of Education, to which grateful acknowledgment is made.

SURFACE AREAS BY ADSORPTION OF A QUATERNARY AMMONIUM HALIDE FROM AQUEOUS SOLUTION

By J. Kivel, F. C. Albers, D. A. Olsen, and R. E. Johnson

Minneapolis-Honeywell Research Center, Hopkins, Minnesota

Received November 19, 1962

A technique has been developed for determining the surface area of powders and flat surfaces by their adsorption of a carbon-14 labeled quaternary ammonium halide. Hexadecyl-1-C^{14}-trimethylammonium bromide has been adsorbed from an aqueous solution onto flat plates and crushed samples of lead glass and onto vacuum deposited iron–nickel thin films. The rate of adsorption and the adsorption isotherms have been determined for these systems. A "monolayer" plateau was found to occur between 3×10^{-4} M and the critical micelle concentration in all systems studied. The effect of the tetrasodium salt of ethylenediaminetetraacetic acid (EDTA) on the effective surface area of lead glass has also been determined. EDTA treatment has been shown to result in a significant roughening of the glass.

Introduction

One approach to obtaining information on surface properties has been to adsorb a monomolecular layer of a long-chain polar organic compound onto the solid surface in the manner of Langmuir and Blodgett.[1] These polar organic compounds, in particular, stearic acid, have been used to determine the specific surface area of powders of such materials as metals[2] and clays.[3]

The availability of radioisotopes of many elements with specific activities high enough to yield statistically reliable results from a square centimeter of surface has made it possible to study surface reactions and determine surface areas that were previously difficult or impossible to analyze.[4] Techniques utilizing carbon-14 or tritium labeled polar organic compounds, such as stearic acid,[5] have made possible determinations of specific surface area of very small powder samples, nonporous materials, and flat surfaces.

In this study, the properties of hexadecyl-1-C^{14}-trimethylammonium bromide (HMAB), an aqueous soluble ionic surfactant, have been utilized to determine surface areas of various materials, to determine the effect of particle size on roughness, and to determine the effect of the tetrasodium salt of ethylenediaminetetraacetic acid (EDTA) on lead glass.

Experimental

Materials. A. Surfaces.—The surfaces used in the study were the following.

1. **Crushed Glass.**—The techniques used to prepare the glass samples were those recommended by the American Ceramic Society.[6] Samples of Corning 0010 lead glass were placed in a flat bottomed steel mortar and crushed by dropping a weight from a constant height onto the samples. The glass was then sieved, and the desired mesh size was transferred to a piece of paper. Foreign particles were removed by magnetic and manual techniques. The sample was then transferred back to the sieve, washed once with distilled water, twice with analytical reagent grade methanol, and stored in a desiccator.

2. **Flat Glass.**—Corning Code No. 2915 microscope cover glasses and 0120 lead glass.

3. **Iron–Nickel Thin Films.**—Iron–nickel thin films were prepared in a bell jar evacuated to 10^{-5} mm. The alloy was heated in an alumina crucible (morganite) by resistance heating and evaporated onto Corning Code No. 2915 microscope cover glasses. The experimental procedure is reported elsewhere[7] in greater detail.

B. Surfactant.—The hexadecyl-1-C^{14}-trimethylammonium bromide was obtained from the Nuclear-Chicago Corp. Analyses by radiochromatography revealed no other radioactive species. A "stock" solution was prepared by diluting the labeled HMAB with inactive HMAB (Eastman Organic Chemical Co.) to a specific activity of 0.50 μcurie/mmole.

C. EDTA.—The tetrasodium salt of ethylenediaminetetraacetic acid was obtained from the Dow Chemical Company and used without further purification.

Procedure.—The steps in the adsorption of HMAB on a surface and the subsequent measurement were as follows:

1. The initial activity in solution was determined. Aqueous solutions containing 25 ml. of varying concentrations of HMAB were prepared in glass tubes that had been pretreated with an identical HMAB solution. Small aliquots (usually 10 μl.) were removed from the solution, placed onto a circular area of 0.25 cm.^{2} in the center of a 1.25 inch diameter aluminum disk, and evaporated to dryness. The samples were then counted using an Atomic Accessories, Inc., Model FC-72A windowless gas-flow counter to determine the initial activity per microliter of solution.

2. The time necessary for adsorption equilibrium to be reached was determined, and the procedure follows for crushed glass. Approximately two grams of crushed glass was added to the 25 ml. of HMAB solution at 25 ± 0.1°. The mixture was stirred manually. Small aliquots of solution were withdrawn at definite time intervals, evaporated onto aluminum disks, and counted.

3. Isotherms for adsorption of HMAB were determined. The crushed glass samples were treated with aqueous solutions of 1.0×10^{-4} to 2.3×10^{-3} M HMAB at 25° for an adsorption time of 30 minutes. Samples of the initial and final solutions were withdrawn, and the adsorption isotherm was determined from the change in activity in solution. The flat glass plates and the iron–nickel deposits were dipped into solutions of similar concentration until equilibrium was reached and then vertically withdrawn at a rate of 2 mm./minute by means of a small motor. At this rate of withdrawal, the samples emerged dry; water did

(1) K. B. Blodgett, *J. Am. Chem. Soc.*, **57**, 1007 (1935); I. Langmuir and V. J. Schaefer, *ibid.*, **58**, 284 (1936).

(2) E. B. Greenhill, *Trans. Faraday Soc.*, **45**, 625 (1949).

(3) C. Orr, Jr., and P. T. Bankston, *J. Am. Ceram. Soc.*, **35**, 58 (1952).

(4) J. E. Willard, *J. Phys. Chem.*, **57**, 129 (1953).

(5) M. C. Kordecki and M. B. Gandy, *Intern. J. Appl. Radiation Isotopes*, **12**, 27 (1962).

(6) D. E. Sharp, *Bull. Am. Ceram. Soc.*, **14**, 181 (1935).

(7) R. J. Prosen, J. O. Holmen, B. E. Gran, and T. S. Cebulla, *J. Appl. Phys.*, **33**, 1150 (1962).

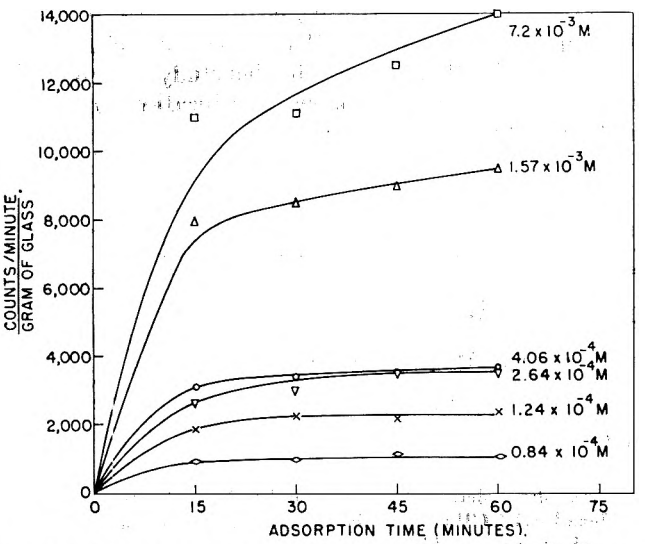

Fig. 1.—Rate of adsorption of HMAB on 25–40 mesh 0010 lead glass at 25°.

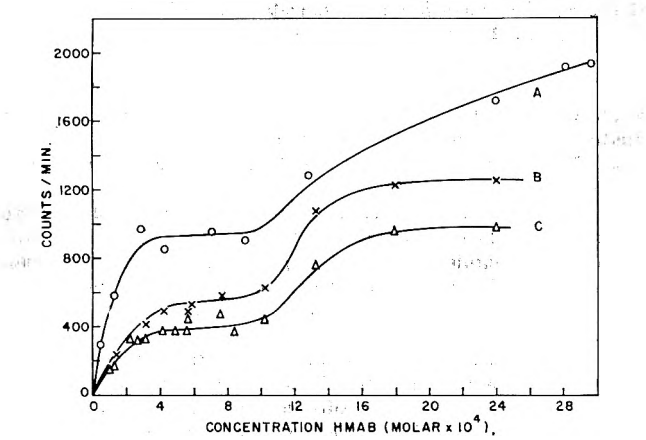

Fig. 2.—Adsorption isotherms of HMAB on (A) crushed 0010 lead glass, (B) iron–nickel thin films, and (C) 2915 microscope cover glasses.

not wet the surface. In the few cases where droplets formed, they were removed by touching a corner of tissue paper to the drops. These adsorption isotherms for the glass and metal plates were determined from the corrected counts/cm.^{2} on the plates.

4. The surface area of each sample was determined. Samples were treated with a 5.72×10^{-4} *M* HMAB solution in the manner described above. Flat samples were withdrawn vertically from solution and counted, whereas the adsorption by crushed glass samples was determined by comparison of the activity of the initial and final solutions.

5. **EDTA Treatment.**—Squares of 0120 lead glass and samples of 7–8 and 50–60 mesh 0010 lead glass were treated with a 0.131 *M* EDTA aqueous solution of pH 12.3 at 96°. Samples were removed from the EDTA solution at time intervals from 0 to 15 hours. The experimental procedure for the EDTA treatment is reported in greater detail elsewhere.[8]

6. **Radioactivity Measurement.**—All samples were compared to the average standards obtained by pipetting several 10-μl. samples of each initial HMAB solution onto aluminum disks, drying them, counting them, and determining the average activity. These standards were calibrated against a 0.19 ± 0.01-μcurie carbon-14 source, assuming a 50% geometry factor, and a backscattering factor of 23%. The backscattering factor of 23% has been determined by others[9] to be the same for aluminum and glass.

Experimental Results

A. Rate of Adsorption.—The rate of adsorption was studied as a function of HMAB concentration and nature of adsorbent. For crushed glass samples a plateau was reached within 30 minutes for all but the most concentrated solutions of HMAB. Maximum adsorption was obtained for the flat glass and the iron–nickel thin films within ten minutes of immersion time. Figure 1 shows the rate of adsorption of HMAB on 25–40 mesh 0010 lead glass as a function of HMAB concentration. Other samples of crushed glass yielded similar curves.

B. Adsorption Isotherms.—Adsorption isotherms were obtained for all materials studied in this investigation. Isotherms obtained for 25–40 mesh 0010 lead glass, 2915 cover glasses, and iron–nickel thin films are shown in Fig. 2. The activity noted for the crushed glass in Fig. 2 is a relative value. The other activities are actual values obtained per sample of cover glass and iron–nickel deposit.

C. Area Determinations.—The surface areas of six different particle sizes of 0010 lead glass have been determined and are listed in Table I. The areas were calculated by determining the fraction of activity in the solution lost due to the adsorption of HMAB onto the glass and multiplying this quantity by the total number of molecules originally present in the solution. The effective area of the molecule has been taken as 20.5 Å.^{2}. Since this value was not redetermined in the present investigation, the quantities reported here should be taken as relative rather than as absolute values.

Roughness factors have been determined for the crushed glass and are also included in Table I. The roughness factor in this investigation is defined as the ratio of surface area determined by using HMAB to that determined by using geometric calculations. Geometric areas were obtained for the crushed glass samples by assuming spherical particles.

TABLE I

AREA AND ROUGHNESS FACTORS OF CRUSHED LEAD GLASS

Mesh range	HMAB surface area (cm.^{2}/g.)	Geometrical surface area (cm.^{2}/g.)	Roughness factor
7–8	121 ± 11	8.3	14.5
20–25	209 ± 29	33.4	6.3
40–45	255 ± 28	56.8	4.5
50–60	296 ± 11	82.4	3.6
80–100	725 ± 40	133	5.4
140–170	1078 ± 105	224	4.8

Surface areas and roughness factors were also determined for the iron–nickel thin films, the cover glasses, and the 0120 lead glass squares. Roughness factors for these materials were found to be 2.8 for iron–nickel thin films, 2.5 for 2915 cover glass, and 4.4 for 0120 lead glass. An effective area of 20.5 Å.^{2} was again attributed to each molecule adsorbed.

D. EDTA Treatment.—The surface area of lead glass was found to increase upon treatment with EDTA. The area of flat 0120 lead glass plates treated with EDTA was found to increase almost linearly with length of treatment for the first seven hours from a roughness factor of 4.4 for the untreated glass to 86 after seven hours treatment. Beyond 7 hr. the increase is more gradual. After 15 hr., the roughness factor of the EDTA treated glass was determined to be 115. Similar results were obtained for crushed lead glass. Table II shows the effect of a 10-hr. EDTA treatment on

(8) D. A. Olsen, R. E. Johnson, J. Kivel, and F. C. Albers, to be published.

(9) J. W. Shepard and J. P. Ryan, *J. Phys. Chem.*, **63**, 1729 (1959).

7–8 and 50–60 mesh 0010 lead glass and on 0120 lead glass plates.

TABLE II
EFFECT OF 10-HR. EDTA TREATMENT ON LEAD GLASS

Glass	Geometrical area	Untreated surface area	EDTA treated surface area
7–8 mesh	8.3 $\frac{cm.^2}{g.}$	121 ± 11 $\frac{cm.^2}{g.}$	811 ± 93 $\frac{cm.^2}{g.}$
50–60 mesh	82.4 $\frac{cm.^2}{g.}$	296 ± 11 $\frac{cm.^2}{g.}$	1541 ± 29 $\frac{cm.^2}{g.}$
0120 plate	1.0 cm.²	4.4 ± 0.2 cm.²	91 ± 6 cm.²

Discussion

A. The Adsorption Isotherm.—Most adsorption isotherms have a plateau or an inflection. The plateau or the beginning of the linear portion above the inflection is believed to represent "first degree saturation"[10] of the surface and is the condition in which all possible sites in the original surface have been filled. Further adsorption can take place only on new surfaces. This degree of coverage is often called a complete "monolayer," although generally the layer may contain solvent as well as solute molecules, consist only of isolated clusters adsorbed on the most active sites, or consist of ionic micelles.[11] Therefore, it is difficult to define the term "monolayer." Willard[4] has arbitrarily defined a monolayer as "the number of ions required to cover the macro surface area of the sample if each ion covers an area equal to the square of its ionic diameters."

The first degree saturation by HMAB has been shown[12,13] to be due to adsorption of long chain cations. Saraga[12] has presented a mechanism of attachment of HMAB onto glass in which the glass is hydrolyzed to yield ≡SiOH groups. These groups are, in turn, to some extent dissociated to ≡SiO^- and H^+. The glass is attacked by the quaternary ammonium cation to produce, according to Saraga, a "surface salt," ≡SiON-$(CH_3)_3C_{16}H_{33}$. Sexsmith and White[13] interpret the initial adsorption of HMAB as a cationic exchange.

Beyond the concentration range of first degree saturation, which is shown in Fig. 2 to occur approximately in the region 3 to 8 × 10^{-4} M, an increase in the amount of adsorption occurs. This has been attributed to an adsorption of ion pairs.[12,13] In the monolayer concentration range the glass is neutral; there is no charge on the surface. Beyond this range, however, the presence of the HMAB cations on the glass gives rise to a positive charge. Therefore, when the glass is removed from the solution it should carry negative ions (Br^- and OH^-) along with it. Saraga[12] in a study of quaternary ammonium bromides, using radiobromine-82, noted that the attachment of bromine onto the glass surface began at concentrations just below the critical micelle concentration. The c.m.c. for HMAB is 1 × 10^{-3} M,[12] which is about that of the concentration at the end of the monolayer plateau.

Comparison of the adsorption isotherms for iron–nickel thin films and the various types of glass indicates that a similar mechanism is responsible for adsorption in these systems. The data for the adsorption of HMAB obtained by Sexsmith and White[13] show that cotton, cordura, and viscose filaments begin to retain bromide and yield a corresponding increase in cation adsorption at approximately 4 to 6 × 10^{-4} M. This concentration range is not very different from that observed in this investigation for the end of the monolayer plateau, again implying a similar type of adsorption mechanism. Preliminary studies in this Laboratory on other substrates also indicate similar adsorption isotherms.

B. Surface Area Measurements.—In order to determine a value for the surface area, the area occupied or "blocked" by each molecule must be known. The value of 20.5 Å.² has been chosen since it has been noted[11] that the irregular shaped projection of long chain hydrocarbons usually results in the effective covering of an area of 20.5 Å.², even though the cross-sectional area of the —CH_2— groups on the hexadecyl chain and the area of the trimethylammonium group are calculable to smaller values. In addition, the value obtained for surface area is influenced by the size of the molecule. A large molecule may not be able to enter pores or fissures in the surface that are accessible to smaller molecules and, therefore, yield a smaller area for the surface. Finally, the effect of the solvent on the substrate must be considered.

The similarity between the adsorption isotherms of HMAB on iron–nickel thin films deposited on 2915 cover glasses and on the glass has been noted above. Figure 2 shows that the amounts of HMAB adsorbed on the two materials do not differ greatly. This result is expected if the deposited metal follows the contours of the glass.

C. EDTA Treatment.—Prolonged treatment of lead glass with EDTA appears to increase appreciably the surface that can adsorb HMAB. Roughness factors of over 100 were noted after 15 hr. treatment. The kinetics of EDTA removal of lead, potassium, and silicon from lead glass to produce the increased surface are reported elsewhere.[8] Interferometric studies of lead glass at this Laboratory have also substantiated these data. The interference patterns were obtained by placing a lead-glass plate on an optical flat, illuminating it with a helium light, and photographing the resultant fringes. After the EDTA treatment, the fringe pattern, which had been sharp and distinguishable, became considerably less distinct and showed jagged variations in intensity along the fringe boundary. These jagged and even discontinuous characteristics of the fringes indicate a microroughness of the surface, in this case a result of the chemical etching of the EDTA salt.

The adsorption of HMAB from aqueous solution has been utilized to determine surface areas of several types of glass and iron–nickel thin films. Similar adsorption isotherms were obtained for these dissimilar systems, indicating that this surface area determination technique may be applicable to other systems. Adsorption isotherms obtained previously for other substrates[12,13] tend to confirm this view. Additional experimental studies with other types of surfaces using HMAB and related compounds are planned.

Acknowledgments.—The authors wish to acknowl-

(10) S. Brunauer, "The Adsorption of Gases and Vapors," Oxford Univ. Press, London, 1944, p. 287.
(11) C. H. Giles, T. H. MacEwan, S. N. Nakhwa, and D. Smith, *J. Chem. Soc.*, 3973 (1960).
(12) L. Ter Minassian-Saraga, *J. chim. phys.*, **57**, 10 (1960).
(13) F. H. Sexsmith and H. E. White, Jr., *J. Colloid Sci.*, **14**, 598 (1959).

edge the assistance of Mr. L. L. Egan and Mr. B. E. Gran, and, in particular, the suggestions of Professor R. S. Hansen of Iowa State University that initiated this investigation.

SPECTROPHOTOMETRIC INVESTIGATION OF THE EXTRACTION OF TRANSITION METAL HALO-COMPLEX IONS BY AMINE EXTRACTANTS

BY S. LINDENBAUM AND G. E. BOYD

Chemistry Division, Oak Ridge National Laboratory, Oak Ridge, Tennessee

Received November 19, 1962

The spectra of the extracted species in the distribution of the halo-complex ions of Fe(III), Co(II), Cu(II), Mn(II), and Ni(II) between organic amine solutions and aqueous chloride and bromide solutions were studied. In each instance the only species observed in the organic phase was the four-coördinated complex ion. In several cases (Fe(III), Co(II), Cu(II), and Ni(II)) it was shown that even when the extraction was from aqueous solutions whose spectra indicated the complete absence of the tetrahedrally coördinated species, the spectra observed in the organic phase were in excellent agreement with spectra shown to be representative of the MCl_4^{-2} and MCl_4^{-} ions. It was not possible to prepare an aqueous solution of Ni(II) which showed any indication of the spectrum characteristic of the $NiCl_4^{-2}$ ion. The spectrum of Ni(II) extracted by a toluene solution of a tertiary amine hydrochloride from 13 *M* LiCl was, however, identical to spectra of compounds containing $NiCl_4^{-2}$.

Introduction

The generally large affinity of quaternary ammonium anion-exchange resins for the transition metal chloro-complex ions, and the dependence of this specificity on the ligand concentration in aqueous solution, has been the basis for many anion-exchange column separations.[1] It has been shown by Smith and Page[2] and others[3-5] that a large selectivity also exists for "liquid ion exchange" systems prepared by dissolving tertiary amine hydrochlorides in water-immiscible solvents. Further, a remarkable similarity in the relative orders of selectivity between liquid and resinous anion exchangers may be demonstrated by comparing published data for a liquid amine extraction system[6] with that for an anion-exchange resin[7] in a plot of the distribution coefficients *vs.* the aqueous hydrochloric acid concentration.

It was the objective of this study to determine the nature of the species involved in the ion-exchange extraction of the halo-complex ions of some of the 3d transition metals and to obtain an understanding of the origins of the large selectivities frequently observed. A liquid amine system was chosen for study because it lends itself more readily to spectrophotometric investigation. Spectra of ions absorbed onto ion-exchange resins have been measured recently.[8-12] In general, it has been found that the species on the anion-exchange resin was the same as that in the liquid amine extractant. In one case, however, Ryan[11] observed that for the anion-exchange resin absorption of hexavalent uranium from nitrate solution, both tri-nitrato and tetranitrato complex ions occurred in the resin phase. The liquid amine system, however, extracts only the trinitrato complex ion $UO_2(NO_3)_3^{-}$.[13] Spectral measurements on ion-exchange resins, however, are beset by difficulties involving scattering of light, obtaining a reproducible blank, and adjusting the concentration of the extracted species. Furthermore, for the extraction of ions from concentrated aqueous solution not all of the ionic species taken up by the resin are necessarily associated with the exchanger sites; some are present in the electrolyte solution imbibed by the resin phase as the result of Donnan "invasion." Measurements have shown[14] that the solubility of electrolytes in solutions of tri-*n*-octyl amine salts in toluene is quite small.

Experimental

Materials.—Triisooctylamine (TIOA) as obtained from Union Carbide Chemicals Company was pale yellow in color, and its neutral equivalent was 375.5 (theor. 357.7). Solutions of TIOA in toluene were shaken with excess aqueous HCl or HBr to form the hydrochloride or hydrobromide. Tri-*n*-octylamine hydrochloride, TOA·HCl, was obtained as a white crystalline solid from Eastman Kodak Co., Rochester, New York. TOA·HBr was prepared from redistilled tri-*n*-octylamine (Eastman) by equilibrating an ether solution of the amine with aqueous HBr. The ethereal solution was dried and the ether evaporated to obtain the pure solid TOA·HBr. Cupric bromide and ferric bromide were prepared by the repeated addition of HBr to the nitrate salt and evaporating to dryness. All other chemicals used were reagent grade.

Spectrophotometric Measurements.—Spectral measurements were performed with a Cary Model 14 recording spectrophotometer. Equal volumes of aqueous HCl or HBr solutions containing known amounts of transition metal chloride or bromide were equilibrated with amine–toluene solutions. Absorption spectra of the organic phase and the *original* aqueous phase were determined, using for the reference cell a solution identical with that in the sample cell except for the presence of the transition metal compound. All measurements were made with 1-cm. path length cells.

Results

Extraction of Fe(III) from HCl and HBr Solutions.—Trivalent iron was extracted from 12 *M* HCl and 1 *M* HCl by 0.225 *M* TIOA·HCl in toluene. The spectra taken on the aqueous and organic phases are shown in

(1) K. A. Kraus and F. Nelson, *Proc. Intern. Conf. Peaceful Uses of Atomic Energy, Geneva*, **7**, 113 (1955).
(2) E. L. Smith and J. E. Page, *J. Soc. Chem. Ind.*, **67**, 48 (1948).
(3) G. W. Leddicotte and F. L. Moore, *J. Am. Chem. Soc.*, **74**, 1618 (1952).
(4) F. L. Moore, "Liquid–Liquid Extraction with High Molecular Weight Amines," National Acad. of Sci. Series on Nucl. Sci., Dec. 15, 1960.
(5) K. B. Brown, C. F. Coleman, D. J. Crouse, C. A. Blake, and A. D. Ryon, *Proc. Intern. Conf. Peaceful Uses of Atomic Energy, 2nd, Geneva*, **3**, 472 (1958).
(6) H. A. Mahlman, G. W. Leddicotte, and F. L. Moore, *Anal. Chem.*, **26**, 1939 (1954).
(7) K. A. Kraus and G. E. Moore, *J. Am. Chem. Soc.*, **75**, 1460 (1953).
(8) D. K. Atwood and T. DeVries, *ibid.*, **83**, 1509 (1961).
(9) E. Rutner, *J. Phys. Chem.*, **65**, 1027 (1961).
(10) J. L. Ryan, *ibid.*, **64**, 1375 (1960).
(11) J. L. Ryan, *ibid.*, **65**, 1099 (1961).
(12) J. L. Ryan, *ibid.*, **65**, 1856 (1961).
(13) W. F. Keder, J. L. Ryan, and A. S. Wilson, *J. Inorg. Nucl. Chem.*, **20**, 131 (1961).
(14) S. Lindenbaum and G. E. Boyd, *J. Phys. Chem.*, **66**, 1383 (1962).

Fig. 1. The spectra for Fe(III) in the organic phase are identical with those reported for $KFeCl_4$ and $HFeCl_4$ in ether by Friedman[15] and Metzler and Myers,[16] which Friedman ascribes to the $FeCl_4^-$ ion. The spectrum shown for Fe(III) in aqueous 12 *M* HCl solution is similar to the organic phase spectra, except for the apparent absence of a peak at 532 mμ. Metzler and Myers[16] have suggested that this peak is overshadowed in HCl solutions by the leading edge of the very intense $FeCl_3$ ultraviolet absorption bands. Good and Bryan[17] have found also that the species extracted by organic amine solutions is the same as the one for which Friedman assigned the $FeCl_4^-$ structure. More recently, Raman spectra[18] and X-ray[19] evidence, consistent with the tetrahedral $FeCl_4^-$ structure for the extracted species, has been presented.

Spectra are shown (Fig. 1) for the extraction of Fe(III) from aqueous 4.5 *M* and from 9 *M* HBr solutions. Identical species appear to be extracted. The spectra of the organic phase species are identical with the spectrum of $(C_2H_5)_4NFeBr_4$ in dimethylformamide obtained by Gill[20] and ascribed by her to the $FeBr_4^-$ ion. The spectrum of Fe(III) in 9 *M* HBr shows a reversal in relative heights of the two prominent peaks from that observed in the organic phase; the molar absorbancy indices are also very much larger. Apparently here, also, the leading edge of an ultraviolet band of one or more complexes less saturated than $FeBr_4^-$ is superimposed on the $FeBr_4^-$ spectrum.

Extraction of Co(II) from HCl Solutions.—Aqueous solutions of $CoCl_2$ exhibit colors ranging from pink in pure water and dilute HCl to blue in concentrated HCl solutions. There is evidence[21,22] that the pink solution contains six-coördinated cobalt and the blue solution the four-coördinated $CoCl_4^{-2}$ species. The spectrum (Fig. 2) of a solution of $CoCl_2$ in concentrated HCl is recognized to be very similar to that obtained by Gill and Nyholm[22] for $[Ph_3CH_3As]_2CoCl_4$ dissolved nitromethane; it also resembles the spectra of solid Cs_2CoCl_4[23,24] and Cs_3CoCl_5[23] (within the resolution obtainable by reflectance methods) in which the presence of the tetrahedral $CoCl_4^{-2}$ ion has been demonstrated crystallographically.[25]

The spectra (Fig. 2) of Co(II) in the organic phases are characteristic of the four-coördinated $CoCl_4^{-2}$ species also. The spectrum of Co(II) in 1 *M* HCl is that due to the aquo ion, $Co(H_2O)_6^{++}$. The species extracted from both dilute and concentrated acid is largely $CoCl_4^{-2}$, even though the spectrum of the dilute HCl aqueous phase shows no indication of the presence of $CoCl_4^{-2}$.

Extraction of Cu(II) from HCl and HBr Solutions.—Solutions of $CuCl_2$ and $CuBr_2$ in water have identical spectra characteristic of the blue, octahedral $Cu(H_2O)_6^{++}$ species. In concentrated aqueous HCl and HBr solutions the spectra differ considerably, the

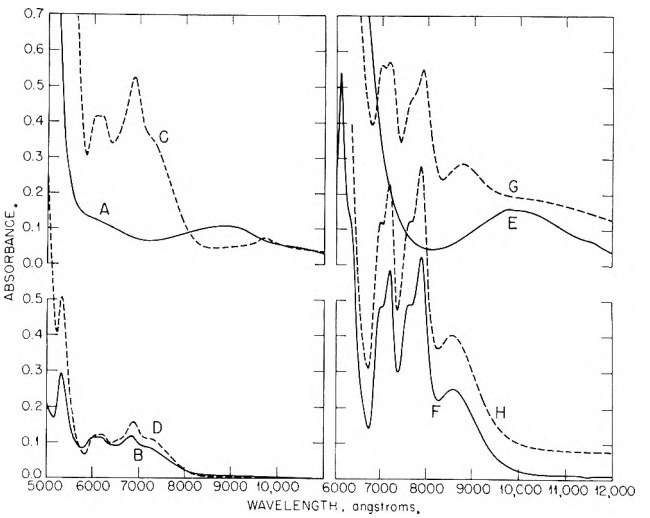

Fig. 1.—Absorption spectra of aqueous and organic phases for the extraction of Fe(III) by TIOA in toluene from aqueous HCl and HBr solutions: A, 1 *M* $FeCl_3$ in 1 *M* HCl; B, 0.225 *M* TIOA·HCl equilibrated with 1 *M* $FeCl_3$ in 1 *M* HCl; C, 1 *M* $FeCl_3$ in 12 *M* HCl; D, 0.225 *M* TIOA·HCl equilibrated with 1 *M* $FeCl_3$ in 12 *M* HCl; E, 0.05 *M* $FeBr_3$ in 4.5 *M* HBr; F, 0.05 *M* TIOA·HBr equilibrated with 0.05 *M* $FeBr_3$ in 4.5 *M* HBr; G, 0.1 *M* $FeBr_3$ in 9 *M* HBr; H, 0.05 *M* TIOA·HBr equilibrated with 0.05 *M* $FeBr_3$ in 9 *M* HBr. Absorbance = optical density = $\log I/I_0$.

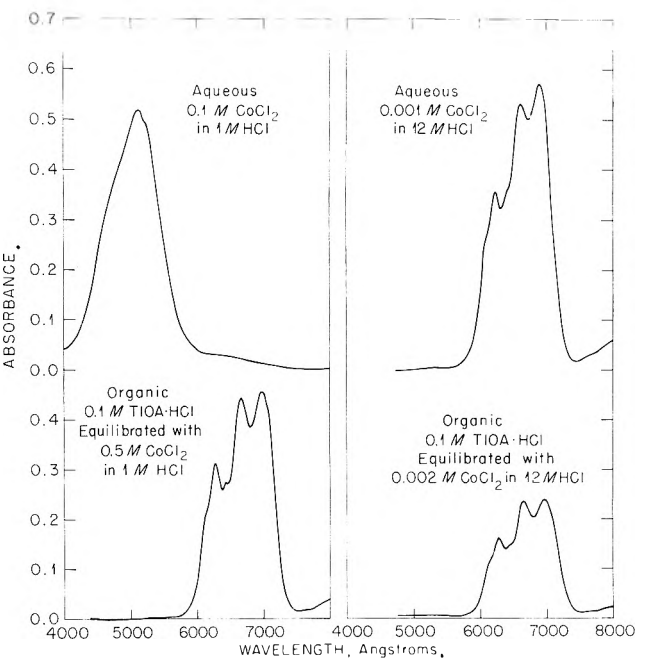

Fig. 2.—Absorption spectra of aqueous and organic phases for the extraction of Co(II) by TIOA·HCl in toluene from aqueous HCl solutions.

predominant species being the yellow $CuCl_4^{-2}$ [22,26] and purple $CuBr_4^{-2}$ [22] complex ions, respectively.

The spectra of the organic and aqueous phases for the extraction of Cu(II) from HCl and HBr solutions are shown in Fig. 3. The organic phase spectra are identical, independent of the concentration of acid in the equilibrium aqueous phase; they differ from those for the concentrated HCl and HBr solutions in that the peak positions are shifted to longer wave lengths. A similar shift in spectra was observed by Moeller upon increasing the chloride to copper ratio in aqueous Cu(II) nitrate solutions. Evidently, Cu(II) in concentrated HCl and HBr solutions is not present exclusively as

(15) H. L. Friedman, *J. Am. Chem. Soc.*, **74**, 5 (1952).
(16) D. E. Metzler and R. C. Myers, *ibid.*, **72**, 3776 (1950).
(17) M. L. Good and S. E. Bryan, *ibid.*, **82**, 5636 (1960).
(18) L. A. Woodward and M. J. Taylor, *J. Chem. Soc.*, 4473 (1960).
(19) C. L. Standley and R. F. Kruh, *J. Chem. Phys.*, **34**, 1450 (1961).
(20) N. S. Gill, *J. Chem. Soc.*, 3512 (1961).
(21) L. I. Katzin and E. Gebert, *J. Am. Chem. Soc.*, **72**, 5464 (1950).
(22) N. S. Gill and R. S. Nyholm, *J. Chem. Soc.*, 3997 (1959).
(23) L. I. Katzin and E. Gebert, *J. Am. Chem. Soc.*, **75**, 2830 (1953).
(24) L. I. Katzin, *ibid.*, **76**, 3089 (1954).
(25) H. M. Powell and A. F. Wells, *J. Chem. Soc.*, 359 (1935).
(26) T. Moeller, *J. Phys. Chem.*, **48**, 111 (1944).

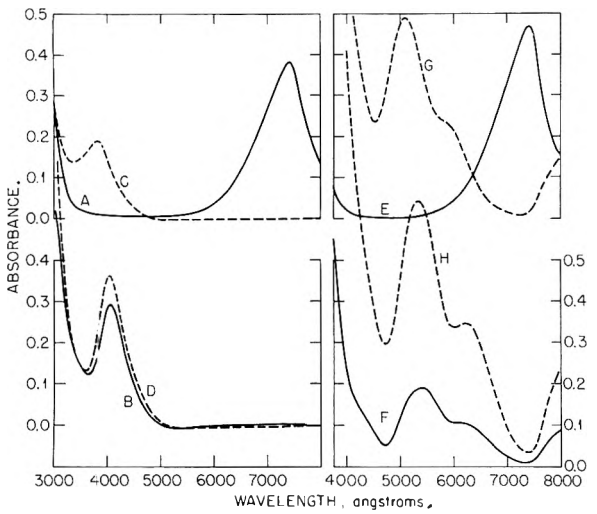

Fig. 3.—Absorption spectra of aqueous and organic phases for the extraction of Cu(II) by TIOA in toluene from aqueous HCl and HBr solutions: A, 0.04 *M* $CuCl_2$ in H_2O; B, 0.1 *M* TIOA·HCl equilibrated with 0.1 *M* $CuCl_2$ in H_2O; C, 0.0001 *M* $CuCl_2$ in 12 *M* HCl; D, 0.1 *M* TIOA·HCl equilibrated with 0.002 *M* $CuCl_2$ in 12 *M* HCl; E, 0.05 *M* $CuBr_2$ in H_2O; F, 0.05 *M* TIOA·HBr equilibrated with 0.2 *M* $CuBr_2$ in H_2O; G, 0.00025 *M* $CuBr_2$ in 9 *M* HBr; H, 0.05 *M* TIOA·HBr equilibrated with 0.0005 *M* $CuBr_2$ in 9 *M* HBr.

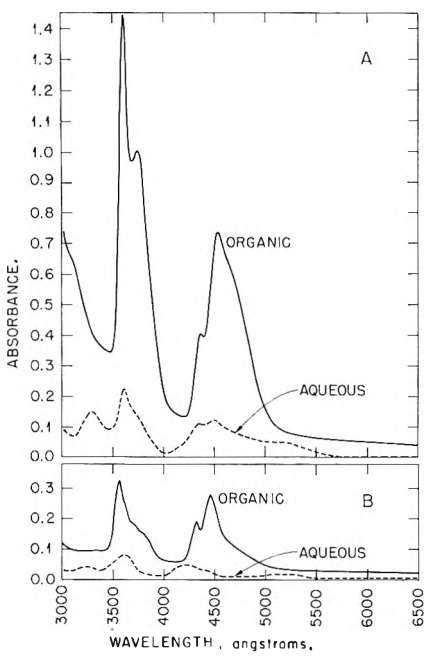

Fig. 4.—Absorption spectra of aqueous and organic phases for the extraction of Mn(II) by: A, 1 *M* TOA·HBr in toluene from 0.36 *M* $MnBr_2$ in 11.4 *M* LiBr; B, 1 *M* TOA·HCl in toluene from 0.60 *M* $MnCl_2$ in 11.4 *M* LiCl.

the $CuCl_4^{-2}$ and $CuBr_4^{-2}$ species, and the presence of less saturated (*e.g.*, $CuCl_3^-$, $CuCl_2$, and $CuCl^+$) species causes a shift in the absorption maximum to shorter wave lengths. Further evidence that the organic phase contains the fully saturated chloro-complex $CuCl_4^{-2}$ is that the peak positions in the spectrum of crystalline Cs_2CuCl_4[27,28] are very close to those observed in the liquid amine phase spectrum. The presence of the $CuCl_4^{-2}$ ion in Cs_2CuCl_4 has been demonstrated by X-ray diffraction.[27,28]

Extraction of Mn(II) from LiCl and LiBr Solutions.—Divalent manganese is only weakly extracted from concentrated HCl or HBr solutions by anion-exchange resins or organic amine solutions. To obtain measurable quantities of Mn(II) in the organic phase, it was necessary to employ concentrated aqueous LiCl or LiBr solutions of Mn(II). The spectra of the aqueous and organic phases for the extraction of Mn(II) from 11.4 *M* LiBr solution by 1 *M* TOA·HBr are shown in Fig. 4A, and from 11.4 *M* LiCl solution by 1 *M* TOA·HCl in toluene in Fig. 4B. The organic phase spectra are nearly identical with the spectra obtained by Gill and Nyholm[22] for $MnCl_4^{-2}$ and $MnBr_4^{-2}$ with solutions of $[Et_4N]_2MnBr_4$ and $[Et_4N]_2MnCl_4$ (or the corresponding triphenylmethylarsonium salts) in nitromethane. Values of λ_{max} observed in Fig. 4A (361, 375, 437, and 453 mμ) may be compared with the values of Gill and Nyholm (371, 437, and 452 mμ) for $MnBr_4^{-2}$. Similarly, in Fig. 4B the values of λ_{max} (357, 433, and 446 mμ) are in good agreement with the values reported (430 and 445 mμ) for $MnCl_4^{-2}$. The lowest wave length absorption bands (361 mμ for $MnBr_4^{-2}$ and 357 mμ for $MnCl_4^{-2}$) were not observed by Gill and Nyholm, however. These bands cannot be measured in nitromethane because this solvent is opaque in this wave length region. The aqueous phase spectra (Fig. 4A and 4B) show some of the same features observed with the organic phase, but at lower intensities and also somewhat distorted. These spectra are probably due to the presence of a small amount of $MnBr_4^{-2}$ and $MnCl_4^{-2}$ and other species intermediate between the hexaaquo and the fully halogen-saturated complex.

Extraction of Ni(II) from LiCl Solutions.—It is well known that divalent nickel is not absorbed appreciably from hydrochloric acid solutions either by ion-exchange resins or liquid anion exchangers; in contrast, divalent cobalt and copper which are adjacent elements to nickel in the periodic table are well absorbed. It is interesting to note that Ni(II) does not form $NiCl_4^{-2}$ complex ions in aqueous solutions, whereas Co(II) and Cu(II) do. Herber and Irvine[29] in fact cite evidence that the only nickel species present even in concentrated HCl are Ni^{++} and $NiCl^+$. It was pointed out by Keder,[30] however, that Ni(II) can be extracted into an amine solution if the aqueous chloride ion activity is made high enough (or the water activity low enough). In Fig. 5 are shown the aqueous and organic phase spectra for the extraction of Ni(II) from 13.0 *M* LiCl solutions into 0.1 *M* TOA·HCl in toluene. The organic phase spectrum is in excellent agreement with that reported by Gill and Nyholm for $NiCl_4^{-2}$ in nitromethane, and also with the spectra of Gruen and McBeth[31] of $NiCl_2$ dissolved in molten pyridinium chloride and Cs_2NiCl_4 in solid solution with Cs_2ZnCl_4. In the latter case it was shown that the solid solution containing nickel is isomorphous with pure tetrahedral Cs_2ZnCl_4.

The aqueous phase spectrum for Ni(II) in 13.0 *M* LiCl (Fig. 5) showed all the bands reported by Gill and Nyholm for $Ni(H_2O)_6^{++}$ except that the entire spectrum was shifted to longer wave lengths. Interestingly, Gruen and McBeth have shown that the spectrum of

(27) L. Helmholz and R. F. Kruh, *J. Am. Chem. Soc.*, **74**, 1176 (1952).
(28) B. Morosin and E. C. Lingafelter, *J. Phys. Chem.*, **65**, 50 (1961).
(29) R. H. Herber and J. W. Irvine, *J. Am. Chem. Soc.*, **78**, 905 (1956).
(30) W. E. Keder, Abstracts of Papers, Division of Physical Chemistry, 140th National Meeting, American Chemical Society, Chicago, Ill., September, 1961.
(31) D. M. Gruen and R. L. McBeth, *J. Phys. Chem.*, **63**, 393 (1959).

Ni(II) in $LiNO_3$–KNO_3 eutectic melt could be shifted toward the red end of the spectrum by the addition of chloride. This shift was interpreted as the consequence of the stepwise formation of chloro-complexes of Ni(II). It is likewise suggested here that the aqueous phase spectrum in Fig. 5 represents Ni(II) partially complexed with chloride ions. The molar absorbancy index for the $NiCl_4^{-2}$ ion is much larger than that for $Ni(H_2O)_6^{++}$; hence, the fact that there is no indication of the $NiCl_4^{-2}$ spectrum in the aqueous phase suggests that even in 13.0 *M* LiCl very little $NiCl_4^{-2}$ can be present.

Discussion

It has been shown for the extraction of Fe(III), Co(II), Cu(II), Mn(II), and Ni(II), by solutions of tertiary amines in toluene from aqueous chloride and bromide solutions that in each case a strong preference for the four-coördinated species exists. This preference is so specific that even when the amine solution is equilibrated with an aqueous phase containing the transition metal almost exclusively in the hexa aquo form (*e.g.*, $Cu(H_2O)_6^{++}$) the visible spectrum of the organic phase shows only the bands associated with the four-coördinated tetrahedral species. However, in all the cases studied the spectral bands for the tetrahedral species are much more intense than those for the corresponding octahedral species. Therefore, small amounts of the metal ion in the organic phase in the octahedral form might not be observed. The absorbance of those bands shown to be representative of the tetrahedral species is in all cases far greater in the organic phase than in the aqueous.[32] In fact, it has been shown for Fe(III), Co(II), Cu(II), and Ni(II) that the tetrahedral species can be observed in an organic phase which has been equilibrated with an aqueous solution showing no sign in its spectrum of bands due to the tetrahedral ion. It has therefore been demonstrated that the "liquid ion-exchange" system has an extremely strong preference for the fully saturated halo-complex ion. Certain MX_6^{-2} species (*e.g.*, $TcCl_6^{-2}$, $ReCl_6^{-2}$)[33] are known to be strongly absorbed by anion exchangers so

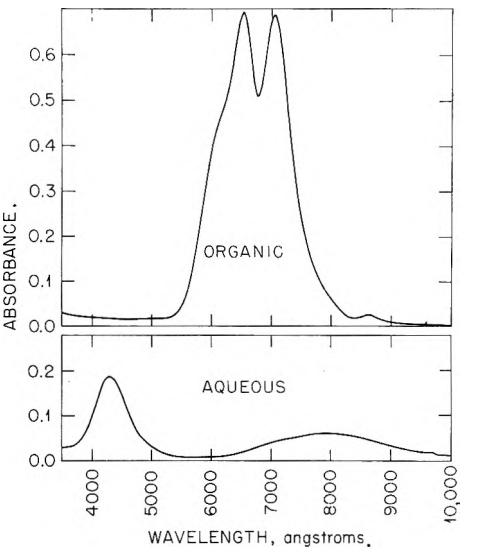

Fig. 5.—Absorption spectra of aqueous and organic phases for the extraction of Ni(II) by 0.1 *M* TOA·HCl in toluene from 0.073 *M* $NiCl_2$ in 13.0 *M* LiCl. (Organic phase diluted 1:5 with 0.1 *M* TOA·HCl in toluene; aqueous phase diluted 1:5 with 13.0 *M* LiCl.)

that the absence of octahedral species in liquid exchangers [for example, $MCl_3(H_2O)_3^-$] probably cannot be attributed solely to the coördination number but rather to the greater stability of tetrahedral species such as MX_4^{-2} in a solvent where excess halide ions are available.

In a paper which appeared while this report was in preparation,[34] Katzin reported the spectra of the species obtained on dissolving transition element chlorides in dimethylformamide. In such a medium of high dielectric constant and low base strength the formation of the tetrahedral configuration was promoted. It was suggested that in this medium the tetrahedral configuration is more stable since the average ligand bond strength is greater than in the octahedral configuration.[35] It was possible, therefore, by using dimethylformamide to study the octahedral–tetrahedral equilibrium in one phase. Our work indicates that in a medium of low dielectric constant and low base strength, the halide complexes of the first transition series assume the tetrahedral configuration to the exclusion of octahedral species within the limits of detection.

(32) It also has been observed by Murrell, Katzin, and Davies, *Nature*, **183**, 459 (1959), that two phases are obtained in the $CoCl_2$–H_2O–acetone system and that the tetrahedral species also predominates in the acetone-rich (organic) phase.

(33) G. E. Boyd and Q. V. Larson, unpublished results of this Laboratory (1961).

(34) L. I. Katzin, *J. Chem. Phys.*, **36**, 3034 (1962).

(35) L. I. Katzin, *ibid.*, **35**, 467 (1961).

THERMAL HYDROGENOLYSIS OF PROPYLENE

BY AKIRA AMANO AND MASAO UCHIYAMA

The Department of Applied Chemistry, Tohoku University, Sendai, Japan

Received November 20, 1962

Thermal decomposition of propylene in the presence of hydrogen was studied in a flow system at atmospheric pressure, and temperatures ranging from 750 to 850°, contact times from 0.2 to 2 sec., and hydrogen to propylene mole ratios from 0 to 10. The main reaction is the hydrogenolysis represented by the stoichiometric relation: $C_3H_6 + H_2 \rightarrow CH_4 + C_2H_4$. The selectivity of the hydrogenolysis is maintained above 95% at low temperatures and high mole ratios. Other products include butadiene, butenes, ethane, propane, and mononuclear aromatic hydrocarbons. Acetylene and allene are present but in extremely minute quantities. The reaction is first order with respect to propylene and one-half order with respect to hydrogen. The values of A-factor and activation energy are, respectively $10^{12.3}$ $l.^{1/2}/mole^{1/2}$-sec. and 55.9 kcal./mole. A close analysis of related elementary reactions reveals the following free-radical chain mechanism to be operative: $C_3H_6 \rightarrow$ allyl + H; H + $C_3H_6 \rightarrow$ *n*-propyl*; H + $C_3H_6 \rightarrow H_2$ + allyl; *n*-propyl* $\rightarrow C_2H_4$ + methyl; methyl + $H_2 \rightarrow CH_4$ + H; methyl + $C_3H_6 \rightarrow CH_4$ + allyl; allyl + $H_2 \rightarrow C_3H_6$ + H; allyl + methyl $\rightarrow C_4H_8$; allyl + H $\rightarrow C_3H_6$. The proposed mechanism accounts for the experimental observations mentioned.

Introduction

Although numerous papers have been published on the pyrolysis of proplyene,[1] the investigations have been mainly confined to establishment of product distributions. A more serious study of the reaction mechanism was initiated by Szwarc,[2] who analyzed experimental results obtained at temperatures ranging from 680 to 870° and pressures from 2 to 14 mm. The main products were allene, ethylene, methane, and hydrogen, and the values of A-factor and activation energy were, respectively, 10^{13} $sec.^{-1}$ and 72 kcal./mole assuming first-order kinetics. The following free-radical chain mechanism was then postulated.

$$C_3H_6 \longrightarrow \text{allyl} + H$$
$$\text{allyl} \longrightarrow C_3H_4 + H$$
$$H + C_3H_6 \longrightarrow H_2 + \text{allyl}$$
$$H + C_3H_6 \longrightarrow C_2H_4 + \text{methyl}$$
$$\text{methyl} + C_3H_6 \longrightarrow CH_4 + \text{allyl}$$
$$\text{allyl} + H \longrightarrow C_3H_6$$

Laidler and Wojciechowski,[3] reinvestigating the reaction at temperatures from 580 to 640° and pressures from 60 to 500 mm., obtained distinctly different results. Although ethylene, methane, and hydrogen were again the main products, no allene was detected while a considerable amount of ethane, propane, and higher boiling materials was formed. They determined the reaction to be three-halves order and reported the values of A-factor and activation energy as $10^{11.84}$ $l.^{1/2}/mole^{1/2}$-sec. and 56.7 kcal./mole, respectively. Attributing these discrepancies to the difference in reaction temperature, Laidler, *et al.*, substituted the reaction

$$C_3H_6 + \text{allyl} \longrightarrow \text{polymer} + H$$

for the second step in the Szwarc mechanism. The difficulty, as is typically exhibited by the discordant results mentioned, is apparently inherent in the dual functioning of olefin; *i.e.*, decomposition predominates at high temperatures, whereas polymerization prevails at low temperatures. Ingold and Stubbs,[4] at conditions similar to those used by Laidler, *et al.*, indeed noted the accumulation of condensation products during an initial stage of the pyrolysis. This suggests the formation of a corresponding amount of hydrogen in the same period. On the other hand, according to preliminary experiments by Frey, *et al.*, and Pease, *et al.*,[5] the product distribution in the pyrolysis of propylene in the presence of added hydrogen was found to be quite similar to that of the *straight pyrolysis* (pyrolysis in the absence of added hydrogen). These observations would strongly indicate that propylene is in reality pyrolyzed in the presence of hydrogen whether or not hydrogen is initially added. The present paper describes our efforts to characterize the pyrolysis in the presence of added hydrogen, to elucidate the reaction mechanism in terms of a few selected elementary reactions, and to clarify the decomposing phase of *straight pyrolysis* of propylene.

Experimental

Materials.—Propylene was prepared by the vapor phase dehydration of isopropyl alcohol using activated alumina as a catalyst. After having been washed by water and dried through a trap cooled at −40°, it was stored in a steel cylinder. Purity of prepared propylene was better than 99.9 mole % with impurities being methane, ethylene, and propane (gas chromatographic). Cylinder hydrogen, 99.8 mole % purity with principal impurities being oxygen and water (mass spectrographic), was used after passing over Deoxo catalyst and silica gel. Cylinder helium of 99.9 mole % purity was used without further purification.

Apparatus and Procedure.—A conventional flow system was used. Hydrogen (or helium) and propylene were separately introduced at controlled constant flow velocities using manually operated regulating valves and soap-film flow meters. The reactant gas mixed at a desired mole ratio was then fed into a reaction vessel after being dried over calcium chloride. The reaction vessel was made of a silica tubing, 20 mm. in inside diameter and 180 mm. in length, and was packed with 10~12 mesh silica tips. The free volume was 47.7% of the volume of the tube. The vessel was fitted in an aluminum-bronze block furnace to which a nichrome heating element was applied. Temperature profiles of the reaction vessel were determined during each run while the reaction was taking place by a movable

(1) F. E. Frey and D. F. Smith, *Ind. Eng. Chem.*, **20**, 948 (1928); C. D. Hurd and R. N. Meinert, *J. Am. Chem. Soc.*, **52**, 4978 (1930); R. V. Wheeler and W. L. Wood *J. Chem. Soc.*, 1819 (1930); V. Schneider and P. K. Frolich, *Ind. Eng. Chem.*, **23**, 1405 (1931); H. P. A. Groll, *ibid.*, **25**, 784 (1933); M. V. Krauze M. S. Nemtzov, and E. A. Soskina, *J. Gen. Chem. U.S.S.R.*, **5**, 356 (1935); *C. A.*, **29**, 6205 (1935); H. Tropsch, C. I. Parrish, and G. Egloff, *Ind. Eng. Chem.*, **28**, 581 (1936); V. G. Moor, N. V. Strigaleva, and A. V. Frost, *J. Gen. Chem. U.S.S.R.*, **7**, 860 (1937); *C.A.*, **31**, 5662 (1937); V. G Moor and N. V. Strigaleva, *J. Gen. Chem. U.S.S.R.*, **7**, 1766 (1937); *C.A.*, **31**, 8330 (1937); S. P. Mitsengendler, *J. Gen. Chem. U.S.S.R.*, **7**, 1848 (1937); *C.A.*, **32**, 30 (1938); H. D. Burnham and R. N. Pease, *J. Am. Chem. Soc.*, **64**, 1404 (1942); R. E. Kinney and D. J. Crowley, *Ind. Eng. Chem.*, **46**, 258 (1954).

(2) M. Szwarc, *J. Chem. Phys.*, **17**, 284 (1949).

(3) K. J. Laidler and B. W. Wojciechowski, *Proc. Roy. Soc.* (London), **A259**, 257 (1960).

(4) K. U. Ingold and F. J. Stubbs, *J. Chem. Soc.*, 1749 (1951).

(5) Location is cited in reference 1.

Pt-Pt·Rh thermocouple in a sheath placed along the central axis of the vessel. The reaction temperature (T_{av}) was then defined by a graphic integration according to the equation

$$T_{av}(°K.) = E/R \ln\left[\int_0^z \exp(-E/RT)dz/z\right]$$

where z is the length along the reactor axis and other symbols have their usual significances. The activation energy used with this equation should coincide with the activation energy determined from the temperature dependence of the reaction rate. This match was obtained by trial-and-error calculations. The corresponding volume (V_r) of the vessel was calculated by the equation

$$V_r(ml.) = v\int_0^z \exp[E/R(1/T_{av} - 1/T)]dz$$

where v is the reactor volume for a unit length (0.964 ml./cm.). Contact time (t) was calculated by the equation

$$t(sec.) = V_r TP/760FT_{av}$$

where F is the flow rate of the reactant mixture (ml./sec.), T the room temperature, and P the atmospheric pressure (mm.). Product gas was passed through a trap, immersed in an ice bath, in which condensable products were collected. Non-condensable components were led to gas sampling tubes after measurement of their flow velocities. The reaction was studied under conditions varied over the following range: temperature, 750~850°; contact time, 0.2~2 sec.; hydrogen/propylene mole ratio, 0, 1, 2, 5, and 10.

Analysis.—Gaseous products, presumably consisting of hydrogen and hydrocarbons from methane up to C_4's, were analyzed by a gas chromatograph (g.l.c.) using the following three different columns: (1) a molecular sieve 13-X column (225 cm.) for hydrogen and methane at 100° with 26.6 ml./min. of nitrogen as a carrier gas, (2) an activated alumina column (300 cm.) for C_2- and C_3-hydrocarbons at 80° with 75 ml./min. of hydrogen as a carrier gas, and (3) an acetonylacetone column (1600 cm.) for C_3- and C_4-hydrocarbons at 0° with 50 ml./min. of hydrogen as a carrier gas. Allene and butadiene in the fractions separated through the columns were identified by infrared absorption spectra. Liquid products were also analyzed by g.l.c. using a high vacuum oil column (225 cm.) at 120° with 45 ml./min. of hydrogen as a carrier gas. Relative errors of the analysis were estimated to be less than ±1% for methane and propylene, and ±2% for ethane, ethylene, and propane.

Results

Gaseous Products.—The most remarkable feature of the reaction was the consumption of hydrogen. This is sharply contrasted with the general observation in *straight pyrolysis* where hydrogen is one of the principal products. A typical *product distribution vs. contact time* relation is illustrated in Fig. 1 for runs at 800° and hydrogen/propylene mole ratio of 10. Methane and ethylene were the main products in accordance with the following stoichiometric reaction, $C_3H_6 + H_2 \rightarrow CH_4 + C_2H_4$. The selectivity of the reaction, being highest at low temperatures and high hydrogen/propylene mole ratios, was in no case below 95%. Contrary to the statements made by many authors,[1] the product distribution as expressed by the above stoichiometry was only maintained up to a certain contact time (~1 sec.) after which the formation of ethylene declined. Small amounts of ethane and propane were also produced. The fact that the formation of these low molecular paraffins became negligible upon reducing the initial pressure of hydrogen and the manner in which they were formed relative to the amount of olefins (Fig. 1) indicate the concurrent hydrogenation of the corresponding olefins. Constituents of C_4-hydrocarbon in the decreasing order were butadiene, straight chain monoölefins, and isobutene. Acetylene and allene were present in still

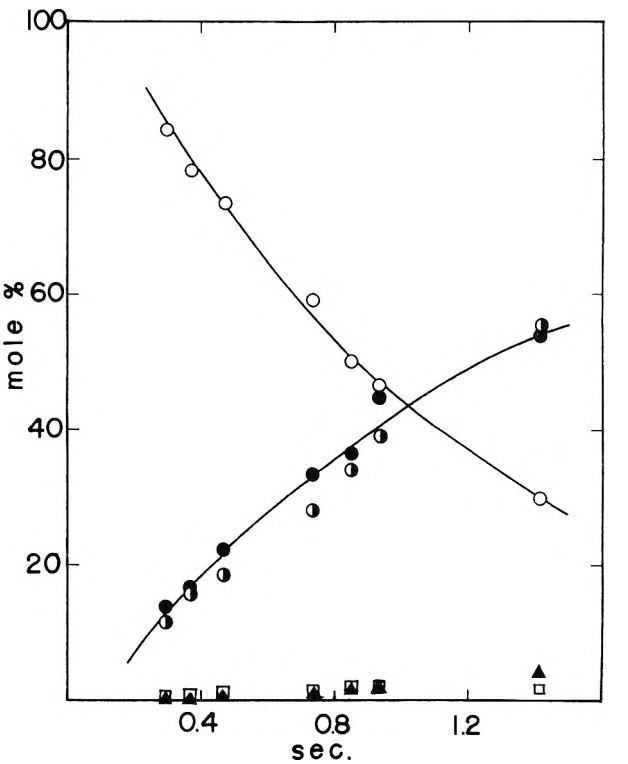

Fig. 1.—Product distribution *vs.* contact time relation at 800° and hydrogen/propylene mole ratio of 10: empty circles, propylene; filled circles, ethylene; half-filled circles, methane; squares, propane; triangles, ethane.

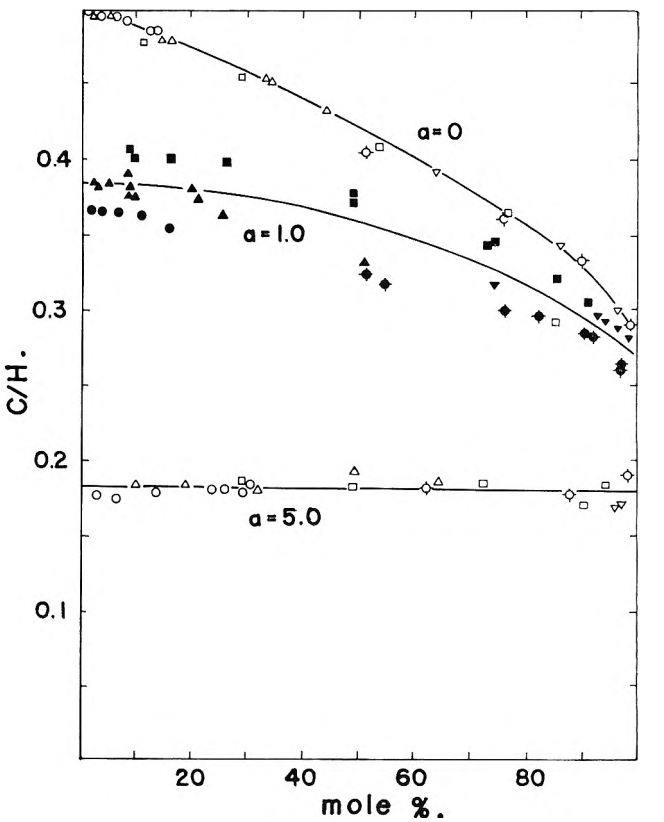

Fig. 2.—Carbon/hydrogen atomic ratio in gaseous products *vs.* conversion of propylene at varying hydrogen/propylene mole ratio (a): circles, 650°; triangles, 700°; squares, 750°; circles with cross, 800°; reversed triangles, 850°.

smaller amounts. These minor products usually totaled less than 0.2 mole % of gases produced and contrary to Frolich's observations[6] did not exceed 5%

(6) Location is cited in reference 1.

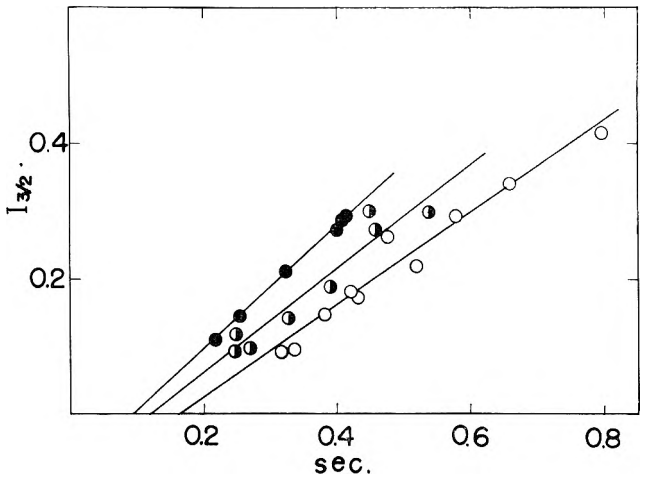

Fig. 3.—Graphic representation of three-halves order rate equation for runs at 800° for ordinate see footnote 7): empty circles, $a = 5$; half-filled circles, $a = 2$; filled circles, $a = 1$.

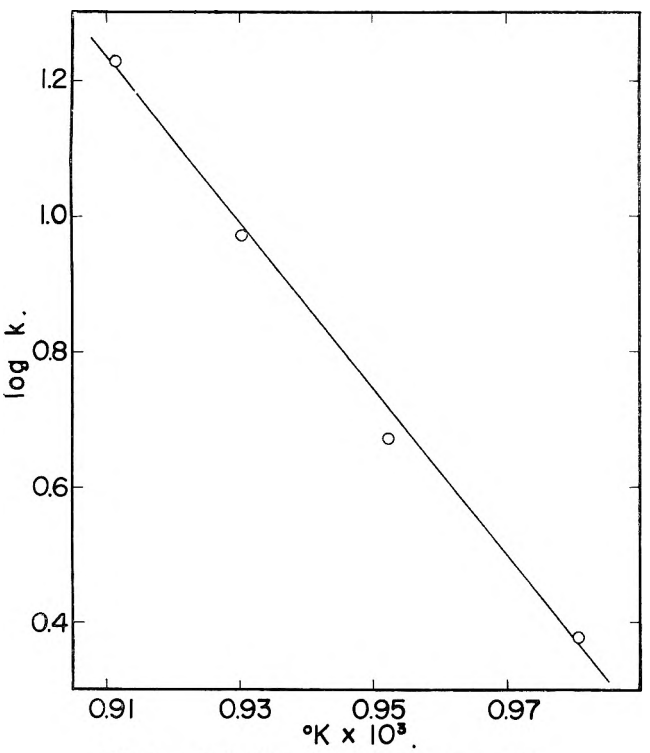

Fig. 4.—Arrhenius plots for runs at $a = 10$.

even when propylene was pyrolyzed without added hydrogen. Butanes and methylacetylene were not detected by g.l.c. The fact that allene was formed in such a trace quantity, while supporting the observation reported by Laidler, *et al.*,[3] and others,[1] does not accord with Szwarc's statement.[2] It should be noted, however, that temperatures and pressures used in the present study were similar to those of the former. Analysis of the related elementary reactions reveals that the formation of allene is favored at higher temperature and lower pressure.

Liquid Products.—Benzene, toluene, xylenes, trimethylbenzenes, and six other unidentified mononuclear aromatic hydrocarbons were separated by g.l.c. as the main constituents of the liquid products. Neither paraffin nor olefin hydrocarbons were detected in the same boiling range. However, the possibility of formation of polynuclear aromatic hydrocarbons could not be excluded Although these higher boiling materials, including carbonaceous matter, were not formed to any noticeable extent when pyrolyzed in the presence of a large excess of hydrogen, they became quite appreciable as the initial concentration of hydrogen was decreased. The effect of hydrogen is illustrated in Fig. 2 in which the atomic ratio of carbon/hydrogen found in the gaseous products is plotted against the conversion of propylene for three different mole ratios. Regardless of reaction temperature, the atomic ratio remained constant through all conversion levels when the hydrogen/propylene mole ratio was 5. For hydrogen-lean mixtures, however, the ratio was decreased with the conversion. This implies, in agreement with our direct observation mentioned above, that the formation of the liquid products becomes appreciable only when the hydrogen/propylene mole ratio is below a certain limit.

Kinetics.—In Table I are collected data which were used for the determination of kinetic parameters. These data were analyzed for the stoichiometric hydrogenolysis assuming a piston flow reactor. The order with respect to propylene was found to be unity using the conventional integration method for runs with hydrogen/propylene mole ratio of 10. The order with respect to hydrogen was preliminarily estimated to be approximately one-half by applying the initial-rate method to an intermediate range of the hydrogen concentration. The one-half order in hydrogen thus obtained was of a limited certainty owing to a relatively narrow range covered for hydrogen concentration. The order was further confirmed, however, by the linear relationship between $I_{3/2}$ and contact time as illustrated in Fig. 3 for over-all three-halves order.[7] It should be noted that the three-halves order is by no means an exact figure but a reasonably rounded expression. Also indicated in Fig. 3 is an approximate magnitude of the induction period (~0.1 sec.) which was again reduced to an unnoticeable extent upon increasing hydrogen concentration and/or temperature. The induction period was also noted by Stubbs, *et al.*[4] Arrhenius plots of the three-halves order rate constants, as illustrated in Fig. 4, correspond to the values of A-factor and activation energy of $10^{12.3}$ $l.^{1/2}/mole^{1/2}$-sec. and 55.9 kcal./mole, respectively. According to our estimation, however, the error involved in the activation energy may be as large as ±4 kcal./mole and the corresponding uncertainty in the A-factor a factor of about 10. For *straight pyrolysis*, the values of A-factor and activation energy are calculated as $10^{12.7}$ $sec.^{-1}$ and 64.6 kcal./mole, respectively, assuming first-order kinetics. These figures are intermediate between those reported by Stubbs, *et al.*,[4] and Szwarc.[2]

Discussion

Initiation Reactions.—Possible radical producing reactions are listed in eq. 1–3 with relevant kinetic parameters.

$$C_3H_6 \longrightarrow \text{allyl} + H; \qquad E = 99.2 - Q, \log A = (15) \quad (1)$$

(7)

$$I_{3/2} = \left(\frac{a+1}{a-1}\right)^{1/2} \times \ln \left\{ \frac{[(a-x)^{1/2} + (a-1)^{1/2}][a^{1/2} - (a-1)^{1/2}]}{[(a-x)^{1/2} - (a-1)^{1/2}][a^{1/2} + (a-1)^{1/2}]} \right\}$$

where a is the hydrogen/propylene mole ratio and x the conversion of propylene.

TABLE I

Reaction temp. (°C.)	Mole ratio	Contact time (sec.)	Propylene consumed (mole %)	Rate[a] constant
746.3	9.4	0.52	7.4	2.10
746.3	10.0	.52	8.6	2.42
746.3	11.4	.92	18.1	2.55
746.3	10.6	1.28	24.1	2.40
746.3	9.3	1.60	29.4	2.35
776.7	9.2	0.19	2.4	4.49
776.7	10.4	.42	13.0	4.65
776.7	9.4	.44	13.6	4.59
776.7	9.7	.57	19.5	4.80
776.7	10.1	.76	25.0	4.54
776.7	10.9	.92	33.2	4.99
776.7	9.9	1.07	35.9	4.67
776.7	11.1	1.36	46.1	4.95
776.7	9.8	1.39	43.2	4.45
801.4	9.9	0.18	15.8	9.93
801.4	10.5	.26	21.7	10.25
801.4	10.1	.33	26.6	8.94
801.4	10.4	.56	40.9	8.59
801.4	10.9	.74	50.0	8.60
801.4	10.1	.82	53.4	9.53
801.4	10.0	1.30	70.1	9.42
823.8	10.6	0.24	35.2	18.2
823.8	10.7	.30	39.9	17.1
823.8	9.6	.38	46.7	16.8
823.8	10.0	.49	55.3	16.7
800.6	5.0	0.22	9.3	8.41
800.6	4.9	.26	12.4	8.37
800.6	5.1	.32	17.3	8.64
800.6	5.1	.40	21.7	8.35
800.6	5.0	.41	22.6	8.58
800.6	5.1	.42	23.4	8.49
800.6	2.11	0.25	7.5	6.80
800.6	1.96	.25	9.1	8.59
800.6	2.03	.27	7.5	6.04
800.6	2.05	.33	11.1	6.46
800.6	1.97	.39	14.1	6.49
800.6	2.04	.45	20.8	8.50
800.6	2.03	.46	19.6	7.51
800.6	1.91	.54	20.8	6.66
800.6	1.01	0.32	6.4	5.80
800.6	0.93	.34	6.3	5.21
800.6	1.02	.38	9.7	6.42
800.6	1.00	.42	12.0	6.68
800.6	1.03	.43	10.7	6.20
800.6	1.04	.48	16.5	7.89
800.6	1.04	.52	14.0	5.77
800.6	0.96	.58	17.6	6.62
800.6	0.98	.66	20.3	6.44
800.6	1.00	.80	24.2	6.15
777.0	0	0.64	4.9	0.187
777.0	0	0.82	6.6	.155
777.0	0	1.36	14.2	.158
777.0	0	1.56	17.2	.155
800.3	0	0.40	8.7	.450
800.3	0	.62	14.2	.366
800.3	0	.80	18.4	.339
800.3	0	.97	26.6	.401
800.3	0	1.02	24.6	.345
800.3	0	1.32	38.0	.426
800.3	0	1.72	42.7	.367
824.3	0	0.36	9.6	.636
824.3	0	.48	17.6	.677
824.3	0	.65	24.7	.631
824.3	0	.87	37.2	.689
824.3	0	1.18	47.3	.650
848.5	0	0.20	19.8	1.28
848.5	0	.29	26.6	1.18
848.5	0	.34	27.7	1.04
848.5	0	.41	36.3	1.18
848.5	0	.48	42.2	1.22

[a] Units are $l.^{1/2}/mole^{1/2}$-sec. for runs with hydrogen and $sec.^{-1}$ for runs without hydrogen.

$C_3H_6 \longrightarrow$ vinyl + methyl;

$$E = 91.0, \log A = (15.6) \quad (2)$$

$H_2 + M \longrightarrow H + H + M$;

$$E = 104.3, \log A = 14.0 \quad (3)$$

The values listed are at 1000°K. in units of kcal./mole for activation energy and either $sec.^{-1}$ or l./mole-sec. for A-factor depending on reaction order. Those in parentheses are the values which are less certain. The stabilization energy of allyl radical has been a controversial subject and is deliberately represented by an undetermined quantity (Q) in reaction 1. This energy is estimated to be more than 20 kcal./mole by Szwarc[8] based on indirect kinetic evidence, although semi-empirical calculations[9] indicate much lower values. If 20 kcal./mole is assumed for Q, reaction 1 is faster than reaction 2 by a factor of about 100 at 1000°K. ignoring the difference in the entropy contribution which slightly favors the latter reaction. The entropy of activation for the rupture of C–C linkage is generally larger than that for the rupture of C–H linkage but by not more than 5 cal./mole-°K. Therefore we conclude that reaction 1 is more important for radical production under the present experimental conditions, although reaction 2 may become significant at higher temperatures. Reaction 3, being by far the slowest process owing to higher activation energy and smaller bimolecular A-factor, can be ignored. It should be mentioned at this point that the bimolecular initiation between propylene molecules

$2C_3H_6 \longrightarrow$ allyl + propyl;

$$E \geq 62.5 - Q, \log A = (8.5) \quad (4)$$

may become important for propylene concentrations exceeding about 10^{-2} mole/l. Thus the mechanism of the high pressure pyrolysis of propylene should be more complex.

Propagation Reactions.—A sequence of metathetical reactions which are induced by either hydrogen atom or allyl radical will be considered. Hydrogen atom first reacts with propylene by the reactions

$H + C_3H_6 \longrightarrow n$-propyl*;

$$E = 1.5, \log A = 10.5 \quad (5)$$

$H + C_3H_6 \longrightarrow H_2 +$ allyl;

$$E = 1.5, \log A = 10.1 \quad (6)$$

The asterisk indicates a *hot radical* which in this case possesses 35 kcal./mole excess energy. The value of $E_5 = 1.5$ kcal./mole is that reported lately by Scheer and Klein.[10] The value assigned to A_5 is based on

(8) M. Szwarc, *J. Chem. Phys.*, **18**, 1660 (1950); see also ref. 2.
(9) J. S. Roberts and H. A. Skinner, *Trans. Faraday Soc.*, **45**, 339 (1949).
(10) M. D. Scheer and R. Klein, *J. Phys. Chem.*, **65**, 375 (1961).

$\Delta S_{8,5}^0$ = 23.2 cal./mole-°K. and $A_8 = 10^{14.5}$ sec.$^{-1}$. The evaluation of the latter will be discussed later. We believe these figures to be more consistent with modern thermodynamic data, hence with discussion which follows; although somewhat different values have been assigned by Allen, Melville, and Robb.[11] These values correspond to $k_5 = 10^9$ l./mole-sec. at 300°K., in excellent agreement with that hitherto reported. The values of kinetic parameters for reaction 6 are based on the experiments by Darwent and Roberts[12] in which they have shown that $E_5 = E_6$ and $0.42A_5 = A_6$. Only *n*-propyl radical is considered in reaction 5, although the association of hydrogen atom with propylene would produce *sec*-propyl radical at a faster rate. A few lines of evidence[13] indicate that *sec*-propyl radical can only decompose to form original species at a reasonable rate. This rules out the possibility that this radical serves as an effective chain carrier.

The subsequent decomposition of *n*-propyl radical is possible by the reactions

$$n\text{-propyl}^* \longrightarrow C_2H_4 + \text{methyl}; \qquad E = 30.4, \log A = 13.4 \quad (7)$$

$$n\text{-propyl}^* \longrightarrow C_3H_6 + H; \qquad E = 38.4, \log A = 14.5 \quad (8)$$

$$n\text{-propyl}^* \longrightarrow H_2 + \text{allyl}; \qquad E = (30), \log A = (13) \quad (9)$$

To evaluate kinetic parameters for reactions 7 and 8, the following values are assumed: D(Me–H) = 102.1 kcal./mole,[14] D(*n*-Pr–H) = 97.4 kcal./mole,[14] $E_5 = 1.5$ kcal./mole,[10] and $E_{-7} = 7$ kcal./mole.[15] By simple calculations based on these best available figures, the activation energies for reactions 7 and 8 are estimated to be 30.4 and 38.4 kcal./mole, respectively. Both of these values are only slightly lower than those recommended by Jackson and McNesby.[16] Using Trotman-Dickenson's experimental rate constants[17] at their average temperatures and our values of the activation energies, $10^{13.4}$ sec.$^{-1}$ and $10^{14.5}$ sec.$^{-1}$ are obtained for the A-factor of reactions 7 and 8, respectively. Considering uncertainties involved, the ratio k_8/k_7 = 0.05 at 500° calculated from our estimated values is in excellent agreement with McNesby's experimental value of $k_8/k_7 = 0.03$ at the same temperature.[16] Of these two competitive reactions, reaction 7 should predominate since the exothermicity of reaction 5 is some 8 kcal./mole in excess of the activation energy of the process. One of the distinctive features of the *hot radical* is that its unimolecular decomposition is concerted with reaction 5. Thus the energy required to surmount the activation barrier is partly supplied from the exothermicity of the preceding reaction. This may be an important reason for ignoring the bimolecular decomposition of the radical even though its pressure is expected to be extremely low. Reaction 9 is a comparatively difficult process since it assumes a four-center arrangement in the transition state. The activation energy of 30 kcal./mole speculated by Gordon and Smith[18] may be the minimum expected for such a reaction. Reaction 9 is kinetically indistinguishable from reaction 6, and it will be ignored in our subsequent discussion. This reaction was considered by Laidler, *et al.*,[3] for *straight pyrolysis* but the values of kinetic parameters were erroneously quoted.

Methyl radical produced by reaction 7 will react with reactant gases by the reactions

$$\text{methyl} + H_2 \longrightarrow CH_4 + H; \qquad E = 10.0, \log A = 8.7 \quad (10)$$

$$\text{methyl} + C_3H_6 \longrightarrow CH_4 + \text{allyl}; \qquad E = 7.7, \log A = 7.8 \quad (11)$$

$$\text{methyl} + C_3H_6 \longrightarrow \text{butyl}; \qquad E = 8.8, \log A = 9.0 \quad (12)$$

The values of kinetic parameters listed are taken from the literature.[19] The rates of reactions 10 and 11 are of comparable magnitude under the present experimental conditions, while the latter alone will be the normal path in the case of *straight pyrolysis*. Reaction 12 is a relatively fast reaction leading to higher boiling products. As indicated by the equilibrium ratio of (methyl)/(butyl) = 10^3, however, the reverse of reaction 12 is still faster. Therefore reaction 12 cannot be an effective process unless butyl radical is eliminated from the system with sufficient rate.

Possible reactions induced by allyl radical are

$$\text{allyl} + H_2 \longrightarrow C_3H_6 + H; \qquad E = 7.3 + Q, \log A = 8.3 \quad (13)$$

$$\text{allyl} + C_3H_6 \longrightarrow \text{higher boiling products}; \qquad E = (15), \log A = (6) \quad (14)$$

$$\text{allyl} \longrightarrow C_3H_4 + H; \qquad E = (50.2 + Q), \log A = (13.6) \quad (15)$$

The values assigned to reaction 13 are estimated from those of the reverse reaction (E_6 and A_6) and the associated change in enthalpy and entropy. The estimation of A_{13} is based on S^0(allyl) = 67.5 cal./mole-°K., which can be obtained from the entropy of propylene with symmetry and electron degeneracy considerations. The stabilization energy term (Q) appears again in E_{13}. Very little has been known about reactions 14 and 15. The values assigned to reaction 14 are due to Laidler, *et al.*[3] Those assigned to reaction 15 are based on the thermodynamic data assuming $E_{-15} = E_5$ and $A_{-15} = A_5$. All of these reactions are invariably slow, undoubtedly by reason of the large stabilization in allyl radical. Among these, reaction 13 will predominate at higher hydrogen concentrations as in the present case. In the case of *straight pyrolysis*, however,

(11) P. E. M. Allen, H. W. Melville, and J. C. Robb, *Proc. Roy. Soc.* (London), **A218**, 311 (1953).

(12) B. deB. Darwent and R. Roberts, *Discussions Faraday Soc.*, **14**, 55 (1953).

(13) J. R. McNesby, C. M. Drew, and A. S. Gordon, *J. Chem. Phys.*, **24**, 1260 (1956); F. P. Lossing and J. B. deSousa, *J. Am. Chem. Soc.*, **81**, 281 (1959); W. M. Jackson and J. R. McNesby, *J. Chem. Phys.*, **36**, 2272 (1962).

(14) S. W. Benson and A. Amano, *ibid.*, **36**, 3464 (1962).

(15) L. Mandelcorn and E. W. R. Steacie, *Can. J. Chem.*, **32**, 474 (1954).

(16) W. M. Jackson and J. R. McNesby, *J. Am. Chem. Soc.*, **83**, 4891 (1961).

(17) J. A. Kerr and A. F. Trotman-Dickenson, *Trans. Faraday Soc.*, **55**, 572 (1959).

(18) A. S. Gordon and S. R. Smith, *J. Chem. Phys.*, **34**, 331 (1961).

(19) E. W. R. Steacie, "Atomic and Free Radical Reactions," Vol. II, Reinhold Publ. Corp., New York, N. Y., 1954, pp. 527; A. F. Trotman-Dickenson and E. W. R. Steacie, *J. Chem. Phys.*, **19**, 169 (1951); M. Miyoshi and R. K. Brinton, *ibid.*, **36**, 3019 (1962).

reaction 14 should be important as was pointed out by Bryce and Ruzicka[20] and postulated by Laidler, *et al.*[3] Reaction 15, suggested by Szwarc,[2] can only become appreciable at higher temperatures and lower pressures.

Termination Reactions.—The termination process is determined mainly by the relative concentration of radicals present in the reaction system, since activation energy of association reactions between radicals can be assumed to be nearly zero. From the foregoing discussion, the steady-state concentration of radicals is apparently in the following order: (allyl) > (methyl), (H) > (propyl). Important termination reactions are therefore

$$\text{allyl} + \text{allyl} \longrightarrow \text{diallyl};\ E = (0) \qquad (16)$$

$$\text{allyl} + \text{methyl} \longrightarrow C_4H_8;\ E = (0),\ \log A = (8) \qquad (17)$$

$$\text{allyl} + \text{H} \longrightarrow C_3H_6;\ E = (0),\ \log A = (9) \qquad (18)$$

Reaction 16, although a reasonable choice from the concentration view point, would not be an effective process. Diallyl, even if once formed by reaction 16, would dissociate at the extremely weak central C–C linkage. Thus allyl radical would be present in such concentrations that it would be consumed through reactions 17 and/or 18. The choice between these latter reactions may be made on the basis of the efficiency of the *concerted reaction*, reaction 5 followed by reaction 7, which in turn determines the rate-controlling step of the chain.

Chain Mechanism.—Based on the preceding considerations, the following set of reactions is selected to best explain the thermal decomposition of propylene in the presence of excess hydrogen.

$$C_3H_6 \xrightarrow{1} \text{allyl} + \text{H}$$

$$\text{H} + C_3H_6 \xrightarrow{5} n\text{-propyl}^*$$

$$\text{H} + C_3H_6 \xrightarrow{6} H_2 + \text{allyl}$$

$$n\text{-propyl}^* \xrightarrow{7} C_2H_4 + \text{methyl}$$

$$\text{methyl} + H_2 \xrightarrow{10} CH_4 + \text{H}$$

$$\text{methyl} + C_3H_6 \xrightarrow{11} CH_4 + \text{allyl}$$

$$\text{allyl} + H_2 \xrightarrow{13} C_3H_6 + \text{H}$$

$$\text{allyl} + \text{methyl} \xrightarrow{17} C_4H_8$$

$$\text{allyl} + \text{H} \xrightarrow{18} C_3H_6$$

This scheme is in conformity with the observed over-all stoichiometry. The prime effect of added hydrogen is to prevent the accumulation of allyl radical through reaction 13 thus minimizing the formation of higher boiling materials. As has been discussed, the presence of excess hydrogen is the reason for ignoring reactions such as (12), (14), and (15) which are otherwise important. It can be shown, *via* the steady-state approximation, that the following rate laws are obtained depending on the mode of termination:

Case I: Chain reaction is controlled by reaction 11 and terminated by reaction 17

$$d(C_2H_4)/dt = (20k_1k_{11}k_{13}/9k_{17})^{1/2}(C_3H_6)(H_2)^{1/2}$$

Case II: Chain reaction is controlled by reaction 5 and terminated by reaction 18

$$d(C_2H_4)/dt = (10k_1k_5k_{13}/9k_{18})^{1/2}(C_3H_6)(H_2)^{1/2}$$

The relations $0.4k_5 = k_6$ and $k_{10}(H_2) = k_{11}(C_3H_6)$ are used in the derivation of the above over-all rate equations. The values of kinetic parameters deduced from these rate laws are $A = 10^{11.8}$ l.$^{1/2}$/mole$^{1/2}$-sec. and $E = 55.9$ kcal./mole for Case I and $A = 10^{12.4}$ l.$^{1/2}$/mole$^{1/2}$-sec. and $E = 54.0$ kcal./mole for Case II. The stabilization energy (Q) of allyl radical is canceled out in the over-all activation energy and the ratio A_1/A_{18} ($\sim A_1/A_{17}$) is replaced by the entropy term in the over-all A-factor. It is expected, therefore, that the final over-all figures do not include any serious amount of errors. It should be noted that $E = 54.0$ kcal./mole for Case II may be the minimum activation energy corresponding to the *concerted reaction* of more than 80% efficiency. Both the order of the reaction and the values of kinetic parameters obtained from the proposed mechanism are in good agreement with the experimental observations. The theoretical rate constant at 1000°K. for Case II is only a factor of three larger than the experimental value, thus we favor the latter mechanism at present.

Acknowledgments.—The authors wish to thank Professor Hiroshi Tokuhisa of the Tohoku University and Professor Sidney W. Benson of the University of Southern California for helpful discussions.

(20) W. A. Bryce and D. J. Ruzicka, *Can. J. Chem.*, **38**, 827, 835 (1960).

THE DEHYDRATION OF POLYHALITE

BY MARCEL W. NATHANS

Lawrence Radiation Laboratory, University of California, Livermore, California

Received November 21, 1962

The kinetics of the reaction $K_2Ca_2Mg(SO_4)_4 \cdot 2H_2O \rightarrow K_2CaMg(SO_4)_3 + CaSO_4 + 2H_2O$ was studied by an isothermal method. The reaction is first order with $\log k\,(\text{min.}^{-1}) = 21.50 - 1.22 \times 10^4/T$. Differential thermal analysis was used to determine the decomposition pressures between 0.5 and 6.1 bars. Below about 1.5 bars the reliability of the measurements is questionable. Between 1.7 and 6.1 bars, the results can be expressed as $\log P_{H_2O} = 27.77 - 1.75 \times 10^4/T$.

Introduction

The interest in the mineral polyhalite, $K_2Ca_2Mg(SO_4)_4 \cdot 2H_2O$ stems from its widespread occurrence in the evaporite deposits of the Salado formation in southeastern New Mexico, the site of the execution of Project Gnome, the first underground nuclear detonation for non-military purposes. Of particular interest is the decomposition reaction

$$K_2Ca_2Mg(SO_4)_4 \cdot 2H_2O \longrightarrow K_2CaMg(SO_4)_3 + CaSO_4 + 2H_2O \quad (1)$$

which occurs above 280° and which is apparently irreversible under ordinary pressure conditions. In differential thermal analysis (d.t.a.) the reaction shows up as a sharp characteristic endothermic peak, the peak temperature occurring at about 360°, the exact value depending upon the heating rate. The shape of the peak[1] indicates a first-order reaction.

Many years ago some work with polyhalite was carried out by the U.S. Bureau of Mines,[2] where the mineral was investigated as a possible source of potassium salts. Several references to the d.t.a. of polyhalite can be found in the literature,[3] including an application of d.t.a. to the quantitative determination in halite, but no study of either the kinetics or the decomposition pressure of reaction 1 is available.

Experimental

The polyhalite was sampled from marker bed 121 in the Salado formation in southeastern New Mexico. Chemical analysis showed less than 1% impurities, consisting mainly of NaCl. The close agreement between the d.t.a. curves of different authors,[3] obtained with material of different origin and impurity content, shows that the impurities have little or no effect on the reaction.

Vapor pressure data were obtained by determining the temperatures at which the d.t.a. curves began to deviate from the base line when steam at various pressures flowed over the sample. The equipment used has already been described elsewhere.[4] The powder sample holder was employed with the thermocouple connections such that the control couple was located in the block and the measuring couple in the sample. The sample size was kept constant at 200 ± 2 mg. Heating rates were 10° per minute and 5° per minute (nominal). The amplification of the differential signal was such that the peak deviation from the base line was about 60 μv.

Isothermal measurements were made by placing a platinum cylindrical cup with the sample on a small platform which was suspended from an Ainsworth Right-A-Way balance in a Marshall furnace. The furnace was lined with a stainless steel tube which had a guide tube welded to it to hold a thermocouple. This assembly was mounted on a platform which could be raised or lowered by means of a motor. The temperature was controlled to about ± 0.5° with a Foxboro potentiometer controller. At the end of each run the sample temperature was determined by placing the thermocouple in the sample and letting the system come to temperature equilibrium.

Results

Decomposition Pressure.—The results of the decomposition pressure measurements are plotted in Fig. 1 as $\log P_{H_2O}$ *vs.* $1/T$(°K.). Above about 1.5 bars the

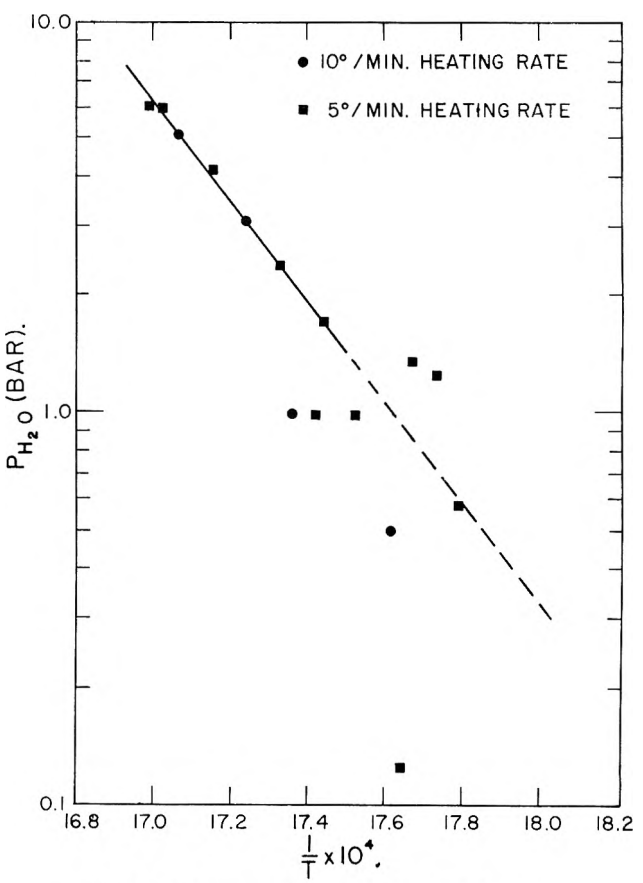

Fig. 1.—Decomposition pressure of polyhalite.

points fall on a straight line, but at lower pressures there is considerable scatter and no line or curve can be defined in this region. The reason is most likely to be found in Borchardt's analysis of the method used.[5] Borchardt has also pointed out that the pressure data may be a little below the equilibrium pressures, but that the slope of the log P *vs.* $1/T$ curve is still $\Delta H/4.57$. We feel, however, that this is not the case here because of the large activation energy of the reaction and the high sensitivity of our equipment; the breaks in the curves are generally quite sharp.

(1) H. E. Kissinger, *J. Res. Natl. Bur. Standards*, **57**, 217 (1956).

(2) See, *e.g.*, J. E. Conley, F. Fraas, and J. M. Davidson, U. S. Bur. Mines Rept. Invest. 3167 (1932); H. H. Storch, *Ind. Eng. Chem.*, **22**, 934 (1930).

(3) See, *e.g.*, I. S. Kurnakov, L. G. Berg, and I. N. Lepeshkov, *J. Appl. Chem.* (U.S.S.R.), **12**, 525 (1939); L. G. Berg, I. N. Lepeshkov, and N. V. Bodaleva, *Compt. rend. Acad. Sci. URSS*, **31**, 577 (1941); G. Cocco, *Periodico di Mineralogica*, **21**, 105 (1952).

(4) M. W. Nathans, *J. Inorg. Nucl. Chem.*, **22**, 231 (1961).

(5) H. Borchardt, *J. Phys. Chem.*, **61**, 827 (1957).

A least squares analysis shows that the data between 1.7 and 6.1 bars can be represented by

$$\log P_{H_2O} = 21.50 - \frac{1.22 \times 10^4}{T}$$

so that $\Delta H = 56$ kcal. per mole of polyhalite. This value is a little lower than the value of 66 ± 5 kcal./mole obtained by Storch by means of direct heat measurements.

It is difficult to assign a value to the probable error of our measurements. The standard deviation in ΔH came out to be less than 1%. This cannot be realistic, however, because our pressure measurements are certainly not better than several per cent. A 5% error in the pressure affects the value of ΔH by about 7%, and this appears to be a reasonable estimate of the actual precision with which ΔH is known.

The value of ΔH is considerably higher than that for the dehydration of simple substances. For example, ΔH for the reaction

$$CaSO_4 \cdot 2H_2O \longrightarrow CaSO_4 + 2H_2O$$

is about 25 kcal./mole. The reason is clearly to be found in the complicated nature of reaction 1.

Isothermal Kinetics.—The weight loss data obtained in air between 300 and 335° on 1.50-g. samples are plotted in Fig. 2 as log $(1 - x)$ *vs.* time, where x is the fraction reacted. The plots clearly show that the reaction is of first order. Sample size had no effect within the limits of our precision as can be seen from Table I. The effect of the humidity of the air may be neglected, because the equilibrium pressure of water vapor is at least two orders of magnitude greater than the ambient water vapor pressure.

TABLE I

COMPARISON BETWEEN OBSERVED AND CALCULATED VALUES OF THE RATE CONSTANTS FOR POLYHALITE DECOMPOSITION

Sample wt., g.	Temp., °C.	k (obsd.), min.$^{-1}$	k (calcd.), min.$^{-1}$
1.50	301	0.00210	0.00199
1.50	312	.00729	.00751
1.78	317	.0169	.0132
2.67	319	.0150	.0168
1.50	319	.0153	.0168
1.50	326	.0403	.0376
1.50	335	.100	.0989

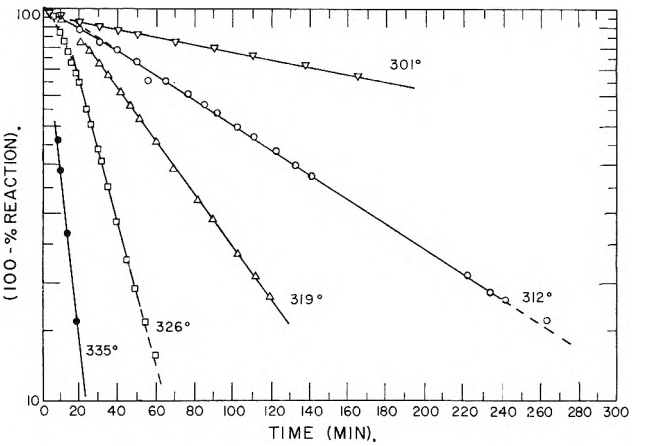

Fig. 2.—Log (1 − fraction reacted) *vs.* time curves of polyhalite at different temperatures.

A least squares analysis of the data yields the rate law

$$\frac{dx}{dt} = \left[-10^{27.774} \exp\left(-\frac{4.03 \times 10^4}{T} \right) \right] (1 - x)$$

The activation energy is 80 kcal./mole, with a standard deviation of 3 kcal./mole.

It appears that the plots in Fig. 2 indicate the presence of an induction period. It could be shown, however, that the initial curvature was caused by the approach of the sample to the steady-state temperature. Fresh samples of 0.8 and of 2.6 g. were placed in the furnace with the thermocouple in the sample and the temperature was followed as a function of time. The small sample reached equilibrium in 7 min., the larger one reached an intermediate state after 15 min., held that temperature for 40 min., then reached the final temperature in another 10 min. This behavior followed very closely the behavior of the initial portions of the rate curves.

Acknowledgment.—This work was performed under the auspices of the U.S. Atomic Energy Commission.

A STUDY OF POLYNUCLEAR AROMATIC HYDROCARBONS USING THE VACUUM SPARK MASS SPECTROGRAPH[1]

BY F. NEIL HODGSON,

Monsanto Research Corporation, Dayton, Ohio

MICHEL DESJARDINS,

University of Cincinnati, Cincinnati, Ohio

AND WILLIAM L. BAUN

Directorate of Materials and Processes Aeronautical Systems Division, Wright-Patterson Air Force Base, Ohio

Received November 24, 1962

The polynuclear aromatic hydrocarbons anthracene, pyrene, triphenylene, chrysene, naphthacene, picene, perylene, benzoperylene, and coronene have been studied in the spark mass spectrograph. Contrary to previous reports that only atomic species can be observed in the spark, ions of masses up to and above the molecular weights of the respective compounds were observed. For each of these compounds, distinct groups of lines have been observed, the number of groups equaling the number of carbon atoms in the molecule. For each compound, also, a strong molecular ion was observed. Associations of carbon atoms occurring in the spark mass spectrum of coronene were compared to those observed for both graphite and amorphous carbon. The carbon associations present in the spectrum of coronene are qualitatively similar to those observed for graphite.

Introduction

Though high frequency spark ionization methods have been used successfully in mass spectrographic studies of inorganic solids for some time,[2] little work has been published concerning the behavior of organic materials in the spark. Indeed it has been reported that, in the spark, organic materials are broken down to their component elements.[3]

Recent investigations by Dörnenburg and Hintenberger[4,5] and by Baun and Fischer[6] have shown that ions up to C_{28}^+ can be observed in the spark mass spectrum of graphite. Since graphite and polynuclear aromatic hydrocarbons are not structurally dissimilar, the latter might logically be the first to be studied in an investigation of the fragmentation and ionization of organic compounds in the radiofrequency spark source. This paper describes an experimental study of fused aromatic structures up to C_{24}, using a spark mass spectrograph.

Experimental

A double focusing mass spectrograph of the Mattauch–Herzog design was used for this work. The instrument, which was built by Bell and Howell Research Center under contract with the United States Air Force, is described in detail by Robinson.[7,8] A prototype of Consolidated Electrodynamics Corporation's Model 21–110, the instrument utilizes a radiofrequency (rf.) spark source operated at an instantaneous voltage of 100–150 kv. of rf. voltage and a photographic recording device, using 2 × 15-in. photographic plates. For this work, Ilford Q2 plates were used and were developed for 3 min. in D-19 developer diluted 10 to 1. Spark repetition rates could be varied from 1 to 10,000 pulses per second (p.p.s.) and the pulse length from 5 to 50 microseconds. In this study, the compounds were sparked at a rate no greater than 1000 p.p.s., the usual rate being 100 p.p.s. The pulse length was kept at a minimum consistent with the production of ions, so that the pressure in the source did not rise prohibitively.

All spectra were obtained by compacting the samples into hollow electrodes of high purity aluminum. These were then used to produce the spark. Exposures were measured by a pair of beam monitors which intercepted 50% of the beam. Exposures were recorded as coulombs of charge and are independent of time. Data shown in the figures were taken from the photographic plate by means of a microdensitometer. The intensities of the lines were read as 100 minus per cent transmission, thus providing an arbitrary scale on which to measure the ion beam intensities. The letters RB on the abscissa of Fig. 1 and 2 indicate reverse blackening; *i.e.*, photographic reversal due to very strong lines.

Results

Coronene.—Since each of the six peripheral rings of coronene has the normal Kekulé structure, the compound is extremely stable and inert, hence was a most suitable starting compound for this study. Masses of fragment ions up to molecular weight are observed as shown in Fig. 1, with the ions being grouped into 24 distinct groups, corresponding to the number of carbon atoms in the molecule. Though not always the strongest line of the group, the first mass of most groups is a multiple of the mass of carbon-12 and it is reasonable to assume that the first lines of the groups are due to ions containing only carbon. Thus groups appear at m/e 12, 24, 36, 48, etc., with the other lines of the group resulting from ions with protons associated.

While intensity of the mass lines generally decreases with increasing mass number, the molecular ion group is quite strong even for high molecular weight compounds. Intense lines in the high mass region tend to be broadened considerably, due to a space-charge effect.[9] Since the lines of the molecular weight group of coronene are greatly broadened, the group is quite prominent. For this reason these lines are drawn heavier than others in Fig. 1. A doubly-charged molecular ion group is seen in the range of mass numbers 144–150 and is recognized by the appearance of lines at fractional mass numbers.

Other Polynuclear Aromatic Hydrocarbons.—In a series of fused aromatic hydrocarbons, the compounds benzoperylene, perylene, picene, naphthacene, chrysene, triphenylene, pyrene, and anthracene, as well as a mixture of triphenylene and perylene, were examined in

(1) Work supported by the United States Air Force, Aeronautical Systems Division, Wright-Patterson Air Force Base, Ohio.

(2) M. G. Inghram, *J. Phys. Chem.*, **57**, 809 (1953).

(3) J. H. Beynon, "Mass Spectrometry and Its Applications to Organic Chemistry," Elsevier Publishing Co., Amsterdam, 1960.

(4) Von E. Dörnenburg and H. Hintenberger, *Z. Naturforsch.*, **14a**, 765 (1959).

(5) Von E. Dörnenburg, H. Hintenberger, and J. Fragen, *ibid.*, **16a**, 532 (1961).

(6) W. L. Baun and D. W. Fischer, *J. Chem. Phys.*, **35**, 1518 (1961).

(7) C. Robinson, *Rev. Sci. Instr.*, **28**, 777 (1957).

(8) C. Robinson, *ibid.*, **29**, 522 (1958).

(9) G. Perkins, private communication.

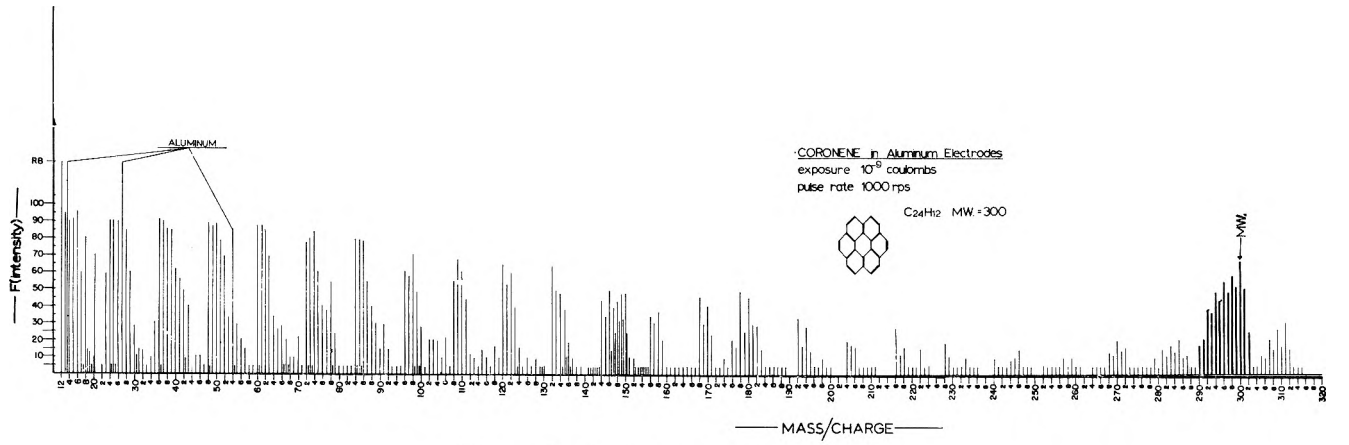

Fig. 1.—Spark mass spectrum of coronene.

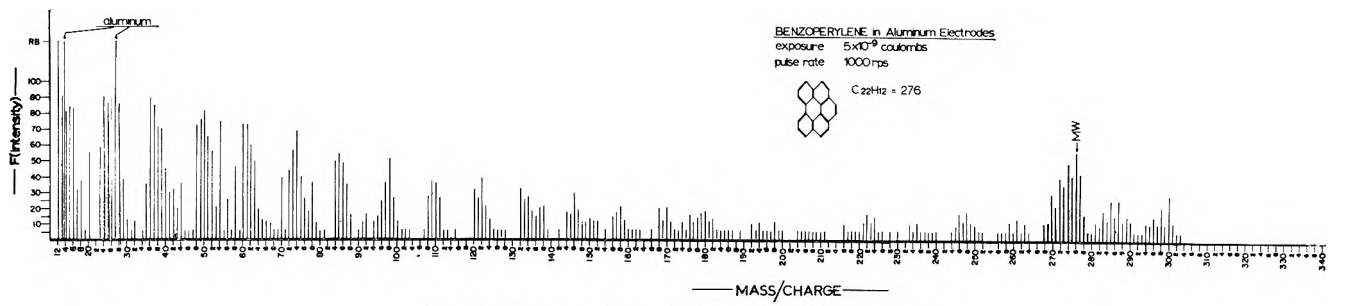

Fig. 2.—Spark mass spectrum of benzoperylene.

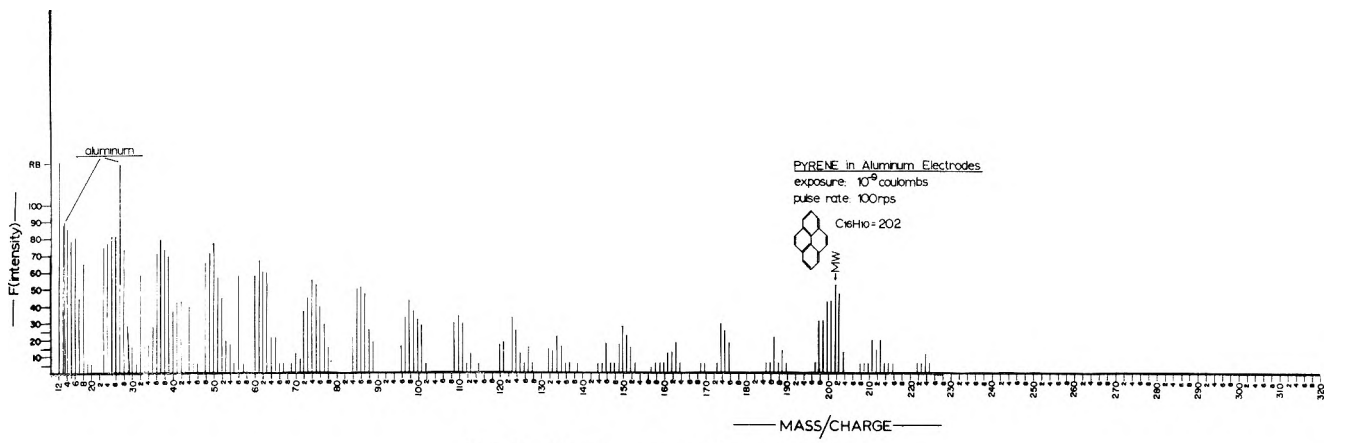

Fig. 3.—Spark mass spectrum of pyrene.

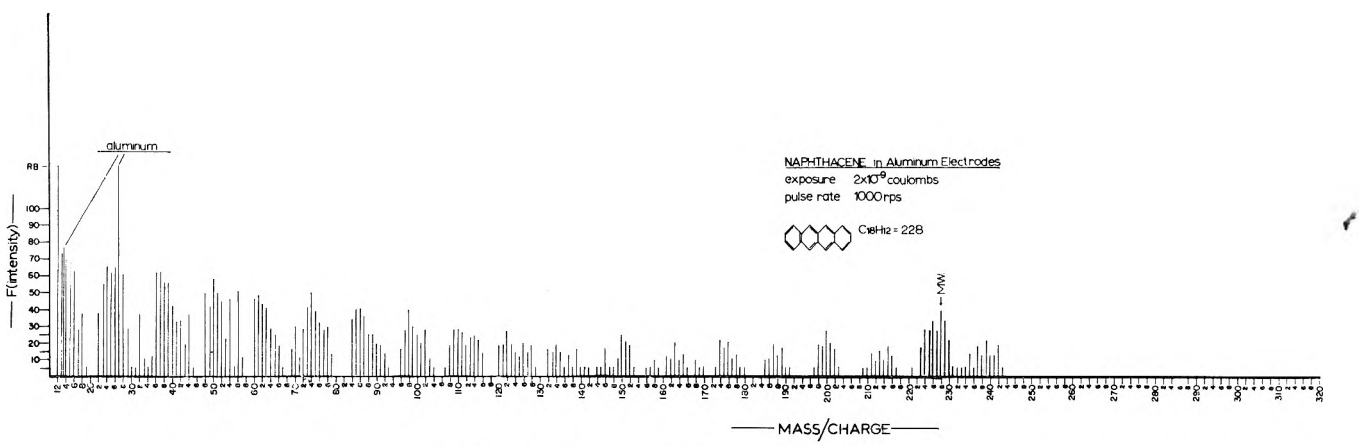

Fig. 4.—Spark mass spectrum of naphthacene.

the spark. The data for each are similar to the data of coronene as is illustrated by the spectra of benzoperylene, pyrene, and naphthacene, Fig. 2, 3, and 4, respectively. That is, the number of groups of lines equals the number of carbon atoms in the molecule and the intensity of the molecular ion is relatively strong compared to intensities of smaller fragments. One point observed consistently was that the first mass lines of the last several groups are not multiples of the mass of carbon-12. This suggests, as might be expected, that high mass fragments which have no protons attached are unlikely to occur. The results

Table I

Summary of Mass Lines and Groups of Lines Due to Fragmentation of Polynuclear Aromatic Hydrocarbons in the Radio-frequency Spark

Compound	Structure	Prominent ions obsd.	First lines of each group mass no.
Coronene $C_{24}H_{12}$		Molecular ion, 300 *m/e* Double charged mol. ion group, 146–150 *m/e*	12, 24, 36, 48, 60, 84, 96, 108, 120, 132, 144, 156, 168, 180, 192, 204, 216, 228, 240, 252, 264, *278*, *290*
Benzo-perylene $C_{22}H_{12}$		Molecular ion, 278 *m/e*	12, 24, 36, ... 204, 216, *233*, *244*, *256*, *268*
Perylene $C_{20}H_{10}$	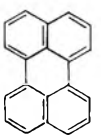	Molecular ion, 252 *m/e*	12, 24, 36, ... 108, 192 *209*, *220*, *233*, *244*
Picene $C_{22}H_{14}$	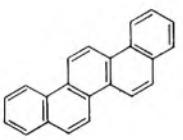	Molecular ion, 278 *m/e*	12, 24, 36, ... 204, 216, *233*, *244*, *256*, *268*
Naphthacene $C_{18}H_{12}$	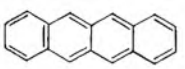	Molecular ion, 228 *m/e*	12, 24, 36, ... 144, 156, *172*, *185*, *197*, *209*, *223*
Chrysene $C_{18}H_{12}$	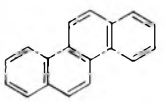	Molecular ion, 228 *m/e* Doubly charged mol. ion group, 111.5–114.5 *m/e*	12, 24, 36, ... 156, 172, *185*, *197*, *209*, *220*
Triphenylene $C_{18}H_{12}$	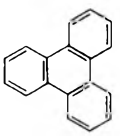	Molecular ion, 228 *m/e* Doubly charged mol. ion group, 111.5–114.5 *m/e*	12, 24, 36, ... 156, 172, *185*, *197*, *209*, *220*
Pyrene $C_{16}H_{10}$	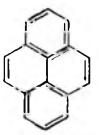	Molecular ion, 202 *m/e*	12, 24, 36, ... 144, 156, *173*, *185*, *197*
Anthracene $C_{14}H_{10}$	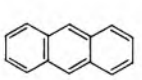	Molecular ion, 178 *m/e* Doubly charged mol. ion group, 87.5–90.5 *m/e*	12, 24, 36, ... 132, 144, *161*, *173*

of the study are summarized in Table I. The first line of each group is given in this table, with the lines which are not multiples of twelve italicized.

Data for the triphenylene–perylene mixture are essentially the addition of the data of the two separate components.

Discussion and Conclusions

Carbon associations in the spark source, as shown in Fig. 5a, were observed for graphite and are in good agreement with observations of previous workers.[4–6] Other studies[10] indicate that only a few associations are

(10) W. Baun, F. N. Hodgson, and M. Desjardins, *J. Chem. Phys.*, in press.

observed for amorphous carbon and the lines, unlike the carbon lines of graphite, decrease steadily in intensity with increasing mass.

Graphite, which may be thought to consist of layers of a practically infinite number of condensed benzene rings with weak van der Waal's binding between layers, can be considered as the limiting case of an infinitely extended polynuclear aromatic hydrocarbon. An aliphatic carbon–carbon bond length is 1.54 Å. while an olefinic carbon–carbon double bond is 1.34 Å. in length. The hybrid bonds of benzene have the intermediate length of 1.39 Å. One might expect that as the number of condensed benzene rings of a compound increases, the average carbon–carbon bond length approaches the value for the carbon–carbon distance of graphite, 1.42 Å.

If the lines of the coronene spark mass spectrum which are due solely to carbon, namely, the first line of each of the groups, are plotted in the same manner as the graphite data of Fig. 5a, the resulting plot, Fig. 5b, is quite similar to that of graphite. This fact doubtlessly derives from the structural similarity of coronene and graphite.

For all compounds studied, the line at mass number 12 was sufficiently intense to cause photographic reversal in exposures that were strong enough for a molecular ion to be observed. Most of the low mass lines are quite intense, indicating that a large portion of the sample was reduced to atomic species. The remainder was preferentially fragmented and produced a mass spectrum characteristic of the structure.

Ions of masses greater than the molecular weight have been observed for most of the compounds. The spectrum of coronene shows a group of lines greater than the molecular weight with the strongest line of the group falling at 311 *m/e*. A spectrum of anthracene recorded at 10^{-9} coulomb exposure showed lines up to the molecular weight, but the spectrum of anthracene recorded at a coulomb exposure 20-fold greater showed ions of masses up to the anthracene dimer. These additional lines are much less intense than the parent ion, however.

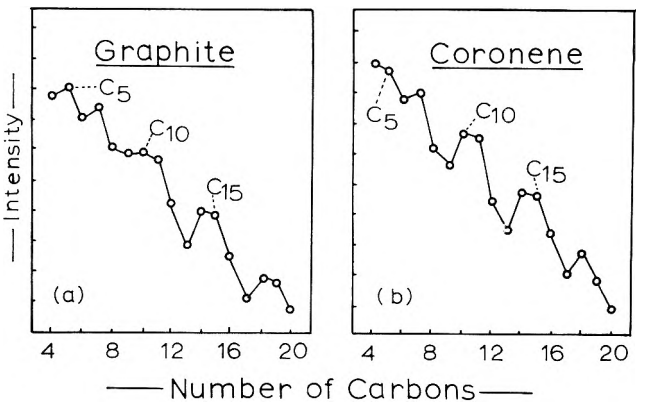

Fig. 5.—Carbon associations observed in the spark: (a) graphite; (b) coronene.

Though photographic plate line blackening measurements cannot be equated directly to ion abundance, they provide an arbitrary scale on which to measure ion beam intensities. Electrometer detection of the ions, which would yield ion abundances directly, would, of course, be more desirable. However, the erratic nature of the spark does not permit its use.

Acknowledgment.—Gratitude is expressed to Dr. B. S. Wildi, Monsanto Chemical Company, for providing the compounds triphenylene, chrysene, naphthacene, picene, benzoperylene, and coronene, and to Mr. A. G. Sharkey, U. S. Bureau of Mines, for providing the compound pyrene.

SORET COEFFICIENTS FOR $CuSO_4$, $CoSO_4$, AND MIXED SALT AQUEOUS SOLUTIONS USING AN IMPROVED DESIGN OF A SORET CELL

BY DANIEL HERSHEY[1] AND JOHN W. PRADOS

College of Engineering, University of Cincinnati, Cincinnati, Ohio

Received November 26, 1962

A Soret cell has been built, incorporating two cellophane DuPont PT-600 membranes. The membranes partitioned the cell so that the "differential" volumes contiguous to the hot and cold zones offered a 0.050-in. diffusion path with the remainder of the cell offering a 0.350-in. diffusion path. The entire "differential" volume could be removed as a sample without disrupting the rest of the cell. It was found for the $CuSO_4$–H_2O system that the Soret coefficient increased monotonically from 9.0–10.3 $\times$ 10^{-3}°C.$^{-1}$ over a 0.1–0.6 molarity range and 7.0–7.4 $\times$ 10^{-3}°C.$^{-1}$ for $CoSO_4$ over the same molarity range. For the mixed salt system, $CuSO_4$–$CoSO_4$–H_2O, no significant change in Soret coefficient of each component was detected as a result of the mixing.

Investigation of the thermal diffusion phenomenon has transcended the merely academic phase. It is recognized that in some cases thermal diffusion can represent an effective means of separating components, such as isotopes in gases, close boiling components, and isotopes in the liquid phase and electrolytes in aqueous solution. Thermal diffusion is a transport process, whereby a temperature gradient imposed upon the system usually causes a migration of molecules with a concomitant concentration gradient. The concentration gradient then gives rise to an ordinary diffusive flux in the opposite direction. A steady state is attained when both fluxes are equal. Phenomenologically, this is represented as

$$J_i = \rho[D_i'\zeta_i(1 - \zeta_i)\ \text{Grad}\ T - D_i\ \text{Grad}\ \zeta_i]\cdot\vec{n} \quad (1)$$

The initial recorded observation of a concentration gradient across a system resulting from a temperature gradient is attributed to Ludwig.[2] Subsequently, Soret[3] investigated this effect more extensively with the

(1) Asst. Prof. Chemical Engineering, Univ. of Cincinnati, Cincinnati, Ohio.

(2) C. Ludwig, *Sitzber. Akad. Wiss. Wien.*, **20**, 539 (1956).

(3) C. Soret, *Arch. Sci.* (Geneva), **2**, 48 (1879).

result that thermal diffusion is sometimes referred to as the Ludwig–Soret or Soret effect.

Separation data are generally obtained in a Soret cell. A Soret or "equilibrium" cell consists essentially of a hot surface, the interstitial liquid, and a cold surface, arranged contiguously. The hot surface is on top to avoid convective currents. There is no flow of material into or out of the cell, only a migration of molecules within the system. A measure of the separations obtained in a thermal diffusion cell is the Soret coefficient, σ, generally calculated from the relation

$$\sigma = \frac{1}{\Delta T} \ln \frac{X_2}{X_1} \qquad (2)$$

Equation 2 can be obtained from eq. 1 at steady state when the net flux, J_i, is set equal to zero. It is implicitly assumed that D'/D is independent of temperature and concentration, and that $(1 - X_1)/(1 - X_2)$ is approximately equal to unity. Soret coefficients vary, depending on the component, its concentration, and temperature. Reports of Soret coefficients in the literature are sparse and subject to disagreement.

Two of the major experimental difficulties involved in obtaining separation data from a Soret cell are sampling techniques and the determination of the point of attainment of a steady-state condition. Sampling difficulties hinge upon the requirement that there must be no disruptive convection currents caused by the technique. Some designs circumvent both of the above difficulties by not removing a sample from the cell. For example, a cell described by Tanner[4] utilized a transparent glass Soret cell and an optical system which measured the deflection of a beam of light passed through the cell. Chipman[5] had two electrodes in the solution. Both of the schemes could monitor the concentration changes and note simultaneously the arrival at steady state and the concentration at that point. There have been many variations of these methods reported in the literature. These methods, however, are not easily applied to the two-salt aqueous solutions since the property measured would now also be a function of the amount of each salt present.

Since one of the aims of this investigation was to determine the change in individual Soret coefficients as a result of mixing two or more salt species in aqueous solution, it was decided to forego the conductivity or optical methods of analysis.

Experimental

Cell Design.—The cell used in this investigation allows the removal of 7-ml. samples from the hot and cold ends without disrupting the remainder of the cell. This is accomplished by cellophane membranes close to each end. Long[6] found that these porous membranes, though resistant to rapid macroscopic flow of solution, apparently did not affect the distribution of the components under conditions of no net transfer. With a Beckman spectrophotometer available for analysis of samples as small as 1 ml., the cell design incorporated: (1) a minimal diffusion path and (2) solution samples that were representative of end conditions. The systems chosen were $CuSO_4$–H_2O, $CoSO_4$–H_2O, and the mixed salt system, $CuSO_4$–$CoSO_4$–H_2O. The concentration, mean temperature, and temperature gradient were varied for the systems.

The cell consisted essentially of three circular sections, two of copper and a plexiglass spacer between the copper sections. Each of the copper sections had an outside diameter of 6.75 in. and an inside diameter of 4 in., with a 0.050-in. diffusion path. Cellophane membranes separated the copper sections from the plastic spacer. The plastic spacer provided the bulk of the diffusion path, 0.350 in., and measured 5.75 in. in outside diameter and 4 in. in inside diameter. The three sections were clamped together. All of the "differential" liquid between the membrane and the end of the cell constituted a sample which was removed from the cell by tipping the cell, opening the sample ports, and drawing the liquid into a hypodermic syringe.

The upper copper section housed a 375-watt "pancake" electric heater. Two copper–constantan thermocouples in the volume between the membrane and the hot well monitored the temperature for a Leeds and Northrup Micromax controller. Provisions were also made for the simultaneous check of the thermocouple signal to the controller, using a Leeds and Northrup portable potentiometer.

The lower copper section incorporated a hollowed portion through which flowed the refrigerant, Freon-12. The refrigeration system was of a standard 0.5 h.p., 6000 BTU/hr. type. Two copper–constantan thermocouples were installed in the space between the membrane and the cold wall, with the e.m.f. signals read on the portable potentiometer.

Experimental Procedure.—A run consisted in tipping the clamped cell vertically, filling the cell by inserting a hypodermic needle filled with solution into the lower sample port of each section, and injecting solution until it overflowed out of the upper sample port of each section. After the sample ports were closed, the cell was returned to a horizontal condition and heating and cooling begun. At the conclusion of the run, the copper sections' sample ports were opened, the empty hypodermic needle inserted, the cell tipped, and the sample drawn out. A steady state was achieved in about 24 hr.

The cellophane membrane was DuPont PT-600 which had been soaked in distilled water to remove the plasticizer. The membrane life was about one month under constant operation, so that a cell had to be dismantled only once a month. Wire mesh screens provided support for the membrane in the cell.

The analysis for the $CuSO_4$–H_2O, $CoSO_4$–H_2O, and $CuSO_4$–$CoSO_4$–H_2O system was made with a Beckman Model DU spectrophotometer.

Discussion of Results

The experimental results for $CuSO_4$, $CoSO_4$ aqueous solutions are summarized in Fig. 1 and 2. It is noted

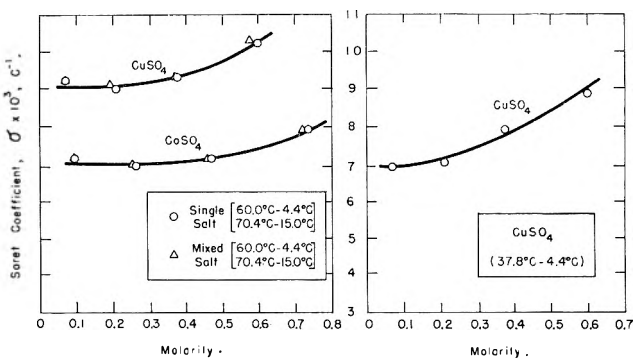

Fig. 1.—Soret coefficients *vs.* concentration for $CuSO_4$ and $CoSO_4$ in aqueous solution.

from Fig. 1 that the Soret coefficient increases with increasing concentration and there did not seem to be a measurable difference in the value of the coefficient for mixed salt and single salt aqueous solutions. For the 100°F. gradient, the experimental results were about 10% higher than the corresponding data of Bosanquet.[7] He used a cell partitioned in two equal halves, separated by a cellophane membrane. Arithmetic average values of concentration and temperature were assumed for each half. Figure 2 is a plot of the temperature dependence of the experimental $CuSO_4$ Soret coefficients.

(4) C. C. Tanner, *Trans. Faraday Soc.*, **49**, 611 (1953).
(5) J. Chipman, *J. Am. Chem. Soc.*, **48**, 2577 (1926).
(6) G. W. Long, M.S. Thesis, The University of Tennessee, 1958.
(7) L. P. Bosanquet, M.S. Thesis, The University of Tennessee, 1960.

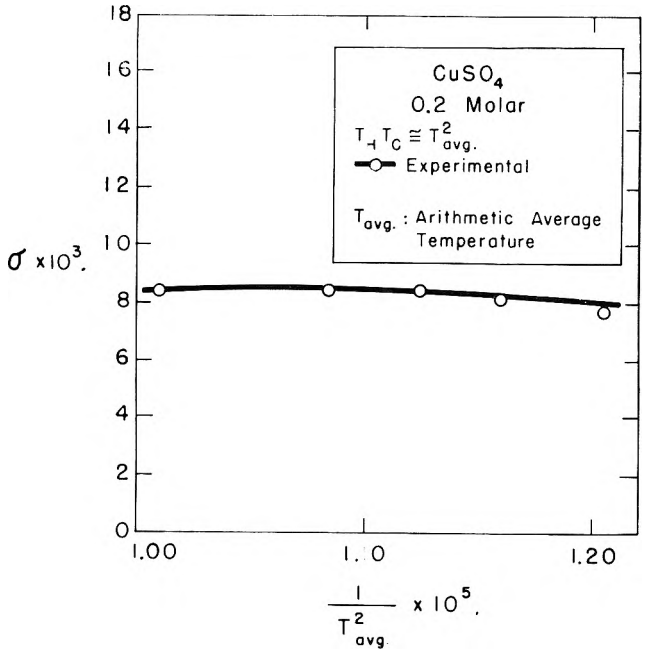

Fig. 2.—Soret coefficient *vs.* the reciprocal of the square of the average temperature for $CuSO_4$.

At the higher average cell temperatures, the Soret coefficients have a small temperature dependence. However for decreasing average cell temperatures the Soret coefficient decreases.

Temperature control on the hot and cold sides was maintained at approximately $\pm 1°$. The two thermocouples in each sample zone were always within two degrees of each other. There was no measurement that introduced an unwarrantable degree of uncertainty.

In summary, a soret cell has been designed which allows the removal of a sample from the hot and cold ends of the cell without disrupting the rest of the contents. Soret coefficients increased monotonically from 9.0–10.3 $\times 10^{-3}$°C.$^{-1}$ over a 0.1–0.6 molarity range for $CuSO_4$ and 7.0–7.4 $\times 10^{-3}$°C.$^{-1}$ for $CoSO_4$ over the same molarity range. For the mixed salt system, no significant change in Soret coefficient of each component was detected as a result of the mixing. At higher average temperatures the Soret coefficient for $CuSO_4$ was essentially constant if the concentration was fixed. Lower average temperatures yielded decreasing values in the coefficient.

List of Symbols

D_i' Coefficient of thermal diffusion of the ith component, eq. 1
D_i Coefficient of ordinary diffusion of the ith component, eq. 1
J_i Diffusive flux of the ith component, eq. 1
T Temperature, eq. 1
ΔT Temperature gradient, eq. 2
$\vec{n}$ Unit normal vector, eq. 1
X Concentration, mole fraction
ζ_i Mole fraction of the ith component, eq. 1.
ρ Molar density, eq. 1
σ Soret coefficient, eq. 2.

THERMAL DIFFUSION. A NON-RIGOROUS SET OF EQUATIONS FOR PREDICTING SEPARATIONS IN GASES AND LIQUIDS

By Daniel Hershey[1] and John W. Prados

College of Engineering, University of Cincinnati, Cincinnati, Ohio

Received November 26, 1962

The derivation of a unified thermal diffusion theory for predicting separations of both gases and liquids has not yet been successful. A non-rigorous set of equations has been derived here which allowed, within about 30%, the successful prediction of separations to be expected for helium–argon, neon–argon, non-polar organic liquid pairs, and electrolytes in aqueous solution. The over-all agreement between predicted and experimental results is encouraging and indicates the equations may be used with reasonable confidence for estimating separations where theoretical and experimental results are lacking.

Thermal diffusion is a transport process, as are heat transfer and ordinary diffusion. It is more complex than heat transfer and ordinary diffusion because the temperature gradient imposed upon the system usually causes a migration of molecules with a concomitant concentration gradient. The concentration gradient then gives rise to an ordinary diffusive flux in the opposite direction. A steady state is attained when both fluxes are equal.

Attempts to present a unified, rigorous theory for thermal diffusion in gases and liquids have been unsuccessful due to a lack of knowledge concerning the liquid state. Though the rigorous mathematical treatment of this non-equilibrium phenomenon in non-uniform gases is complex, it has been treated extensively by Chapman and Cowling,[2a] Chapman,[2b] Enskog,[3] Clark Jones,[4] and others with good results. The approach is from the kinetic theory point of view utilizing assumptions concerning intermolecular interactions. A comprehensive survey of thermal diffusion in gases is to be found in a text by Grew and Ibbs.[5]

Liquid thermal diffusion theories have been far less satisfactory since they are encumbered by the anomalous and abstruse behavior of liquids. Kinetic theories such as those proposed by Nernst,[6] Wirtz,[7] and Denbigh[8] conceived of liquid thermal diffusion as the transport of activated solute molecules from one equilibrium site to another in discrete jumps, requiring an "energy of activation." Eastman[9] and Wagner[10] used a thermodynamic approach to liquid thermal diffusion, introducing a "heat of transfer." In developing an irreversible

(1) Asst. Prof. Chemical Engineering, Univ. of Cincinnati, Cincinnati, Ohio.

(2) (a) S. Chapman and T. G. Cowling, "Mathematical Theory of Non-uniform Gases," Cambridge Univ. Press, Cambridge, England, 1939; (b) S. Chapman, *Phil. Trans. Roy. Soc.* (London), **A211**, 433 (1912).

(3) D. Enskog, Ph.D. Thesis, Upsala University, 1917.

(4) R. Clark Jones, *Phys. Rev.*, **58**, 111 (1940).

(5) K. E. Grew and T. L. Ibbs, "Thermal Diffusion in Gases," Cambridge Univ. Press, Cambridge, England, 1952.

(6) Nernst, *Z. physik. Chem.*, **2**, 613 (1888).

(7) K. Wirtz, *Z. physik.*, **124**, 482 (1948).

(8) D. G. Denbigh, *Trans. Faraday Soc.*, **48**, 1 (1952).

(9) E. D. Eastman, *J. Am. Chem. Soc.*, **48**, 1482 (1926).

(10) C. Wagner, *Ann. Physik*, **3**, 629 (1928).

thermodynamic theory, de Groot[11] introduced a "heat of transport," similar to the terms described previously. Other non-rigorous theories have been published by Porter,[12] Wereide,[13] Chapman,[14] and others.

A mathematical development is presented here, based on the postulation that irreversible thermible diffusion can be represented as a quasistatic transport process with the Boltzmann distribution function applicable. Gases are considered as being composed of ideal particles and liquids as condensed gases.

Derivation of Equations for Predicting Thermal Diffusion Separations.—Because of the slowness of the thermal diffusion process, it will be considered not as an irreversible transport phenomenon but rather as a quasistatic process. The system will be envisioned as being initially in equilibrium, at a uniform temperature, T_0, with $N_i/V = \eta_i$. With the imposition of the temperature gradient, thermal diffusion proceeds quasistatically, during which time the system is at all times infinitesimally near a state of equilibrium, so that the Boltzmann distribution function is applicable.

Ideal Gas Derivation.—If at a time, t_s, the thermal gradient has been imposed and thermal diffusion is imminent but has not yet commenced, then

$$\sum_{i=1}^{m} \eta_i = \frac{T_0}{T} \sum_{i=1}^{m} \frac{N_i}{V} \tag{1}$$

and the system possesses an energy per unit volume

$$\left(\frac{E}{V}\right)_{t_s} = \left(\sum_{i=1}^{m} \sum_{j=0}^{n} E_{ij}\eta_{ij}\right)_{t_s} \tag{2}$$

If the Boltzmann function is introduced

$$\frac{\eta_{ij}}{\eta_{in}} = e^{-(E_{ij}-E_{in})/kT}$$

and the partition function P_i is substituted along with the definition $\sum_{j=0}^{n} \eta_{ij} = \eta_i$, it is possible to arrive at another form of equation 2, namely

$$\left(\frac{E}{V}\right)_{t_s} = \sum_{i=1}^{m} \sum_{j=0}^{n} \frac{N_i}{V} \frac{T_0}{T} \frac{Q_i}{P_i} \tag{3}$$

After time t_s, thermal diffusion proceeds until a steady-state condition is attained. At steady state it is assumed that the energy per unit volume is equal approximately to that value at t_s. Since the number of atoms per unit volume that have migrated is small compared to the number that have not, the net energy change resulting from the difference between the energy of those atoms that have migrated and the ones that have replaced them will be small compared to the total energy of the unit volume. It can be shown[15] therefore that for a two component system

$$\eta_1 = \frac{T_0}{T}\left[\left(\frac{N_1}{V}\right) + \alpha\left(\frac{N_2}{V}\right)\right] - \eta_2\alpha \tag{4}$$

where $\alpha = P_1Q_2/P_2Q_1$. With the following conditions

$$\frac{\eta_2}{\eta_1} = re^{H^*/T} \tag{5}$$

$$N_1 = S\int_0^L \eta_1 dX \tag{6}$$

$$N_2 = S\int_0^L \eta_2 dX \tag{7}$$

equation 8 can be obtained.

$$\left(\frac{N_1}{N_1 + \alpha N_2}\right) \ln \frac{T_H}{T_C} = \int_{1/T_H}^{1/T_C} \frac{d\left(\frac{1}{T}\right)}{\left(\frac{1}{T}\right)(1 + \alpha re^{H^*/T})} \tag{8}$$

In equation 5, H^* is related to the heat of transport and r is an unspecified parameter defined by equation 5. Unfortunately no method has been found for integrating eq. 8 in a closed form. It was necessary to resort to an expansion of the integrand in a Taylor series, make appropriate assumptions pertaining to uniform convergence of this series, and then integrate term by term.[10] The final result is eq. 9.

$$H^* = \frac{C}{B}\left[-A\alpha r + (1 - 2A) + \frac{(1 - A)}{\alpha r}\right] \tag{9}$$

where

$$A = \frac{N_1}{N_1 + \alpha N_2}$$

$$B = \frac{T_H - T_C}{T_H T_C}$$

$$C = \ln \frac{T_H}{T_C}$$

If H^* and r were known, it would be possible to predict separation from eq. 4 and 5. Additional information is obtained from equations derived from Fig. 1

$$\eta_1 = \frac{N_1}{V} = \frac{T_0}{T_A}\left[\frac{N_1 + \alpha N_2}{V}\right]/(1 + \alpha re^{H^*/T_A}) \tag{10}$$

$$\frac{\eta_2}{\eta_1} = re^{H^*/T_B} = \frac{N_2/V}{(\eta_1)_{T_B}} = \frac{N_2/V}{\frac{T_0}{T_B}\left[\frac{N_1 + \alpha N_2}{V}\right]/(1 + \alpha re^{H^*/T_B})} \tag{11}$$

and

$$(\eta_1)_{T_B} + (T_A - T_B)\left(\frac{d\eta_1}{dT}\right)_{T_B} \cong \frac{N_1}{V} \tag{12}$$

with

$$T_0 = \frac{T_H - T_C}{\ln T_H/T_C} \tag{13}$$

Equations 9–13 in conjunction with a knowledge of α, T_H, and T_C enable the calculation of the separation to be expected for two perfect gases without resort to experiment. The evaluation of α from available literature

(11) S. R. de Groot, "The Soret Effect," North Holland Publ. Co., Amsterdam, Holland, 1945.
(12) A. E. Porter, *Trans. Faraday Soc.*, **23**, 314 (1927).
(13) T. Wereide, *Ann. Phys.*, **2**, 55 (1914).
(14) S. Chapman, *Proc. Roy. Soc.* (London), **A119**, 34 (1948).
(15) D. Hershey, Ph.D. Thesis, Univ. of Tennessee, 1961.

information is dealt with extensively in the Ph.D. thesis by Hershey.[15] Involved is the evaluation of the ratios of partition functions. This is an area in which little is known and consequently "pragmatic" assumptions were necessitated. The method for calculating α is shown in the Appendix of this report.

For example, it was necessary to assume that the partition function for each energy mode (translation, rotation, vibration, electronic, etc.) could be represented as $P = Cm^a\beta^{-b}$, where a, b, and c are constants, $\beta = 1/kT$, and m is the mass of the atom.

Liquids.—All that has been written and assumed for gases including the postulation of a quasistatic process and the validity of the Boltzmann distribution will be assumed to hold for liquids. However, because of the relatively small coefficient of expansion of liquids, no temperature dependence will be indicated for η_i at t_s. That is

$$\eta_i \cong \frac{N_i}{V} \tag{14}$$

or

$$\sum_{i=1}^{m} \eta_i \cong \sum_{i=1}^{m} \frac{N_i}{V} \tag{15}$$

The derivation of the governing equations proceeds as before and consequently

$$H^* = \frac{C}{B}\left[-A\alpha r + (1 - 2A) + \frac{(1 - A)}{\alpha r}\right] \tag{16}$$

where

$$A = \frac{N_1}{N_1 + \alpha N_2}$$

$$B = \ln \frac{T_H}{T_C}$$

$$C = T_H - T_C$$

and

$$\frac{\eta_2}{\eta_1} = \frac{N_2}{N_1} = re^{H^*/T_A} \tag{17}$$

$$\left(\frac{\eta_2}{\eta_1}\right)_{T_H} = re^{H^*/T_H} = \frac{(\eta_2)_H}{(\eta_1)_H} = \frac{(\eta_2)_{T_A} + \left(\frac{d\eta_2}{dT}\right)_{T_A}(T_H - T_A)}{(\eta_1)_{T_A} + \left(\frac{d\eta_1}{dT}\right)_{T_A}(T_H - T_A)} \tag{18}$$

In summary, eq. 16–18 are sufficient to predict separations.

Discussion of Results

The per cent separation was calculated for the helium–argon and neon–argon systems. The temperature gradient was fixed but the concentration was varied, as shown in Fig. 2 and 3. The calculated curve is compared with the data of Van Itterbeek[16], Ibbs and Grew,[17] and the plot of the calculations

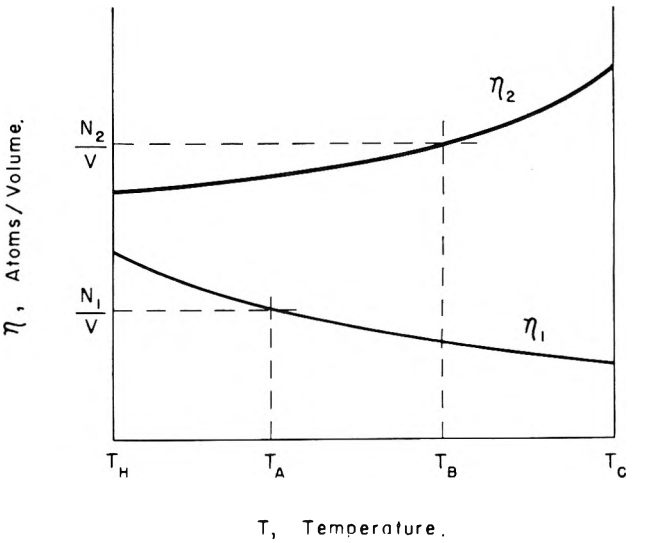

Fig. 1.—Concentration *vs.* temperature at steady state.

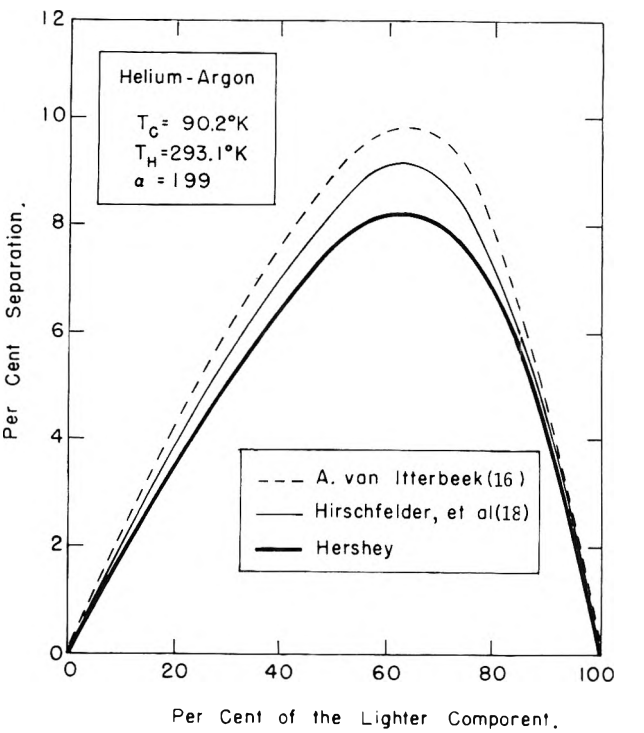

Fig. 2.—Per cent separation *vs.* concentration for helium—argon.

of Hirschfelder, Curtiss, and Bird,[18] based on the Lennard-Jones 6, 12 model. It is apparent from Fig. 2 and 3 that the calculated results based on eq. 9–13 not only predict the proper shape of the curve but also lie within about 30% of the experimental line. As pointed out previously, the rigorous mathematical treatment, epitomized by the Hirschfelder, *et al.*, curve is quite adequate for non-uniform gas transport.

For liquids, Soret coefficients (a measure of the separations) were calculated for various values of α, with a fixed temperature gradient and concentration. The calculated curve shown in Fig. 4 is for a 50 mole % concentration of various organic and inorganic liquid pairs with experimental data superimposed. Figure 5 shows a similar calculated curve for a 1.8 mole % concentration of 15 aqueous electrolyte solutions, including sulfates, chlorides, bromides, iodides, and nitrates of potassium,

(16) A. Van Itterbeek and A. de Troyer, *Physica*, **16**, 329 (1950).
(17) T. L. Ibbs and K. E. Grew, *Proc. Phys. Soc.*, **43**, 142 (1931).
(18) J. O. Hirschfelder, *et al.*, "Molecular Theory of Gases and Liquids," John Wiley and Sons, Inc., New York, N. Y., 1954, p. 584.

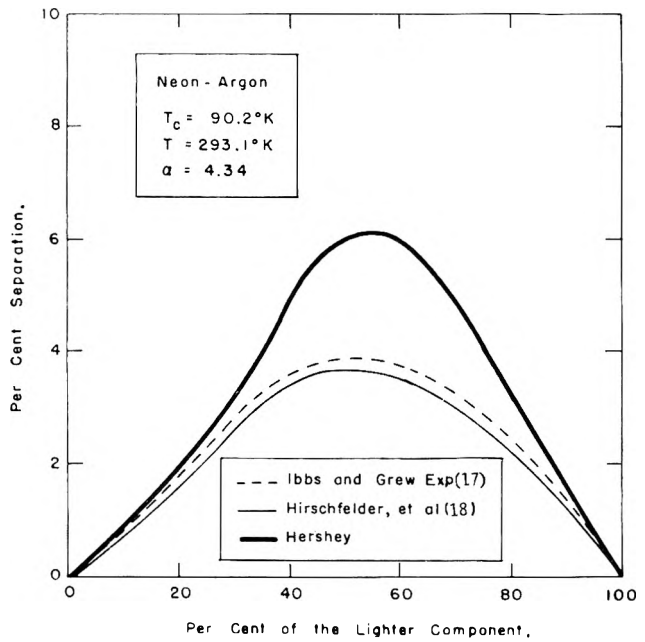

Fig. 3.—Per cent separation *vs.* concentration for neon—argon.

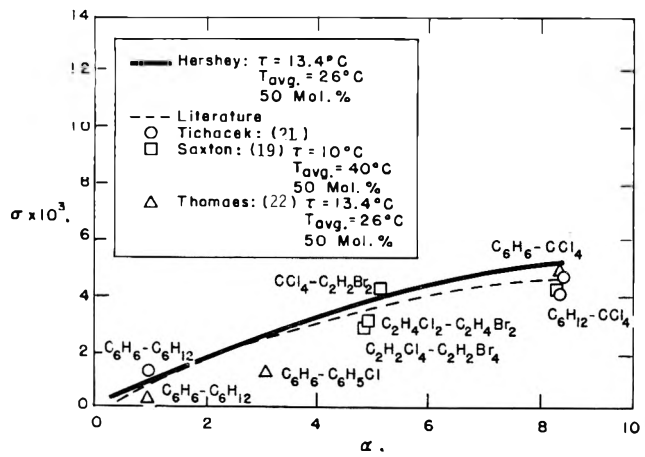

Fig. 4.—Soret coefficient *vs.* α for organic liquids.

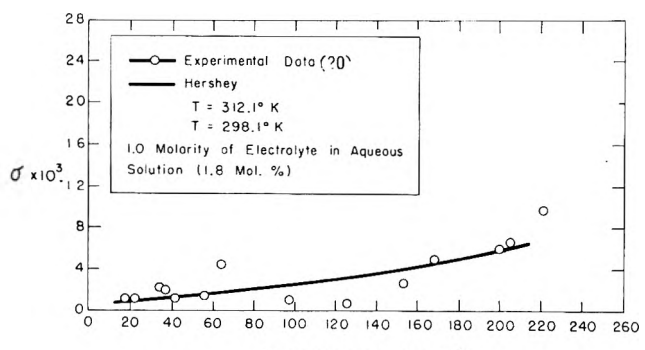

Fig. 5.—Soret coefficient *vs.* corrected α for various electrolytes in aqueous solution.

sodium, strontium, cobalt, copper, nickel, zinc, and silver.

Non-polar liquid pairs seem to conform as a group to the calculated line in Fig. 4. Polar liquid pairs tend to deviate from the line, implying some sort of interaction or molecular association. If the system is limited to "ideal" liquid pairs such as non-polar groups, it appears as if the calculations are satisfactory within about 25% over the range of α examined. Figure 5 shows a "reasonable" agreement between the calculated curve and experimental data for the electrolyte solutions. The nature of the correction factor for α in Fig. 5 is covered thoroughly in the Ph.D. thesis from which this report is extracted.

This correction factor represents a deviation of the electrolyte in solution from its "ideal" behavior and is related to deviations in expected colligative properties—as measured by the reciprocal of the osmotic coefficient, φ^{-1}. It should be pointed out, however, that this correction factor, φ^{-1}, like α, is evaluated from a knowledge of the properties of the components, obtainable from the literature. There is no need to resort to experimentation.

In summary, with the system of equations derived, it was possible to predict within about 30%, the separations to be expected in helium–argon, neon–argon, non-polar liquid pairs, and electrolytes in aqueous solution. It was also possible (though not shown here) to predict the dependence of the separation upon concentration and temperature.

The over-all agreement between predicted and experimental results is encouraging, and while it obviously does not provide justification for any specific steps in the development, it does indicate that the equations may be used with reasonable confidence for estimating separations where theoretical and experimental results are lacking.

List of Symbols

E_{ij}	Energy of an atom of component i, in energy level j
E	Total energy of the system
H^*	Defined by eq. 5
L	Length of the cell along the temperature gradient
N_i, N_1, N_2	Total no. of atoms of component i, 1, 2, respectively
P_i	Partition function for ith component: $P_i = \sum_{j=0}^{n} e^{-E_{ij}/kT}$
Q_i	$-\frac{\partial}{\partial\beta} P_i$
r	Defined by eq. 5
S	Cross-sectional area
T	Temperature
T_H, T_C	Temperature of hot and cold sides, respectively
T_0	Initial temperature of the system
T_A, T_B	Intermediate temperatures between T_H and T_C
V	Volume of the cell
X	Linear distance along the cell
k	Boltzmann constant
t_s	Time of implementation of the temperature gradient
α	$\frac{P_1Q_2}{P_2Q_1}$
β	Reciprocal of kT
η_1, η_2	Atoms per unit volume of components 1 and 2, respectively
η_{ij}	Number of atoms of component i, at energy level j, per unit volume
η_{in}	Number of atoms of component i, at energy level n, per unit volume
σ	Soret coefficient

Appendix

The Evaluation of α for a Perfect Monatomic Gas.

$$\alpha = \frac{P_1Q_2}{P_2Q_1}$$

Let E_S denote the total energy per atom. Therefore

(19) R. L. Saxton, *et al.*, *J. Chem. Phys.*, **22**, 1287 (1954).
(20) C. C. Tanner, *Trans. Faraday Soc.*, **49**, 611 (1953).
(21) L. J. Tichacek and H. G. Drickamer, *J. Phys. Chem.*, **60**, 820 (1956).
(22) G. Thomaes, *Physica*, **17**, 885 (1951).

$$E_S = E_{TR} + E_{ROT} + E_{VIB} + E_{ELECT} + E_{MISC} \quad (A\text{-}1)$$

where

E_{TR} = translational energy
E_{ROT} = rotational energy
E_{VIB} = vibrational energy
E_{ELECT} = electronic energy
E_{MISC} = miscellaneous energy terms

For a perfect monatomic gas, E_{ROT} and E_{VIB} are equal to zero. At the temperature considered, it is assumed that a negligible number of atoms are in excited electronic states, that is, all the atoms are in their ground state, indicated by $E_{ELECT} \sim E^0$.

From the principle of equipartition of energy and the definition of a partition function

$$P = P_{TR}\, P_{ELECT}\, P_{ROT}\, P_{VIB}\, P_{MISC} \quad (A\text{-}2)$$

Classical statistical mechanics and quantum theory predict

$$P_{TR} = (2\pi mkT)^{3/2}\frac{V}{h^3} = cm^a\beta^{-b} = f(m,\beta) \quad (A\text{-}3)$$

where a, b, and c are constants of $\beta = 1/kT$. Assume P_{MISC} can be expressed similarly

$$P_{MISC} = c'm^{a'}\beta^{-b'} = g(m,\beta) \quad (A\text{-}4)$$

and note for an ideal monatomic gas

$$P_{ROT} = P_{VIB} = 1 \quad (A\text{-}5)$$

Then equation (A-2) becomes

$$P = (cm^a\beta^{-b})(c'm^{a'}\beta^{-b'})e^{-E^0\beta} \quad (A\text{-}6)$$

From the definition of Q, it can be shown that

$$Q = -\frac{\partial}{\partial\beta}P \quad (A\text{-}7)$$

and, therefore

$$Q = -\frac{\partial}{\partial\beta}[(cc')(m^{a+a'})\beta^{-(b+b')}e^{-E^0\beta}]$$

or

$$Q = -(cc')(m^{a+a'})[e^{-E^0\beta}\beta^{-(b+b')}[-E^0 - (b+b')\beta^{-1}]$$

Since E^0 generally ranges from several thousand electron volts to higher values, and $\beta^{-1} = 0.026$ electron volt, it seems reasonable to assume $(b + b')\beta^{-1} << E_0$. Then

$$Q = (cc')m^{a+a'}e^{-E^0\beta}\beta^{-(b+b')}E^0 \quad (A\text{-}8)$$

and

$$\alpha = \frac{P_1}{P_2}\frac{Q_2}{Q_1} = \frac{E_2^0}{E_1^0}$$

The significance of α is discussed by Hershey.[15] It is called an "interaction coefficient," a measure of the influence of one atom upon another by virtue of the presence of their electronic fields.

The calculation of E_2^0/E_1^0, the ratio of the ground state electronic energies of components 1 and 2, is obtained by summing the energy of every electron of the atom. The electronic energy is the energy necessary to remove an electron in its ground state from its orbit to infinity, that is, the ionization potential.

INTERACTION IN SALT VAPORS AND ACTIVITY COEFFICIENTS IN THE POTASSIUM CHLORIDE–MAGNESIUM CHLORIDE SYSTEM[1,2]

BY EUGENE E. SCHRIER[3] AND HERBERT M. CLARK

Department of Chemistry, Rensselaer Polytechnic Institute, Troy, New York

Received November 29, 1962

The vapor pressures of the pure molten salts KCl, $MgCl_2$, and CsCl and of mixtures of KCl and $MgCl_2$ have been determined at temperatures between 900 and 1150° by boiling point and transpiration methods. The data from the boiling point and transpiration experiments on the pure salts were combined to yield the average molecular weight of the vapor. Association into dimers is postulated for all the pure salts studied and the equilibrium constants for dissociation of the dimers and heats and entropies of dimerization are calculated. For the KCl–$MgCl_2$ system the vapor pressure obtained by the boiling point method was found to exhibit a minimum near the composition 66.7 mole % KCl-33.3 mole % $MgCl_2$ at all temperatures. The presence of the mixed dimer or compound, $KMgCl_3$, in the vapor was inferred from a study of transpiration measurements made on various KCl–$MgCl_2$ mixtures. A model is postulated for the vapor over KCl–$MgCl_2$ mixtures which includes the monomers and dimers of the pure salts and the compound $KMgCl_3$. Activity coefficients calculated from this model are compared with the results of other investigators and with those calculated from the liquid phase model of Flood and Urnes.

Introduction

The vapor phase over pure molten halides and halide solutions has been the subject of a number of recent investigations.[4-14] Mass spectrometric studies have given direct evidence for unsuspected polymerization in these vapors. However, the restriction of such studies to Knudsen conditions has limited the range of investigation of this strongly pressure-dependent type of interaction. Furthermore, difficulties in the measurement of accurate ionization cross-sections impair the utility of the method for obtaining quantitative data.

In the investigation to be described, vapor pressure measurements were used to study the nature of vapor

(1) Abstracted from a thesis presented by Eugene E. Schrier to Rensselaer Polytechnic Institute in partial fulfillment of the requirements for the Ph.D. degree.

(2) Presented in part at the 18th IUPAC Congress in Montreal, August, 1961.

(3) International Nickel Fellow 1956–1958. National Science Foundation Predoctoral Fellow 1958–1960.

(4) J. Berkowitz and W. A. Chupka, *J. Chem. Phys.*, **29**, 653 (1958).

(5) J. Berkowitz and W. A. Chupka, *Ann. N. Y. Acad. Sci.*, **79**, 1073 (1960).

(6) S. Datz, U.S.A.E.C ORNL-2933 (1960).

(7) L. Friedman, *J. Chem. Phys.*, **23**, 477 (1955).

(8) R. Miller and P. Kusch, *ibid.*, **25**, 865 (1956).

(9) T. A. Milne, H. M. Klein, and D. Cubicciotti, *ibid.*, **28**, 718 (1958).

(10) S. A. Rice and W. Klemperer, *ibid.*, **27**, 573 (1957).

(11) R. C. Schoonmaker and R. F. Porter, *ibid.*, **29**, 116 (1958).

(12) C. Beusman, U.S.A.E.C. ORNL-2323 (1957).

(13) J. L. Barton and H. Bloom, *J. Phys. Chem.*, **63**, 1785 (1959).

(14) J. L. Barton and H. Bloom, *Trans. Faraday Soc*, **55**, 1792 (1959).

phase interactions between salt species for three pure salts, KCl, CsCl, and $MgCl_2$, and for binary mixtures of KCl and $MgCl_2$. Included in the study was the formulation of a model for the vapor phase over the binary mixture which could account for the data obtained. Since liquid phase activity coefficients for the components have been calculated using this model, a measure of the validity of the model is provided by comparison of the calculated activity coefficients with experimental values determined by previous workers using e.m.f. and equilibrium measurements.[15-20] The liquid phase of the KCl–$MgCl_2$ system has also been treated theoretically by Flood and Urnes.[21] It was of interest to see whether the liquid phase complexes proposed by Flood and Urnes would be present in the vapor.

Experimental

Reagent grade potassium chloride was purified by melting under vacuum. The best crystals obtained were selected for the measurements. Anhydrous magnesium chloride was obtained from the Carborundum Company as the by-product of the Kroll reduction of zirconium tetrachloride. It was purified by a modification of the method used by Laitinen, Ferguson, and Osteryoung.[22] Cesium chloride (Maywood Company) was dried in air and used without further purification. The purified salts and KCl–$MgCl_2$ mixtures were stored and handled in a drybox.

The furnaces used in these experiments were constructed by winding Kanthal wire on 18-in. long, cylindrical, grooved alundum cores. Insulation was provided by embedding the cores in layers of high temperature pipe lagging. The use of four separately controllable windings in the furnace provided a 4-in. long zone having a temperature uniform to ±1°. Temperature control (±1°) was accomplished by manual adjustment of variable transformers connected to the furnace windings.

The boiling point apparatus was similar to that used by Barton and Bloom.[23] Mullite (Morganite Company) tubes were used as containing-vessels for the salt samples. Introduction of nitrogen into the melt in the form of a fine stream of bubbles to prevent superheating was found to be unnecessary presumably because of the nature of the mullite surface. The pressure in the system was controlled by the method of O'Gorman[24] and measured with an estimated uncertainty of ±0.1 mm. using a mercury manometer and a Gaertner cathetometer.

At the conclusion of a boiling point experiment a sample of the melt was removed from the cell and analyzed using the Fajans method for chloride and an EDTA titration for magnesium. Similar procedures were used for analysis of samples obtained during transpiration measurements.

Some of the transpiration measurements for the pure salts were made in a horizontal type apparatus resembling that used by Beusman.[12] However, it was found that reproducible results could not be obtained for $MgCl_2$ in this apparatus. A vertical type apparatus was designed and used successfully for measurements involving $MgCl_2$. The apparatus consisted of (1) a main cylindrical quartz vessel (38 mm. o.d.) in which the salt was placed, (2) an inner cylindrical tube (10 mm at top) which was open at the bottom (25 mm.) and dipped into the molten salt, (3) a removable condenser which was positioned axially and supported by the inner tube, (4) a thermocouple well, and (5) gas inlets and outlets. A quartz capillary tube at the bottom of the condenser was ring-sealed and extended upward within the condenser to provide a small well to retain the condensate, whose weight (about 200 mg.) was determined by the increase in weight of the condenser. The use of several interchangeable condensers allowed vapor analyses to be made at different temperatures for the same sample of salt.

In the vertical type apparatus the chance for creep of liquid $MgCl_2$ was greatly diminished and at the same time mixing of salt vapor and carrier gas was improved. The carrier gas (nitrogen) passed downward through the annular space between the main vessel and the inner cylinder and then bubbled through the salt before passing through the condenser.

To alter the composition of the salt mixture it was merely necessary to remove the condenser and add a predetermined quantity of salt. The composition of the molten salt was checked by analysis of samples pipetted from the apparatus. Changes in composition of the melt resulting from vaporization during a series of measurements over a range of temperature were shown to be insignificant. Transpiration data for KCl obtained with the original and modified arrangements were consistent.

The effect of flow rate on the amount of salt collected per unit volume of carrier gas at a given temperature was studied in both forms of the apparatus. In each case, a range of carrier gas flow was found (usually 10–30 cc./min.) in which the amount of salt collected per unit volume of carrier gas was independent of flow rate. The amount of carrier gas used was determined by water displacement.

Temperatures in boiling point and transpiration vessels were measured with a Rubicon portable precision potentiometer and calibrated Pt–Pt (10% Rh) thermocouples. The estimated uncertainty of a temperature measurement was ±1.5°.

Results and Discussion

Pure Salts.—The vapor pressures for the pure salts as determined using the boiling point technique were correlated using equations of the form

$$\log p = -\frac{\Delta H_0}{4.576T} + \frac{\Delta C_P}{1.987}\log T + I \quad (1)$$

where

p = The vapor pressure of the salt in mm.
T = The absolute temperature in °K.
ΔH_0 = The constant of integration derived from the Kirchoff equation, kcal./mole
ΔC_p = C_p(vapor) − C_p(liquid) at the mean temp. of the experiments, cal./mole °K.
I = A constant

The values for ΔC_p were the same as those used by Kelley[25] for KCl and CsCl. For $MgCl_2$, the value of ΔC_p was amended from −10 to −8.1 cal./mole °K. in view of more recent heat capacity data for the liquid.[26]

Table I contains values obtained for ΔH_0 and I for the pure salts. The standard deviation in ΔH_0, calculated from a least squares treatment of the data, and the extreme variation in I, a measure of precision suggested by Kelley,[25] are given for each salt in the table. The vapor pressure data presented here are considered accurate to ±2%. For KCl and CsCl, the data for a given vapor pressure agree to 1–3°K. with the values reported by previous investigators.[12,23,27,28] The values for $MgCl_2$ are in poor agreement with the results of Maier.[29] Maier himself suggested the possibility of a systematic error in his determinations of the vapor pressure of this salt.

The results of the transpiration measurements for the pure salts may be used to determine the average molecular weight of the vapor at the temperature of the measurement. For any transpiration measurement, the following form of Dalton's law holds

(15) B. Chu and J. Egan, *Ann. N. Y. Acad. Sci.*, **79**, 908 (1960).
(16) B. F. Markov, J. K. Delimarsky, and I. D. Panchenko, *J. Polymer Sci.*, **31**, 263 (1958).
(17) D. E. Neil, Dissertation, Rensselaer Polytechnic Institute, 1959.
(18) I. L. Resnikow, *J. Appl. Chem. U.S.S.R.*, **23**, 950 (1950).
(19) W. D. Treadwell and A. Cohen, *Helv. Chim. Acta*, **22**, 433 (1939).
(20) R. Tsuchiya, *Sci. Rept. Tohoku Univ.*, F. Isikawa Anniversary Vol., **37**, 9 (1953).
(21) H. Flood and S. Urnes, *Z. Elektrochem.*, **59**, 834 (1955).
(22) H. A. Laitinen, W. S. Ferguson, and R. A. Osteryoung, *J. Electrochem. Soc.*, **104**, 516 (1957).
(23) J. L. Barton and H. Bloom, *J. Phys. Chem.*, **60**, 1413 (1956).
(24) J. M. O'Gorman, *Anal. Chem.*, **19**, 506 (1947).
(25) K. K. Kelley, U. S. Bur. Mines Bull. No. 383 (1935).
(26) G. E. Moore, *J. Am. Chem. Soc.*, **65**, 1700 (1943).
(27) W. H. Rodebush and E. Fiock *ibid.*, **48**, 2522 (1926).
(28) H. Von Wartenburg and H. Schulze, *Z. Elektrochem.*, **27**, 568 (1921).
(29) C. G. Maier, U. S. Bur. of Mines Tech. Paper No. 360 (1929).

TABLE I

VAPOR PRESSURE PARAMETERS FOR MOLTEN HALIDES

Salt	No. of determ.	Temp. range, °K.	ΔH_0, kcal./mole	ΔC_p, kcal./mole	I	Extreme variation in I
KCl	31	1189–1418	50.8 ± 0.2	-7.0	20.83	0.10
$MgCl_2$	18	1208–1413	53.7 ± 0.2	-8.1	23.15	0.08
CsCl	13	1102–1387	46.0 ± 0.1	-7.0	20.51	0.02

$$p_s' = \frac{W_s/M_F}{W_s/M_F + n_{c.g.}} P_T \qquad (2)$$

where

p_s' = The apparent vapor pressure of the salt in mm.
W_s = The weight in g. of salt vapor collected during the run
M_F = The formula weight of the salt in g.
$n_{c.g.}$ = The no. of moles of carrier gas used during the run
P_T = The average total pressure of salt vapor and carrier gas throughout the run in mm.

It should be noted that p_s' will be equal to the vapor pressure determined by an absolute method, *i.e.*, one which does not depend on a knowledge of the molecular weight, only if the vapor phase is not associated. If the salt vapor phase is associated, equation 2 may be rearranged to give equation 3

$$\bar{M}_s = \frac{W_s}{n_{c.g.}} \left[\frac{P_T}{p_s} - 1 \right] \qquad (3)$$

where

$\bar{M}_s = W_s/n_s$ = The average molecular weight of the salt vapor at the temp. of the measurement
p_s = The vapor presssure of the salt as determined by an absolute method.

Average molecular weights for the salt vapors investigated are given at several temperatures in Table II. Each value is the result of a single measurement. The two values for KCl at 1297° and for $MgCl_2$ at 1255° reflect the precision of the measurements. If it is assumed that the predominant species in the vapor are monomer and dimer only, the mole fractions of these species are obtained by solving the following simultaneous equations for X_1 and X_2

$$\bar{M}_s = X_1 M_F + 2X_2 M_F$$

$$1 = X_1 + X_2$$

The above assumption is substantiated for KCl and CsCl by mass spectrometric data.[4] While there is no direct evidence regarding the vapor states of $MgCl_2$, the salts $BeCl_2$ and $FeCl_2$, which are chemically similar to $MgCl_2$, have been shown to consist primarily of monomers and dimers in the vapor state.[5,11] From the mole fractions in each species in the vapor phase partial pressures of the monomers and dimers and equilibrium constants, heats and entropies for the dissociation of the dimers were obtained for the three salts. Equilibrium constants were correlated as a function of temperature by means of the integrated form of the van't Hoff equation

$$\log K_p = -\frac{\Delta H_D^0}{2.303RT} + \frac{\Delta S_D^0}{2.303R} \qquad (4)$$

where K_p is expressed in atmospheres and ΔH_D^0 and ΔS_D^0 are the enthalpy and entropy, respectively, for

TABLE II

AVERAGE MOLECULAR WEIGHT OF HALIDE VAPORS AS DETERMINED FROM TRANSPIRATION MEASUREMENTS

Salt	Temp., °K.	$\bar{M}$
KCl	1153	97.9
	1161	94.8
	1282	94.8
	1291	94.9
	1297	95.0
	1297	97.3
	1298	95.9
	1314	95.5
	1326	94.8
	1352	94.6
$MgCl_2$	1255	125.4
	1255	123.1
	1275	120.9
	1279	121.8
	1301	123.7
	1309	124.6
	1316	126.5
	1339	129.2
	1346	126.6
CsCl	1209	214.8
	1240	213.9
	1278	219.5
	1320	221.5
	1350	217.5

dissociation of the dimer at the mean temperature of the experiments. It has been assumed that ΔH_D^0 is independent of temperature over the short range investigated. Table III gives the values of ΔH_D^0 and

TABLE III

ENTHALPIES AND ENTROPIES FOR THE DISSOCIATION OF THE DIMER IN HALIDE VAPORS AT 1300°K.

Salt	ΔH_D^0, kcal./mole	ΔS_D^0, cal./mole °K.
KCl	45.7 ± 4.1[a]	29.3 ± 2.2[a]
	40.8 ± 0.6[b]	
	43.8 ± 2.3[c]	27.1 ± 1.7[c]
$MgCl_2$	32.0 ± 4.5[a]	18.8 ± 2.0[a]
CsCl	32.2 ± 3.1[a]	21.0 ± 2.5[a]
	37.3 ± 1.1[c]	25.3 ± 1.0[c]

[a] This work. [b] Barton and Bloom.[13] [c] Datz.[6]

ΔS_D^0 along with the results of other investigators. The uncertainties expressed are the standard deviations as calculated from the least squares treatment of the data. It is of interest to note that the equilibrium constant for dissociation of the dimer of KCl is essentially equal to that for $MgCl_2$.

Potassium Chloride–Magnesium Chloride Mixtures.—Vapor pressures were obtained as a function of temperature using the boiling point method for twelve mixtures of potassium chloride and magnesium chloride over the entire composition range in the temperature range 950–1150°. These data were correlated by the method of least squares. The resulting equations were used to compute the vapor pressure as a function

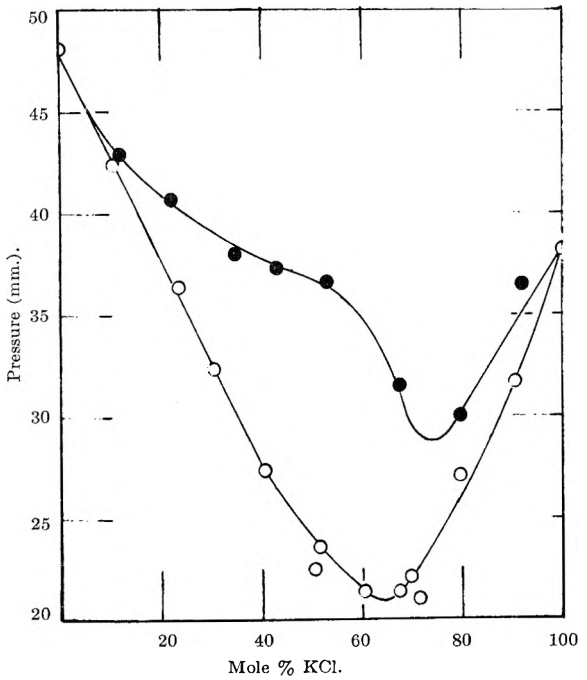

Fig. 1.—Apparent total vapor pressure (●) and observed total vapor pressure (○) of KCl–$MgCl_2$ mixtures *vs.* liquid composition at 1075°.

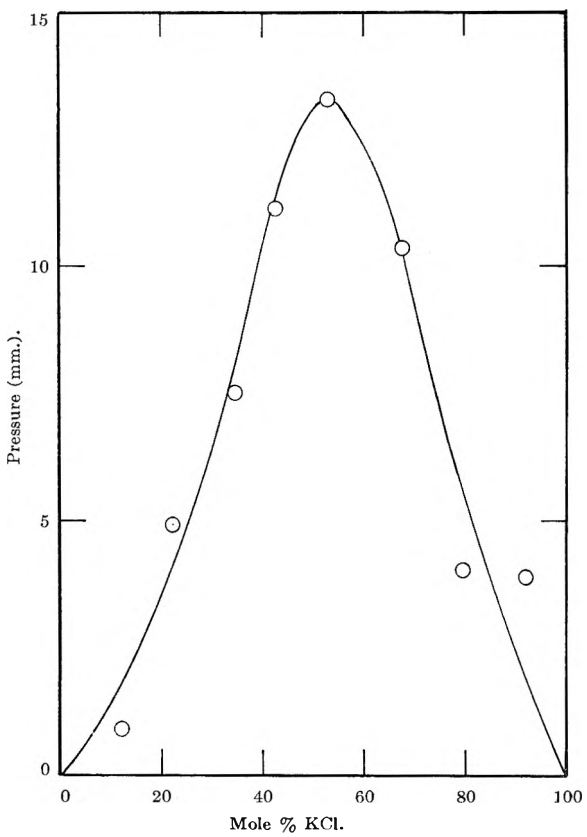

Fig. 2.—Difference between apparent total vapor pressure and observed total vapor pressure *vs.* liquid composition at 1075°.

of composition at various temperatures. Transpiration measurements were made as a function of temperature for eight mixtures of KCl and $MgCl_2$ over the entire composition range. From these data, apparent partial pressures could be obtained for each component. These pressures were calculated on the assumption that only monomers and dimers of each salt exist in the vapor and that there are no vapor phase interactions between the components. A least squares correlation

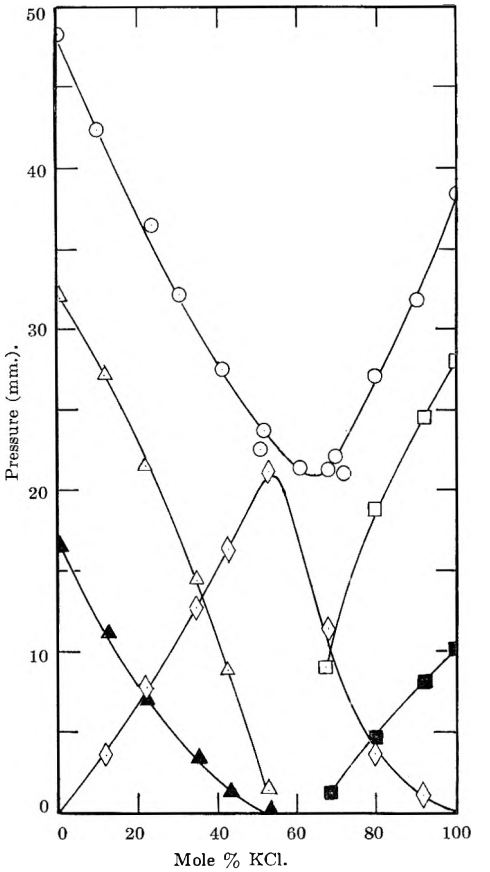

Fig. 3.—Calculated partial pressures of the components and observed total pressure for KCl–$MgCl_2$ mixtures at 1075°: ○, total (b.p.) pressure; △, $MgCl_2$ monomer; ▲, $MgCl_2$ dimer; □, KCl monomer; ■, KCl dimer; ◇, $KMgCl_3$.

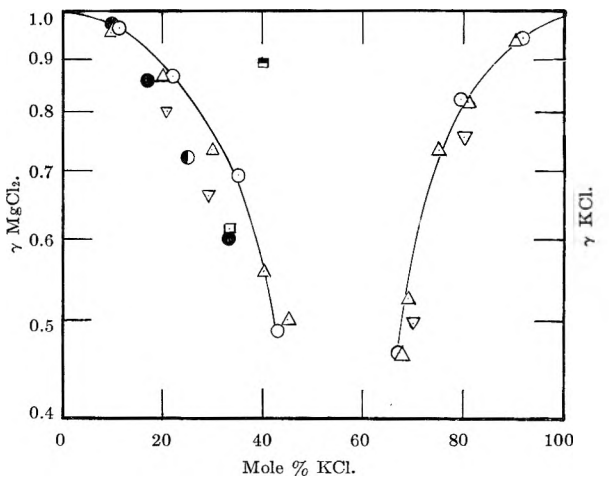

Fig. 4.—Activity coefficients of $MgCl_2$ and KCl *vs.* composition: ○, this work at 1075°; ▽, Neil[17] at 800°; ▀, Markov, *et al.*,[16] at 718°; △, Chu and Egan[15], ●, Tsuchiya[20] at 800°, ◐, Resnikow[18] at 950°; □, Treadwell[19] at 650°.

of these data similar to that made for the boiling point measurements provided apparent vapor pressures as a function of composition for various temperatures. The lower solid curve in Fig. 1 gives the vapor pressure as a function of liquid composition as determined from boiling point measurements at 1075°. The upper curve is a plot of the sum of the apparent partial vapor pressures, *i.e.*, the apparent total vapor pressure, as determined from transpiration measurements at 1075°. It can be seen that the two curves do not coincide indicating that there is a vapor phase interaction between the components. It is assumed that the

interaction involves a mixed compound of the type $(KCl)_i(MgCl_2)_j$, where i and j are integers.

Evidence for the nature of the interaction compound is provided by Fig. 2. Here, the difference between the apparent and observed total vapor pressures shown in Fig. 1 is plotted as a function of liquid composition. The maximum in the region of 50 mole % of each component is taken as evidence that the compound is of the 1:1 type, *i.e.*, $KMgCl_3$.

As a model of the vapor phase it is postulated that the species present are $MgCl_2$, Mg_2Cl_4, $KMgCl_3$, K_2Cl_2, and KCl. On the basis of this model the partial pressures for each of the components for various mixtures were calculated using the scheme suggested by Beusman[12] which involves combining the transpiration data with the boiling point data. The calculated partial pressures were restricted to those of $MgCl_2$, Mg_2Cl_4, and $KMgCl_3$ when $MgCl_2$ was the major formal component in the vapor and to $KMgCl_3$, KCl, and K_2Cl_2 when KCl was the major formal component. Figure 3 shows the calculated partial pressures of the various components and the observed total vapor pressure as a function of liquid composition at 1075°.

Activity coefficients for $MgCl_2$ and KCl calculated from the partial pressures of $MgCl_2$ monomer and KCl monomer[30] are shown in Fig. 4. The agreement with the results of other investigators[15-20] for $MgCl_2$ in the liquid composition range 0 to 42.9 mole % KCl is better than 10% while the activity coefficients calculated for KCl in the range 67.2 to 100 mole % KCl agree to better than 5% with previously reported results.[15,17] In Table IV the activities obtained at 1075° are compared with those computed from the model of Flood and Urnes.[21]

TABLE IV

COMPARISON OF ACTIVITIES OBTAINED IN THE PRESENT INVESTIGATION WITH THOSE COMPUTED FROM THE MODEL OF FLOOD AND URNES

Comp., mole % KCl	a_{MgCl_2}		a_{KCl}	
	Exptl.	Calcd.	Exptl.	Calcd.
11.7	0.853	0.815	...	...
22.0	.676	.641	...	...
34.6	.455	.418	...	...
42.9	.278	.268	...	...
67.2	...	...	0.313	...
79.4	...	...	.658	0.650
91.9	...	...	.868	0.903

It appears from the above comparisons that the proposed vapor phase model leads to activities which are in substantial agreement with other work.

Although, according to Flood and Urnes,[21] the predominant complex species in the liquid is K_2MgCl_4, the vapor appears to contain $KMgCl_3$ under our experimental conditions. Such a difference is not unexpected since dissociation of the larger complex in the vapor would be favored at low pressures. Further work is necessary to ascertain the thermodynamic stability of these vapor phase complexes over a wider range of pressures. A study of the dependence of the stability of such complexes of magnesium on the nature of the alkali cation would also be of interest.

Acknowledgment.—The authors gratefully acknowledge a grant for equipment from the International Nickel Company. We are indebted to Dr. E. W. Dewing of the Aluminum Company, Ltd., of Canada for a helpful discussion.

(30) I. Prigogine and R. Defay, "Chemical Thermodynamics," Longmans, Green and Company, London, 1954, p. 410.

THE RADIOLYSIS OF THE XYLENE ISOMERS AND ETHYLBENZENE

BY D. VERDIN

Wantage Research Laboratory, U.K. Atomic Energy Authority, Wantage, Berkshire, England

Received December 10, 1962

The G-values for the formation of H_2 and CH_4 in the ^{60}Co γ-radiolysis of the xylene isomers and ethylbenzene have been compared. The presence of iodine does not affect G_{H_2}, but reduces G_{CH_4} to a limiting value. For *p*-xylene the yields of H_2 and CH_4 are independent of dose rate, and G_{H_2} and the unscavengeable CH_4 are independent of temperature from 20 to 110°, whereas the total CH_4 yield increases sixfold over this range. The H_2 and CH_4 yields are greatly reduced in the solid state, and in the liquid state benzene shows a protective effect on the yields of both gases. The formation of CH_4 and C_2-hydrocarbons was compared with the C_6- and C_7-products for *p*-xylene and ethylbenzene, and isomerization has been shown to occur to a negligible extent. The production of high molecular weight products was measured for the xylenes, and is independent of dose rate and temperature for liquid *p*-xylene, but is decreased in the solid state. The results are qualitatively consistent with the reactions of radicals and excited molecules.

The radiation chemistry of toluene has been studied in detail,[1-5] but other alkylbenzenes have received comparatively little attention. The yields of the gaseous products from the radiolysis of toluene, mesitylene, and ethylbenzene[2] and of isopropylbenzene and *t*-butylbenzene[6] have indicated the influence of the number and complexity of alkyl groups in the molecule. In addition it has been demonstrated that the gas yields of alkyl benzenes vary with the type of radiation.[3,7] The spectrum of products of lower molecular weight has been established for isopropylbenzene.[7,8]

To extend the study of the effect of structure to that of the ring position of substituents on the radiation chemistry of simple alkyl-aromatic hydrocarbons the ^{60}Co γ-radiolysis of the xylene isomers and ethylbenzene

(1) J. P. Manion and M. Burton, *J. Phys. Chem.*, **56**, 560 (1952).
(2) R. R. Hentz and M. Burton, *J. Am. Chem. Soc.*, **73**, 532 (1951).
(3) T. J. Sworski and M. Burton, *ibid.*, **73**, 3790 (1951).
(4) R. B. Ingalls, *J. Phys. Chem.*, **65**, 1605 (1961).
(5) J. Hoigné and T. Gaumann, *Helv. Chim. Acta*, **44**, 2141 (1961).
(6) T. J. Sworski, R. R. Hentz, and M. Burton, *J. Am. Chem. Soc.*, **73**, 1998 (1951).
(7) M. A. Sweeney, Univ. of California Radiation Laboratory Report, UCRL-9983, March, 1962.
(8) R. R. Hentz, *J. Phys. Chem.*, **66**, 1622 (1962).

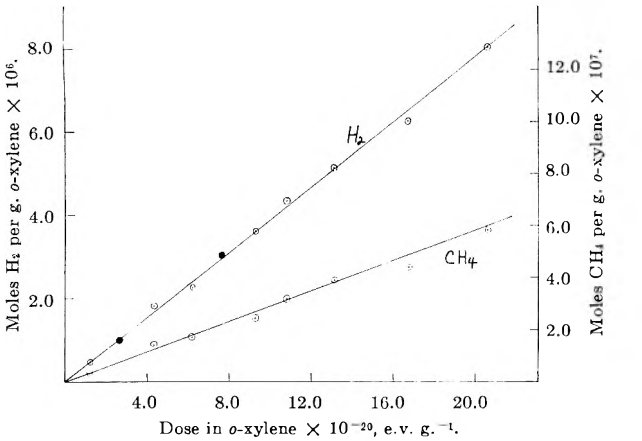

Fig. 1.—The formation of H_2 and CH_4 in the ^{60}Co γ-radiolysis of *o*-xylene at 20°. Dose rate = 3.97×10^{15} e.v. g.$^{-1}$ sec.$^{-1}$. Samples degassed at −119° (⊙) and −196° (●).

has been investigated. Since the influence of temperature has generally been neglected, the radiolysis of *p*-xylene has been examined over a wide temperature range.

Experimental

Materials.—All hydrocarbons were Phillips research grade. They were further purified by repeated shaking with concentrated H_2SO_4 until the acid layer was colorless, and then washing with 10% Na_2CC_3 solution and several times with distilled water. After drying with anhydrous $CaSO_4$ and filtering, the hydrocarbons were distilled under vacuum in a greaseless system, the middle 80% fraction being collected and stored in evacuated vessels until used.

Iodine was Fisher Scientific Company, certified reagent (resublimed). Oxygen was General Dynamics Corporation 99.5% pure. Tetrachloroethylene (Eastman Organic Chemicals, spectro grade) was dried with anhydrous $CaSO_4$, filtered, and distilled under vacuum, the middle fraction of 50% being collected and used immediately.

Irradiation Technique.—The previously degassed hydrocarbons were distilled under vacuum into a calibrated tube and after volume determination distilled into the irradiation vessels fitted with break-seals. Mixtures, and solutions of I_2 or C_2Cl_4, were prepared with hydrocarbons which had been distilled twice under vacuum, and were pipetted into the vessels, degassed, and sealed off under vacuum. Samples containing O_2 were sealed off at measured pressures of O_2. The volumes of liquid used were from 5 to 15 ml.

An underwater ^{60}Co γ-facility was employed and the samples were irradiated in air at the ambient temperature of the source (20 ± 1°), in an oilbath controlled to ±1° or in dewar vessels containing cooling liquids. The rates of energy absorption in the hydrocarbons and in solutions were calculated on the basis of electron densities from dose rates measured with the ferrous sulfate dosimeter assuming $G_{Fe^{3+}} = 15.5$.[9]

Analysis.—After irradiation the sample tubes were sealed on to a modified Saunders–Taylor apparatus[10] and the total quantity of gas which could be obtained by repeated freezing, expansion, and melting cycles was measured. Degassing at −196° did not remove all the CH_4 from the samples, but the gas collected by degassing at −119° (C_2H_5Br slush) contained all the H_2 and CH_4 produced. When C_2Cl_4 solutions were irradiated the −119° fraction contained HCl which was removed by a plug of crushed KOH pellets located between the sample and the measuring apparatus. The C_2-hydrocarbons were completely removed by degassing at −23° (CCl_4 slush). The collected gases were transferred in calibrated tubes for gas chromatographic analysis.

Analyses were performed with a Perkin–Elmer Model 154 vapor fractometer, using a thermistor detector, 1 mv. recorder, helium carrier gas, and columns supplied by Perkin–Elmer. H_2 and CH_4 (and O_2) were determined on a 2-meter activated charcoal column at 45° and their identities and ratio of yields confirmed by mass spectrometry. For samples collected at −23° the ratio of each of the C_2 gases to CH_4 was determined on a 2-meter silica gel column at 45°. Analyses on this column of samples collected at −119° indicated less than 1% of C_2-hydrocarbons in this fraction. The identities of the C_2-hydrocarbons were confirmed by their retention times on a 2-meter modified (di-2-ethylhexyl sebacate added) silica gel column at 52°.

To study the higher molecular weight products ampoules were filled and irradiated just prior to analysis to minimize any post-irradiation effects. Samples of the irradiated liquid were analyzed on a 4-meter, 7,8-benzoquinoline column at 95°. This column resolves benzene, toluene, and three xylene isomers and ethylbenzene, but does not separate *m*-xylene, *p*-xylene, and ethylbenzene when one of these is present in large excess.

The total irradiation products which are less volatile than the parent xylenes, *i.e.*, "polymer," were isolated by vacuum distillation of the irradiated liquids, kept at 20°, until a piece of solid CO_2 pressed against the neck of the tube from which the hydrocarbon was being distilled caused no condensation of liquid at that point. In all cases this gave viscous yellow liquids which by chromatographic analysis were shown to contain always less than 7.5% of the parent hydrocarbon. After weighing, the average molecular weights of the residues were measured in toluene solution using a Mechrolab, Inc., vapor pressure osmometer Model 301 calibrated with biphenyl and *p*-terphenyl.

Results

Formation of Gaseous Products.—The yields of H_2 and CH_4 obtained on the radiolysis of the pure liquid hydrocarbons at 20° were in all cases proportional to the absorbed dose over the range 1×10^{20} to 2×10^{21} e.v. g.$^{-1}$ at a dose rate of 4×10^{15} e.v. g.$^{-1}$ sec.$^{-1}$. Figure 1 shows the results for *o*-xylene and the yields from the hydrocarbons studied are summarized in Table I, which also shows the yields of H_2 and CH_4 from the hydrocarbons containing iodine at concentrations in the range 3×10^{-3} to 5×10^{-2} *M*, the *G*-values being independent of the I_2 concentration. G_{H_2} increases slightly on adding I_2 to the hydrocarbons, whereas for benzene Schuler[11] obtained a slight decrease at comparable I_2 concentrations. The ratio G_{CH_4}/G_{H_2} (0.164) for ethylbenzene agrees closely with the data of Hentz and Burton[2] for 1.8 Mev. electrons, but the individual *G*-values are about 10% lower than obtained by these authors.

In the case of *p*-xylene ampoules were sealed off containing approximately measured pressures of oxygen. After irradiation at 20° and a dose rate of 4×10^{15} e.v. g.$^{-1}$ sec.$^{-1}$ the H_2, CH_4, and excess O_2 were collected and analyzed. For O_2 pressures exceeding 50 mm. the yields were $G_{H_2} = 0.217$ and $G_{CH_4} = 0.0029$. At lower O_2 pressures G_{H_2} was unchanged but G_{CH_4} increased progressively to its value for the pure hydrocarbon, indicating competition between O_2 and *p*-xylene for the methyl radicals. Irradiation under the same conditions of *p*-xylene containing tetrachloroethylene at concentrations from 0.014 to 0.15 *M* caused no change in the values of G_{H_2} or G_{CH_4}. C_2Cl_4 is known to scavenge H atoms produced in the radiolysis of hexane,[12] but it apparently does not scavenge methyl radicals produced in the radiolysis of *p*-xylene. This behavior is consistent with the reported methyl affinity of C_2Cl_4.[13]

For *p*-xylene the yields of H_2 and CH_4 were measured over a range of dose rates and the results, included in Table I, show the formation of both products is independent of dose rate from 8.5×10^{14} to 1.3×10^{16} e.v. g.$^{-1}$ sec.$^{-1}$. The effect of temperature on the gas yields from liquid and solid *p*-xylene is shown in Table II. The production of H_2 and CH_4 was linear with ab-

(9) R. H. Schuler and A. O. Allen, *J. Chem. Phys.*, **24**, 56 (1956).
(10) K. W. Saunders and H. A. Taylor, *ibid.*, **9**, 616 (1941).
(11) R. H. Schuler, *J. Phys. Chem.*, **60**, 381 (1956).
(12) T. J. Hardwick, *ibid.*, **64**, 1623 (1960).
(13) R. P. Buckley and M. Szwarc, *J. Am. Chem. Soc.*, **78**, 5696 (1956).

sorbed dose except for the CH_4 yields at 82 and 110° which decreased slightly at doses exceeding 8×10^{20} e.v. g.$^{-1}$ so that the G-values were calculated from the initial slopes of the yield curves. In the liquid phase the yields were also measured in the presence of iodine at concentrations from 5×10^{-3} to 5×10^{-2} M. The gases formed in solid p-xylene (m.p. 13°) were isolated by melting and then degassing by the usual procedure.

The radiolysis of p-xylene and ethylbenzene produced ethane, ethylene, and acetylene with the yields given in Table III. The G-values were independent of dose in the range 6 to 30×10^{20} e.v. g.$^{-1}$. No propane was detected in p-xylene samples irradiated to the higher doses.

TABLE I

100 E.V. YIELDS FROM ^{60}Co γ-RADIOLYSIS OF HYDROCARBONS AT 20 ± 1°

Hydrocarbon	Dose rate × 10^{-15}, e.v. g.$^{-1}$ sec.$^{-1}$	Pure hydrocarbon G_{H_2}	Pure hydrocarbon G_{CH_4}	Hydrocarbon + I_2 G_{H_2}	Hydrocarbon + I_2 G_{CH_4}
Ethylbenzene	3.73	0.158	0.0259	0.163	0.0058
o-Xylene	3.97	.235	.0171	.246	.0028
m-Xylene	3.73	.184	.0142	.197	.0028
p-Xylene	3.97	.209	.0144	.219	.0030
	0.852	.203	.0145	...	...
	72.7	.200	.0138	...	...
	128	.216	.0147	...	...

TABLE II

G-VALUES FOR p-XYLENE IRRADIATED AT DOSE RATE OF 3.73×10^{15} E.V. G.$^{-1}$ SEC.$^{-1}$

Temp., °C.	Pure p-xylene G_{H_2}	Pure p-xylene G_{CH_4}	p-Xylene + iodine G_{H_2}	p-Xylene + iodine G_{CH_4}
−196	0.0112	6.4×10^{-4}	...	...
−80	.0196	7.3×10^{-4}	...	...
0	.0493	10.5×10^{-4}	...	...
20[a]	.209	0.0144	0.219	0.0030
49.5	.194	.0154	.203	.0026
82	.200	.0224	.201	.0024
110	.199	.0867	.208	.0024

[a] Dose rate = 3.97×10^{15} e.v. g.$^{-1}$ sec.$^{-1}$.

TABLE III

G-VALUES FOR THE FORMATION OF C_2-PRODUCTS AT 20°

Hydrocarbon	Dose rate × 10^{-15}, e.v. g.$^{-1}$ sec.$^{-1}$	$G_{C_2H_2}$	$G_{C_2H_4}$	$G_{C_2H_6}$
p-Xylene	3.44	0.0033	0.0002	0.0001
Ethylbenzene	3.52	0.0021	0.0071	0.0057

Formation of C_6 and Higher Products.—For p-xylene irradiated at 20° at a dose rate of 7.02×10^{16} e.v. g.$^{-1}$ sec.$^{-1}$ to doses in the range 5 to 14×10^{21} e.v. g.$^{-1}$, toluene was produced with a G-value of 0.014. No benzene or o-xylene was detected and analysis of test mixtures indicated that if they are formed they must have G-values less than 0.002. The products of o-xylene irradiated under the same conditions contained no benzene, ethylbenzene, or p-xylene, but did contain toluene (G = 0.023) and m-xylene (G = 0.042). Similarly radiolysis of ethylbenzene produced benzene (G = 0.016) and toluene (G = 0.018) but no detectable o-xylene. For m-xylene irradiated to lower total doses no benzene, toluene, or o-xylene was detected, indicating their G-values to be less than 0.05. In none of the irradiated samples did the chromatograms show any unidentified peaks which eluted before o-xylene, so that the liquid products are predominantly of higher molecular weight than the parent compounds.

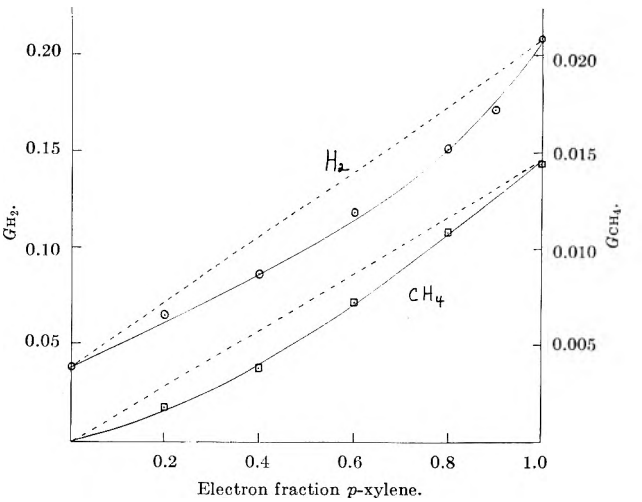

Fig. 2.—The G-values for the formation of H_2 and CH_4 in the ^{60}CO γ-radiolysis of mixtures of benzene and p-xylene at 20°. Dose rate = 7.27×10^{16} e.v. g.$^{-1}$ sec.$^{-1}$.

The yields and average molecular weights of the "polymer" produced from the xylene isomers irradiated under various conditions are summarized in Table IV. The G-values calculated as loss of the irradiated hydrocarbon are independent of dose over the ranges studied, and the molecular weights increase continuously, but not linearly, with dose.

Radiolysis of p-Xylene–Benzene Mixtures.—To determine whether the radiolysis of p-xylene could be influenced by the presence of a second aromatic molecule the formation of H_2 and CH_4 was measured in the radiolysis of mixtures of p-xylene and benzene over the full range of compositions. From Fig. 2, in which each point is the average of three measurements, it is seen that the values of G_{H_2} and G_{CH_4} based on total energy absorbed in such mixtures are both less than predicted (dotted lines) simply on the basis of electron fraction.

Discussion

The yields of H_2 from the radiolysis of ethylbenzene and the xylenes are effectively unchanged by radical scavengers so that none of the H_2 results from H atoms which have escaped from the solvent cage of their parent molecules. Similar conclusions were made by Schuler[11] in the case of benzene, and are consistent with the high rate constants for addition of H atoms to these hydrocarbons[14] which prevent their escape from the solvent cage. If initially formed H atoms were to abstract a second H atom from an adjacent xylene molecule then the activation energy of this reaction[15] would cause G_{H_2} to be temperature dependent, whereas for p-xylene the activation energy for G_{H_2} is 0.0 ± 0.3 kcal. mole^{-1}. Furthermore, the fact that the G-value for scavengeable CH_4 is greater for ethylbenzene than for the xylenes (although it contains fewer CH_3 groups) indicates the ease of H atom abstraction from the methylene group in ethylbenzene. Consequently the fact that G_{H_2} is smaller for ethylbenzene than for the xylenes, which contain no methylene groups, indicates a nonradical mechanism for H_2 formation.

These results may be interpreted in terms of the type of mechanism discussed by Burns[16,17] and Burr[18,19] in

(14) T. J. Hardwick, *J. Phys. Chem.*, **66**, 117 (1962).
(15) R. B. Ingalls and J. R. Hardy, *Can. J. Chem.*, **38**, 1734 (1960).

TABLE IV

G-VALUES AND AVERAGE MOLECULAR WEIGHTS OF THE "POLYMER" PRODUCED ON RADIOLYSIS OF THE ISOMERIC XYLENES

Hydrocarbon	Temp., °C.	Dose rate × 10^{-16}, e.v. g.$^{-1}$ sec.$^{-1}$	Dose range, e.v. g.$^{-1}$	*G*(-hydrocarbon)	Range of mol. wt.
o-Xylene	20	6.86	9.88×10^{20} to 1.18×10^{22}	1.34	253 to 289
m-Xylene	20	7.01	1.26×10^{21} to 1.97×10^{22}	0.99	272 to 308
p-Xylene	20	7.02	6.06×10^{21} to 1.40×10^{22}	1.10	282 to 299[a]
p-Xylene	20	0.344	5.94×10^{20} to 3.00×10^{21}	1.07	260 to 269
p-Xylene	110	0.344	8.15×10^{20} to 2.09×10^{21}	1.17	267[b]
p-Xylene	−80	0.344	1.42×10^{21} to 3.66×10^{21}	0.43	230[c]

[a] Repeat sample irradiated to dose of 1.4×10^{22} e.v. g.$^{-1}$ and in which residue was kept at 50° and evacuated for 72 hours gave residue of molecular weight 345 instead of 299. [b] Dose = 1.89×10^{21} e.v. g.$^{-1}$. [c] Dose = 3.66×10^{21} e.v. g.$^{-1}$.

which the gaseous and some of the higher molecular weight products of the radiolysis of aromatic hydrocarbons are considered to arise from the reactions of the excited species produced on irradiation. In the liquid phase a small proportion of the H_2 may result from a temperature independent unimolecular dissociation of an excited molecule

$$C_8H_{10}^* \longrightarrow [C_8H_9\cdot + H\cdot] \longrightarrow H_2 + C_8H_8 \quad (1)$$

the possibility of the reaction occurring in two stages being included in equation 1, in which the brackets enclose species which have not been separated by diffusion from the solvent cage in which they were formed. However, in the liquid state the majority of the H_2 is produced by bimolecular reactions of the excited molecules, reaction 4 being included to explain LET effects.[16]

$$C_8H_{10}^* + C_8H_{10} \longrightarrow 2C_8H_{10} \quad (2)$$

$$C_8H_{10}^* + C_8H_{10} \longrightarrow H_2 + C_{16}H_{18} \quad (3)$$

$$2C_8H_{10}^* \longrightarrow H_2 + C_{16}H_{18} \quad (4)$$

Reactions 2, 3, and 4 must each have zero activation energy to account for the temperature independence of G_{H_2}. Moreover, the experimental results make it necessary to assume that the excited molecules do not react with radical scavengers. On passing from liquid to solid *p*-xylene G_{H_2} decreases sharply to a value which varies slightly with temperature. In the solid state, where the probability of collisional deactivation is small owing to the limited diffusion of the active species, H_2 must arise predominantly by reaction 1. Immobilization of the activated molecules undergoing reaction 1 should not interfere with their unimolecular decomposition, whereas the greater diffusion in the liquid phase favors the bimolecular reactions 2, 3, and 4, which therefore produce the majority of the H_2 formed in that state. Thus the increase in H_2 yield with temperature in the solid state must result from the small, but increasing, contribution from reactions 3 and 4 as the temperature rises and the probability of diffusion of active species increases.

According to Ingalls[4] the hydrogen from toluene radiolysis is derived mainly from the methyl group, but some can arise from the aromatic ring by a H atom adding to toluene and the adduct disproportionating with a second atom from another toluene molecule. Scavengers should compete for reaction with this second H atom, and also with the first H atom if it diffuses from the solvent cage in which it is formed, and reduce the H_2 yield so that a similar reaction apparently does not occur in the xylenes. Moreover, the disproportionation reaction would be expected to have an activation energy and so result in a temperature variation of G_{H_2}.

At 20° the presence of I_2 or O_2 decreases the CH_4 yields to a limiting value about 20% of that in the absence of scavengers, so that the majority of the CH_4 is formed by abstraction reactions of freely diffusing methyl radicals formed in reaction 5. The yield of C_2H_6 from *p*-xylene shows combination of methyl radicals to be negligible.

$$CH_3\cdot C_6H_4\cdot CH_3^* \longrightarrow CH_3\cdot C_6H_4\cdot + CH_3\cdot \quad (5)$$

The increase in G_{CH_4} with temperature, which rises too steeply to give an Arrhenius type plot, may be due to the increased probability of escape of methyl radicals from the solvent cage in which they are formed and to the higher activation energy for abstraction compared with addition reactions of these radicals. Since the yield of CH_4 in solid *p*-xylene is much less than the unscavengeable yield in the liquid phase, the latter, which is independent of temperature, must arise by two or more processes, which may be analogous to those for H_2 production.

There is evidence[20] that in aromatic mixtures the unimolecular formation of hydrogen (*i.e.*, both H atoms from the same molecule) is uninfluenced by the nature of the solvent, but that the bimolecular production of hydrogen does vary with the solvent. Toluene is the only other alkyl benzene for which the radiolysis of its mixtures with benzene has been studied over the full concentration range.[1] The H_2 and CH_4 (but not C_2H_2 and C_2H_4) formation obeyed the simple mixture law, so that its behavior differs from that of *p*-xylene. Since the ionization potentials of toluene and *p*-xylene are both less than that of benzene,[21] it is unlikely that charge transfer is the cause of the protection. Preferential addition of H atoms and CH_3 radicals to one component of the mixture does not appear to be an explanation, at least for H_2, since a small proportion of benzene produces a marked fall in G_{H_2} and the rate constant for addition of H atoms to *p*-xylene exceeds that for addition to benzene.[14] A greater probability for the occurrence of reaction 2, if the unexcited species is benzene, could explain the observations in these mixtures, that is, the protective effect is due to excitation energy transfer, but the present work provides no direct evidence on this point.

The lack of influence of scavengers or temperature on the H_2 yield would be expected if it arose entirely from

(16) W. G. Burns, Rass. Intern. Elettron. Nucl., Rome, 1959, Atti Congr. Sci, Sez. Nucl., **6**, 99 (1959).
(17) W. G. Burns, *Trans. Faraday Soc.*, **58**, 961 (1962).
(18) J. G. Burr and J. M. Scarborough, *J. Phys. Chem.*, **64**, 1367 (1960).
(19) J. G. Burr, *Nucleonics*, **19**, No. 10, 49 (1961).
(20) P. J. Dyne and J. Denhartog, *Can. J. Chem.*, **40**, 1616 (1962).
(21) G. F. Crable and G. L. Kearns, *J. Phys. Chem.*, **66**, 436 (1962).

the reactions of "hot" hydrogen atoms; however, rapid collisional deactivation of such atoms would cause them to be accompanied by some thermal H atoms. Consequently scavengers would be expected to decrease the H_2 yield, as has been observed in the radiolysis of saturated hydrocarbons, where the "molecular" yield is considered to result from the reactions of hot H atoms.[22] The similar dependence of the yields of H_2 and C_2H_2 on the LET value of the radiation in the radiolysis of benzene suggests that they are produced by similar mechanisms,[17] so that if hot H atoms were involved in the formation of H_2 it would be necessary to assume their interaction with benzene could form acetylene, a reaction which is difficult to envisage. Moreover, there is evidence that the reaction of recoil tritium atoms with the benzene ring is predominantly addition.[23] These considerations indicate that in the radiolysis of simple aromatic hydrocarbons the H_2 does not arise by hot atom mechanisms, whereas the CH_4 yield, which is affected by scavengers and temperature, may result partly from hot methyl radicals.

The very low yields of C_2 products from *p*-xylene indicate that ring fission is much less important than in the case of benzene where the acetylene yield is sixfold higher, and amounts to one-third of the total gas yield.[1]

Comparable yields of CH_4 and toluene were obtained on radiolysis of either *o*-xylene or *p*-xylene at 20°, so that reaction 5 followed by both radicals abstracting H atoms must be the principal source of toluene, and has been shown to account for 80% of the CH_4. Similarly for ethylbenzene the sum of the C_2 hydrocarbon yields is of the same order of magnitude as the benzene yield. In the case of toluene G_{benzene}[5] is nearly twice the value of G_{CH_4}[1] so that ethylbenzene and the xylenes should be formed with a total yield of approximately G_{CH_4}, but these yields have not yet been reported.

The very small or zero yields for isomerization of the xylenes obtained in this work are contrary to a preliminary report by Gelbshtein, *et al.*,[24] who stated that under γ-irradiation at room temperature each of the three xylenes is isomerized into the other two, the *G*-values for the products being between 2 and 6.

The *G*-values for the conversion of xylene molecules to products of higher molecular weight are of the same order of magnitude as the corresponding values for benzene[25] and toluene,[2] and show the formation of "polymer" to be independent of dose rate and temperature in liquid *p*-xylene. The formation of polymer in *p*-xylene by pile irradiation has been observed[26] but no absolute yield was determined. The molecular weights of the products indicate a progressive increase in the average size of the polymer molecules with dose, and show that the average number of monomer units per polymer molecule is close to that for the case of benzene at similar doses.[27] If all the H_2 from liquid *p*-xylene were formed by reactions 3 and 4, then $G_{(p\text{-xylene})}$ for the formation of polymer would be $2G_{H_2}$ and the molecular weight would be 210. Therefore, other processes which are independent of temperature and dose rate must account for the majority of the polymer. These could involve excited molecules[17] or be the subsequent addition reactions with each other, with xylene molecules, or with polymer molecules of the radicals resulting by reactions 6 and 7 from the dissociation of *p*-xylene in the solvent cage.

$$C_8H_{10}^* + C_8H_{10} \longrightarrow [C_8H_9\cdot + H\cdot + C_8H_{10}] \quad (6)$$

$$[H\cdot + C_8H_{10}] \longrightarrow C_8H_{11}\cdot \quad (7)$$

The molecular weight of the polymer formed in *p*-xylene irradiated in the solid state shows it to be mainly dimer. This probably results from the combination of the radicals formed in reactions 6 and 7, either at −80° or as the solid is warmed up prior to analysis: the low yield of H_2 in the solid state signifies negligible contribution of reactions 3 and 4 to polymer formation in the solid.

The stability of the xylenes with regard to the formation of H_2, CH_4, and high molecular weight products decreases in the order *meta*, *para*, *ortho*. No significance can be attached to a comparison of stabilities with ionization potentials since these differ little between the xylenes,[21] however, the sequence of stabilities is the same as that of the C–H bond dissociation energies.[28] The influence of the positions of ring substituents have been examined for the terphenyls[29] and substituted toluenes[30] but the results are not directly comparable with the present work.

Acknowledgment.—This work was performed in part under the auspices of the U. S. Atomic Energy Commission at Brookhaven National Laboratory, Upton, New York. The author thanks the U. K. Atomic Energy Authority for his support on an exchange scheme during the course of this work. He is indebted to N. Carciello for the molecular weight measurements, and to Drs. R. Barker, W. G. Burns, and C. H. Collins for helpful discussions.

(22) T. J. Hardwick, *J. Phys. Chem.*, **66**, 1611 (1962).

(23) A. N. Nesmeyanov, *et al.*, *Radiokhimiya*, **4**, 116 (1961).

(24) A. I. Gelbshtein, *et al.*, All-Union Conference on Radiation Chemistry, Moscow, 1957. Abstracts of papers AEC-TR-2925, Part 4, p. 27. N.B. Full paper did not appear in the Proceedings of the Conference.

(25) S. Gordon, A. R. Van Dyken, and T. F. Doumani, *J. Phys. Chem.*, **62**, 20 (1958).

(26) F. Van Hecke, *Nature*, **186**, 382 (1960).

(27) W. N. Patrick and M. Burton, *J. Am. Chem. Soc.*, **76**, 2626 (1954).

(28) M. Szwarc, *Chem. Rev.*, **47**, 75 (1950).

(29) E. L. Colichman and R. H. J. Gercke, *Nucleonics*, **14**, No. 7, 50 (1956).

(30) R. M. Wagner and L. H. Towle, WADC Technical Report 58-683 (1959).

SPECTROSCOPIC STUDIES ON THE COLOR REACTION OF ACID CLAY. III. THE COLORATION WITH POLYENES AND POLYACENES

BY HAJIME HASEGAWA

Department of Applied Chemistry, Faculty of Science and Engineering, Waseda University, Tokyo, Japan

Received December 11, 1962

The color reactions in benzene of acid clay with diphenylpolyenes, carotenoids, and polyacenes were studied by measuring the absorption spectra of the colored clay suspensions between 350 and 1000 mμ by the opal glass transmission method for translucent materials. The absorption bands of these hydrocarbons shift toward longer wave lengths when they are adsorbed on the clay. The shifts are as large as 156–386 mμ, and a close linear relationship exists between the wave lengths of absorption maxima of diphenylpolyenes and β-carotene with acid clay and without the clay. The similarity of the spectra of the colored clay suspensions to those of the hydrocarbons in concentrated sulfuric acid solutions indicated that the coloration is due to the formation of cation radicals of these hydrocarbons on the clay.

Introduction

It has been known that a blue color is developed on acid clay of the Montmorillonite group when it comes into contact in non-polar solvents with aromatic amines or hydrocarbons with a long chain of conjugated double bonds such as vitamin A,[1-3] β-carotene,[2,3] and diphenyloctatetraene.[4] Spectroscopic observations were made on the color reaction with aromatic amines in previous studies[5,6] in which clearly defined absorption spectra of colored clay suspensions were obtained by use of the opal glass transmission method[7] for translucent materials. The results elucidated the mechanism of the coloration, which involves two chemical reactions, the formation of the semiquinone radicals of amines and the successive change into quinoidal compounds.

At nearly the same time as the author's publication[6] and during the further investigation described here, Hall[8] reported the spectral changes of anthracene, perylene, pyrene, and 3,4-benzopyrene due to the adsorption on a silica–alumina catalyst, and concluded that the remarkable changes are due to the formation of cation radicals of these hydrocarbons on the catalyst, referring to his data of electron spin resonance and the absorption spectra in a concentrated sulfuric acid solution obtained by Aalbersberg, Hoijtink, Mackor, and Weijland.[9] This conclusion is in accord with the mechanism clarified by the author for the coloration of amines, since the formation of semiquinone radicals involves the transfer of electrons from amines to the clay. Described herein are the results obtained in a systematic study on the coloration of acid clay in benzene with various hydrocarbons; diphenylpolyenes with different chain lengths, anhydro vitamin A, β-carotene, and condensed aromatic hydrocarbons including naphthalene, anthracene, and tetracene. The spectra of the colored clay suspensions were compared with those in sulfuric acid.

(1) A. Lowmann, *Science*, **101**, 182 (1945).
(2) K. Kobayashi, *Kogyokagaku-Zasshi*, **27**, 937, 1010 (1924).
(3) P. Meunier, *Compt. rend.*, **215**, 470 (1942).
(4) L. Zechmeister, *Science*, **101**, 585 (1945).
(5) H. Hasegawa, *J. Phys. Chem.*, **65**, 292 (1961).
(6) H. Hasegawa, *ibid.*, **66**, 834 (1962).
(7) K. Shibata, "Spectrophotometry of Translucent Biological Materials—Opal Glass Transmission Method," in "Methods of Biochemical Analysis," D. Glick, ed., Vol. VII, Interscience Publishers Inc., New York, N. Y., 1959.
(8) W. K. Hall, *J. Catalysis*, **1**, 53 (1962).
(9) W. I. Aalbersberg, G. J. Hoijtink, E. L. Mackor, and W. P. Weijland, *J. Chem. Soc.*, **162**, 3049, 3055 (1959).

Experimental

Reagents.—ω,ω'-Diphenylethylene, -butadiene, -hexatriene, -octatetraene, -decapentaene, and -dodecahexaene were purified, recrystallizing several times from their solutions in acetic anhydride; melting points, 124, 152, 195, 225, 252, and 267°, respectively. Anhydro vitamin A was synthesized from vitamin A using *p*-toluenesulfonic acid as the dehydrating catalyst,[10] and the product was purified on an alumina column with benzene as the solvent. Crystalline β-carotene, which was commercially available, also was purified chromatographically; melting point, 178°. These preparations of reagents were found to be in the *trans* form by the analysis of their infrared absorption spectra. Naphthalene, anthracene, and tetracene of reagent grade were recrystallized from the tetrachloroethane solutions and purified further chromatographically on alumina with benzene as the solvent; melting points, 80, 217, and 331°, respectively.

Acid Clay.—The Itoigawa Clay of the Montmorillonite group was activated with 3 *N* H_2SO_4 at 100° as described previously.[6] The clay was washed with water and dried. By this treatment, the coloration of the natural clay was intensified to the maximal extent.

Preparation of Colored Mixtures.—The acid-treated clay (0.5 g.) in a glass vessel was heated at 100° in a reduced pressure of 10^{-3} mm. to remove water and gases adsorbed on the acid clay. After cooling, the vessel was filled with dry hydrogen gas, and then 15 ml. of dry benzene was added to the clay. To this suspension of acid clay, 2.5–20 ml. of a reagent solution in benzene was added, and the colored suspension thus obtained was subjected to spectroscopic observations. The reagents and their concentrations to be added to the clay suspension were 2×10^{-5} *M* ω,ω'-diphenylpolyenes and carotenoids and 2×10^{-4} *M* polyacenes.

Spectroscopic Observations.—The absorption spectra of colored clay suspensions were observed between 350 and 1000 mμ by the opal glass transmission method[7] with a Shimadzu recording spectrophotometer Model RS-27, using cells of 1 mm. optical path length. The same clay suspension with no reagent was used as the reference in the measurements.

Results

(I) The Coloration with Polyacenes.—The coloration occurs immediately after mixing of a solution of polyacenes with a clay suspension. The colors developed, however, fade rapidly in the presence of oxygen, but very slowly with hydrogen or nitrogen. The coloration experiments were, therefore, conducted with hydrogen as described in the Experimental part.

The spectra of colored clay with naphthalene, anthracene, and tetracene are shown in Fig. 1. The acid clay is colored weakly with naphthalene and strongly with anthracene and tetracene. The spectrum observed for the clay suspension with naphthalene shows a weak band at 510 mμ with two shoulders around 410 and 455 mμ. On the other hand, the suspensions with anthracene and tetracene show four absorption bands above 500 mμ and two bands below 500 mμ.

(10) P. Budowski and A. Bondi, *Analyst*, **82**, 751 (1957).

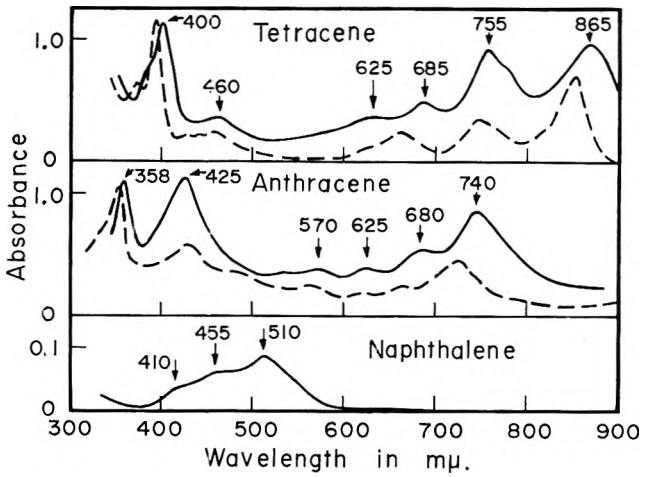

Fig. 1.—Absorption spectra of the colored clay suspensions with polyacenes and the sulfuric acid solutions of the reagents: ———, colored clay; – – – –, sulfuric acid solution.

The wave lengths of absorption maxima of these bands and shoulders are indicated with arrows in the figure. The band at the longest wave length is the highest of the bands observed above 500 mμ for each polyacene, and the band height decreases progressively in the order of decreasing wave length. The bands observed around 400 mμ with anthracene and tetracene are very sharp and even higher than the bands at the longest wave length. Trials to observe the spectral change upon addition of benzene to a clay suspension in hexane were unsuccessful.

The spectra of sulfuric acid solutions of anthracene and tetracene were measured and the results are shown by dashed curves in Fig. 1. The band positions were 720, 660, 620, 560, 428, and 354 mμ for anthracene and 848, 743, 660, 620, 455, and 393 mμ for tetracene. The spectrum of naphthalene in sulfuric acid could not be measured, since it was insoluble in the acid. The positions and shapes of the bands of the sulfuric acid solutions are similar to those of the colored clay with the same polyacene, although they shifted slightly toward shorter wave lengths. This fact strongly suggests that the colored substances formed in the acid clay are the cation radicals of anthracene and tetracene. The results obtained by Hall[8] and by Aalbersberg and others[9] also support this point of view. The slight shift between the band positions in sulfuric acid and with the clay may be due to a small change of electronic state by the interaction of acid clay.

(II) **The Coloration with Polyenes.**—The color reactions with diphenylpolyenes, β-carotene, and anhydro vitamin A were carried out also in the presence of hydrogen. In atmospheric oxygen, the colors developed fade rapidly. The colored substances formed on acid clay in hydrogen are stable enough to observe their absorption spectra. The absorption spectra between 350 and 1000 mμ of the clay suspensions colored with diphenylpolyenes, Ph·(CH=CH)$_n$·Ph, of n = 1–6 are shown by solid curves in Fig. 2. These spectra show from one to three absorption peaks with a shoulder at a shorter wave length. The colored clay suspension with diphenylethylene has a very weak band, but the clay with other diphenylpolyenes has strong absorption bands, and the height of the band at the shorter wave length is relatively more increased with increasing chain length. The plot of the wave length of

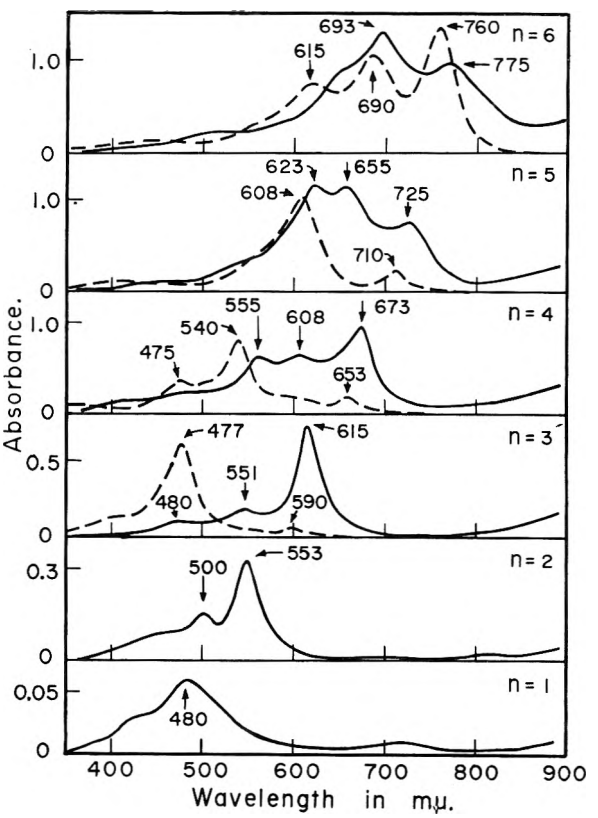

Fig. 2.—Absorption spectra of the colored clay suspensions with diphenylpolyenes, Ph·(CH=CH)$_n$·Ph, and the sulfuric acid solutions of the reagents: ———, colored clay; – – – –, sulfuric acid solution.

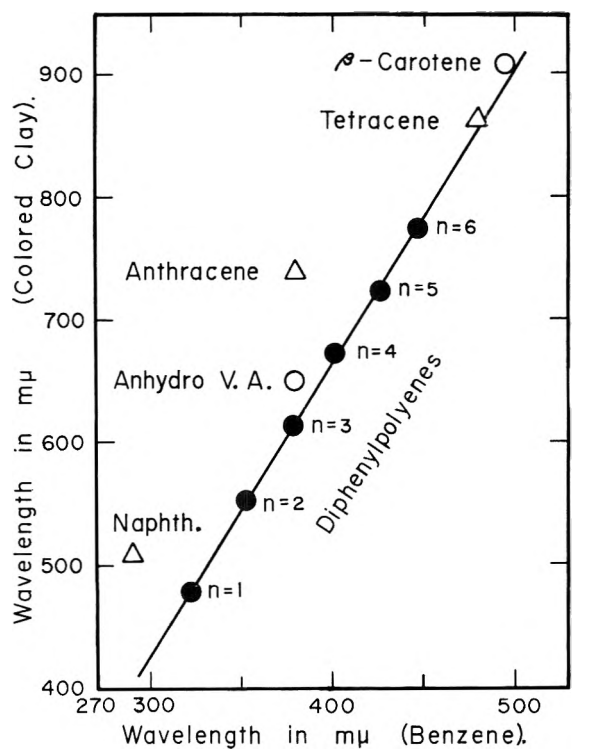

Fig. 3.—The relation between the wave length of the absorption maximum at the longest wave length observed for the colored clay and that observed for the benzene solution.

the absorption maximum at the longest wave length observed with acid clay against that observed without the clay indicated a close linear relationship between these wave lengths (solid circles in Fig. 3).

The clay suspension colored with β-carotene shows two distinct bands at 590 and 910 mμ with a shoulder

between 720 and 780 mμ. The height of the band at 910 mμ is roughly six times that of the band at 590 mμ. A plot of the longer wave length against the wave length of absorption maximum without clay gave a point approximately on the line of the linear relationship found for diphenylpolyenes (open circle in Fig. 3). The clay suspension colored with anhydro vitamin A shows a band at 650 mμ. The point in the similar plot deviates slightly from the line (open circle in Fig. 3). Similar plots were made between the wave lengths with and without the clay for polyacenes. The point for tetracene lies on the line of the linear relationship for diphenylpolyenes, but the points for other polyacenes deviate considerably (open triangles in Fig. 3).

Attempts were made to obtain the spectra of these diphenylpolyenes in sulfuric acid. Diphenylethylene and diphenylbutadiene were practically insoluble in the acid. When diphenylpolyenes were dissolved in sulfuric acid, colored products were formed and then faded. The rate of fading is very slow with diphenyldodecahexaene but becomes progressively more rapid with decreasing chain length. The spectra of the colored solutions were observed immediately after the preparation, and are shown by dashed curves in Fig. 2. The three bands observed for the stable sulfuric acid solution of diphenyldodecahexaene are located at roughly the same positions of the bands of the colored clay suspension, and their relative heights are not widely different from those of the colored clay bands. With decreasing chain length, however, the height, in particular, of the band at the longest wave length decreases markedly. This may result from the successive reaction of fading. In fact, the shoulder on the shorter wave length side of the second rises with the lowering of the weak band at the longest wave length. In this transformation, the second strong band is lowered, but no parallelism exists between the lowerings of the first and the second bands. This implies that complicated reactions of fading occur in these transformations of bands. It may, however, be worth noticing that the positions of the weak bands of these polyenes of $n = 3$–5 are located at a slightly shorter wave length of the corresponding band position of the colored clay with the same diphenylpolyene. It may, therefore, be inferred that the initial product in sulfuric acid is similar in its chemical structure to the colored product on the acid clay, so that the same conclusion of the formation of a cation radical may be drawn from the above results.

Discussion

On the color reaction, the bands of the polyenes and polyacenes without acid clay disappear completely and are shifted markedly. This suggests that the coloration is not due to the enhancement of a weak band of these reagents by the interaction of the acid clay, such as the enhancement of a band of the singlet–triplet transition. This view is supported by the fact that a very concentrated solution of these reagents showed no band in the visible and near-infrared regions. The coloration may, therefore, be described as the shift of the bands in the ultraviolet region toward longer wave lengths. The great shifts of absorption bands on the coloration of acid clay with polyenes and polyacenes are certainly remarkable as compared with the shifts or color changes which are commonly observable when various chemicals or pigments are adsorbed on solid materials. To effect the large shift observed, which was as much as 156–386 mμ, the energy gap between the ground level and the first excited level of the molecule has to be reduced by 26.6–42.8 kcal./mole, which is as much as the energies of chemical bonds. This would result in a marked change of the electronic structure of the reagent molecule adsorbed in acid clay. The colored substances formed on the acid clay were labile and were easily bleached in the presence of oxygen. This implies that the reagent molecule is unstabilized to a great extent. This fact also supports the conclusion described above that the color reaction is due to the formation of a cation radical on the acid clay. The color products formed on the clay are more stable as compared with those formed in sulfuric acid. Probably, the color reaction with the acid clay is a useful tool to observe the absorption spectra of the cation radicals of various organic compounds.

Acknowledgment.—The author wishes to express his hearty thanks to Prof. K. Shibata for his kind guidance and valuable suggestions and to Asahi Glass Corp. for their financial support in carring out this investigation.

SOLVENT EFFECTS ON THE PHOTOCHEMISTRY OF THE IODIDE ION

BY JOSHUA JORTNER, MICHAEL OTTOLENGHI, AND GABRIEL STEIN

Department of Physical Chemistry, Hebrew University, Jerusalem, Israel

Received December 12, 1962

The photochemistry of the I^- ion in D_2O, ethanol, methanol, isopropyl alcohol, and methyl cyanide is investigated and the results compared to those previously obtained in H_2O solutions. It is shown that solvated electrons appear as a detectable intermediate in all these solvents and that the cross section for primary dissociation, Γ, is solvent dependent. The kinetic behavior in the case of D_2O is analogous to that previously proposed for H_2O solutions. The rate constant of the cage scavenging reaction $H + H^+$ in H_2O is found to be equal to that of $D + D^+$ in D_2O.

In a previous series of papers,[1-5] the photochemistry of the I^- ion in aqueous solutions was investigated. The use of specific scavengers enabled the identification of intermediates. The kinetic study of the dependence of the quantum yield of the final products on scavenger concentration indicated the operation of photochemical cage effects. The results may be represented by the general scheme

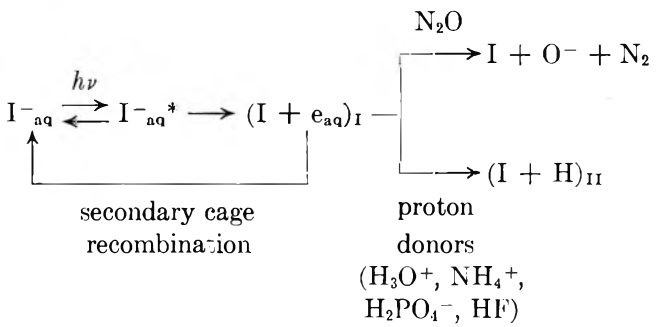

I_{aq}^{*-}, the excited aqueous ion, is formed by excitation of an outer 5p electron of I^- to an s-type expanded orbital[6] in the polarization field of the oriented solvent medium.[6a,b] This excited state may dissociate thermally into an iodine atom and a solvated electron, e_{aq}, both in the same solvent cage—$(I + e_{aq})_I$. Alternatively it may decay back to the ground state. The competition between these processes determines the quantum yield, Γ, for the formation of the pair e_{aq} and I in the photochemical cage. At high scavenger concentrations a constant quantum yield of the final products, independent of scavenger concentration, was observed. This value, $\gamma_{max} = 0.290 \pm 0.05$ at 25° and 2537 Å. for all scavenger systems,[2-5] corresponds to total scavenging of solvated electrons from the cage $(I + e_{aq})_I$ and may thus be identified as the primary dissociation yield of the excited state, Γ.

Specific scavengers, *e.g.*, proton donors,[1,2,5] oxygen,[4] or nitrous oxide,[3] react with the solvated electron competing with cage recombination. The kinetics of the scavenging process could be well represented on the basis of the treatment proposed by Noyes,[7] adapted by us to more complex systems in which parallel and consecutive scavenging occur over a large range of scavenger concentrations.[2]

(1) J. Jortner, R. Levine, M. Ottolenghi, and G. Stein, *J. Phys. Chem.* **65**, 1232 (1961).

(2) J. Jortner, M. Ottolenghi, and G. Stein, *ibid.*, **66**, 2029 (1962).

(3) J. Jortner, M. Ottolenghi, and G. Stein, *ibid.*, **66**, 2037 (1962).

(4) J. Jortner, M. Ottolenghi, and G. Stein, *ibid.*, **66**, 2042 (1962).

(5) J. Jortner, M. Ottolenghi, J. Rabani, and G. Stein, *J. Chem. Phys.*, in press.

(6) (a) R. Platzman and J. Franck, "Farkas Memorial Volume," Jerusalem, 1952, p. 21; (b) G. Stein and A. Treinin, *Trans. Faraday Soc.*, **55**, 1087 (1959).

(7) R. M. Noyes, *J. Am. Chem. Soc.*, **77**, 2042 (1955).

Both the kinetic analysis and the fact that $\gamma_{max} < 1$ indicated that the scavenging process does not involve a direct interaction of the scavenger with the spectroscopic excited state of the ion.

In the present paper we report our experiments in which solvents other than H_2O (*i.e.*, D_2O, alcohols, and CH_3CN) were used, in an attempt to establish whether the mechanisms, previously derived are of general validity, and in particular whether the solvated electron appears as a detectable intermediate in solvents other than H_2O.

Spectroscopic studies[8] indicate that the ultraviolet absorption spectra of I^- in the solvents employed by us involves charge transfer bands. We are therefore dealing with the same type of excited state as that previously described for I^- in H_2O. As to previous photochemical studies, Edgecombe and Norrish[9] have used flash photolysis techniques for an investigation of the intermediates in ultraviolet irradiated solutions of I^-. Their results indicate that the species I_2^- is not restricted to aqueous solutions, thus demonstrating that I atoms are also formed, in a primary photochemical stage, in solvents such as alcohols and methyl cyanide.

Experimental

Irradiations were carried out at 25° and 2537 Å. as described previously.[1,2]

Materials.—D_2O was purified as described previously.[2] Methanol and ethanol, BDH Analar, were dried by refluxing over Mg metal in the presence of I_2 and then redistilled twice. Isopropyl alcohol, BDH laboratory reagent grade, was freed of peroxides by refluxing over $SnCl_2$, redistilled twice, and dried over $CaSO_4$. Methyl cyanide was obtained in spectroscopic grade from Eastman Kodak Co. and used without further purification.

Actinometry.—In all solutions used the optical path was 3 cm. and conditions of total absorption were attained. Therefore, the actinometric data were as described previously[1,2]; the light intensity was $J = 1.5 \times 10^{-6}$ einstein $l.^{-1}$ $sec.^{-1}$.

Gas Analysis.—Nitrogen produced in N_2O containing solutions was determined by a McLeod and a Pirani gage after freezing the N_2O and solvent vapor in a liquid air trap.

Results

Solutions in D_2O.—It was found that the molar extinction coefficient of I_3^- in D_2O was equal to that measured under the same conditions in H_2O,[1] so that the same calibration could be used for the determination of the I_2 liberated. Evacuated solutions of 0.15 *M* KI were irradiated and the D^+ concentration was adjusted by adding concentrated H_2SO_4 diluted with D_2O. $[D^+]$ was calculated from the amount of H_2SO_4 added, using[10] $K_{DSO_4^-} = 8 \times 10^{-3}$ (while the corre-

(8) (a) I. Burak and A. Treinin, to be published; (b) M. Smith and M. C. R. Symons, *Discussions Faraday Soc.*, **24**, 206 (1957).

(9) F. H. C. Edgecombe and R. G. W. Norrish, *Proc. Roy. Soc.* (London), **A253**, 154 (1959).

(10) E. C. Noonan and V. K. La Mer, *J. Phys. Chem.*, **43**, 247 (1939).

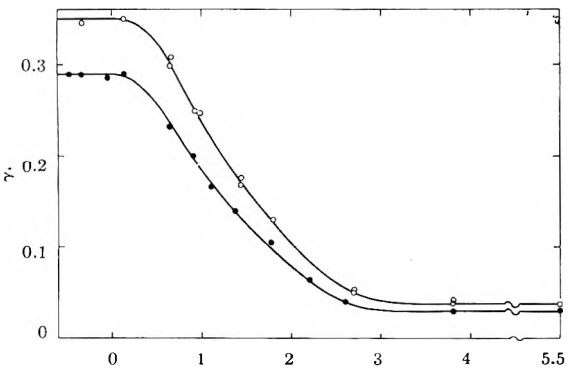

Fig. 1.—Solutions of I^- (0.15 M) in D_2O, O. Dependence of $\gamma(I_2)$ on pD (= −log [D^+]). For comparison results[1] in H_2O are shown, ●.

sponding value for H_2O is $K_{HSO_4^-} = 2 \times 10^{-2}$). $\gamma(I_2)$, the quantum yield for iodine formation, was determined in the range $10^{-6}\ M < [D^+] < 2\ M$. The values derived from the initial slopes of $[I_2]$ *vs.* the irradiation time, t, are shown in Fig. 1 and compared with those obtained in H_2O solutions.[1]

As in the case of H_2O solutions[1,2] the pH dependence of $\gamma(I_2)$ in this pH region should be attributed to the competition

$$(I + D)_{II} \longrightarrow I^- + D^+ \text{ (cage recombination)} \quad (1)$$

$$(I + D)_{II} + D^+ \longrightarrow \text{radicals in bulk of soln.}$$
$$\text{(cage scavenging[11])} \quad (2)$$

The value of $\Gamma = \gamma_{max}(I_2)$, the maximum quantum yield reached when total scavenging occurs from both cages $(I + e_{aq})_I$ and $(I + D)_{II}$, is 0.35 in D_2O compared with 0.29 in H_2O. The value $\Gamma = 0.35$ in D_2O obtained from $\gamma_{max}(I_2)$ in acid solutions (pD < 0.9) agrees with that obtained previously[2] in D_2O for $\gamma_{max}(HD)$ when methanol or isopropyl alcohol, instead of D^+, was used as the D atom scavenger at pD 2.9.

When dealing with acid H_2O solutions at pH < 2.5 it was shown[1,2] that at the initial stages of the reaction, when very small amounts of I_2 are present, each H atom scavenged by H^+ is converted ultimately into H_2^+ which is capable of oxidizing another I^- ion according to

$$I^- + H_2^+ \longrightarrow I + H_2 \quad (3)$$

followed by

$$I + I \longrightarrow I_2 \quad (4)$$

However, when $[I_2]$ becomes considerable, the back reactions: $I_2 + H_2^+ \rightarrow I_2^- + 2H^+$ and $I_2 + H \rightarrow I_2^- + H^+$ should also be taken into account. These reactions cause a lowering of $\gamma(I_2)$ and $\gamma(H_2)$ and are therefore responsible for the deviations of the plots of $[I_2]$ *vs.* t from linearity. In such a case it was shown that the dependence of $[I_2]$ (or $[H_2]$) on t is given by[1]

$$\frac{t}{[I_2]} = \frac{1}{\gamma_i J} + \frac{k_r[I_2]}{k_{ox} 2J\gamma_i[I^-]} \quad (5)$$

where t is the duration of irradiation, $[I_2]$ and $[I^-]$ the concentrations of iodine and iodide ion at time t, γ_i is the initial quantum yield of I_2, k_r and k_{ox} are complex rate constants depending on $[H^+]$. To investigate whether the mechanism derived in the case of H_2O solutions holds for D_2O as a solvent, $t/[I_2]$ is plotted as a function of $[I_2]$. Straight lines are obtained (Fig. 2) in agreement with equation 5. Thus in accordance with the considerations previously given,[1,2] the mechanism including competition in the bulk between I_2 and I^- for H_2^+ is pertinent. The values of $A = k_r/k_{ox} = 2 \times [I^-] \times$ slope/intercept are given in Table I together with the corresponding values in H_2O,[1] showing that there is no significant change in the value of this ratio while passing from H_2O to D_2O. From the intercepts of Fig. 2 the initial $\gamma(I_2)$ values could be obtained. These are compared in Table II with the experimental values of Fig. 1.

The pD dependence of the initial quantum yields should be interpreted in terms of a consecutive scavenging by the D^+ ion[1,2]

$$(I + e_{aq})_I \xrightarrow{D^+} (I + D)_{II} \xrightarrow{D^+} \text{radicals in bulk}$$

Remembering that in the region pD < 2 the scavenging of e_{aq} from $(I + e_{aq})_I$ is complete,[2] the dependence of $\gamma(I_2)$ on $[D^+]$ will be given by Noyes' scavenging equation[7]

$$\gamma = \gamma_r + 2a_{II}\Gamma_{II}\sqrt{\pi k_{D+D}[D^+]} \quad (6)$$

which is valid at small $[D^+]$ values. γ_r is the "residual yield" of radicals escaping cage recombination in the absence of external scavengers, Γ_{II} is the cross section for formation of the cage $(I + D)_{II}$ and a_{II} a constant related to microscopic parameters[12] of the radicals in the cage $(I + D)_{II}$. The theoretical significance of γ_r, Γ_{II}, and a_{II} in such a consecutive scavenging system was previously discussed.[2] Figure 3 shows the extrapolated values of $\gamma(I_2)$ as a function of $\sqrt{(D^+)}$. A straight line is obtained, confirming the operation of the mechanism involving scavenging from the photochemical cage.[1,2] The intercept in Fig. 3 gives $\gamma_r = 0.13$ in D_2O compared[1] with $\gamma_r = 0.09$ for H_2O. From the slope of Fig. 3, $\Gamma_{II}2a_{II}\sqrt{\pi k_{D+D^+}} = 0.4$ l.$^{1/2}$ mole$^{-1/2}$. Setting[2] $\Gamma_{II} = \Gamma = 0.35$, $2a_{II}\sqrt{\pi k_{D+D^+}} = 1.14$ l.$^{1/2}$ mole$^{-1/2}$. Setting $\Gamma_{II} = \Gamma - \gamma_r = 0.22$ this parameter will be 1.8 l.$^{1/2}$ mole$^{-1/2}$. These results are compared in Table III with the corresponding ones in H_2O solutions.[1] Thus the main difference between solutions of I^- in H_2O and D_2O lies in the value of Γ. The subsequent steps in the mechanism are equal in both cases, and support the kinetic analysis given for H_2O.[12]

TABLE I

THE DEPENDENCE OF THE RATIO k_r/k_{ox} ON pD AND pH IN D_2O AND H_2O SOLUTIONS, RESPECTIVELY

D_2O Soln.		H_2O Soln.[1]	
pD	$\frac{k_r}{k_{ox}} \times 10^{-4}$	pH	$\frac{k_r}{k_{ox}} \times 10^{-4}$
0.65	0.65	0.65	0.58
0.95	1.2	0.90	0.71
1.44	3.2	1.10	1.46
1.82	5.9	1.36	2.25
...	...	1.78	5.20

An examination of Table III shows that no significant difference exists between the ratio $\gamma_r^{extrapol}/\Gamma$ in the two solvents (0.37 in D_2O compared to 0.32 in H_2O).

(11) The exact nature of this process, involving either a direct formation of D_2^+ or a charge transfer from D to D^+, was previously discussed.[2]

(12) R. M. Noyes. *J. Am. Chem. Soc.*, **78**, 5486 (1956).

TABLE II

INITIAL QUANTUM YIELDS IN THE PHOTOCHEMISTRY OF I^- ($[I^-] = 0.15\ M$) IN D_2O

	$\gamma_i(I_2)$	
pD	Exptl. value	From intercepts of Fig. 2
0.65	0.300	0.314
0.95	.244	.278
1.44	.175	.220
1.82	.130	.190

This implies that the cage parameter β_{II}', related to γ_r and Γ_{II} by the equation[1] $\gamma_r = \Gamma_{II}(1 - \beta_{II}')$, has not changed markedly. Theoretical equations relating a and β' with microscopic parameters of diffusion have been developed by R. M. Noyes.[12] According to this study β' is related to ρ, the encounter diameter of the caged radicals, and to σ, the root mean square displacement distance for relative diffusive motion of the radicals. As the values of ρ in D_2O cannot differ from those in H_2O, σ should also be equal in the two solvents. The parameter a is related[12] to ρ, σ, and D, the diffusion coefficient of relative motion of the radicals. However only $\sqrt{D}$ appears in the expression for a so that, after taking into consideration the relatively small effect of the change in viscosity of D_2O compared to H_2O, we may conclude that a_{II} is also similar in the two solvents. These considerations imply (see Table III for the values of $2a_{II}\sqrt{\pi k}$) that the rate constant ratio $(k_{H^++H})_{H_2O}/(k_{D^++D})_{D_2O}$ is near to unity.

TABLE III

COMPARISON OF PHOTOCHEMICAL SCAVENGING DATA AND CAGE PARAMETERS FOR I^- IN H_2O[1,2] AND D_2O AT 2537 Å. AND 25°

(See ref. 1 for the back bulk reactions explaining the difference between the experimental value and the extrapolated value of γ_r)

Parameter	H_2O	D_2O
Γ	0.29	0.35
γ_r (experimental value)	0.030	0.045
γ_r (from extrapolation of eq. 6)	0.092	0.130
$2a_{II}\sqrt{\pi k_{H^++H}}$ and $2a_{II}\sqrt{\pi k_{D^++D}}$	1.57	1.8

The reaction $H + H_{aq}^+$ could involve the formation of H_2^+. If so, the absence of an isotope effect shows that H_2^+ is not formed by a proton transfer from H_3O^+ to an H atom, a process which would involve an O–H bond rupture. The results could also be consistent with charge transfer from H to H_{aq}^+. Some charge transfer processes indeed show an isotope effect, due to different interatomic distances within the primary hydration layer in the activated complex prior to the electron transfer, but others do not and the existence of such an effect depends markedly on the nature of the transition state.[13] The charge transfer mechanism is however excluded by the results in γ-irradiated solutions where no isotope exchange reaction of H atoms occurs in acid D_2O solutions[14] (see also ref. 2). A possible mechanism, consistent with both the absence of an isotope effect in the scavenging reaction now described and lack of isotope exchange of H atoms in γ-irradiated

(13) R. A. Marcus, *J. Chem. Phys.*, **26**, 867 (1957).

(14) (a) T. W. Davis, S. Gordon, and E. J. Hart, *J. Am. Chem. Soc.*, **80**, 4487 (1958); (b) H. L. Friedman and A. H. Zeltman, *J. Chem. Phys.*, **28**, 878 (1958); (c) K. C. Kurien and M. Burton, Summary of Proceedings of the 4th Informal Conference on the Radiation Chemistry of Water, University of Notre Dame, Indiana, March 23–25, 1961.

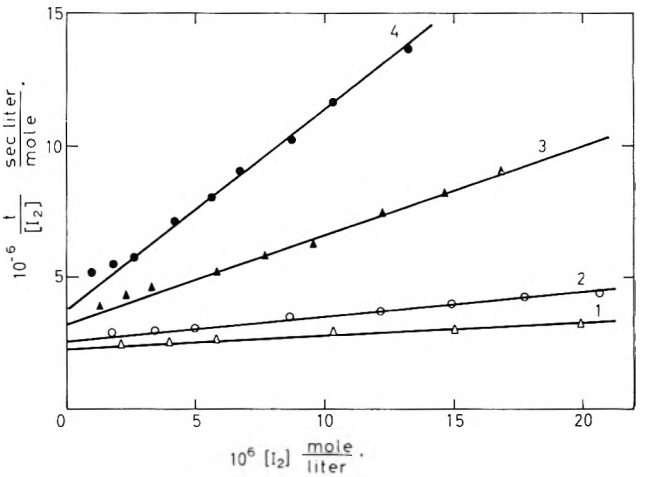

Fig. 2.—Determination of initial quantum yields in D_2O solutions of I^- by method of extrapolation: (1) pD = 0.65; (2) pD = 0.95, (3) pD = 1.44; (4) pD = 1.82.

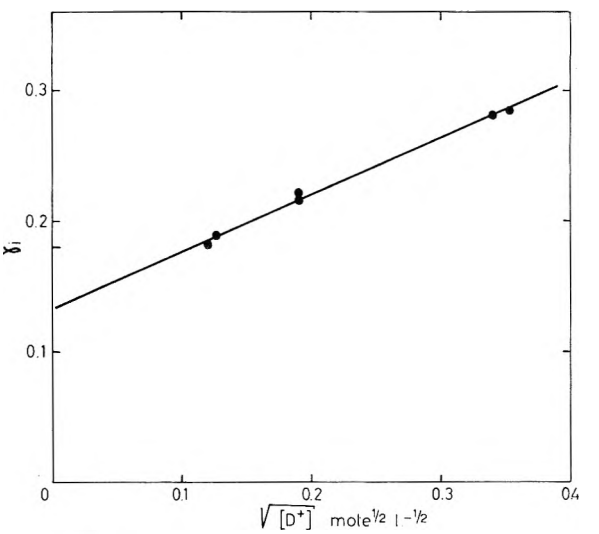

Fig. 3.—Initial quantum yield in D_2O solutions of I^- as a function of $\sqrt{[D^+]}$.

D_2O, may involve the formation of an H_2^+ complex in which H atoms are not equivalent, *e.g.*, $\{H\text{–}H\text{–}O<\begin{matrix}H\\H\end{matrix}\}^+$ The velocity constant[1,2] of the reaction $H + H_{aq}^+$ is $< 10^5$ liter mole^{-1} sec.$^{-1}$; it does not therefore belong to that category of very fast diffusion controlled reactions which do not show isotope effects for this reason.

Primary Dissociation Yields in Some Non-aqueous Solvents.—The photochemistry of the I^- ion in methanol, ethanol, isopropyl alcohol, and methyl cyanide was investigated. N_2O was used as a radical scavenger.[3] Its solubility in methanol and ethanol is known[15] to be some 5 times greater than in H_2O. The I^- concentration was 0.15 M in methanol and 0.045 M in ethanol. In the case of isopropyl alcohol and methyl cyanide saturated solutions were used and $[I^-]$ was determined spectroscopically from measurements of the absorption of these solutions at wave lengths corresponding to $\epsilon = 5.5$. For I^- in methyl cyanide where $\epsilon = 5.5$ at 280 mμ,[8a] we found $[I^-] \cong 0.2\ M$. For $[I^-]$ in isopropyl alcohol only $h\nu_{max} \cong 130.5$ kcal. is known.[8b] However, for all solvents[8a] $h\nu_{max} - h\nu_{\epsilon=5.5} \cong 18$ kcal., so that for I^- in isopropyl alcohol $h\nu_{\epsilon=5.5} \cong 111.5$ kcal, and the value $[I^-] \cong 0.35\ M$ was found in this

(15) A. Siedell, "Solubility of Inorganic and Organic Compounds," D. Van Nostrand Co., Suppl. to 3rd Edition, 1952.

solvent. Measurements showed that at 2537 Å. total absorption could be assumed for all those solutions at 3 cm. path length. Table IV shows $\gamma(N_2)$, the quantum yield of N_2, at two N_2O pressures. The identity of the two sets of results shows that the quantum yield is independent of N_2O concentrations, hence $\gamma(N_2) = \Gamma$. Control tests were carried out for the evolution of H_2 in the absence of dissolved N_2O in the above solvents. No detectable amount of H_2 was found.

TABLE IV

NITROGEN QUANTUM YIELDS IN THE PHOTOCHEMISTRY OF I^- IN ORGANIC SOLVENTS

Solution	$\gamma(N_2)$ P_{N_2O} = 500 mm.	$\gamma(N_2)$ P_{N_2O} = 280 mm.
0.15 *M* KI in methanol	0.60 ± 0.02	0.59 ± 0.02
0.045 *M* KI in ethanol	.66 ± .02	.65 ± .02
~0.2 *M* KI in isopropyl alcohol	.70 ± .02	.71 ± .02
~0.3 *M* KI in methyl cyanide	.75 ± .02	.75 ± .02

Discussion

The question arises whether the species reacting with N_2O in the various non-aqueous solvents may be unambiguously identified as the solvated electron, as in the cases of H_2O and D_2O. An alternative process may be[3] $H + N_2O \rightarrow N_2 + OH$, with H atoms which may be formed (in methanol and ethanol) *via* a dissociative electron capture by the solvent. This possibility is ruled out by the observation that no hydrogen gas is evolved when irradiating alcoholic solutions of I^- in the absence of N_2O. Hence H atoms are not formed in these solutions, where the solvent itself may act as an efficient scavenger for H atoms,[2,16] *via* dehydrogenation, leading to the evolution of H_2. In all cases the value $\gamma_{max} = \Gamma < 1$ indicates that N_2O does not interact directly with the spectroscopic excited state.

We may thus conclude that solvated electrons appear as reactive intermediates in the photochemistry of the iodide ion in all the solvents investigated in the present work, according to the scheme

$$I^-_{sol} \overset{h\nu}{\rightleftarrows} I^{-*}_{sol} \longrightarrow (I + e_{sol}) \xrightarrow{N_2O} I + O^- + N_2 \quad (7)$$

The existence of solvated electrons, which have sufficiently long life time to react with chemical scavengers, in solutions of methanol and ethanol was recently confirmed by a radiation chemical study.[17]

The independence of the quantum yields, $\gamma(N_2)$, in Table IV, of $[N_2O]$ indicate that total electron scavenging by N_2O occurs in this concentration range. This supports the previous assumption that all solvents employed by us react relatively slowly with solvated electrons, thus $k_{e+N_2O}[N_2O] >> k_{e+solv}[solv.]$. As $[N_2O] = 10^{-2}\,M$ and $[solv.] \cong 20\,M$, we get $k_{e+N_2O}/k_{e+solv} >> 2 \times 10^3$.

Another conclusion which may be derived from these data is that the O^- ion (or the OH radical) produced according to eq. 7 reacts with the solvent (in the case of the alcohols probably by H atom abstraction) and does not contribute to the yield of gaseous products. A reaction between N_2O and the organic radicals formed by the reaction of OH or O^- with the solvent (CH_2OH and CH_3CHOH for methanol and ethanol, respectively) should be ruled out as it would lead to a chain reaction and consequently to too high N_2 yields. We confirmed this conclusion by measuring the N_2 yields in aqueous solutions saturated with N_2O and irradiated with 200 kv. X-rays. We found that the addition of 1 *M* ethanol did not change the value of G_{N_2} (the yield of N_2). In these solutions the same organic radicals as those appearing in our photochemical systems are produced by dehydrogenation of the alcohol by OH radicals. We may therefore rule out any reaction between the organic radicals and N_2O which can ultimately lead to the formation of N_2 or any other gaseous product.

The similar photochemical behavior of all these systems is consistent with the interpretation of their absorption spectra as due in all these solvents to electron transfer. In all cases a fraction Γ of these excited states is thermally converted to solvated electrons, capable of decomposing N_2O with the formation of N_2. The scavenging process by N_2O may thus serve as a photochemical criterion for the identification of charge transfer bands of anions in solution. The value of Γ is a result of the competition between deactivation of the spectroscopic excited state and its decomposition into the solvated electron in the photochemical cage. Changing the solvent changes the rates of both processes. The results reported so far do not enable us to decide their relative changes, as they probably depend simultaneously on a number of factors. To determine the nature of the two competing processes, which determine the value of Γ, it is desirable to study the effects of specific parameters, *e.g.*, temperature, wave length, and nature of dissolved ion. We hope to publish our results in this respect separately.

(16) J. T. Allan and G. Scholes, *Nature*, **187**, 218 (1960).

(17) J. H. Baxendale and F. W. Mellows, *J. Am. Chem. Soc.*, **83**, 4720 (1961).

THE EFFECT OF $LiClO_4$, LiCl, AND LiBr ON THE POLAROGRAPHIC BEHAVIOR AND ULTRAVIOLET SPECTRUM OF PRASEODYMIUM(III) IN ETHANOL

BY SHELDON H. COHEN, REYNOLD T. IWAMOTO, AND JACOB KLEINBERG

Department of Chemistry, University of Kansas, Lawrence, Kansas

Received December 15, 1962

Polarographic and spectrophotometric studies of perchlorate-, bromide-, and chloride-containing ethanolic praseodymium(III) solutions, both in the absence and presence of added water, give strong evidence that these anions and the tripositive lanthanide form ion-associates. These ion-associates are more readily reduced than the tripositive praseodymium ion solvated by ethanol or ethanol–water combinations.

Introduction

Reduction of tripositive praseodymium in aqueous solution at the dropping mercury electrode has been studied extensively. However, the experimental results reported by various workers have not been in agreement, and, indeed, the interpretation of the same results has varied among different workers.

A number of investigators[1-3] have obtained a two-step wave for the reduction of aqueous praseodymium(III) solutions. Noddack and Brukl ascribed the two-step wave they observed for the reduction of 0.01 *F* aqueous praseodymium(III) sulfate in the absence of supporting electrolyte to the stepwise reduction of Pr(III) to Pr(II) and of Pr(II) to the metal. This interpretation is doubtful because no definitive evidence for the existence of dipositive praseodymium in aqueous solution has ever been obtained. Kolthoff and Lingane[4] attribute the first step to the reduction of hydrogen ion and the second to the reduction of the tripositive ion to the metal. This explanation does not account for a third step, with a half-wave potential considerably less negative than either potential reported by Noddack and Brukl, found in the polarograms for acidified praseodymium(III) sulfate solutions.[2] A number of other investigators have reported only a single step, that for the reduction of tripositive praseodymium to the metal.[5-7] Recently, Misumi and Masuda[8] obtained a one-step wave for the reduction of both praseodymium(III) sulfate and perchlorate in aqueous 0.1 *F* lithium perchlorate, and a two-step wave in 0.1 *F* tetramethylammonium iodide medium. These investigators postulated from their data that the praseodymium(III) cation can form complexes in certain media and that through a bridge-type mechanism these complexes are more easily reduced than the aquo ion.

Current interest in how the nature and make-up of the solvation sphere of metal ions affect the behavior of these ions in solution has prompted a further study of the polarographic behavior of praseodymium(III) in halide medium. However, because tripositive praseodymium is strongly solvated by water, the formation of other complexes in this solvent is difficult. Our studies, therefore, were undertaken in ethanol, a much less strongly solvating medium than water. Attempts have been made to correlate the polarographic data obtained with spectrophotometric information on corresponding solutions.

(1) W. Noddack and A. Brukl, *Angew. Chem.*, **50**, 362 (1937).
(2) A. Purushottam and B. S. V. Raghava Rao, *Anal. Chim. Acta*, **12**, 89 (1955).
(3) V. A. Zarinskii, *Zh. Fiz. Khim.*, **24**, 662 (1950).
(4) I. M. Kolthoff and J. J. Lingane, "Polarography," 2nd Ed., Interscience Publishers, Inc., New York, N. Y., 1952, p. 436.
(5) A. W. Swensen and G. Glockler, *J. Am. Chem. Soc.*, **71**, 1641 (1949).
(6) S. Misumi and A. Iwase, *Nippon Kagaku Zasshi*, **76**, 231 (1955); *C. A.*, **51**, 12706 (1957).
(7) A. Iwase, *ibid.*, **80**, 1133 (1959); *C. A.*, **55**, 6208 (1961).
(8) S. Misumi and Y. Masuda, *Mem. Fac. Sci. Kyushu Univ., Ser. C*, **3**, 171 (1960).

Experimental

Reagents.—The following procedure was used for the preparation of praseodymium(III) perchlorate hydrate. An amount of praseodymium oxide (Pr_6O_{11}) in excess of the stoichiometric quantity was treated with 6 *F* perchloric acid. On gentle heating the acid reacted rapidly with the oxide to give a solution of pH 5. Unreacted oxide was removed by filtration, and the clear green filtrate was evaporated at 140° to a dark green sirup. Cooling of the sirup yielded green crystals which were removed by filtration. The crystals were powdered and dried to constant weight at 80° under a pressure of 5 cm. The praseodymium content of the salt was determined by oxalate precipitation and ignition of the oxalate to Pr_6O_{11}. From the praseodymium analysis, the formula $Pr(ClO_4)_3 \cdot 4.5H_2O$ was obtained for the salt.

Both praseodymium chloride and bromide were prepared by treatment of Pr_6O_{11} with an excess of concentrated hydrohalic acid. After removal of unreacted acid by heating, the solution was treated as described above for the preparation of the perchlorate. Praseodymium was determined by the method cited previously and halide gravimetrically as the silver salt. The formulas obtained for the salts were $PrCl_3 \cdot H_2O$ and $PrBr_3 \cdot 3H_2O$.

Anhydrous ethanol was obtained by treatment of absolute ethanol with magnesium metal activated by iodine, followed by fractional distillation. The water content, determined by the Karl Fischer method, varied for different batches of the alcohol from 0.9×10^{-2} to 1.4×10^{-2} *M*.

All other chemicals employed were of reagent grade.

Procedure.—The polarographic data were obtained with a Sargent Model XV recording polarograph. An H-type cell with the two compartments separated by a sintered glass disk was used. A saturated calomel electrode, which served both as auxiliary and reference electrode, was placed in one compartment of the cell and the d.m.e. in the other. All solutions were adjusted to a temperature of 25.0 ± 0.1°. The solutions were deaerated with purified nitrogen and protected from atmospheric oxygen during the course of measurement by passage of nitrogen over the top. Half-wave potentials were corrected for *iR* drop across the cell. Resistance measurements for this correction were made with a Model RC-1B Industrial Instruments Inc. conductivity bridge.

The background scans obtained for solutions containing lithium chloride, bromide, or perchlorate in the potential region of interest were similar, and background currents were sufficiently small that they could be ignored.

All ultraviolet spectra were taken with a Cary Model 14 recording spectrophotometer, at a scan rate of 5 Å. per sec. Reproducibility of absorbancy and wave length values were 0.02 unit and 5 Å., respectively. Reference and test solutions contained the same concentration of lithium halide for studies involving the effect of chloride or bromide ion on the spectrum of praseodymium(III) in ethanol.

Results

Polarographic Studies.—The interaction of perchlorate, of chloride, and of bromide anions with tripositive praseodymium in ethanol was investigated polarographically. Extremely drawnout waves for the reduction of the metal ion in perchlorate, chloride, and

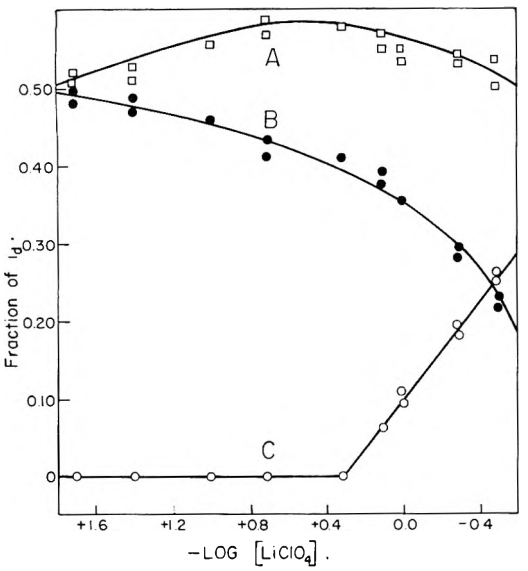

Fig. 1.—Distribution of the diffusion currents for the reduction of praseodymium(III) in ethanol as a function of the logarithm of lithium perchlorate concentration. (All solutions are 10^{-3} F in $Pr(ClO_4)_3$.) A, first step; $E_{1/2}$ between -1.55 and -1.61 volts; B, second step; $E_{1/2} < -1.70$ volts; C, third step, $E_{1/2} \sim -1.45$ volts.

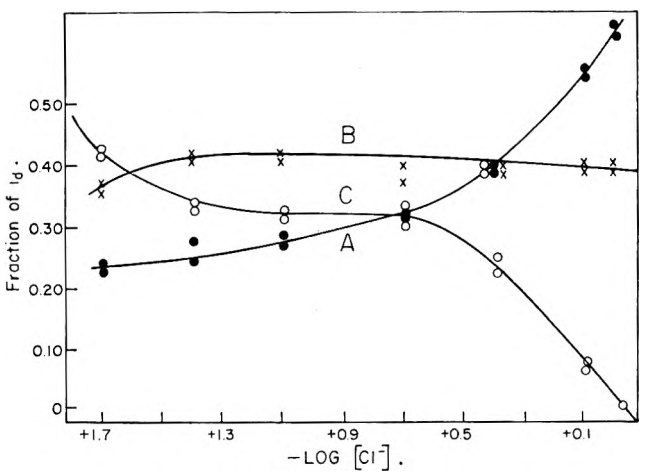

Fig. 2.—Distribution of the diffusion currents for the reduction of praseodymium(III) in ethanol as a function of the logarithm of lithium chloride concentration. (All solutions are 2×10^{-3} F in $Pr(ClO_4)_3$.) A, first step; $E_{1/2}$ between -1.60 and 1.73 volts; B, second step; $E_{1/2}$ between -1.78 and -1.83 volts, C, third step; $E_{1/2}$ between -1.86 and -1.91 volts.

bromide media were obtained, and indicate that the electrode processes in these media are irreversible. Whereas Misumi and Masuda[8] observed only a single wave for the reduction of praseodymium(III) in aqueous perchlorate medium, either two or three steps, depending upon the ratio of metal ion to perchlorate, were found by us for the reduction carried out in ethanolic solutions which were 10^{-3} F in praseodymium(III) perchlorate and contained varying amounts of lithium perchlorate. At low perchlorate concentrations, two steps, with half-wave potentials in the range -1.55 to -1.61 v. for the first step and more negative than -1.70 v. for the second step, were observed. (All potentials reported are *vs.* s.c.e.) A third step with a half-wave potential in the neighborhood of -1.45 v. was found at high perchlorate concentrations. Distribution of the diffusion currents for the various steps as a function of the logarithm of the lithium perchlorate concentration is shown in Fig. 1. Since the various steps tended to merge, an error as great as 10% is possible in the evaluation of the separate diffusion currents. Because of this large uncertainty, the data summarized in Fig. 1 are only of semiquantitative significance.

The polarographic data for the reduction of 2×10^{-3} F praseodymium(III) perchlorate in ethanol containing varying amounts of lithium chloride showed three steps in all, except in the most concentrated (1 F) chloride solutions. The half-wave potentials for these steps were in the respective ranges -1.60 to -1.73, -1.78 to -1.83, and -1.86 to -1.91 v. Only the first two steps were found in the polarograms of solutions 1 F in lithium chloride. Distribution of the diffusion currents for the separate steps as a function of the logarithm of the lithium chloride concentration is given in Fig. 2.

Polarograms for the reduction of 10^{-3} F praseodymium(III) perchlorate in ethanol in the presence of lithium bromide showed from one to four steps over the concentration range 4×10^{-2} to 1 F for the latter salt. The number of steps was the greatest in the intermediate concentration range of 10^{-1} to 2×10^{-1} F. The half-wave potentials for the four steps observed were: -1.55; -1.65; -1.75; and -1.80 v. Because of the large overlap of the steps, no attempt was made to evaluate the distribution of the total diffusion current among the separate steps.[9]

The effect of water on the reduction of praseodymium(III) in the various ethanolic solutions was investigated. Some typical polarograms for ethanol solutions 10^{-3} F in praseodymium(III) perchlorate, 2×10^{-1} F in lithium bromide, and containing varying amounts of added water are shown in Fig. 3. There is little difference between the curve containing no added water (curve A) and that with 4.5×10^{-3} F added water (curve B); both polarograms show four reduction steps. The probable reason for this is that lithium ion, which is present in relatively high concentration, ties up the small amount of added water. As the concentration of water is increased (curve C), the heights of the first two steps decrease and finally, with still greater concentrations of water (curve D), the steps disappear. Curve D is similar to that obtained by Swensen and Glockler[5] for the reduction of aqueous praseodymium(III) sulfate.

Spectrophotometric Studies.—The ultraviolet absorption spectrum of praseodymium(III) perchlorate in ethanol showed the beginnings of a broad band starting at 260 mμ and extending beyond 220 mμ, the cut-off point of measurement. Because of this spectral characteristic, no further spectrophotometric studies were carried out in perchlorate medium.

The effect of added bromide on the ultraviolet absorption spectrum of praseodymium(III) bromide in ethanol is shown in Fig. 4. There are two features worthy of special mention. The first feature is that in solutions of low bromide concentration (< about 10^{-2} F) a sharp band with λ_{max} at 232 mμ and a shoulder at *ca.* 225 mμ are obtained. As the concentration of bromide is increased beyond 10^{-2} F, the band at 232 mμ shifts in the direction of the shoulder and eventually merges with the shoulder into a single band at 225 mμ (curves 3, 4, 5, and 6). The second noteworthy feature

(9) For detailed polarographic data for the praseodymium(III)–bromide system the reader is referred to S. H. Cohen, Ph.D. Thesis, University of Kansas, 1962.

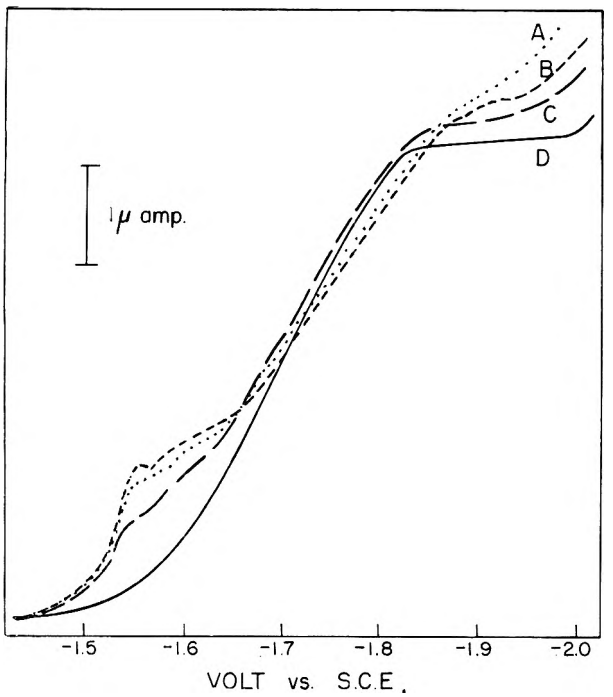

Fig. 3.—Effect of water on reduction of 1×10^{-3} *F* praseodymium(III) perchlorate in 2×10^{-1} *F* ethanolic lithium bromide. Added H_2O concentration: A, 0; B, 4.5×10^{-3} *F*; C, 4.5×10^{-2} *F*; D, 2.66 *F*.

is the appearance of a second band with λ_{max} at 255 mμ in solutions with added bromide ion concentration of 4×10^{-1} *F* and greater (curves 4, 5, and 6). The intensity of this band increases with increasing bromide concentration.

The ultraviolet spectrum of praseodymium(III) chloride contains only a single band at 227 mμ. This band is not affected significantly by added chloride ion (from LiCl).

The effect of water on the ultraviolet spectrum of praseodymium(III) bromide in ethanol was investigated and the results are shown in Fig. 5. Small amounts of added water (up to 1.8×10^{-2} *F*) do not affect the shape of the curve. With added water concentrations between 9×10^{-2} *F* and 4.4×10^{-1} *F* the band originally at 232 mμ shifts toward the violet (curves 3, 4, and 5). At a high added water concentration (2.2 *F*) the single band disappears leaving the foot of a band extending beyond 220 mμ, the cut-off point of measurement.

Discussion

Our polarographic and spectrophotometric studies of perchlorate-, bromide-, and chloride-containing ethanolic praseodymium(III) solutions, both in the absence and presence of added water, strongly indicate the formation of ion-associates which are more readily reduced than the tripositive praseodymium ion solvated by ethanol or ethanol–water combinations. The following observations are pertinent.

(1) Changes in distribution of the diffusion currents of the various reduction steps in the bromide-containing ethanolic solutions closely parallel the changes in absorbancy of the several bands observed in the ultraviolet region for the same system. The single band in the ultraviolet found in the praseodymium(III)–chloride system in ethanol, which showed little dependence on chloride concentration, appears to correspond to curve B in Fig. 2, arising from a reduction step

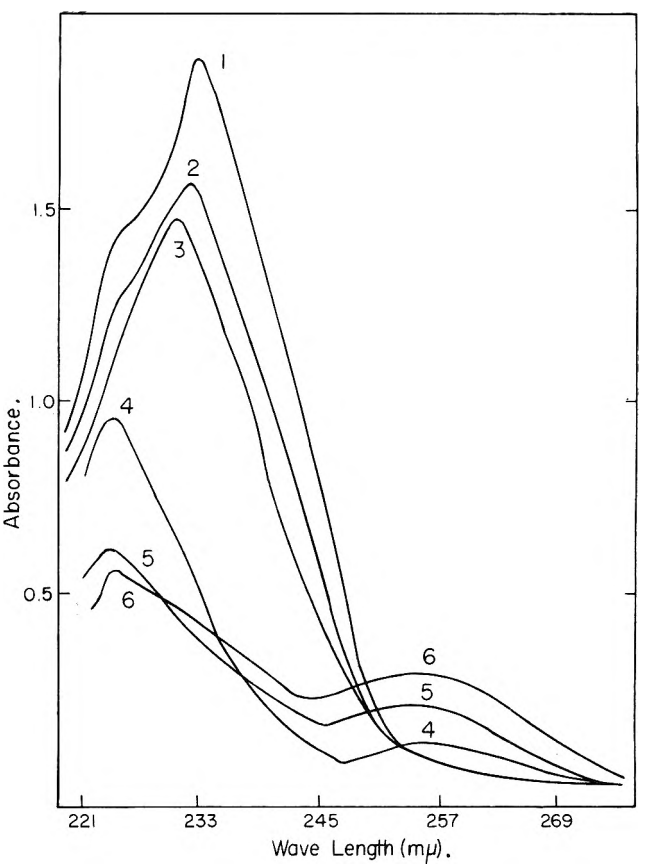

Fig. 4.—Effect of bromide ion on the ultraviolet spectrum of praseodymium(III) bromide in ethanol. (Concentration of $PrBr_3$: 1×10^{-3} *F*.) LiBr concentration: 1, 7×10^{-3} *F*; 2, 2.3×10^{-2} *F*; 3, 4.3×10^{-2} *F*; 4, 4×10^{-1} *F*; 5, 8×10^{-1} *F*; 6, 1.5 *F*.

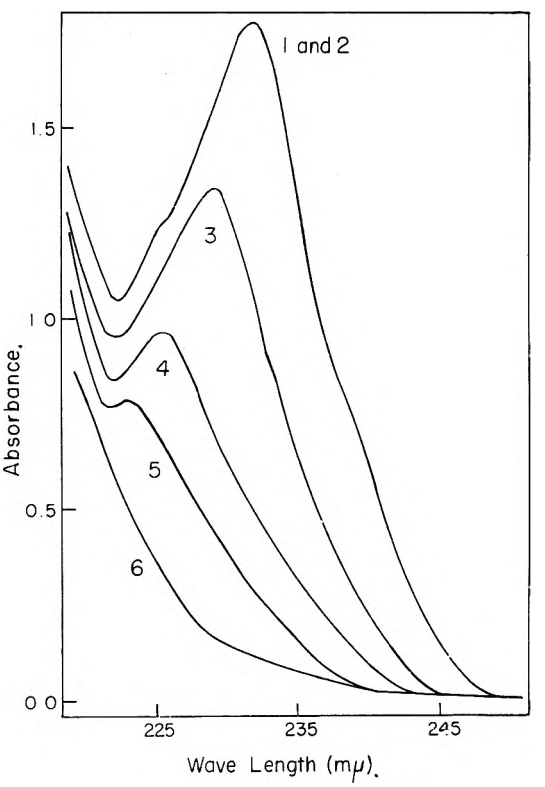

Fig. 5.—Effect of water on the ultraviolet spectrum of praseodymium(III) bromide in ethanol containing lithium bromide. Concentration of $PrBr_3$: 1×10^{-3} *F*; concentration of LiBr: 8×10^{-3} *F*; added H_2O concentration: 1, 0; 2, 1.8×10^{-2} *F*; 3, 9×10^{-2} *F*; 4, 2.7×10^{-1} *F*; 5, 4.4×10^{-1} *F*; 6, 2.2 *F*.

which also is relatively unaffected by changes in chloride ion concentration. Although no ultraviolet spectrophotometric study could be carried out for the praseodymium(III)–perchlorate system, the polarographic data are similar to those obtained for the chloride system.

(2) The fact that the polarographic reduction of praseodymium(III) in the presence of halide ion occurs through multiple steps both in ethanol and in water[2,3,8] strongly indicates that such behavior must be attributed to a common complexing role of halide ion in both solvents rather than to praseodymium(III)–solvent interactions.

(3) The close agreement of the polarographic results and the spectrophotometric results cited above rules out the possibility that reduction of hydrogen ion accounts for one of the polarographic steps in ethanolic solutions.

(4) The behavior of praseodymium(III) in halide media at the dropping mercury electrode is similar to that of indium(III) and nickel(II) in aqueous halide and thiocyanate media,[10-16] where there is strong evidence that halo and thiocyanato complexes, more readily reduced than the aquated ions, are formed.

The interesting observation that praseodymium(III) and perchlorate form ion-associates in ethanol is not completely surprising in view of the recent work of Choppin and Dinius.[17] These investigators in ion-exchange studies found evidence for such ion-associates with a number of tripositive lanthanide ions in 12 *M* aqueous perchloric acid.

(10) Reference 4, pp. 519–520, 486–489.
(11) E. D. Moorhead and W. M. MacNevin, *Anal. Chem.*, **34**, 269 (1962).
(12) E. D. Moorhead and N. H. Furman, *ibid.*, **32**, 1507 (1960).
(13) J. W. Grenier and L. Meites, *Anal. Chim. Acta*, **14**, 482 (1956).
(14) N. Tanaka, *Bull. Chem. Soc. Japan*, **23**, 253 (1950).
(15) N. Tanaka, *ibid.*, **33**, 14 (1960).
(16) I. V. Nelson and R. T. Iwamoto, unpublished results.
(17) G. R. Choppin and R. H. Dinius, *Inorg. Chem.*, **1**, 140 (1962).

The polarographic behavior of praseodymium(III) has also been investigated in acetonitrile.[18] The results of this investigation differ from our findings in two respects. First, with regard to the effect of halide ion, a single reduction wave at a potential (−1.95 v.) *more negative* than that at which the metal ion is reduced in tetraethylammonium perchlorate solutions (1.5 v.) was observed with tetraethylammonium bromide as supporting electrolyte. Addition of water shifted the wave to *more positive* potentials. In our work, on the other hand, a single wave is obtained only with 1 *F* lithium bromide solution, and, furthermore, with added halide the reduction waves are shifted to *more positive* potentials. Second, the two-step polarograms obtained at high concentrations of praseodymium(III) (generally above 1 millimolar) in acetonitrile containing tetraethylammonium perchlorate were attributed to reduction of the water of hydration and of the metal ion to the metal amalgam. The multiple step waves observed in our studies in ethanol in the presence of halide ion cannot be interpreted in this manner, because it is difficult, if not impossible, to explain the changes in the ultraviolet spectra of ethanol solutions containing praseodymium(III) with variation in the concentration of halide ion except through the formation of halide complexes. Such praseodymium(III) complexes have been proposed to explain the single wave obtained in the presence of halide in acetonitrile.[18] This single wave in acetonitrile for the reduction of praseodymium(III), even at relatively high concentrations, in the presence of bromide indicates that the halide-containing praseodymium species are not sufficiently acidic to undergo the combined hydrolysis and reduction reactions.

Acknowledgment.—The authors wish to express their thanks to the Dow Chemical Company and the University of Kansas for grants in support of this work.

(18) I. M. Kolthoff and J. F. Coetzee, *J. Am. Chem. Soc.*, **79**, 1852 (1957).

SURFACE CONDUCTIVITY OF HIGH SURFACE AREA ADSORBENT DUE TO THE PRESENCE OF ADSORBED MOLECULES

BY S. LEVY AND M. FOLMAN

Department of Chemistry, Technion-Israel Institute of Technology, Haifa, Israel

Received December 17, 1962

Surface conductivity of high surface area porous silica adsorbent has been studied at low surface coverages using ammonia and methanol as adsorbates. For both adsorbates a marked increase in the surface conductivity was found on adsorption. The conductivities measured were of the order 10^{-15}–10^{-10} mho cm.$^{-1}$. For ammonia, an exponential relationship was obtained between the conductivity and the degree of surface coverage. For methanol, such relationship was found for lower coverages only. The surface conductivity increased in all cases with increase in temperature, suggesting an ionic type of mechanism. In the case of NH_3, a linear relationship between the activation energy and the amount adsorbed was found, ranging from 9 to 5 kcal./mole. For CH_3OH, the activation energy for surface conductivity remained practically constant. Measurements on a modified surface where the concentration of the surface OH groups was markedly decreased showed an enhancement of the surface conductivity. In the light of the results obtained, possible mechanisms for surface conductivity are suggested.

Introduction

There exist few works on surface conductivity of a solid adsorbent in the presence of adsorbed layers. In most cases water vapor served as adsorbate. Meakins[1] studied the surface conductivity of glass in the presence of water vapor at high relative pressures where multilayers were formed. The increase in conductivity was ascribed to diffusion of alkali ions from the adsorbent's surface to the adsorbed layer.

Le Clerc,[2] working on a similar system, found similar

(1) R. J. Meakins, *Australian J. Appl. Sci.*, **1**, 120 (1950).

(2) P. Le Clerc, *Silicates Ind.*, **13**, 237 (1954).

effects and ascribed them to solubility of the glass. Kuznetsov[3] gave an identical explanation for his results.

More recently Kawasaki[4] found an exponential relationship between the conductivity and the number of adsorbed water layers. At higher amounts adsorbed the exponential relationship changed into a linear one. This was explained by a transition to a liquid-like layer.

Kurosaki[5] used in his work a non-alkali glass as well as fused silica. Here again a marked influence of the adsorbate on the measured conductivity was found. According to him, the current carriers were not Na^+ but OH^- and H^+ ions from dissociation of water. Kinetic effects in conductivity were found by Deryagin.[6] They were explained as being due to redistribution of the adsorbate as a result of heterogeneity of the adsorbent's surface.

A different system was used by Cook,[7] *et al.* Synthetic silica–alumina catalyst powder was used as adsorbent, quinoline and water vapor as adsorbates. The influence of quinoline on the surface conductivity was much more pronounced than that of water. According to these authors, this is explained by the fact that the catalyst, which is a strong Lewis acid, reacts with quinoline—a strong Lewis base—and leads to a change in the coördination number of the aluminum ions which are the current carriers.

Voltz and Weller[8] used a synthetic silica–alumina powder as adsorbent, ammonia and amines as adsorbates. It was suggested by these authors that the adsorbed NH_3 molecules react with the protons present on the surface to give NH_4^+ ions, which are the main current carriers.

In the present work a single plate of porous silica Vycor glass was chosen as adsorbent, with NH_3 and CH_3OH vapor serving as adsorbates. It seemed that in order to obtain a clearer picture the measurements ought to be done at low surface coverages—below a monolayer—and the changes in conductivity be measured as a function of the amount adsorbed.

Experimental

The measuring system consisted of a measuring cell, an apparatus for adsorption measurements, and a "High-Meg" meter for measurements of the d.c. resistance of the sample. The "High-Meg" meter was based on the one described by Kurosaki[5]; it was slightly improved. The resistance of the sample was measured by comparison with a standard resistor in a potential dividing system. The potential drop on the standard resistor was compensated using a K-2 Leeds and Northrup potentiometer. The compensation was effected using a Victoreen 5800 electrometer tube and a Scalamp galvanometer with a maximum sensitivity of 92 mm./μa. In order to extend the working range of the "Meg-Meter" the reference resistor could be substituted by another one. This permitted measurements of resistance in the region from 6×10^{10} ohms up to 2×10^{15} ohms.

The adsorption apparatus was of a conventional volumetric type. Pressures were measured with an accuracy of 0.02 mm. using a cathetometer. The cell consisted of two parts. The upper part was made of fused silica. Two Kovar-to-silica seals on top of it permitted two nickel electrodes to be vacuum-sealed. The electrodes were in close contact with a porous Vycor glass sample, on whose both ends silver deposits were prepared.

The lower part of the cell provided with a ground joint was attached to the vacuum system. A small side arm with vacuum tungsten seals permitted mounting of a chromel–alumel thermocouple, with its end resting on the adsorbent. The sample was cut from tubing supplied by Corning Glass, 25 mm. in length, 11 mm. wide, and 1.1 mm. thick.

The whole cell was shielded by means of a metal enclosure, in order to obtain the necessary stability of the measuring system.

The cell could be heated up to 450° to permit proper evacuation of the samples. When measurements were taken it was immersed in a constant-temperature bath.

The description of the porous Vycor glass adsorbent is given by Nordberg.[9] The surface area of the sample used was measured by the B.E.T. method using argon as adsorbate at liquid-oxygen temperature. The area obtained was 151 m.^{2}/g.

Materials and Sample Preparation.—NH_3 was obtained from cylinders supplied by Matheson. It was of purest grade. The gas was dried by condensing into a small bulb, distilled several times over metallic sodium, and freed from air and hydrogen by bulb-to-bulb distillation. Finally, it was transferred to a storage bulb, the first and the last fractions being rejected.

Analytical pure-grade methanol was refluxed over metallic magnesium for 24 hours. It was freed from air by bulb-to-bulb distillation and evacuation after freezing. For measurements, only the middle fraction was used.

The solid adsorbent was heated at 450° in oxygen for 2 hours in order to burn off the organic matter always present on its surface. After it had become colorless and transparent, it was heated at 400° and evacuated for six hours until the pressure measured was less than 10^{-5} mm.

As will be described later, some of the experiments were carried out on a methylated surface.

This methylation was performed in order to decrease the concentration of the surface OH groups. The procedure of replacing the OH groups is described in detail elsewhere.[10]

Results

1. Surface Conductivity in the Presence of Adsorbed NH_3.—After heating and evacuation of the sample as described in the previous section, the conductance measured at room temperature was beyond (below 10^{-15} ohm^{-1}) the range of the measuring system. For the first amounts of gas admitted no noticeable changes occurred. When the amount adsorbed reached about 10 cc./g., the conductance of the sample increased and from that coverage onward it continued to increase with each dose of gas admitted.

Already at the beginning of the experiments, it became obvious that some kinetic effects were taking place. These were especially pronounced for the first doses of adsorbate for which the effect of presence of adsorbed layer could be detected and measured. When a dose of gas was admitted to the adsorption cell, an increase in conductance occurred; this lasted for a few minutes, and was in accordance with the fact that adsorption is not instantaneous and achievement of equilibrium is a time-consuming process. Moreover, instead of reaching some constant value, the conductance passed through a maximum and then decreased with time, until some equilibrium value was reached. This phenomenon was noticed especially for the first doses of gas adsorbed, for which changes in conductance were detected. On desorption no similar kinetic effects occurred.

Since it appeared that the surface conductance is not only a function of the amount adsorbed but also depends on the surface properties of the adsorbent, a plot of log σ/V against V for 2 and $-23°$ was pre-

(3) A. Y. Kuznetsov, *Zhur. Fiz. Khim.*, **27**, 657 (1953).

(4) K. Kawasaki, *et al.*, *J. Phys. Soc. Japan*, **2**, 222 (1958); *J. Appl. Phys. Japan*, **27**, 216 (1958).

(5) S. Kurosaki, *et al.*, *J. Chem. Phys.*, **23**, 1846 (1955).

(6) J. F. Abrakhmanova and B. V. Deryagin, *Doki. Akad. Nauk SSSR*, **120**, 94 (1958).

(7) M. A. Cook, *et al.*, *J. Phys. Chem.*, **58**, 358 (1954).

(8) S. E. Voltz and S. W. Weller, *ibid.*, **62**, 574 (1958).

(9) M. E. Nordberg, *J. Am. Ceram. Soc.*, **27**, 299 (1944).

(10) M. Folman and D. J. C. Yates, *Proc. Roy. Soc.* (London), **A246**, 32 (1958).

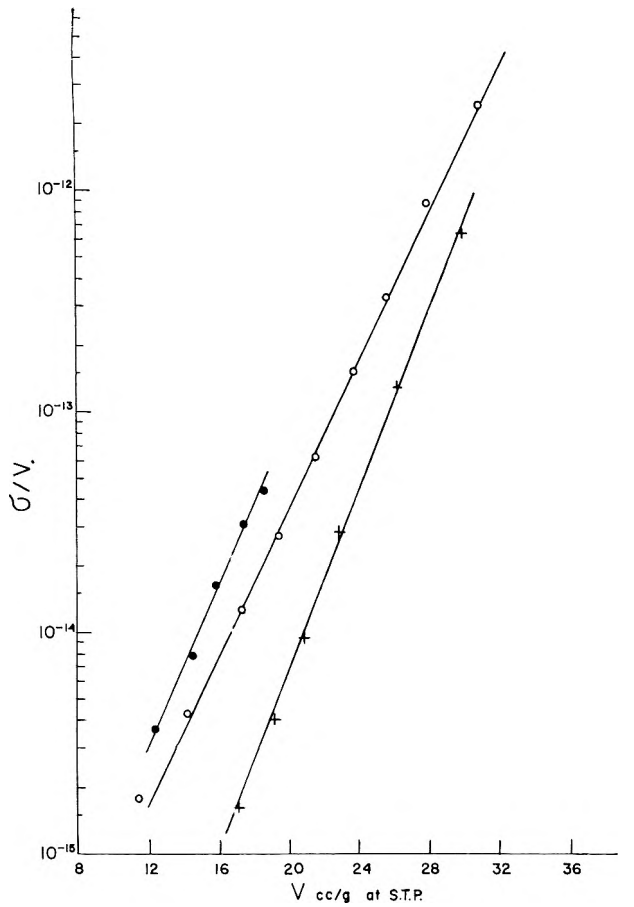

Fig. 1.—Log σ/V *vs.* V for adsorption of NH_3: O, at 2°; +, at −26°; ●, at 2° after methylation.

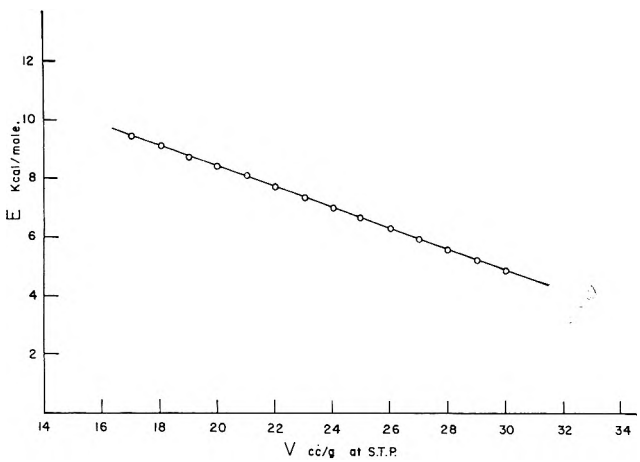

Fig. 2.—Activation energy for surface conductivity *vs.* the amount of NH_3 adsorbed.

pared and is given in Fig. 1. Here σ is the specific conductance (below, it will be referred to as conductivity) and V the amount of gas adsorbed in cc. per 1 g. of adsorbent.

It may be easily seen that the conductivity per one cc. of adsorbate changes exponentially with the amount adsorbed, increasing with surface coverage. The conductivity isotherm for the higher temperature lies higher, which means that for the same total amount adsorbed the conductivity increases with temperature.

The total conductivity for our system may be expressed as composed of two contributions (1): the bulk conductivity of the solid and the surface conductivity due to the presence of adsorbed layer.

$$\sigma = \sigma_b + \sigma_s \qquad (1)$$

In the absence of adsorbate the conductivity measured was below 10^{-15} ohm^{-1} cm.$^{-1}$. If we assume that the adsorbate does not influence the bulk conductivity, the changes in conductivity upon adsorption will be due to changes in σ_s only.

Generally σ for the ionic type of conductivity may be expressed as

$$\sigma = \sigma_0 e^{-E/RT} \qquad (2)$$

where σ_0 includes the number of ions and E is the energy of activation for conduction. This energy of activation can be calculated from two conductivity isotherms taken at temperatures not far apart. This was done in our case, using the isotherms given in Fig. 1. It appeared that E is not constant and changes with the amount adsorbed. A plot of E *vs.* V is shown in Fig. 2. A good linear relationship was obtained. The energy of activation changed from about 9.4 kcal./mole for 16 cc./g. to about 5.0 kcal./mole for 30 cc./g. adsorbed.

When measurements were done on adsorption, it appeared that analogously to hysteresis in the adsorption isotherm (already reported previously for this system), hysteresis was present in the conductivity isotherm as well. This is shown for room temperature in Fig. 3. The resistance (R) curve (resistance is directly obtained from measurements) on adsorption lies below the desorption curve, which means that, for the same amount adsorbed, lower values are always obtained on adsorption compared with the desorption values.

The methylation of the glass, performed in order to remove the surface OH groups, leads to an exchange of about 80%. The adsorption isotherm on such a surface is different compared with the isotherm for a non-methylated surface. It lies much lower.

The isosteric heat of adsorption on this sample is also much lower compared with the non-methylated sample and practically constant. The time effects in conductivity measurements reported for the non-methylated glass are not present in this case. After admission of a dose of adsorbate, the approach to equilibrium is in this case faster and no maxima are present in the conductivity *vs.* time curves.

The conductivity *vs.* amount adsorbed curve for 2°, shown in Fig. 1, reveals the same linear dependence between log σ/V and V. It may be seen that this line lies above the one for non-methylated glass, which indicates that for the same amount of gas adsorbed the conductivity is always higher for the methylated sample. In this case, the highest surface coverage was 19 cc./g. only, since, as already stressed, the adsorption was much weaker and the measuring apparatus was not adapted to work at pressures above 1 atm.

2. Surface Conductivity in the Presence of Adsorbed CH_3OH.—The kinetic effects reported for NH_3 were found also with CH_3OH, being even more pronounced in this case. They were present in adsorption as well as in desorption. In the latter case the conductance always dropped to some minimum value and then rose slightly until it reached some equilibrium value.

The log σ/V *vs.* V for CH_3OH is shown in Fig. 4 for 21 and 2°. Here, in contrast to the previous findings with NH_3, the surface conductivity increases markedly already at low surface coverages and measurable changes are observed at an amount adsorbed of 6 cc./g. In both curves two portions can be distinguished. For

lower surface coverages log σ/V changes linearly with V, as in the NH_3 case. For higher surface coverages, the linear dependence disappears and a small but distinctive curvature is present.

The conductivity again increases with increasing temperature. From the two conductivity isotherms, the energy of activation for surface conductivity was calculated. A nearly constant value of 12.7 kcal./mole was obtained in the region between $V = 7$ cc./g. and $V = 18$ cc./g. This corresponds to surface coverages from $\theta = 0.22$ to $\theta = 0.58$, respectively.

Hysteresis in adsorption and conductivity isotherms were found in desorption. The hysteresis loop in this case is not as wide as with NH_3, still the phenomenon is in evidence for this system too.

For CH_3OH in desorption, the approach to equilibrium was always much more time-consuming than in measurements on adsorption.

Methanol vapors adsorbed on the methylated surface showed a similar relationship between log σ/V and V as that obtained for the non-methylated sample. For the first amounts adsorbed, a linear relationship between log σ/V and V was obtained while for higher surface coverages the change in log σ/V became less rapid. This may be seen from Fig. 4, where the curve of log σ/V *vs.* V is given for the methylated glass together with the curve for the non-methylated glass.

Comparing the two conductivity isotherms for the methylated and non-methylated glass it became obvious, as in the NH_3 case, that over the whole range of adsorption measured the conductivity for the methylated sample is always higher.

Discussion

The conductivity of the heated and evacuated adsorbent was, at room temperature, outside the measuring range of the apparatus, and only became measurable at much higher temperatures of about 200°. Most probably it is of an ionic type usually observed in solid dielectrics. Since in the present work the main interest was in conductivities due to the presence of adsorbed layers, no further details of the conductivity of the solid adsorbent will be given.

The kinetic effects described in the previous section and obtained in adsorption, and in desorption, may be explained as due to the existence of a high concentration of OH groups on the surface of the adsorbent. These groups act apart from the Si and O atoms as adsorption sites. It has been shown that the two types of sites differ in their adsorption kinetics. NH_3 and CH_3OH are more rapidly adsorbed on the OH groups. If the contribution to conductivity by the adsorbate was larger when adsorbed on the OH groups, the conductivity kinetics should follow the adsorption kinetics and an initial rise of conductivity after admission of a dose of gas should be followed by a decrease gradually approaching an equilibrium value. Moreover, after decreasing the concentration of the OH groups by methylating the surface the kinetic effects should become much smaller, and this is what actually happens. There may exist an additional reason for the effect observed. The diffusion of adsorbed molecules to the inner regions of the glass adsorbent is certainly not instantaneous. If the contribution to conductivity from the molecules situated at the very narrow capillaries were lower compared with more accessible sites and time is needed to reach these places, a similar effect should be observed.

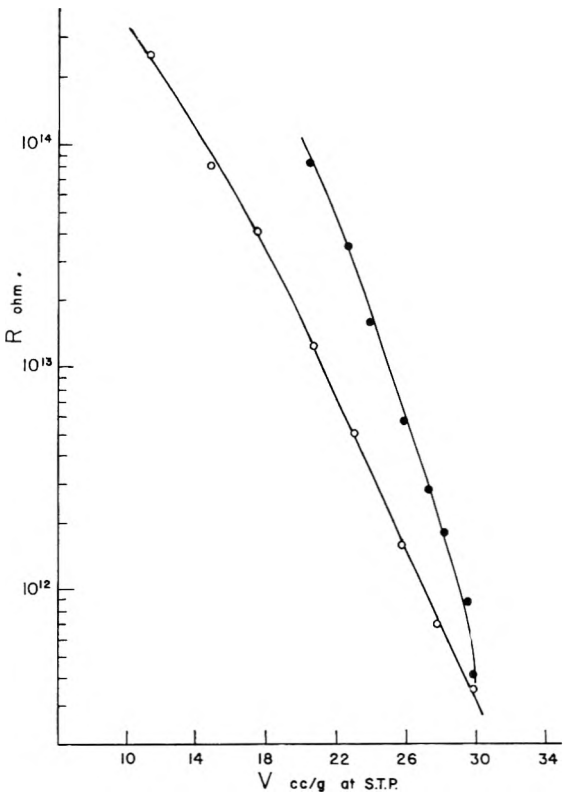

Fig. 3.—Hysteresis in surface resistance for NH_3: O, adsorption; ●, desorption.

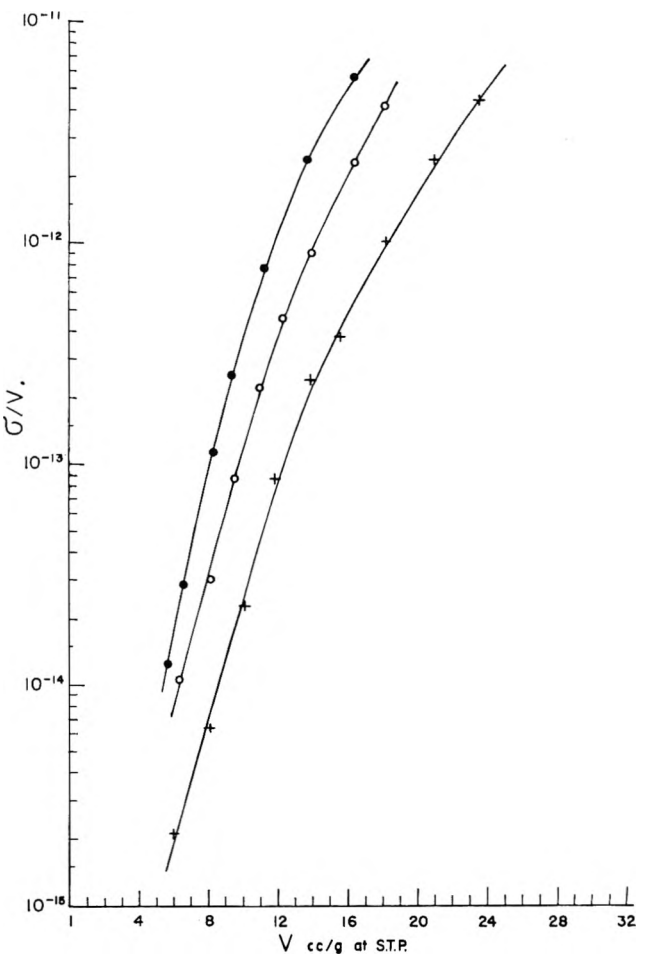

Fig. 4.—Log σ/V *vs.* V for adsorption of CH_3OH: +, at 2°; O, at 21°; ●, at 21° after methylation.

The dependence of conductivity on temperature found suggests, as already mentioned, an ionic type of mechanism for which eq. 2 usually applies. The exponential relationship between σ/V and V found for NH_3 in the whole region of measurements suggests that E should vary linearly with V if eq. 2 is valid in our case. Such a linear relationship actually exists, as is evident from Fig. 2.

The energy of activation for the conductivity may be written as composed of two contributions[11]

$$E = {}^1/_2E_1 + E_2 \qquad (3)$$

where E_1 is the energy required for formation of current carriers, or the energy of dissociation of a molecule into two ions, and E_2, in our case, the activation energy for surface migration of the ions. Since the surface of the adsorbent is energetically heterogeneous, it is quite justifiable to assume that the activation energy for surface migration depends on surface conditions and will be higher for regions where the energy of adsorption is higher (namely, for the regions occupied first in the process of adsorption), falling off with increasing amounts adsorbed. It seems justified to accept that this energy of activation will change roughly in the same way as the heat of adsorption, since it may be seen that in ideal cases its value is a fraction ($^1/_2$ or $^2/_3$) of the heat of adsorption.[12]

For ammonia, q_{is} changes more or less linearly with V from a coverage of about $V = 20$ cc./g.

The increase in surface conductivity on the modified surface, compared with the non-methylated surface, may be explained by lowering of the activation energy for surface migration, parallel to that of the energy of adsorption.

In the initial stage of the work, it was supposed that the surface OH groups, giving hydrogen bonding with the adsorbate, are responsible for the large increase in conductivity by a mechanism in which a proton transfer from these groups to the NH_3 molecule occurs, and as a result NH_4^+ ions are formed. These ions may serve as the current carriers on the surface.

Accordingly, the removal of the OH groups, or a marked decrease in their concentration, should cause a decrease in the conductivity which however did not take place. This does not yet disprove the mechanism postulated. Actually, 20–25% of the OH groups still remained on the surface and these are still able to act as proton donors. In parallel, methylation also resulted in lowering of the activation energy for surface conductivity. Thus two mutually counteractive factors were present, and as an over-all increase in conductivity took place, lowering of the activation energy outweighed the decrease in concentration of surface OH groups. In order to prove the validity of the proton transfer mechanism the OH groups should be removed completely.

Methanol as Adsorbate.—The kinetic effects obtained in adsorption and desorption of methanol may be explained in the same way as those for ammonia.

In the log σ/V *vs.* V plots two portions were obtained. From a coverage of about 12 cc./g. the change in log σ/V becomes less rapid and the plot begins to deviate from linearity. This would imply that if the previous explanation given for NH_3 holds in this case as well, the energy of activation for conductivity changes linearly only for the first amounts adsorbed, while later on this change becomes much slower. On the other hand, the energy of activation calculated from two conductivity isotherms was found practically constant and did not change much with surface coverage. By contrast, σ_0/V was found to increase with surface coverage, which means that the number ratio of current carriers to adsorbed molecules increases with V.

The mechanism postulated for NH_3 may equally well explain the conductivity caused by the presence of adsorbed CH_3OH through formation of $CH_3OH_2^+$ ions, still it does not explain why the log σ/V *vs.* V are different in this case and why σ_0/V increases with the amount adsorbed. Accordingly, the presence of a second type of mechanism may be suggested such as conduction through autoprotolysis, where two CH_3OH molecules give two ions.

$$2CH_3OH \rightleftharpoons CH_3OH_2^+ + CH_3O^-$$

Autoprotolysis is supposed to be the cause of ionic conductivity in liquid methanol. This would explain the increase in σ_0/V *vs.* V. Although the present experiments remained far below monolayer coverage, there exists the possibility that the molecules are adsorbed in clusters. The probability of such clustering increases with surface coverage and this explains the increase of σ_0/V with V since autoprotolysis may be present in clusters only. That clustering is possible at all at low θ values may be due to the fact that the energy of hydrogen bonds formed between the adsorbed molecules and the surface is very nearly the same as that of the H-bonds between two molecules in the liquid state, as may be judged by comparing the corresponding infrared spectra.[13]

For the methylated adsorbent, the conductivity was generally higher than for the non-methylated one. The same was the case with NH_3, and it may again be explained by the fact that the activation energy for surface migration is in this case lower. Here, however, another factor may be present. As on the methylated surface the adsorption of CH_3OH is weaker, it was necessary to work at higher relative pressure in order to obtain similar surface coverages and it is quite possible that a fraction of the adsorbate is obtained as capillary condensate.

Apart from the two possible mechanisms discussed, a third explanation of the surface conductivity on adsorption of NH_3 and CH_3OH may be based on migration of H^+ ions, along the lines of the accepted views on conductivity of pure water where an H^+ ion jumps from one molecule to another in hydrogen-bonded systems. In this case H^+ ions would be the main current carriers. Such a picture necessitates the existence of chains of hydrogen bonds, which is possible at higher surface coverages. At low surface coverages, where no possibility of long chains exists, the conductivity by H^+ ion may be similarly ascribed to the accepted mechanism in hydrogen-bonded molecular crystals, such as RCOOH,[14] where the H^+ ion leaves

(11) N. F. Mott and R. H. Gurney, "Electronic Processes in Ionic Crystals," Clarendon Press, 1957, p. 43.

(12) J. H. DeBoer, "The Dynamical Character of Adsorption," Clarendon Press, 1953, p. 96.

(13) M. Folman and D. J. C. Yates, *Trans. Faraday Soc.*, **54**, 1684 (1958).

(14) J. McPollock and A. R. Ubbelohde, *ibid.*, **52**, 1112 (1956).

the hydrogen bond and migrates between the H-bonded molecules in the crystal lattice.

The mechanisms advanced above for surface conductivity are nearly equally probable. Additional experiments would be required in order to clarify which of them is the predominant one.

ELECTRON IMPACT INVESTIGATIONS OF SULFUR COMPOUNDS. III. 2-THIAPROPANE, 3-THIAPENTANE, AND 2,3,4-TRITHIAPENTANE[1]

BY BRICE G. HOBROCK AND ROBERT W. KISER

Department of Chemistry, Kansas State University, Manhattan, Kansas

Received December 19, 1962

In addition to reporting basic electron impact data for 2,3,4-trithiapentane, 2-thiapropane, and 3-thiapentane, comparisons of heats of formation of various series of related ions containing one, two, and three sulfur atoms are made. It is observed that, in general, successive addition of sulfur atoms has little effect on the heats of formation of the ions. This is also found to be true for variation of the R group. The addition of hydrogen atoms is observed, in almost all of the cases we studied, to have a significant effect in decreasing the heats of formation of the ions. The heats of formation for the principal ions from the three compounds, in agreement with postulated processes, are given. The ionization potentials of the molecules are discussed as well as the derived values for the ionization potentials of C_2H_5SH and CH_3S_2H.

Introduction

In the course of our study of the ions resulting from the ionization and dissociation of organic sulfur compounds by electron impact in a mass spectrometer,[2-4] we have noted many unusual and interesting species. In our initial studies, we paid particular attention to the ease with which hydrogen atoms rearrange onto sulfur atoms (*i.e.*, H_3S^+, CH_5S^+, $H_2S_2^+$, etc.). In an attempt to observe and study more of these intriguing species, such as $H_2S_3^+$, $CH_3S_2H^+$, $CH_3S_3H^+$, and S_3^+, we have studied 2,3,4-trithiapentane. Not all of the species just cited were observed experimentally; however, a number of other different ions were found. We describe herein our methods of study and the results observed and then we discuss these latter ions. In addition, we also include new electron impact data for 2-thiapropane and 3-thiapentane. Appearance potentials for the positive ions of interest are measured and probable ionization and dissociation processes are given in agreement with heat of formation data. Heats of formation of the ions are calculated and intracomparisons are made and discussed for various series of related ions.

Experimental

The experimental techniques employed are the same as those described previously.[2-5] The samples of 2-thiapropane and 3-thiapentane were obtained from Aldrich Chemical Co. and were used as received. Gas–liquid partition chromatography suggested that both compounds were pure; however, a small non-sulfur-containing impurity was noted in the mass spectrum of 3-thiapentane. The only interference with the mass spectrum of 3-thiapentane was noted at $m/e = 58$; however, this was not a serious interference. The sample of 2,3,4-trithiapentane was very graciously supplied to us by S. Meyerson of American Oil Company, Whiting, Indiana. An impurity of about 2% 2,3-dithiabutane was noted[6] and our calculations from the mass spectrum and relative vapor pressures confirm this amount of impurity. After standing on the inlet system of the mass spectrometer for a short period of time, the impurity in the 2,3,4-trithiapentane became quite small and no interference was noted in the subsequent measurements of appearance potentials. Appropriate subtraction of impurities from the mass spectrum obtained gave results which agreed very closely with serial 1222 in the API Tables[7] determined from the same sample by S. Meyerson. Good agreement was also obtained with serial 909 and serial 497 for 2-thiapropane and 3-thiapropane, respectively.

Results and Discussion

Heats of formation for the various ions in accord with their respective postulated processes are listed in Tables I, and II and III. The experimentally measured appearance potentials and partial mass spectra are also given. The calculated heats of formation are based upon the appearance potentials, the appropriate heats of formation of the molecules, and the proposed radicals. The heats of formation employed for 2-thiapropane and 3-thiapentane were -8.79[8] and -19.77 kcal./mole,[9] respectively. The calculations for 2,3,4-trithiapentane are based, however, on our estimated value for its heat of formation of 0.0 kcal./mole. This estimation was made by extrapolation from values for 2-thiapropane and 2,3-dithiabutane. Good agreement with known or previously determined heats of formation for ions are obtained using this value. A heat of formation of 51 kcal./mole for CH_2S has been employed. This value is 25 kcal./mole less than that used by Gallegos and Kiser.[10]

The ionization potentials determined for the three compounds in this study agree very well with literature values. The value of 8.70 e.v. for 2-thiapropane agress closely with 8.73 e.v. determined by Issacs, *et al.*,[11] and 8.684 e.v. determined by Watanabe[12] by photo-

(1) This work was supported by the U. S. Atomic Energy Commission under contract No. AT(11-1)-751 with Kansas State University. This is a portion of a dissertation to be presented by B. G. Hobrock to the Graduate School of Kansas State University in partial fulfillment of the requirements for the degree of Doctor of Philosophy. Presented at the 144th National Meeting of the American Chemical Society, Los Angeles, California, March 31, 1963.

(2) B. G. Hobrock and R. W. Kiser, *J. Phys. Chem.*, **66**, 1214 (1962).

(3) B. G. Hobrock and R. W. Kiser, *ibid.*, **66**, 1648 (1962).

(4) B. G. Hobrock and R. W. Kiser, *ibid.*, **67**, 648 (1963).

(5) E. J. Gallegos and R. W. Kiser, *J. Am. Chem. Soc.*, **83**, 773 (1961).

(6) S. Meyerson, private communication.

(7) "Mass Spectral Data," American Petroleum Institute Research Project 44, National Bureau of Standards, Washington, D. C.

(8) J. P. McCullough, W. N. Hubbard, F. R. Frow, I. A. Hossenlopp, and G. Waddington, *J. Am. Chem. Soc.*, **79**, 561 (1957).

(9) W. N. Hubbard, W. D. Good, and G. Waddington, *J. Phys. Chem.*, **62**, 614 (1958).

(10) E. J. Gallegos and R. W. Kiser, *ibid.*, **66**, 136 (1962).

(11) L. D. Issacs, W. C. Price, and R. G. Ridley, "Vacuum Ultraviolet Spectra and Molecular Ionization Potentials," in "The Threshold of Space," edited by M. Zelikoff, Pergamon Press, Ltd., London, 1957, pp. 143–151.

(12) K. Watanabe, T. Nakayama, and J. Mottl, "Final Report on Ionization Potentials of Molecules by a Photoionization Method," December, 1959. Department of Army No. 5B99-01-115 ORD TB2-001- OGR-1624. Contract No. DA-04-200ORD 480 and 737.

TABLE I

APPEARANCE POTENTIALS AND HEATS OF FORMATION OF THE PRINCIPAL IONS FROM 2-THIAPROPANE

m/e	70 e.v. R.a.	A.p. (e.v.)	Process	ΔH_f^+ (kcal./mole)
13	2.1			
14	7.6			
15	14.0	17.0 ± 0.4	$C_2H_6S \rightarrow CH_3^+ + CH_2 + SH$	284
27	25.0	15.4 ± 0.3	$\rightarrow C_2H_3^+ + H + H_2S$	299
29	1.5			
34	1.3			
35	32.0	14.8 ± 0.2	$\rightarrow H_3S^+ + (???)$	
37	1.3			
44	5.1	15.0 ± 0.5 (?)		
45	51.9	15.6 ± 0.2	$\rightarrow CHS^+ + CH_4 + H$ (?)	317
			$\rightarrow CHS^+ + CH_3 + H_2$ (?)	
46	42.0	11.2 ± 0.2	$\rightarrow CH_2S^+ + CH_4$ (?)	
47	100.0	11.7 ± 0.2	$\rightarrow CH_3S^+ + CH_3$	229
48	3.1			
49	4.7			
57	2.6			
58	3.4			
59	3.1			
61	32.5	11.8 ± 0.2	$\rightarrow C_2H_5S^+ + H$	211
62	83.0	8.70 ± 0.20	$\rightarrow C_2H_6S^+$	192

TABLE II

APPEARANCE POTENTIALS AND HEATS OF FORMATION OF THE PRINCIPAL IONS OF 3-THIAPENTANE

m/e	70 e.v. R.a.	A.p. (e.v.)	Process	ΔH_f^+ (kcal./mole)
15	3.6			
26	18.0	16.3 ± 0.5		
27	91.1	16.7 ± 0.5	$C_5H_{10}S \rightarrow C_2H_3^+ + C_2H_5 + S + H_2$	290
29	62.7	14.5 ± 0.3	$\rightarrow C_2H_5^+ + C_2H_5 + S$	239
34	4.3			
35	18.0	15.6 ± 0.4	$\rightarrow H_3S^+ + 2C_2H_3 + H$	160
41	6.4			
45	32.9	15.3 ± 0.5	$\rightarrow CHS^+ + C_2H_4 + CH_3 + H_2$ (?)	289
46	16.4	12.5 ± 0.3	$\rightarrow CH_2S^+ + C_2H_5 + CH_3$	215
47	82.4	13.5 ± 0.2	$\rightarrow CH_3S^+ + CH_3 + C_2H_4$	247
48	2.1			
49	4.2			
57	5.6			
58	16.0 (?)			
59	11.7	14.6 ± 0.4	$\rightarrow C_2H_3S^+ + CH_3 + CH_2 + H_2$	217
60	11.1	11.2 ± 0.2	$\rightarrow C_2H_4S^+ + C_2H_4 + H_2$	226
61	59.1	12.0 ± 0.2	$\rightarrow C_2H_5S^+ + C_2H_5$	235
62	56.2	10.4 ± 0.2	$\rightarrow C_2H_6S^+ + C_2H_4$	208
63	3.8			
64	1.9			
75	100.0	11.6 ± 0.2	$\rightarrow C_3H_7S^+ + CH_3$	216
76	3.2			
77	6.2			
89	2.5			
90	60.4	8.49 ± 0.19	$\rightarrow C_4H_{10}S^+$	176
92	2.3			

ionization techniques, but poorly with a value of 9.4 e.v. determined by Sugden, *et al.*,[13] by electron impact methods. A calculated value of 8.73 e.v. by Gallegos and Kiser[14] is also in agreement.

For 3-thiapentane, our value of the ionization potential of 8.49 e.v. agrees with literature values of 8.43 e.v.[11] and 8.48 e.v.[12] and with a calculated value of 8.58 e.v.[14]

The ionization potential for 2,3,4-trithiapentane of 8.80 e.v. which we report here is new and appears to be a quite reasonable value. One may attempt to calculate the ionization potentials of some other trisulfides by an equivalent orbital method[2,3,15] but results are inconclusive as the values are very sensitive to small changes in the ionization potential selected for H_2S_3. The calculation is based upon an interpolated value for the ionization potential of this molecule.

Other ionization potential data may be derived from our experimental results. From 3-thiapentane, the ion at $m/e = 62$ is $C_2H_6S^+$ but probably has the structure $C_2H_5SH^+$ for reasons to be discussed next. Using a heat of formation of −11.03 kcal./mole for the molecule[8] and our heat of formation for the ion of 207 kcal./mole, the ionization potential of $C_2H_6S^+$ is calculated to be 9.45 e.v. which agrees with a literature value of

(13) T. M. Sugden, A. D. Walsh, and W. C. Price, *Nature*, **148**, 373 (1951).

(14) E. J. Gallegos and R. W. Kiser, *J. Phys. Chem.*, **65**, 1177 (1961).

(15) J. L. Franklin, *J. Chem. Phys.*, **22**, 1304 (1954).

TABLE III

APPEARANCE POTENTIALS AND HEATS OF FORMATION OF THE PRINCIPAL IONS OF 2,3,4-TRITHIAPENTANE

m/e	70 e.v. R.a.	A.p. (e.v.)	Process	ΔH_f^+ (kcal./mole)
15	7.9			
32	4.1			
44	2.5			
45	59.0	14.5 ± 0.3	$CH_3SSSCH_3 \rightarrow CHS^+ + CH_3 + S_2 + H_2$	272
46	21.3	13.4 ± 0.3	$\rightarrow CH_2S^+ + CH_3S_2 + H$	234
			$\rightarrow CH_2S^+ + CH_3S + SH$	240
47	35.9	12.9 ± 0.2	$\rightarrow CH_3S^+ + CH_3 + S_2$	236
48	2.4			
61	7.9			
64	22.3	14.4 ± 0.3	$\rightarrow S_2^+ + CH_2S + CH_4$	299
65	2.2			
66	2.5			
78	7.0			
79	50.6	12.3 ± 0.2	$\rightarrow CH_3S_2^+ + CH_3S$	246
80	14.1	10.8 ± 0.2	$\rightarrow CH_3SSH^+ + CH_2S$	198
81	3.4			
111	16.2	11.4 ± 0.2	$\rightarrow CH_3S_3^+ + CH_3$	231
126	100.0	8.80 ± 0.15	$\rightarrow CH_3S_3CH_3^+$	203
128	10.5			

$I(C_2H_5SH)$ = 9.285 e.v.[12] Therefore, the structure of the ion is believed to be $C_2H_5SH^+$, instead of $CH_3SCH_3^+$, which has an ionization potential of 8.70 e.v., as reported above.

One may also attempt to derive an ionization potential for the ion at m/e = 80, $CH_4S_2^+$, from 2,3,4-trithiapentane.

One may estimate a heat of formation for the CH_3SSH molecules of −5 kcal./mole, using Franklin's method.[16] Using $\Delta H_f^+(CH_3SSH)$ = 198 kcal./mole, one may calculate an ionization potential of 8.8 e.v. An equivalent orbital calculation[4] gives a value of 9.15 e.v., in fair agreement with the value derived from our data.

If one assumes that the neutral fragments are CS + H_2, $\Delta H_f(CH_3SSH)$ = 196 which leads to $I(CH_3SSH)$ = 8.7 e.v.

Correlations of Heats of Formation

Our observations of the various species in the mass spectrum of 2,3,4-trithiapentane allow us to make a number of correlations of heats of formation of various series of related ions (see Table IV).

Since we observed S_2^+ from $CH_3S_2CH_3$, it was hoped that the S_3^+ ion might be observed from 2,3,4-trithiapentane. However, S_3^+ did not appear in the mass spectrum of 2,3,4-trithiapentane; this ion may well be too unstable to exist in the gas phase. An examination of the literature[17] reveals that S_3^{-2} exists in aqueous solution, but no information concerning S_3 and S_3^+ is available. By extrapolation using the known $\Delta H_f^+(S)$ = 304[18] and $\Delta H_f^+(S_2)$ = 282 (see Table IV) a value of approximately 260 kcal./mole is expected for $\Delta H_f^+(S_3)$. Similarly, one can extrapolate $\Delta H_f(S)$ and $\Delta H_f(S_2)$ to obtain $\Delta H_f(S_3)$ = 7 kcal./mole. Combination of these estimates leads one to estimate $I(S_3)$ = 11.0 e.v.

The addition of hydrogen atoms to the S^+, S_2^+, and S_3^+ series appears to stabilize the ΔH_f at a nearly constant value. This is not too surprising when one notes also the addition of hydrogen atoms in the CS^+ and $C_2H_2S^+$ series (see Table IV).

The series, CH_3S^+, $CH_3S_2^+$, $CH_3S_3^+$, wasco mpleted in this study as $CH_3S_3^+$ occurred in the mass spectrum of 2,3,4-trithiapentane. The decreasing value for the heats of formation of the S^+, S_2^+, S_3^+ series apparently is arrested by the addition of a CH_3 radical. We note that the series experienced only a very minor (and

TABLE IV

COMPARISONS OF THE HEATS OF FORMATION OF RELATED IONS

Species	"best," ΔH_f^+, kcal./mole	Molecule
S^+	304	S
S_2^+	282	$C_2H_5S_2C_2H_5$
S_3^+	(255)	
H_2S^+	236	
$H_2S_2^+$	239	
$H_2S_3^+$	(242)	
CH_3S^+	226	$CH_3SC_2H_5$
$CH_3S_2^+$	229	$C_2H_5S_2C_2H_5$
$CH_3S_3^+$	231	$CH_3S_3CH_3$
CH_3SH^+	205	$CH_3S_2CH_3$, $CH_3Sn\text{-}C_3H_7$
$CH_3S_2H^+$	198	$CH_3S_3CH_3$
CH_3S_3H	(190)	
CH_3S^+	226	$CH_3SC_2H_5$
$C_2H_5S^+$	225	$CH_3SC_2H_5$
$C_3H_7S^+$	217	$CH_3Si\text{-}C_3H_7$
CH_3SH^+	205	$CH_3S_2CH_3$, $CH_3Sn\text{-}C_3H_7$
$C_2H_5SH^+$	207	$C_2H_5SC_2H_5$
$C_3H_7SH^+$	(200)	
$CH_3S_2H^+$	198	$CH_3S_3CH_3$
$C_2H_5S_2H^+$	219	$C_2H_5SSC_2H_5$
$C_2H_7S_2H^+$	(216)	$n\text{-}C_3H_7SSn\text{-}C_3H_7$
CHS^+	270	$C_2H_5SSC_2H_5$
CH_2S^+	225	$CH_3SC_2H_5$
CH_3S^+	226	$CH_3SC_2H_5$
CH_4S^+	205	$CH_3S_2CH_3$, $CH_3Sn\text{-}C_3H_7$
CH_5S^+	163	(Av.)
$C_2H_2S^+$	284	$C_2H_5SSC_2H_5$
$C_2H_3S^+$	234	$CH_3Si\text{-}C_3H_7$
$C_2H_4S^+$	226	$C_2H_5SC_2H_5$
$C_2H_5S^+$	225	$CH_3SC_2H_5$, $CH_3Si\text{-}C_3H_7$
$C_2H_6S^+$	192–208	CH_3SCH_3, $C_2H_5SC_2H_5$
$C_2H_7S^+$	(175)	

(16) J. L. Franklin, *Ind. Eng. Chem.*, **41**, 1070 (1949).

(17) F. D. Rossini, D. D. Wagman, W. H. Evans, S. Levine, and I. Jaffe, "Selected Values of Chemical Thermodynamic Properties," National Bureau of Standards Circular 500, U. S. Government Printing Office, Washington, D. C., 1952.

(18) F. H. Field and J. L. Franklin, "Electron Impact Phenomena and the Properties of Gaseous Ions," Academic Press, New York, N. Y., 1957.

possibly unreal) increase. We conclude that the subsequent addition of one or two sulfur atoms has little or no effect on the ΔH_f^+ of the ions of the $CH_3S_x^+$ type.

$CH_3S_3H^+$ was not observed. By comparison to CH_3SH^+ and $CH_3S_2H^+$, it would appear that if the trend is followed, the heat of formation of $CH_3S_3H^+$ might be slightly smaller than for CH_3SH^+ and $CH_3S_2H^+$. We note also that in the other series, the addition of H atoms to sulfur atoms results in ions with lower heats of formation. $\Delta H_f^+(CH_3S_3H)$ is estimated to be ~190 kcal./mole. It is anticipated that $CH_3S_3H^+$ may be experimentally observed in planned studies of 3,4,5-trithiaheptane or 2,3,4-trithiahexane.

The effect of changing the R group also is noted in the series CH_3SH^+, $C_2H_5SH^+$, and $C_3H_7SH^+$. No $\Delta H_f^+(C_3H_7SH)$ has yet been calculated but the ion has been observed in significant quantities in *n*-propyl and isopropyl sulfides. It is estimated, however, that $\Delta H_f^+(C_3H_7SH) = 200$ kcal./mole. Again, we see no significant effect on ΔH_f^+ for these ions when changing R.

The value of 216 kcal./mole for $\Delta H_f^+(C_3H_7S_2H)$ has not been previously reported but was determined from 4,5-dithiaoctane.[19] With reference to the various preceding series, one would expect that the heats of formation of these ions would remain constant around 215 kcal./mole. If $\Delta H_f^+(CH_3S_2H)$ were then also 215 kcal./mole, the ionization potential of CH_3S_2H then is calculated to be 9.23 e.v., in good agreement with the calculated value of 9.15 e.v. discussed earlier.

The effect of adding successive hydrogen atoms to CS^+ is shown and, as in most of the preceding series, it is noted that the heats of formation of the ions become smaller. Large decreases in ΔH_f^+ are found for CHS^+ and CH_2S^+. No apparent decrease in ΔH_f^+ is seen for $CH_2S^+ \xrightarrow{+H} CH_3S^+$, as the heats of formation are essentially the same. Addition of an H atom to CH_3S^+ and CH_4S^+ then again continues the trend to lower ΔH_f^+.

The same type of series is investigated by noting successive addition of H atoms to $C_2H_2S^+$. The same trends are dominant as in the preceding series; lower ΔH_f^+ for $C_2H_3S^+$ and $C_2H_4S^+$, but the heats of formation for $C_2H_3S^+$ and $C_2H_5S^+$ are alike. And again, lower ΔH_f^+ subsequently are found for $C_2H_6S^+$ and $C_2H_7S^+$. The value of 175 kcal./mole for $\Delta H_f^+(C_2H_7S)$ is an estimated one. We plan to be able to report experimental data for this ion in a future publication, since it has been observed in measurable quantities in both $C_2H_5Sn\text{-}C_3H_7$ and $C_2H_5Si\text{-}C_3H_7$.

Acknowledgments.—We gratefully acknowledge the gift of the sample of 2,3,4-trithiapentane by S. Meyerson of American Oil Company, Whiting, Indiana, and we also wish to thank him for the details of its source and purity.

(19) B. G. Hobrock and R. W. Kiser, unpublished results, 1962.

INFRARED SPECTRA OF SOLID BOROXINE[1]

BY SURESH K. GUPTA AND RICHARD F. PORTER[2]

Department of Chemistry, Cornell University, Ithaca, N. Y.

Received December 20, 1962

Solid boroxine ($B_3O_3H_3$) has been isolated at liquid nitrogen temperatures from the high temperature reaction products of $H_2O(g)$ with $B\text{–}B_2O_3$ mixtures. Low temperature infrared analyses of thin films of the solid may be interpreted on the basis of the six-membered ring structure characteristic of boroxine derivatives, although the spectra suggest that the atoms in the ring are not coplanar. Structural changes in the solid are noted by observing the spectra of films as they are warmed and evolve diborane. The thermal decomposition product at 25° has the approximate composition $B_4O_5H_2$. Similarities in the decomposition behavior of boroxine and its trifluoro and trichloro derivatives are noted.

Introduction

Mass spectrometric studies[3] of the low pressure reactions of $H_2(g)$ with $B\text{–}B_2O_3$ mixtures and of $H_2O(g)$ with elemental boron have shown that gaseous boroxine, $B_3O_3H_3$, is a reaction product at temperatures of about 1400°K. A condensed form of boroxine has not previously been reported as an isolated compound although a number of its alkyl derivatives have been prepared. Difficulty in isolating the unsubstituted compound is noted from the observation[3] that the product condensed in a liquid nitrogen trap from the high temperature gas-solid reaction disproportionates at room temperature to diborane. The present work is an outgrowth of the mass spectrometric studies and we have utilized the high temperature reaction to produce quantities of this material for chemical and structural studies.

Experimental

Samples of solid were obtained by condensing the gaseous product generated when $H_2O(g)$ is passed over a mixture of boron and boric oxide at temperatures between 1350 and 1400°K. The reactant mixture was contained in a molybdenum boat in contact with a cylindrical piece of molybdenum foil used as a liner in a quartz reaction tube. This tube was sealed to a Pyrex vacuum system and $H_2O(g)$ was passed through a glass frit over the reactants while the pressure in the system was maintained at about 1 mm. by continual pumping. The reaction tube was heated by a resistance-type furnace. Gaseous H_2O reacts completely at the high temperature and the measured gas pressure in the system is due mainly to hydrogen which is the main product in a reaction that also produces additional boron oxide. The vacuum system was constructed to permit isolation of milligram quantities of solid by passing the reaction products through a U-tube held in a liquid nitrogen trap. A further modification was the replacement of the U-tube by a low temperature infrared cell through which the product gases could pass. Solid was deposited on a 1-in. NaCl disk which was held within the cell in a copper jacket fastened to a copper block which was cooled by a liquid nitrogen reservoir. The cell was made from a piece of stainless steel tubing 2.5 in. in diameter and about 4 in. in length and was joined to the vacuum system by Kovar glass seals. The external NaCl windows were sealed with Glyptal to the ends of the cell for vacuum-tight operation. Accumulation of moisture on the outside of the windows was observed unless warm air was passed over the cell. Under these conditions the temperature of the internal window was found to be −150° with liquid nitrogen as coolant. Spectra were obtained with a Perkin-Elmer

(1) Supported by the Advanced Research Projects Agency.

(2) Alfred P. Sloan Fellow.

(3) W. P. Sholette and R. F. Porter, *J. Phys. Chem.*, **67**, 177 (1963).

Model 21 spectrophotometer. Mass spectrometric data[3] show that the equilibrium constant for the reaction

$$^3/_2H_2(g) + (B + B_2O_3) = B_3O_3H_3(g)$$

is of the order of unity at 1400°K. Thus when the H_2 pressure is about 10^{-4} atmosphere the equilibrium pressure of $B_3O_3H_3(g)$ would be about 10^{-6} atm. This most probably represents an upper limit to the pressure since the reaction may not reach complete equilibrium under the flow condition imposed. At these low pressures $B_3O_3H_3(g)$ behaves as a permanent gas and is transported through the vacuum line. Deposits of a dark brown solid appeared at the cooler portions of the quartz tube beyond the reaction zone. This is attributed to condensation of $B_2O_2(g)$ which is also a product of a condensed phase reaction of B and B_2O_3 at high temperatures.[4]

Results

A sample of solid condensed in a U-tube was warmed to room temperature and the $B_2H_6(g)$ evolved was removed by condensing it in a bulb with liquid nitrogen. The quantity of B_2H_6 was determined from its pressure and volume. The residual solid material was then heated to about 185° until decomposition was complete and the additional B_2H_6 was measured. A small residual amount of hydrogen gas could not be removed by trapping with liquid nitrogen. In a typical analysis of a sample obtained in a 6-hr. run it was found that 2.0×10^{-3} mole of B_2H_6 was produced at room temperature and 3.4×10^{-3} mole was obtained upon complete decomposition. In addition 1.43×10^{-3} mole of H_2 and 0.42 g. of solid residue were recovered. It cannot be ascertained whether the hydrogen is formed by direct decomposition of the original solid or by subsequent decomposition of diborane. Previous observations[3] have shown that the solid residue which exhibits a yellow discoloration has a B:O ratio as high as 1:1.38. These data allow us to establish an approximate composition of $B_{1.10}O_{1.00}H_{1.31}$ for the original solid. The departure of this compound from the ideal value for $B_3O_3H_3$ most probably results from the presence of excess B_2H_6 (about 5 mole %) which is formed by decomposition of material deposited on the warmer regions of the system and is condensed with boroxine in the liquid nitrogen trap. A small amount of monohydroxyboroxine, if present, does not appreciably alter the over-all composition. The mass spectral data[3] indicate that this latter compound may be present to less than 10%. The decomposition behavior also indicates that the solid material at room temperature has retained almost 40% of the available B_2H_6 and has a nominal over-all composition of $B_4O_5H_2$. This solid dissolves readily in water with evolution of hydrogen. It also dissolves exothermically in methyl alcohol but is insoluble in $CHCl_3$ and CCl_4.

Solid films for infrared analysis were obtained from the high temperature reaction using $H_2O(g)$ and $D_2O(g)$ as the reactant gases. Spectra were obtained with films maintained at −150°. At this film temperature diborane does not condense for pressures below 1 mm. Frequency measurements are given in Table I. Several features of these spectra are to be noted. The absence of bridged hydrogen and hydroxyl groups is apparent. Hydroxyboroxine which is observed in small concentration in the vapor[3] is apparently not present in significant amount. A frequency corresponding to a B=O stretch in the region of about 2000 cm.$^{-1}$ is also absent. Terminal B–H stretching frequencies are present in the region 2500 to 2650 cm.$^{-1}$. The corresponding frequencies in the B–D spectrum are noticably split into two bands while for the B–H system one band appears only as a shoulder. This splitting is too large to result from a normal ^{10}B isotope effect. The isotope shift is typical of that observed for molecules like $HB(OCH_3)_2$ and $DB(OCH_3)_2$ with the ratio of B–H/B–D frequencies of approximately 1.34.[5] The appearance of two bands in the B–H stretching region will deserve special consideration later. The appearance of two strong bands in the region of 1300–1400 cm.$^{-1}$ is indicative of single bond B–O stretching frequencies. A similar situation exists for the compounds $B_3O_3F_3$[6] and $B_3O_3(CH_3)_3$[7] from which two intense bands in this region have been atrributed to ring stretching frequencies. The isoelectronic molecule $C_3N_3H_3$[8,9] also exhibits two strong ring stretching frequencies. A comparison of these data is given in Table IV. For these frequencies the deuterium isotope shift is small as expected. The broad bands at 903 and 1115 cm.$^{-1}$ may be taken as the B–H out-of-plane and in-plane bending frequencies, respectively. The corresponding frequencies in $HB(OCH_3)_2$ are 910 and 1114 cm.$^{-1}$. Shifts in these bands with deuterium substitutions are quite large although the broadening makes it difficult to locate the exact portion of the shifted band heads.

TABLE I

INFRARED SPECTRA OF SOLIDS CONDENSED FROM GASEOUS PRODUCTS IN THE REACTION OF $H_2O(g)$ AND $D_2O(g)$ WITH A MIXTURE OF B AND B_2O_3 (REACTION TEMPERATURE 1325°K., NaCl WINDOW 120°K.)

Frequency (cm.$^{-1}$) (H_2O reactant)	Intensity[a]	Frequency (cm.$^{-1}$) (D_2O reactant)	Intensity[a]
2620[c]	m	1970	ms
2530	ms	1895	ms
1560	w	...	...
1404	s	1375	s
1335	s	1310	s
1195	ms	1180	ms
1115	sb	1202[b]	s, vb
903	sb	815	s, b

[a] m, medium; ms, medium to strong; s, strong; vs, very strong; b, broad; vb, very broad. [b] Position of band uncertain due to broadening. [c] Shoulder.

TABLE II

PARTIAL VIBRATIONAL ASSIGNMENTS FOR $B_3O_3H_3$ AND $B_3O_3D_3$

Fundamental	Symmetry species[a]	($B_3O_3H_3$) cm.$^{-1}$	($B_3O_3D_3$) cm.$^{-1}$
ν_1(symmetric B–H stretch)	A_1'	2530	1895
ν_6(asymetric B–H stretch)	E′	2620	1970
ν_7(ring stretch)	E′	1404	1375
ν_8(ring stretch)	E′	1335	1310
ν_9(in-plane B–H bend)	E′	1115	(1020)[b]
ν_{11}(out-of-plane B–H bend)	A_2''	903	815

[a] Classification follows procedure of ref. 6 and 9. [b] Uncertain due to peak broadening.

(4) (a) M. G. Inghram, R. F. Porter, and W. A. Chupka, *J. Chem. Phys.*, **25**, 498 (1956); (b) M. D. Scheer, *J. Phys. Chem.*, **62**, 490 (1958).

(5) W. J. Lehmann, T. P. Onak, and I. Shapiro, *J. Chem. Phys.*, **30**, 1215 (1959).

(6) H. D. Fisher, W. J. Lehmann, and I. Shapiro, *J. Phys. Chem.*, **65**, 1166 (1961).

(7) (a) J. Goubeau and D. Hummel, *Z. Physik. Chem.* (Frankfurt), **20**, 15 (1959); (b) W. J. Lehmann, *Spectroscopia Mol.*, **9**, 62 (1960).

(8) J. Goubeau, E. L. Jahn, A. Kreutzberger, and C. Gundmian, *J. Phys. Chem.*, **58**, 1078 (1954).

(9) J. E. Lancaster and N. B. Colthup, *J. Chem. Phys.*, **22**, 1149 (1954).

TABLE III

INFRARED SPECTRA OF ROOM TEMPERATURE DECOMPOSITION PRODUCT OF BOROXINE

Frequency (cm.$^{-1}$) (H_2O reactant)	Intensity[a]	Frequency (cm.$^{-1}$) (D_2O reactant)	Intensity[a]
2600	ms	1950	ms, b
2560	ms	1865	ms
1265(B_2O_3)	vs	1265(B_2O_3)	vs
...	...	1183	ms
1110	s, b	(985)[b]	s, vb
903	s, b	775	m, b
725(B_2O_3)	s, b	725(B_2O_3)	s, b

[a] m, medium; ms, medium to strong; s, strong; vs, very strong; b, broad; vb, very broad. [b] Position of band uncertain due to broadening.

TABLE IV

COMPARSION OF THE RING STRETCHING FREQUENCIES OF $B_3O_3H_3$ AND RELATED COMPOUNDS

Compound	ν_7, cm.$^{-1}$	ν_8, cm.$^{-1}$	Ref.
$B_3O_3H_3$[a]	1404	1335	Present work
$^{11}B_3O_3F_3$	1450	1381	6
$^{11}B_3O_3(CH_3)_3$	1389	1227	7
$C_3N_3H_3$	1560	1410	8, 9

[a] Spectra obtained with samples having the natural boron isotope abundances.

In a series of experiments the liquid nitrogen reservoir was replaced by an oil bath and the solid films were warmed first to room temperature and then successively to 85 and 200°. After the films were maintained at each of these temperatures for a few minutes under vacuum, they were then cooled to room temperature and their spectra were recorded. We also have listed frequencies for the room temperature sample in Table III. Some features of the low temperature spectra are clearly retained by the decomposition product at room temperature. A split in the B–H stretching frequency is quite evident in the latter case while the B–O stretching frequencies are partially masked by the appearance of a strong band at 1265 cm.$^{-1}$ and broad bands at higher frequencies. A new band at 725 cm.$^{-1}$ is also evident in the room temperature spectrum. Spectra of room temperature deuterated samples show marked splittings in the B–D stretching frequencies and a new band at 775 cm.$^{-1}$ which appears to be an out-of-plane B–D bending frequency. The structure between 900–1100 cm.$^{-1}$ is too broad to be of much aid in structure analysis. Bands in the spectra of films heated to 85° were not shifted appreciably from those observed at room temperature although the bands arising from B–H groups were lower in intensity. The spectra of the solid produced at 200° retained only the strong band structure at 1265 cm.$^{-1}$ and the weaker band at 725 cm.$^{-1}$. The spectra of the decomposition products were identical for the hydrogenerated and deuterated sample. This spectrum is very similar to that reported for boric oxide films[10] and that reported by Bauer and Wiberley[11] for the final oxidation product of B_5H_9.

Discussion

On the basis of the observed infrared spectrum of solid $B_3O_3H_3$ and comparison with spectra of its derivatives, $B_3O_3F_3$ and $B_3O_3(CH_3)_3$ it is reasonable to postulate that the basic six-membered ring structure

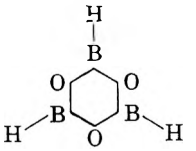

is retained in the solid. For a gaseous molecule with D_{3h} symmetry (as proposed for $C_3N_3H_3$)[8,9] seven infrared active frequencies are predicted from the selection rules. Assuming this symmetry for $B_3O_3H_3$ we would then anticipate only the asymmetrical B–H stretch to be infrared active. The appearance of two fairly intense B–H stretching frequencies require therefore, that the molecule in the solid phase assume a configuration that will give the hydrogen stretching vibrations a dipole component perpendicular to the ring. This indicates that the boron, oxygen, and hydrogen atoms are not coplanar. The influence of lattice interactions on the spectra may be important and the intense broadening of the B–H bending frequencies may reflect this effect. The selection rules for D_{3h} symmetry as assumed in the vibrational assignment (Table II) are therefore not obeyed rigorously. The in-plane and out-of-plane B–O bending frequencies probably occur below 650 cm.$^{-1}$ and are beyond the spectral region studied. The remaining unassigned frequencies listed in Table I may be due to combination bands and to other fundamentals pending a definite symmetry assignment. The asymmetrical B–H stretching frequency (2620 cm.$^{-1}$) is higher than that observed in borane derivatives but corresponds closer to that observed in $B_2O_3H_2$[12] (2667 cm.$^{-1}$) which may also have a ring structure. The infrared spectrum of solid trifluoroboroxine[6] has been interpreted on the basis of a planar structure. In this case, however, resonance interaction of the fluorine atoms with the ring may tend to stabilize the planar configuration. Shifts in the B–D frequencies observed for the solid at room temperature show that structural changes have occurred upon decomposition of the low temperature solid. The higher thermal stability of the decomposition product indicates that this material is not a simple mixture of solid boroxine and boric oxide.

Similarities in the properties of the X–B–O systems (X = H, F, and Cl) may be noted. At low temperatures boroxine, trifluoro-,[13,14] and trichloroboroxine[15] can apparently be isolated as condensed materials. At higher temperatures they undergo thermal decomposition to produce B_2H_6, BF_3, and BCl_3 gases, respectively. At room temperature the solid decomposition product always has a composition ratio of B_2O_3:BX_3 greater than unity. For products from $B_3O_3H_3$, $B_3O_3F_3$, and $B_3O_3Cl_3$ the ratio is about 2.5, 2.1, and 5.0, respectively. These observations suggest an interrelation in the chemical behavior of these compounds. The enhanced thermal stability of the decomposition product from $B_3O_3F_3$ also suggests that structural changes are occurring in the solid during decomposition.

Acknowledgment.—Helpful discussions with Professor A. W. Laubengayer are gratefully acknowledged.

(10) T. A. Sidorov and N. N. Sobolev, *Optika i Spectroskopiya*, **3**, 9 (1958).
(11) W. H. Bauer and S. E. Wiberley, Advances in Chemistry Series No. 32, American Chemical Society, Washington, D. C., 1961, p. 115.
(12) J. F. Ditter and I. Shapiro, *J. Am. Chem. Soc.*, **81**, 1022 (1959).
(13) P. Baumgarten and W. Bruns, *Ber. Chem. Ges.*, **72B**, 1753 (1939).
(14) E. M. Magee, *J. Inorg. Nucl. Chem.*, **22**, 155 (1961).
(15) J. Goubeau and H. Keller, *Z. anorg. allgem. Chem.*, **265**, 72 (1951).

VAPORIZATION PROPERTIES OF IRON PHOSPHIDES[1]

By Gordon Lewis and Clifford E. Myers

State University of New York, College of Ceramics at Alfred University, Alfred, New York

Received December 22, 1962

The equilibrium dissociation of FeP_2, FeP, and Fe_2P to phosphorus vapor and the next lower phosphide has been studied by the effusion method using a direct mass loss technique, employing a vitreous silica helix as a microbalance. A "second law" treatment of the dependence of the dissociation pressure upon temperature yielded the following heats of dissociation per mole of P_2 vapor: FeP_2 $\Delta H^0_{1000} = 70.6 \pm 2$ kcal., $\Delta S^0_{1000} = 52.9 \pm 1$ cal. mole^{-1} deg.$^{-1}$; FeP $\Delta H^0_{1250} = 84.8 \pm 2$ kcal., $\Delta S^0_{1250} = 50.3 \pm 1$ cal. mole^{-1} deg.$^{-1}$; Fe_2P $\Delta H^0_{1350} = 111.2 \pm 2$ kcal. Combination of these data with appropriate data from the literature yielded the following heats of formation of the iron phosphides from solid iron and red phosphorus at 900°K.: Fe_3P, -35.2 kcal. (not determined in this work); Fe_2P, -35.2 ± 2 kcal.; FeP, -28.6 ± 2 kcal.; and $1/2\,FeP_2$, -21.8 ± 2 kcal.

Introduction

The refractory character of some of the iron phosphides, their importance to the iron and steel industry, and their possible use as corrosion resistant electrodes for electro-organic synthesis[2] provide justification for expanding the present meager thermodynamic data for this system. The definitive work on the number and composition of compounds in the system was done by Franke, Meisel, and Juza[3] and Le Chatelier and Wologdine.[4] The phase diagram[5] is shown in Fig. 1. In their study of the iron–phosphorus system, Franke, *et al.*, carried out equilibrium vapor pressure measurements over the two-phase regions, FeP–Fe_2P and FeP_2–FeP. They worked at temperatures (1200–1500°K.) where the vapor pressures of P_2 and P_4 were of the order of millimeters of mercury and varied the composition of the mixtures by their "phosphorus valve" technique. While useful free energies of dissociation were calculated from their data, the temperature ranges (40 and 80°, respectively) were not great enough to give reliable "second law" heats of dissociation. Measurements of the heat capacities and entropies needed for a "third law" calculation have not been reported.

Weibke and Schrag[6] measured the heats of formation at 908°K. of Fe_3P and Fe_2P in a high temperature calorimeter. Their determinations lead directly to the following

$$3Fe(s) + P(s, red) = Fe_3P(s) \qquad \Delta H_{908} = -35.2 \text{ kcal.}$$

$$2Fe(s) + P(s, red) = Fe_2P(s) \qquad \Delta H_{908} = -34.5 \text{ kcal.}$$

The present work was undertaken to extend the dissociation pressure data to lower temperatures in order to obtain meaningful second law heats of dissociation of the iron phosphides. Accordingly, the method chosen was the Knudsen effusion method.[7] The temperature range covered in this study, as well as in the work of Franke, *et al.*,[3] are indicated in Fig. 1. The dissociation of Fe_3P was not studied since the pressures developed below the Fe_3P–Fe eutectic were too low to be measured by the technique used.

(1) This work was supported in part by a grant from the National Science Foundation which the authors are pleased to acknowledge. Partial support for initial phases of the research at Lynchburg College, Lynchburg, Virginia, was provided by the Research Corporation.

(2) D. W. Wood, Ph.D. Thesis, University of Illinois, 1953.

(3) W. Franke, K. Meisel, and R. Juza, *Z. anorg. allgem. Chem.*, **218**, 346 (1934).

(4) H. L. Le Chatelier and S. Wologdine. *Compt. rend.*, **149**, 709 (1910).

(5) M. Hansen and K. Anderko, "Constitution of Binary Alloys," McGraw-Hill Book Co., New York, N. Y., 1958.

(6) F. Weibke and G. Schrag, *Z. Elektrochem.*, **47**, 222 (1941).

(7) M. Knudsen, *Ann. Phys.*, **28**, 999 (1909); **29**, 179 (1909).

Experimental

A quartz-helix microbalance was mounted in a high-vacuum system so that vitreous silica effusion cells (2 cm. high by 2 cm. dia.) could be suspended in a mullite protection tube inserted in a furnace. The system was designed to allow determinations of the mass lost during a run without breaking vacuum. During a run, the background pressure in the system was held below 5×10^{-6} mm. Changes in the extension of the silica spring were measured with a filar-eyepiece microscope. The spring was surrounded by a thermostated water jacket (±0.02°), and that portion of the apparatus containing the spring and microscope was enclosed in a thermostated box (±0.5°). The microbalance system was capable of detecting weight changes of less than 0.03 mg. in a one gram sample. The Kanthal-wound furnace was controlled by a Variac and a Sola constant-voltage transformer. Temperature variation over the course of a run was usually less than ±2°K. The temperature in the vacuum chamber was constant to ±2°K. over a six centimeter region at 1240°K., with an increase in the zone length at lower temperatures. Temperatures were measured by a chromel–alumel thermocouple protected with a fused silica sheath. The thermocouple was calibrated *in situ* under experimental conditions against a previously standardized thermocouple. Above 900°K., an empty cell showed an increase in weight due to carbon deposition on the external surface. This effect was checked over the experimental temperature range, and an appropriate correction (generally less than 1%) was applied to the data.

The iron phosphide mixtures were prepared by two methods: (1) direct synthesis *in vacuo* from iron powder[8] and phosphorus for Fe_2P–Fe_3P and FeP–Fe_2P mixtures, and (2) electrolysis[9] of a molten sodium metaphosphate–iron oxide bath at approximately 1100°K. to obtain FeP and FeP_2. Direct synthesis was accomplished both by distilling phosphorus vapor onto iron at 800–900° and by heating mixtures of iron and phosphorus slowly to 800–900° and holding at temperature for over ten hours. Preparations by the latter technique were made using both technical and semiconductor grade red phosphorus.[10] X-Ray analysis on a General Electric XRD-5 using Co radiation was to establish the phases present before and after a run.

Surface area measurements were carried out on a modified gas chromatography apparatus.[11]

Results and Calculations

At a given temperature, the primary measurement was extension of the silica helix as a function of time. Figure 2 shows selected samples of the experimental data for FeP dissociation for different temperatures and starting materials. At the temperatures where P_2 was the predominates species, a steady pressure was calculated from the least-squares slope of the extension *vs.* time curve by the equation

$$P = \frac{(r)\quad(s)\quad(T/M)^{1/2}}{(44.33 \times 10^3)\,(a)\,(60)}$$

where

(8) Iron sample generously donated by U. S. Steel Corporation.

(9) M. Chêne, *Compt. rend.*, **207**, 571 (1938).

(10) Ultrapure red phosphorus purchased from the American Agricultural Chemical Co.

(11) F. M. Nelsen and F. T. Eggertsen, *Anal. Chem.*, **30**, 1387 (1958).

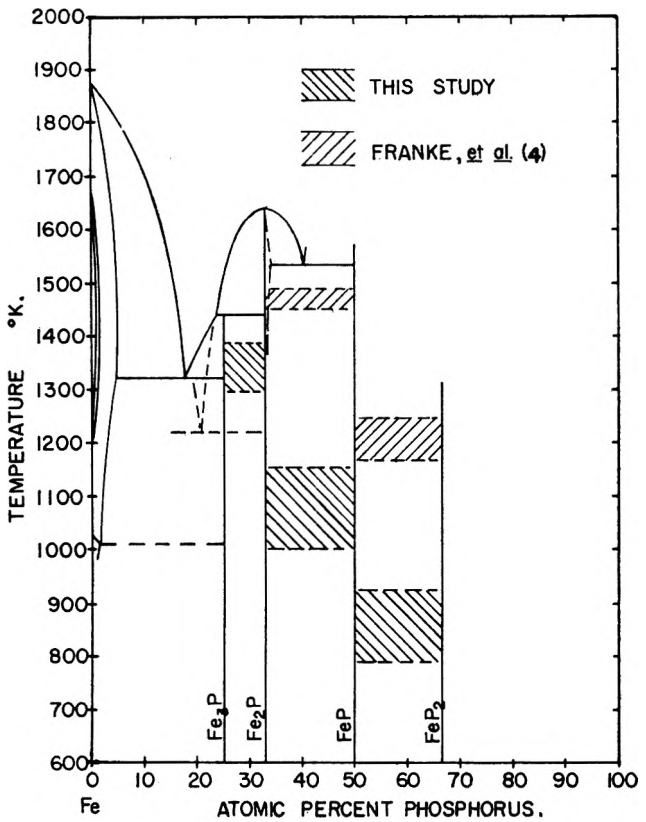

Fig. 1.—Iron–phosphorus phase equilibrium diagram.

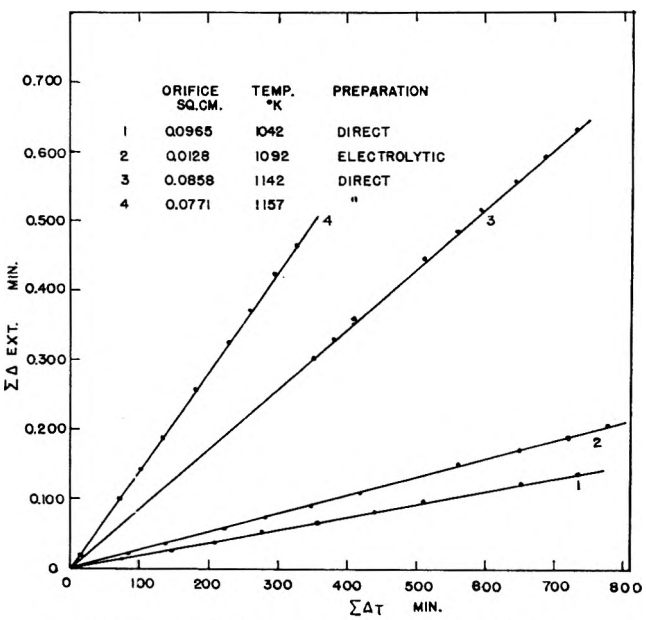

Fig. 2.—Typical raw data: dissociation of FeP.

P = pressure, atmospheres
r = rate of change of the extension of the spring, mm./min.
T = absolute temperature
M = molecular weight of the P_2 molecule
a = orifice area, cm.^{2}
s = sensitivity of spring, mg./mm.

No correction was made for a Clausing factor[12] since the orifices had a "knife-edged" profile. In the temperature range where the effusing vapor was not predominately of one species, the following equation was used with equilibrium constants calculated from the compilation of data by Stull and Sinke[13]

$$P_{(\text{of } P_2)} = \frac{Kp}{2\sqrt{2}}\left[\left\{\frac{1 + 4(r)\ (s)\left(\frac{2T}{M}\right)^{1/2}}{Kp(44.33 \times 10^3)\ (60)\ (a)}\right\}^{1/2} - 1\right]$$

where

M = molecular weight of P_2
Kp = equilibrium constant per mole in atmospheres for the dissociation of P_4.

Professor R. F. Porter, of Cornell University, was kind enough to make a preliminary investigation of the vapor composition above FeP_2, using a mass spectrometer. Although difficulty was encountered with the fragmentation of P_4, the resulting P_2^+/P_4^+ ratios are in general accord with calculated ratios assuming that the gas phase is equilibrated.

The dissociation pressure results for FeP_2 are presented in Table I and are shown graphically in Fig. 3, which also includes the data of Franke and associates.[3] As can be seen from Fig. 3, there is no consistent dependence of calculated pressure on orifice area; hence, it is assumed that the calculated pressures are equilibrium pressures. Furthermore, the lack of curvature indicates that the change in heat capacity is near zero. A least-squares solution of the combined data leads to the following thermodynamic quantities at 900°K.

$$2FeP_2(s) = 2FeP(s) + P_2(g),\ \Delta H^0 = 70.6 \pm 2.0 \text{ kcal.}$$
$$\Delta S^0 = 52.9 \pm 1.0 \text{ cal. mole}^{-1} \text{ deg.}^{-1}$$

Results of effusion studies on the dissociation of FeP are presented in Table II and Fig. 4, which also includes the data of Franke and co-workers.[3] There is no apparent dependence of behavior on preparative technique. It is noted that the calculated pressures with the 0.0965 sq. cm. orifice are consistently lower than with the smaller orifices, among which there is no consistent difference. Accordingly, it was assumed that the data with the large orifice showed the effects of a low vaporization coefficient, while the calculated pressures with smaller orifices are equilibrium pressures. The two points with the large orifice were thus not used in subsequent thermodynamic calculations. Again, ΔC_P appears to be near zero. A least-squares solution of the combined data leads to the following thermodynamic quantities at 1100°K.

$$4FeP = 2Fe_2P(s) + P_2(g),\ \Delta H^0 = 84.8 \pm 2.0 \text{ kcal.}$$
$$\Delta S^0 = 50.3 \pm 1.0 \text{ cal. mole}^{-1} \text{ deg.}^{-1}$$

Data for effusion runs on Fe_2P are given in Table III. In the samples used for the first two orifice sizes, there was X-ray evidence of unreacted iron before runs and of melting during runs; in addition, no Fe_2P was observed after these runs. This behavior was taken to indicate that the phases present in these samples under operating conditions were Fe_3P and liquid.

When the excess iron in these samples was removed by leaching with 6 N hydrochloric acid, the resulting product gave higher pressures and did not show evidence of melting. The sample of Fe_2P prepared with ultrapure red phosphorus did not show evidence of melting and also gave the higher pressures. Hence, only the last six points listed in Table III were con-

(12) P. Clausing, *Ann. Phys.*, **12**, 961 (1932).
(13) D. R. Stull and G. C. Sinke, "Thermodynamic Properties of the Elements," American Chemical Society, Washington, D. C., 1956.

TABLE I

SUMMARY OF RESULTS FOR THE REACTION:

$2FeP_2(s) = 2FeP(s) + P_2(g)$

Temp., °K.	$(Temp.)^{-1}$	Pressure, atm.	$-\text{Log } P$
	Orifice 7.992×10^{-3} cm.^{2}		
825	1.212×10^{-3}	1.24×10^{-7}	6.9073
871	1.148	1.01×10^{-6}	5.9974
873	1.145	1.12×10^{-6}	5.9501
894	1.119	2.33×10^{-6}	5.6324
906	1.104	2.73×10^{-6}	5.5632
	Orifice 8.344×10^{-3} cm.^{2}		
888	1.126	1.78×10^{-6}	5.7503
914	1.094	5.19×10^{-6}	5.2846
	Orifice 10.16×10^{-3} cm.^{2}		
884	1.131	8.28×10^{-7}	6.0817
926	1.080	5.44×10^{-6}	5.2647
	Orifice 63.03×10^{-3} cm.^{2}		
804	1.244	3.09×10^{-8}	7.5096
825	1.212	8.10×10^{-8}	7.0916
827	1.209	8.33×10^{-8}	7.0793
841	1.189	1.49×10^{-7}	6.8276
844	1.185	1.92×10^{-7}	6.7171
	Orifice 117.2×10^{-3} cm.^{2}		
787	1.271	5.60×10^{-9}	8.2251
805	1.242	1.94×10^{-8}	7.7113
827	1.209	6.37×10^{-8}	7.1810
	Orifice 117.2×10^{-3} cm.^{2}		
805	1.242	1.86×10^{-8}	7.7294
805	1.242	1.64×10^{-8}	7.7839

TABLE II

SUMMARY OF RESULTS FOR THE REACTION:

$4FeP(s) = 2Fe_2P(s) + P_2(g)$

Temp., °K.	$(Temp.)^{-1}$	Pressure, atm.	$-\text{Log } P$	Preparation technique
	Orifice 1.332×10^{-3} cm.^{2}			
1123	8.904×10^{-4}	3.22×10^{-6}	5.4924	Direct combination
1152	8.680	9.11×10^{-6}	5.0405	(D.C.)
	Orifice 4.623×10^{-3} cm.^{2}			
1075	9.302	4.57×10^{-7}	6.3402	(D.C.) (Ultrapure)
1118	8.945	1.99×10^{-6}	5.7005	
	Orifice 7.706×10^{-3} cm.^{2}			
1051	9.515	2.26×10^{-7}	6.6449	D.C.
1086	9.209	1.02×10^{-6}	5.9922	
1116	8.959	2.65×10^{-6}	5.5775	
1157	8.646	9.72×10^{-6}	5.0123	
	Orifice 8.593×10^{-3} cm.^{2}			
1070	9.345	3.83×10^{-7}	6.4163	D.C. (almost all FeP)
1098	9.108	1.07×10^{-6}	5.9702	
1142	8.756	5.22×10^{-6}	5.2820	
	Orifice 12.75×10^{-3} cm.^{2}			
1002	9.982	3.80×10^{-8}	7.4199	Electrolytic preparation
1092	9.158	1.06×10^{-6}	5.9732	
	Orifice 96.51×10^{-3} cm.^{2}			
1000	10.000	1.78×10^{-8}	7.7503	D.C.
1042	9.596	9.81×10^{-8}	7.0084	

sidered significant. The temperature range of these points was too small to give meaningful heat and entropy values from the slope and intercept of a "second law" plot. However, since the calculated entropies

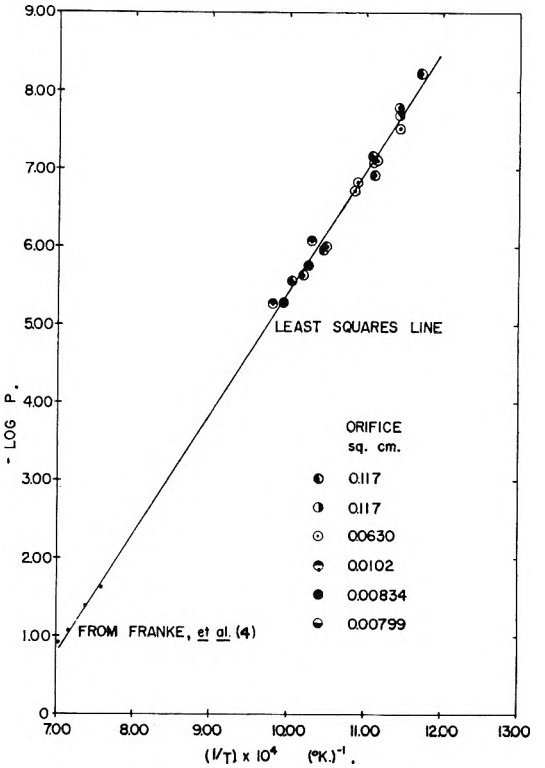

Fig. 3.—Second law plot for the reaction: $2FeP_2(s) = 2FeP(s) + P_2(g)$.

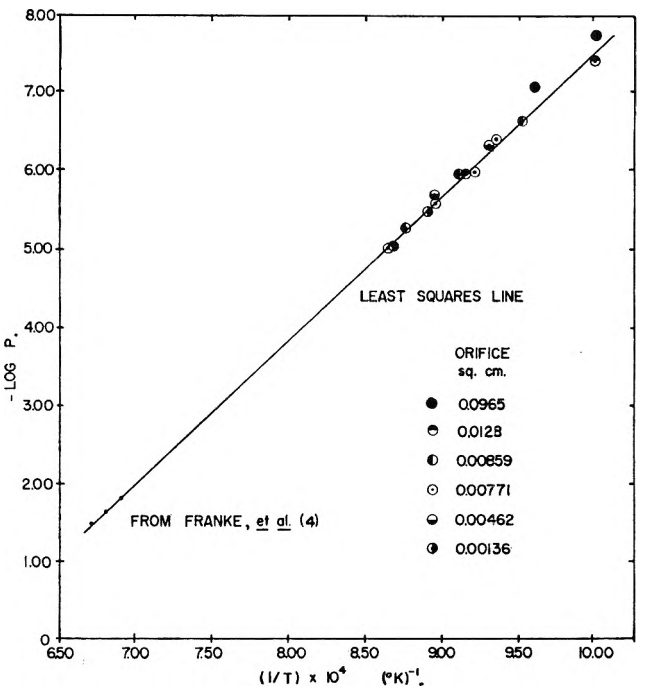

Fig. 4.—Second law plot for the reaction: $4FeP(s) = 2Fe_2P(s) + P_2(g)$.

from the dissociations of FeP_2 and FeP appeared to be nearly the same within experimental error, it was assumed that the entropy of dissociation of Fe_2P would be closely approximated by the average of these two values, *i.e.*, 51.6 cal. mole^{-1} deg.$^{-1}$. Heats of dissociation were then calculated as shown in Table III.

The heats of dissociation of FeP_2, FeP, and Fe_2P obtained above were combined with the calorimetric heat of formation of Fe_3P given by Weibke and Schrag[6] and the heat of vaporization of red phosphorus[13] to obtain the heats of formation of the iron phosphides

TABLE III

SUMMARY OF RESULTS FOR THE REACTION:

$$6Fe_2P(s) = 4Fe_3P(s) + P_2(g)$$

Temp., °K.	Pressure, atm.	−Log P	ΔH_T^{0a} (kcal.)	Preparation technique
	Orifice 6.971×10^{-3} cm.²			
1363	1.01×10^{-7}	6.9968		D.C.
1364	1.31×10^{-7}	6.8815		
1384	1.76×10^{-7}	6.7546		
	Orifice 8.112×10^{-2} cm.²			
1330	6.70×10^{-8}	7.1736		D.C.
1365	1.64×10^{-7}	6.7842		
	Orifice 8.345×10^{-3} cm.²			
1295	4.82×10^{-8}	7.3166	110.2	D.C. ultra-pure
1330	7.47×10^{-7}	6.8731	110.5	
1376	1.81×10^{-7}	6.7423	113.4	
	Orifice 10.06×10^{-3} cm.²			
1332	1.18×10^{-7}	6.9312	111.0	D.C. *Fe removed*
1334	1.52×10^{-7}	6.8183	110.4	
1365	2.73×10^{-7}	6.5643	111.4	
	av. of values		111.2 ± 2.0 kcal.	

[a] Calculated with average entropy: $\Delta S_{av}^0 = 51.60$ cal. mole^{-1} deg.$^{-1}$.

listed in Table IV. The values obtained by Weibke and Schrag are included for comparison. The good agreement for Fe_2P should be noted.

TABLE IV

HEATS OF FORMATION OF IRON PHOSPHIDES AT 900°K. FROM IRON AND RED PHOSPHORUS

	This work	Weibke and Schrag[6]
1/2 FeP_2	−21.8 kcal.	
FeP	−28.6	
Fe_2P	−35.2	−34.5 kcal.
Fe_3P		−35.2

The two non-equilibrium runs on the dissociation of FeP provide the basis for a rough estimate of the vaporization coefficient for this process, by use of Speiser and Johnston's equation[14] where α is the

$$\alpha = \frac{a}{A}\left(\frac{P_{ss}}{P_{eq} - P_{ss}}\right)$$

vaporization coefficient, A is the effective vaporizing surface area, a is the orifice area, P_{eq} is the equilibrium pressure, and P_{ss} is the observed steady-state pressure. Now the gross sample area is an upper limit and the cell cross-sectional area is a lower limit to the effective vaporizing surface area, and the values on the least-squares line may be taken as the equilibrium pressures. α is thus estimated to be between 4×10^{-5} and 6×10^{-2} for the dissociation of FeP.

Discussion

The treatment of the experimental data outlined above was predicated on the assumptions of narrow, near stoichiometric homogeneity ranges and a constancy of compositional limits of the phases. Wood[2] did not find any noticeable changes in composition of phosphides with temperature of preparation, and the analyzed compositions were well within 1% of theoretical. Furthermore, there was no observed difference in the positions of X-ray diffraction lines of FeP in the FeP_2–FeP or FeP–Fe_2P regions, and similarly, the positions of the X-ray lines of Fe_2P were the same in both the FeP–Fe_2P and Fe_2P–Fe_3P regions. Hence, it would appear that the assumptions regarding homogeneity and composition are justified.

While no great error is involved in taking the entropy of an ordered alloy as being the sum of the entropies of the components,[15] the applicability of this procedure to semimetallic compounds is problematical. If the assumption is made that the atomic entropies of iron and phosphorus are the same, respectively, in each iron phosphide, a reasonable value for the atomic entropy of phosphorus is not obtained. Under the above assumption, the atomic entropy of phosphorus is given by

$$S_P = \frac{S^0(P_2) - \Delta S^0}{2}$$

where S_P is the atomic entropy of phosphorus in an iron phosphide, $S^0(P_2)$ is the entropy of the gaseous dimer, and ΔS^0 is the average entropy change during reaction, determined experimentally. This leads to an atomic entropy of phosphorus, at 298°K., near zero. This is unlikely, and implies that the assumption regarding the constancy of the respective atomic entropies is not valid for the iron phosphides.

While this research was not directly oriented toward an elucidation of the evaporation mechanism, some inferences can be drawn as to which step may be rate determining. The pertinent observations are the linearity, over long period of time, of the $\Sigma\Delta$ext *vs.* $\Sigma\Delta t$ plots, and the apparent equilibration between P_2 and P_4 in the gas phase. Effusion is the rate-controlling step in the equilibrium runs. Bulk diffusion is not likely to be the rate-controlling step in the non-equilibrium runs since there is no diminution of steady-state pressure as the diffusion path becomes longer. Because of the long mean free path of the gaseous molecules, it is problematical whether there are sufficient gas-phase molecular collisions to account for the apparent equilibration between P_2 and P_4. If it is assumed that the number of gas-phase collisions is insufficient, then P, P_2, and P_4 must be in equilibrium on the surface prior to desorption, and the desorption step cannot then be rate determining since the same rates would not be expected for both P_2 and P_4. Also, the equilibration step must be relatively fast, if it occurs on the surface, since P_2 and P_4 would not appear in equilibrium amounts if it were slow. Thus, it appears likely that the rate-controlling step for large orifices involves the promotion of phosphorus atoms from the bulk to the surface layer.

The heats of formation of the iron phosphides calculated from the results of this study show that these compounds are more stable than corresponding carbides and nitrides, are of comparable stability with other phosphides and sulfides, and are less stable than corresponding oxides.

(14) R. Speiser and H. L. Johnston, *Trans. Am. Soc. Metals*, **42**, 283 (1950).

(15) O. Kubaschewski and E. L. Evans, "Metallurgical Thermochemistry," Pergamon Press, 1958.

CHARACTERIZATION OF COUNTERION DISTRIBUTION IN POLYELECTROLYTE SOLUTIONS. II. THE EFFECT OF THE DISTRIBUTION OF ELECTROSTATIC POTENTIAL ON THE SOLVOLYSIS OF CATIONIC ESTERS IN POLYMERIC ACID SOLUTION[1,2]

BY H. MORAWETZ AND J. A. SHAFER

Department of Chemistry, Polytechnic Institute of Brooklyn, Brooklyn, N. Y.

Received December 22, 1962

A polyion is expected to inhibit reactions of two low molecular weight species if one is positively and the other negatively charged, while reactions of two species carrying charges of the same sign should be accelerated. The theory of the effect as a means to characterize the distribution of electrostatic potential in polyelectrolyte solutions is developed. The effect is then demonstrated on the inhibition of the hydroxyl ion-catalyzed hydrolysis of cationic esters carrying one and two positive charges by partially ionized polycarboxylic acids. The data are interpreted on the basis of a simple model for the polyelectrolyte solution, in which a region containing a uniform density of fixed charges is in Donnan equilibrium with a region from which the fixed charges are excluded.

In previous communications from this Laboratory[2,3] it was pointed out that the rates of reactions involving two charged low molecular weight species should be affected by the uneven distribution of electrostatic potential in solutions containing polymeric ions. A comparison of the rates of such reactions in conventional buffers and in polyelectrolyte solutions should, therefore, yield a parameter related to the distribution of the potential. Using then reactions involving different combinations of charged species it should, in principle, be possible to obtain a number of parameters from which the counterion distribution could be approximated to a high degree of precision. In the present work these ideas were applied to the hydroxyl ion-catalyzed hydrolysis of singly and doubly charged cationic esters in buffers and solutions of polymeric acids.

Theory

Consider a second-order reaction involving species A and B which carry m and n unit charges, respectively. Assume that these species are added to a polyelectrolyte solution at such low concentration that the distribution of the electrostatic potential ψ is not altered significantly. The local concentration at a point characterized by a potential ψ is then

$$C_A = C_A^0 x^m$$

$$C_B = C_B^0 x^n$$

$$x = \exp\,[-e\psi/kT] \qquad (1)$$

where e is the magnitude of the electronic charge, k is the Boltzmann constant, and T the temperature.

In any small volume element the reaction rate will depend on the local reagent concentration. Since no work is carried out against the field of the polyion in bringing the two reagents together to form the transition-state complex, the reaction rate constant in any volume element will be equal to the intrinsic rate constant k^0 observed in simple electrolyte solutions at low ionic strength. The observed rate R will then be

$$R = k^0 \langle C_A C_B \rangle = k^0 C_A^0 C_B^0 \langle x^{m+n} \rangle \qquad (2)$$

where the square brackets indicate an averaging process over the volume of the system. But the observed rate constant k is conventionally expressed in terms of the volume average concentration of the reagents

$$R = k \langle C_A \rangle \langle C_B \rangle = k C_A^0 C_B^0 \langle x^m \rangle \langle x^n \rangle \qquad (3)$$

Comparing (2) and (3) we obtain for the relationship of the intrinsic and the observed rate constant

$$k^0/k = \langle x^m \rangle \langle x^n \rangle / \langle x^{m+n} \rangle \qquad (4)$$

Qualitatively, this result predicts $k > k^0$ if m and n have the same sign, while $k < k^0$ if the signs of the charges carried by the reagents are opposite. This may be understood by considering that reagents of the same sign are concentrated into the same region of space, being either attracted or repelled by the polyion. If the reagents carry charges of opposite sign, the polyion will tend to separate them, since it will attract one and repel the other.

If we have data for only one combination of m and n, we have to assume the general form of the distribution of x and eq. 4 will then yield one parameter characterizing that distribution. Obtaining then data for reagents of other charge types, we obtain other ratios of volume average values of various powers of x which will allow us to refine gradually our model, so that all the parameters can be fitted simultaneously.

In interpreting the data from the present investigation, we used a model in which the vicinity of each polyion contains a sufficient excess of counterions over by-ions to render the region electroneutral. The mobile ions in the polymer regions may then be assumed to be in Donnan equilibrium with the electrolyte in that part of the system from which the polyions are excluded. The applicability of such a model to polyelectrolyte solutions has been discussed by many workers.[4-8] We have used as a first approximation a model in which the fixed charge densities have a constant value p in the region containing the polyions, so that the electrostatic potential has only two values defined as $\psi_0 = 0$ outside and $\psi = \psi_i$ inside the regions containing the polyions corresponding to $x_0 = 1$ and

(1) This research was supported by grants of the Office of Naval Research and the National Institutes of Health. It is part of a Ph.D. thesis to be submitted by J. A. Shafer to the Graduate School of the Polytechnic Institute of Brooklyn in June, 1963.

(2) Part I of this series: *J. Polymer Sci.*, **42**, 125 (1960).

(3) H. Morawetz and E. W. Westhead, Jr., *ibid.*, **16**, 273 (1955).

(4) G. E. Kimball, M. Cutler, and H. Samelson, *J. Phys. Chem.*, **56**, 57 (1952).

(5) P. J. Flory, *J. Chem. Phys.*, **21**, 162 (1953).

(6) F. Oosawa, N. Imai, and I. Kagawa, *J. Polymer Sci.*, **13**, 93 (1954).

(7) F. T. Wall and J. Berkowitz, *J. Chem. Phys.*, **26**, 114 (1957).

(8) S. Lifson, *ibid.*, **27**, 700 (1957).

$x = x_i$, respectively. If the fraction of the total volume assigned to the regions containing polyions is φ and if the system contains only polyions with univalent counterions and a uni-univalent electrolyte of a volume average concentration s, then the electrolyte concentration s_0 outside the polymer region is obtained from

$$s = s_0 [(1 - \varphi) + \varphi x_i] \quad \text{(cationic polymers)}$$

$$s = s_0 [(1 - \varphi) + \varphi x_i^{-1}] \quad \text{(anionic polymers)} \quad (5)$$

From the requirement of equal chemical potential of the mobile ions inside and outside the polymer regions

$$s_0^2 = s_0 x_i (s_0 x_i + p) \quad \text{(cationic polymer)}$$

$$s_0^2 = s_0 x_i^{-1} (s_0 x_i^{-1} + p) \quad \text{(anionic polymers)} \quad (6)$$

Solving (6) for x_i, we obtain then

$$x_i = [-p + (p^2 + 4s_0^2)^{1/2}]/2s_0 \quad \text{(cationic polymers)}$$

$$x_i^{-1} = [-p + (p^2 + 4s_0^2)^{1/2}]/2s_0 \quad \text{(anionic polymers)} \quad (7)$$

We may then use the x_i values from (7) in relation 4, so that the ratio of the intrinsic and the observed rate constant will be interpreted in terms of the model for the polyelectrolyte solution described above by

$$k^0/k = [(P/p)x_i^m + 1 - (P/p)] [(P/p)x_i^n + 1 - (P/p)]/[(P/p)x_i^{m+n} + 1 - (P/p)] \quad (8)$$

since $\varphi = P/p$ where P is the bulk average concentration of fixed charges.

We may note that for any experimental value of s and P the value of x_i depends only on the choice of p, so that the rate constant ratio k^0/k is also a function of this single adjustable parameter.

Results and Discussion

To test the theory outlined in the previous section and to use it in the characterization of the distribution of electrostatic potential in polyelectrolyte solutions, we have studied the effect of four polymeric acids, PMA, PAA, PAA/MA, and PVME/MA, on the hydroxide ion catalyzed hydrolysis of esters I, II, and III.

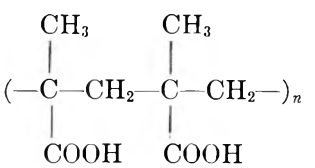

PMA

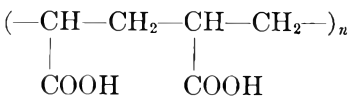

PAA

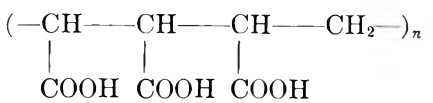

PAA/MA

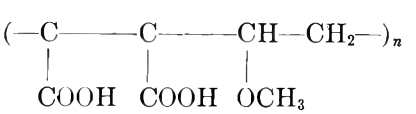

PVME/MA

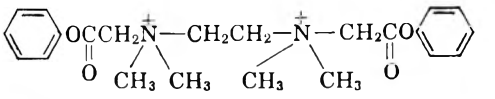

I

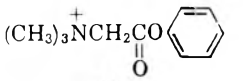

II

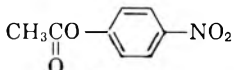

III

In the case of reagent I carrying two ester functions the two steps of the hydrolysis are characterized by different rate constants designated as k_1 and k_2. It was found that k_1 was reduced substantially below the value k_1^0 observed in buffer solution, when a polymeric acid was added to the system, while k_2 was reduced below k_2^0 by a much smaller factor. Qualitatively, this is the expected pattern of behavior, since the polyanions will interact much more powerfully with the unreacted reagent with its doubly positive charge than with the half-reacted species IV which has a net charge of only

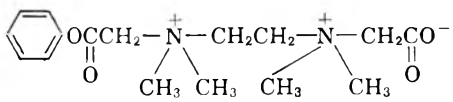

IV

+1. Table I lists inhibition factors k_1^0/k_1 and k_2^0/k_2 for the reaction of ester I in PMA solutions at a pH of 7.87 and at varying concentrations of added simple electrolyte. The trend of k_1^0/k_1 is also illustrated in Fig. 1. The inhibition effect decreases sharply with increasing counterion concentration reflecting the decreasing electrostatic potential in the neighborhood of the polyion. It may be noted that this happens in spite of a slight increase in the degree of ionization α of the polyion as salt is being added to the system while the pH is kept constant. It is estimated that α rises from a value of 0.75 at the lowest electrolyte concentration employed, to about 0.97 in solutions containing 0.3 N sodium ion.

TABLE I

THE EFFECT OF COUNTERION CONCENTRATION ON THE EFFICIENCY OF 0.01 N PMA AS AN INHIBITOR IN THE HYDROLYSIS OF (I) AND (IV)[a]

$T = 25.8°$; pH 7.87 ± 0.04; $\alpha \geq 0.75$

Counterion concn. (moles/l.)	k_1^0/k_1	k_2^0/k_2
0.0099	5.20	1.98
.0125	4.37	1.61
.0325	2.14	1.35
.0575	1.43	1.20
.1093	1.17	0.98
.3156	1.09	1.01

[a] k_1^0 and k_2^0 correspond to the rate constants for k_1 and k_2 in the absence of polymer and at the same pH at which k_1 and k_2 were measured.

Table II illustrates the effect of polyion charge density and charge distribution on the inhibition factor in the absence of simple electrolyte. As would be expected, PAA/MA which carries three ionizable carboxyls for four carbon atoms in the chain backbone as against one carboxyl on every second backbone atom of PMA, is a more powerful inhibitor if the two polymeric acids are compared at equal degrees of ionization. The effect of the charge density along the chain backbone on the inhibition factor is shown in Fig. 2. It

TABLE II

THE EFFECT OF SOME POLYANIONS ON THE HYDROLYSIS OF (I) IN THE ABSENCE OF ADDED SIMPLE ELECTROLYTE

Polymer	Concn. (base moles/l.)	α	Charges per backbone atom	pH	Inhibition factor[a]
MA	0.0100	0.333	0.167	6.62	1.65
PMA	.0100	.667	.333	7.54	3.43
PMA	.100	.667	.333	6.83	1.03
PAA	.0100	.667	.333	7.42	4.23
PMA	.0100	.750	.375	8.02	6.68
PVME/MA	.0100	.750	.375	9.05	21.6
PAA/MA	.0112	.591	.443	7.88	12.3
PAA/MA	.0112	.668	.501	8.67	26.3

[a] Calculated from k_1^0/k_1, where k_1^0 is calculated from the equation $k_1^0 = 4.8 \times 10^{-1} + (1.28 \times 10^{-10})/(H^+)$ and k_1 is the observed rate constant for the hydrolysis of (I) at 25.8°.

may be seen that on this basis the effect of PMA, PAA, and PAA/MA appear to be quite similar, while PVME/-MA falls sharply out of line. This can be easily understood since neighboring carboxyl groups are not expected to ionize in PAA/MA if the degree of ionization is below two-thirds. In this range, the charge distribution will, therefore, be similar at equal charge densities for PAA/MA, PMA, and PAA. By contrast, carboxyls attached to neighboring atoms of the chain backbone must ionize in PVME/MA for degrees of ionization above 0.5 (*i.e.*, at charge densities higher than 0.25 per atom of the chain backbone), resulting in higher values of the local electrostatic potential. The larger effect on reaction kinetics observed with polyions deviating further from a uniform distribution of ionizable groups along the chain is a consequence of the same situation which leads for such polyanions to a steeper titration curve.

Before considering in greater detail the quantitative interpretation of the inhibition by the polyanions of the hydroxide-catalyzed hydrolyses of the cationic esters, we have to assess the possible contribution of non-electrostatic forces to the formation of molecular association complexes between the polyanion and the ester. This was done by comparing the rate of basic hydrolysis of *p*-nitrophenyl acetate (III) in buffer solution and in 2/3 ionized PAA/MA. These two rates were found to be identical within the experimental error, indicating that the fluctuations in the local concentration of the uncharged ester are negligible.

Applying now eq. 7 and 8 to the hydroxide ion catalyzed hydrolysis of the doubly charged cationic ester I (*i.e.*, $m = +2, n = -1$) we obtain for the inhibition factors k_1^0/k_1 at a constant counterion concentration as a function of the bulk average concentration of fixed charges P a family of curves, each corresponding to a given value of p, the assumed concentration of fixed charges within the region assigned to the polyelectrolyte. The relation of these theoretical curves to the observed inhibition factors in solutions containing 2/3 ionized PAA/MA and counterion concentrations of 0.0367 and 0.0184 N, respectively, is shown in Fig. 3. For both counterion concentrations, the experimental data fall into the range between the curves calculated for $p = 0.2$ and $p = 0.3$ N. Our model can now be tested by comparing the inhibition factor which would be predicted for the hydrolysis of the singly charged cationic ester II with that observed under conditions where the values given above for the parameter p are applicable. It can be seen in Table III that the values of p which fit the results with the doubly charged ester lead to a calculated inhibition factor which agrees closely with that observed with the singly charged ester II.

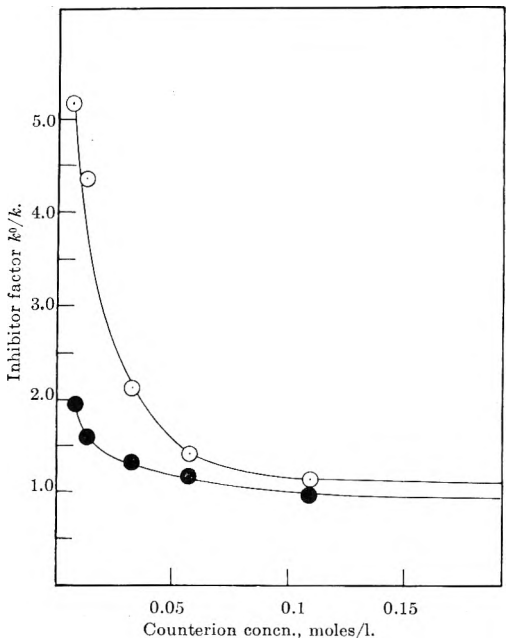

Fig. 1.—The effect of counterion concentration on the inhibition of the hydrolysis of cationic esters by PMA. Ester I, ⊙; ester IV, ●. PMA concn. 0.01 N, temp. 25.8°, pH 7.87 ± 0.04, $\alpha \geq 0.75$.

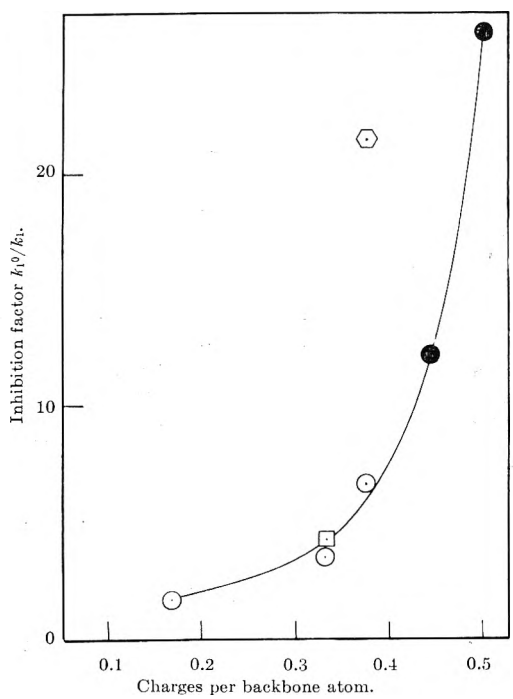

Fig. 2.—The effect of polyanion charge density on the hydrolysis rate of ester I. PMA, ⊙; PAA, ⊡; PAA/MA, ●; PVME/MA, ⊙. Polyanion concn. 0.01 N, temp. 25.8°, no simple electrolyte added.

It has been pointed out by Strauss and Ander[9] that the radius of curvature of a polyion chain is generally large compared to the distance over which the forces due to the fixed charges affect the distribution of the counterions in the presence of a simple electrolyte. They have therefore proposed that when treating the polyelectrolyte solution as a Donnan system, the region assigned

(9) U. P. Strauss and P. Ander, *J. Am. Chem. Soc.*, **80**, 6494 (1958).

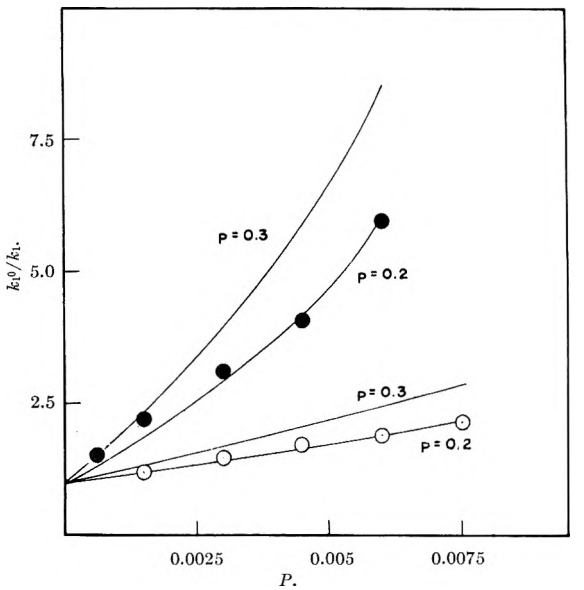

Fig. 3.—Dependence of inhibition factor on the concentration of 2/3 neutralized PAA/MA. $[Na^+]$ = 0.0367, ⊙; $[Na^+]$ = 0.0184, ●. Temp. 1.8°. Full lines calculated from equations 5–8.

TABLE III

THE EFFECT OF 0.0112 *N* PAA/MA ON THE HYDROLYSIS OF SOME ESTERS[a]

$\alpha \backsim 2/3$, pH = 8.96 ± 0.02

Ester	Temp., °C.	Obsd. inhibition factor k^0/k	Calcd. inhibition factor from eq. 7 and 8 p = 0.2 *M*	p = 0.3 *M*
p-Nitrophenyl acetate	25.8	1.00	1.00	1.00
N,N,N-Trimethyl-2-acetoxyphenyl-ammonium cation	1.8	1.18	1.17	1.19
Ester IV	1.8	1.16	1.17	1.19
Ester I	1.8	2.13	2.12	2.83

[a] Cation concentration = 0.0367 *M* Na^+, k^0 was obtained within 0.03 unit of the pH at which k was measured. The value of k^0 was corrected to the pH at which k was measured by assuming that k^0 is proportional to hydroxide ion concentration in this range.

to the fixed charges should be represented by a cylinder whose radius r is given by

$$r = d - S/\kappa \qquad (9)$$

where d is the radius of the rod representing the polyion, κ is the Debye–Hückel parameter, and S is a constant close to unity. Basing the calculations of κ on the concentration of mobile ions[10] we obtain for the counterion concentrations of 0.0184 and 0.0367 *N* with the polyelectrolyte concentrations used, values of $1/\kappa$ ranging from 23.9 to 24.8 Å. and 16.2 to 17.0 Å., respectively. These values may be compared to r = 32 Å. corresponding to a cylindrical region within which the fixed charge concentration p is 0.2 *N* and a radius of r = 26 Å. corresponding to p = 0.3 *N*. In these calculations the charge density of the polyanion is based on an all-*trans* conformation of the chain backbone. Considering the uncertainties of the proper values of d and S the agreement of r with $1/\kappa$ may be considered satisfactory.

Yet another check of our analysis is available in a comparison of the observed inhibition factors with the titration behavior of the polymeric acid used as an inhibitor. The titration of polymeric acids may be represented by[11]

$$K_{app} = K^0 \exp(-e\psi/kT) = K^0 x_i \qquad (10)$$

where K_{app} is the apparent ionization constant given by

$$K_{app} = (H^+)\alpha/(1 - \alpha) \qquad (11)$$

while K^0 is the intrinsic ionization constant to be expected in the absence of the electrostatic interaction of the charges of a polyion. The x_i values corresponding to the inhibition factors observed in this study lead to predicted $pK_{app} - pK^0$ values of 1.4 or less, while potentiometric titration gave for 2/3 neutralized PAA/MA $pK_{app} - pK^0$ = 3.5. This discrepancy indicates that the Donnan model is not adequate for predicting the titration behavior in this case. Qualitatively this is not surprising, since the small hydrogen ion can approach the polyion much more closely (and thus can penetrate to regions of much higher electrostatic potential) than the bulky ester reagent. It should also be noted that the treatment outlined above for the interpretation of the effect of a polyion on the reaction rate of a multiply charged reagent does not take into account the spatial separation of the charges carried by the reagent. The limitations of such a treatment have become apparent in a recent investigation of the dialysis equilibrium involving polyanions and bis-quaternary ammonium ions, which indicates that the interaction of a polyion with a bolaform counterion is quite sensitive to the spacing of the two cationic charges.[12]

Experimental

Materials.—The preparation of phenyl 2-bromoethanoate, ethylene bis-[N,N-dimethyl-N-(phenyl)-carboxymethylammonium] bromide, and the copolymerization of acrylic acid and maleic anhydride are described elsewhere.[13] Poly-(methacrylic acid)(PMA) was prepared by heating (1.5 hours under nitrogen at 60°) 120 ml. of methacrylic acid with 350 mg. of azobisisobutyronitrile in 550 ml. of butanone. The resulting polymer was collected by suction filtration, washed repeatedly with ether, and freeze-dried from a water solution. Poly-(acrylic acid) (PAA) was prepared by heating (2 hours under nitrogen at 60°) 100 ml. of acrylic acid in 700 ml. of benzene containing 500 mg. of azobisisobutyronitrile. The same procedure employed to collect and purify poly-(methacrylic acid) was also used here. The copolymer of vinyl methyl ether and maleic anhydride (PVME/MA) was from General Aniline and Film Corp. (Batch No. 31).

N,N,N-Trimethyl-N-(phenyl)-carboxymethylammonium Bromide.—Anhydrous trimethylamine (4.0 g., 0.068 mole) was added to phenyl 2-bromoethanoate (4.0 g., 0.019 mole) in 50 ml. of dry acetone (dried over type 4A molecular sieve). After 1 hour the precipitated product was filtered and washed with acetone (dec. 197–198°).

Anal. Calcd. for $C_{11}H_{16}BrNO_2$: C, 48.19; H, 5.88; Br, 29.15; N, 5.11. Found: C, 48.20; H, 5.96; Br, 29.05; N, 5.20.

Polyacid Solutions.—The letter *N* when used to indicate concentrations, refers to the normality of carboxyl groups in the solution. In all cases only sodium and ester cations were present. When the counterion concentration exceeded the concentration of the formally ionized carboxyls on the polyanion, the excess counterions were introduced from stock solutions of partially neutralized sodium hydrogen phosphate and partially neutralized boric acid. The degree of neutralization of these acids was such that these stock solutions had a pH equal to the final pH of the polyacid solution.

(10) A. Katchalsky and S. Lifson, *J. Polymer Sci.*, **11**, 409 (1956).

(11) J. T. G. Overbeek, *Bull. soc. chim. Belges*, **57**, 252 (1948).

(12) H. Morawetz and A. Kandanian, in preparation.

(13) H. Morawetz and J. Shafer, *Biopolymers*, **1**, 71 (1963).

The pH measurements were made with a Cambridge Research Model pH meter.

The symbol α refers to the ratio of equivalents NaOH added to equivalents of carboxyl originally present.

Poly-(acrylic acid–maleic acid) 1–1 copolymer stock solution (0.1128 N) was prepared by dissolving poly-(acrylic acid–maleic anhydride) 1–1 copolymer (6.400 g., 0.1128 carboxyl equivalent) in a 1 liter volumetric flask and making up to volume with de-ionized water. The solution was then kept in a 85° bath overnight to hydrolyze the anhydride groups.

3/4-Neutralized Poly-(vinylmethyl ether–maleic acid) Copolymer Stock Solution (0.100 N).—The anhydride copolymer was dried to constant weight in a vacuum oven and 3.90 g. (0.05 carboxyl equivalent) was placed in a 500-ml. volumetric flask containing 17.53 ml. of 2.139 M (0.0375 mole) sodium hydroxide. De-ionized water (approximately 350 ml.) was added to the flask. The flask was then kept in a 60° bath overnight in order to hydrolyze the anhydride groups. The solution was cooled to room temperature and filled to volume with de-ionized water.

Rate Measurements.—In the case of the cationic esters, release of phenol was followed by the rise in the optical density at 273 mμ on a Beckman DU spectrophotometer. A special water-jacketed cylindrical cell equipped with a mechanical stirrer-designed to prevent bubble formation was used. The cell was 10 cm. long and had a capacity of 50 ml. An aliquot of the ester stock solution (in the neighborhood of 0.1 ml.) was introduced by means of a blow-out pipet to start a kinetic run. Prior to each run stock solutions of esters I and II were prepared in 0.01 N HCl and methanol, respectively. In the 10 cm. cell, esters I and II were present in concentrations of 0.6 mg./50 ml. and 0.7 mg./50 ml., respectively.

The rate of disappearance of p-nitrophenyl acetate was followed at 273 mμ. The test solution containing 0.64 mg. of the ester in 50 ml. was thermostated and at various time intervals aliquots were removed from the flask. The optical densities were measured in a 1 cm. cell.

In all cases the temperature was controlled to at least 0.05°.

Kinetics.—The hydrolysis of I in basic solution may be depicted by

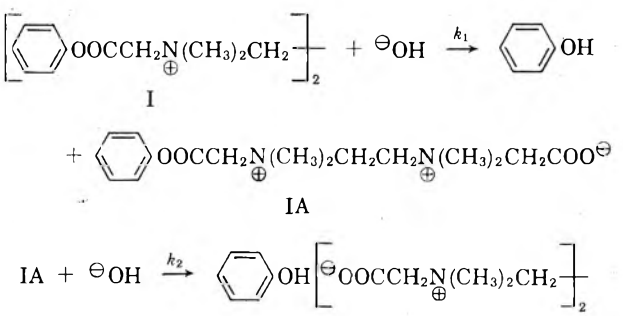

For the two consecutive reactions shown above, the fraction of ester groups (E) at any time (t) is given by[14]

$$E = \frac{C_E}{2C_0} = (1 - \gamma)\exp[-k_1 t] + \gamma \exp[-k_2 t]$$

where C_E represents the molar concentration of ester bonds, C_0 the molar concentration of (I) at $t = 0$ and $\gamma = k_1/2$ ($k_1 - k_2$). The fraction of ester bonds at any time was calculated from the optical density D of the solution

$$D = C_E e_E + (2C_0 - C_E)e_p + U$$

where e_E and e_p are the extinction coefficients associated with the ester bonds, and with phenol, respectively, and U is the optical density due to background which is unaffected by the reaction.

The initial slope of a plot of $-\ln(D_\infty - D)$ against time (where D_∞ is the optical density at the conclusion of the reaction) equals $k_1/2$, and the final slope is equal to k_2 if $k_1 > k_2$ and to k_1 if $k_2 > k_1$. Although the initial slopes could be used to give good estimates of k_1, the final slopes could not be used for an accurate estimate of k_2, because k_1/k_2 was not large enough to observe the disappearance rate of ester bonds in II without some contribution from I. Thus, the method of initial slopes was used when only values of k_1 were desired. In order to calculate easily both k_1 and k_2 a graphical method was employed in which the observed dependence of $\ln E$ on t was compared with curves calculated for various values of γ.

As expected, the pseudo-first-order rate constants of ester hydrolysis in conventional buffer solutions varied with hydrogen ion concentration according to

$$k = k_{(H_2O)} = \frac{k_{(OH)}K_W}{(H^+)}$$

In order to represent the data, the following values were taken for $k_{(H_2O)}$ and $k_{(OH)}$. At 25.8°

Ester I, $k_{(H_2O)} = 4.8 \times 10^{-4}$ sec.$^{-1}$,

$k_{(OH)}K_W = 1.28 \times 10^{-10}$ l. mole^{-1} sec.$^{-1}$

Ester IV, $k_{(H_2O)} = 1.0 \times 10^{-4}$ sec.$^{-1}$,

$k_{(OH)}K_W = 0.375 \times 10^{-10}$ l. mole^{-1} sec.$^{-1}$

The kinetics of the hydrolysis of esters II and III in buffer solution were first order. Plots of $-\ln(D_\infty - D)$ were linear in time, and were used to obtain the pseudo-first-order rate constants.

(14) A. A. Frost and R. G. Pearson, "Kinetics and Mechanism," John Wiley and Sons, New York, N. Y., 1953, p. 153.

ADSORPTION STATISTICS AND THE PHYSICAL PROPERTIES OF TRANSITION METAL CATALYSTS

BY CHARLES P. POOLE, JR.

Gulf Research & Development Company, Pittsburgh, Pennsylvania

Received December 26, 1962

The number of small clusters of transition metal ions formed on an alumina surface by adsorption from solution was calculated from a statistical model, and the resulting variation of clusters with metal content was correlated with electron spin resonance, nuclear magnetic resonance, magnetic susceptibility, and gas adsorption data for alumina impregnated with chromium, cobalt, and nickel salts.

I. Introduction

Over the past few years several members of this Laboratory have been studying catalysts prepared by impregnating silica, alumina, and silica–alumina with transition metal oxides. For example, chromia on alumina was studied by electron spin resonance,[1,2] magnetic susceptibility,[3] nuclear magnetic resonance (n.m.r.),[4] and catalytic techniques[5]; cobalt on alumina was studied by magnetic susceptibility,[6] X-ray ab-

(1) D. E. O'Reilly, *Advan. Catalysis*, **12**, 31 (1960).

(2) D. E. O'Reilly and D. S. MacIver, *J. Phys. Chem.*, **66**, 276 (1962).

(3) J. R. Tomlinson and G. T. Rymer, Preprints, Division of Petroleum Chemistry, American Chemical Society National Meeting, April 5–10, 1959, Boston, Mass.

(4) D. E. O'Reilly and C. P. Poole, Jr., to be published.

(5) J. M. Bridges, D. S. MacIver, and H. H. Tobin, Paper No. 110, Second International Congress on Catalysis, Paris, France (July, 1960).

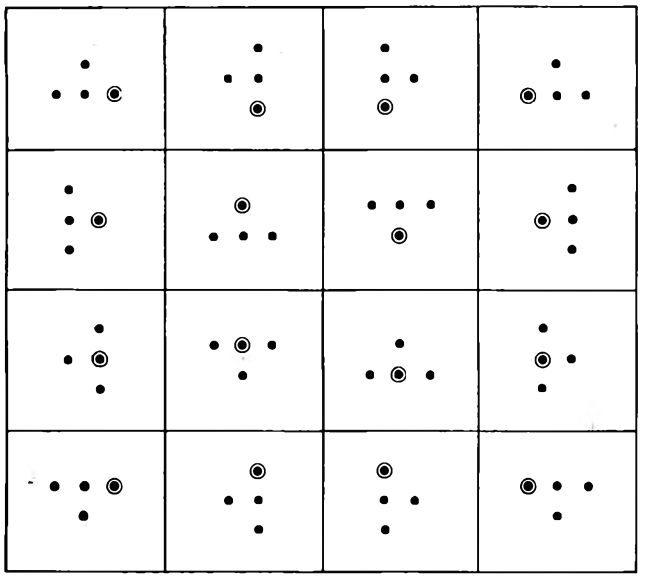

Fig. 1.—Various possible arrangements of three ions (●) around a particular ion (◉) to form the Q_T cluster.

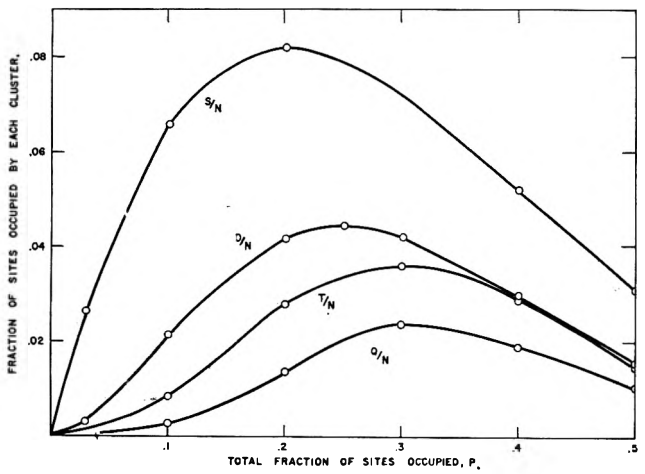

Fig. 2.—Fraction of sites occupied by single (S/N), double (D/N), triple (T/N), and quadruple (Q/N) isolated clusters for a plane square lattice.

sorption edge spectroscopy,[7] nuclear magnetic resonance,[4] and chemical kinetics[6]; nickel on alumina was studied by magnetic susceptibility,[8] nuclear magnetic resonance,[4] and chemical kinetics.[8] At low chromium concentrations the electron spin resonance spectra of reduced chromia on alumina[1,2] were produced by isolated Cr^{+3} ions (δ-phase Cr^{+3}) and at high chromium concentrations the spectra were produced by "clumped" Cr^{+3} ions (β-phase). Intermediate concentration spectra were superpositions of these two cases. The cobalt on alumina and nickel on alumina catalysts each showed the presence of a low concentration δ-phase and a high concentration β-phase; these phases are discussed in detail in references 6 and 8. More recently these phases have been studied in coprecipitated chromia–alumina.[9]

The purpose of this note is to show that such a two-phase behavior is expected if it is assumed that the metal ions are adsorbed randomly on available alumina surface sites during the impregnation process. The theory of random adsorption will be developed in section II; it will be compared with experiment in section III and discussed in section IV. In section V several concluding remarks will be made.

(6) J. R. Tomlinson, R. O. Keeling, Jr., G. T. Rymer, and J. M. Bridges, Paper No. 90, Second International Congress on Catalysis, Paris, France (July, 1960).

(7) R. O. Keeling, Jr., *J. Chem. Phys.*, **31**, 279 (1959).

(8) G. T. Rymer, J. M. Bridges, and J. R. Tomlinson, *J. Phys. Chem.*, **65**, 2152 (1961).

(9) C. P. Poole, Jr., W. L. Kehl, and D. S. MacIver, *J. Catalysis*, **1**, 407 (1962).

II. Theory

It is assumed that the base or adsorbent contains N adsorption sites and that PN metal ions are adsorbed randomly on PN of these sites, where P is the fraction of the sites covered by the metal ions. Multilayer adsorption will not be considered for the present. The probability of a given site being unoccupied is $(1 - P)$. In a square plane lattice, each site has four nearest neighbors, so the probability S/N finding a given site occupied by an isolated adsorbed ion is the probability of the site being occupied (P) times the probability of the four nearest neighbors being unoccupied $(1 - P)^4$. The number of isolated metal ions S is therefore

$$S = NP(1 - P)^4 \qquad (1)$$

for a square lattice, and

$$S = NP(1 - P)^6 \qquad (2)$$

for a plane triangular lattice which has six nearest neighbor sites. Similar expressions may be obtained for the number of ions in isolated pairs D, triplets T, and quadruplets Q, and these are listed in Table I. As an illustration of how a complicated formula from this table is derived, consider Q_T for the square lattice. The probability of occupying a particular lattice site with an ion is P and the probability of occupying three more previously designated sites to form this cluster is P^3. The probability that the eight nearest neighbor sites to the cluster are empty is $(1 - P)^8$, so $P^4 (1 - P)^8$ is the probability of finding this particular cluster. Now once the site under consideration is occupied there are sixteen ways in which three nearby sites may be occupied to form Q_T, as shown in Fig. 1, so the probability must be multiplied by 16, as shown in Table I. Figure 2 shows a graph of the fraction of ions in single, double, triple, and quadruple sites for the plane square lattice. Similar graphs have been given for three dimensional lattices by Behringer.[10]

The formulas in Table I were checked by observing that the sum of all possible clusters is NP, and therefore the sum $S + D + T + Q$ cannot contain terms in P^2, P^3, and P^4. This check ensures that no clusters are omitted. It will be useful to notice that these formulas may be used for the number of unoccupied sites by interchanging P and $(1 - P)$.

All of the formulas in Table I are of the form $KP^m \cdot (1 - P)^n$ where K is a constant, so the value of $P = P_{mn}$ which corresponds to a maximum in the number of sites occupied by a given cluster is obtained by the formula

$$\frac{d}{dP}\left[KP^m (1 - P)^n\right] = 0 \qquad (3)$$

with the solution $P = P_{mn}$ given by

$$P_{mn} = \frac{m}{m + n} \qquad (4)$$

(10) R. E. Behringer, *J. Chem. Phys.*, **29**, 537 (1958).

TABLE I

NUMBER OF ADSORBED ATOMS IN SINGLE S, DOUBLE D, TRIPLE T, AND QUADRUPLE Q ISOLATED GROUPS

Plane triangular lattice

$S = NP(1-P)^6$

$D = 6NP^2(1-P)^8$

$T_0 = 6NP^3(1-P)^9 = P(1-P)D$

$T_1 = 9NP^3(1-P)^{10} = 3/2(1-P)T_0$

$T_< = 18NP^3(1-P)^{10} = 2T_1$

$T = T_0 + T_1 + T_<$

$Q_0 = 12NP^4(1-P)^{10} = 4PT_1/3$

$Q_1 = 12NP^4(1-P)^{12} = (1-P)^2Q_0$

$Q_\triangle = 48NP^4(1-P)^{11} = 4(1-P)Q_0$

$Q_\frown = 24NP^4(1-P)^{12} = 2Q_1$

$Q_N = 24NP^4(1-P)^{12} = 2Q_1$

$Q_< = 48NP^4(1-P)^{12} = 4Q_1$

$Q_\lambda = 8NP^4(1-P)^{12} = 2/3\,Q_1$

$Q = Q_0 + Q_1 + Q_\triangle + Q_\frown + Q_N + Q_< + Q_\lambda$

Plane square lattice

$S = NP(1-P)^4$

$D = 4NP^2(1-P)^6 = 4P(1-P)^2S$

$T_L = 12NP^3(1-P)^7 = 3P(1-P)D$

$T_1 = 6NP^3(1-P)^8 = 1/2(1-P)T_L$

$T = T_1 + T_L$

$Q_0 = 4NP^4(1-P)^8 = 2/3PT_1$

$Q_T = 16NP^4(1-P)^8 = 4Q_0$

$Q_L = 32NP^4(1-P)^9 = 8(1-P)Q_0$

$Q_1 = 8NP^4(1-P)^{10} = 2(1-P)^2Q_0$

$Q_N = 16NP^4(1-P)^8 = Q_T$

$Q = Q_0 + Q_T + Q_L + Q_1 + Q_N$

On a square lattice, for a given size cluster (given m) a single linear chain has the lowest P_{mn} and a square has one of the largest P_{mn} values (a configuration which more closely approximates a circle has a larger P_{mn} than a square) as shown in Table II. Figure 3 shows the variation with cluster size of these two P_{mn} values and the analogous quantities for a triangular lattice. For each lattice the average P_{mn} for all clusters of a given size will lie between the corresponding limits on the graph, and Fig. 2 illustrates such average maxima for T and Q clusters. The symbols S_0, D_0,. . .will be used to denote the maximum in the number of sites occupied by atoms in the corresponding clusters S, D,. . ., and for isolated atoms we have $m = 1$, and

$$S_0 = NP_{1n}(1 - P_{1n})^n \qquad (5)$$

For the square lattice where $n = 4$

$$S_0 = 0.082N \text{ and } P_{14} = 1/5$$

while for the triangular lattice where $n = 6$, we have

$$S_0 = 0.057 \text{ and } P_{16} = 1/7$$

at their respective maxima.

TABLE II

VALUES OF P_{mn} FOR FOUR TYPES OF CLUSTERS

The Quantity k is defined by the expression $m = \sum_{j=1}^{k} j$

Lattice type	Arrangement of atoms	P_{mn}
Plane square	In single straight line	$\frac{m}{3m+2}$
Plane square	In square	$\frac{m}{m+4\sqrt{m}}$
Plane triangular	In single straight line	$\frac{m}{3m+4}$
Plane triangular	In equilateral triangle	$\frac{m}{m+3(k+1)}$

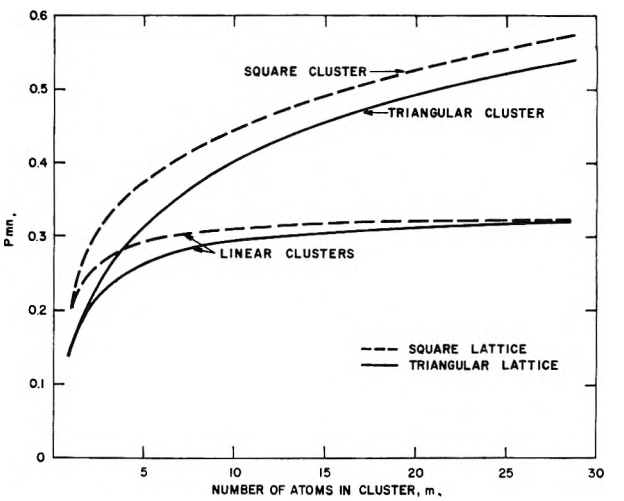

Fig. 3.—Variation of P_{mn} with cluster size m for four particular cluster shapes.

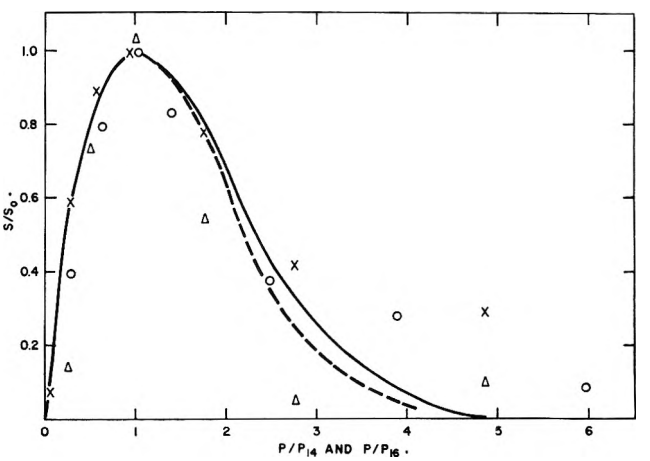

Fig. 4.—Comparison of plane square lattice (------) and plane triangular lattice (——) theoretical curves with experimental data from the Cr^{+3} δ-phase detected by the e.s.r. of reduced Cr/Al_2O_3 (X), from the Al^{27} n.m.r. of reduced Cr/Al_2O_3 (Δ) and from the Co^{+2} δ-phase detected by the magnetic susceptibility of Co/Al_2O_3 (O).

III. Comparison with Experiment

A. Electron Spin Resonance and Magnetic Susceptibility Data.—As mentioned above, the electron spin resonance spectrum from alumina impregnated with a low concentration of chromia originates from isolated Cr^{+3} ions.[1,2] The present theory may be compared with these experimental data by normalizing the experimental results in such a way that both the abscissa and ordinate in the graph of the number of isolated Cr^{+3} atoms against the chromium concentration are set equal to one at the maximum point. For the present case this maximum corresponds to 8.1×10^{19} spins/g. and 2.1 weight % chromium.[2] The normalized experimental data are given on Fig. 4, and they are

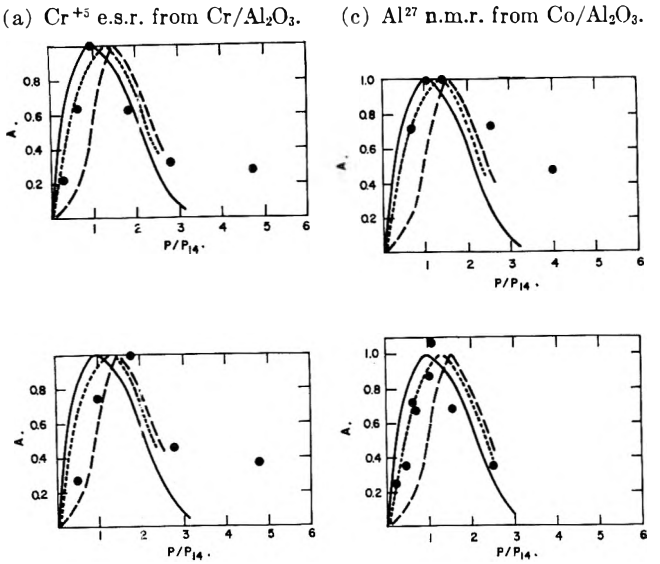

Fig. 5.—Comparison of theoretical curves with Cr^{+5} (γ-phase) e.s.r. and Al^{27} n.m.r. data for oxidized samples. In the figure $A = S/S_0$ (——), $A = (S + D + T + Q)/(S + D + T + Q)_0$ (....) and $A = Q/Q_0$ (------) where A is normalized to unity at its maximum and plotted against P/P_{14} for a square planar lattice.

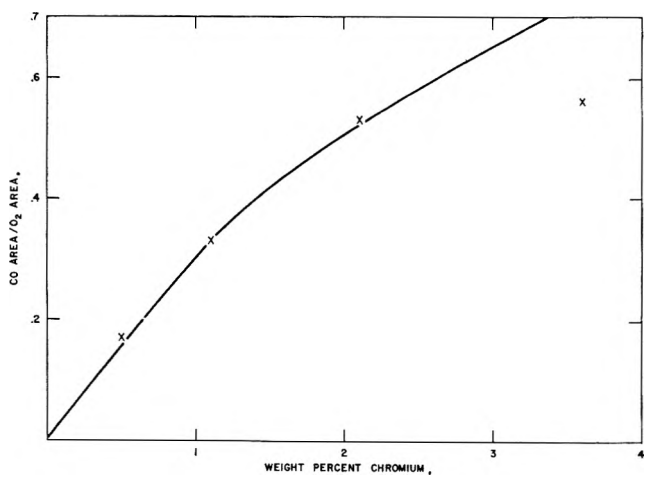

Fig. 6.—A comparison of the calculated (——) and measured (x) ratios of CO to O_2 surface areas. The CO/O_2 surface areas are assumed to be proportional to the ratio of the number of sites available for double site to that available for single site adsorption.

compared with the theory by plotting on the same figure S/S_0 *vs.* P/P_{1n} for the plane square ($n = 4$) and plane triangular ($n = 6$) lattices. It will be noticed that the theory agrees with the experiment except at high chromium concentrations. The Cr^{+5} (γ-phase) e.s.r. data obtained after oxidizing these samples produce a maximum at 2.1 wt. % Cr, and these data were normalized in the same way and plotted on Fig. 5a.

The low concentration magnetic susceptibility data for cobalt on alumina were normalized in a similar way with $S_0 = 1.17$ wt. % Co and plotted on Fig. 4. These data agree with the theory at low cobalt concentrations and deviate at high concentrations.

B. Nuclear Magnetic Resonance Data.—When alumina is impregnated with a transition metal, the amplitude of the Al^{27} n.m.r. absorption envelope at first decreases with increasing metal content, reaches a minimum, and then increases for higher concentrations.[4] The decrease in Al^{27} amplitude was attributed by O'Reilly and Poole to the removal from detection of Al^{27} nuclei near small clusters of transition metal ions. The number of aluminum nuclei removed from detection by chromium, cobalt, and nickel ions was normalized to the maximum number and the resulting data are plotted on Fig. 5b, 5c, and 5d for the oxidized samples, and in Fig. 4 for reduced Cr/Al_2O_3. The values of S_0 used were 2.1, 1.17, and 4.3 wt. % Cr, Co, and Ni, respectively. The data show a general qualitative agreement with the theoretical curves except at high metal concentrations.

C. Gas Adsorption Data.—Bridges, MacIver, and Tobin have shown that the amount of oxygen adsorbed at 77°K. on a chromia–alumina surface is proportional to the Cr_2O_3 surface area,[5] and the lower areas obtained by CO adsorption were attributed by them to a two-site adsorption mechanism.[11] In Fig. 6 their experimental points for the ratio of the surface area from CO adsorption to that from O_2 adsorption are plotted against the chromium concentration and the data are seen to fit the curve computed for the ratio of the number of chromium ions available for double-site adsorption to the number available for single-site adsorption. This double site calculation was made with the plane square lattice and assumes that cluster D can adsorb one CO molecule, Q_0 can adsorb two, Q_T can adsorb one, etc. Again the high concentration point deviated from the curve.

IV. Discussion

The simple assumption that the alumina surface contains randomly distributed transition metal ions has allowed us to calculate the distribution of various small clusters as a function of the transition metal concentration. The dispersed or δ-phase Cr^{+3} and Co^{+2} concentrations detected by e.s.r. and magnetic susceptibility correlate quite well except at relatively high metal concentrations with the theoretical curve S/S_0 for isolated ions, as Fig. 4 indicates. The high concentration deviations occur because during the impregnation process most of the metal ions are adsorbed directly from low concentration impregnating solutions, while as the solution concentration increases, more and more of the total number of metal ions originate from the solution which is trapped in the pores and evaporated during the drying process, as previously noted by Rymer, Tomlinson, Keeling, and Bridges.[6,8] This latter mechanism probably results in multilayer adsorption and explains the deviations from the theory at high metal concentrations.

Oxidized chromia on alumina samples contain Cr^{+5} ions (referred to as the γ-phase) with a maximum concentration of 1.6×10^{19} spins/g. at 2.1 wt. % Cr and a concentration dependence similar to that of the δ-phase, but with only a fifth of the number of spins. Because the δ-phase Cr^{+3} spins are insensitive to oxidation, while both the bulk or β-phase and the γ-phase are oxidation dependent, O'Reilly and MacIver associated the Cr^{+5} ions with the β-phase[1,2] which is most susceptible to oxidation when in rather small clusters. Figure 5a indicates that the Cr^{+5} ions may predominate in small clusters of chromic ions. Again the 5 wt. % Cr point deviates due to condensation of chromium in the pores.

The magnetic susceptibility data of the $Ni–Al_2O_3$

(11) D. S. MacIver and H. H. Tobin, *J. Phys. Chem.*, **64**, 451 (1960).

system did not allow a calculation of the δ-phase as a function of concentration, but the δ-phase was detected in this work.[8]

It was previously deduced[4] that the Al^{27} n.m.r. signal from transition metals on alumina is affected by small clusters of metal ions on the surface. The suitably normalized Al^{27} results presented on Fig. 4 and on Fig. 5b, 5c, and 5d show a general qualitative agreement with the theoretical curves except at high concentrations, and this supports the postulated origin of the Al^{27} n.m.r. results. The data shown in Fig. 5 scatter much more than those shown in Fig. 4. When the $Cr–Al_2O_3$ sample is oxidized, the maximum in the number of aluminum nuclei relaxed beyond detection shifts to larger chromia concentrations in the manner shown on Fig. 4 and 5b, and this may originate from the partial oxidation of medium size clusters of chromium. Figure 3 shows that for clusters larger than the Q cluster the maximum P_{mn} changes only very slowly with the number of atoms m in the cluster, so the fit of theoretical curves to experimental data becomes insensitive to m.

The metal concentration S_0 for the maximum in the δ-phase was 1.17, 2.1, and 4.3 for the three ions Co^{+2}, Cr^{+3}, and Ni^{+2}, respectively, and this indicates that the amount of surface accessible to each ion is not the same. Part of this difference may result from the use of separate alumina preparations in each series. Sacconi[12] had discussed the order of adsorption of various cations when their solutions are passed through an alumina chromatographic column, but this order differs from the variation in S_0 observed for the three cations discussed above. Gas adsorption studies of chromia–alumina catalysts[5,9] showed that less than 20% of the total alumina area is available for adsorbing chromium. The present treatment assumed random adsorption on those regions of the alumina surface which are accessible to the metal ions.

(12) L. Sacconi, *Discussions Faraday Soc.*, **7**, 173 (1949).

When silica is put in an aqueous solution of Ni^{+2} it does not appreciably adsorb the nickel, in contrast to the strong adsorption that occurs on alumina.[8] The magnetic susceptibility measurements of cobalt catalysts[6] indicate that the cobalt concentration which produces a maximum in the δ-phase on silica is less than one-fifth as large as that which produces a δ-phase maximum on alumina. One may conclude that silica has considerably fewer adsorption sites for adsorbing these transition metals than alumina has. This makes it very difficult to obtain experimental data on a silica base for comparison with the theory, and at the present time such data are not available. It would be particularly instructive to study a series of silica alumina–transition metal catalysts from the viewpoint of this paper.

V. Conclusions

By making the assumption that transition metal ions are randomly adsorbed from an impregnating solution on an alumina surface, and that the distribution of these ions remains random after drying and calcination, it has been possible to explain a large body of experimental data. For example, electron spin resonance, magnetic susceptibility, and nuclear magnetic resonance data give δ-phase spin concentrations which correlate quantitatively with the number of isolated single ions computed from the theory, and the $CO–O_2$ adsorption data agree with the ratio of the number of chromium double sites to the total number of chromium sites on a $Cr–Al_2O_3$ surface. The theory breaks down at high metal concentrations due to the condensation from solution left in the pores.

Acknowledgment.—The author wishes to thank Dr. D. S. MacIver, Dr. Joanne M. Bridges, Dr. J. R. Tomlinson, Dr. D. E. O'Reilly, Mr. G. T. Rymer, and Mr. H. H. Tobin for helpful discussions of their experimental data.

ENERGY VOLUME RELATIONS OF OCTAMETHYLCYCLOTETRASILOXANE AND ITS MIXTURES WITH CARBON TETRACHLORIDE

By Marvin Ross and Joel H. Hildebrand

Department of Chemistry, University of California, Berkeley, California

Received January 9, 1963

Values of $(\partial P/\partial T)_V$ have been determined for octamethyltetrasiloxane, $c\text{-}Si_4O_4(CH_3)_8$, over the range from 22 to 45°. At 25° and a molal volume of 312.02 cc., it is 7.879 atm. deg.$^{-1}$, and $(\partial E/\partial V)_T$ is 56.88 cal. cc.$^{-1}$. If, following the suggestion of Frank, we set the potential energy of a liquid $E = -a/V^n$, then $(\partial E/\partial V)_T = na/V^{n+1}$ and $n = V(\partial E/\partial V)_T/\Delta E^v$, where ΔE^v is energy of vaporization. The second expression yields $n = 2.3$ and the third $n = 1.38$, instead of $n = 1$ for a van der Waals liquid. Both values are consistent with an intermolecular potential of the Kihara type. Values $(\partial E/\partial V)_T$ for mixtures of this siloxane with CCl_4 are only slightly greater than additive on a volume fraction basis, differing as expected from the mixture, $n\text{-}C_6H_{12}$ + $n\text{-}C_6F_{12}$, investigated by Dunlap and Scott.

The purpose of this research is that stated by Hildebrand and Scott[1] in their recent book, "for practical purposes," the most useful theory is likely to be the one which is built "close to the ground," and which evaluates its parameters under conditions closely approximating those where they will be applied. For this reason, we prefer to relate the properties of liquid solutions to those of pure liquids, rather than to dilute gases at very different densities and temperatures.

Of these parameters, $(\partial E/\partial V)_T$, which we will call internal pressure, is one of the most significant, and is also easy to determine with precision, because it can be calculated from $(\partial P/\partial T)_V$, which is constant over a wide range of pressure. Extensive data for pure liquids

(1) J. H. Hildebrand and R. L. Scott, "Regular Solutions," Prentice-Hall, Inc., Englewood Cliffs, New Jersey, 1962.

and their mixtures are now available.[2-7] In earlier papers, rather good agreement was reported between observed values of $(\partial E/\partial V)_T$ for mixtures and those calculated from the same function for the pure components when the calculation was based upon the old Berthelot relation, the geometric mean between the van der Waals a's, $a_{12} = (a_1a_2)^{1/2}$ and[7a] $(\partial E/\partial V)_T = a/V^2$.

Smith and Hildebrand[5] found, however, that the exponent of V, as obtained by comparing $(\partial E/\partial V)_T$ with the energy of vaporization per cc., the "energy density," increases with increasing molecular size, becoming 2.49 for C_7F_{16} and 2.44 for c-$C_6F_{11}CF_3$ (*vide infra*). Our early value[2] of the exponent for CCl_4, 2.09, has been confirmed by Benninga and Scott.[7] It is obvious that the dimensions of the "constant," a, change with the exponent, and that the simple Berthelot relation is no longer appropriate. It seems important, therefore, to express the value of $(\partial E/\partial V)_T$ for mixtures in terms of the same function for the pure components, and to increase the rigor of the test by using components for which the volume dependence is very different. We chose mixtures of CCl_4 and octamethylcyclotetrasiloxane, c-$Si_4O_4(CH_3)_8$. The latter consists of a core, c-Si_4O_4, well buried under eight methyl groups. It is quasi-spherical in form. We have used it in other studies[8-11] of the effects of disparity in molal volumes.

Experimental

The apparatus was essentially the same as that used by Smith and Hildebrand.[5] The temperature of the bath was controlled within 0.1°; the temperature inside the bomb fluctuated about 0.03°. A P–T point was considered acceptable when four make-and-break cycles agreed to 0.01°. The previously calibrated Heise–Bourdon gage could be read to ±0.1 atmosphere. Metal rings of the sort used in distillation columns were placed in the space between the cell and the walls of the bomb in order to hasten thermal equilibrium.

The octamethylcyclotetrasiloxane was from the stock used in previous investigations that had kindly been donated by the General Electric Company. Its purity was estimated from its melting point to be 99.6%. The CCl_4, of C.P. grade, was distilled over Drierite and allowed to stand over mercury.

From 5 to 8 points were determined on the P–T line for each volume. The range was from 1 to from 100 to 140 atm. The root mean square deviation is 0.01°. The observed values of $(\Delta P/\Delta T)_V$ were corrected in the usual manner for the compression of the glass.

Results

The results for pure c-$Si_4O_4(CH_3)_8$ are given in Table I. The values of the molal volume were calculated from the densities published by Hurd.[12] The values of $(\partial P/\partial T)_V$ represent the corrected slopes of the ΔP–ΔT lines. The figures for $(\partial E/\partial V)_T$ were calculated by the equation

$$\left(\frac{\partial E}{\partial V}\right)_T = T\left(\frac{\partial P}{\partial T}\right)_V - P \qquad (1)$$

The figures for the compressibility, β, were obtained by dividing $(\partial P/\partial T)_V$ by the coefficient of expansion. The value interpolated for 25.0°, 1.543×10^{-4}, is near the figure obtained by Shinoda and Hildebrand,[6] 1.56×10^{-4}.

Results for two mixtures of the siloxane with CCl_4 of mole fraction x_1 are given in Table II. For the internal pressure of pure CCl_4, needed for dealing with the mixtures, we use the data of Benninga and Scott.[7] We measured the densities of the two mixtures with the results

$$x_{CCl_4} = 0.500,\ d = 1.1354 - 1.350 \times 10^{-3}t \text{ g./cc.} \qquad (2)$$

$$x_{CCl_4} = 0.7627,\ d = 1.2989 - 1.530 \times 10^{-3}t \text{ g./cc.} \qquad (3)$$

We calculated the excess molal volumes of the mixtures to be 0.8 cc. at $\phi_1 = 0.500$ and −0.4 at $\phi_1 = 0.237$.

TABLE I

RESULTS FOR PURE c-$Si_4O_4(CH_3)_8$

t, °C.	v, cc. mole^{-1}	$(\partial P/\partial T)_V$, atm. deg.$^{-1}$	$(\partial E/\partial V)_T$, cal. cc.$^{-1}$	$10^4\beta$, atm.$^{-1}$	n
22.26	311.09	8.030	57.45	1.511	1.385
24.45	311.93	7.905	56.96	1.537	1.385
25.00	(312.02)	(7.879)	(56.88)	(1.543)	(1.38)
29.56	313.90	7.663	56.19	1.595	1.390
35.65	316.27	7.271	54.37	1.691	1.375
44.84	319.91	6.726	51.80	1.844	1.350

TABLE II

RESULTS FOR MIXTURES OF (1) CCl_4, (2) c-$Si_4O_4(CH_3)_8$

x_1	ϕ_1	t, °C.	v	$(\partial P/\partial T)_V$	$(\partial E/\partial V)_T$ Exptl.	$(\partial E/\partial V)_T$ Calcd.
1.000	1.0000	25.00	97.09	11.22	81.04	...
0.763	0.500	25.00	148.92	9.69	69.97	68.96
.763	.500	31.76	...	9.19	67.87	...
.500	.237	24.57	204.29	8.82	63.60	...
.500	.237	25.00	(204.56)	(8.786)	63.46	62.60
0	0	25.00	312.02	7.879	56.88	...

Discussion

(a) **The Pure Siloxane.**—We begin by analyzing the data for the pure siloxane in the way first proposed by Frank[13] and applied by Smith and Hildebrand.[5] The potential energy of the liquid is assumed to vary with volume in accord with the expression

$$E = -a/V^n \approx -\Delta E^v \qquad (4)$$

where ΔE^v is energy of vaporization. If n is constant, differentiation gives

$$(\partial E/\partial V)_T = na/V^{n+1} \qquad (5)$$

and, for molal quantities, v and E^v

$$n = v(\partial E^v/\partial V)/\Delta E^v \qquad (6)$$

We may obtain a value of n by means of eq. 5 from the slope of a line obtained by plotting log $(\partial E/\partial V)_T$ *vs.* log v. The interval is not large enough, in view of some scatter of the points, to fix the slope accurately; we find $n = 2.3 \pm 0.2$.

(2) W. Westwater, H. W. Frantz, and J. H. Hildebrand, *Phys. Rev.*, **31**, 135 (1928).
(3) J. H. Hildebrand and J. M. Carter, *J. Am. Chem. Soc.*, **54**, 3592 (1932).
(4) B. J. Alder, E. W. Haycock, J. H. Hildebrand, and H. Watts, *J. Chem. Phys.*, **22**, 1060 (1954).
(5) E. B. Smith and J. H. Hildebrand, *ibid.*, **31**, 145 (1959).
(6) K. Shinoda and J. H. Hildebrand, *J. Phys. Chem.*, **65**, 183 (1961).
(7) H. Benninga and R. L. Scott, *J. Chem. Phys.*, **23**, 1911 (1955).
(7a) *Cf.* ref. 1, p. 80.
(8) K. Shinoda and J. H. Hildebrand, *J. Phys. Chem.*, **61**, 789 (1957).
(9) J. E. Jolly and J. H. Hildebrand, *ibid.*, **61**, 791 (1957).
(10) K. Shinoda and J. H. Hildebrand, *ibid.*, **62**, 295, 481 (1958).
(11) K. Shinoda and J. H. Hildebrand, *ibid.*, **65**, 1885 (1961).
(12) C. B. Hurd, *J. Am. Chem. Soc.*, **68**, 364 (1946).
(13) H. S. Frank, *J. Chem. Phys.*, **13**, 495 (1945).

In order to obtain n by aid of eq. 6, we use the values of $(\partial E/\partial V)_T$ in Table I with values of ΔE^v calculated at the corresponding temperatures from the expression for the heat of vaporization given by Osthoff and Grubb,[14] $\Delta H^{vap} = 20.7 - 0.0245T$ kcal. mole^{-1}. This procedure yields the values of n given in the last column of Table I.

We see that the value of n obtained from eq. 5, 2.3, is much larger than that obtained from eq. 6, 1.38, indicating that n is far from constant, but diminishes with increasing v. The nature of the discrepancy is to be seen in Fig. 1. The curve AC is drawn with $n = 1$. In this case both the slope at point A and the area under the curve between V_1 and V_2 would yield the value $n = 1$. The curve BC represents what may be expected for a liquid such as our siloxane, where intermolecular attractive forces depend mainly upon the distances between the peripheral, methyl groups, and increase as volume diminishes more rapidly than they would if they were radial and central. The greater slope at B yields a larger value for n, from eq. 5, but since V_1 is but little altered from A to B, the area under the curve BC would give nearly the same value of n as the area under AC. This substance is obviously one for which a Kihara-type of potential is appropriate.

(b) **Mixtures.**—The question we set for this investigation was how the internal pressures of the mixtures are related to those of the pure components in a case where the latter show very different dependence upon volume. We found long ago that $n = 1.09$ for CCl_4, a value since reconfirmed. Obviously, values of attraction constants dependent upon such different powers of v as 2.38 and 2.09 have such different dimensions that they cannot be properly included in the simple Berthelot relation. We must therefore seek to relate the thermodynamic quantities themselves.

We find, first of all, that the values of $(\partial E/\partial V)_T$ are nearly additive with respect to volume fraction (but of course, very far from additive with respect to mole fraction) as shown in the last column of Table II. This accords with the symmetry of the curves of volume fraction *vs.* temperature for many non-polar *liquid mixtures*.[15] This fact, the near additivity of volumes, and the solubility parameter for the siloxane obtained from its solutions with iodine[8] and c-$C_6F_{11}CF_3$,[9] 8.2, close to the parameter of CCl_4, 8.6, all combine to indicate that the present mixture is probably nearly ideal. We have undertaken a study of vapor pressures.

It is instructive to compare the behavior of our mixture with that of the mixture of n-C_6F_{14} and n-C_6H_{14}, investigated by Dunlap and Scott.[16] Instead of being nearly ideal, this one deviates very strongly, separating into two liquid phases at 22.65°. In Fig. 2 the values of $(\partial E/\partial V)_T$ are plotted against volume fractions; our mixture at 25°, the mixture of the two hexanes at 35° instead of 25°, in order be a little farther from the critical point. The components of the latter system differ less than those of the former in "internal pressure," $(\partial E/\partial V)_T$, but very strongly in their solubility parameters, $\delta = (\Delta E^v/V)^{1/2}$, 5.9 and 7.3, for n-C_6F_{14} and n-C_6H_{14}, respectively. As Dunlap and Scott point out, the excess free energy of mixing of this system, like other mixtures of paraffins with perfluoroparaffins, is much greater than predicted from differences in their solubility parameters.

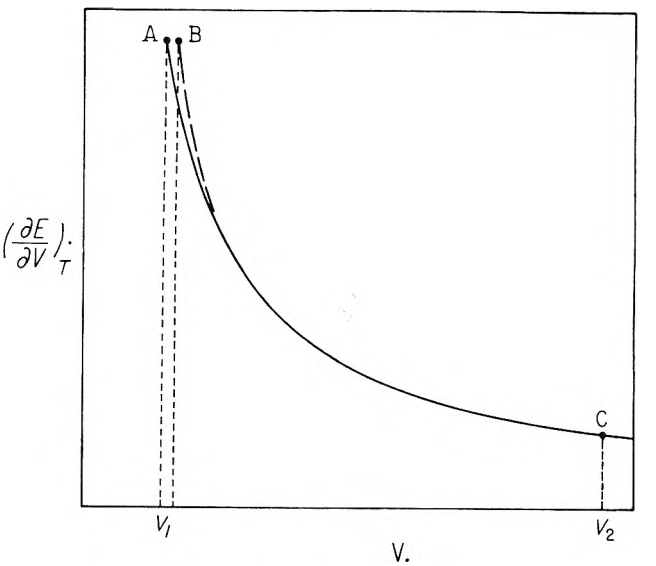

Fig. 1.—Illustrating why eq. 5 and 6 yield different values of n.

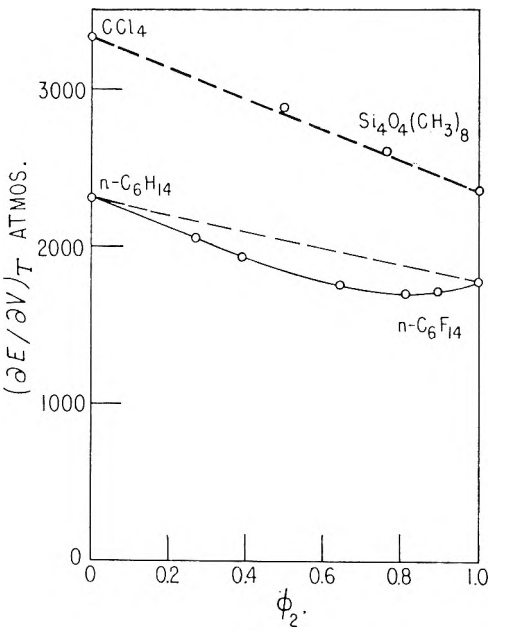

Fig. 2.—Comparing the mixture CCl_4 + c-$Si_4O_4(CH_3)_8$ with the mixture of the two hexanes investigated by Dunlap and Scott.

Acknowledgment.—We express our appreciation to the General Electric Company for the supply of siloxane and to the National Science Foundation for the support of the investigation.

(14) R. C. Osthoff and W. T. Grubb, *J. Am. Chem. Soc.*, **76**, 399 (1954).
(15) Reference 1, pp. 140–141.
(16) R. D. Dunlap and R. L. Scott, *J. Phys. Chem.*, **66**, 631 (1962).

SIGNIFICANCE OF NEW VALUES FOR IONIC RADII TO SOLVATION PHENOMENA IN AQUEOUS SOLUTION

By M. J. Blandamer and M. C. R. Symons

Department of Chemistry, The University, Leicester, England

Received January 10, 1963

The behavior of ions with rare gas structure in solution is discussed in terms of radii derived from electron density maps of sodium chloride and those estimated indirectly. It is concluded that the former "experimental" values are preferable.

Introduction

Although the term "ionic radius," when applied to ions in solution, cannot be given a rigid definition,[1] nevertheless, many attempts have been made to relate the thermodynamic changes associated with the dissolution of an electrolyte in water to the radii of the positive and negative ions.[2] The major problem is to find a satisfactory method of dividing both the experimentally determined interionic distances in the crystal and the free energies of solvation in water of the salt into separate contributions from cations and anions. Some workers, for example Bernal and Fowler,[3] and more recently, Noyes,[4] have equated radii of ions in water to those suggested by Pauling[5] for ions in crystals.

Crystal Radii.—Radii of ions in crystals, as proposed by Pauling,[5] are derived in a semi-empirical fashion in order to obtain a set of values which are self consistent with observed interionic distances. The method is based on the postulate that the sizes of a pair of isoelectronic ions are inversely proportional to the effective nuclear charges operating on the peripheral electron shells. Radii so obtained are assumed to be independent of the counterion in the crystal and electron distribution maps obtained over thirty years ago[6] indicated that this assumption was valid for the fluoride ion in the series sodium fluoride, lithium fluoride, and calcium fluoride, although the radius reported, *i.e.*, 1.25 Å., was smaller than that calculated by Pauling.[5] In contrast, however, the radius for the sodium ion was found to decrease from sodium chloride to sodium fluoride.

On the basis of electron density maps obtained more recently by Witte and Wölfel[7] for sodium chloride, Gourary and Adrian[8] have arrived at the new set of ionic radii for simple ions with rare gas structure shown in Table I. The maps demonstrate the ionic character of this salt and indicate only slight deformity of the ions from spherical symmetry. Further, the maps show that along the [100] line joining the sodium and chloride ions, the electron density falls sharply to zero. The ionic radii were equated to the distance between the point of zero electron density and the center of either ion. This gave 1.17 Å. for r_{Na^+} and 1.64 Å. for r_{Cl^-}. Gourary and Adrian adopted these values and proceeded to calculate, from known interatomic distances, the radii of other ions. The values so obtained reproduce these distances within an error of about 1% with one expection, lithium fluoride. In this case, electron density maps[9] do not show a position of zero electron density between the ions but only a minimum and it is suggested[8] that the values for the ionic radii of the lithium and fluoride ions, calculated on this basis, are too small because of the ability of the small cation to penetrate the large anion. In Table II, a comparison is made of the interatomic distances calculated from the two sets of ionic radii together with those observed,[10] and it would appear that the new radii give slightly better agreement.

Table I

Comparison of Values for Ionic Radii

	F^-	Cl^-	Br^-	I^-	Li^+	Na^+	K^+	Rb^+	Cs^+
Pauling[5] radii, Å.	1.36	1.81	1.95	2.16	0.60	0.95	1.33	1.48	1.69
Gourary and Adrian[8] radii, Å.	1.16	1.64	1.80	2.05	0.94	1.17	1.49	1.63	1.86

Table II

A Comparison of Observed[10] and Calculated Interionic Distances, Å.

		Li^+	Na^+	K^+	Rb^+	Cs^+
F^-	Obsd.	2.01	2.31	2.67	2.82	3.01
	Pauling	1.96	2.31	2.69	2.84	3.05
	Gourary and Adrian	2.10	2.33	2.65	2.79	3.04
Cl^-	Obsd.	2.57	2.81	3.14	3.27	
	Pauling	2.41	2.76	3.14	3.29	
	Gourary and Adrian	2.58	2.81	3.13	3.27	
Br^-	Obsd.	2.75	2.98	3.29	3.43	
	Pauling	2.55	2.90	3.28	3.43	
	Gourary and Adrian	2.74	2.97	3.29	3.43	
I^-	Obsd.	3.02	3.23	3.53	3.66	
	Pauling	2.76	3.11	3.49	3.64	
	Gourary and Adrian	2.99	3.22	3.54	3.68	

The new radii,[8] which for brevity are described as "experimental" do not differ greatly from those calculated by Pauling,[5] but as shown in the following outline, the differences are sufficient to alter several correlations significantly. In Fig. 1, the "experimental" ionic radii and the radii of rare gas atoms[11] are compared and it will be noted that the fluoride ion is now about equal in size to the sodium ion, rather than the potassium ion as suggested earlier.[5]

Ions in Solution.—In the following, various properties of ions in aqueous solution which have been related empirically or theoretically to ionic radii are discussed.

(1) K. H. Stern and E. S. Amis, *Chem. Rev.*, **59**, 1 (1959).

(2) B. E. Conway and J. O'M. Bockris, in "Modern Aspects of Electrochemistry," J. O'M. Bockris and B. E. Conway, Ed., Butterworths, London, 1954, p. 47.

(3) J. D. Bernal and R. H. Fowler, *J. Chem. Phys.*, **1**, 515 (1933).

(4) R. M. Noyes, *J. Am. Chem. Soc.*, **84**, 513 (1962).

(5) L. Pauling, "The Nature of the Chemical Bond and the Structure of Molecules and Crystals," 3rd. Ed., Cornell University Press, Ithaca, N. Y., 1960.

(6) R. J. Havighurst, *Phys. Rev.*, **29**, 1 (1927).

(7) H. Witte and E. Wölfel, *Z. physik. Chem.* (Frankfurt), **B3**, 296 (1955).

(8) B. S. Gourary and F. J. Adrian, *Solid State Phys.*, **10**, 127 (1960).

(9) J. Krug, H. Witte, and E. Wölfel, *Z. physik. Chem.* (Frankfurt), **4**, 36 (1955).

(10) N. K. Adam, "Physical Chemistry," Clarendon Press, Oxford, 1956, p. 197.

(11) These values are taken from ref. 4, Table II, although other compilations, *e.g.*, R. B. Heslop and P. L. Robinson, "Inorganic Chemistry," Elsevier, London, 1960, p. 237, give widely different values for the radius of the helium atom. Hydride is omitted because its radius is very variable.

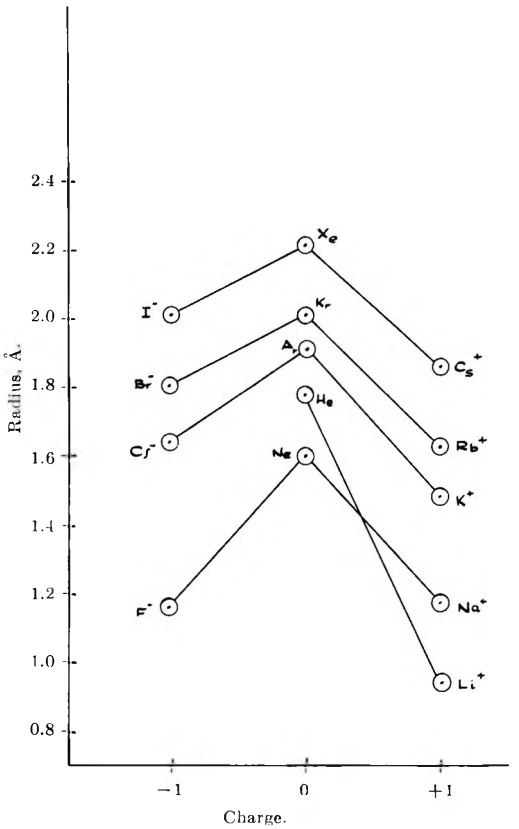

Fig. 1.—Comparison of the radii of rare gas atoms with "experimental" radii of iso-electronic ions.

These have been selected from a literature abounding in such correlations.

Entropy of Solvation.—There have been many attempts to correlate partial molar entropies of solvation of ions in water with their radii and although the equations used differ in form, it seems[12] that most of these correlations are about equally effective in predicting experimental values. A common feature of such correlations is that "effective" ionic radii are proposed, with different increments added to the radii of cations and anions. Partial molar entropies of ions taken from the compilation of Powell and Latimer[13] but adjusted to the scale proposed by Gurney[14] have been plotted in Fig. 2 against $1/r_i^2$ for both sets of radii. It seems that a single smooth curve is almost adequate for both cations and anions when "experimental" radii are used, so that it appears no longer necessary to differentiate between anion–water and cation–water interactions with respect to entropy considerations.

Ionic Mobility.—That the limiting equivalent conductivities of ions with rare gas structure in water[15] decrease with decrease in ionic radius is well known and has been discussed in classical terms as evidence for a corresponding increase in ion–solvent interaction through the series. However, the correlation for cations and anions collectively with "experimental" ionic radii is better than that with Pauling radii. This is shown in Table III, where the ions are placed in order of increasing size.

(12) G. N. Lewis and M. Randall, "Thermodynamics," 2nd. Ed., K. S. Pitzer and L. Brewer, Ed., McGraw-Hill Book Co., London, 1961, p. 524.
(13) R. E. Powell and W. M. Latimer, *J. Chem. Phys.*, **19**, 1139 (1951).
(14) R. W. Gurney, "Ionic Processes in Solution," McGraw-Hill Book Co., London, 1953, p. 175.
(15) R. A. Robinson and R. H. Stokes, "Electrolyte Solutions," 2nd. Ed., Butterworths, London, 1959, p. 463.

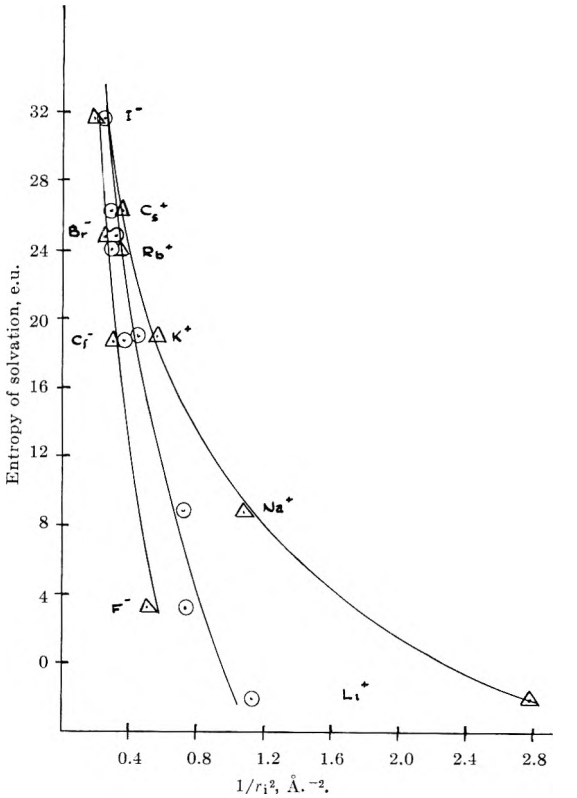

Fig. 2.—Correlation diagram between entropy of solvation,[13,14] in water and both Pauling, △, and "experimental," ⊙, radii.

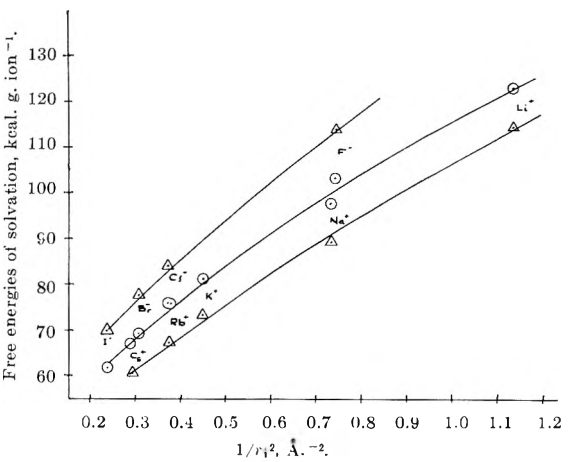

Fig. 3.—Correlation diagram between "experimental" ionic radii and free energies of solvation in water derived from the data for rubidium chloride, ⊙, and those suggested by Latimer, Pitzer, and Slansky,[16] △.

TABLE III

LIMITING EQUIVALENT CONDUCTIVITIES OF IONS IN WATER AT 25°, CM.² OHM⁻¹ EQUIV.⁻¹, AND IONIC RADII

Pauling radii		Experimental radii	
Li^+	(38.7)	Li^+	(38.7)
Na^+	(50.1)	F^-	(55.4)
K^+	(73.5)	Na^+	(50.1)
F^-	(55.4)	K^+	(73.5)
Rb^+	(77.8)	Rb^+	(77.8)
Cs^+	(77.3)	Cl^-	(76.3)
Cl^-	(76.3)	Br^-	(78.1)
Br^-	(78.1)	Cs^+	(77.3)
I^-	(76.8)	I^-	(76.8)

Free Energy of Solvation.—In deriving the contributions of individual ions to the total free energy of solvation in water, the method introduced by Bernal and Fowler[3] has been adopted. These authors divided the

heats of solvation on the basis of the similarity in Pauling radii for potassium and fluoride ions but, if the new values are adopted this method is no longer justified, and it is more reasonable to use rubidium and chloride ions as shown in Table I. In this manner, the total free energy of solvation, −151.5 kcal./mole,[16] for this salt has been divided into two equal contributions and the values for other ions obtained by difference through the chloride and rubidium series of salts. These values are plotted, in Fig. 3, against $1/r_i^2$ since such a dependence results if the main free energy contribution arises from the interaction between the ion and the contiguous water molecules.[17] Included on the graph are the free energies obtained by Latimer, Pitzer, and Slansky,[16] who fitted the free energies of solvation to the Born equation in terms of another set of effective ionic radii. The plot demonstrates that the simple procedure adopted here results in a dependence which does not differentiate between anion and cation.

TABLE IV

FREE ENERGIES OF SOLVATION IN WATER FOR ALKALI AND HALIDE IONS

	Li^+	Na^+	K^+	Rb^+	Cs^+	F^-	Cl^-	Br^-	I^-
$\Delta G_{s,i}$, −kcal. g. ion^{-1}	122.9	97.6	81.3	75.8	67.0	103.3	75.8	69.2	61.8

Discussion

When Pauling radii are used, it is found that anions invariably have greater free energies of solvation than cations of equal size and charge. In particular, differences in enthalpies have been explained[4] on the grounds that for oriented water molecules, the center of the positive charge is closer to the "edge" of the water molecule and thus interacts more effectively with anions. This argument is not convincing since the "lone-pair" electrons contribute very greatly to the over-all dipole of the water molecule, and hence its ability to stabilize cations should be at least as great as its ability to stabilize anions. By using "experimental" radii, the energy differences are largely lost together with this apparent anomaly.

On balance, we conclude that "experimental" ionic radii without arbitrary adjustments are more appropriate to consideration of the properties of ions in solution than are "Pauling" radii with or without adjustments and, while we do not suggest any theoretical justifications for the relationships observed, it appears that anion/solvent and cation/solvent interactions are similar. However, it should be stressed that, so far, these values are based entirely on experimental results for sodium chloride. It would be very helpful if data for other alkali halides were available, but it appears that there are important experimental difficulties involved in their measurement.[9] The most serious objection to the new values for ionic radii must be that sodium ions appear approximately equal in radius to fluoride ions. This result is perhaps puzzling if it is considered in connection with the radius for the isoelectronic rare-gas atom, neon, as shown in Fig. 1. It seems that at least in the fluoride case there has been a dramatic decrease in radius as a result of the very powerful crystal forces which must therefore be taken into account when radii are compared.

(16) K. S. Latimer, K. S. Pitzer, and C. Slansky, *J. Chem. Phys.*, **7**, 108 (1939).

(17) Reference 14, p. 51.

PERFLUOROPIPERIDINE: ENTROPY, HEAT OF FORMATION, AND VAPOR PRESSURE; N–F BOND ENERGY; AND SOLID-STATE TRANSITIONS[1,2]

BY W. D. GOOD, S. S. TODD, J. F. MESSERLY, J. L. LACINA, J. P. DAWSON, D. W. SCOTT, AND J. P. MCCULLOUGH

Contribution No. 118 from the Thermodynamics Laboratory of the Bartlesville Petroleum Research Center, Bureau of Mines, U. S. Department of the Interior, Bartlesville, Okla.

Received January 12, 1963

Measurements were made of the thermodynamic properties of perfluoropiperidine, $C_5F_{11}N$. The experimental studies provided the following information: values of heat capacity for the solid above 12°K. and the liquid below 320°K.; temperature of two transitions in the solid state; triple-point temperature; heats of transition, fusion, and vaporization; vapor pressure (302–355°K.); and the standard heats of combustion and formation at 298.15°K. A value for the N–F thermochemical bond energy was calculated from the results.

The Bureau of Mines is conducting systematic investigations of the thermodynamic properties of organic fluorine compounds in this Laboratory. The first work was concerned primarily with compounds of low to moderate fluorine content.[3] Modification of the early experimental techniques later allowed studies of completely fluorinated compounds, such as fluorocarbons.[4] This paper reports application of these techniques to perfluoropiperidine, a completely fluorinated compound that also contains nitrogen.

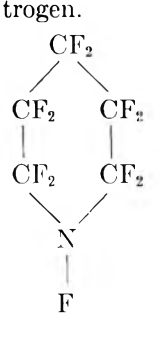

(1) The research reported in this article was supported by the United States Air Force through the Air Force Office of Scientific Research of the Air Research and Development Command under Contract No. CSO-680-57-4. Reproduction in whole or in part is permitted for any purpose of the United States Government.

(2) Presented in part at the 133rd National Meeting of the American Chemical Society, San Francisco, Calif., April 13–18, 1958, and in part at the Southwest Regional Meeting of the American Chemical Society, Tulsa, Oklahoma, December 4–6, 1957.

(3) (a) D. W. Scott, J. P. McCullough, W. D. Good, J. F. Messerly, R. E. Pennington, T. C. Kincheloe, I. A. Hossenlopp, D. R. Douslin, and G. Waddington, *J. Am. Chem. Soc.*, **78**, 5457 (1956); (b) D. W. Scott, D. R. Douslin, J. F. Messerly, S. S. Todd, I. A. Hossenlopp, T. C. Kincheloe,

The results of low temperature calorimetric studies, vapor pressure determinations, and heat of combustion measurements are reported in the Experimental section. In the following two sections, the N–F thermochemical bond energy and the low temperature phase behavior of perfluoropiperidine are discussed separately.

The N–F Thermochemical Bond Energy

The heat of formation of gaseous perfluoropiperidine is -475.78 kcal. mole^{-1}, as reported in the Experimental section. Calculation of the N–F thermochemical bond energy based on this result was approached through consideration of the hypothetical gas phase reaction

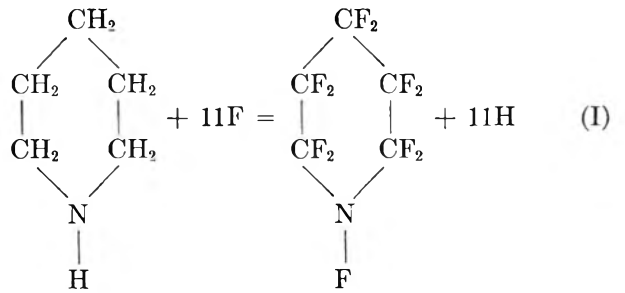

(I)

The heat of formation of gaseous piperidine from an unpublished result of this Laboratory is $\Delta Hf°_{298.15}(g) = -11.32$ kcal. mole^{-1}. When values of $\Delta Hf°_{298.15}$ for piperidine and perfluoropiperidine are combined with values of $\Delta Hf°_{298.15}$ for monatomic hydrogen[5] and fluorine,[6] $\Delta H°_{298.15}$ for reaction I is calculated to be -99.41 kcal.

Both molecules in reaction I have six-membered rings, and perfluoropiperidine differs from piperidine only in having each hydrogen atom replaced by a fluorine atom. Because the ring strain energy should be about the same in the two molecules, the heat of reaction I can be calculated directly from the thermochemical bond energies for those bonds created or destroyed in the reaction.

$$\Delta H°_{298.15}(\text{reaction I}) = 10E(\text{C–H}) + E(\text{N–H}) - 10E(\text{C–F}) - E(\text{N–F}) \quad (1)$$

E is the thermochemical bond energy of the indicated bond. The foregoing equation was rearranged to emphasize that only the difference between E(C–F) and E(C–H) is required.

$$E(\text{N–F}) = -\Delta H°_{298.15}(\text{reaction I}) - 10[E(\text{C–F}) - E(\text{C–H})] + E(\text{N–H}) \quad (2)$$

An earlier publication of this Laboratory[4] has shown that E(C–F) $-$ E(C–H) $= 12.0$ kcal. mole^{-1} for bonds in a $>CF_2$ group relative to those in a $>CH_2$ group. The N–H thermochemical bond energy, based on the heats of formation of ammonia[7] and monatomic hydrogen[5] and nitrogen,[8] is 93.4 kcal. mole^{-1}. When these values are substituted in equation 2, E(N–F) is found to be 73 kcal. mole^{-1}. For comparison, the average N–F thermochemical bond energy recently was reported to be 66 kcal. mole^{-1} in both NF_3[9] and N_2F_4.[10] The difference between E(N–F) in perfluoropiperidine and the nitrogen fluorides probably is due to the difference in molecular environments.

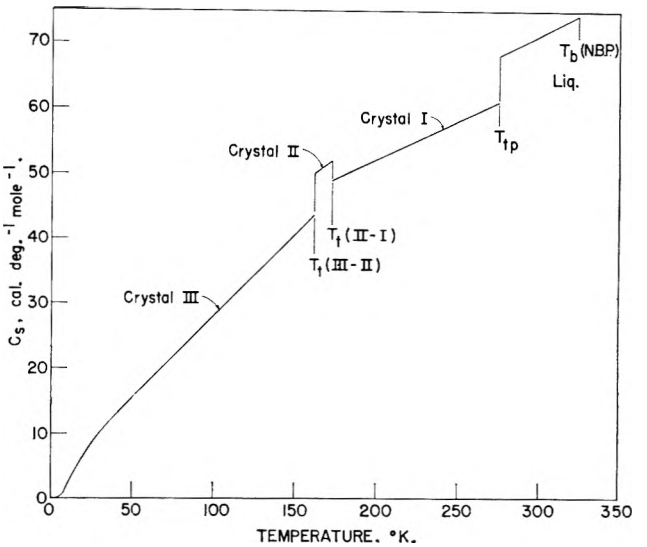

Fig. 1.—Heat capacity curve of perfluoropiperidine.

Phase Behavior of Perfluoropiperidine

The heat capacity of perfluoropiperidine is plotted as a function of temperature in Fig. 1. Two essentially isothermal phase transitions (Type I)[11] take place about 100° below the melting point (274.12°K.). Two other saturated, six-membered ring compounds—cyclohexane[12] and thiacyclohexane[13]—show similar phase behavior, but unpublished studies of piperidine show that it does not undergo a solid–solid phase change. Table I summarizes data on the phase changes in these four structurally similar compounds. These results provide valuable insight into the nature of the so-called plastic crystals formed by nearly globular molecules.[14,15]

As shown by the low entropies of fusion, the first three compounds in Table I form high temperature phases (Crystal I) with such extensive orientational disorder that they may be considered as rotator phases, in the sense distinguished by Andrew.[16] Because the degree of disorder is so high, the interpretive scheme of Guthrie and McCullough[17]—involving alignment of molecular with crystal symmetry elements—cannot be applied to explain the observed entropy increments. Nevertheless, the statistical approach does show that the results in Table I are consistent with modern concepts of the mechanism of phase changes. It is necessary to assume, first, that the extent of orientational

and J. P. McCullough, *J. Am. Chem. Soc.*, **81**, 1015 (1959); (c) W. D. Good, D. W. Scott, and G. Waddington, *J. Phys. Chem.*, **60**, 1080 (1956).

(4) W. D. Good, D. R. Douslin, D. W. Scott, A. George, J. L. Lacina, J. P. Dawson and G. Waddington, *ibid.*, **63**, 1133 (1959).

(5) A. G. Gaydon, "Dissociation Energies," Chapman and Hall, London, 1953.

(6) W. H. Evans, T. R. Munson, and D. D. Wagman, *J. Res. Natl. Bur. Std.*, **55**, 147 (1955).

(7) F. D. Rossini, D. D. Wagman, W. H. Evans, S. Levine, and I. Jaffe, "Selected Values of Chemical Thermodynamic Properties," Natl. Bur. Std. Circ. 500, 1952.

(8) L. Brewer and A. W. Searcy, *Ann. Rev. Phys. Chem.*, **7**, 259 (1956).

(9) G. T. Armstrong, S. Marantz, and C. F. Coyle, *J. Am. Chem. Soc.*, **81**, 3798 (1959).

(10) G. T. Armstrong, S. Marantz, and C. F. Coyle, Natl. Bur. Std., Report No. 6584 (1961).

(11) J. P. McCullough, *Pure Appl. Chem.*, **2**, 221 (1961).

(12) (a) R. A. Ruehrwein and H. M. Huffman, *J. Am. Chem. Soc.*, **65**, 1620 (1943); (b) J. G. Aston, G. J. Szasz, and H. L. Finke, *ibid.*, **65**, 1135 (1943).

(13) J. P. McCullough, H. L. Finke, W. N. Hubbard, W. D. Good, R. E. Pennington, J. F. Messerly, and G. Waddington, *ibid.*, **76**, 2661 (1954).

(14) J. Timmermans, *Bull. soc. chim. Belges*, **44**, 17 (1935).

(15) Proceedings of the Symposium on Plastic Crystals and Rotation in the Solid State, *J. Phys. Chem. Solids*, **18**, No. 1 (1961).

(16) E. R. Andrew, *J. Chem. Phys.*, **18**, 607 (1950).

(17) G. B. Guthrie, Jr., and J. P. McCullough, *J. Phys. Chem. Solids*, **18**, 53 (1961).

TABLE I

DATA ON PHASE CHANGES IN PERFLUOROPIPERIDINE AND RELATED COMPOUNDS

Compound	Phase change[a]	T, °K.	ΔS,[b] cal. deg.$^{-1}$ mole^{-1}
Perfluoropiperidine	1	161.0	9.839
	1	171.9	2.557
	Fusion	274.12	2.455
	Total		14.851
Cyclohexane[c]	3I	186.09	8.656
	Fusion	279.81	2.287
	Total		10.943
Thiacyclohexane[d]	2I	201.4	1.303
	3N	207[e]	
	1	240.01	7.743
	Fusion	292.24	2.002
	Total		11.048[f]
Piperidine[g]	Fusion	262.12	13.544

[a] The symbols of ref. 11 are used to denote solid–solid phase changes. [b] Entropy increments for phase changes. [c] Reference 12a. [d] Reference 13. [e] Temperature of peak heat capacity. [f] Does not include estimate of entropy increment for the non-isothermal order–disorder process. [g] Unpublished work of this Laboratory.

disorder in the liquid phase is about the same for all of these compounds if disorder due to the hetero-atoms is accounted for separately. Next, it must be assumed that each compound forms crystals of similar structure. If these assumptions be true, the total entropy of phase change, including fusion, for each hetero-compound should equal that of cyclohexane plus a contribution from disorder of the hetero-atoms. Thus, considering the ring hetero-atoms only, the total entropy of phase change for the hetero-compounds should be $10.943 + R \ln 6 = 14.504$ cal. deg.$^{-1}$ mole^{-1}, because there are six distinguishable orientations of a hetero-compound for each one of cyclohexane.

As pointed out earlier,[13] part of the order–disorder process in thiacyclohexane occurs non-isothermally, probably occurring at the maximum rate in the region of the Type 3N transition (207°K.), and reasonable allowance for the non-isothermal entropy increment makes the total entropy of phase change consistent with the foregoing estimate. The net observed entropy of phase change for perfluoropiperidine, on the other hand, is 0.35 cal. deg.$^{-1}$ mole^{-1} *greater* than the estimate. Because the assessment of the isothermal entropy increment of a phase change from experimental data is arbitrary to a certain extent, and because a portion of the disordering process in a crystal may actually occur non-isothermally, the discrepancy between the experimental and estimated total entropy increment for perfluoropiperidine probably is not significant. However, it is possible that partial or complete disorder of the F atom in the N–F group of perfluoropiperidine between axial and equatorial positions would occur, so the first estimate would be increased by as much as $R \ln 2$, or to a total of 15.881 cal. deg.$^{-1}$ mole^{-1}. At least partial conformational disorder of this type seems likely in liquid perfluoropiperidine, if not in the highly disordered Crystal I.

If piperidine itself has a crystal structure similar to the other compounds listed in Table I, the absence of any solid–solid phase changes may be an indication that orientational order is preserved in the crystal of this compound by some type of hydrogen bonding or dipolar interaction. The net entropy of phase change for piperidine is 0.96 cal. deg.$^{-1}$ mole^{-1} *less* than the estimate for the hetero compounds. There are at least two possible explanations for this discrepancy. First, if the crystal structure of piperidine differs significantly from that of cyclohexane, one of the assumptions on which the estimate was based is invalid. Second, liquid piperidine undoubtedly is hydrogen-bonded to some extent near the melting point, so the extent of orientational disorder in the liquid phase very likely is less than that for the other compounds.

Experimental

The apparatus and methods used in the continuing program of this Laboratory evolve as a result of improvements and modifications suggested by experience or required in studies of different substances. Not all these improvements have been described in the literature, but the basic experimental techniques used for perfluoropiperidine are presented in published descriptions of apparatus and methods for low temperature calorimetry,[18] comparative ebulliometry,[19] and combustion calorimetry.[3c,4]

The reported values are based on a molecular weight of 283.058 for perfluoropiperidine (1951 International Atomic Weights),[20a] the 1951 values of the fundamental physical constants,[20b] and the relations: 0°C. = 273.15°K. and 1 cal. = 4.184 (exactly) j. Measurements of temperature were made with platinum resistance thermometers calibrated in terms of the International Temperature Scale[21] between 90 and 500°K. and the provisional scale[22] of the National Bureau of Standards between 11 and 90°K. All electrical and mass measurements were referred to standard devices calibrated at the National Bureau of Standards.

Material.—The original sample of perfluoropiperidine, supplied by the Minnesota Mining and Manufacturing Company through the courtesy of Dr. W. H. Pearlson, was a combination of three distillation fractions having a boiling range of 0.3°. This material was distilled in a semimicro fractionating column by C. J. Thompson and H. J. Coleman of this Center. Middle fractions of essentially the same refractive index were combined to give a higher purity sample, hereinafter designated sample A, n^{20}D 1.27777. The end fractions, all of lower refractive index, were combined to give a lower purity sample, hereinafter designated sample B. Sample A was used for low temperature calorimetry, comparative ebulliometry, and combustion calorimetry. Sample B also was used for combustion calorimetry. The purity of sample A, as determined by a calorimetric study of the melting point as a function of fraction melted, was 99.49 mole %. Gas–liquid chromatography showed the presence of an impurity with longer emergence time in both samples. The concentration of impurity in sample B was estimated to be 50% greater than in sample A.

Heat Capacity in the Solid and Liquid States.—Low temperature calorimetric measurements were made with 0.36142 mole of sample sealed in a platinum calorimeter with helium (3 cm. pressure at room temperature) added to promote equilibration. The observed values of heat capacity at saturation pressure, C_s, are given in Table II. The chronological sequence of measurements is not indicated in this table. Over the temperature range studied, C_s does not differ significantly from C_p, the heat capacity at constant pressure. The temperature increments used in the measurements were small enough that corrections for curvature were unnecessary: 10% of the absolute temperature

(18) H. M. Huffman, *Chem. Rev.*, **40**, 1 (1947); H. M. Huffman, S. S. Todd, and G. D. Oliver, *J. Am. Chem. Soc.*, **71**, 584 (1949); D. W. Scott, D. R. Douslin, M. E. Gross, G. D. Oliver, and H. M. Huffman, *ibid.*, **74**, 883 (1952).

(19) G. Waddington, J. W. Knowlton, D. W. Scott, G. D. Oliver, S. S. Todd, W. N. Hubbard, J. C. Smith, and H. M. Huffman, *ibid.*, **71**, 797 (1949).

(20) (a) E. Wichers, *ibid.*, **74**, 2447 (1952); (b) F. D. Rossini, F. T. Gucker, Jr., H. L. Johnston, L. Pauling, and G. W. Vinal, *ibid.*, **74**, 2699 (1952). Use of the unified atomic weight scale [*Chem. Eng. News*, Nov. 20, 1961, p. 43] would not change any of the results significantly.

(21) H. F. Stimson, *J. Res. Natl. Bur. Std.*, **42**, 209 (1949); H. F. Stimson, *Am. J. Phys.*, **23**, 614 (1955).

(22) H. J. Hoge and F. G. Brickwedde, *J. Res. Natl. Bur. Std.*, **22**, 351 (1939).

below 60°K.; about 6° for the solid above 60°K., except about 3° for the measurements on crystal II; and 5 to 10° for the liquid. Corrections for premelting caused by impurities have not been applied to the results in Table II, but corrections for vaporization (0.03% or smaller) have been applied to the values above 210°K. Above 30°K. the accuracy uncertainty is estimated to be no greater than 0.2% except in the vicinity of phase changes. The heat capacity of the liquid varies linearly with temperature between the melting and boiling points and may be represented by the equation

$$C_s(\text{liq}) = 35.359 + 0.11933T, \text{ cal. deg.}^{-1} \text{ mole}^{-1} \quad (3)$$

with a maximum deviation of 0.04%.

TABLE II

THE MOLAL HEAT CAPACITY OF PERFLUOROPIPERIDINE, CAL. DEG.$^{-1}$

T, °K.[a]	C_s[b]	T, °K.[a]	C_s[b]	T, °K.[a]	C_s[b]
Crystal III		59.84	17.799	Crystal I	
11.82	2.758	65.03	19.122	180.29	49.969
11.92	2.807	70.40	20.450	181.45	50.116
12.88	3.274	75.89	21.844	185.97	50.617
12.91	3.272	81.46	23.322	192.04	51.320
14.22	3.944	85.90	24.530	193.12	51.405
14.30	4.000	87.12	24.844	199.20	52.158
15.73	4.697	90.48	25.699	205.66	52.927
16.02	4.836	96.03	27.071	211.93	53.682
17.43	5.509	101.82	28.548	218.52	54.479
17.90	5.727	107.80	30.029	225.53	55.337
19.33	6.361	113.97	31.550	232.44	56.189
19.94	6.613	119.88	32.997	233.66	56.341
21.57	7.269	125.97	34.472	239.25	57.044
22.19	7.515	132.16	35.964	241.52	57.329[d]
24.10	8.259	137.39	37.186	249.72	58.394[d]
24.77	8.522	138.08	37.377	256.36	59.343[d]
26.76	9.172	138.68	37.535	262.84	62.253[c,d]
27.65	9.474	143.10	38.586	Liquid	
29.69	10.085	143.80	38.800	279.33	68.679
30.74	10.409	144.88	39.068	284.80	69.337
32.95	11.048	150.40	40.739	286.38	69.550
34.21	11.397	Crystal II		291.66	70.170
37.00	12.155	162.76	50.332	293.80	70.441
38.12	12.448	164.07	50.603	302.00	71.385
42.02	13.419	164.97	50.857	307.19	72.018
42.17	13.469	165.67	50.835	309.76	72.303
46.55	14.493	167.20	51.217	312.15	72.622
47.43	14.728	167.85	51.303	313.95	72.812
51.49	15.721	168.54	51.403	318.97	73.429
54.71	16.510				

[a] T is the mean temperature of heat capacity measurement. [b] C_s is the heat capacity of the condensed phase at saturation pressure. [c] Values of C_s for crystals are not corrected for the effects of premelting caused by impurities. [d] The temperature increments of these measurements are in order of increasing T, °K.; 9.702, 6.679, 6.580, and 6.364.

The Heat of Fusion, Triple-Point Temperature, Cryoscopic Constants, and Purity of Sample.—Three determinations of the heat of fusion gave an average value of 673 ± 5 cal. mole^{-1}, corrected for the effect of premelting caused by impurities. The relatively low precision of this measurement is partly the result of poor thermal equilibration in the premelting region, which was particularly troublesome because of the large amount of impurity in the sample.

The results of a study of melting temperature, T_F, as a function of fraction of total sample melted, F, are given in Table III. Also listed in Table III are values obtained for the triple-point temperature, T_{tp}, the mole fraction of impurity in the sample, N_2^*, and the cryoscopic constants, $A = \Delta Hm/RT_{tp}^2$ and $B = 1/T_{tp} - \Delta Cm/2\Delta Hm$, calculated from the observed values of T_{tp}, ΔHm and from $\Delta Cm = 6.95$ cal. deg.$^{-1}$ mole^{-1} (Table IV).

The melting point study was not made in enough detail to define the melting curve precisely because the approach to equilibrium after a fraction was melted was extremely slow. Apparent equilibrium was reached only in the observations for F = 0.9422.

TABLE III

SUMMARY OF MELTING POINT STUDY

$T_{tp} = 274.12$°K.; $N_2^* = AF/(T_{tp} - T_F) = 0.0051$

$A = 0.004507$ deg.$^{-1}$; $B = -0.00151$ deg.$^{-1}$

F	1/F	T_F, °K.	T_{graph}, °K.[b]
0.5313	1.882	272.1326	271.98
.7407	1.350	272.5865[a]	272.5865
.9422	1.061	272.9138[a]	272.9138
1.0000	1.000		272.9829
Pure	0.0		274.1154

[a] A straight line through these points was extrapolated to 1/F = 0 to obtain T_{tp}. [b] Temperatures from the straight line of footnote *a*.

TABLE IV

THE MOLAL THERMODYNAMIC PROPERTIES OF PERFLUOROPIPERIDINE IN THE SOLID AND LIQUID STATES[a]

T, °K.	$-(F_s - H°_0)/T$, cal. deg.$^{-1}$	$(H_s - H°_0)/T$, cal. deg.$^{-1}$	$H_s - H°_0$, cal.	S_s, cal. deg.$^{-1}$	C_s, cal. deg.$^{-1}$
		Crystal III			
10	0.167	0.488	4.876	0.655	1.837
15	.517	1.352	20.278	1.869	4.340
20	1.048	2.394	47.88	3.442	6.635
25	1.695	3.441	86.01	5.136	8.568
30	2.411	4.433	132.97	6.844	10.182
35	3.164	5.358	187.52	8.522	11.609
40	3.937	6.223	248.90	10.160	12.920
45	4.718	7.035	316.58	11.753	14.141
50	5.499	7.806	390.3	13.305	15.352
60	7.052	9.270	556.1	16.322	17.843
70	8.588	10.675	747.2	19.263	20.350
80	10.103	12.044	963.5	22.147	22.930
90	11.600	13.404	1206.3	25.004	25.580
100	13.082	14.745	1474.5	27.827	28.073
110	14.550	16.070	1767.7	30.620	30.565
120	16.005	17.381	2085.7	33.38	33.03
130	17.447	18.678	2428.1	36.12	35.44
140	18.878	19.960	2794.4	38.83	37.82
150	20.299	21.239	3185.8	41.53	40.59
160	21.711	22.552	3608	44.26	43.87
161.0	21.85	22.68	3652	44.53	44.19
		Crystal II			
161.0	21.85	32.52	5236	54.37	49.94
165	22.65	32.95	5437	55.61	50.77
171.9	24.02	33.69	5792	57.71	51.97
		Crystal I			
171.9	24.02	36.25	6231	60.27	49.03
180	25.70	36.84	6632	62.55	49.94
190	27.71	37.56	7137	65.28	51.07
200	29.66	38.27	7654	67.93	52.23
210	31.54	38.96	8182	70.51	53.42
220	33.37	39.65	8722	73.02	54.62
230	35.15	40.32	9275	75.47	55.83
240	36.88	40.99	9839	77.88	57.04
250	38.56	41.66	10416	80.23	58.24
260	40.21	42.32	11004	82.54	59.44
270	41.82	42.98	11604	84.80	60.63
273.15	42.32	43.18	11797	85.51	61.01
274.12	42.48	43.25	11856	85.73	61.12
		Liquid			
274.12	42.48	45.70	12529	88.18	68.07
280	43.45	46.18	12930	89.63	68.77
290	45.08	46.98	13624	92.06	69.96
298.15	46.40	47.62	14199	94.02	70.93
300	46.69	47.76	14330	94.46	71.15
310	48.27	48.54	15047	96.81	72.35
320	49.82	49.30	15777	99.12	73.54

[a] The values tabulated are the free energy function, enthalpy function, enthalpy, entropy, and heat capacity of the condensed phases at saturation pressure.

The values of T_F at F = 0.5313 and 0.7407 given in Table III were obtained from the observed time–temperature curve for each point with the assumption of exponential approach to equilibrium. For these reasons, the values of T_{tp} and N_2* are subject to uncertainties greater than normal.

Even from the limited portion of the melting point curve that was determined, it is apparent that the impurity forms a solid solution with perfluoropiperidine. The heat capacity data in the premelting region support this conclusion. When the heat capacity data in Table II were corrected for premelting using N_2* = 0.0051, the "corrected" curve had negative slope and curvature just below the melting point. To obtain a corrected heat capacity curve with positive slope and zero curvature below the melting point, N_2* = 0.00069 had to be chosen as the mole fraction of solid-*insoluble* impurity. The values in Table IV, discussed later, were corrected for premelting by use of the mole fraction of solid-*insoluble* impurity selected from the premelting heat capacity data.

The Transition Temperatures and Heats of Transitions.—Neither of the two solid–solid phase transformations was strictly isothermal, both taking place over about 1° temperature intervals. For the transformation from Crystal III to Crystal II, the equilibrium temperatures observed for two fractions transposed, 0.4667 and 0.8198, were 160.5250 and 160.8086°K.; the extrapolated value for complete transposition was selected as the transition temperature, T_t(III–II) = 161.0°K. Equilibration in the transition from Crystal II to Crystal I was very slow, and only one observation was made of the transition temperature at 0.50 transposed. The result of this observation was chosen as the transition temperature, T_t(II–I) = 171.9°K. It is possible that the transition temperatures of pure perfluoropiperidine differ significantly from those found for the sample studied because of the effects of about 0.5% solid-soluble impurity. However, the effect of the solid-soluble impurity on the entropy and other properties of the liquid, discussed in a following section, should not be significant.

Duplicate determinations of the heat of each transition gave the following values: 1584.0 ± 0.6 cal. mole^{-1} for transition III–II; and 439.5 ± 0.1 cal. mole^{-1} for transition II–I. The indicated uncertainty in each value is the deviation of the two results from the mean.

Thermodynamic Properties in the Solid and Liquid States.—Values of the thermodynamic properties of the condensed phases were computed from the calorimetric data for selected temperatures between 10 and 320°K. The results are given in Table IV. The values at 10°K. were computed from a Debye function for 6.5 degrees of freedom with θ = 79.1°; these parameters were evaluated from the heat capacity data between 11.8 and 20.0°K. Corrections for the effect of premelting were applied in calculating the "smoothed" data recorded in Table IV.

Vapor Pressure.—The vapor pressure of sample A of perfluoropiperidine (99.49 mole % pure) was determined by comparative ebulliometry. The difference in the boiling and condensation temperatures at 906 mm. pressure was 0.004°. This small difference shows that the impurity in the sample had nearly the same volatility as the major component and, therefore, had little effect on the observed vapor pressure. The results are listed in Table V. The Antoine[23] and Cox[24] equations selected to represent these results are

$$\log p = 6.85082 - 1058.558/(t + 217.023) \quad (4)$$

and

$$\log (p/760) = A(1 - 322.766/T) \quad (5)$$

where

$$\log A = 0.892699 - 1.01968 \times 10^{-3}T + 1.13381 \times 10^{-6}T^2$$

In these equations, p is in mm., t in °C., and T in °K. Ebulliometric vapor pressure measurements for perfluoropiperidine could not be extended into the usual lower vapor pressure range because of the relatively high freezing point (274.12°K.). The normal boiling point calculated from the Antoine equation is 49.62° (322.77°K.).

(23) C. Antoine, *Compt. rend.*, **107**, 681 (1888).
(24) E. R. Cox, *Ind. Eng. Chem.*, **28**, 613 (1936).

TABLE V

THE VAPOR PRESSURE OF PERFLUOROPIPERIDINE

Boiling point, °C. Water[a]	Perfluoropiperidine	p(obsd.), mm.	p(obsd.) − p(calcd.), eq. 4	eq. 5
80.000	29.138	355.22	−0.05	0.00
85	34.191	433.56	.00	+ .02
90	39.290	525.86	− .01	.00
95	44.421	633.99	+ .23	+ .23
105	54.847	906.06	− .08	− .05
110	60.117	1074.6	.0	+ .1
115	65.437	1268.0	− .2	− .1
120	70.798	1489.1	− .2	− .1
125	76.201	1740.8	.0	.0
130	81.646	2026.0	+ .3	.0

[a] N. S. Osborn, H. F. Stimson, and D. C. Ginnings, *J. Res. Natl. Bur. Std.*, **23**, 261 (1939).

Heat of Vaporization.—The heat of vaporization at 298.15°K. was computed from the Cox equation, the exact form of the Clapeyron equation, and an estimated value of −1.9 liter mole^{-1} for the second virial coefficient. The value for the heat of vaporization to the real gas is $\Delta Hv_{298.15}$ = 7.10 ± 0.05 kcal. mole^{-1}. From an unpublished correlation, the correction for gas imperfection is estimated to be 0.06 kcal. mole^{-1}, so the standard heat of vaporization is $\Delta Hv^\circ_{298.15}$ = 7.16 ± 0.05 kcal. mole^{-1}.

The Entropy.—The experimental and derived results given in the previous sections were used to calculate the entropy in the ideal gas state, S°, at 298.15°K., as shown in Table VI.

TABLE VI

MOLAL ENTROPY OF PERFLUOROPIPERIDINE IN THE IDEAL GAS STATE AT 298.15°K. IN CAL. DEG.$^{-1}$

S_s(liq.)[a]	94.02 ± 0.20[b]
$\Delta Hv/T$	23.81
S(ideal) − S(real)[c]	0.12
$R \ln P$[d]	−1.85
S°, ideal gas	116.10 ± 0.25[b]

[a] From Table IV. [b] Estimated accuracy uncertainty. [c] Estimated from an unpublished correlation. [d] Calculated by use of eq. 5.

Heat of Combustion.—The bomb, laboratory designation Pt-5 (volume, 0.353 l.), and calorimeter, laboratory designation BMR-2, have been described.[3c] The auxiliary oil, polyester film used for sample containers, and fuse also are described in ref. 3c. In trial combustion experiments with perfluoropiperidine with 30 atm. initial oxygen pressure in the bomb, a light deposit of "soot" formed on the walls, and a resinous deposit remained on the crucible. These difficulties were largely eliminated when the initial oxygen pressure was increased to 40 atm. Two of the ten calorimetric experiments required small corrections for incomplete combustion.

In the combustion of perfluoropiperidine under conditions of the calorimetric experiments, 79 to 81% of the fluorine appeared in the combustion products as CF_4; the remainder of the fluorine appeared as aqueous hydrofluoric acid. About 5 to 6% of the nitrogen appeared in the products as aqueous HNO_3; the remainder appeared as elemental nitrogen. Samples of HF-free gas from the combustion experiments, some of which were reduced in oxygen content by treatment with alkaline pyrogallate solution, were examined with a mass spectrometer. No fluorine-containing gases other than CF_4 were present in significant amounts.

The presence of nitrogen in the sample required two changes in the procedure normally used for fluorocarbons.[4] Because a significant amount of nitric acid was produced in the combustion experiment, nitric acid as well as hydrofluoric acid was needed in the initial solution for the comparison experiments.[3c,4] The presence of elemental nitrogen in the gaseous phase also necessitated appropriate changes in the reduction of the data to standard states.

Five determinations of energy of combustion including the accompanying comparison experiments were performed for each of the two samples, A and B, of perfluoropiperidine. It is im-

practical to report the results of all experiments, but detailed results of two determinations selected as typical are given in Table VII. The results of all experiments are summarized in Table VIII. The symbols in these tables are the same as those of ref. 3c. The values of $\Delta Ec^\circ/M$ for perfluoropiperidine apply to reaction II.

TABLE VII

SUMMARY OF TYPICAL DETERMINATIONS OF ENERGY OF COMBUSTION[a]

	Comparison experiments	
	Sample A	Sample B
m(benzoic acid), g.	0.73922	0.75354
m(auxiliary oil), g.	.29512	.28667
$n^i(H_2O)$, mole	.4938	.4943
n^i(HF), mole	.04451	.04472
$n^i(HNO_3)$, mole	.001110	.001104
Δt_c, deg.	1.97323	1.97257
$m\Delta Ec^\circ/M$(benzoic acid), cal.	−4666.63	−4757.03
$m\Delta Ec^\circ/M$(auxiliary oil), cal.	−3241.51	−3148.70
$m\Delta Ec^\circ/M$(fuse), cal.	−5.18	−5.35
$-\Delta E^i$ dec. (HNO_3), cal.	−0.89	−1.04
$-\Delta E$, cor. to st. states, cal.	−9.75	−9.78
$-\Delta E$, ign., cal.	−0.80	−0.54
ε(cont.)$(-\Delta t_c)$, cal.	26.11	26.15
ε_{app}(Calor.)$(-\Delta t_c)$, cal.	−7898.65	−7896.29
ε_{app}(Calor.), cal. deg.$^{-1}$	4002.90	4003.05
	Combustion experiments	
	Sample A	Sample B
m(perfluoropiperidine), g.	5.74513	5.75961
m(polyester), g. (at % rel. hum.)	0.13013 (54)	0.13167 (59)
$n^i(H_2O)$, moles	0.5523	0.5523
Δt_c, deg.	1.97856	1.98680
ε_{app}(Calor.)$(-\Delta t_c)$, cal.	−7919.98	−7953.26
ε(cont.)$(-\Delta t_c)$, cal.	−30.16	−30.29
ΔE, ign., cal.	0.64	0.89
ΔE, cor. to st. states, cal.	23.58	23.68
ΔE^i dec. (HNO_3), cal.	16.79	16.68
$-m\Delta Ec^\circ/M$(fuse), cal.	3.89	4.62
$-m\Delta Ec^\circ/M$(polyester), cal.	710.83	719.07
Cor. to st. CF_4 conversion, cal.[b]	40.93	42.22
$m\Delta Ec^\circ/M$(perfluoropiperidine), cal.	−7153.48	−7176.39
$\Delta Ec^\circ/M$(perfluoropiperidine), cal. g.$^{-1}$	−1245.14	−1245.99

[a] Physical properties of perfluoropiperidine at 25°: ρ = 1.730 g. ml.$^{-1}$, $(\partial E/\partial P)_T$ = −0.0069 cal. atm.$^{-1}$ g.$^{-1}$, c_p = 0.251 cal. deg.$^{-1}$ g.$^{-1}$. [b] Correction to the % of fluorine appearing as CF_4 in the combustion products according to reaction II; based on the value of the heat of hydrolysis of CF_4 determined in this Laboratory.[3c]

$$C_5F_{11}N(l) + 2.25O_2(g) + 21H_2O(l) = 2HF\cdot10H_2O(l) + 2.25CF_4(g) + 2.75CO_2(g) + 0.5N_2(g) \quad (II)$$

The average values of $\Delta Ec^\circ/M$ for samples A and B differ significantly. The value for pure perfluoropiperidine was calculated on the assumption of a linear variation of $\Delta Ec^\circ/M$ with concentration of impurity as found by gas–liquid chromatography. However, the accuracy uncertainty assigned is large enough to include the value for sample A and all values within twice the standard deviation of the mean thereof. Thus, $\Delta Ec^\circ/M$ for the pure compound is taken to be −1242.5 ± 2.7 cal. g.$^{-1}$. The 0.2% uncertainty is the penalty for samples that are inadequately pure for precision combustion calorimetry.

TABLE VIII

SUMMARY OF ENERGY OF COMBUSTION RESULTS

	Sample A	Sample B
$\Delta Ec^\circ/M$, cal. g.$^{-1}$ at 298.15°K.	−1245.15	−1246.92
	1244.86	1245.85
	1244.35	1245.35
	1244.39	1245.47
	1245.14	1245.99
Mean and std. dev.	−1244.78 ± 0.18	−1245.92 ± 0.28
Selected value	−1242.5 ± 2.7	

TABLE IX

THERMOCHEMICAL PROPERTIES OF PERFLUOROPIPERIDINE

Property	Value at 298.15°K., in kcal. mole^{-1}	
	Liquid	Ideal gas
ΔEc°[a]	−351.70 ± 0.80	
ΔHc°[a]	−349.77 ± 0.80	
ΔHf°[b]	−482.94	−475.78
ΔSf°[b]	−202.13	−180.05
ΔFf°[b]	−422.67	−422.10
log Kf	309.81	309.39

[a] For reaction II. [b] For the reaction: 5C(c, graphite) + $^{11}/_2F_2(g)$ + $^1/_2N_2(g)$ = $C_5F_{11}N$(l. or g.)

The Heat of Formation and Related Properties.—Molal values of ΔEc° and ΔHc° for reaction II are given in Table IX. The value for ΔHc° was combined with values of the heats of formation of H_2O(l), $HF\cdot10H_2O$(l) and CO_2(g) from N.B.S. Circular 500[7] and the value of the heat of formation of CF_4(g) obtained in this Laboratory[3c] to compute the heat of formation of liquid perfluoropiperidine, $\Delta Hf^\circ_{298.15}$(l). This value was combined with the value of heat of vaporization from a previous section to calculate $\Delta Hf^\circ_{298.15}$(g). The values of heat of formation were used with the standard entropy of perfluoropiperidine and entropy values for C(graphite),[7] N_2(g),[7] and F_2(g)[8] to compute values of the standard entropy of formation, free energy of formation, and logarithm of the equilibrium constant of formation given in Table IX.

1,2-BIS-DIFLUOROAMINO-4-METHYLPENTANE: HEATS OF COMBUSTION, FORMATION, AND VAPORIZATION; VAPOR PRESSURE; AND N–F THERMOCHEMICAL BOND ENERGY[1]

By W. D. Good, D. R. Douslin, and J. P. McCullough

Contribution No. 119 from the Thermodynamics Laboratory of the Bartlesville Petroleum Research Center, Bureau of Mines, U. S. Department of the Interior, Bartlesville, Okla.

Received January 12, 1963

The heat of combustion of 1,2-bis-difluoroamino-4-methylpentane was measured by rotating-bomb calorimetry, and the vapor pressure was measured between −20 and +20° with an inclined-piston gage. Experimental techniques suitable for studying compounds of this class were developed. The results were used to calculate the following thermochemical data in kcal. mole^{-1} at 298.15°K.: standard heat of formation of the liquid, −60.09; heat of vaporization, 10.51; and standard heat of formation of the gas, −49.58. The N–F thermochemical bond energy in this compound was found to be 67 kcal. mole^{-1}, about the same as the N–F thermochemical bond energy in NF_3 and N_2F_4 but significantly less than that in perfluoropiperidine.

In continuing studies of organic fluorine compounds, the Federal Bureau of Mines has made accurate thermodynamic measurements on 1,2-bis-difluoroamino-4-methylpentane.

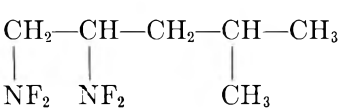

The heat of combustion of a purified sample was measured in a rotating-bomb calorimeter, and the vapor pressure was measured with a recently developed inclined-piston gage. The heat of vaporization and the standard heats of formation in the liquid and gas states at 298.15°K. were computed from the experimental results. The N–F thermochemical bond energy in this compound was compared with that in NF_3, N_2F_4, and perfluoropiperidine, the only other compounds for which the N–F bond energy has been determined accurately. This report also describes the purification of the sample used in the experiments and new techniques developed for combustion calorimetry and vapor-pressure measurements on compounds of this class.

Experimental

A. Material and Purification.—A sample of 1,2-bis-difluoroamino-4-methylpentane was provided through the courtesy of Dr. R. W. Walker, Rohm and Haas Co., Huntsville, Alabama. The material was purified by a preparative-scale g.l.c. method by T. C. Davis of the Bureau's Laramie (Wyo.) Petroleum Research Center. About 2-g. samples were charged to the purification unit, and fractions of about 1.5 g. were trapped and sealed in individual glass ampoules under nitrogen.

The purified sample was analyzed on a 0.25-in. by 40-ft. analytical g.l.c. column, operated at 120° and packed with 20 parts of Dow Corning 550 silicone oil per 100 parts of 30–42 mesh firebrick. The chromatogram showed one major component and three minor components. Analysis by a microhydrogenation technique[2] showed that the major component was 1,2-bis-difluoroamino-4-methylpentane and that the minor components were isomeric $C_6H_{12}N_2F_4$ compounds and a $C_5H_{10}N_2F_4$ compound. From these results, it was concluded that the sample was 99.8 mole % $C_6H_{12}N_2F_4$, with about 0.2 mole % $C_5H_{10}N_2F_4$ (probably 1,2-bis-difluoroamino-3-methylbutane). Also, the sample was shown to contain about 4.5 mole % of $C_6H_{12}N_2F_4$ isomers other than 1,2-bis-difluoroamino-4-methylpentane. These isomeric impurities (probably including some components with unbranched carbon skeletons) would not cause significant error in the experimental results. A small correction for the $C_5H_{10}N_2F_4$ impurity was applied in calculating the heats of combustion and formation.

B. Safety Precautions.—Compounds of this type are shock and spark sensitive. Consequently, the sample was always handled in 2-g. or smaller quantities, and it was possible in all the experimental procedures to provide shielding equipment adequate to prevent dangerous exposure of the investigator to an explosion. The samples were handled by tongs behind explosion shields while the investigator's hands and arms were protected by gauntlets. An ionizing radiation source was used to avoid accumulation of static electricity. Pipets were used instead of ground-glass syringes for transferring liquid samples to avoid frictional effects that might cause detonation. The compound probably is toxic and was handled as if it were.

C. Calorimetric Technique. Apparatus.—The rotating-bomb calorimeter, laboratory designation BMR-III, is similar to that previously described.[3] The modified platinum-lined bomb, Pt-5, internal volume 0.347 l., also has been described.[4]

Units of Measurements and Auxiliary Quantities.—For consistency with related published data, results reported herein are based on the 1951 International Atomic Weights[5] and fundamental constants[6] and the definitions: 0°C. = 273.15°K.; 1 cal. = 4.184 (exactly) joules. The laboratory weights had been calibrated at the National Bureau of Standards.

For reducing weights in air to *in vacuo*, converting the energy of the actual bomb process to the isothermal process, and reducing to standard states, the following estimated values, all for 298.15° K., were used for the difluoroamino compound: density, 1.15 g. ml.$^{-1}$; specific heat, 0.4 cal. deg.$^{-1}$ g.$^{-1}$; and $(\partial E/\partial P)_T$, −0.007 cal. atm.$^{-1}$ g.$^{-1}$.

The paraffin oil, polyester film, and fuse material have been described.[3,4]

Calibration.—The energy equivalent of the calorimetric system, $\mathcal{E}$(calor.), was determined by combustion of benzoic acid (National Bureau of Standards standard sample 39h, which was certified to evolve 26,434 ± 3 j. g.$^{-1}$ when burned under specified conditions). Five calibration experiments gave the value, $\mathcal{E}$(calor.) = 4030.98 ± 0.19 cal. deg.$^{-1}$ (mean and standard deviation).

Procedures.—The calorimetric and analytical procedures generally were those previously described for organic fluorine compounds.[3,4] However, ignition of the undiluted difluoroamino compound in the bomb resulted in detonation or other violent and incomplete reaction, as evidenced by unburned carbon in the products. Smooth and complete combustion reactions were obtained when the sample was diluted with a paraffin oil in such proportion that 58 to 75% of the evolved energy came from the diluent. Even such mixtures did not burn completely in

(1) This research was supported by the United States Air Force and the Advanced Research Projects Agency through the Air Force Office of Scientific Research of the Air Research and Development Command under Contract No. CSO 59-9, ARPA Order No. 24-59, Task 3. Reproduction in whole or in part is permitted for any purpose of the United States Government.

(2) C. J. Thompson, H. J. Coleman, C. C. Ward, and H. T. Rall, *Anal. Chem.*, **32**, 424 (1960).

(3) W. D. Good, D. W. Scott, and G. Waddington, *J. Phys. Chem.*, **60**, 1080 (1956).

(4) W. D. Good, D. R. Douslin, D. W. Scott, A. George, J. L. Lacina, J. P. Dawson, and G. Waddington, *ibid.*, **63**, 1133 (1959).

(5) E. Wichers, *J. Am. Chem. Soc.*, **74**, 2447 (1952). Use of the recently adopted unified atomic weight scale (*Chem. Eng. News*, Nov. 20, 1961, p. 42) would not change the results significantly.

(6) F. D. Rossini, F. T. Gucker, Jr., H. L. Johnston, L. Pauling, and G. W. Vinal, *J. Am. Chem. Soc.*, **74**, 2699 (1952).

several experiments, data from which were rejected in computing the final results.

To prepare a diluted sample, the appropriate quantity of nonvolatile paraffin oil,[3] USBM-P3a, empirical formula $CH_{1.891}$, was placed in a previously weighed bag of polyester film, and the mass of oil plus bag was determined. A sample of the difluoroamino compound was then introduced by a pipet, the bag was sealed, the components were mixed, and the filled bag was weighed. In this way, the mass of each component of the combustion sample, including container, was determined accurately. To obtain a perfect closure of the bag, these operations were carried out so that no liquid touched the edges to be sealed, and it was necessary to leave a small air bubble in the neck of the bag.

For the comparison experiments,[3] the combustion example was paraffin oil ($\Delta Ec^\circ/M$ = 10984.12 cal. g.$^{-1}$), and enough aqueous HF and HNO_3 were added to the bomb to produce final states essentially the same as those obtained in the experiments with the difluoroamino compound.

D. Vapor Pressure Measurements.—The Bureau of Mines recently developed an apparatus, to be described elsewhere, for accurate vapor pressure measurements in the range 0.01–40 mm., a range in which previous devices were not satisfactory for many thermodynamic purposes. It was especially designed for studies of sensitive or high-boiling substances, and its first application other than tests with water was in the measurements reported here. The instrument, an inclined-piston gage, is a novel adaptation of the piston–cylinder principle long used in dead-weight gages at high pressures. In these experiments, a one-gram sample was contained in a glass bulb immersed in a thermostat. The sample was thoroughly outgassed by cycles of freezing in liquid nitrogen, evacuation, and thawing. It was necessary to distil several small portions from the bulb before reproducible vapor pressure results could be obtained on the remaining sample. This procedure probably removed a small quantity of volatile impurity and residual dissolved nitrogen. The precision of the measurements was about ±0.001 mm., and the estimated absolute accuracy (not including the effect of impurities) ranges from ±0.001 mm. at the lowest pressures to ±0.02 mm. at the highest.

Results

Calorimetric Results.—Seven satisfactory combustion experiments and corresponding comparison experiments were performed. Data for a single pair of combustion and comparison experiments, selected as typical of all experiments, are given in Table I. The final results of all experiments are given at the bottom of Table I. The values of $\Delta Ec^\circ/M$ in this table refer to the idealized combustion reaction 1.

$$C_6H_{12}N_2F_4(\text{soln. in oil}) + 8O_2(g) + 196H_2O(l) = 6CO_2(g) + N_2(g) + 4[HF\cdot 50H_2O](l) \quad (1)$$

In computing the results, the heat of mixing of the substance and paraffin oil was neglected. This heat effect should be small enough to be included in the stated uncertainty interval, for no significant trend was noted in the results for samples of varying composition.

Analysis of the products of the combustion reactions indicated that the HF formed represented 99.9 ± 0.3% of that to be expected from reaction of pure $C_6H_{12}N_2F_4$. This result is confirming evidence for the purity of the sample and the assumed stoichiometry of the combustion reaction.

Vapor Pressure and Heat of Vaporization.—The results of vapor-pressure measurements in the range −20 to +20° are given in Table II. These results are represented by the Antoine equation

$$\log p = 6.88576 - 1427.201/(209.946 + t) \quad (2)$$

where p is in mm. and t is in °C. Equation 2 does not represent the experimental results within their precision (see Table II), but it is satisfactory for most purposes.

TABLE I

TYPICAL PAIR OF COMBUSTION AND COMPARISON EXPERIMENTS[a]

	Combustion experiment	Comparison experiment
m(compound), g.	0.53218	
m(auxiliary oil), g.	.41913	0.71285
m(polyester), g. (at % rel. hum.)	.07774 (52)	
$n^i(H_2O)$, mole	.55344	.54599
n^i(HF), mole		.01131
$n^i(HNO_3)$, mole		.00101
Δt_c, deg.	2.00401	1.93876
ε(calor.)$(-\Delta t_c)$, cal.	−8081.1	−7818.0[b]
ε(cont.)$(-\Delta t_c)$, cal.[c]	−27.0	−25.6
$\Delta E_{ign.}$, cal.	0.7	0.5
ΔE, cor. to st. states, cal.	6.6	6.0
ΔE, cor. for impurity	−0.5	
$\Delta E^f_{dec.}(HNO_3)$, cal.	14.2	1.4
$-m\Delta Ec^\circ/M$(fuse), cal.	5.1	5.7
$-m\Delta Ec^\circ/M$(oil), cal.	4603.8	7830.0
$-m\Delta Ec^\circ/M$(polyester), cal.	424.7	
$m\Delta Ec^\circ/M$(compound), cal.	−3053.5	
$\Delta Ec^\circ/M$(compound), cal. g.$^{-1}$	−5757.7	

$\Delta Ec^\circ/M$, cal. g.$^{-1}$, all results: −5748.2, −5739.9, −5732.5, −5734.8, −5731.4, −5737, −5734.6.

$\Delta Ec^\circ/M$, cal. g.$^{-1}$, mean and std. dev.: −5737.0 ± 2.2.

[a] The symbols and terminology are, except as noted, those of W. N. Hubbard, D. W. Scott, and G. Waddington, "Experimental Thermochemistry," F. D. Rossini, Ed., Interscience Publishers, Inc., New York, N. Y., 1956, Chapter 5, pp. 75–128. [b] Value used to determine ε(calor.) for the corresponding combustion experiment. [c] ε^i(Cont.)$(t_i - 25°) + \varepsilon^f$(Cont.)$(25° - t_f + \Delta t_{corr.})$.

The Clapeyron equation and eq. 2 were used to compute the standard heat of vaporization, $\Delta Hv^\circ_{298.15}$ = 10.51 ± 0.05 kcal. mole^{-1}.

TABLE II

VAPOR PRESSURE OF 1,2-BIS-DIFLUOROAMINO-4-METHYLPENTANE

t, °C.	p(obsd.), mm.	p(obsd.) − p(calcd.), mm.
−20.000	0.236	0.000
−15.000	.364	− .003
−10.000	.560	.000
− 5.000	.843	+ .007
0.000	1.235	+ .010
+ 5.000	1.743	− .019
10.000	2.466	− .028
15.000	3.478	+ .002
20.000	4.812	+ .036

Heat of Formation.—Table III lists derived thermochemical data, including the heat of formation. The values of ΔEc° and ΔHc° apply to the idealized reaction, eq. 1. The values of heat of formation, ΔHf°, refer to equation 3 and were computed from ΔHc°, ΔHv°, and heat of formation data for carbon dioxide,[7] water,[7] and aqueous HF.[7]

$$6C(c, \text{graphite}) + 6H_2(g) + N_2(g) + 2F_2(g) = C_6H_{12}N_2F_4(l \text{ or } g) \quad (3)$$

Discussion of Results

The thermodynamic data given herein are the first accurate values reported for any organic difluoroamino compound, a new class[8] of much theoretical interest. The only other compounds containing N–F bonds for

(7) F. D. Rossini, D. D. Wagman, W. H. Evans, S. Levine, and I. Jaffe, "Selected Values of Chemical Thermodynamic Properties," Natl. Bur. Std. Circ. 500, 1952.

(8) R. C. Petry and J. P. Freeman, *J. Am. Chem. Soc.*, **83**, 3912 (1961).

TABLE III

THERMOCHEMICAL DATA FOR 1,2-BIS-DIFLUOROAMINO-4-METHYLPENTANE IN KCAL. MOLE^{-1} AT 298.15°K.

$\Delta Ec°$	Liquid	-1079.54 ± 0.80[a]
$\Delta Hc°$	Liquid	-1080.13 ± 0.80[a]
$\Delta Hf°$	Liquid	-60.09
$\Delta Hv°$		$+10.51 \pm 0.05$
$\Delta Hf°$	Gas	-49.58

[a] Uncertainty is the uncertainty interval equal to twice the final "over-all" standard deviation.

which accurate thermochemical data are available are NF_3,[9] N_2F_4,[10] and perfluoropiperidine.[11] The N–F thermochemical bond energy, E(N–F), in the last three compounds is reported to be 66,[9] 66,[10] and 73[11] kcal. mole^{-1}, respectively. Although bond energy calculations are arbitrary for complex organic compounds, a reasonable estimate can be made of E(N–F) in 1,2-bis-difluoroamino-4-methylpentane for comparison with the foregoing values. Consider the following hypothetical reaction

$$\begin{array}{l} CH_2\text{—}CH\text{—}CH_2\text{—}CH\text{—}CH_3(g) + H_2(g) = \\ \quad|\quad\;|\quad\quad\;|\quad\quad\;\; \\ NF_2\;\;NF_2\quad\;\;CH_3 \end{array}$$

$$\begin{array}{l} CH_3\text{—}CH_2\text{—}CH_2\text{—}CH\text{—}CH_3(g) + N_2(g) + 2F_2(g). \\ \qquad\qquad\qquad\qquad\quad|\quad\quad\;\; \\ \qquad\qquad\qquad\qquad CH_3 \end{array}$$

for which

$$\Delta H = \Delta Hf°_{298.15}[C_6H_{14}(g)] - \Delta Hf°_{298.15}[C_6H_{12}N_2F_4(g)] = 4E(\text{N–F}) + 2E(\text{C–N}) + E(\text{H–H}) - E(\text{N–N}) - 2E(\text{F–F}) - 2E(\text{C–H})$$

where the E's are thermochemical bond energies. From this relationship, the heats of formation of the difluoroamino compound and 2-methylpentane,[12] and a consistent set of bond energies [E(H–H) = 104.204[13]; E(F–F) = 37.806[14]; E(N≡N) = 226.090[15]; E(C–H) = 99.297, from the heat of formation of methane[7] and the heat of atomization of carbon[15]; E(N–H) = 93.4, from the heat of formation of ammonia[7]; and E(C–N) = 67.41, from the heat of formation of dimethylamine[16]], the N–F bond energy in 1,2-bis-difluoroamino-4-methylpentane was calculated to be E(N–F) = 67 kcal. mole^{-1}. This value is about the same as those for NF_3 and N_2F_4, but it is significantly less than that for perfluoropiperidine.

(9) G. T. Armstrong, S. Marantz, and C. F. Coyle, *J. Am. Chem. Soc.*, **81**, 3798 (1959).

(10) G. T. Armstrong, S. Marantz, and C. F. Coyle, Natl. Bur. Std., Report No. 6584 (1961).

(11) W. D. Good, S. S. Todd, J. F. Messerly, J. L. Lacina, J. P. Dawson, D. W. Scott, and J. P. McCullough, *J. Phys. Chem.*, **67**, 1306 (1963).

(12) "Selected Values of Physical and Thermodynamic Properties of Hydrocarbons and Related Compounds," American Petroleum Institute Research Project 44, Carnegie Press, Pittsburgh, Penna., 1953.

(13) A. G. Gaydon, "Dissociation Energies," Chapman and Hall, London, 1953.

(14) W. H. Evans, T. R. Munson, and D. D. Wagman, *J. Res. Natl. Bur. Std.*, **55**, 147 (1955).

(15) L. Brewer and A. W. Searcy, *Ann. Rev. Phys. Chem.*, **7**, 259 (1956).

(16) W. H. Johnson, I. Jaffe, and E. J. Prosen, *J. Res. Natl. Bur. Std.*, **65A**, 71 (1961).

THE THREE ELECTRON (OR HOLE) CUBIC LIGAND FIELD SPECTRUM[1]

BY ANDREW D. LIEHR[2]

Bell Telephone Laboratories, Inc., Murray Hill, New Jersey, and Mellon Institute, Pittsburgh 13, Pennsylvania

Received January 14, 1963

The theoretical dependence of the energy with respect to the ligand field coulombic (Dq), spin-orbit (ζ), and electron correlation parameters (B and C) for $kd^{3,7}$ (k = 3, 4, 5), transition metal systems is applied to a variety of fresh experimental situations, and a number of surprising new results are obtained. First, it is found that the use of the "exact" ligand field energy level scheme to interpret the spectral features of a number of carefully chosen test systems introduces fundamental alterations in the established theory of nephelauxetic shifts [that is, the displacements of the energy levels due to reductions in the magnitude of the electron correlation parameter B as compared with its free ion value]. Second, the experimental rule of systematic variation of spectral frequency with alternant ligands [the so-called spectrochemical variation] is subject to strict reservations in crystalline media. Third, the effects of next nearest neighbor polarizations are important in fixing the magnitude of the ligand field coulombic parameter Dq. And fourth, an unambiguous determination of all the ligand field parameters can only be accomplished upon experimental resolution of the large number of distinct spin forbidden multiplets permitted by the exact theory. Sample systems are discussed to illustrate each of these results, and precautionary words are spoken to dampen some of the wild enthusiasm currently prevalent in the use of elementary ligand field concepts.

Introduction

The most general set of secular equations for a kd,[3,7] (k = 3, 4, 5), transition metal complex in a cubic environs which is allowed by the fundamental approximations of ligand field theory has recently been derived by Eisenstein,[3] and subsequently has been utilized by him to interpret the magnetic and optical properties of K_2ReCl_6 and IrF_6. Concomitantly, Weakliem,[4] Racah,

(1) This paper was originally scheduled to appear under the joint by-line of Andrew D. Liehr, James Ferguson, and Darwin L. Wood, and was so referenced in previous advertisements of the author. The author most firmly believes that the by-line should still so read. However, Drs. Ferguson and Wood believe otherwise and have most firmly pressed upon the author the duty of changing this by-line to its present form. The work reported in this article is a direct result of over two years of close collaborative effort with Drs. Wood and Ferguson, and hence, is in nowise the sole production of the author. Indeed, most of the figures and tables here recorded and much of the text are joint preparations of all three of us. Thus, in reading and referencing this work please be sure to associate it most intimately with the several works of Drs. Ferguson and Wood on the experimental and interpretive aspects of the three electron and hole ligand field problem (ref. 28a, 37m, 38f, and 39d). This paper was presented, in part, by the three of us at the Symposia on Molecular Structure and Spectroscopy, Ohio State University, Columbus, Ohio, June, 1961 (A. D. L.), and 1962 (A. D. L., J. F., and D. L. W.).

(2) Mellon Institute, Pittsburgh 13, Penna.

(3) J. C. Eisenstein, *J. Chem. Phys.*, **32**, 1887 (1960); **33**, 1530 (1960); **34**, 1628 (1961) [*Errata, ibid.*, **35**, 2246 (1961)].

Schonfeld, and Low,[5] and Runciman and Schroeder[6] also have derived complete secular determinants for the $kd^{3,7}$ systems in the crystalline field approximation.[7] These papers represent the first real advancement made in the theory of the $kd^{3,7}$ transition metal compounds since the classic work of Finkelstein and Van Vleck in 1940.[8] However, none of these authors has utilized their theory to characterize chemically and physically the optical behavior of the three electron (or hole) transition metal compounds: they confined their considerations to a detailed examination of quite specific complexes. What we wish to do here is to investigate critically and circumscribe carefully the realm of applicability of ligand field theory, in particular of the crystalline field approximation, for three particle (and hole) transition metal chemicals. This study represents a continuation of our previous indagations into the utility of the crystalline field approximation in the "exact" theory of ligand fields.[9,10]

Critique

Since the relevant theory has been outlined a number of times now,[3-6,8,10-16] we shall content ourselves with a few specific comments. Firstly, we must recognize at the outset its inherent limitations. As we use the Slater–Condon–Shortley[17] method, our theory can be no more accurate than the method employed. It is well known that the conventional Slater–Condon–Shortley technique cannot predict accurately the locations and symmetries of all the atomic (free ion) kd^n energy levels.[17,18] In Tables I through IV and Fig. 1 through 4 we illustrate this fact for vanadium(III), chromium(III), cobalt(II), and nickel(II).[19] We see that the standard three parameter theory yields tolerably good agreement, but that the minimum spin valued configurations generally are poorly represented. Indeed, for chromium(III) the ^2P configuration is actually computed to be in the wrong spectral region (look at Table II and Fig. 2). The reasons for these discrepancies are well understood: they arise from a neglect of higher lying configurations, such as $d^{n-1}s^1$, and of electronic correlations in the computations.[20] What must be remembered, however, is that these same discrepancies will be carried over into the molecular complex. Hence, we cannot expect our computations to be any more accurate than the Slater–Condon–Shortley procedure upon which they are based.

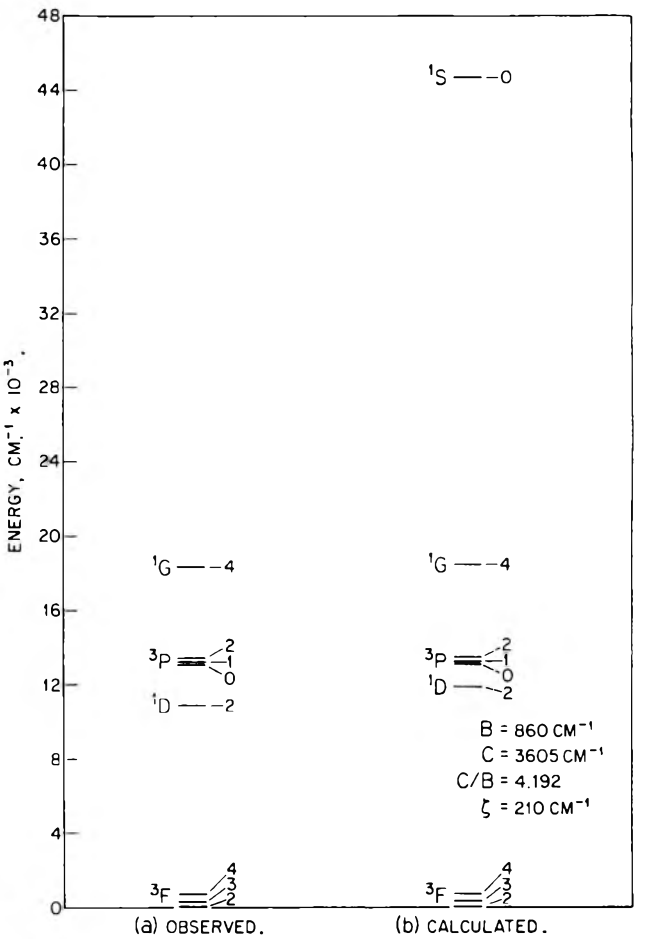

Fig. 1.—Plot of the experimental and theoretical energy levels for the vanadium(III) free ion.

TABLE I

PREDICTED AND OBSERVED SPECTRA FOR THE V(III) FREE ION IN CM.$^{-1}$

Level	Obsd.[a]	Calcd. (B = 860, C = 3605, ζ = 210 cm.$^{-1}$)
$^3F_2$	0	0
$^3F_3$	318	323.9
$^3F_4$	730	741.3
$^1D_2$	10,960	11,887.9
$^3P_0$	13,121	13,110.5
$^3P_1$	13,238	13,223.9
$^3P_2$	13,453	13,493.7
$^1G_4$	18,389	17,961.4
$^1S_0$	....	44,592.3

[a] C. E. Moore, "Atomic Energy Levels," Vol. I, Circular of the National Bureau of Standards 467, Washington, D. C., 1949.

(4) H. A. Weakliem, Jr., private communication, 1960, and Document No. 7139, ADI Auxiliary Publications Project, Photoduplication Service, Library of Congress, Washington 25, D. C. (the Appendices of ref. 21b).

(5) G. Racah, G. Schonfeld, and W. Low, private communication, 1960, and G. Schonfeld, Thesis, Hebrew University, Israel, 1959.

(6) W. A. Runciman and K. A. Schroeder, *Proc. Roy. Soc.* (London), **265A**, 489 (1962).

(7) We shall denote here by the crystalline field approximation that modification of ligand field theory which substitutes for the general molecular orbital electron–electron repulsion integrals and spin–orbit interaction integrals suitable averages such that the resultant mathematics adopts the mien of an ionic hypothesis.

(8) R. Finkelstein and J. H. Van Vleck, *J. Chem. Phys.*, **8**, 790 (1940).

(9) By an "exact" theory we signify a complete eigenvalue–eigenvector calculation carried out within the confines of a pseudo kd^n basis. The complete computation of this type reported here was performed on the IBM 7090 data processing machine at the Murray Hill Bell Telephone Laboratories, programmed by J. D. Sautter.

(10) (a) A. D. Liehr and C. J. Ballhausen, *Ann. Phys.* [N. Y.], **6**, 134 (1959); (b) A. D. Liehr, *J. Phys. Chem.*, **64**, 43 (1960).

(11) A. Abragam and M. H. L. Pryce, *Proc. Roy. Soc.* (London), **206A**, 173 (1951).

(12) Y. Tanabe and S. Sugano, *J. Phys. Soc. Japan*, **9**, 753 (1954), *et seq.*

(13) L. E. Orgel, *J. Chem. Phys.*, **23**, 1004 (1955), *et seq.*

(14) (a) C. J. Ballhausen and C. K. Jørgensen, *Dan. Mat. Fys. Med.*, **29**, No. 14, 1955; (b) C. K. Jørgensen, *Acta Chem. Scand.*, **9**, 116 (1955).

(15) (a) H. Hartmann and H.-H. Kruse, *Z. physik. Chem.* (Frankfurt), **5**, 9 (1955); (b) H. Hartmann and H.-H. Schmidtke, *ibid.*, **19**, 43 (1959).

(16) B. Jezowska-Trzebiatowska and W. Wojciechowski, *Bull. Acad. Pol. Sci. Ser. Sci. Chim.*, **9**, 693 (1961).

(17) (a) E. U. Condon and G. H. Shortley, "The Theory of Atomic Spectra," Cambridge University Press, London and New York, 1953; (b) J. C. Slater, "Quantum Theory of Atomic Structure," Vol. I and II, McGraw-Hill, New York, N. Y., 1960.

(18) J. S. Griffith, "The Theory of Transition-Metal Ions," Cambridge University Press, Cambridge, 1961.

(19) We here employ the more logical chemical rather than the spectroscopical notation.

(20) (a) C. K. Jørgensen, *Acta Chem. Scand.*, **9**, 717 (1955); (b) K. Hijikata, *Bull. Am. Phys. Soc. Ser. II*, **2**, 315 (1957); (c) G. Racah and Y. Shadmi, *Bull. Res. Counc. Israel*, **8F**, 15 (1959); (d) W. Low and M. Weger, *Phys. Rev.*, **118**, 1119 and 1130 (1960); [*Errata*, *ibid.*, **120**, 2277 (1960)]; (e) H. B. Gray and C. J. Ballhausen, *Acta Chem. Scand.*, **15**, 1327 (1961); (f) R. E. Trees and C. K. Jørgensen, *Phys. Rev.*, **123**, 1278 (1961).

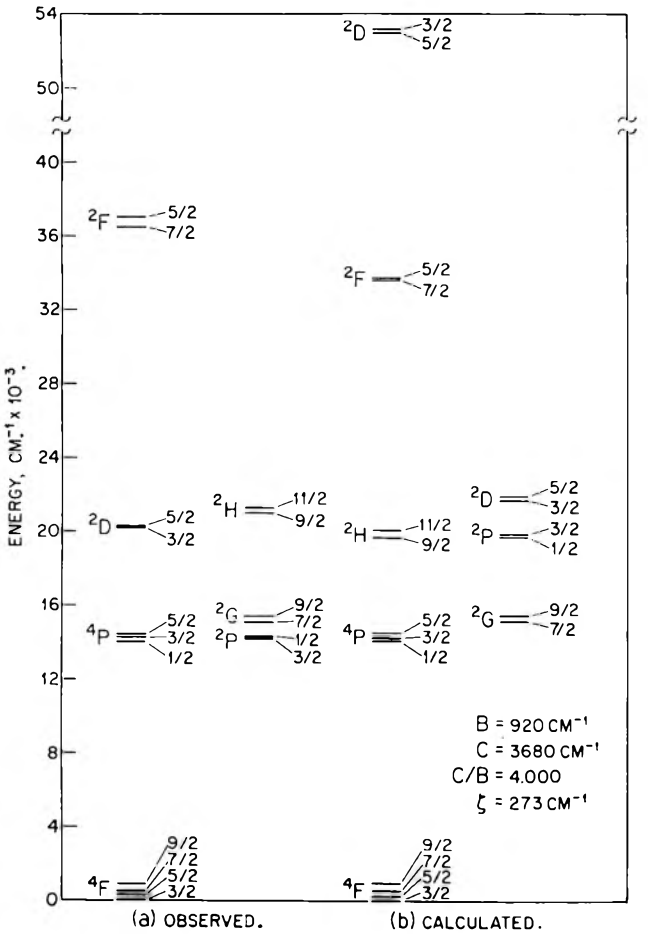

Fig. 2.—Plot of the experimental and theoretical energy levels for the chromium(III) free ion.[1,37m]

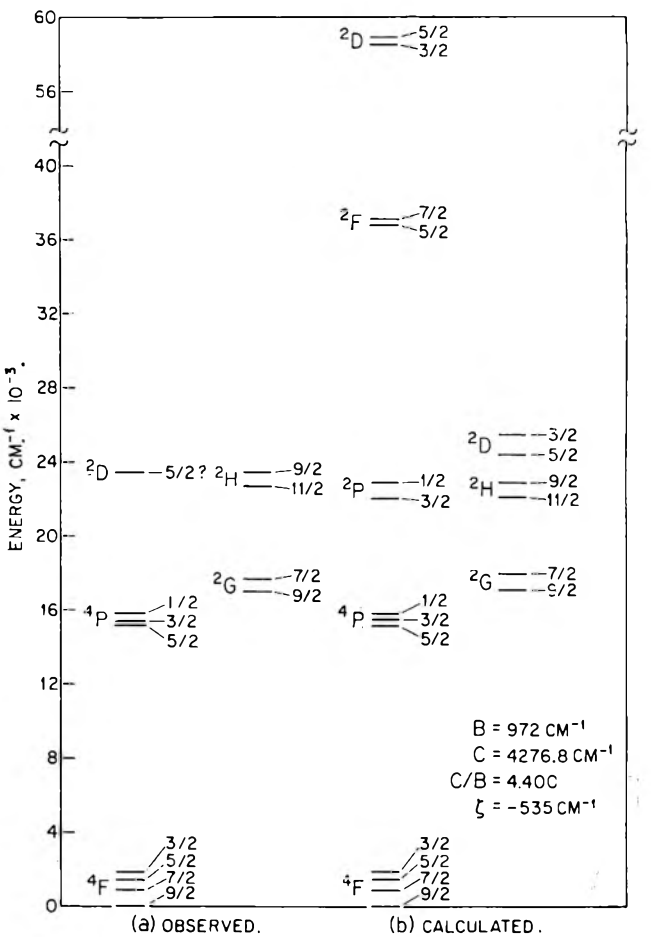

Fig. 3.—Plot of the experimental and theoretical energy levels for the cobalt(II) free ion.[1,28a]

TABLE II

PREDICTED AND OBSERVED SPECTRA FOR THE Cr(III) FREE ION IN CM.$^{-1}$

Level	Obsd.[a]	Calcd. (B = 920, C = 3680, ζ = 273 cm.$^{-1}$)
$^4F_{3/2}$	0	0
$^4F_{5/2}$	244	235.5
$^4F_{7/2}$	561	557.2
$^4F_{9/2}$	956	958.0
$^4P_{1/2}$	14,072	14,113.1
$^4P_{3/2}$	14,215	14,216.9
$^4P_{5/2}$	14,481	14,489.2
$^2G_{7/2}$	15,064	15,076.1
$^2G_{9/2}$	15,414	15,412.3
$^2P_{1/2}$	14,317	19,720.1
$^2H_{9/2}$	21,078	19,763.2
$^2P_{3/2}$	14,185	19,838.4
$^2H_{11/2}$	21,328	20,017.8
$^2D_{3/2}$	20,218	21,679.3
$^2D_{5/2}$	20,667	21,891.0
$^2F_{7/2}$	36,490	33,617.6
$^2F_{5/2}$	37,062	33,765.0
$^2D_{5/2}$	....	52,945.8
$^2D_{3/2}$	....	53,109.4

[a] C. E. Moore, "Atomic Energy Levels," Vol. II, Circular of the National Bureau of Standards 467, Washington, D. C., 1952.

TABLE III

PREDICTED AND OBSERVED SPECTRA FOR THE Co(II) FREE ION IN CM.$^{-1}$

Level	Obsd.[a]	Calcd. (B = 972, C = 4276.8, ζ = −535 cm.$^{-1}$)
$^4F_{9/2}$	0	0
$^4F_{7/2}$	841.2	830.9
$^4F_{5/2}$	1,451.3	1,441.5
$^4F_{3/2}$	1,866.8	1,860.4
$^4P_{5/2}$	15,201.9	15,129.2
$^4P_{3/2}$	15,428.2	15,436.7
$^4P_{1/2}$	15,811.4	15,806.1
$^2G_{9/2}$	16,977.7	17,148.2
$^2G_{7/2}$	17,766.2	17,959.8
$^2P_{3/2}$	.....	22,016.6
$^2H_{11/2}$	22,720.3	22,155.0
$^2P_{1/2}$	.....	22,843.0
$^2H_{9/2}$	23,434.3	22,878.3
$^2D_{5/2}$	23,058.8 ?	24,405.5
$^2D_{3/2}$	.....	25,557.6
$^2F_{5/2}$	.....	36,799.9
$^2F_{7/2}$	.....	37,153.4
$^2D_{3/2}$	.....	58,492.9
$^2D_{5/2}$	.....	58,830.7

[a] See ref. *a* of Table II.

Secondly, it must be borne in mind that the ligand field theory is itself just an approximation to a complete molecular orbital theory, and therefore has certain innate qualifications. For one, the influence of the charge transfer states on the kd^n molecular orbital states of the complex is neglected.[20,21] Two, the usual reduction of the ten[22] independent kd^n electron–electron coulombic

(21) (a) C. J. Ballhausen and A. D. Liehr, *J. Mol. Spectry.*, **2**, 348 (1958) [*Errata, ibid.*, **4**, 190 (1960)]; (b) H. A. Weakliem, Jr., *J. Chem. Phys.*, **36**, 2117 (1962).

(22) Actually only eight electron repulsion integrals are required,[23e] as one of the original ten integrals, together with the totally symmetric electron-nuclear interactions, serves solely to fix the energy zero for the system, and the other contributes exclusively to the ligand field strength, Dq.[23c,e]

TABLE IV

PREDICTED AND OBSERVED SPECTRA FOR THE Ni(II) FREE ION IN CM.$^{-1}$

Level	Obsd.[a]	Calcd. (B = 1042, C = 4060, ζ = −666 cm.$^{-1}$)
$^3F_4$	0	0
$^3F_3$	1,360.7	1,352.5
$^3F_2$	2,269.6	2,262.9
$^1D_2$	14,031.6	14,032.8
$^3P_2$	16.661.6	16,721.8
$^3P_1$	16,977.8	16,982.5
$^3P_0$	17,230.7	17,239.7
$^1G_4$	23,108.7	21,664.0
$^1S_0$	.....	52,439.3

[a] A. G. Shenstone, *J. Opt. Soc. Am.*, **44**, 749 (1954).

repulsion integrals and the two independent kd^n spin-orbit integrals[3,12,18,23,24] to but three repulsion integrals, the (average) ligand field Racah parameters A, B, C, and but one spin–orbit integral,[10b,15b,18,23d,f,24] the (average) ligand ζ parameter, is invoked.[25] Three, the use of complete electron-hole complementarity is unfounded.[26] Four, the interaction of nuclear and electronic motions which give rise to Franck–Condon, Herzberg–Teller, and Jahn–Teller envelopes is ignored.[27] Five, the contributions of the environment which produce electron–lattice (either solid or liquid) and magnetic–magnetic exchange profiles are suppressed[28]; and so on.

Thirdly, the intrinsic reservations of the molecular orbital technique must be recognized. It is extremely doubtful whether such things as molecular orbitals, even when they are not constructed from atomic functions, exist. Certainly, the indications of current attempts at the rigorous solution of atomic and molecular problems are that they definitely do not.[17b,29,30] What is of general authenticity in the orbital procedure are the principles of symmetry. All results from the orbital employment which derive from symmetry concepts alone are universally valid. Hence, only those deductions of molecular orbital theory which are based solely upon symmetry precepts are to be regarded as final.[31]

We must expect theoretical incertitude of these sorts to temper our mathematical derivations and to condition our physical inferences. However, as will be seen in what follows, despite these incertitudes much use can be made of the simplified theory we employ. Indeed, new physical notions may be uncovered by its application. In this paper on the kd^n, (n = 3,7), transition metal compounds, as in its predecessors,[10a,b] (n = 1, 2, 8, 9), and its successors,[32] (n = 4, 5, 6), we shall demonstrate, by example, both this pragmatic utility and this detective capacity of the simple ligand field approach to transition metal spectroscopy, as well as to underscore explicitly its practical bounds.

Analysis

Although a large number of $kd^{3,7}$ transition metal chemicals have been spectroscopically investigated of late,[33] relatively few of these have been viewed with the utmost in precision and detail under wide ranges of

(23) (a) K. W. H. Stevens, *Proc. Roy. Soc.* (London), **219A**, 542 (1953); (b) C. K. Jørgensen, *Acta Chem. Scand.*, **12**, 903 (1958); (c) H. S. Jarrett, *J. Chem. Phys.*, **31**, 1579 (1959); (d) Y. Tanabe, *Progr. Theoret. Phys., Suppl.*, No. **14**, 17 (1960); (e) G. F. Koster, "Multiplet Structure in Crystalline Fields," Quart. Progr. Rept. Solid State and Mol. Theory Group M.I.T., Jan. 15, 1960, pp. 3–15; (f) S. Sugano, *J. Appl. Phys. Suppl.*, **33**, 303 (1962).

(24) (a) Y. Tanabe and H. Kamimura, *J. Phys. Soc. Japan*, **13**, 394 (1958). Please note that if the crystalline or molecular symmetry is lower than cubic, one (or two if the symmetry is less than trigonal) additional spin–orbit integral is needed [read for instance reference 15b and (b) H. Kamimura, *Phys. Rev.*, **128**, 1077 (1962)].

(25) The justification of this procedure runs as follows. It is anticipated that the five independent coulomb and five independent exchange integrals of the form $(ab|e^2/r_{12}|cd)$, will each be expressible in terms of generalized Racah parameters, A_j, B_j, and C_j, say (j = 0, 1, 2, 4), where the index j specifies the occupancy number of the e type molecular orbitals (this conversion is *not* exact as the expansions in terms of the parameters for j equals 2 and 4 are over determined and under determined by one relation, apiece). It is further expected that the spread in value of these three sets of parameters, A_j, B_j, C_j, (j = 0, 1, 2, 4), and of the two spin–orbit parameters, ζ_j, (j = 0, 1), about their respective means, A, B, C, and ζ will be small (in reckoning this average the null valued quantities A_1 and C_1 are excluded). Thus, it is concluded that a four variable theory will be applicable.

(26) This assertion may be readily verified upon comparison of Eisenstein's[3] energy matrices for kd^3 chemicals with those expected for kd^7 compounds. Griffith has independently uncovered this same truth and has given an elegant proof of its ecumenicity.[18]

(27) (a) H. Sponer and E. Teller, *Rev. Mod. Phys.*, **13**, 76 (1941); (b) R. S. Mulliken and C. A. Rieke, *Rept. Prog. Phys.*, **8**, 231 (1941); (c) D. P. Craig, *J. Chem. Soc.*, 2146 (1950); (d) C. J. Ballhausen, "Progress in Inorganic Chemistry," Vol. 2, F. A. Cotton, Ed., Interscience Publishers, Inc., New York and London, 1960, pp. 251–265; (e) R. Englman, *Trans. Faraday Soc.*, **57**, 236 (1961); (f) A. D. Liehr, "Advances in Chemical Physics," Vol. V, I. Prigogine, Ed., Interscience Publishers, Inc., New York and London, 1962, pp. 241–259; (g) S. Koide and Y. Mizuno, to be published.

(28) (a) J. Ferguson, to be published; (b) K. Knox, R. G. Shulman, and S. Sugano, *Bull. Am. Phys. Soc. Ser. II*, **5**, 415 (1960), and to be published.

(29) "Papers from the Conference on Molecular Quantum Mechanics Held at the University of Colorado, Boulder, Colorado, June 21–27, 1959," *Rev. Mod. Phys.*, **32**, 169 (1960).

(30) Both in the atomic and molecular cases the need for the explicit introduction of configurational interaction and/or electron correlation in computations shows the circumscribed nature of the orbital assumption.[17b,29]

(31) A most powerful method for obtaining such deductions is that of irreducible tensorial sets [(a) M. E. Rose, "Multipole Fields," John Wiley and Sons, Inc., New York, N. Y., 1955; (b) M. E. Rose, "Elementary Theory of Angular Momentum," John Wiley and Sons, Inc., New York, N. Y., 1957; (c) A. R. Edmonds, "Angular Momentum in Quantum Mechanics," Princeton University Press, Princeton, N. J., 1957; (d) U. Fano and G. Racah, "Irreducible Tensorial Sets," Academic Press, Inc., New York, N. Y., 1959; (e) J. S. Griffith, "The Irreducible Tensor Method for Molecular Symmetry Groups," Prentice-Hall, Inc., Englewood Cliffs, N. J., 1962; (f) G. F. Koster, *Phys. Rev.*, **109**, 227 (1958)], a method which was first applied to ligand field theory by Abragam and Pryce.[11] Samples of its potency are underscored by general affirmations of the kind: (1) the weak field representation of ligand field theory is just that representation in terms of the basic irreducible tensorial sets of order l equals two for e and t_2 type functions combined in direct product form to yield irreducible tensorial sets of order L and finally of order J, where $\vec{J}$ equals $\vec{S} + \vec{L}$; (2) the operator equivalent description of addend field relations can be succinctly justified by means of the universalized Wigner–Eckart theorem of irreducible tensorial set theory; (3) the spin Hamiltonian picturization of augend field effects may be neatly derived by considerations of either tensorial invariants or of transformational equivalents; (4) the barycenter invariance regulations of ligand field theory are quickly proved by the generalized trace theorem of irreducible tensorial set theory; and so forth. Some of these samples, as well as others, have been independently noted and commented upon previously.[11,12,18,20d,23c,d,24,31e,f,g,h,i] [(g) G. F. Koster and H. Statz, *Phys. Rev.*, **113**, 445 (1959); (h) H. Statz and G. F. Koster, *ibid.*, **115**, 1568 (1959); (i) N. K. Hamer, *Mol. Phys.*, **5**, 455 (1962). In this conjunction it is interesting to compare the spin Hamiltonian treatments of references 31e,f,g,h with those of (j) M. H. L. Pyrce, *Proc. Phys. Soc.* (London), **63A**, 25 (1950); (k) A. Abragam and M. H. L. Pyrce, *Proc. Roy. Soc.* (London), **205A**, 135 (1951); (l) H. A. Buckmaster, *Can. J. Phys.*, **40**, 1670 (1962); and (m) C. F. Davis, Jr., and M. W. P. Strandberg, *Phys. Rev.*, **105**, 447 (1957)].

(32) A. D. Liehr, J. Ferguson, and D. L. Wood, to be published.

(33) For a survey of these measurements consult the books of C. J. Ballhausen [(a) "Introduction to Ligand Field Theory," McGraw-Hill Book Co., New York, N. Y., 1962], and J. S. Griffith,[16] and C. K. Jørgensen [(b) "Absorption Spectra and Chemical Bonding in Complexes," Pergamon Press, Ltd., London and New York, N. Y., 1962], and the review articles of C. K. Jørgensen [(c) Report to the Xth Solvay Council, Brussels, May, 1956; *J. Chim. Phys.*, **56**, 889 (1959), and "Solid State Physics," F. Seitz and D. Turnbull, Ed., Vol. 13, Academic Press, New York and London, 1962, pp. 375–462], W. A. Runciman (d) *Rept. Progr. Phys.*, **21**, 30 (1958)], D. S. McClure [(e) "Solid State Physics," F. Seitz and D. Turnbull, Ed., Vol. 9, Academic Press, Inc., New York and London, 1959, pp. 399–525], T. M. Dunn [(f) "Modern Coördination Chemistry," J. Lewis and R. G. Wilkins, Ed., Interscience Publishers, Inc., New York and London, 1960, pp. 229–300; *Pure Appl. Chem.* (London), **6**, 1 (1963)], and W. Low [(g) "Quantum Electronics," C. H. Townes, Ed., Columbia University Press, New York, N. Y., 1960, pp. 410–427].

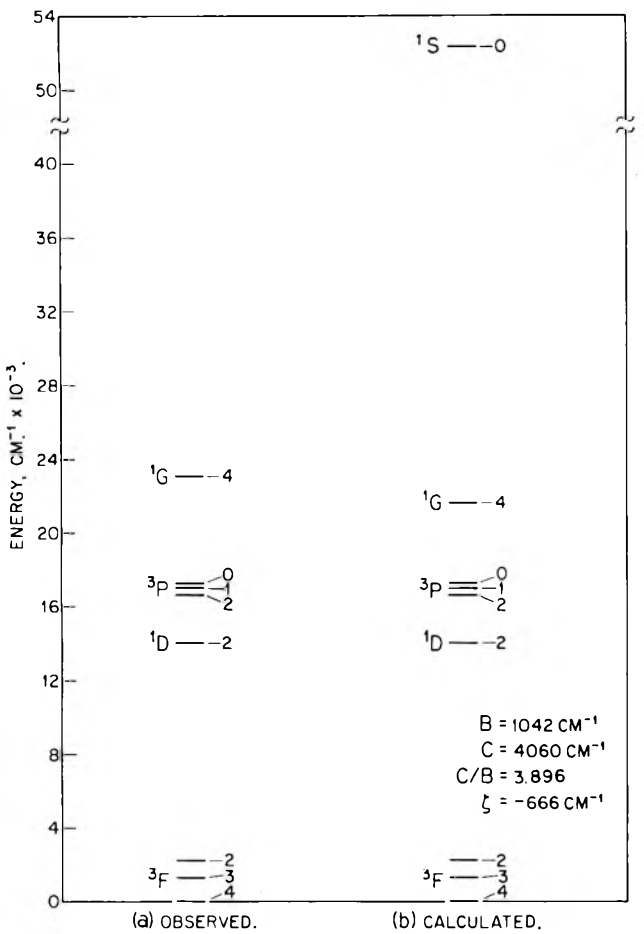

Fig. 4.—Plot of the experimental and theoretical energy levels for the nickel(II) free ion.

physical conditions. Only a few specific compounds and solid solutions have been so studied, and these have been of chromium(III) and cobalt(II).[34] Since it is the aim of this article, as well as that of its antecedents[10] and its subsequents,[32] to critically test the domain of applicability of the ligand field theory of transition metal complexes, we shall confine our examination to a critical spectral analysis of these few select systems alone. Figures 5 through 8 illustrate the essence of the theoretical expectations for these particular complexes.

Tetrahedral, Hexahedral, and Tetradecahedral Chromium(III)

To date no compounds or solute–solvent mixtures containing tetrahedrally, hexahedrally, or tetradecahedrally coördinated chromium(III) have been synthesized.[35] Thus the energy dependence sketched in Fig. 5 for dispositions of this kind is at present largely indicative. However, we may expect that this situation will not long endure. The inorganic chemist and experimental chemical physicist will inevitably succeed to construct such chromium(III) arrangements.[35,36]

Octahedral Chromium(III)

Because of the beautiful colors associated with octahedrally coördinated chromium(III), as seen for example in the many gem stones and glasses (and costume jewelries) which contain chromium, the optical properties of this system have been studied extensively and intensively.[18,33,34a,m,37] Figure 6 outlines the anticipated energy pattern of trivalent chromium in an octahedral structure and Tables V through VII summarize some derived energy levels and ligand field parameters. It is apparent that a fairly satisfactory fit of the observed spectral features of chromium(III) complexes can be obtained on the basis of the simple ligand field theory. However, the physical significance of the parameters thus educed is somewhat unclear. The values of the ligand field strength Dq and of the electron–electron repulsion energies B and C seem to be little correlated

(34) Other examples of compounds and solid solutions which latterly have obtained attention are vanadium(II)[14a] [(a) O. G. Holmes and D. S. McClure, *J. Chem. Phys.*, **26**, 1686 (1957); (b) C. K. Jørgensen, "Absorption Spectra of Complexes of Heavy Metals," Report to the European Research Office, U. S. Department of the Army, Frankfurt am Main, Contract No. DA-91-508EUC-247, October, 1958, and *Acta Chem. Scand.*, **12**, 1537 (1958); (c) R. M. Bennett and O. G. Holmes, *Can. J. Chem.*, **38**, 2319 (1960); (d) D. M. Gruen and R. L. McBeth, *J. Phys. Chem.*, **66**, 57 (1962); (e) M. D. Sturge, to be published]; manganese(IV) [(f) Y. Shimura, H. Ito, and R. Tsuchida, *J. Chem. Soc. Japan*, **75**, 560 (1954), and Y. Shimura and R. Tsuchida, *Bull. Chem. Soc. Japan*, **30**, 502 (1957); (g) M. R. Lorenz and J. S. Prener, *J. Chem. Phys.*, **25**, 1013 (1956); (h) C. K. Jørgensen, *Acta Chem. Scand.*, **12**, 1539 (1958), and *Mol. Phys.*, **3**, 201 (1960); (i) G. Kemeny and C. H. Haake, *J. Chem. Phys.*, **33**, 783 (1960); (j) S. Geschwind, P. Kisliuk, M. P. Klein, J. P. Remeika, and D. L. Wood, *Phys. Rev.*, **126**, 1684 (1962)]; nickel(III) [(k) G. A. Barclay and A. K. Barnard, *J. Chem. Soc.* (London), 4269 (1961); (l) S. Geschwind and J. P. Remeika, *J. Appl. Phys. Suppl.*, **33**, 370 (1962); (m) D. S. McClure, *J. Chem. Phys.*, **36**, 2757 (1962)]; niobium(II) [(n) D. Cozzi and S. Vivarelli, *Z. anorg. allgem. Chem.*, **279**, 165 (1955)]; molybdenum(III)[6,34b,37a] [(o) H. Hartmann and H. J. Schmidt, *Z. physik. Chem.* (Frankfurt), **11**, 234 (1957); (p) C. K. Jørgensen, *Acta Chem. Scand.*, **11**, 73 (1957); (q) D. E. LaValle, R. M. Steele, M. K. Wilkinson, and H. L. Yakel, Jr., *J. Am. Chem. Soc.*, **82**, 2433 (1960); (r) M. I. Wilkinson, E. O. Wollan, H. R. Child, and J. W. Cable, *Phys. Rev.*, **121**, 74 (1961)]; technetium(IV)[33b,34b] [(s) J. Dalziel, N. S. Gill, R. S. Nyholm, and R. D. Peacock, *J. Chem. Soc.*, 4012 (1958); (t) K. Knox and C. E. Coffey, *J. Am. Chem. Soc.*, **81**, 5 (1959)]; palladium(III)[34r] [(u) M. A. Hepworth, K. H. Jack, R. D. Peacock, and G. J. Westland, *Acta Cryst.*, **10**, 63 (1957)]; tungsten(III) [No compounds seem to have been adequately individualized as yet]; rhenium(IV)[3,16,34b,h] [(v) C. K. Jørgensen, *Acta Chem. Scand.*, **9**, 710 (1955), and *Mol. Phys.*, **2**, 309 (1959)]; and iridium(VI)[3,6,34b,h,v] [(w) W. Moffitt, G. L. Goodman, M. Fred, and B. Weinstock, *Mol. Phys.*, **2**, 109 (1959)]. The interpretation of the $4d^3$ and $5d^3$ [with the notable exception of palladium trifluoride[34r,u] no $4d^7$ or $5d^7$ compounds have been well characterized either chemically or physically] ligand field spectra are complicated by the overlap of low energy charge transfer transitions.[33b,34b,v]

(35) There exists some evidence though for a tetrahedral vanadium(II) species.[34d] Attempts are being made to produce a tetrahedral chromium(III) entity also [D. M. Gruen, private communication, June, 1961].

(36) Witness the rapid progress in tetrahedral nickel(II) chemistry and physics since 1957.[21b] [(a) O. Schmitz-DuMont, H. Gössling, and H. Brokopf, *Z. anorg. allgem. Chem.*, **300**, 159 (1959); (b) F. A. Cotton, O. D. Faut, and D. M. L. Goodgane, *J. Am. Chem. Soc.*, **83**, 344 (1961); (c) R. Pappalardo, D. L. Wood, and R. C. Linares, Jr., *J. Chem. Phys.*, **35**, 1460 (1961); (d) R. Pappalardo and R. E. Dietz, *Phys. Rev.*, **123**, 1188 (1961); (e) J. R. Miller, "Advances in Inorganic and Radiochemistry," H. J. Emeléus and A. G. Sharpe, Ed., Vol. 4, Academic Press, Inc., New York, N. Y., 1962, pp. 133–195; (f) R. G. Hayter and F. S. Humiec, *J. Am. Chem. Soc.*, **84**, 2004 (1962); (g) L. Sacconi, P. L. Orioli, P. Paoletti, and M. Ciampolini, *Proc. Chem. Soc.*, 225 (1962)].

(37) (a) H. Hartmann and H. L. Schläfer, *Z. Naturforsch.*, **6a**, 760 (1951), E. König and H. L. Schläfer, *Z. physik. Chem.* (Frankfurt), **26**, 371 (1960), and H. L. Schläfer and H. P. Opitz, *Z. Chem.*, **2**, 216 (1962), and others; (b) C. K. Jørgensen, *Acta Chem. Scand.*, **8**, 1502 (1954), and *Mol. Phys.*, **5**, 485 (1962); (c) C. E. Schäffer, *J. Inorg. Nucl. Chem.*, **8**, 149 (1958); (d) W. Low, *Phys. Rev.*, **105**, 801 (1957); and *Ann. N. Y. Acad. Sci.*, **72**, 69 (1958); (e) S. Sugano, A. L. Schawlow, and F. Varsanyi, *Phys. Rev.*, **120**, 2045 (1960); (f) R. A. Ford and O. F. Hill, *Spectrochim. Acta*, **16**, 493, 1318 (1960), and R. A. Ford, *ibid.*, **16**, 582 (1960); (g) C. Furlani, G. Morpurgo, and G. Sartori, *Z. anorg. allgem. Chem.*, **303**, 1 (1960); (h) S. Sugano and M. Peter, *Phys. Rev.*, **122**, 381 (1961); (i) A. L. Schawlow, A. H. Piksis, and S. Sugano, *ibid.*, **122**, 1469 (1961); (j) W. Kaiser, S. Sugano, and D. L. Wood, *Phys. Rev. Letters*, **6**, 605 (1961); (k) H. A. Weakliem, Jr., and D. S. McClure, *J. Appl. Phys. Suppl.*, **33**, 347 (1962); (l) A. L. Schawlow, *ibid.*, **33**, 395 (1962); (m) D. L. Wood, J. Ferguson, K. Knox, and J. W. Dillon, Jr., to be published; and (n) T. S. Piper and R. L. Carlin, *J. Chem. Phys.*, **36**, 3330 (1962). In addition to the above spectroscopic investigations at set chromium(III) composition, a number of researches have been designed to examine the effects of structural change by a variable chromium(III) content or a variable temperature in a variety of solid solute–solvent combinations: (o) R. Ritschl and R. Müller, *Z. Physik*, **133**, 237 (1952); (p) E. Thilo, J. Jander, and H. Seeman, *Z. anorg. allgem. Chem.*, **279**, 2 (1955); (q) O. Schmitz-DuMont and D. Reinen, *Z. Elektrochem.*, **63**, 978 (1959); (r) A. Neuhaus, *Z. Kristallog.*, **113**, 195 (1960); (s) J. Graham, *J. Phys. Chem. Solids*, **17**, 18 (1960).

with one another. We shall find that this happenstance is not confined to trivalent chromium but seems to be of general occurrence for transition metal ions in crystalline environments. Its interpretation is attempted in the Discussion.

TABLE V

PREDICTED AND OBSERVED SPECTRUM FOR DIPOTASSIUM SODIUM CHROMIUM HEXAFLUORIDE IN CM.$^{-1}$

A level designated by an asterisk is essentially a spin doublet, one by a dagger essentially a spin seven-tenths quartet:three-tenths doublet hybrid, and one by an asterisk–dagger essentially a spin three-quarter doublet:one-quarter quartet hybrid

Observed[37m]	Calculated (Dq = 1610, B = 760, C = ^4B, ζ = 170 cm.$^{-1}$)			
~16,100(s)	$\Gamma_8 \rightarrow \Gamma_8$*	14,586	$\Gamma_8 \rightarrow \Gamma_8$	36,353
~23,400(s)	Γ_8*	15,296	Γ_6†	36,440
~36,500(m)	Γ_6*	15,345	Γ_8†	36,509
	Γ_7	16,032	Γ_7*	41,823
	Γ_8	16,077	Γ_8*	41,853
	Γ_6	16,165	Γ_7*	43,466
	Γ_8	16,174	Γ_6*	46,753
	Γ_8*	21,773	Γ_8*	46,832
	Γ_7*	21,858	Γ_7*	48,542
	Γ_8	23,333	Γ_8*	48,652
	Γ_7	23,345	Γ_8*	51,496
	Γ_8	23,387	Γ_6*	54,471
	Γ_6	23,410	Γ_8*	54,554
	Γ_6*	28,270	Γ_8*	69,989
	Γ_7*	30,582	Γ_7*	70,112
	Γ_8*	30,622	Γ_8*	70,501
	Γ_6*	31,027		
	Γ_8*	31,171		
	Γ_8*	32,832		
	Γ_8*†	36,114		
	Γ_6*†	36,147		
	Γ_7	36,346		

TABLE VI

PREDICTED AND OBSERVED SPECTRUM FOR CHROMIUM(III) DISSOLVED IN MAGNESIUM OXIDE UNDER THE ASSUMPTION OF AN OCTAHEDRAL SITE SYMMETRY IN CM.$^{-1}$

A level designated by an asterisk is essentially a spin doublet, one by a dagger essentially a spin seven to eight-tenths quartet: three to two-tenths doublet hybrid, and one by an asterisk–dagger essentially a spin seven to eight-tenths doublet:three to two-tenths quartet hybrid

Observed[37d]	Calculated (Dq = 1620, B = 650, C = 3250, ζ = 135 cm.$^{-1}$)			
14,200(w)	$\Gamma_8 \rightarrow \Gamma_8$*	14,547	$\Gamma_8 \rightarrow \Gamma_7$	35,641
15,350(w)	Γ_8*	15,102	Γ_8	35,646
15,750(w)	Γ_6*	15,139	Γ_6†	35,734
16,200	Γ_7	16,145	Γ_8†	35,772
20,850(w)	Γ_8	16,180	Γ_7*	40,167
22,700	Γ_6	16,245	Γ_8*	40,216
29,700	Γ_8	16,251	Γ_7*	41,554
46,000 (?)	Γ_8*	21,743	Γ_6*	46,771
	Γ_7*	21,805	Γ_8*	46,842
	Γ_8	22,691	Γ_7*	48,407
	Γ_7	22,706	Γ_8*	48,478
	Γ_8	22,715	Γ_8*	49,976
	Γ_6	22,724	Γ_6*	53,180
	Γ_6*	28,555	Γ_8*	53,250
	Γ_7*	30,596	Γ_8*	67,935
	Γ_8*	30,627	Γ_7*	68,044
	Γ_6*	30,923	Γ_8*	70,213
	Γ_8*	31,033		
	Γ_8*	32,711		
	Γ_7*†	35,464		
	Γ_6*†	35,489		

Tetrahedral, Hexahedral, and Tetradecahedral Cobalt(II)

After a number of years of relative neglect, a renewed interest has been taken in the spectra of cobalt(II) compounds of a regular polyhedral structure.[38] The expected energy diagram for such systems in their tetrahedral, hexahedral, or tetradecahedral aspect is pictured in Fig. 7. We see that for geometries of these sorts an extremely rich spectrum is predicted. From the data of Tables VIII and IX we see that this prediction is amply realized. Because of the low value of the ligand field strength Dq for (cubically) four, eight, and twelve coördinated transition metal complexes, we see from Fig. 7 and 9 that the spin–orbit interactions are of paramount importance for the comprehension of their spectral lineaments. However, as will be mentioned in the discussion, the simple ligand field theory here used is inadequate to fully understand the detailed features of the spin forbidden portion of the tetrahedral spectrum.

Octahedral Cobalt(II)

The beautiful pink to red color of octahedrally coordinated oxygen ligated cobalt(II), as distinguished from the blue color of tetrahedrally ligated cobalt(II), is well known to every child with a chemistry set. Indeed, this color distinction is often cited in popular as well as scientific sources as symptomatic of an octahedral and tetrahedral geometry for cobalt–oxygen containing compounds. However, this differentiation is not rigorous: it was to prove this assertion that the present work on the three electron-hole transition metal energy spectrum was begun.[39] The upshot of the proof

(38) (a) C. J. Ballhausen and C. K. Jørgensen, *Acta Chem. Scand.*, **9**, 397 (1955); (b) W. Low, *Phys. Rev.*, **109**, 256 (1958); (c) R. Stahl-Brada and W. Low, *ibid.*, **113**, 775 (1959); (d) R. Pappalardo, D. L. Wood, and R. C. Linares, Jr., *J. Chem. Phys.*, **35**, 2041 (1961); (e) G. W. Pratt, Jr., and R. Coelho, *Phys. Rev.*, **116**, 281 (1959); (f) J. Ferguson, D. L. Wood, and K. Knox, to be published. [All these measurements were made on spin free cobalt(II) chemicals. No regular polyhedral spin paired divalent cobalt compounds have yet been synthesized (octahedral spin paired complexes of trivalent nickel[34k,l,m] and palladium[34r,u] are known, however).] Closely allied with these studies are those of the distorted (either slightly or grossly) regular polyhedra[21b,34a,36d,37a,k,38f,39d,e]: (g) D. S. McClure, *J. Phys. Chem. Solids*, **3**, 311 (1957); (h) R. Pappalardo, *Phil. Mag.*, [8] **4**, 219 (1959); (i) R. Newman and R. M. Chrenko, *Phys. Rev.*, **115**, 1147 (1959); (j) J. Ferguson, *J. Chem. Phys.*, **32**, 528 and 533 (1960); (k) F. A. Cotton and R. H. Holm, *J. Am. Chem. Soc.*, **82**, 2979 and 2983 (1960); F. A. Cotton, D. M. L. Goodgame, and M. Goodgame, *ibid.*, **83**, 4690 (1961); A. Sacco and F. A. Cotton, *ibid.*, **84**, 2043 (1962), and more; (l) C. Furlani and M. Geroni, *Ricerca Sci.*, **30**, 1016 (1960), and C. Furlani and F. diTella, *Gazz. chim. ital.*, **90**, 280 (1960); (m) L. I. Katzin, *J. Chem. Phys.*, **35**, 467 (1961); **36**, 3034 (1962), and antecedents; (n) A. Turco, C. Pecile, and M. Nicolini, *J. Chem. Soc.*, 3008 (1962); (o) H. Nishikawa, S. Yamada, and R. Tsuchida, *Z. anorg. allgem. Chem.*, **316**, 278 (1962); (p) C. K. Jørgensen, *Acta Chem. Scand.*, **16**, 2017 (1962). Other indagations have been aimed at the analysis of the influence of tectonics and thermics on cobalt(II) spectra in sundry solid solute–solvent media: (q) O. Schmitz-DuMont, H. Brokopf, and K. Burkardt, *Z. anorg. allgem. Chem.*, **295**, 7 (1958); (r) E. Banks and M. Robbins, *Nature*, **191**, 1387 (1961); and M. Robbins, "Fluoride-Compensated Cation Substitutions in Oxides," Thesis, Polytechnic Institute of Brooklyn, 1962.

(39) In 1958 S. Geller brought to the attention of the authors (A. D. L. and D. L. W.)[1] the anomalous blue color of octahedral divalent cobalt in the garnets [(a) S. Geller, C. E. Miller, and R. G. Treuting, *Acta Cryst.*, **13**, 179 (1960); (b) S. Geller, *J. Appl. Phys. Suppl.*, **31**, 30S (1960)] and in the tungstates [(c) these latter samples were made by L. G. Van Uitert]. To explain the anomaly this study was undertaken. Since the initial recognition of the existence of unusual chromaticity by Geller and Van Uitert other samples have been uncovered: octahedral divalent nickel in magnesium tungstate is orange[39c] [(d) J. Ferguson, K. Knox, and D. L. Wood, *J. Chem. Phys.*, **35**, 2236 (1961), and *Errata*, *ibid.*, **37**, 193 (1962)], and in anhydrous nickel sulfate is yellow, divalent cobalt in cobaltous silicate is purple [(e) M. Goodgame and F. A. Cotton, *J. Phys. Chem.*, **65**, 791 (1961)], and trivalent chromium in dipotassium sodium chromium hexafluoride is yellow-green.[39d] From these examples it is thus apparent that color cannot be used with impunity to infer structure or magnetism.

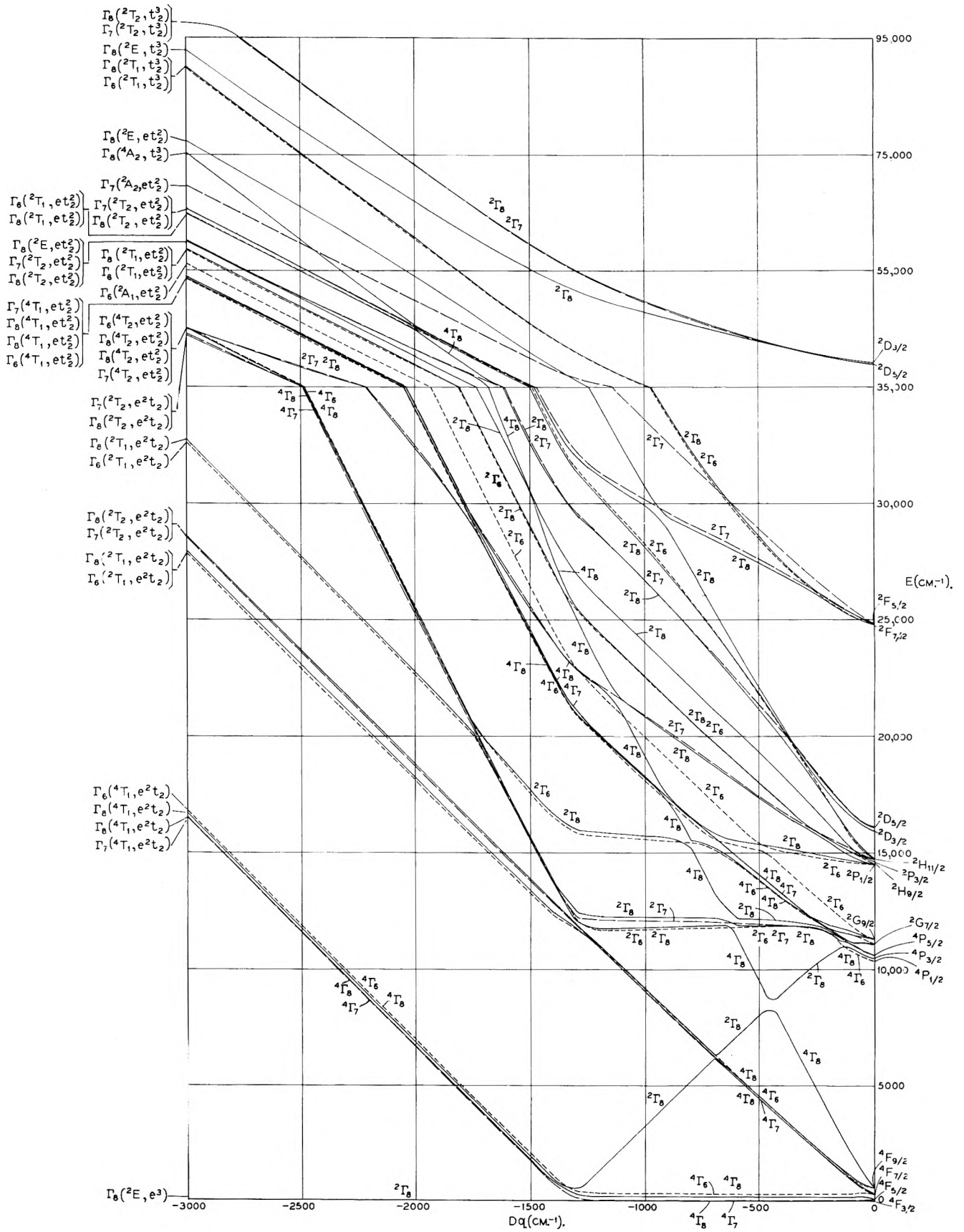

Fig. 5.—Energy level diagram for a d^3 electronic configuration encompassed by a field of tetrahedral, hexahedral, or tetradecahedral symmetry for ζ equals 175 cm.$^{-1}$, B equals 680 cm.$^{-1}$, and C equals $4B$.

was a dramatic demonstration of the influence of structure, as separate from coördination number, on spectra (see the Discussion).

Figure 8 maps the energy level plan for octahedral divalent cobalt complexes, and Tables X and XI demonstrate its usefulness. We see from the tables that again spin–orbit forces contribute importantly to the intelligibility of the six coördinate cobalt(II) spectrum. That the physical meaningfulness of the elicited ligand field parameters leaves something yet to be desired is

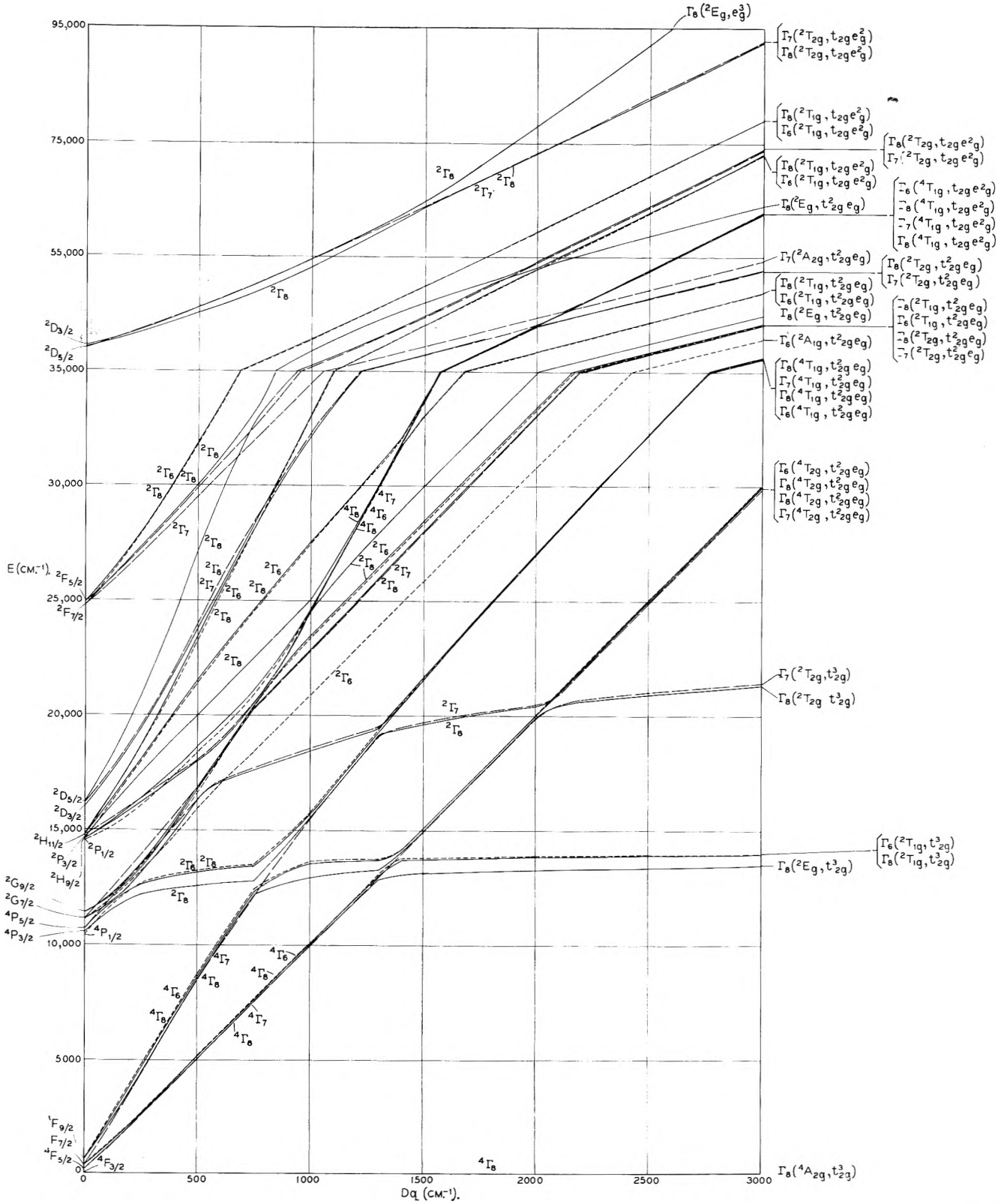

Fig. 6.—Energy level diagram for a d^3 electronic configuration encompassed by a field of octahedral symmetry for ζ equals 175 cm.$^{-1}$, B equals 680 cm.$^{-1}$, and C equals $4B$.

clearly underlined by the résumé of Table XII (read the Discussion).

Discussion

Two things become quite plain from the previous analysis: (a) The comparative change in the ligand field strength, Dq, the electron–electron repulsion integral, B, and the ratio of the electron–electron repulsion integrals, C/B, is quite irregular even for a fixed addend group (Tables VII and XII)[40]; and (b) the resolution and classification of the myriad of optical absorption lines is at times fraught with ambiguity when both spin–orbit and non-cubic electron–nuclear interactions (either static or dynamic) must be taken into account. The initial perplexity has its explanation in several

(40) This phenomena is not confined to chromium(III) and cobalt(II), but is quite general as is witnessed by the existence of orange and yellow paramagnetic varieties of hexacoördinated nickel(II) oxide lattices.[39]

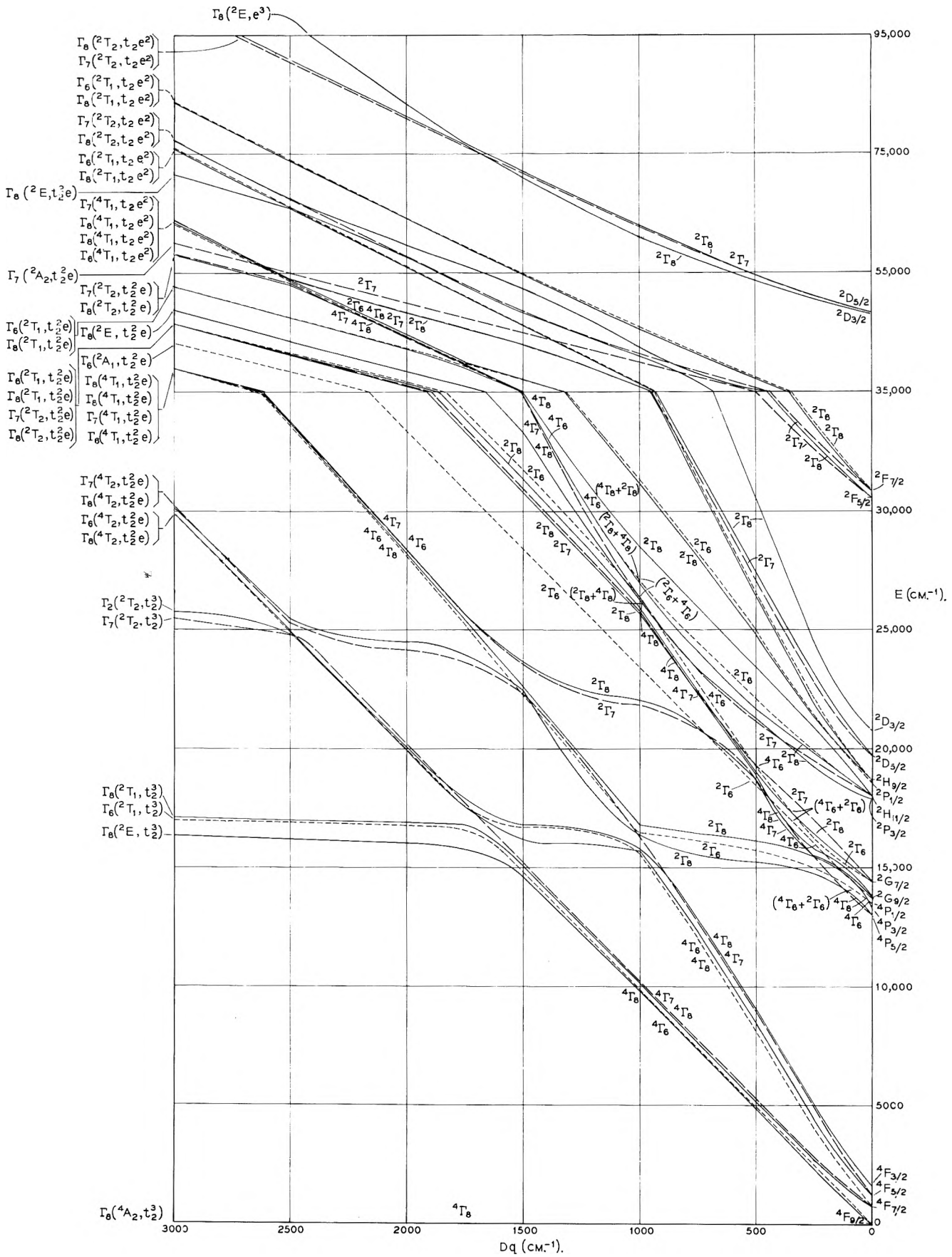

Fig. 7.—Energy level diagram for a d^7 electronic configuration encompassed by a field of tetrahedral, hexahedral, or tetradecahedral symmetry for ζ equals -450 cm.$^{-1}$, B equals 835 cm.$^{-1}$, and C equals $4B$.

directions. Firstly, the electrical asymmetries at the site of the ligand in a given crystal has a profound influence on the value of the ligand field strength, Dq. For example, the imbalance of positive attractive power in the cubic (O_h) potassium sodium chromium hexafluoride crystal and in the rhomboidal (C_{2h}) cobalt tungstate crystal about their augends, fluorine and oxygen, respectively, due to their chromium–fluorine–

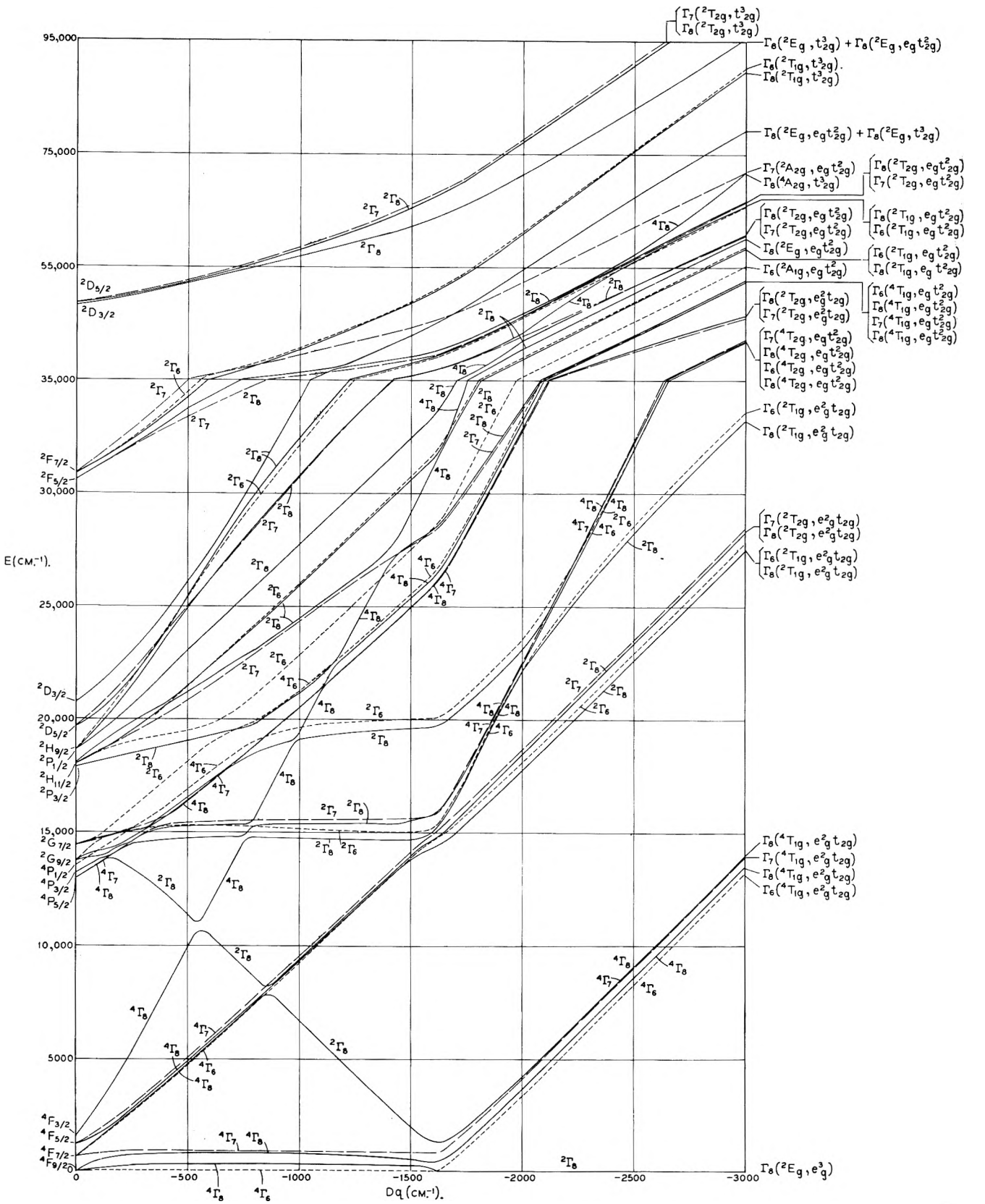

Fig. 8.—Energy level diagram for a d^7 electronic configuration encompassed by a field of octahedral symmetry for ζ equals -450 cm.$^{-1}$, B equals 835 cm.$^{-1}$, and C equals $4B$.

sodium and cobalt–oxygen–tungsten linkages, enhances the chromium–fluorine ligand field in potassium sodium chromium hexafluoride and diminishes the cobalt–oxygen ligand field in cobalt tungstate.[41] Secondly, the alteration of the e and t_2 molecular orbitals due to the differential expansion of the metallic basis kd orbitals and to the selective modification of the covalent linkage of the addend orbitals because of structural and steric

(41) Similarly, in chromium trifluoride the imbalance created by the bent chromium–fluorine–chromium bond increases the chromium ligand field over that for a correspondent cubic (linear) arrangement. P. Cosse [(a) *J. Inorg. Nucl. Chem.*, **8**, 483 (1958)] has invoked an analogous argument to explain the anomalous paramagnetism of trivalent cobalt in lanthanum cobalt trioxide [in this regard view also (b) C. S. Naiman, *Mol. Phys.*, **5**, 539 (1962)].

TABLE VII

A COMPEND OF THE CHROMIUM(III) SPECTRAL VARIABLES[37m]

	Free ion	Yttrium–gallium–garnet	Yttrium–aluminum–garnet	Ruby	Emerald	K_2NaCrF_6	CrF_3	$CrCl_3$	$CrBr_3$
Dq, cm.$^{-1}$	0	1650	1640	1800	1630	1610	1460	1370	1340
B, cm.$^{-1}$	920	570	650	640	780	760	740	550	370
C, cm.$^{-1}$	3680	3400	3250	3300	2960	3020	...	3400	3700
C/B	4.0	5.95	5.0	5.15	3.8	3.97	...	6.3	10.0
ζ, cm.$^{-1}$	273	172	172	172	172	172	172	172	172
Cr ligand distance, Å.	...	1.93	1.92	1.90	1.94	1.90	1.90	2.38	2.54

TABLE VIII

PREDICTED AND OBSERVED SPECTRUM FOR COBALT(II) DISSOLVED IN ZINC OXIDE UNDER THE ASSUMPTION OF TETRAHEDRAL SITE SYMMETRY IN CM.$^{-1}$

A level designated by an asterisk is essentially a spin doublet

Observed[38d]	Calculated (Dq = 390, B = 700, C = 3150, ζ = −500 cm.$^{-1}$)			
6,045.9	$\Gamma_8 \rightarrow \Gamma_8$	3,714.2	$\Gamma_8 \rightarrow \Gamma_8^*$	19,109
6,101.3	Γ_6	3,851.5	Γ_6^*	19,485
6,188.1	Γ_8	4,099.6	Γ_8^*	20,626
6,289.3	Γ_7	4,200.6	Γ_8^*	21,542
6,535.9	Γ_6	6,251.5	Γ_6^*	21,706
6,666.6	Γ_8	6,676.0	Γ_8^*	22,826
6,788.8	Γ_7	7,202.6	Γ_6^*	22,963
6,944.4	Γ_8	7,304.4	Γ_7^*	23,450
7,168.4	Γ_8^*	13,809	Γ_8^*	23,879
7,317.9	Γ_6^*	14,137	Γ_8^*	26,176
7,401.9	Γ_8^*	14,576	Γ_7^*	30,258
7,499	Γ_8	15,338	Γ_8^*	30,599
7,692.3	Γ_7	15,346	Γ_7^*	30,904
8,000	Γ_8	15,620	Γ_8^*	31,968
8,196	Γ_6	15,885	Γ_6^*	32,132
15,384	Γ_6^*	16,452	Γ_8	46,948
15,674	Γ_8^*	16,794	Γ_7	47,657
15,949	Γ_7^*	17,218	Γ_8	47,721
16,260	Γ_7^*	18,627		
17,652	Γ_8^*	18,758		
20,202(vw)				

TABLE IX

PREDICTED AND OBSERVED SPECTRUM FOR COBALT(II) DISSOLVED IN CALCIUM FLUORIDE IN CM.$^{-1}$

A level designated by an asterisk is essentially a spin doublet

Observed[38c]	Calculated (Dq = 350, B = 930, C = 4185, ζ = −515 cm.$^{-1}$)			
3,200	$\Gamma_8 \rightarrow \Gamma_8$	3,317.7	$\Gamma_8 \rightarrow \Gamma_6^*$	24,182
3,440	Γ_6	3,460.4	Γ_8^*	25,566
5,800	Γ_8	3,728.9	Γ_8^*	26,230
6,100	Γ_7	3,819.1	Γ_6^*	26,346
6,600	Γ_6	5,653.6	Γ_8^*	27,135
17,800	Γ_8	6,104.8	Γ_6^*	27,280
18,550	Γ_7	6,661.8	Γ_7^*	28,252
19,220(w)	Γ_8	6,774.3	Γ_8^*	28,693
19,580(w)	Γ_8^*	18,020	Γ_8^*	30,536
20,450(w)	Γ_7	18,190	Γ_7^*	38,489
21,750(w)	Γ_8	18,198	Γ_8^*	38,863
22,000(w)	Γ_6^*	18,346	Γ_7^*	39,090
25,750(w)	Γ_8	18,411	Γ_8^*	39,885
28,000–37,000(vw)	Γ_6	18,823	Γ_6^*	40,043
44,250	Γ_8^*	19,018	Γ_8^*	60,180
48,200	Γ_6^*	20,103	Γ_7^*	60,816
	Γ_8^*	20,554	Γ_8^*	60,828
	Γ_7^*	21,102		
	Γ_8^*	23,426		
	Γ_7^*	23,617		
	Γ_8^*	24,077		

effects and incompatibilities (such as the fixture of a transition metal ion into too large or too small a lattice hole or into a distorted site) induces strong fluctuations

TABLE X

PREDICTED AND OBSERVED SPECTRUM FOR COBALT(II) DISSOLVED IN MAGNESIUM OXIDE IN CM.$^{-1}$

A level designated by an asterisk is essentially a spin doublet, one by a dagger essentially a spin six-tenths quartet: four-tenths doublet hybrid, one by a dagger–asterisk essentially a spin six to seven-tenths doublet: four to three-tenths quartet hybrid, and one by an asterisk–dagger essentially a spin eight-tenths doublet: two-tenths quartet hybrid

Observed[38d]	Calculated (Dq = −930, B = 840, C = 3700, ζ = −475 cm.$^{-1}$)			
8,146.6	$\Gamma_6 \rightarrow \Gamma_8$	314.6	$\Gamma_6 \rightarrow \Gamma_6$	23,523
8,163.2	Γ_8	821.5	Γ-	25,297
8,203	Γ_7	903.7	Γ_8	25,516
8,319.4	Γ_6	8,629.5	Γ_8	26,635
8,350.7	Γ_8	8,648.1	Γ_6	26,706
8,403.3	Γ_8	8,737.6	Γ_8	28,583
8,547	Γ_8^*†	8,898.0	Γ_7	31,380
8,598.4	Γ_7	8,939.1	Γ_8	31,452
8,633.3	Γ_8	16,098	Γ_6	32,606
18,559	Γ_6	16,556	Γ_8	32,988
18,797	Γ_8	16,777	Γ_8	34,518
19,723	Γ_7	16,996	Γ_7	36,902
20,555	Γ_8	18,073	Γ_8	37,500
20,833	Γ_8†	19,771	Γ_7	40,278
	Γ_7	19,997	Γ_8	40,663
	Γ_8	20,003	Γ_6	41,020
	Γ_6^*†	20,311	Γ_8	58,894
	Γ_8†*	21,290	Γ_8	59,960
	Γ_6†*	21,334	Γ_7	60,392

TABLE XI

PREDICTED AND OBSERVED SPECTRUM FOR POTASSIUM COBALT TRIFLUORIDE IN CM.$^{-1}$

A level designated by an asterisk is essentially a spin doublet

Observed[38f]	Calculated (Dq = −785, B = 880, C = 4.4B, ζ = −500 cm.$^{-1}$)			
~ 7,200(m)	$\Gamma_6 \rightarrow \Gamma_8$	332.8	$\Gamma_6 \rightarrow \Gamma_8^*$	25,146
~15,100(w)	Γ_8	875.2	Γ_8^*	25,940
~17,500(sh)	Γ_7	966.8	Γ_6^*	25,974
~19,300(s)	Γ_6	7,313.8	Γ_8^*	27,883
~21,600(w)	Γ_8	7,356.2	Γ_7^*	30,479
22,840(vw)	Γ_8	7,451.8	Γ_8^*	30,535
	Γ_7	7,641.6	Γ_6^*	31,431
	Γ_8^*	10,793	Γ_8^*	31,829
	Γ_8	15,293	Γ_8^*	32,620
	Γ_8^*	16,640	Γ_7^*	37,480
	Γ_6^*	17,160	Γ_8^*	38,037
	Γ_8^*	17,297	Γ^*	39,882
	Γ_7^*	17,501	Γ_7^*	40,206
	Γ_7	19,363	Γ_6^*	40,242
	Γ_8	19,364	Γ_8^*	59,396
	Γ_8	19,405	Γ_8^*	59,906
	Γ_6	19,856	Γ_7^*	60,340
	Γ_8^*	21,577		
	Γ_6^*	21,662		
	Γ_6^*	22,761		
	Γ_7^*	24,870		

TABLE XII

A DIGEST OF THE COBALT(II) SPECTRAL VARIABLES[38f]

	Free ion	$KCoF_3$	$KMg(Co)F_3$	$CoCl_2$	$CoBr_2$	$CoWO_4$
Dq, cm.$^{-1}$	0	770	800	690	640	690
B, cm.$^{-1}$	972	880	880	780	760	760
C, cm.$^{-1}$	4276.8	3872	3872	3432	3344	3344
C/B	4.40	4.40	4.40	4.40	4.40	4.40
ζ, cm.$^{-1}$	535	500	500	500	500	500
Co ligand distance, Å.	...	2.04	~2.01	...	...	~2.10

in the electron–electron repulsive forces as measured by the Racah parameters B and C,[42] hence the large vacillation of the ratio C/B.[42–45]

The second encumbrance has its origin in the circumstance that the spin–orbit and nuclear–electronic interactions are equi-energetic in some instances. Consequently, it is difficult to separate spectral splittings due to spin–orbit forces and Jahn–Teller–Renner (pseudo and real), Herzberg–Teller, and steric nuclear-electronic forces. An excellent example of this difficulty is to be found in the analysis of the spectrum of the cobalt tetrachloride anion.[28a] The use of purely electronic ligand field model in such circumstances is almost ineffectual.[46]

A further enigma yet to be unraveled is that of the cause of absorptive power in the cubic and skew-cubic $kd^{3,7}$ compounds.[23d,37e,47] Research on this problem is still in progress.[48] It seems clear, however, that the spectral intension of the lowest spin forbidden transition in octahedral chromium(III) chemicals is predominantly magnetic dipole in character in some instances,[37e,48a] and mostly vibronic and/or static electric dipole in nature in others.[37f,m,47b] Also, it is a fact that the intensity of the spin forbidden bands of tetrahedral cobalt(II) apparently is taken from non-ligand field spin allowed transitions, or else is not electric dipole in quality (this latter possibility is most unlikely).[28a] The chromium(III) and cobalt(II) spin allowed transitions are certainly electric dipole in constitution [but see ref. 48a for a caution against untested generalization], but it has not yet been ascertained how much of their optical strength is due to intrinsic static architectural asymmetry and how much due to induced dynamic structural asymmetry, although some attempts have been made at the assessment of both.[34m,37m,38f,47,48] Further, the question as to the relative proficiency of the general lattice modes, as compared to the localized modes, in the production of optical absorptive power remains to be settled. There is definite evidence in the cubic and skew-cubic cobalt(II) compounds for the existence of both lattice and localized contributions.[28a,38f]

It is quite perplexing to find that the tetrahedral–octahedral ligand field strength ratio is embarassingly close to the multipole field value of $-4/9$ (as an instance, the ratio for cobalt tetrachloride to cobalt di-

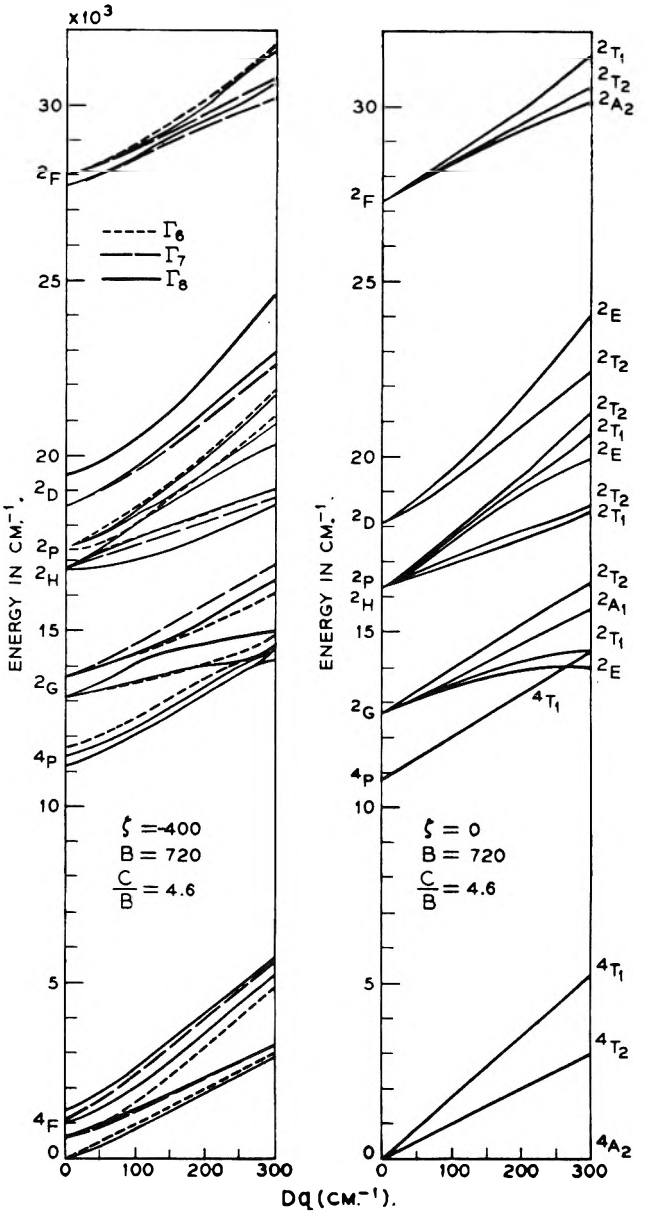

Fig. 9.—Comparative energy level diagrams for a d^7 electronic configuration encompassed by a field of tetrahedral, hexahedral, or tetradecahedral symmetry for ζ equals -400 cm.$^{-1}$ (left) and ζ equals 0 cm.$^{-1}$ (right), for B equals 720 cm.$^{-1}$, and C equals $4.6B$.[1,28a]

(42) These statements hold true also for the exact wave functions and are not limited to their molecular orbital (approximate) representations alone.

(43) In the one electron molecular orbital approximation B is determined by transitions which change the e and t_2 molecular orbital occupancy numbers, while C is fixed by transitions which do not alter (to good approximation) these numbers. Therefore, C as thus determined is relatively insensitive to the transilient covalency effects which normally accompany optical excitations. [Actually, in the elementary ligand field theory it is a linear combination of B and C ($3B + C$) which is so specified. Hence, a great deal of ambiguity attends the selection of a proper magnitude for C.]

(44) The invalidity of the electron-hole correlative relation is clearly apparent in the striking behavioral difference of the C/B ratio as a function of structure and composition for trivalent chromium (three electrons) and divalent cobalt (three holes).

(45) The cause of the diminution of the electron–electron repulsive forces in inorganic compounds over that in the dissociated free ions has been speculated upon and discussed a number of times heretofore. Those interested in further discourse should consult (a) J. Owen, *Proc. Roy. Soc.* (London), **227A**, 183 (1955); (b) C. K. Jørgensen, *Acta Chem. Scand.*, **11**, 53 (1957); O. Bostrup and C. K. Jørgensen, *ibid.*, **11**, 1223 (1957); and C. K. Jørgensen, *Discussions Faraday Soc.*, **26**, 110 (1958); (c) D. P. Craig and E. A. Magnusson, *ibid.*, 116 (1958); D. P. Craig and C. Zauli, *Gazz. chim. ital.*, **90**, 1700 (1960); Final Report, Air Research and Development Command, U. S. Air Force, Contract AF61(052)-61, January, 1961, and *J. Chem. Phys.*, **37**, 601, 609 (1962); (d) T. M. Dunn, *J. Chem. Soc.*, 623 (1959); (e) R. L. Belford and M. Karplus, *J. Chem. Phys.*, **31**, 394 (1959); (f) A. J. Freeman and R. E. Watson, *Phys. Rev.*, **117**, 742 (1960); **118**, 1168 (1960); **127**, 2058 (1962); R. E. Watson, *ibid.*, **118**, 1036 (1960); **119**, 1934 (1960); and others; (g) N. F. Lane and C. C. Lin, to be published; and (h) L. S. Forster and K. de Armond, *Spectrochim. Acta*, in press.

(46) An attempt has been made by McClure (unpublished) to treat simultaneously the electron–nuclear and spin–orbit interactions for tetrahedral cobalt(II). However, the worthiness of this treatment has not yet been established.

(47) (a) S. Koide, *Phil. Mag.*, [8] **4**, 243 (1959); (b) S. Sugano, *Progr. Theoret. Phys. Suppl.*, No. **14**, 66 (1960); (c) R. Englman, *Mol. Phys.*, **3**, 48 (1960).

(48) A. D. Liehr, to be published.

(48a) NOTE ADDED IN PROOF.—J. Ferguson, H. J. Guggenheim, L. F. Johnson, and H. Kamimura (to be published) have recently found that a similar statement can be made for the lowest spin allowed transition in certain nickel(II) chemicals also.

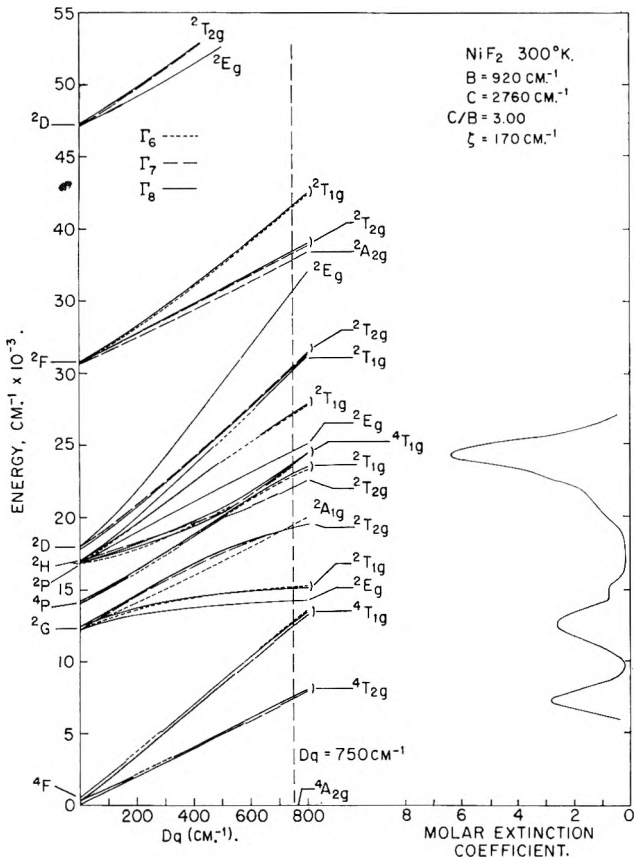

Fig. 10.—Energy level diagram (left) for nickel difluoride treated as a d^3 electronic configuration with ζ equals 170 cm.$^{-1}$, B equals 920 cm.$^{-1}$, and C equals $3B$. The experimental single crystal absorption spectrum at 300°K. is shown on the right for comparison.[39d]

chloride is $-3.9/9$).[10,49] This happenstance is puzzling in that one would not expect offhand that the radial multipole field strength was of equal magnitude for such different types of structure (recall that the factor $-4/9$ for kd^n configurations derives solely from the fixed tetrahedral and octahedral geometric angular factors in the multipole expansion of the coulombic potential field[10]). We must assign it as fortuitous until a more rigorous comparative molecular orbital treatment, like that of Shulman and Sugano,[23f,50] is attempted. This suspension of judgment is required as the same ratio for the hexahedral to octahedral field is only $-4.0/9$ for cobalt(II) in calcium difluoride[38c] and in potassium cobalt trifluoride,[38f] instead $-8/9$ as predicted by the multipole distension.[10b,38c,d] Evidently geometrical factors such as structural misfits are important in settling this ratio (the normal cobalt(II) ionic radius is ~0.68 Å., while that of the calcium(II) hole in calcium difluoride is ~0.99 Å., hence a diminished cobalt–fluorine covalency must be expected under a structural mismatch of this sort). The magnitudes of the electron–electron repulsion parameters B and C/B are not correspondent in the several cases as can be seen from their values of 700 cm.$^{-1}$ and 4.8, and 780 cm.$^{-1}$ and 4.4, in cobalt tetrachloride[28a] and cobalt dichloride,[38f] respectively, and 880 cm.$^{-1}$ and 4.4, and 933 cm.$^{-1}$ and 4.5, in potassium cobalt trifluoride[38f] and cobalt(II) in calcium difluoride,[38c] each. There is, however, some conflict as to the correct choice of these latter parameters even for the free ion, so not too much reliance should be placed on their absolute magnitudes; their relative magnitudes are of interest though.[51]

The substance of this discussion is best summarized in an example. Consider the yellow-green compound nickel difluoride to be a kd^3 configuration, say due to a sample mix up with the similar looking yellow-green chromium trifluoride,[52] and attempt to fit its spectrum with the aid of the complete energy matrices of Eisenstein.[3] It turns out that this can actually be done! Figure 10 and Table XIII epitomize the result. It is thus quite evident that extreme caution must be utilized in the use of a ligand field theory more sophisticated than the simple four parameter theory in crystalline media, and that no small amount of doubt and skepticism should accompany any itemized rationalization of the magnitudes of even the ordinary usual four addend field characteristics Dq, B, C, and ζ in such media (and perhaps in liquid solution also, but here lack of spectral detail mitigates all harsh verdicts).

Conclusion

Our main finds may be put briefly as follows.

(1) The elementary conception of nephelauxetic displacement[18,33a,b,53] (that is, the shift of a spectral pattern because of a diminution of the electron correlation integral, B, from its free ion magnitude) is of strictly restricted utility in crystalline media.

(2) The empirical principle of progressive change of optical frequency with different addends[54] (named the spectrochemical change) is of sharply delimited validity in rigid milieu.

(3) The electrical inductive effects of circumjacent

(49) C. J. Ballhausen, *Dan. Mat. Fys. Med.*, **29**, No. 4 (1954).

(50) R. G. Shulman and S. Sugano, *Phys. Rev. Letters*, **7**, 157 (1961); *J. Chem. Phys.*, **36**, 3496 (1962), and to be published.

(51) For example, compare the initial[38b,c] and revised[33g] B and C values of Low for cobalt(II) in magnesium oxide and calcium difluoride and of Pappalardo, Wood, and Linares,[36c] Pappalardo and Dietz,[36d] Pappalardo, Wood, and Linares,[38d] and Weakliem[21b] for nickel(II) and cobalt(II) in zinc oxide and cadmium sulfide. In the present study[28a,37m,38f,39d] B has always been chosen to fit the spin allowed transitions and the ratio C/B to fit the *lowest* spin forbidden transition [the higher spin forbidden transitions are less reliable and subject to large perturbations. See Griffith,[18] for instance]. It is most important to realize that redundancy can exist even when a rule such as this latter is followed. As a sample, consider the assignment of the "red" or "second" band of the hexaaquonickel(II) cation located at ~13,000–15,000 cm.$^{-1}$ [(a) C. K. Jørgensen, *Acta Chem. Scand.*, **9**, 1362 (1955)]. Here the first spin forbidden transition cannot be unambiguously identified. If water is assumed to bond "covalently" as does ammonia [the hexaamminenickel(II) spectrum is reported in ref. 51a], one identification is made; if it is assumed to bond "ionically" as does fluoride [the hexafluoronickel(II) spectrum is recorded in reference 28b and in (b) W. Rüdorff, J. Kandler, and D. Babel, *Z. anorg. allgem. Chem.*, **317**, 261 (1962); (c) C. K. Jørgensen, to be published; (d) W. Hayes, to be published; (e) J. Ferguson, to be published], a different, but equally good identification is constructed.[10a,18,28b,33,51a,c,d,e] [Please remember that the words "covalent" and "ionic" are here used in a classical, not a quantum mechanical sense. Read (f) G. E. Kimball and E. M. Loebl, *J. Chem. Educ.*, **36**, 233 (1959); (g) A. D. Liehr, *ibid.*, **39**, 135 (1962); (h) K. Ruedenberg, *Rev. Mod. Phys.*, **34**, 326 (1962); (i) P.-O. Löwdin, *J. Appl. Phys. Suppl.*, **33**, 251 (1962); (j) H. Shull, *ibid.*, **33**, 290 (1962); (k) J. C. Phillips and M. H. Cohen, *ibid.*, **33**, 293 (1962); and references 23f and 50. For the experimental aspects of this semantic question as related to chromium(III), manganese(IV), and nickel(II) chemistry see (l) L. Helmholz, A. V. Guzzo, and R. N. Sanders, *J. Chem. Phys.*, **35**, 1349 (1961) and ref. 50.] Thus ensues a dilemma: does water ligate more in the fashion of fluoride or more in the manner of ammonia [Perhaps the controversy[10] surrounding the nickel(II) tris-(*o*-phenanthrolene) spectrum permits a similar reduction]? Chemically, the latter alternative would be chosen.[10a] Spectroscopically, however, it is not at all clear which option should be selected. The four parameter ligand field theory *per se* equivocates and gives no answer. Hence, only refined experiment and rigorous computation can resolve and decide the question.

(52) This hypothetical situation has actually occurred.[39d]

(53) (a) C. E. Schäffer and C. K. Jørgensen, *J. Inorg. Nucl. Chem.*, **8**, 143 (1958); (b) C. K. Jørgensen, "Progress in Inorganic Chemistry," Vol. 4, F. A. Cotton, Ed., Interscience Publishers, Inc., New York, N. Y., 1962, pp. 73–124.

(54) R. Tsuchida, *J. Chem. Soc. Japan*, **13**, 388, 436 (1938), and R. Tsuchida and M. Kobayashi, *ibid.*, **13**, 471 (1938).

TABLE XIII

PREDICTED AND OBSERVED SPECTRUM FOR NICKEL DIFLUORIDE TREATED AS AN OCTAHEDRAL THREE ELECTRON SYSTEM IN CM.$^{-1}$

A level designated by an asterisk is essentially a spin doublet

Observed[39d]	Calculated (Dq = 750, B = 920, C = 2760, ζ = 170 cm.$^{-1}$)		
~ 7,500	$\Gamma_8 \rightarrow \Gamma_7$	7,435.2	$\Gamma_8 \rightarrow \Gamma_8^*$ 24,595
~13,000	Γ_8	7,476.9	Γ_6^* 27,141
~15,000(w)	Γ_8	7,534.9	Γ_8^* 27,223
~21,000(w)	Γ_6	7,547.6	Γ_6^* 30,158
~22,500(w)	Γ_7	12,510	Γ_8^* 30,196
~24,000	Γ_8	12,519	Γ_8^* 30,403
	Γ_8	12,690	Γ_7^* 30,493
	Γ_6	12,800	Γ_8^* 35,806
	Γ_8^*	14,197	Γ_7^* 37,868
	Γ_8^*	15,073	Γ_7^* 38,331
	Γ_6^*	15,155	Γ_8^* 38,474
	Γ_8^*	19,241	Γ_6^* 41.543
	Γ_7^*	19,269	Γ_8^* 41,605
	Γ_6^*	19,481	Γ_8^* 55,889
	Γ_8^*	22,072	Γ_8^* 58,155
	Γ_7^*	22,081	Γ_7^* 58,192
	Γ_6^*	22,843	
	Γ_8^*	23,007	
	Γ_6	23,595	
	Γ_8	23,690	
	Γ_8	23,746	
	Γ_7	23,762	

ions and molecules are at times decisive in setting the value of the ligand field constant Dq.

(4) The unequivocal particularization of the augend field parameters can be executed only upon docimastical specification of the variety of diverse spin forbidden multiplets allowed a kd^n system.[55]

Despite these bounds, and in special instances because of them, great use can still be made of the theory of ligand fields. Samples of such use are plentiful: (a) to probe site symmetries in inorganic compounds and solutions (as in "perfect"[18,28,32-34,36-39] and "defect"[56] crystals, solid "ionic" solutions,[18,21b,32-34,36-39] glasses and costume jewelries,[57] gems and minerals,[34m,37,38,58] fused salts and fused salt solutions,[34d,59] liquid[18,33,34,36-38] and solid[60] molecular solutions, gases,[34w,57g,61] etc.; (b) to obtain knowledge of the chemical bond, electronic distribution, wave functions, and so on[18,21,23,24,33,45,50]; (c) to ascertain geometries of ground and excited electronic states and to particularize nuclear–electronic interactions[18,28a,33,34m,36,38f,39,47,48,51e,62]; (d) to construct new materials for specific uses and devices ("materials engineering)[63]; (e) to elucidate variform optical phenomena as absorption, fluorescence and phosphorescence, optical rotatory power, photosensitization, and many others[18,33,37l,45h,64]; (f) to understand photochemical syntheses, decompositions, and metamorphoses[65]; (g) to interpret magnetical observations as paramagnetism, paramagnetic and nuclear magnetic resonance, and so forth[3,11,18,23,24,33,50,56,66]; (h) to tender an explanation of the coöperative acts of antiferromagnetism, ferromagnetism, metallicism, *cum multis aliis*[67]; and the like. However, most certainly hesitancy, caution, and prudence must surely be the bywords in applications of this sort if dialectical fallacy is to be sidestepped.

Acknowledgments.—This paper owes much to many people. To S. Geller for providing the necessary stim-

(55) Mark that the usual nephelauxetic, spectrochemical, and chemical inductive effects associated with coördination by substitutionally related ligands such as water, alcohols, phenols, ethers, aldehydes, ketones, organic, and inorganic oxyacids, and so on,[53,54] may also be viewed as due to "lattice" and "structural" effects of circumjacent groups, only in this case the close bordering atoms are chemically attached to the coördinating atom (here oxygen), rather than merely crystallographically placed opposite it [it should not be inferred from the last statement that the crystallographic pulls need necessarily be weak compared to the chemical ties: they may in special instances be quite comparable (*viz.*, in the crystalline and gaseous monometallic halides, oxides, sulfides, and the like). Estimates of the inductive effects, both direct and indirect, have been given by J. H. Van Vleck (*J. Chem. Phys.*, **7**, 61 (1939)) for lattices which contain hydrated cationic species such as the alums (they are found to be small)].

(56) Peruse "Papers Presented at the Northwestern University 1961 International Conference on the Chemical Physics of Nonmetallic Crystals," *J. Appl. Phys. Suppl.*, **33**, 251 (1962).

(57) (a) T. Bates and R. W. Douglas, *J. Soc. Glass Technol.*, **43**, 289 T (1959) [chromium(III)]; (b) S. Kumar and P. Sen, *Phys. Chem. Glasses*, **1**, 175 (1960) [manganese(III) and vanadium(II)]; (c) W. A. Weyl, "Colored Glasses," Dawson's of Pall Mall, London, 1959; (d) R. W. Douglas, "Progress in Ceramic Science," Vol. 1, J. E. Burke, Ed., Pergamon Press, New York, and London, 1961, pp. 200–223; (e) T. Bates, "Modern Aspects of the Vitreous State," Vol. 2, J. D. Mackenzie, Ed., Butterworths, Washington, D. C., 1962, pp. 195–254; (f) R. E. Tischer and H. G. Drickamer, *J. Chem. Phys.*, **37**, 1554 (1962); (g) D. J. Williams, Progress Report No. 8, Wave Mechanics Group, Mathematical Institute, University of Oxford, 1961–1962, pp. v, 32, and 33.

(58) (a) E. H. Kraus and C. B. Slawson, "Gems and Gem Materials," Third Edition, McGraw-Hill Book Co., New York and London, 1939; (b) "The Spectroscope and its Applications to Gemmology," a series of forty articles by B. W. Anderson and C. J. Payne, *The Gemmologist*, **22** through **25**, 1953 through 1956 [index in **26**, 13 (1957)]; (c) S. V. Grum-Grzhimailo and G. V. Klimusheva, *Optics and Spectroscopy*, **8**, 179 (1960); (d) E. A. D. White, *Quart. Rev.*, **15**, 1 (1961).

(59) For a comprehensive and thorough review see (a) G. P. Smith (especially), to be published; (b) D. M. Gruen and R. L. McBeth, *Pure Appl. Chem.* (London), **6**, 23 (1963); and (c) B. R. Suncheim, to be published.

(60) (a) C. M. Herzfeld, *Phys. Rev.*, **107**, 1239 (1957); (b) C. M. Herzfeld and H. Goldberg, *J. Chem. Phys.*, **34**, 643 (1961).

(61) (a) R. A. Berg and O. Sinanoglu, *ibid.*, **32**, 1082 (1960); (b) J. T. Hougen, G. E. Leroi, and T. C. James, *ibid.*, **34**, 1670 (1961), and G. E. Leroi, T. C. James, J. T. Hougen, and W. Klemperer, *ibid.*, **36**, 2879 (1962); (c) G. L. Goodman, to be published; (d) K. D. Carlson, Progress Report No. 8, Wave Mechanics Group, Mathematical Institute, University of Oxford 1961–1962, p. 27.

(62) A detailed theory of the stereochemical vibronic problem and a critical appraisal of the current experimental situation is given in (a) A. D. Liehr, *J. Phys. Chem.*, **67**, 389 (1963). [Note in this regard that the ground state of octahedral cobalt(II) is Jahn-Teller stable since it is a Kramers doublet. Look up (b) J. H. Van Vleck, *Discussions Faraday Soc.*, **26**, 96 (1958), and *Physica*, **26**, 544 (1960), and (c) A. D. Liehr, *Bell Syst. Tech. J.*, **39**, 1617 (1960).]

(63) The coinage of the term and the concept of "molecular engineering" although done independently by the author several years ago, is not original: others have had similar dreams. Peruse for example A. R. von Hippel, *Science*, **138**, 91 (1962).

(64) (a) L. G. Van Uitert, to be published; (b) A. D. Liehr, Sixth International Conference on Coördination Chemistry, Wayne State University, Detroit, Michigan, 1961, and to be published; (c) N. K. Hamer, *Mol. Phys.*, **5**, 339 (1962); (d) T. S. Piper and A. Karipides, *ibid.*, **5**, 475 (1962); (e) M. Shinada and S. Sugano, "International Symposium on Molecular Structure and Spectroscopy," Tokyo, 1962, and to be published.

(65) (a) F. Basolo and R. G. Pearson, "Mechanisms of Inorganic Reactions," John Wiley and Sons, Inc., New York, N. Y., 1958; (b) H. L. Schläfer, *Z. physik. Chem.* (Frankfurt), **11**, 65 (1957); (c) A. W. Adamson, *J. Inorg. Nucl. Chem.*, **13**, 275 (1960); (d) J. R. Perumareddi, "The Photochemistry and Ligand Field Theory of Some Transition-Metal Complexes," Thesis, University of Southern California, 1962.

(66) (a) B. N. Figgis and R. S. Nyholm, *J. Chem. Soc.*, 338 (1959); (b) R. H. Holm and F. A. Cotton, *J. Chem. Phys.*, **32**, 1168 (1960); (c) M. Kotani, *Progr. Theoret. Phys. Suppl.*, No. **14**, 1 (1960); (d) H. Kamimura, S. Koide, H. Sekiyama, and S. Sugano, *J. Phys. Soc. Japan*, **15**, 1264 (1960); (e) D. H. Busch, "Cobalt," R. S. Young, Ed., A. C. S. Monograph Series, Reinhold Publ. Corp., 1960, Chap. 6, and in journals; (f) A. Bose, A. S. Chakravarty, and R. Chatterjee, *Proc. Roy. Soc.* (London), **261A**, 43 (1961); (g) R. C. Stoufer, D. W. Smith, T. E. Norris, and E. A. Clevenger, to be published; (h) A. D. Liehr, to be published; (i) D. J. E. Ingram, "Spectroscopy at Radio and Microwave Frequencies," Butterworths, London, 1955; (j) W. Low, "Solid State Physics Supplement 2," F. Seitz and D. Turnbull, Ed., Academic Press, New York and London, 1960; (k) J. S. Griffith and L. E. Orgel, *Trans. Faraday Soc.*, **53**, 601 (1957); (l) C. J. Ballhausen and R. W. Asmussen, *Acta Chem. Scand.*, **11**, 479 (1957); (m) C. G. Windsor, J. H. M. Thornley, J. H. E. Griffiths, and J. Owen, *Proc. Phys. Soc.* (London), **80**, 803 (1962).

(67) (a) J. C. Slonczewski, *J. Appl. Phys. Suppl.*, **30**, 310S (1959); (b) P. W. Anderson, *Phys. Rev.*, **115**, 2 (1959); (c) J. B. Goodenough, *ibid.*, **117**, 1442 (1960); **120**, 67 (1960); (d) F. J. Morin, "International Conference on Semiconductor Physics, Prague, 1960," Academic Press, New York and London, 1961, pp. 858–863.

ulation to begin, to J. C. Eisenstein, J. Ferguson, and D. L. Wood for contributing the wherewithal to do, to J. D. Sautter for affording the numerical data to work, to J. C. Eisenstein, W. Low, W. A. Runciman, and H. A. Weakliem, Jr., for furnishing the confidence to continue, to C. J. Ballhausen, E. Banks, D. H. Busch, F. A. Cotton, D. P. Craig, R. E. Dietz, R. Englman, L. S. Forster, S. Geschwind, D. M. Gruen, R. G. Hayter, W. Hayes, K. Hijikata, J. T. Hougen, J. S. Jarrett, C. K. Jørgensen, H. Kamimura, L. I. Katzin, K. Knox, S. Koide, C. C. Lin, F. J. Morin, R. Pappalardo, M. Robbins, H.-H. Schmidtke, R. G. Shulman, O. Sinanoglu, J. C. Slonczewski, D. W. Smith, G. P. Smith, M. D. Sturge, S. Sugano, B. R. Sundheim, and L. G. Van Uitert, for supplying the background (preprints and conversations) to fill in, and to each of us (A. D. L., T. F., and D. L. W.) to the other for the strength to endure and accomplish.

THE KINETICS OF THE THERMAL ISOMERIZATION OF CYCLOBUTENE[1,2]

BY WILLIAM P. HAUSER AND W. D. WALTERS

Department of Chemistry, University of Rochester, Rochester, New York

Received January 14, 1963

The homogeneous isomerization of cyclobutene to 1,3-butadiene has been studied at 150° for initial pressures from 23 to 0.015 mm. The first-order rate constant has been observed to decrease as the initial pressure is lowered, the rate constant at 0.015 mm. pressure being about one-eighth the value of the high pressure rate constant. Measurements near 0.02 mm. in a packed reaction vessel have shown that the reaction is not influenced significantly by wall effects under the experimental conditions used in this study. Evaluation of the activation energy at initial pressures from about 5 to 0.05 mm. on the basis of experiments at various temperatures in the range 130–175° indicated that the activation energy decreases slightly as the pressure is lowered. Inert gases added to cyclobutene in the fall-off region raise the rate constant; preliminary values of the efficiencies of various inert gases have been obtained.

In an earlier study[3] of the kinetics of the isomerization of cyclobutene preliminary experiments at initial pressures of 0.7–0.1 mm. indicated that a decrease in the first-order rate constant occurs as the initial pressure is lowered. Therefore, the present work was undertaken to investigate the fall-off in rate constant and the effect of the addition of inert gases.

Experimental

Materials.—The cyclobutene used in this study was obtained from two sources. The material for most of the experiments was prepared by Cooper[3] and fractionated in a Podbielniak low-temperature distillation column. During the course of the present investigation this sample was split into four fractions. After trap-to-trap distillation two samples (I and IV) were shown by gas chromatography to be about 99.9% pure. Two small samples were further purified on a Perkin–Elmer Model 154B vapor fractometer using a column packed with tetraisobutylene on a firebrick base. These two samples were designated as II and III. Another sample, prepared by a different synthesis, was kindly furnished by Dr. W. R. Moore of the Massachusetts Institute of Technology. A portion of this sample after some purification in this Laboratory was designated as V. Infrared absorption spectra were obtained for samples I and V. Both spectra, having nearly identical maxima, compared favorably with the spectrum in the literature.[4] Of the samples tested only sample V showed a significant absorption in the region of wave lengths used for rate measurements. It appeared to contain an impurity with an absorption equivalent to 1.4% 1,3-butadiene and in the one experiment in which it was used the results were corrected accordingly.

Samples of 1,3-butadiene (Matheson, 99.4%) were purified by vacuum distillation and were found by gas chromatography to possess a minimum purity of 99.5%. The materials which were used as inert gases were usually commercially available and obtainable from cylinders. The stated minimum purities were: 99.9% or greater, ethane, ethylene, and nitrogen; 99.5–99.8%, dimethyl ether, helium, hydrogen, and methane; 99%, *n*-butane, *cis*-2-butene, *trans*-2-butene, carbon dioxide, and propane. Condensable gases were purified by vacuum distillation; noncondensable gases were passed through a trap kept at −196° in order to eliminate any condensable impurity.

Apparatus and Procedure.—A grease-free vacuum system employing mercury cut-off valves was used for all rate studies. Pressures less than 4.5 mm. were measured with a McLeod gage and pressures greater than this were measured by means of a wide-bore mercury manometer read with a Gaertner cathetometer. Since the reaction product, 1,3-butadiene, absorbs strongly in the region 204–230 mμ, the rate of reaction was followed by determining the increase in the optical density of the reaction mixture. In the majority of the experiments this was accomplished by the use of a quartz cell (vol. 22 ml., about 2.5 cm. diameter, and 5 cm. long) which was situated between the monochromator and photomultiplier of a Beckman DU spectrophotometer.

Two methods were used for the measurement of the isomerization of cyclobutene. In the first method the quartz cell was heated in an apparatus constructed to provide suitable spatial uniformity of temperature and temperature regulation (±0.1°). The increase in the optical density of the reaction mixture was measured *in situ*. The temperature could be determined by the use of two platinum, platinum–13% rhodium thermocouples (B and S gage 28) which were placed along the top and bottom of the reaction cell. The temperatures indicated by both thermocouples were essentially the same. Precautions were taken in the construction of the reaction cell to minimize the volume of the dead space (~3.8%). The relationship of the optical density to the pressure of butadiene was found from calibration curves (essentially linear) determined for the wave lengths and temperatures used for the kinetic experiments. From absorption measurements taken during the course of the reaction the first-order rate constants could be calculated. Appropriate corrections for dead space were applied. The isomerization was studied for experiments *in situ* between 25 and 0.18 mm. At the lower pressures measurements were made at 209.5 mμ and at higher pressures wave lengths of 221, 226, and 232 mμ were used.

In the second method employed for rate measurements the reaction was carried out in a larger cylindrical Pyrex vessel (vol. 522 ml., about 7 cm. diameter, and 14 cm. long). The temperature at the center of the reaction vessel was measured by means of a platinum, platinum–13% rhodium thermocouple (24 gage) standarized at the melting point of an N.B.S. sample of tin (231.9°). The two thermocouples used in the measurements *in situ* were standardized against this thermocouple. Usually the reaction was allowed to proceed to 15–20% isomerization and then the entire reaction mixture was removed by condensation at

(1) This work was supported by a research grant from the National Science Foundation. Presented at the 18th IUPAC Congress, Montreal, 1961.

(2) Abstracted from the Ph.D. thesis submitted by W. P. Hauser, who held an E. H. Hooker fellowship during 1958–1960.

(3) W. Cooper and W. D. Walters, *J. Am. Chem. Soc.*, **80**, 4220 (1958).

(4) J. D. Roberts and C. W. Sauer, *ibid.*, **74**, 3192 (1952).

−196°. In most of the discontinuous experiments the ultraviolet absorption of the vaporized reaction mixture was measured in the 22-ml. quartz cell kept at room temperature. From the determination of the total pressure, the pressure of butadiene, and the time of reaction the first-order rate constants were calculated. By this procedure the rate was measured at pressures between 1.2 and 0.035 mm. In separate experiments the time of removal of the sample had been determined and a small correction was applied for the reaction occurring during removal. To extend the pressure range to 0.015 mm., the entire reaction mixture was transferred to a small quartz cell which could be sealed off and placed in a Cary Model 11 spectrophotometer for measurement of the optical density.

In order to study the effect of surface on the rate at low initial pressures another Pyrex vessel was packed with 10-mm. Pyrex tubes. For this vessel (327-ml. capacity) the packing increased the surface to volume ratio to almost eight times that of the unpacked 522-ml. vessel. In order to have a deactivated surface for each vessel, preliminary experiments with cyclobutene were carried out and samples of 2-butene or 1,3-butadiene were allowed to stand in the vessel for several hours. Most kinetic measurements involving the use of inert gases were carried out in the quartz cell *in situ*. A gas mixture of cyclobutene and inert gas was prepared in a grease-free portion of the vacuum system. To ensure that the composition of the sample was homogeneous the sample was mixed thoroughly in a gas buret.

Results

Preliminary Observations.—In the previous investigation at pressures of 5–50 mm. it was found that the reaction

$$\begin{array}{l} CH=CH \\ | \quad\quad | \\ CH_2—CH_2 \end{array} \longrightarrow CH_2=CH—CH=CH_2 \quad (1)$$

is the only one of significance at 130–175°. The reaction proceeded homogeneously and did not appear to involve chain processes. During the present study additional observations were made to ascertain whether the course of the reaction remains unaltered under the present experimental conditions. Measurements made for the low-pressure experiments (in the 522-ml. reaction vessel) showed that non-condensable gases constitute much less than 0.1% of the reaction mixture. Gas chromatographic analysis of the reaction mixture from a 3.8 mm. experiment at 150° carried to about 50% reaction in the quartz cell showed peaks only for 1,3-butadiene and cyclobutene and indicated that there is less than 0.1–0.2% of other substances present. Other experiments demonstrated that the low intensity ultraviolet light used for the absorption measurements *in situ* had a negligible effect on the rate of isomerization.

First-Order Rate Constants and their Pressure Dependence.—The results from experiments *in situ* were treated in several ways to determine the order under the present conditions and to evaluate rate constants. One method was to plot the data as log $[P_0/(P_0 - P_B)]$ *vs.* t where P_0 is the initial pressure of cyclobutene and P_B is the pressure of 1,3-butadiene formed at time t (Fig. 1). The linearity of such plots indicated that during the course of an experiment the isomerization obeys a first-order relationship. The effect of decreasing initial pressure upon the rate constant is shown in Fig. 1 where the slope of line 1 for the reaction at 0.202 mm. is less than half of that of line 2 representing an experiment with 5.97 mm. also at 150°. Other treatments of the data confirmed that the first-order law is followed during an experiment even though the reaction is in a region where the first-order rate constant decreases with the lowering of the initial pressure. For seven experiments *in situ* with initial pressures from 0.25 to 1.47 mm. at 175° the values for the half-time ($t_{1/2}$) and the quarter-time ($t_{1/4}$) were obtained from plots of P_B *vs.* t. After corrections for diffusion between the reaction cell and the dead space, the ratio $(t_{1/2}/t_{1/4})$ averaged 2.41 ± 0.02 in agreement with the value of 2.41 expected for a first-order process. For ten experiments *in situ* in the pressure range 0.18–0.98 mm. at 150° the ratio $t_{1/4}/t_{1/8}$ had an average value of 2.15 ± 0.03 in accord with the value of 2.15 for a first-order reaction. It is to be noted that first-order rate constants were calculated also from the fractional times in each experiment and they were in good agreement with the constants obtained from the first-order plots.

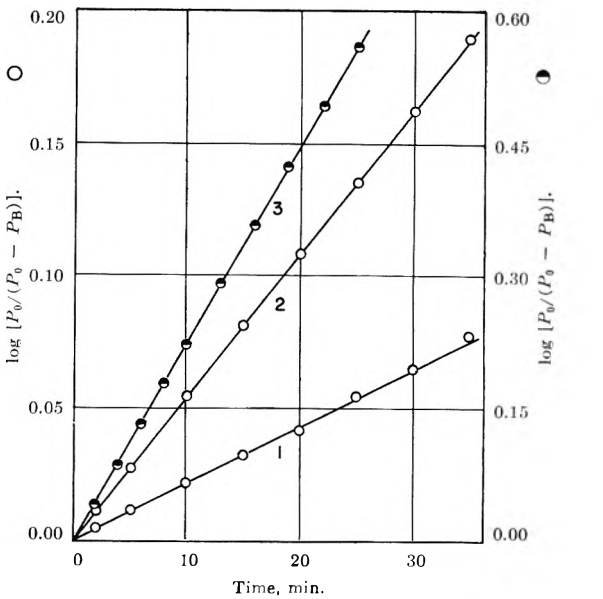

Fig. 1.—First-order plots for the isomerization of cyclobutene: curve 1, 0.202 mm. at 150°; curve 2, 5.97 mm. at 150°; curve 3, 0.555 mm. at 175°. Curves 1 and 2 (but not 3) have been corrected for dead space.

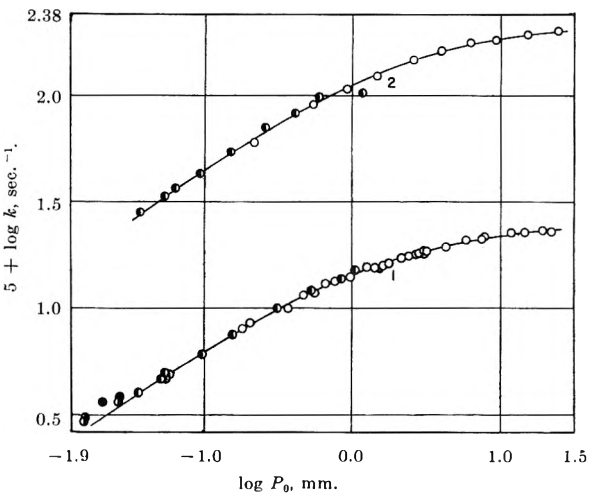

Fig. 2.—Change of the first-order rate constant with decreasing initial pressure: curve 1, 150.4°; curve 2, 175.4°. Experiments: ○, *in situ* (quartz cell); 522-ml. Pyrex vessel with analysis on the Beckman spectrophotometer, ◐, and Cary spectrophotometer, ◑. Packed bulb experiments, ●.

At lower pressures the isomerization was studied by the discontinuous technique and the rate constants were calculated on the basis of the integrated first-order equation

$$k = (1/t) \ln [P_0/(P_0 - P_B)]$$

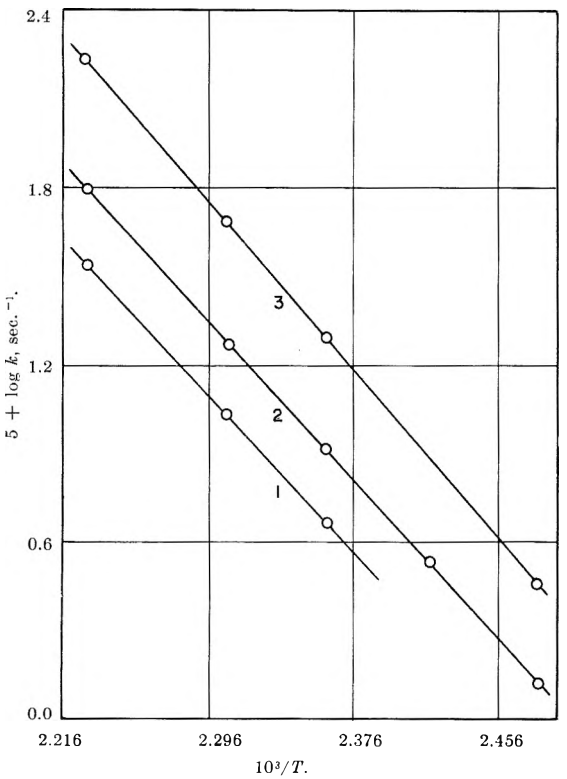

Fig. 3.—Temperature dependence of the first-order rate constants at different initial pressures: curve 1, 0.055 mm. initial pressure; curve 2, 0.22 mm.; curve 3, 5.4 mm.

The rate constants from several experiments at 150° are shown in Table I. The fact that in the fall-off region the first-order rate constant remains essentially the same as the reaction proceeds (considering the experimental error and the variation in the initial pressure) indicates that 1,3-butadiene is approximately as efficient as cyclobutene in the collisional energy transfer process.

TABLE I

COMPARISON OF THE FIRST-ORDER RATE CONSTANTS AT VARIOUS PERCENTAGES OF REACTION AT 150.3°

P_0, mm.	% Isomerization	10^4k, sec.$^{-1}$
0.0575	17.0	0.470
.0564	49.4	.465
.0550	18.3	.490
.0508	53.0	.462

The decrease of the first-order rate constant as the initial pressure is lowered is shown in Fig. 2. When necessary, small corrections have been applied to bring the data to the same temperature. The plotted fall-off curves indicate that the data obtained by different experimental techniques and with different purified samples of cyclobutene are in reasonably good agreement with each other. The points for the three experiments with the lowest initial pressures (0.015–0.026 mm.) at 150° in the 522-ml. unpacked vessel lie slightly above the curve for the other results. In these experiments the technique of analysis which involved the use of the Cary spectrophotometer was different from that used in the other discontinuous experiments. Since the higher values might conceivably be due to a wall effect, two experiments at 0.020 and 0.027 mm. pressure were performed in the packed vessel with almost eight times the surface to volume ratio. The inside diameter of the tubes used for packing was only one-ninth the diameter of the unpacked vessel. The resulting rate constants (two filled circles at the low pressure end of curve 1 in Fig. 2) are about 5–9% higher than comparable experiments in the unpacked vessel. On this basis no indication of significant wall effects in the unpacked vessel has been obtained.

Both of the sets of data shown in Fig. 2 give clear evidence for the fall-off of the first-order rate constant with decreasing pressure. Similar behavior at 130 and 160° had been observed in this study for an earlier (but less extensive) series of experiments carried out *in situ* at 130, 150, 160, and 175° with pressures of about 0.23 to 8 mm. A comparison of curve 2 at 175° with curve 1 at 150° in Fig. 2 reveals that for a given pressure the percentage decrease in the rate constant is somewhat greater at 175°.

Activation Energy.—In the present investigation activation energies have been determined at three pressures in the fall-off region. From the first series of measurements *in situ* at 130.4, 150.4, 160.4, and 175.4° rate constants representing experiments with an initial pressure of about 5 mm. were taken from the fall-off curves drawn through the experimental points at each temperature. The values of log k *vs.* $1/T$ are shown as curve 3 in Fig. 3. It was observed that the values of k obtained at 175 and 150° for similar pressures (~5 mm.) in the second series of experiments *in situ* (shown in Fig. 2) are within 1.1 and 2.3% of the values of k shown in Fig. 3. The activation energy was evaluated graphically from the slope of this plot and also by a least squares analysis of the data with an IBM 650 computer. A value of 32.7 ± 0.2 kcal./mole was found. With the activation energy set at 32.7 kcal./mole the Arrhenius pre-exponential factor was obtained by solving for A in the expression $k = A \exp(-32700/RT)$ sec.$^{-1}$ for each value of k. For the determination of the activation energy at an initial pressure of about 0.2 mm. a series of experiments was performed *in situ* at 130.4, 140.4, 150.4, 160.4, and 175.4° (curve 2, Fig. 3). An attempt was made to keep the cyclobutene concentration constant by the use of slightly greater pressures at the higher temperatures. The pressures obtained experimentally averaged within 0.005 mm. of the desired value for constant concentration. The activation energy determined in the 0.2 mm. experiments was 30.7 ± 0.2 kcal./mole. A value of the pre-exponential factor for these experiments was found as mentioned above.

To ascertain the temperature dependence at lower pressures (~0.055 mm.) experiments were performed by the use of the discontinuous technique. For each temperature the values of log k were plotted against log P_0 and the interpolated value of log k was taken from each plot at a pressure which would give a concentration corresponding to that for 0.055 mm. at 160°. The plot of log k *vs.* $1/T$ for the experiments at 0.055 mm. is shown as curve 1 in Fig. 3. The slope of the line gives a value of 30.2 kcal./mole for activation energy.

The results obtained for the pre-exponential factors and the activation energies at various pressures are listed in Table II. The experimental data indicate that there is a decrease in the activation energy as the initial pressure is lowered.

Although the rate constant was not measured at high pressures, it was desirable to have an expression

TABLE II

VALUES OF THE ACTIVATION ENERGY AND THE ARRHENIUS PRE-EXPONENTIAL FACTOR FOR THE ISOMERIZATION OF CYCLOBUTENE AT VARIOUS PRESSURES

Exptl. temp. range, °C.	P_0,[a] mm.	$E_{act.}$, kcal./mole	$10^{-13}A$, sec.$^{-1}$
130–175	5.4	32.7	1.5
130–175	0.22	30.7	0.056
150–175	0.055	30.2	0.018

[a] Pressure at 160°; experiments at other temperatures at essentially the same concentration.

for the rate constant at infinite pressure so that fall-off curves could be obtained from various theoretical treatments of unimolecular reactions for comparison with the experimental results. To this end reciprocals of the rate constants were plotted first against the reciprocal of the initial pressure and also against the reciprocal of the square root of the pressure as suggested by Schlag and Rabinovitch.[5] Neither of the curves was exactly linear and the extrapolated values at $(1/P_0) = 0$ were not quite coincident. The value for $(1/k_\infty)$ at each temperature was calculated from the mean of the two intercepts. The extrapolation would have been subject to less uncertainty if data at higher pressures had been available. As a result of several methods of calculating the temperature dependence of k_∞ from the two series of experiments *in situ*, it was concluded that the best value for E_∞ obtainable from the present results would be 32.7 kcal./mole with a maximum deviation of 0.8 kcal./mole to cover the range of values plus their deviations. With this value for the activation energy the rate expression $k_\infty = 1.8 \pm 0.1 \times 10^{13} \exp(-32700/RT)$ sec.$^{-1}$ was found to represent the high pressure rate constant determined by extrapolation.

Effect of Inert Gases.—As was expected, the addition of an inert gas to cyclobutene in the fall-off region was observed to raise the first-order rate constant toward the high pressure limit. Typical results which were obtained for some of the inert gases are shown in Table III. To determine the relative efficiencies of various substances in transferring energy, the method described by Trotman-Dickenson[6] was employed. Experiments were performed with a series of gases increasing in molecular complexity from helium to cyclobutane and differing in some cases with respect to the type of bonds and polarity. The experimental measurement involved the determination of the rate constant k_B when a pressure P_I of inert gas was added to a low pressure P_C of cyclobutene. Comparison of the value of k_B with the fall-off curve for pure cyclobutene gave the pressure of cyclobutene P_b which would have the same rate constant k_B. The efficiency of the inert gas relative to that of cyclobutene in transferring energy by collision was taken as $(P_b - P_C)/P_I$. The efficiencies on this pressure for pressure $(E_{p/p})$ basis are shown in Table IV. In each case the value given represents the average of only two or three experiments and in some cases k_B fell in a region where the rate constant did not change rapidly with pressure. The mean deviation of the values given in Table IV averaged 7%, but the uncertainty of the values may be 10–20%. For each substance the efficiency on a collision for collision basis, $E_{c/c}$, was calculated by the use of the collision diameter, σ, shown in Table IV, together with a diameter of 5.3 Å. for cyclobutene. In some cases values of the collision diameter were chosen to coincide with those used in the studies for cyclopropane,[7] cyclobutane,[8] and methylcyclopropane[9] so that comparisons of relative efficiencies would not be distorted by differences in σ. As noted in an earlier section, the constancy of the first-order rate constant during the course of the reaction in the fall-off region indicates that 1,3-butadiene has an efficiency (relative to cyclobutene) close to one. In view of the uncertainties in the measurements of $E_{p/p}$ and in the selection of σ the tabulation of $E_{c/c}$ to more significant figures than those used in Table IV did not seem warranted. In a comparison with the results of earlier studies[7-9] of other unimolecular reactions, the inert gases seem to fall in the same order with respect to efficiency and even though the reacting molecules are not the same, the relative values of the efficiency of energy transfer are not greatly different. In the present work no marked difference due to the type of bond or its polarity has been observed. The limited nature of the present study precluded the possibility of ascertaining whether the efficiency depends upon the reference pressure and the pressure interval covered.[10]

TABLE III

EFFECT OF VARIOUS INERT GASES UPON THE RATE OF ISOMERIZATION OF CYCLOBUTENE AT 150°

Inert gas	P_I,[a] mm.	P_C, mm.	10^4k, sec.$^{-1}$
None	0	0.202	0.86
H_2	4.26	.212	1.37
N_2	3.86	.203	1.29
CO_2	4.35	.211	1.53
CH_4	4.44	.200	1.63
None	0	3.41	1.86
None	0	4.33	1.93

[a] P_I is the pressure of inert gas and P_C is the pressure of cyclobutene.

TABLE IV

EFFICIENCIES OF INERT GASES FOR THE ISOMERIZATION OF CYCLOBUTENE AT 150°[c]

	He	H_2	N_2	CO_2	CH_4	C_2H_4	C_2H_6	C_3H_8
$E_{p/p}$	0.034	0.16	0.12	0.27	0.35	0.54	0.60	0.88
σ, Å.	2.2	2.7	3.8	4.0	4.1	4.5	4.5	5.0
$E_{c/c}$	0.03	0.08	0.13	0.3	0.3	0.5	0.6	0.9

	CH_3OCH_3	n-C_4H_{10}	2-C_4H_8 (*cis*)	2-C_4H_8 (*trans*)	C_4H_8 (cyclo)
$E_{p/p}$	0.79	0.95	0.92	0.95	0.96
σ, Å.	5.0	5.1	5.1	5.1	5.5
$E_{c/c}$	0.8	1.0	1.0	1.0	0.93

Discussion

In this study the isomerization of cyclobutene at 150.4° has been examined over a 1500-fold pressure range; at an initial pressure of 0.015 mm. the first-order rate constant has decreased to slightly less than 13% of the value at 22.6 mm. (where $k = 2.31 \times 10^{-4}$ sec.$^{-1}$). The rate constants at 150.4° in the present

(5) E. W. Schlag and B. S. Rabinovitch, *J. Am. Chem. Soc.*, **82**, 5996 (1960).

(6) A. F. Trotman-Dickenson, "Gas Kinetics," Academic Press, Inc., New York, N. Y., 1955, p. 83.

(7) H. O. Pritchard, R. G. Sowden, and A. F. Trotman-Dickenson, *Proc. Roy. Soc.* (London), **A217**, 563 (1953).

(8) H. O. Pritchard, R. G. Sowden, and A. F. Trotman-Dickenson, *ibid.*, **A218**, 416 (1953).

(9) J. P. Chesick, *J. Am. Chem. Soc.*, **82**, 3277 (1960).

(10) M. Volpe and H. S. Johnston, *ibid.*, **78**, 3903 (1956).

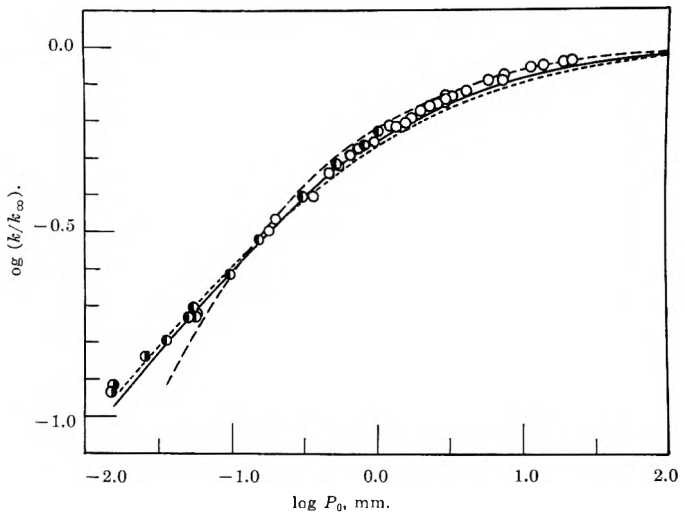

Fig. 4.—Comparison of the experimental data at 150.4° with the fall-off curves calculated from Kassel theory: - - - - quantum form, $s = 13$; - - - - - - - - - modified quantum form, $s = 12$; ——— classical form, $s = 10$. Symbols for the data are the same as those in Fig. 2.

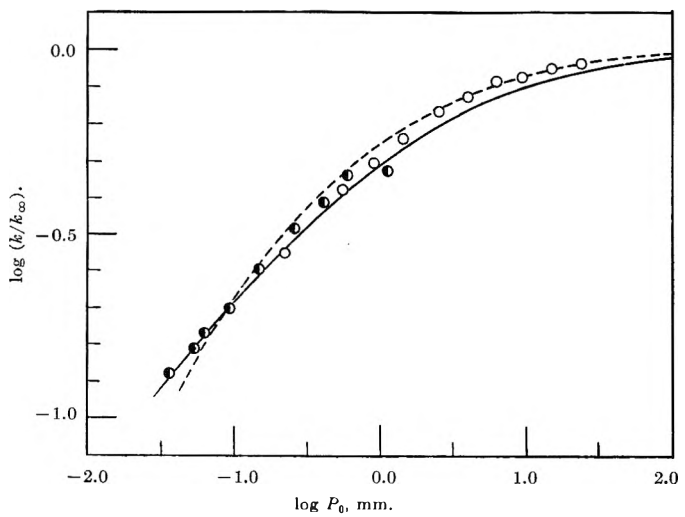

Fig. 5.—Comparison of the experimental data at 175.4° with the fall-off curves calculated from Kassel theory: - - - - quantum form, $s = 13$; ——— classical form, $s = 10$. Symbols for the data are the same as those in Fig. 2.

work[11] were found to be in agreement with those in the previous work[3] at 4–8 mm. which was the region of greatest accuracy, but at higher pressures the present values are 5–15% larger than the earlier values. The activation energy of 32.7 kcal./mole found for the 5 mm. experiments in this work agrees with the earlier value of 32.5 ± 0.5 kcal./mole for the 8–14 mm. region.

In comparison with the behaviors of cyclobutane[8,12,13] and cyclopropane[7,14,15] the decrease in the first-order rate constants for the isomerization of cyclobutene occurs in about the pressure region observed for the fall-off of cyclobutane (at slightly greater pressure than that for cyclobutane), but at a significantly smaller pressure than that for cyclopropane. It is to be noted that these three reactions are not strictly comparable. The reactions of both cyclobutane and cyclopropane proceed at much higher temperatures and have greater activation energies and frequency factors than those for cyclobutene.

Figure 4 shows the relationship between the present data at 150.4° and the fall-off curve obtained from the quantum form[16] of the Kassel theory with the number of oscillators $s = 13$, $\nu = 2.3 \times 10^{13}$ sec.$^{-1}$, $\sigma = 5.3$ Å., $E_{act} = 32.7$ kcal./mole, and $A = 1.8 \times 10^{13}$ sec.$^{-1}$. The symbols are defined and used as in the standard Kassel treatment.[16] Other curves with $s = 12$ and $s = 14$ did not give as good agreement with the experimental points. The difficulty in deciding upon the best fit lies to some extent upon the weight to be given to the points at the lowest pressures which were obtained with a different experimental technique and which seem to be higher than an extrapolation of the curve from higher pressures might indicate.

Values of k/k_∞ in the fall-off region were calculated also by the use of a modified form of the Kassel quantum theory on an IBM 650 computer with a program which was furnished by Dr. David Wilson of these Laboratories and which involved the replacement of the quantity (A/aN) found in the original Kassel expression.[17] In this comparison which concerned only the curvature of the plot the calculated curve was moved along the pressure axis to see whether a satisfactory fit could be obtained. Of the several curves calculated with an oscillator frequency of 4.48×10^{12} sec.$^{-1}$ the best fit was found with the curve for $s = 12$. This curve is shown also in Fig. 4.

For the classical form of the Kassel theory[18] the fall-off curve for $s = 10$ (and the other parameters as given above) was obtained first by the use of a Bendix G-15 computer with the program of Schlag.[19] The values of k/k_∞ were checked subsequently with an IBM 7090 computer. The comparison with the experimental results is shown in Fig. 4. That the classical form of the Rice–Ramsperger–Kassel theory gives agreement with the fall-off data for unimolecular reactions frequently with a value of s considerably smaller than the number of vibrational degrees of freedom in a molecule has been observed in previous work[7,9,13,14] and the shortcomings of the usual classical formulation have been pointed out.[20]

The experimental data at 150° were compared also with fall-off curves predicted on the basis of a simplified form of the classical Slater theory[21] with various values of n, the effective number of normal vibration modes which contribute to the extension of the reaction coordinate. For predicting the correct pressure region for the fall-off, the curve for $n = 16$ gave the best agreement, but it was somewhat too flat to reproduce the experimental behavior. From the standpoint of curva-

(11) On the basis of curve 1 in Fig. 2 the value of the rate constant at 5.25 mm. is 2.0×10^{-4} sec.$^{-1}$ at 150.4.

(12) F. Kern and W. D. Walters, *Proc. Natl. Acad. Sci. U. S.*, **38**, 937 (1952).

(13) D. F. Swinehart and R. W. Vreeland, Abstracts, National Meeting, Sept., 1960, Am. Chem. Soc., p. 37S; R. W. Vreeland, Ph.D. Thesis, University of Oregon, 1961.

(14) T. S. Chambers and G. B. Kistiakowsky, *J. Am. Chem. Soc.*, **56**, 399 (1934).

(15) E. S. Corner and R. N. Pease, *ibid.*, **67**, 2067 (1945).

(16) L. S. Kassel, "The Kinetics of Homogeneous Gas Reactions," Chemical Catalog Co. (Reinhold Publ. Corp.), New York, N. Y., 1932, p. 100.

(17) D. J. Wilson, private communication.

(18) From eq. 23 and 24 on p. 103 of ref. 16.

(19) E. W. Schlag, B. S. Rabinovitch, and F. W. Schneider *J. Chem. Phys.*, **32**, 1599 (1960).

(20) R. A. Marcus and O. K. Rice, *J. Phys. Colloid Chem.*, **55**, 894 (1951); B. S. Rabinovitch and J. H. Current, *J. Chem. Phys.*, **35**, 2250 (1961); E. W. Schlag, *ibid.*, **35**, 2117 (1961); M. Vestal, A. L. Wahrhaftig, and W. H. Johnston, *ibid.*, **37**, 1276 (1962); G. M. Wieder and R. A. Marcus, *ibid.*, **37**, 1835 (1962).

(21) N. B. Slater, "Theory of Unimolecular Reactions," Cornell Univ. Press, Ithaca, N. Y., 1959, pp. 164–187.

ture the curve for $n = 15$ gave the best fit, but to agree satisfactorily with the experimental data the curve for $n = 15$ would have to be shifted about 0.25 of a log unit toward lower pressures.

It was of interest to compare the fall-off curves predicted at 175.4° with the experimental data since no further adjustment of parameters is possible in such calculations. The Kassel curves for the quantum form with $s = 13$ and the classical form with $s = 10$ were calculated at 175.4° as in the case of the curves at 150.4°. These curves are compared with the experimental results in Fig. 5. Over the limited range of the available data both curves predict approximately the shift in the fall-off region along the pressure axis which is caused by a change in temperature. It is hoped that it will be possible to study the isomerization of cyclobutene at pressures below 0.0365 mm. in a larger reaction vessel, thereby overlapping the lowest pressure range at 150° shown in Fig. 2 and extending the range of available data at 175°.

As has been shown in Table II, the change in the fall-off behavior of the isomerization of cyclobutene with temperature results in a decrease in activation energy from a value of 32.7 kcal./mole at the high pressure limit (and at 5 mm.) to a value of 30.7 kcal./mole at 0.2 mm. and 30.2 kcal./mole at 0.055 mm. Both the Kassel and Slater theories predict a pressure dependence of the activation energy in the fall-off region. On the basis of the simplified form of the Slater theory[21] with $n = 15$ the predicted decrease in activation energy from the high pressure limit to the 0.055 mm. region is 2.6 kcal./mole; with the Kassel theory the decrease in activation energy ranges from about 1.7 to 2.4 kcal./mole depending on whether the fall-off behavior is estimated from the quantum form with $s = 13$ or the classical version with $s = 10$. In view of the considerable effect of the possible experimental error upon the difference in two large quantities (E_∞ and $E_{0.055}$), satisfactory agreement seems to exist between the experimental and predicted decreases in activation energy with decreasing pressure according to either the Slater or the Kassel theory.

Acknowledgment.—The authors wish to thank Dr. E. W. Schlag and Dr. David Wilson for their computer programs and Mr. Carl Whiteman, Jr., for his assistance in connection with the least squares calculations and the computer operations.

THE MULTI-DIMENSIONAL GLASS TRANSITION

BY ADI EISENBERG

Contribution No. 1513 from the Department of Chemistry, University of California, Los Angeles, California

Received January 24, 1963

The glass transition in polymeric materials is discussed as a phenomenon which can occur upon a change in any of the variables affecting its free volume, *i.e.*, temperature, pressure, diluent concentration, and molecular weight. Depending on which one of these variables is being changed, we can regard the glass transition as a glass transition temperature T_g, a glass transition pressure P_g, a glass transition concentration C_g, and, in a formal sense, also a glass transition molecular weight M_g. A phenomenologically derived equation is presented giving the position of the glass transition in a four-dimensional space of T, P, C, and M, which enables one to calculate any one of these glass transitions from a knowledge of the three other variables.

I. Introduction

The glass transition is normally regarded as a phenomenon which occurs when a glass former is heated or cooled through a specific temperature range. Since the glass transition depends very strongly on the free volume (which, while lacking an operational definition, has been very helpful in the formulation of phenomenological theories of the glassy state), it is normally determined by following some property dependent on the free volume, for instance the specific volume, as a function of temperature, *i.e.*, in one dimension. Since the expansion coefficients of the liquid and the glass are approximately linear except in the transition region, the intersection of the extrapolation of the linear portions of those lines through the transition region is called the glass transition temperature, T_g. However, the glass transition can be obtained by varying any of the other parameters which influence the free volume of a homopolymer, notably the pressure, molecular weight, and concentration of diluent. It has been shown[1] that rates also have a very pronounced influence on the position of the glass transition, but these will be neglected in this discussion, and constant rates assumed throughout.

Thus, the glass transition is clearly a multi-dimensional phenomenon, the dimensions being temperature T, pressure P, molecular weight M, and concentration of diluent C. If one wishes to observe the transition rather than merely describe its location within these four dimensions, one must add a fifth, say the specific volume V, which would show some type of a discontinuity at the transition.

The first part of this work will present a discussion of sections through this five-dimensional space keeping all but two of the variables constant, *i.e.*, varying only the volume and one of the others, T, P, M, or C. Subsequently, a simple, phenomenologically derived equation will be presented, which correlates the location of the transition obtained by varying any one of the above parameters with all the others, *i.e.*, a correlation of T_g, P_g, M_g, and C_g.

II. The Individual Glass Transitions

A. The Glass Transition Temperature, T_g.—Since a change in temperature is the most obvious way of bringing about a glass transition, the glass transition temperature has been investigated extensively,[2,3] and will not be described here further, except to mention

(1) A. J. Kovacs, *J. Polymer Sci.*, **30**, 131 (1958).

(2) W. Kauzmann, *Chem. Rev.*, **43**, 219 (1948).

(3) H. A. Stuart, "Die Physik der Hochpolymeren," Vol. III, Springer, 1955, Chapters 10 and 11.

that a volume–temperature plot shows a change in slope at the glass transition temperature.

B. The Glass Transition Concentration, C_g.—Lewis and Tobin[4] have recently investigated the dynamic-mechanical behavior of a series of polymers as a function of diluent concentration at room temperature, and at a certain concentration (depending on the polymer–diluent system), they observed an inflection point in the modulus–temperature curve and a maximum in the damping–temperature curve, *i.e.*, behavior characteristic of a glassy transition. The concentration of polymer at that point was called the glass transition concentration, C_g. It is quite obvious that C_g would vary with temperature, although no data were given.

Glass transition temperatures as a function of concentration have, of course, been determined for a number of polymer–diluent systems and are discussed in the literature.[5,6] It is obvious that any plot of T_g *vs.* C can also be regarded as a plot of C_g *vs.* T, and the glass transition concentration for any temperature obtained from such a graph. Various expressions correlating T_g and C have also been given.[5,6]

C. The Glass Transition Molecular Weight, M_g.—Because of the difference in free volume associated with chain ends and chain middles, a method of changing the free volume of a homopolymer at constant temperature (at atmospheric pressure and in the absence of diluent) is to change the degree of polymerization. This cannot, of course, be done *continuously*, but present techniques of polymerization permit excellent control of molecular weights and distributions so that this may be regarded as more than just a formal way of changing the free volume.

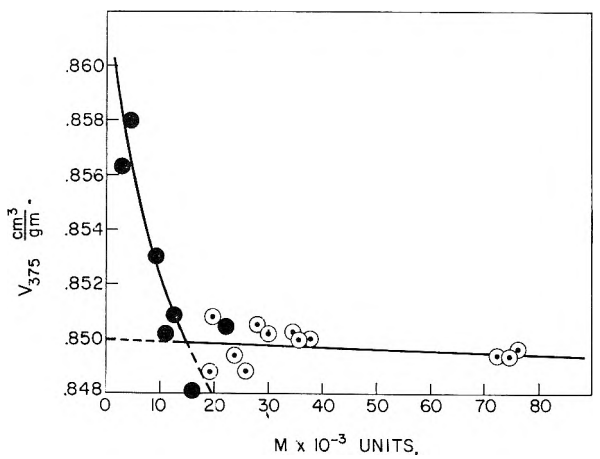

Fig. 1.—$V_{375°}$ *vs.* M for poly-(methyl methacrylate)[7]: ○, glass; ●, liquid.

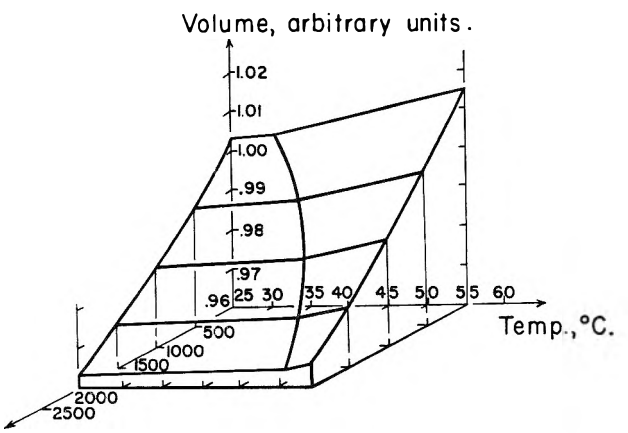

Fig. 2.—Pressure–volume–temperature for selenium.[8]

If the specific volume of a polymer is investigated isothermally as a function of molecular weight in the temperature region of the glass transition, one would expect to encounter a discontinuity at the molecular weight for which this temperature is the T_g. While no direct data are given in the literature for this type of experiment, a plot of the data of Beevers and White[7] for methyl methacrylate gives the density of the material at any temperature, in the range investigated, for a number of molecular weights. A plot of specific volume *vs.* molecular weight, given in Fig. 1 for 375°K., shows a definite discontinuity at a molecular weight of *ca.* 15,000 which can be taken as the M_g at that temperature. Similar to the results on concentration, a plot of T_g *vs.* M (or, preferably, $1/M$ since this is linear) gives simultaneously M_g *vs.* T. The formulas of Beevers and White[7] give for 375°K. a value of the molecular weight of $(1.8 \pm 0.3) \times 10^4$; close to the above graphic estimate. The concept of an M_g, therefore, seems quite well founded on experimental fact.

D. The Glass Transition Pressure, P_g.—An early systematic investigation of vitrification under pressure was undertaken by Tamman and Jellinghaus[8] on three glass-formers, selenium, salicin, and colophony. Since subsequent investigations on other materials do not differ in their conclusions from those of the above work (with one exception which will be discussed below), those of importance to this discussion will be reviewed briefly at this point.

Assuming the validity of the free-volume concept of the glass transition, the effect of pressure on T_g can be predicted qualitatively. If hydrostatic pressure simply "squeezes out" free volume in a liquid in addition to compressing the material itself, vitrification will take place as soon as the free volume of the glass transition is reached. Therefore, the effect of hydrostatic pressure is to raise the glass transition temperature. The simultaneous effect of temperature and pressure can perhaps be visualized best in a three-dimensional plot of V–T–P for amorphous selenium constructed from the data of Tamman and shown in Fig. 2. This plot illustrates the fact that while the volume–temperature curves at any pressure are linear, the volume–pressure curves at constant temperature are not, and also that the curvatures of the $(\partial V/\partial P)_T$ curves are different for the glass and the liquid, as was found by Tamman. To illustrate this last point, two volume–pressure curves are shown in Fig. 3, one for the liquid at 70° and the other for the glass at 10°. A volume–pressure plot at 40° is shown in Fig. 4, which shows the intersection of the glass-like curve at high pressures with that of the liquid-like curve at low pressures to lie at *ca.* 1100 atm. This would be the transition pressure at the temperature. A much more precise estimate of the transition pressure at that or any other temperature within the region investigated can be obtained by a projection on the P–T plane of the line of intersection of the glass and

(4) A. F. Lewis and M. C. Tobin, *Trans. Soc. Rheol.*, **6**, 27 (1962).
(5) F. N. Kelley and F. Bueche, *J. Polymer Sci.*, **50**, 549 (1961).
(6) H. A. Stuart, ref. 3, Vol. IV, Ch. 9.
(7) R. B. Beevers and E. F. T. White, *Trans. Faraday Soc.*, **56**, 744 (1960).
(8) G. Tamman and W. Jellinghaus, *Ann. Phys.*, [5] **2**, 264 (1929).

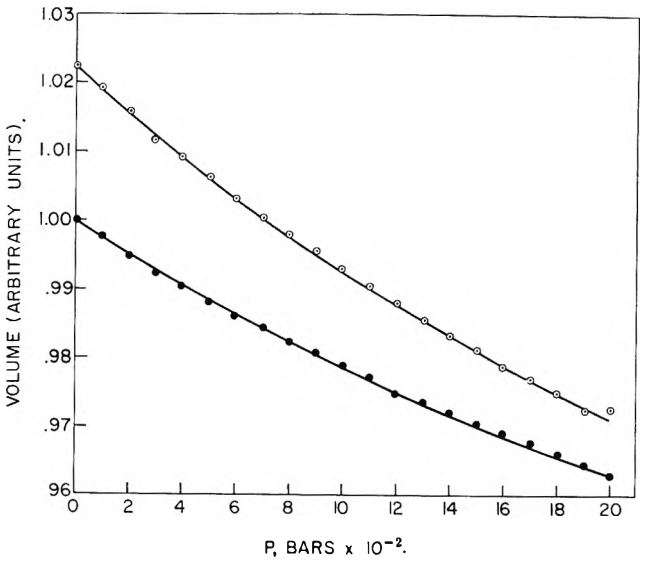

Fig. 3.—Volume *vs.* pressure for selenium[8]: ⊙, 70°, liquid; ●, 10°, glass.

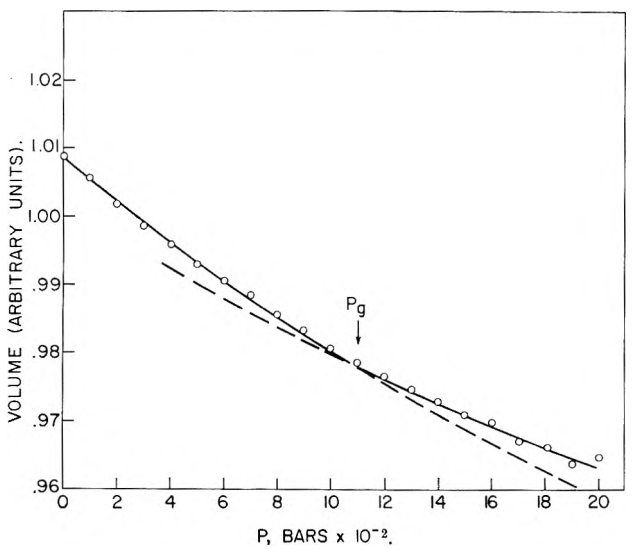

Fig. 4.—Volume *vs.* pressure for selenium[8]; 40°.

liquid planes. This projection, shown in Fig. 5 together with those for other materials to be discussed later, gives, as in the other cases, both the variation of T_g with P and of P_g with T. It is noteworthy that of all the materials investigated, only in the case of selenium is the P–T graph non-linear. It has been shown before[9] that amorphous selenium is a mixture of Se_8 and of polymeric selenium, and since the compressibilities of these two species are, most probably, not identical, it is not surprising that the $(\partial T_g/\partial P)_{C,M}$ plot is curved.

Vitrification under pressure was investigated by Shishkin[10] for phenolphthalein, rosin, a phenol–formaldehyde resin, B_2O_3, poly-(methyl methacrylate), and styrene. The last material was also studied by Matsuoka and Maxwell.[11] O'Reilly[12] studied the variation of T_g with P for polyvinyl acetate, and it was he who defined the glass transition pressure as that pressure at which molecular rearrangements can no longer follow the applied pressure; at that point, the polymer exhibits a glass-like compressibility. The

(9) A. Eisenberg and A. V. Tobolsky, *J. Polymer Sci.*, **46**, 19 (1960).
(10) N. I. Shishkin, *Zh. Tekhn. Fiz.*, **25**, 188 (1955); *Fiz. Tverd. Tela*, **2**, 350 (1960).
(11) S. Matsuoka and B. Maxwell, *J. Polymer Sci.*, **32**, 131 (1948).
(12) J. M. O'Reilly, *ibid.*, **57**, 429 (1962).

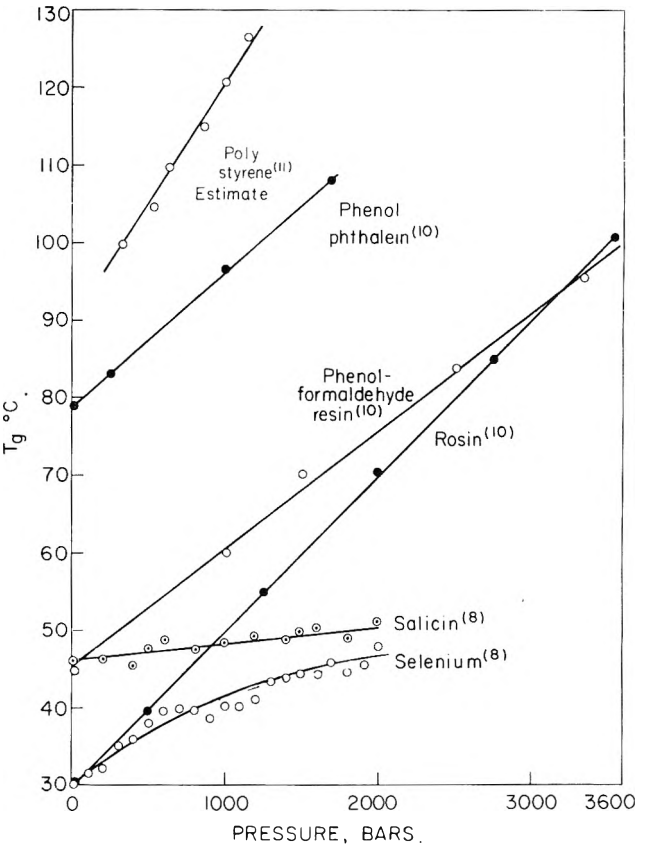

Fig. 5.—T_g *vs.* P or P_g *vs.* T for various materials.

$(\partial T/\partial P)_{M,\,C=0}$ plots for some characteristic materials which have been studied and the results on which are reported in the literature or can be estimated therefrom are given in Fig. 5. They all show an unambiguous rise of T_g with P. The only exception to this phenomenon was found by Weir,[13] who, in an investigation of volume–temperature curves of sulfur-vulcanized rubber at various pressures, found no change in T_g with pressure. No explanation seems to be available for this unique behavior. In view of the results on all the other materials, however, the glass transition pressure is certainly an experimental fact.

III. Relation between T_g, C_g, M_g, and P_g

While it is impossible to show graphically the relation between these four variables, an analytical expression can be derived easily.

The influence of molecular weight on T_g has been investigated by several authors[7,14–16] and an equation developed which describes this influence in the high molecular weight region. This equation is

$$T_g = T_g^{\infty}(0) - A/M_g \qquad (1)$$

where $T_g^{\infty}(0)$ is the glass transition temperature of a polymer of infinite molecular weight at zero pressure, A is a constant equal to $-[\partial T_g/\partial(1/M)]_{P,C}$, and $M_g(0)$ is the molecular weight, the subscript g having been added to indicate that this equation expresses the simultaneous variation of T_g with M and M_g with T.

Since, as shown in Fig. 5, all materials consisting of only one species show a linear dependence of T_g on P (and *vice versa*), we can introduce the effect of pressure on T_g by expanding equation 1 to

(13) C. E. Weir, *J. Res. Natl. Bur. Std.*, **50**, 311 (1953).
(14) T. G Fox and P. J. Flory, *J. Appl. Phys.*, **21**, 581 (1950).
(15) K. Uberreiter and G. Kanig, *J. Coll. Sci.*, **7**, 569 (1952).
(16) T. G Fox and P. J. Flory, *J. Polymer Sci.*, **14**, 315 (1954).

$$T_g = T_g^{\infty}(0) - A/M_g(0) + DP_g \qquad (2)$$

where D is a constant equal to $(\partial T_g/\partial P)_M$ and is assumed to be independent of M. It should be mentioned that Ferry[17] proposed the relationship $(\partial T/\partial P)_f = \beta_f/\alpha_f$ for the change of T_g with P at constant free volume, where β_f is the "free volume compressibility," approximately equal to $\beta_l - \beta_g$, and α_f is the "free volume expansion coefficient," approximately equal to $\alpha_l - \alpha_g$, the subscripts l and g referring to liquid and glass, respectively. A similar relation was also proposed by Shishkin,[10] and, in a somewhat more complicated form, by Singh and Nolle.[18]

Finally, the behavior of plasticized polymers can be approximated by[6]

$$1/T_g = C_1/T_{g1} + C_2/T_{g2} \qquad (3)$$

where C_1 and C_2 are the weight fractions of diluent and polymer, respectively. Recalling that the diluent has only one molecular weight, so that we can rewrite equation 2 for diluent as

$$T_{g1} = T_{g1}(0) + D_1P \qquad (2\text{-d})$$

we can combine all equations to yield

$$1/T_g = (1 - C_g)/[T_{g1}(0) + D_1P_g] + C_g/[T_{g2}^{\infty}(0) - A/M_g + D_2P_g] \qquad (4)$$

where C_g is the weight fraction of polymer. Thus, if we know A, D_1, $T_{g2}^{\infty}(0)$, and $T_{g1}(0)$, which are constants for the materials involved, we can correlate the simultaneous variation of all four variables influencing the glass transition and calculate any one from a knowledge of three of the four.

Acknowledgment.—It is a great pleasure to acknowledge the benefit of stimulating discussions with professors R. L. Scott and M. E. Baur in the course of this work.

(17) J. D. Ferry and R. A. Stratton, *Kolloid Z.*, **171**, 107 (1960).
(18) H. Singh and A. W. Nolle, *J. Appl. Phys.*, **30**, 337 (1959).

CATALYTIC ACTIVITY AND SINTERING OF PLATINUM BLACK. II. DEMETHANATION AND HYDROGENOLYSIS OF CYCLOPROPANE[1]

BY DOUGLAS W. McKEE

General Electric Research Laboratory, Schenectady, New York

Received January 25, 1963

The kinetics of the demethanation (cracking) and hydrogenolysis of cyclopropane on unsupported platinum black have been studied between 100 and 250° by a static method. The specific catalytic activity of the metal decreased rapidly during sintering due to the elimination of active sites. Both reactions were found to occur simultaneously, the products of the catalytic dissociation of cyclopropane being methane, ethane, propane, and a surface residue of average composition $CH_{1.1}$. The apparent activation energy for demethanation on sintered platinum black was 14 kcal./mole but this reaction was strongly inhibited by the presence of hydrogen. Hydrogenolysis showed an activation energy of about 8.0 kcal./mole and was approximately zero order in both reactants at low hydrogen concentrations but a large excess of hydrogen tended to retard the formation of propane. Possible mechanisms for these reactions are discussed.

Introduction

Gas phase hydrocarbon reactions have rarely been studied on unsupported metal catalysts owing to the difficulty of preparing and maintaining a metal surface of sufficiently high area for appreciable activity. Metal blacks, however, although sintering readily when freshly reduced, provide materials of high surface area and avoid complications such as the uncertain influence of a catalyst support and unknown and possible metastable surface morphology of evaporated metal films. It is of interest to compare the behavior of metal catalysts in different states so that the role of these factors can be assessed. The kinetics of propane cracking on platinum black have been discussed in part I[2] of this series and the influence of sintering on the activity of the metal was investigated. This paper describes reactions involving dissociation of cyclopropane on a similar catalyst.

Several recent studies[3] have been concerned with the hydrogenolysis of cyclopropane and its derivatives on supported nickel and platinum catalysts, and it is generally agreed that in this reaction cyclopropane appears to have properties intermediate between those of olefins and alkanes. These previous investigations have however mostly overlooked the simultaneous occurrence of catalytic cracking (demethanation), the products of which are likely to confuse the kinetic picture for the hydrogenolysis reaction. In addition, although it is agreed that cyclopropane chemisorbs readily on metal surfaces at elevated temperatures, neither the mode of attachment nor the mechanism of the subsequent cleavage has been established. The present investigation represents a further attack on these problems in the case where the hydrocarbon is present both alone and pre-mixed with hydrogen over the catalyst.

Experimental

Materials.—The platinum black used in this work was the same as in the previous investigation. The unreduced metal had a B.E.T. nitrogen surface area of 19.5 m.²/g., but this was reduced to about 12 m.²/g. after careful reduction with pure hydrogen. Most of the measurements were carried out using sintering platinum black obtained by reduction with hydrogen at 180° for over 2 hr. This material had a surface area of 5–6 m.²/g. and little further sintering occurred on further reduction and evacuation. Samples of platinum black weighing approximately 0.8 g. were used.

The cyclopropane was obtained from the Matheson Co. Analysis showed this material to be better than 99.8% pure, the main impurities being ethane and propylene. The gas was

(1) This work was made possible by the support of the Advanced Research Projects Agency (Order No. 247-61), through the United States Army Engineer Research and Development Laboratories, Fort Belvoir, Virginia, under Contract No. DA-44-009-ENG-4853.
(2) D. W. McKee, *J. Phys. Chem.*, **67**, 841 (1963).
(3) For a review of the recent literature see, *e.g.*, G. C. Bond, "Catalysis by Metals," Academic Press, New York, N. Y., 1962, pp. 270–276.

condensed and fractionally distilled from a trap cooled in liquid nitrogen before being admitted to the apparatus.

Pure hydrogen was obtained by diffusion through a heated palladium thimble.

Apparatus and Procedure.—The volumetric apparatus and experimental techniques were similar to those used previously.[2] Gold foil traps were used to protect the catalyst surface from mercury vapor as it has recently been shown[4] that the hydrogenolysis of cyclopropane can be poisoned by chemisorbed mercury on metal surfaces. The gaseous products of cyclopropane dissociation and hydrogenolysis were studied as a function of time, temperature, and the partial pressures of the reactants. Analyses of the products and reactants were carried out in a temperature-programmed gas chromatograph, using an 8-ft. silica gel column and helium as carrier gas. In order to remove the carbonaceous residue remaining on the metal after reaction, the sample was reduced in flowing hydrogen at 150° or above for at least 2 hr. after each run and then evacuated at the same temperature for a further 2 hr. By this procedure the original activity of the sintered platinum black could be completely restored.

Results

Demethanation of Cyclopropane above 150°.—The gaseous products of the catalytic dissociation of cyclopropane on platinum black between 100 and 250° were found to be methane, propane, and small amounts of ethane. In addition, a carbonaceous residue of approximate composition $CH_{1.1}$ remained on the surface, as in the case of propane and ethylene decomposition.[2,5] This residue could only be removed by prolonged reduction with hydrogen at elevated temperatures as described above. No hydrogen, propylene, or higher molecular weight products were found in the gaseous products.

As in the previous investigation, the specific activity of the platinum black depended to a large extent on the amount of sintering which had taken place. Figure 1 shows the specific rate of methane formation from cyclopropane (molecules $sec.^{-1}$ $cm.^{-2}$) plotted as a function of B.E.T. surface area (determined from nitrogen adsorption at −195°). Each point in this diagram represents a separate determination, the catalyst being re-reduced and evacuated after each measurement, the surface area being measured between each demethanation run. The rapid decrease in specific activity with surface area, indicated in Fig. 1, is consistent with the idea that the sintering process involves a decrease in the density of active sites on the metal surface.

Immediately when the gaseous hydrocarbon was brought into contact with the metal catalyst a rapid chemisorption of the cyclopropane took place which resulted in an initial decrease in pressure. Subsequent liberation of methane and other products caused the pressure to rise again after falling to a minimum value and the rate of pressure increase was generally linear for an extended period until the carbonaceous residue began to poison an appreciable fraction of the metal surface and other by-products began to accumulate in the gas phase. Typical pressure *vs.* time curves are shown in Fig. 2 for a variety of temperatures and catalyst areas. As the rate of propane formation by hydrogenolysis was usually considerably less than that of methane formation (demethanation), the linear curves shown in Fig. 2 suggest that the rate of methane production was approximately zero order with respect to the cyclopropane partial pressure. At temperatures of 150° and below a greater

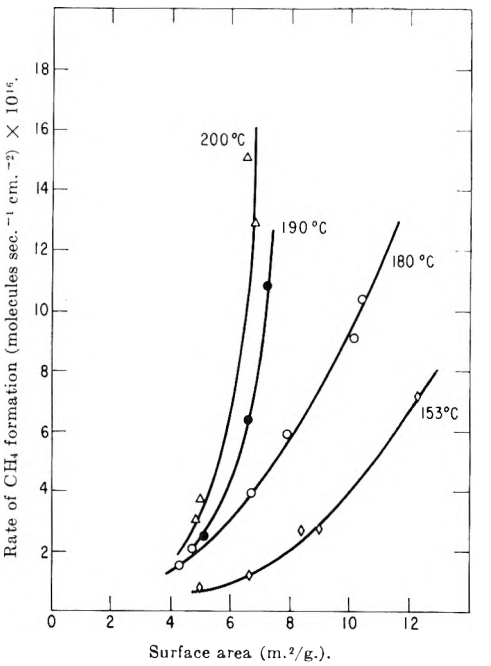

Fig. 1.—Specific rate of methane formation (molecules $sec.^{-1}$ $cm.^{-2}$) as a function of B.E.T. surface area of Pt black: $P^0_{C_3H_6} \approx$ 14 mm.; 1 hr. contact time.

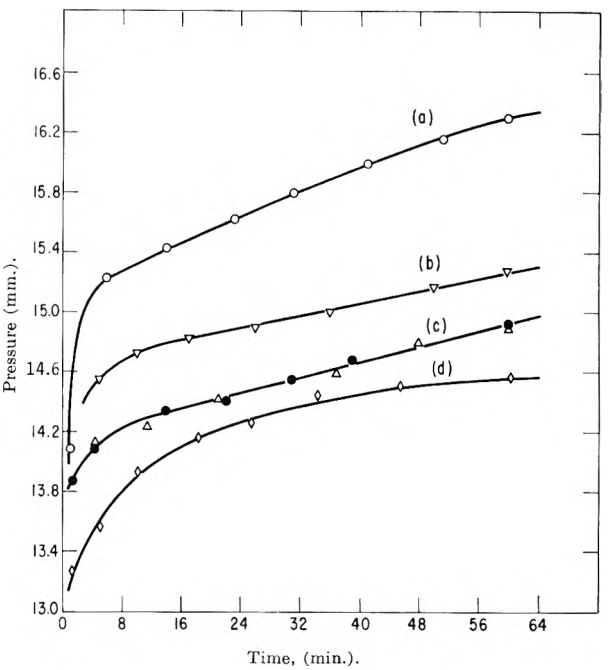

Fig. 2.—Decomposition of cyclo-C_3H_6 on Pt black: Pressure (mm.) *vs.* time (min.); $P^0_{C_3H_6} \approx$ 14 mm.: (a) 10.4 $m.^2/g.$, 180°; (b) 7.4 $m.^2/g.$, 180°; (c) 6.5 $m.^2/g.$, 200°; (d) 12.3 $m.^2/g.$, 153°.

proportion of propane was found in the products and this may account for the slight curvature shown by the 153° curve in Fig. 2.

The rate of methane formation on the sintered platinum black was measured by direct analysis of the gas phase at a number of different temperatures between 150 and 250° but with constant initial cyclopropane pressure $P^0_{C_3H_6}$. The results are shown in Fig. 3 in the form of an Arrhenius plot. This gave an apparent activation energy for the demethanation reaction of 14 ± 1 kcal./mole and a frequency factor A (in molecules $sec.^{-1}$ $cm.^{-2}$) given by $\log A = 17.0 \pm 0.3$.

Hydrogenolysis with Simultaneous Demethanation.—In order to study the effect of hydrogen concentration

(4) K. C. Campbell and S. J. Thomson, *Trans. Faraday Soc.*, **55**, 985 (1959).

(5) D. W. McKee, *J. Am. Chem. Soc.*, **84**, 1109 (1962).

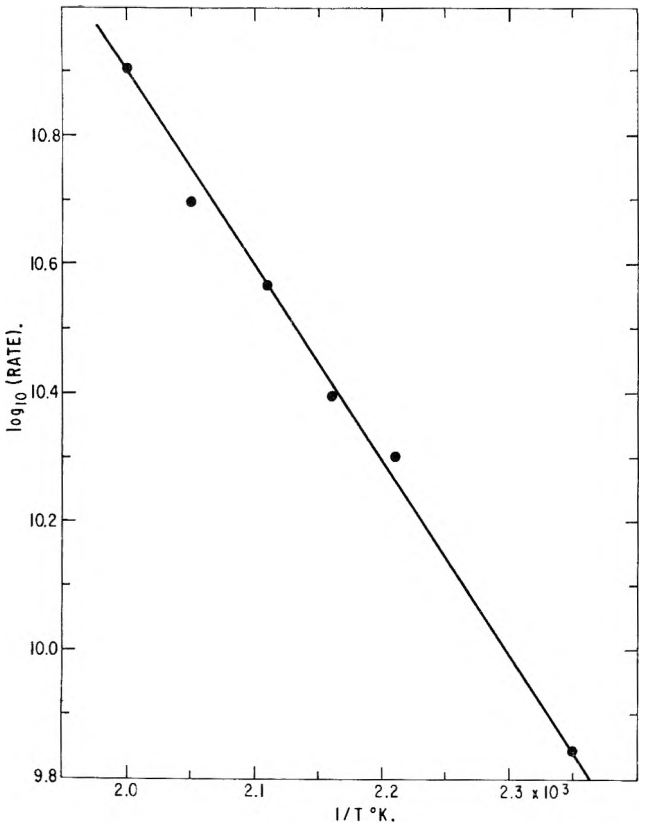

Fig. 3.—Rate of demethanation of cyclopropane: log [rate CH_4 formation (molecules sec.$^{-1}$ cm.$^{-2}$)] *vs.* $1/T$ (°K). $P^0_{C_3H_6} \approx$ 14 mm.; area of Pt = 5 m.²/g.

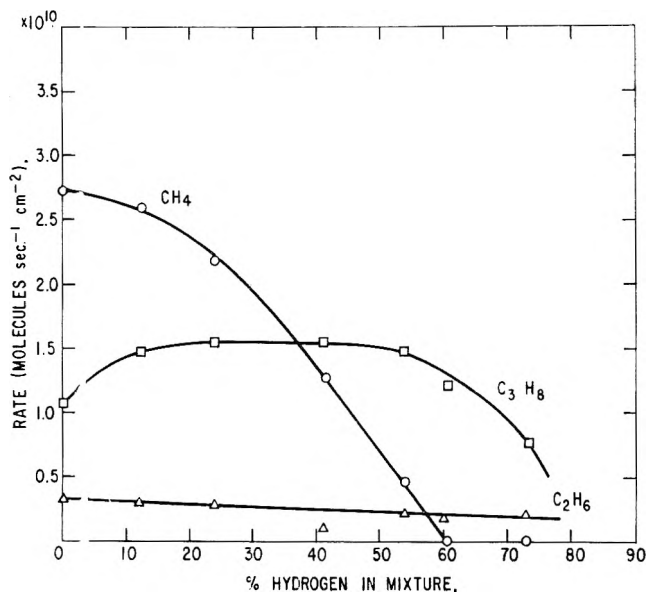

Fig. 4.—Products of reaction of C_3H_6–H_2 mixtures on sintered Pt black. Rate (molecules sec.$^{-1}$ cm.$^{-2}$) *vs.* % H_2 in mixture. Temp. = 180°; $P^0_{C_3H_6}$ = 17.7 mm.; surface area of Pt = 6 m.²/g.; 1 hr. contact time.

on the rates of the hydrogenolysis and demethanation reactions, the composition of the gas products was determined as a function of hydrogen content in the initial gas mixture. The results are shown in Fig. 4 for a series of hydrogen–cyclopropane mixtures of constant cyclopropane partial pressure. In this diagram, the composition of the gaseous products after 1 hr. contact at 180° are plotted against per cent hydrogen in the mixture. It is apparent that the rate of methane formation decreases with increasing hydrogen

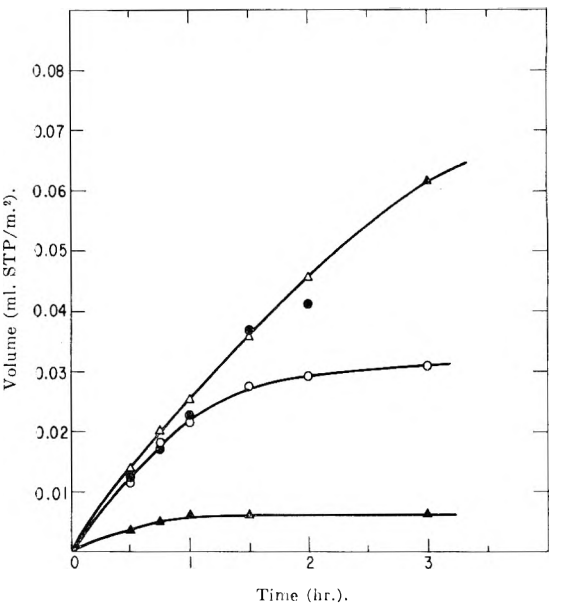

Fig. 5.—Rates of CH_4 and C_3H_8 formation at 180° on sintered Pt black. Surface area of Pt = 6 m.²/g. Volume of products (ml. STP/m.²) *vs.* time; $P^0_{C_3H_6}$ = 5.5 mm. 0% H_2: ○, C_3H_8, ●, CH_4; 55% H_2: △, C_3H_8, ▲, CH_4.

content, whereas the concentration of propane in the products remains constant between 10 and 60% hydrogen, although some decrease in the rate of hydrogenolysis appears to occur with mixtures containing higher concentrations of hydrogen. The amount of ethane produced remains small but decreases slightly with hydrogen content.

Additional data on the rates of methane and propane formation at 180° are shown in Fig. 5 for pure cyclopropane and for a mixture containing 55% hydrogen. The initial rate of propane formation is only slightly less from pure cyclopropane than when hydrogen is present, although the concentration of surface hydrogen is apparently insufficient to maintain the high initial rate in the former case.

Analysis of these data suggests that the rate of the demethanation reaction in the presence of hydrogen follows the relation

$$\text{rate} = kP^0_{C_3H_6}P_{H_2}{}^{-n}$$

where n lies between 0.5 and 1.8.

The hydrogenolysis reaction was approximately zero order in both reactants at low hydrogen concentrations, although the data were not precise enough to distinguish between zero and small negative orders. At high hydrogen concentrations, the rate of hydrogenolysis followed a relation of the type

$$\text{rate} = k'P^0_{C_3H_6}P_{H_2}{}^{-m}$$

where m was approximately 0.8.

It is also probable that the presence of high concentrations of chemisorbed propane on the metal surface may inhibit the demethanation of cyclopropane. Thus experiments carried out with pure cyclopropane on partially sintered platinum black indicated that the rate of methane formation varied inversely with the amount of propane formed, although the rate of the demethanation reaction was initially greater than that of hydrogenolysis. Typical results are shown in Table I for several different samples of platinum black.

TABLE I

SIMULTANEOUS DEMETHANATION AND HYDROGENOLYSIS ON Pt BLACK

Temp., °C.	Surf. area, m.²/g.	$P^0_{C_3H_6}$, mm.	Contact time, hr.	Products, ml. STP CH_4	Products, ml. STP C_3H_8
180	7.9	13.5	1	0.48	0.01
180	7.0	4.4	1.5	.41	.005
180	6.5	4.3	1.5	.22	.122
180	6.5	4.1	1.5	.18	.135
180	6.5	4.2	2	.13	.18

The composition of the residue remaining on the metal surface was calculated in the form $(CH_n)_x$ where n was given by the expression

$$n = \frac{2[3\Delta n_{C_3H_6} - (2n_{CH_4} + 3n_{C_2H_6} + 4n_{C_3H_8})]}{3\Delta n_{C_3H_6} - (n_{CH_4} + 2n_{C_2H_6} + n_{C_3H_8})}$$

where $\Delta n_{C_3H_6}$ is the decrease in the number of moles of cyclopropane during the reaction and the other symbols refer to the molar quantities of the other components in the gas product. The value of n was found to vary between 0.7 and 1.2 with 1.1 being the most common value. The residue from cyclopropane thus contained less hydrogen than that from propane for which n = 1.6.[2]

Chemisorption of Cyclopropane and Hydrogen on Platinum Black at Low Temperatures.—Some measurements were made of the extent of chemisorption of cyclopropane and hydrogen, both separately and from 50:50 mixtures, at temperatures too low for decomposition of cyclopropane to be observed. Typical results are shown in Table II for sintered platinum black. At temperatures below 100°, the amounts of the individual gases chemisorbed were about the same as when adsorption took place from a 50:50 mixture. Although the chemisorption of hydrogen remained fairly constant and considerably larger than that of cyclopropane, the latter increased with temperature until the point when reaction products were observed in the gas. It is interesting that at low temperatures the rate of hydrogenolysis was larger than that of demethanation. The apparent activation energy for the former reaction at low hydrogen concentration was approximately 8.0 ± 1 kcal./mole, which may be compared with the value of 8.4 kcal./mole obtained by Bond and Newham[6] for platinum–pumice over the same temperature range.

TABLE II

ADSORPTION OF CYCLOPROPANE AND HYDROGEN ON SINTERED PLATINUM BLACK

Surface area = 6 m.²/g.; wt. of metal = 0.77 g.

Temp., °C.	Vol. ads. separately, ml. STP H_2	Vol. ads. separately, ml. STP C_3H_6	Products from C_3H_6 decomp. CH_4	Products from C_3H_6 decomp. C_3H_8	Vol. ads. from mixt., ml. STP H_2	Vol. ads. from mixt., ml. STP C_3H_6	Products from mixt., ml. STP CH_4	Products from mixt., ml. STP C_3H_8
0	0.35	0.095						
27.5	.32	.067			0.28	0.07		
76	.25	.089			.28	.062		0.02
100	.28	.098	..	0.035	.20	.11		.03
124	.26	.17	0.01	.06	.26	.11	..	.047
150	.29	.26	0.04	.11	.36	.15	0.01	.10

Discussion

As in the case of propane cracking,[2] the specific activity of the metal for the demethanation of cyclopropane was found to be a strong function of the degree of sintering which had taken place. This finding is in agreement with the previous conclusion that the sintering process involves a decrease in both surface area and density of active sites which are responsible for the catalytic behavior. The rate of demethanation of cyclopropane above 150° was found to be greater than that of propane under the same conditions. Typical values are shown in Table III. The greater ease of C–C bond fission in cyclopropane is undoubtedly associated with the strain energy of the ring, which has been calculated to be about 30 kcal.[7]

TABLE III

COMPARISON OF THE RATES OF CRACKING OF PROPANE AND CYCLOPROPANE ON PLATINUM BLACK

Surf. area of Pt, m.²/g.	Temp., °C.	—Rate of cracking, molecules sec.$^{-1}$ cm.$^{-2}$— C_3H_8	Cyclo-C_3H_6
10	150	1.5×10^{10}	4.2×10^{10}
10	180	4.8×10^{10}	9.7×10^{10}
6	200	5.7×10^{10}	9.0×10^{10}

The observed kinetics for the hydrogenolysis reaction are of similar form to those recorded before for platinum–pumice[8] and for nickel–silica–alumina[9] and in general show only slight pressure dependence for both reactants. Minor changes in the order of reaction for the two components seem to occur over different temperature ranges and for different catalysts, but the rate is generally of negative order in hydrogen at high concentrations of the latter. Although these earlier results ignore the occurrence of the demethanation reaction, which must certainly complicate the mechanism, the observed kinetics and those of the present work can be explained qualitatively on the basis of a Langmuir–Hinschelwood scheme in which both reactants are strongly adsorbed. Assuming that the rate-determining step involves the addition of chemisorbed hydrogen to adsorbed cyclopropane, then the rate of hydrogenolysis

$$v = k \frac{b_c P_{C_3H_6} \sqrt{b_H P_H}}{(1 + b_c P_{C_3H_6} + \sqrt{b_H P_H})^2}$$

If the adsorption of hydrogen is so strong that $b_H P_H >> 1$, then $v \approx P_{C_3H_6} P_H^{-1}$, but when cyclopropane is also strongly adsorbed, the rate will be essentially independent of $P_{C_3H_6}$. The simultaneous occurrence of demethanation and the accumulation of the products of both reactions on the surface may, however, completely invalidate such a mechanism.

Even when cyclopropane is present alone, the simultaneous appearance of methane and propane in the gas phase suggests that hydrogen is present on the surface. Some feasible modes of cyclopropane chemisorption and dissociation are shown in Table IV although there are many other possibilities.

Reaction 1 may always occur to some extent and probably accounts for the occurrence of some hydrogenolysis even in the absence of hydrogen in the initial mixture. Also the exchange of cyclopropane and deuterium over evaporated metal films[10] and on platinum–pumice[11] produced some deuteriocyclopropanes as a result of this reaction. However the low yields of cyclopropane ex-

(6) G. C. Bond and J. Newham, *Trans. Faraday Soc.*, **56**, 1501 (1960).

(7) J. E. Kilpatrick and R. Spitzer, *J. Chem. Phys.*, **14**, 463 (1946).

(8) G. C. Bond and J. Addy, *Trans. Faraday Soc.*, **53**, 388 (1957).

(9) J. E. Benson and T. Kwan, *J. Phys. Chem.*, **60**, 1601 (1956).

(10) J. R. Anderson and C. Kemball, *Proc. Roy. Soc.* (London), **A226**, 472 (1954).

(11) G. C. Bond and J. Turkevich, *Trans. Faraday Soc.*, **50**, 1335 (1954).

TABLE IV
CHEMISORPTION, HYDROGENOLYSIS, AND DEMETHANATION OF CYCLOPROPANE

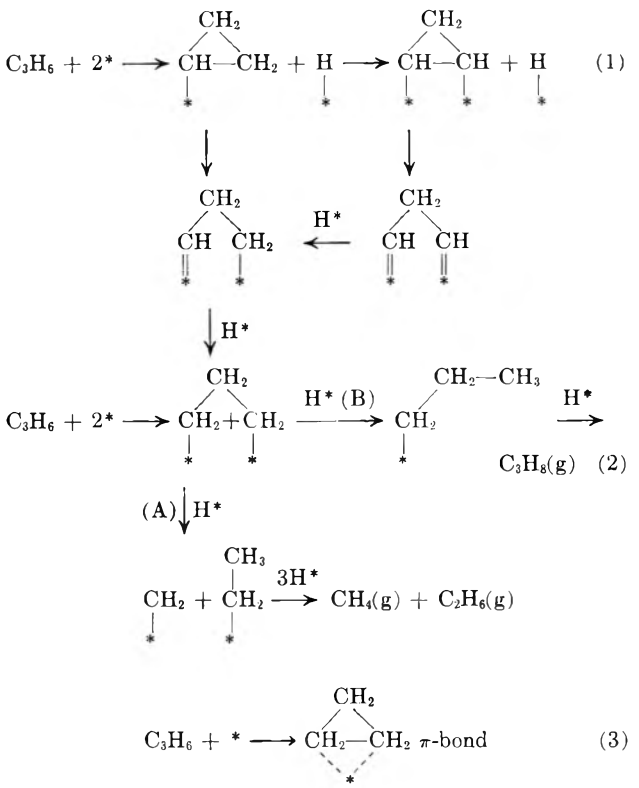

change products and the kinetics of the hydrogenolysis reaction suggest that reaction 1 is not the most important step.

Reaction 2 involving ring opening would be expected to occur more readily than with propane. However, if this were the rate-controlling step, either the demethanation or the hydrogenolysis reaction would be first order in cyclopropane which is not found experimentally. An alternative mode of chemisorption of cyclopropane (3), suggested by Bond and Newham,[6] involves π-bond formation between the delocalized electrons of the ring and unfilled d orbitals of the metal. This relatively weak chemisorption may be an intermediate in the subsequent fission of the ring by reaction 2, which Bond suggests as the rate-determining step in the hydrogenolysis. The formation of this weakly bonded intermediate may account for the initial adsorption which was found to precede reaction in the present work.

The formation of a 1,3-diadsorbed radical on the metal surface can also take place starting from reaction 1 by means of several unsaturated intermediates, as recently suggested by Newham and Burwell.[12] Once formed, the adsorbed radical can react with chemisorbed hydrogen by reaction (A) involving a further C–C bond fission and subsequent formation of methane and ethane. The fact that the ethane concentration in the products is much less than that of methane suggests that simultaneous cracking of ethane also occurs to some extent. A similar result was observed in the products of cracking of propane on nickel.[13] The alternative reaction (B) can give rise to a 1-adsorbed propyl radical and hence propane. As the concentration of hydrogen in the system increases, reaction (A) is suppressed more rapidly than reaction (B). However, the displacement of cyclopropane from the surface by the more strongly adsorbed hydrogen would be expected to inhibit both reactions by decreasing the surface concentration of the 1,3-diadsorbed radical. It is possible that hydrogenolysis also takes place simultaneously to some extent by means of a Rideal–Eley mechanism involving chemisorbed hydrogen and gas phase or physically adsorbed cyclopropane. Such a process has been postulated for the exchange of cyclopropane and deuterium on supported platinum[11] and for the self-hydrogenation of ethylene on nickel at low temperatures.[5] The build-up of carbonaceous residues represents the accumulation of the more strongly bonded intermediates and radicals which do not readily react with chemisorbed hydrogen except at high temperatures.

In spite of the obvious complexity of this system several authors have proposed that the fission of the cyclopropane ring may be rate-controlling. However, too little attention has apparently been given to the possibility that the desorption of the final product, in this case propane or methane, may control the kinetics to a large extent. No information, however, is available on this subject although the heat of chemisorption, and hence the activation energy for desorption, of propane on a clean platinum surface might be expected to be quite high.

Acknowledgments.—The author wishes to thank E. J. Cairns and W. T. Grubb for many helpful discussions during the course of this investigation.

(12) J. Newham and R. L. Burwell, Jr., *J. Phys. Chem.*, **66**, 1431 (1962).
(13) D. W. McKee, *J. Am. Chem. Soc.*, **84**, 4427 (1962).

THE EFFECT OF LIGHT INTENSITY AT 313 mμ ON THE PHOTOCHEMICAL DISAPPEARANCE OF BENZOPHENONE IN ISOPROPYL ALCOHOL

BY A. C. TESTA

Lever Brothers Company, Research Center, Edgewater, N. J.

Received January 26, 1963

Results obtained indicate that the quantum yield for the photochemical disappearance of benzophenone in isopropyl alcohol at 313 mμ is intensity dependent. This effect is attributed to two competing processes. At high light intensities, the quantum yield approaches one, which arises from a predominance of the direct coupling of the ketyl radicals, $(C_6H_5)_2\dot{C}OH$, formed by hydrogen abstraction from isopropyl alcohol by an excited benzophenone molecule. As the intensity is lowered, the contribution of an additional reaction path becomes significant, namely, one in which two hydrogen atoms are abstracted from each isopropyl alcohol molecule and two benzophenone molecules react for each quantum of absorbed light. This latter scheme corresponds to $\Phi = 2$ for benzophenone disappearance. As a result of these competing reactions, the quantum yield for benzophenone disappearance has one as its lower limit and a maximum value close to two. In the experiments described, the quantum yield varied between 1.12 and 1.62, while the intensity was changed by a factor of one hundred. A plot of the reciprocal square root of light intensity *vs.* quantum yield was linear and a least squares calculation of the slope yielded a value of $2.43 \pm 0.25 \times 10^6$ molecules-quanta$^{-1/2}$-sec.$^{-1/2}$. The linearity of the plot is indicative of the predominance of radical recombination reactions.

Introduction

The mechanism of the photochemical disappearance of benzophenone in isopropyl alcohol has been an active problem in the photochemical literature.[1-5] There appears to be some disagreement as to whether the quantum yield for benzophenone disappearance should be one or two in degassed solutions.

In the results reported by Pitts, *et al.*,[1] the quantum yield at 366 mμ for benzopinacol formation in a 0.5 *M* benzophenone solution in isopropyl alcohol is 0.93, which corresponds to $\Phi = 1.86$ for benzophenone disappearance.

In the experiments of Hammond, *et al.*,[4] the quantum yield for benzophenone disappearance was equal to one. The intensity in these experiments was 4.66×10^{17} quanta/sec., in contrast to the value of 1.16×10^{15} quanta/sec. in Pitts' experiments.

Preliminary experiments at 313 mμ for a 1.32×10^{-2} *M* solution of benzophenone in isopropyl alcohol were performed by the author,[6] and quantum yields in nitrogen flushed solutions were found to be in agreement with results reported by Pitts, *et al.*[1] In these experiments it was also observed that in air-saturated solutions the quantum yield for benzophenone disappearance was 0.31 with a standard deviation of 0.03 for nine determinations. It is noteworthy that changing the fractional disappearance of benzophenone from 4 to 67% caused no significant change in the quantum yield, which would make the system suitable as an actinometer.

Results obtained in degassed solutions indicated a tendency for quantum yields to be greater than one; however, data were insufficient to establish this with certainty. The aim of the present study was to determine if the quantum yield for benzophenone disappearance can be greater than one by investigating the intensity dependence of the quantum yield.

Experimental

Materials.—The benzophenone (Matheson, Coleman and Bell) used in this work was recrystallized from absolute ethanol and from hexane.[1] Spectrograde isopropyl alcohol was used as the solvent, and the concentration of benzophenone used in these experiments was 1.32×10^{-2} *M*.

Apparatus.—The 313-mμ mercury line from a BH-6 mercury arc was isolated with a Farrand UV monochromator. The entrance and exit slits of the monochromator were set at 2.0 and 0.75 mm., respectively. Photolyses were performed in 1 cm. fused silica cells with a ground glass joint fused on top to accommodate a stopcock attachment. Each sample was degassed three or more times on a vacuum line with alternate cycles of freezing and vacuum boiling. Experiments were performed at $24.5 \pm 0.5°$.

Filters and Actinometry.—Intensity determinations were made using the potassium ferrioxalate actinometer described by Hatchard and Parker,[7] and the sensitive uranyl oxalate actinometer described by Pitts, *et al.*[8]

The light intensity was changed over a range of one hundred and corresponded to intensities from 3.30×10^{15} to 3.40×10^{13} quanta/sec. Intensity determinations were made before and after each photolysis run, and the constancy was estimated to be approximately 2%.

Analysis of Residual Benzophenone.—The benzophenone disappearance was measured by the method described by Pitts, *et al.*,[1] namely, by following the optical density changes at 335 mμ. The fractional change in benzophenone was kept below 10% in order to minimize interference, if any, from an absorbing intermediate formed during the photochemical exposure. A Beckman DU spectrophotometer was used for absorbance measurements.

Results

To eliminate the possibility of erroneous intensity measurements, it was found convenient to use two independent actinometers, which are sensitive over different ranges and have different quantum yields. A comparison of intensities determined at 254 and 313 mμ with the uranyl oxalate and potassium ferrioxalate actinometers indicated a maximum difference of approximately 4%.

Twenty-seven determinations were made of the quantum yield for the disappearance of benzophenone. Results indicated no significant variation of this quantity when the fractional change of benzophenone varied from 2.1 to 8.3%. It was further observed that the quantum yield increased as the intensity was lowered.

(1) J. N. Pitts, Jr., R. L. Letsinger, R. P. Taylor, J. M. Patterson, G. Recktenwald, and R. B. Martin, *J. Am. Chem. Soc.*, **81**, 1068 (1959).

(2) G. O. Schenck, W. Mader, and M. Pape, *Proc. of the Intern. Conf. Peaceful Uses At. Energy*, **29**, 352 (1958).

(3) V. Franzen, *Ann. Chem.*, **633**, 1 (1960).

(4) W. M. Moore, G. S. Hammond, and R. P. Foss, *J. Am. Chem. Soc.*, **83**, 2789 (1961).

(5) G. Porter and F. Wilkinson, *Trans. Faraday Soc.*, **57**, 1686 (1961).

(6) A. C. Testa, unpublished work.

(7) C. G. Hatchard and C. A. Parker, *Proc. Roy. Soc.* (London), **A235**, 518 (1956).

(8) J. N. Pitts, Jr., J. D. Margerum, R. P. Taylor, and W. Brim, *J. Am. Chem. Soc.*, **77**, 5499 (1955).

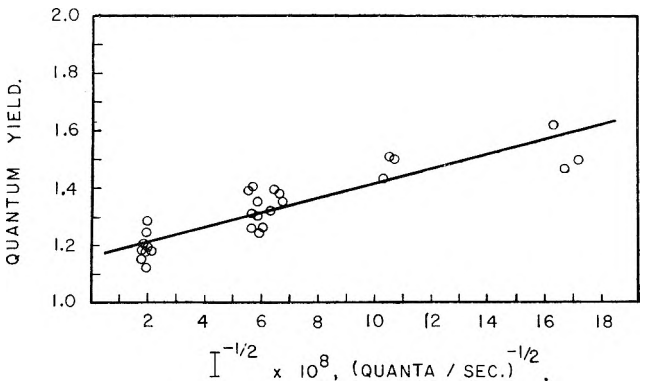

Fig. 1.—Variation of the quantum yield with the reciprocal square root of light intensity for the photochemical disappearance of benzophenone in isopropyl alcohol at 313 mμ (1.32×10^{-2} *M* benzophenone). Intensity range: 3.30×10^{15} to 3.40×10^{13} quanta/sec. Least squares calculation of slope: $2.43 \pm 0.25 \times 10^6$ molecules-quanta$^{-1/2}$-sec.$^{-1/2}$.

Reference to Fig. 1 indicates that a plot of the reciprocal square root of the light intensity *vs.* quantum yield was linear and a least squares calculation yielded a slope of $2.43 \pm 0.25 \times 10^6$ molecules-quanta$^{-1/2}$-sec.$^{-1/2}$.

Since the uncertainty in the quantum yield determinations is estimated to be approximately 10%, the dependence of the quantum yield on the reciprocal square root of the light intensity is probably real. If the quantum yield is inversely proportional to the square root of the light intensity, a recombination process second order with respect to the atoms or radicals concerned predominates in the mechanism by which the radicals disappear.[9]

In view of the results of Hammond, *et al.*,[4] and those reported in the present study, it is expected that above a limiting light intensity the quantum yield should be one. Similarly, as the intensity is lowered, the quantum yield approaches a value close to two.

Discussion

Since the results described above show an inverse square root dependence of the light intensity with the quantum yield an explanation was desired to account for this behavior. In addition, it seemed possible to eliminate certain schemes in the literature which have been proposed to explain the quantum yields for benzophenone disappearance.

For the case when the light intensity is sufficiently high, the dimerization of ketyl radicals, $(C_6H_5)_2\dot{C}OH$, predominates, and the quantum yield for benzophenone disappearance is unity. Under these experimental conditions, the destruction of the dimethylcarbinol radical, $CH_3\dot{C}OHCH_3$, occurs predominantly by dimerization to form the following pinacol, $(CH_3)_2C(OH)$-$(OH)C(CH_3)_2$. This reaction has been observed in the photolysis of an acetone–isopropyl alcohol mixture and in the photolysis of azodicarboxylic esters in isopropyl alcohol.[2,10] Some crossed product between the dimethylcarbinol and ketyl radicals also occurs according to the data reported by Hammond, *et al.*[4] In their work, the ratio of (Δ benzopinacol/$-\Delta$ benzophenone) was 0.39 instead of the expected value of 0.5.

Under the conditions of low intensity the formation of benzopinacol by one or more alternate paths must play a significant part in the over-all disappearance of benzophenone. On the basis of recent work by Schenck, *et al.*,[2] and Franzen[3] it seems reasonable to consider the formation of a hemiacetal radical as an intermediate in the over-all disappearance of benzophenone

$$(C_6H_5)_2CO + CH_3\dot{C}OHCH_3 \longrightarrow$$

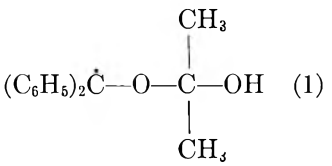

(1)

hemiacetal radical

Further evidence regarding this intermediate species was noted in a recent publication by Pitts, *et al.*[11] The hemiacetal radical couples with the ketyl radical formed from hydrogen abstraction from isopropyl alcohol.

$$(C_6H_5)_2\dot{C}OH + (C_6H_5)_2\dot{C}O—C(CH_3)_2OH \longrightarrow$$

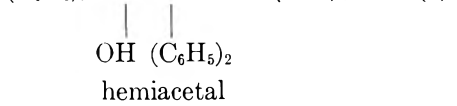

(2)

hemiacetal

and finally a hemiacetal cleavage results in a molecule of benzopinacol and one of acetone

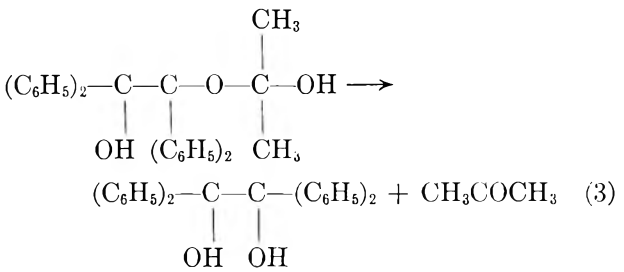

(3)

It seems, therefore, that there are two concomitant modes for the disappearance of benzophenone, *i.e.*, (a) dimerization of ketyl radicals, $(C_6H_5)_2\dot{C}OH$, and (b) reaction *via* eq. 1–3.

According to the proposed reaction scheme, the quantum yield for benzophenone disappearance varies between one and two depending on the relative importance of each of the two possible modes of benzophenone disappearance. Since the formation of benzopinacol presumedly occurs from radical coupling of $(C_6H_5)_2\dot{C}OH$ with itself and with the hemiacetal radical formed in eq. 1, it is not unexpected that the reciprocal square root dependence of light intensity should be maintained.

Although the reaction scheme proposed is qualitatively consistent with quantum yield determinations, this is not the only possible mechanism to account for the experimental results. Indeed, Schenck and coworkers[2] have postulated that intermediates I and II participate in the over-all disappearance of benzophenone.

In view of the quantum yields greater than one obtained in the present study, species II is not favored, since by this scheme two quanta are consumed, one

(9) W. A. Noyes, Jr., and P. A. Leighton, "The Photochemistry of Gases," Reinhold Publ. Corp., New York, N. Y., 1941, p. 197.

(10) G. O. Schenck and H. Formanek, *Angew. Chem.*, **70**, 505 (1958).

(11) J. N. Pitts, Jr., T. Kuwana, and A. Marchetti, Fifth Intl. Symp. Free Radicals held at Uppsala, Sweden, July, 1961, preprint no. 51.

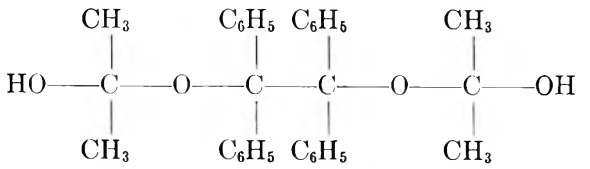

I

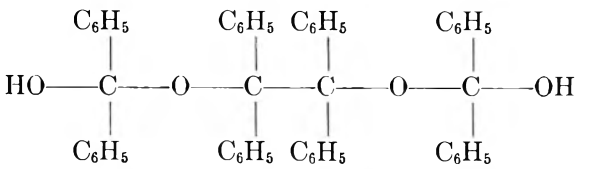

II

molecule of benzopinacol is produced, and two benzophenone molecules are released by hemiacetal cleavage—this would correspond to a quantum yield of one for benzophenone disappearance. The existence of species I is reasonable, since by this scheme, two ketyl radicals dimerize and hemiacetal cleavage of species I leads to another molecule of benzopinacol, thereby resulting in a quantum yield of two for benzophenone disappearance or unity for the formation of benzopinacol.

Conclusion

The quantum yield for the photochemical disappearance of benzophenone in isopropyl alcohol at 313 mμ has been shown to be dependent on the inverse square root of the light intensity. This relationship indicates the importance of recombination processes, second order with respect to the radicals concerned. Results obtained indicate that the quantum yield can exceed one and approach a value close to two as the light intensity is lowered. A reaction scheme is proposed which is consistent with experimental results and attributes the variation in quantum yield to two competing processes. A hemiacetal radical, $(C_6H_5)_2\dot{C}OC(CH_3)_2OH$, is presumed to contribute more to the over-all disappearance of benzophenone as the intensity is lowered.

At high light intensities, the quantum yield of unity is attributed to the direct coupling of ketyl radicals.

At low light intensities, the quantum yield is larger than one and is attributed to the disappearance of benzophenone by two concomitant processes; (1) dimerization of ketyl radicals and (2) hemiacetal cleavage of $(C_6H_5)_2C(OH)C(C_6H_5)_2C(CH_3)_2OH$.

ELECTROSTRICTION IN POLAR SOLVENTS. I[1]

BY DEBBIE FU-TAI TUAN[2] AND RAYMOND M. FUOSS

Contribution No. 1727 from the Sterling Chemistry Laboratory of Yale University, New Haven, Connecticut

Received January 28, 1963

Viscosities and densities of a series of quaternary salts have been measured in acetonitrile and several other solvents; some electro-neutral solutes were also investigated. Up to about 0.2 mole/l., viscosities satisfy the equation $\eta/\eta_0 = 1 + Ac^{1/2} + Bc$ and the densities are given by $\rho/\rho_0 = 1 + (Mc/1000)(v_0 - v_s)$ where v_s is the specific volume of the solute in solution and the other symbols have their usual meanings. Assuming the Einstein viscosity mechanism (spheres in a continuum), $B = Mv_s/400$. It was found that B and $V = 10^{-3}Mv_s$ are additive in contributions from the constituent ions. For large ions (*e.g.*, Bu_4N^+, Ph_4B^-), the radii calculated from B and V agree, confirming the theory and model. But, for small ions, the B-values are larger than the values computed from V, and the more so, the smaller the ion. Neutral molecules, on the other hand, give smaller B's than expected from the V's. Electrostriction in the first case and slipping in the second are proposed as explanations. This suggestion is confirmed by the behavior of dipolar solutes.

The properties of aqueous solutions of inorganic electrolytes are in general highly specific to the individual ions, and generalizations are difficult to find. The B-coefficients in the viscosity equation (concentration, moles/l.)

$$\eta/\eta_0 = 1 + Ac^{1/2} + Bc \qquad (1)$$

are, however, approximately additive[3-5] in contributions from the two ions of a given salt for aqueous systems. Very few data are available for non-aqueous systems, where, by and large, the situation should be simpler because complications due to water structure are excluded. In particular, one would hope to find good additivity and a good correlation between structure and the value of B, because in the case of the idealized model of spheres in a continuum B should be given by the Einstein relation

$$B = 5\phi/2c$$
$$= (N\pi/300)(R_+^3 + R_-^3) \qquad (2)$$

where ϕ is volume fraction of solute, N is Avogadro's number and R_+ and R_- are, respectively, the radii of the spheres representing cation and anion. (We are neglecting the contribution to B from higher electrostatic terms arising from the same source as the $Ac^{1/2}$ term.)

Furthermore, we expect a correlation between viscosity and density data for non-aqueous systems, which is masked in water by the marked effect of ions on the structure of water. Suppose we take x g. of solute of molecular weight M and $(1 - x)$ g. of solvent of specific volume v_0 (density $\rho_0 = 1/v_0$) to make one gram of solution at concentration c moles/l. with specific volume $v = 1/\rho$. Clearly

$$x = Mc/1000\rho \qquad (3)$$

(1) This paper is based on a thesis presented by Debbie Fu-Fai Tuan to the Graduate School of Yale University in partial fulfillment of the requirements for the Degree of Doctor of Philosophy, June, 1961.

(2) Heyl Research Fellowship, 1960–1961.

(3) W. M. Cox and J. H. Wolfenden, *Proc. Roy. Soc.* (London), **A145**, 475 (1934).

(4) H. S. Harned and B. B. Owen, "The Physical Chemistry of Electrolytic Solutions," Third Edition, Reinhold Publ. Corp., New York, N. Y., 1958, pp. 236–242.

(5) R. W. Gurney, "Ionic Processes in Solution," McGraw-Hill Book Company, Inc., New York, N. Y., 1953, Chapter 9.

Let us assume that the solute has a specific volume v_s *in solution* and that v_s is independent of concentration. Then

$$v = (1 - x)v_0 + xv_s \quad (4)$$

whence

$$\rho/\rho_0 = 1 + (Mc/1000)(v_0 - v_s) \quad (5)$$

Again representing the ions by spheres, we have

$$v_s = (4\pi N/3M)(R_+^3 + R_-^3) \quad (6)$$

Elimination of the radii between (6) and (2) then gives

$$B = Mv_s/400 = 2.5V \quad (7)$$

The purpose of this paper is to present viscosity and density data for a variety of electrolytes (and several related non-electrolytes) in acetonitrile (and for a few compounds, in several other solvents). Good additivity is found for both B and Mv_s, and eq. 7 is satisfied in the limiting case of large ions such as those of the quaternary tetraphenylborides. Furthermore, the values of radii calculated from (2) and (6) are quite reasonable in magnitude and agree fairly well with each other and with ionic radii derived from conductance data.

Experimental

Materials.—Acetonitrile (Matheson 2726) was refluxed overnight with Drierite and fractionated; b.p. 80.0–80.8°. Fisher A412 certified methanol or Mallinckrodt 3016 analytical reagent methanol was used as received. **Nitromethane** (Matheson 124) was refluxed overnight with Drierite and fractionated; b.p. 100.5–101.5°. **Methyl ethyl ketone** (Matheson 2609) was refluxed over activated alumina for 24 hr. and distilled; b.p. 78.5–79.5°; another lot was refluxed for 4 hr. over a mixture of potassium hydroxide and permanganate; b.p. 78.3–79.0°. The second batch gave about 0.2% lower viscosity. Fisher carbon tetrachloride (certified reagent C187) was used as received. The above were used as solvents, and also to calibrate the viscometers. Additional calibrating liquids were water, Fisher certified reagent benzene and toluene, dioxane[6] and ethylene chloride (b.p., 83.7°; central cut from a Todd still), and Cannon Instrument Company *n*-hexane, *n*-decane, and methylcyclohexane.

Tetra-*n*-butylammonium bromide (Eastman) was recrystallized from benzene and *n*-hexane[7]; m.p. 117.0–117.5°. **Tetraethylammonium bromide** (Eastman) was recrystallized from absolute ethanol. **Tetramethylammonium bromide** (Eastman) was recrystallized from a 50:50 ethanol–methanol mixture (5 g. of salt/100 ml. of solvent). **Tetra-*n*-butylammonium iodide** was from laboratory stock; m.p. 145.5–146.3°. **Tetra-*n*-propylammonium iodide** (Fisher) was purified by dissolving 4 g. in 8 ml. of 95% ethanol at 80°, adding 45 ml. of *n*-hexane, and allowing to cool. The product (45% first crop) was pure white. Tetraphenylborides were prepared from tetraalkylammonium halides and sodium tetraphenylboride[8] and recrystallized from 3:1 acetone–water mixtures; **tetrabutylammonium tetraphenylboride**, m.p. 230–235°; **tetrapropylammonium tetraphenylboride**, m.p. 206–207°. Picrates were prepared by neutralizing tetraalkylammonium hydroxide solutions by picric acid and were recrystallized from ethanol; **tetra-*n*-butylammonium picrate**, m.p; 91.6–91.9°; **tetra-*n*-propylammonium picrate**, m.p. 117.1–118.1°; **tetraethylammonium picrate**, m.p. 255–256°; **tetramethylammonium picrate**, m.p. 319–322°. Amine picrates were prepared by addition: **tripropylammonium picrate**, m.p. 115°; **tri-*n*-butylammonium picrate**, m.p. 108.3°. **Picric acid** was recrystallized from water. **Diphenylmethane** and **diphenyl ether** were fractionally crystallized. **Diphenylamine** (Matheson) was used as received, after allowing the ammonium carbonate stabilizer to evaporate.

Viscometer.—The viscometer is shown in Fig. 1. The instrument is designed so that a series of dilutions can be made on a sample of solute without opening the viscometer between check runs at a given concentration. In this way, evaporation errors are eliminated, and contamination of the viscometer contents by dust or moisture are minimized. The viscometers fit into spring clips in racks in the thermostat (25.00 ± 0.02°) which position them accurately vertical, and which permit rapid removal and remounting. The working volume is refilled by taking the viscometer out of the thermostat for about 10 sec. in order to tip it and run liquid through the side tube C from the dilution chamber A to the top chamber B. The viscometer is then placed back in the thermostat at about 30° from vertical on the side of tube C while the bulb D fills through the tube E. For acetonitrile, this operation takes about 2 min. Then the viscometer is taken out of the bath for a few seconds and tipped to run most of the excess liquid in B back into A through C; it is then immediately clamped in its vertical position. It will be noted that tube E projects 6–8 mm. above the floor of B; the liquid hold-up in E above the mark P gives the operator ample time to position the viscometer and focus the telescope on P before the meniscus passes it, when the electric timer is started.

The working volume (bulb D) is 20–25 ml. The lower capillary is 8.0 cm. long and 0.0356 cm. in diameter. The filling capillary E and the ones above and below D are 2 mm. in internal diameter; liquid flows from B through E into D much faster than it can drain out through the 0.0356 cm. capillary under D. The 5 mm. spherical cavity at the T-juncture of the capillaries is important; if constant 2 mm. bore is maintained, an air bubble is usually trapped. With the sphere, the bubble escapes through D and H. Two viscometers were used, with flow times of 3175 and 2635 sec. for water at 25°. All solutions and solvents were filtered into the viscometers through a coarse frit. When eventually dust did get into the viscometer, the latter was cleaned by filling with filtered concentrated nitric acid and heating for 8 hr. in a water bath at 80–90°.

The viscometers were calibrated, using water[9] (η = 0.008903), dioxane[10] (η = 0.011937), *n*-hexane[11] (η = 0.002952), *n*-decane[11] (η = 0.008555), and methylcyclohexane[11] (η = 0.006824). Literature values, if not based on the standard value of 0.010020 for water[9] at 20°, were recomputed to this standard before use. Eight other liquids were used as secondary standards. The Poiseuille equation

$$\eta = \pi\rho g h r^4 t/8lV - m\rho V/8\pi lt$$

was put into the familiar form

$$\eta/\rho t = C - D/t^2$$

The values of D (0.140 and 0.126 for viscometers I and II, respectively) were computed from viscometer dimensions, using m = 1.2. Then D/t^2 was added to the average values of $\eta/\rho t$ for each calibrating liquid. The final results are 10^6C = 2.831 ± 0.004 for viscometer I and 3.399 ± 0.005 for II. Since we are primarily concerned with *relative* viscosities of *dilute* solutions, this precision in calibration is adequate. The flow times for a given liquid gave a standard deviation of 0.02% or less.

Methods.—All solutions were prepared by weight. Viscosities were measured at a series of concentrations, the lowest concentration being about 0.01 mole/l. Usually the highest concentration was about 0.2, which was found empirically to be the practical limit of the linear equations 1 and 5. At higher concentrations, the viscosity plots usually became concave-up. Densities were measured over the same range of concentrations, using a Sprengel pycnometer (V_0 = 21.5743 ml.) which was calibrated with distilled water at 25°.

Results.—Since both the viscosity and the density data can be reduced to linear functions of c up to about 0.2 mole/l. for the systems studied, a compact summary of the results can be presented by giving the numerical values of the constants of eq. 1 and 5. Back-calculation showed that the constants reproduce the densities and viscosities to about ±0.02%, averaged over all the systems. Table I gives the solute–solvent pairs investigated, together with an identification code. (The symbol "Pi" stands for the picrate ion; the other symbols are familiar. The last

(6) J. E. Lind, Jr., and R. M. Fuoss, *J. Phys. Chem.*, **65**, 999 (1961).
(7) F. Accascina, S. Petrucci, and R. M. Fuoss, *J. Am. Chem. Soc.*, **81**, 1301 (1959).
(8) D. S. Berns and R. M. Fuoss, *ibid.*, **82**, 5585 (1960).
(9) J. F. Swindells, J. R. Coe, Jr., and T. B. Godfrey, *J. Res. Natl. Bur. Std.*, **48**, 1 (1952).
(10) J. A. Geddes, *J. Am. Chem. Soc.*, **55**, 4832 (1933).
(11) M. R. Cannon, *Anal. Chem.*, **32**, 355 (1960).

three compounds, disubstituted benzenes, are all *para*.) Table II describes the solvents. Table III gives the constants v_s, Mv_s, and B which were derived from the data. In order to obtain B, $[(\eta - \eta_0)/\eta_0 C^{1/2}]$ was plotted against the square root of concentration; the slope gives B, and the intercept at $c = 0$ gives the Falkenhagen coefficient A when the system is electrolytic. The $Ac^{1/2}$ term was quite small for our systems in the range $0.01 \leq c \leq 0.2$; within experimental error, the coefficient A agreed with the theoretical value.[12] For the non-electrolytic solutes, A is, of course, zero; in these cases, B was obtained as the weighted average of $[(\eta_0 - \eta_0)/\eta_0 c]$. The values of $100A$ for the electrolytes are: A, 1.6; B, 2.1; C, 1.9; D, 3.0; E, 1.7; F, 1.5; G, 2.1; H, 1.9; I, 2.5; J, 2.2; K, 2.0; L, 1.9; M, 1.7; N, 1.6.

TABLE I

DESCRIPTION OF SYSTEMS

Key	Solute	Solvent	Key	Solute	Solvent
A	Me_4NBr	MeOH	N	Me_4NPi	MeCN
B	Bu_4NBr	MeOH	O	Bu_3NHPi	MeCN
C	Bu_4NBr	$MeNO_2$	P	Pr_3NHPi	MeCN
D	Bu_4NBr	MeCOEt	Q	HPi	MeCN
E	Bu_4NBr	MeCN	R	Bu_3N	MeCN
F	Et_4NBr	MeCN	S	Ph_2CH_2	MeCN
G	Bu_4NI	MeCN	T	Ph_2O	MeCN
H	Pr_4NI	MeCN	U	Ph_2NH	MeCN
I	Bu_4NBPh_4	MeCN	V	Ph_2CH_2	CCl_4
J	Pr_4NBPh_4	MeCN	W	Ph_2NH	CCl_4
K	Bu_4NPi	MeCN	X	MeC_6H_4Me	MeCN
L	Pr_4NPi	MeCN	Y	$O_2NC_6H_4NO_2$	MeCN
M	Et_4NPi	MeCN	Z	$H_2NC_6H_4NO_2$	MeCN

TABLE II

Solvent	$100\eta_0$	ρ_0
MeOH	0.5417	0.7870
$MeNO_2$	.6175	1.1262
MeCOEt	.3820	0.8010
MeCN	.3427	0.7777
CCl_4	.904	1.5846

TABLE III

CONSTANTS FOR DENSITY AND VISCOSITY EQUATIONS

Key	v_s	$10^{-3}Mv_s$	B	q
A	0.643	0.099	0.42	4.25
B	.912	.294	.84	2.85
C	.931	.300	.75	2.50
D	.885	.285	1.01	3.54
E	.894	.288	0.93	3.23
F	.714	.150	.69	4.60
G	.834	.308	.87	2.83
H	.764	.239	.71	2.96
I	1.010	.567	1.35	2.38
J	0.985	.498	1.24	2.49
K	.854	.402	1.13	2.81
L	.801	.332	0.90	2.71
M	.721	.278	.85	3.06
N	.662	.200	.78	3.90
O	.821	.340	.99	2.91
P	.768	.286	.88	3.08
Q	.563	.129	.48	3.72
R	1.301	.241	.157	0.65
S	1.001	.168	.207	1.23
T	0.946	.161	.205	1.27
U	.913	.155	.274	1.77
V	.981	.165	.196	1.19
W	.900	.152	.30	1.97
X	1.173	.125	.042	0.34
Y	0.694	.117	.169	1.44
Z	0.721	.100	.294	2.94

Discussion

We first consider the coefficients B and $V = 10^{-3} \cdot Mv_s$ l./mole with respect to each other. In the last column of Table III is given q, the ratio B/V. According to eq. 7, this ratio should be 2.5, if (1) the linear term in the viscosity is due to the Einstein volume effect and if (2) the volume determined *via* the density is a true measure of the volume occupied by the solute. Two salts, Bu_4NBPh_4 and Pr_4NBPh_4 in acetonitrile, satisfy the ratio test for the validity of the model. These are the two salts among those studied both of whose ions are large and centrally symmetric; if any of the salts should agree with the working hypotheses, it should be these two. Since Bu_4N^+ and Ph_4B^- have nearly the same mobility,[13] we shall divide B and V for $Bu_4N \cdot BPh_4$ equally in order to obtain single ion values for these two ions. Then, if the coefficients B and V are additive properties of the constituent ions, we can assign single ion values to the ions of the other salts studied. There are six cases among the systems of Table I which permit a test of additivity; they are summarized in Table IV.

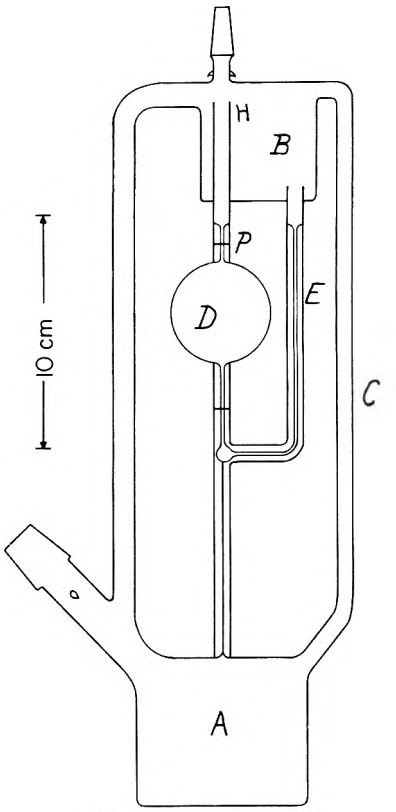

Fig. 1.—Viscometer.

TABLE IV

ADDITIVE PROPERTIES OF B AND V

	Ph_4B'	Pi'	I'
	B		
Pr_4N^+	1.20	0.96	0.71
Bu_4N^+	1.35	1.10	0.87
	V		
Pr_4N^+	0.50	0.33	0.24
Bu_4N^+	0.57	0.40	0.31

It is seen that pair-wise differences are constant, thereby establishing additivity for these six cases at least. We shall assume that it is general, *i.e.*

$$B = B^+ + B^-, \quad V = V^+ + V^- \qquad (8)$$

Next, we note that the other salts of Table III (with

(12) Reference 4, eq. 4-2-28, p. 104.

(13) R. W. Kunze and R. M. Fuoss, *J. Phys. Chem.*, **67**, 385 (1963).

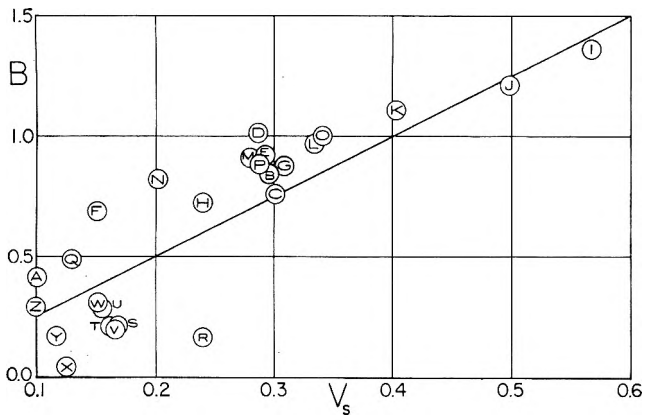

Fig. 2.—Comparison of viscosity and density coefficients; key in Table I.

the single exception of Bu_4NBr in nitromethane) all give q-values larger than 2.5. This is shown best in Fig. 2, where B is plotted against V; the solid line is drawn in accordance with eq. 7. The systems are identified by the code given in the first and fourth columns of Table I. All the electrolyte points lie *above* the line, except the two tetraphenylborides and the nitromethane point. For the tetraphenylborides, we found that v_s, as determined from the slopes of the density curves, is nearly equal to the reciprocal of the density ρ_s of the dry salt: $Bu_4N \cdot BPh_4$, $v_s = 1.01$, $1/\rho_s = 0.98$; $Pr_4N \cdot BPh_4$, $v_s = 0.98$, $1/\rho_s = 0.95$. The salts required a little more space in solution than in the rigid crystal lattice. Let us assume that, for all the salts, v_s is a valid measure of the static volume occupied by the ions in solution. (It should be mentioned that conductance measurements show that association is negligible in acetonitrile, due to the high dielectric constant; for $Me_4N \cdot NO_3$, where both ions are small,[14] K_A, the association constant, is only 23, and still smaller values of K_A are to be expected for the salts of Table I, with the exception of Me_4NBr.) Then the fact that the points lie *above* the solid line of Fig. 2 can have only one interpretation: most of the salts produce a viscosity increment greater than that corresponding to their volumes. In other words, if we assume that the V-values are physically correct, then the B-values are "too large." One explanation would be failure of the ion to conform to the spherical model which leads to the Einstein coefficient of 5/2; cylindrical ions, for example, would give much larger viscosity increments than spherical at the same volume fraction.[15] But Me_4NBr, Et_4NBr, Bu_4NBr, Pr_4NI, and Bu_4NI have spherical anions, and yet their q values are, respectively, 4.25, 4.60, 3.23, 2.96, and 2.83, all significantly larger than 2.5.

The discrepancy can be rationalized as follows. The Einstein model is spheres in a continuum. Real liquids contain a certain amount of unoccupied space ("holes" of one sort or another) and transport by slip without paying the price in friction is possible. Hence in general we would expect real solutes in real solvents to give a smaller contribution to viscosity than corresponds to their volumes. This is precisely what is observed for the non-electrolytic solutes Bu_3N, Ph_2CH_2, Ph_2O, and Ph_2NH (systems R, S, T, U) in either the highly polar acetonitrile, or in the non-polar carbon tetrachloride (V, W). We therefore conclude that the small ions in acetonitrile pull solvent dipoles to themselves (electrostriction) and thereby produce two effects which increase viscosity: (1) the holes in the vicinity of the ions are squeezed shut and (2) the kinetic entity which corresponds to a moving ion effectively is the ion plus a certain number of solvent dipoles which, on a time average, accompany it ("solvation").

If we use the spherical model, and split the B and V coefficients equally for Bu_4NBPh_4, then radii can be computed for the various ions of Table I. The results of these calculations are shown in Table V, where r_B is $(300B_j/N\pi)^{1/3}$ and r_V is $(750V_j/N\pi)^{1/3}$, and B_j and V_j are the appropriate single ion values obtained on the assumption of additivity, assuming also, as already mentioned, equal division for $Bu_4N \cdot BPh_4$. (Parentheses indicate which value of a pair was assumed.)

TABLE V

RADII FROM VISCOSITY AND DENSITY

Salt	$10^8 r_B^+$	$10^8 r_B^-$	$10^8 r_V^+$	$10^8 r_V^-$
Bu_4NBPh_4	(4.74)	(4.74)	(4.81)	(4.81)
Pr_4NBPh_4	4.37	(4.74)	4.40	(4.81)
Bu_4NPi	(4.74)	4.06	(4.81)	3.61
Pr_4NPi	4.39	(4.06)	4.39	(3.61)
Et_4NPi	4.22	(4.06)	3.81	(3.61)
Me_4NPi	3.96	(4.06)	3.18	(3.61)
Bu_3NHPi	4.49	(4.06)	4.44	(3.61)
Pr_3NHPi	4.17	(4.06)	4.05	(3.61)
Bu_4NI	(4.74)	3.15	(4.81)	2.37
Pr_4NI	4.34	(3.15)	4.34	(2.37)
Bu_4NBr	(4.74)	3.35	(4.81)	1 44
Et_4NBr	4.14	(3.35)	3.84	(1 44)

In a general way, the radii of Table V are quite satisfactory: they are of the right order of magnitude, and sequences are in the expected direction (Bu > Pr, etc.). The r_V values for the first four quaternary ions, Me_4N^+, . . , Bu_4N^+ are only a little smaller than the values 3.47, 4.00, 4.52, 4.92 calculated by Robinson and Stokes[16] from the molar volumes of the corresponding paraffins. These values are larger than the Stokes radii calculated from limiting conductances in water[16] (2.04, 2.81, 3.92, 4.71) and strikingly different from the values (2.83, 3.94, 5.55, 6.05) calculated from the B coefficients determined from the viscosity of aqueous solutions of the quaternary salts.[17] As mentioned in the introduction, aqueous solutions do not belong to the general class of solutions, and we merely say that we are not surprised at the lack of agreement between constants derived from measurements in water and in acetonitrile.

Study of the table reveals some significant details. For the larger ions (Bu_4N^+, Pr_4N^+, Ph_4B^-, Bu_3HN^+, Pr_3HN^+), the agreement between r_V and r_B is excellent, and confirms our feeling that the model ought to be satisfactory in these cases. But as the size of the ion decreases, r_B decreases much more slowly than one would expect on the basis of the simple model; see values for Et_4N^+ and Me_4N^+, for example. This point is best demonstrated by the halide ions; for bromide, r_V, which by hypothesis is a measure of the actual ionic size, is 1.44 Å., while r_B is 3.35, over twice

(14) D. S. Berns and R. M. Fuoss, *J. Am. Chem. Soc.*, **83**, 1321 (1961).
(15) F. Perrin, *J. phys. radium*, **7**, 1 (1936).
(16) R. A. Robinson and R. H. Stokes, "Electrolyte Solutions," 2nd Ed., Academic Press, New York, N. Y., 1959, Table 6.2, p. 124.
(17) E. R. Nightingale, Jr., *J. Phys. Chem.*, **66**, 894 (1962).

as large. That is, the bromide ion affects a volume about ten times its own in the flow process. The discrepancy between r_V and r_B thus supports our suggestion of electrostriction.

The non-electrolytic solutes also show evidence of electrostatic interaction with the solvent. The nonpolar or slightly polar solutes give B-values which are considerably smaller than one would expect from the corresponding volumes. The sequence of the last three compounds of Table III is especially informative; the three molecules have roughly the same shape and size, so the geometrical contributions to B should be not greatly different. The q-values, however, increase by nearly an order of magnitude in the sequence MeC_6H_4Me, $O_2NC_6H_4NO_2$, $O_2NC_6H_4NH_2$. The first two components have zero dipole moments, the first due to absence of electrical asymmetry and the second by compensation of vectorially opposed moments. The value of B for the dinitro compound is, however, over four times that for p-xylene; strong local interaction between the individual nitro-dipoles and solvent molecules is clearly indicated. The value for p-nitroaniline neatly confirms the argument; the net dipole moment is very large ($\approx$7 Debyes) and has an intense field at both ends. The value of B (2.94) is greater than the ideal 2.5, which shows the strong dipoles can also produce electrostriction in their vicinity.

Finally, a comparison of tributylammonium picrate with tributylamine and picric acid also leads to the conclusion that electrostatic interaction, in addition to purely geometrical effects, determines viscosity. The sum of V's for picric acid and the amine is 0.37, which is in fair agreement with 0.34, the value of V for the amine picrate. But the sum of the B's is only 0.64 as compared with 0.99 for the amine picrate. The field at the nitrogen end of the Bu_3NH^+ ion is of course much stronger than that at the Bu_3N nitrogen, and a large B is expected and found for the amine picrate.

THE McDEVIT–LONG EQUATION FOR SALT EFFECTS ON NON-ELECTROLYTES[1]

By N. C. Deno and Charles H. Spink[2]

College of Chemistry and Physics, the Pennsylvania State University, University Park, Penna.

Received January 31, 1963

Evidence is presented supporting the theory that the salting-out and salting-in of non-electrolytes depends on the molecular volume of solute and on the changes in internal pressure of the solvent which take place on addition of salt.

The familiar salting-in or salting-out of non-electrolytes is correlated by the equation

$$\log f = k_s c_s \qquad (1)$$

where f is the activity coefficient of the non-electrolyte, k_s is the Setschenow constant, and c_s is the concentration of salt in moles/liter.[3]

Based on the concept of volume energies, Long and McDevit[4] derived the equation

$$k_s = \bar{V}_i^0(V_s - \bar{V}_s^0)/2.3RT\beta_0 \qquad (2)$$

Equation 2 requires that salt effects are determined by the molecular volume of the solute molecule and the extent of electrostriction, $(V_s - \bar{V}_s^0)$, of the solvent by the salt. Long and McDevit used the compressibility data of Gibson[5] to evaluate the electrostriction. The resulting evaluation of k_s for salt effect on the solubility of benzene in water gave the correct salt order and correct sign of k_s for a variety of salts.

The concept of volume energies also has been used to correlate solubility and distribution data for a large number of hydrocarbons in water,[6,7] sulfur dioxide,[7] and ammonia.[7] In these systems, the activity coefficient of the non-electrolyte is again related to the volume energies

$$RT \ln f = V\Delta P_e \qquad (3)$$

In eq. 3, V is the molecular volume of the solute and ΔP_e is an empirical parameter that depends only on the two liquid phases and is interpreted to be the difference in internal pressures.[8]

If eq. 3 is differentiated with respect to salt concentration for solutions of non-electrolytes in varying salt concentrations, eq. 4 results.

$$\mathrm{d} \log f/\mathrm{d}c_s = k_s = (V/2.3RT)(\mathrm{d}\Delta P_e/\mathrm{d}c_s) \qquad (4)$$

Since V is approximately equal to $\bar{V}_i^0$ for non-electrolytes, eq. 2 and 4 are equivalent. The change in internal pressure with salt concentration, $\mathrm{d}\,\Delta P_e/\mathrm{d}c_s$ in eq. 4, is equal to the internal pressure factor, $(V_s - \bar{V}_s^0)/\beta_0$, of the McDevit–Long eq. The success of eq. 3, independent of eq. 2, supports the McDevit–Long eq. (eq. 2) and suggests that eq. 2 or 4 deserves more experimental testing than has previously been given.[3,4,9]

Experimental

The solubilities of tetralin, diphenylmethane, and 2,4-diphenyl-2-methyl-2-pentene were measured in sodium sulfate solutions. Concentrations of the hydrocarbons in solution were determined by conventional spectrophotometric methods using a Beckman DU spectrophotometer. All hydrocarbons were distilled and,

(1) This work was supported in part by the Petroleum Research Fund administered by the American Chemical Society. Grateful acknowledgment is hereby made of this support.

(2) Recipient of a du Pont Fellowship.

(3) F. A. Long and W. F. McDevit, *Chem. Rev.*, **51**, 119 (1952).

(4) F. A. Long and W. F. McDevit, *J. Am. Chem. Soc.*, **74**, 1773 (1952).

(5) R. E. Gibson, *ibid.*, **56**, 4, 865 (1934); **57**, 284 (1935).

(6) J. C. McGowan, *J. Appl. Chem.*, **2**, 323 (1952); **4**, 41 (1954).

(7) N. Deno and H. Berkheimer, *J. Chem. Eng. Data*, **4**, 1 (1959).

(8) The original notation of McGowan (ref. 6 and 7) has been changed in order to be more consistent with the underlying concepts and with the notations of Gibson (ref. 5) and Long and McDevit (ref. 4). The original expression of McGowan was ($\log f = k_M P$), where k_M is a constant for a given solvent pair and P is the Parachor, a measure of molecular volume. McGowan's expression for the molecular volume near the m.p., 0.42 P (J. C. McGowan, *Rec. trav. chim.*, **75**, 199 (1956)), is the most convenient way to estimate V in eq. 3 in view of the availability of Tables of Parachor increments (O. R. Quayle, *Chem. Rev.*, **53**, 484 (1953)).

(9) M. A. Paul, *J. Am. Chem. Soc.*, **74**, 5274 (1952).

prior to each experiment, chromatographed through activated alumina.

The general procedure was to mix about 0.5 ml. of hydrocarbon with 30 ml. of salt solution in glass stoppered flasks and to allow the samples to equilibrate with gentle agitation at 25°. Aliquots were withdrawn from the aqueous phase intermittently for spectral measurement. When the optical densities were constant within 2%, equilibration was regarded as complete. Spectral measurements were made at a number of wave lengths for each compound in order to check for possible oxidation and colloidal dispersion. Beer's law tests were made on each hydrocarbon. The sodium sulfate was analyzed for water content by ignition. The salt solutions were checked for optical purity in the ranges where measurements were made.

The solubilities of the above hydrocarbons were also determined in aqueous tetramethylammonium bromide solutions. In the wave length region 230 to 250 mμ, there was a low absorption which increased slowly with time. For the tetralin and diphenylmethane experiments this absorption was not significant. As a precaution, however, fresh salt solutions were prepared immediately before use.

Discussion

The Setschenow constants were determined from eq. 1. The data in Table I demonstrate that the proportionality between molecular volume and k_s, required by eq. 2, is exhibited for both salting-out and salting-in. The deviation for molecules of small volumes such as ethylene arises from occupation of interstitial space as explained for similar deviations from eq. 3.[7]

Table I

Correlation of the Setschenow Constant (k_s) with Molecular Volume for Na_2SO_4 and $(CH_3)_4N^+Br^-$ Solutions

Non-electrolyte	V[a] (ml./mole)	Na_2SO_4 k_s	Na_2SO_4 $k_s/V \times 10^3$	$(CH_3)_4N^+Br^-$ k_s	$(CH_3)_4N^+Br^-$ $k_s/V \times 10^3$
Ethylene	42	0.42[b]	10		
Benzene	86	.54[c]	6.3	−0.15	−1.8
Naphthalene	131	.72[d]	5.5		
1,2,3,4,-Tetrahydronaphthalene	139	.74	5.3	− .28	−2.0
Biphenyl	160	.84[d]	5.3		
Diphenylmethane	177	.88	5.0	− .37	−2.1
2,4-Diphenyl-2-methyl-2-pentene	251	1.05	4.2		

[a] Estimated as suggested in footnote 8. [b] J. Billitzer, *Z. physik. Chem.*, **40**, 535 (1902). [c] Ref. 3. [d] Ref. 9.

The relatively small drift in k_s/V values in Table I may be due to the Kirkwood interaction term, $r_c/(r_c + r_n)$, which was proposed as a possible additional factor for eq. 2.[3] In this term, r_c is the radius of the cation in solution and r_n is the radius of the non-electrolyte.[10] The radii are unambiguous for spherical molecules, but in more complex molecules, such as those approaching cylindrical shapes, r_n is more nearly approximated by the radius of a cross section of the cylinder. Thus r_n does not necessarily continue to increase with increasing molecular volume.

The term, $(V_s - \bar{V}_s^0)/2.3RT\beta_0$, has also been tested beyond the initial considerations of Long and McDevit.[3] Table II summarizes the test and again a reasonable fit is found for both salting-out and salting-in. For V_s, the volume of the salt in solution, the formulations of Mukerjee[11] were used. In the case of the large tetraalkylammonium salts, where Mukerjee's method is not applicable, V_s was estimated by the relation, $V = 0.42P$, where P is the Parachor.[8] The $\bar{V}_s^0$ values for the $R_4N^+Br^-$ salts were measured in this work and are reported in Table III.

Table II

Comparison of Calcd. and Exptl. Values of k_s for Benzene

Salt	$V_s - V_s^0$	$(0.3k_s)$[a] (calcd. from eq. 2)	k_s (exptl.)[b]
$Al_2(SO_4)_3$	214	2.5	1.2
Na_2SO_4	53	0.58	0.55
$BaCl_2$	41	.47	.33
NaOH	22.3	.26	.26
NaF	18.6	.21	25
NaCl	12.8	.16	20
KCl	10.3	.12	17
NaBr	13.6	.14	16
LiCl	10.4	.12	14
RbCl	9.0	.10	.14
KBr	10.1	.12	.12
NH_4Cl	9.0	.10	.10
CsCl	8.7	.10	.09
$C_6H_5CO_2Na$	− 4.4	− .05	− .05
$C_6H_5SO_3Na$	− 9.0	− .10	− .09
$(CH_3)_4NBr$	−10.0	− .11	− .15
$(C_2H_5)_4NBr$	−23	− .26	− .25
$(C_3H_7)_4NBr$	−32	− .37	− .41

[a] The 0.3 factor is an arbitrary factor introduced to improve the agreement. It is evident that eq. 2 in its present form is more successful in calculating relative values for k_s rather than absolute values. In using eq. 2, the compressibility of water, β_0, was taken as 39.6×10^{-6} bar^{-1} and the molar volume of benzene, $\bar{V}_1^0$, was taken as 86 ml./mole. [b] Most of the values are from ref. 3 and 4.

Table III

Densities of Aqueous Salt Solutions at 25°

Salt	Wt. %	Density, g./ml.
$(CH_3)_4NBr$	0.00	0.9971
	3.95	1.0074
	6.00	1.0122
	7.97	1.0186
	$\bar{V}_s^0$ = 112.1 ml./mole	
$(CH_3CH_2)_4NBr$	4.15	1.00480
	6.11	1.00861
	8.15	1.01270
	$\bar{V}_s^0$ = 170.3 ml./mole	
$(CH_3CH_2CH_2)_4NBr$	4.07	1.00282
	6.11	1.00502
	8.09	1.00831
	$\bar{V}_s^0$ = 225.8 ml./mole	

The only major deviation is for $Al_2(SO_4)_3$. This salt differs from the others in Table II in that one of the ions, Al^{+3}, is strongly bonded to water by covalent bonds.[12] It would be more proper to regard the ion as $Al(H_2O)_6^{+3}$. The formation of covalent bonds lowers the value of $\bar{V}_s^0$ beyond the electrostriction effect so that $(V_s - \bar{V}_s^0)$ and k_s calculated by eq. 2 are too large.

The tests of eq. 2 can be extended to include polar molecules. Equation 3 has been extended to include solutes which specifically bond to solvent

$$RT \ln f = V\Delta P_e + \Delta F_H \qquad (5)^{6,7}$$

Since such bondings are usually hydrogen bonds, the symbol ΔF_H was used. It was found that ΔF_H was characteristic of the type of functional group and exactly proportional to the number of such groups.[7]

(10) J. G. Kirkwood, *Chem. Rev.*, **24**, 233 (1939).
(11) P. Mukerjee, *J. Phys. Chem.*, **65**, 740, 744 (1961).
(12) H. Taube, *ibid.*, **58**, 523 (1954).

If eq. 5 is differentiated in respect to salt concentration, eq. 6 results. This equation predicts that the Setsche-

$$RT\ (\mathrm{d}\ \ln f/dc_s) = V(\mathrm{d}\ \Delta P_e/\mathrm{d}c_s) + \mathrm{d}\ \Delta F_H/\mathrm{d}c_s \quad (6)$$

TABLE IV

VALUES OF k_s/V FOR POLAR SOLUTES COMPARED TO BENZENE (25°) USING $(NH_4)_2SO_4$ AS THE SALT

Solute	k_s[a]	V (ml./mole)[b]	$k_s/V \times 10^3$
Benzene	0.396[c]	86	4.6
Methanol	.154	42	3.6
Ethanol	.249	59	4.0
1-Propanol	.336	76	4.5
1-Butanol	.417	93	4.3
2-Butanol	.40	91	4.5
Diethyl ether	.42	89	4.8
1,2-Dimethoxyethane	.37	97	3.8
Diisopropyl ether	.54	119	4.5
Dipropyl ether	.62	122	5.0
Acetone	.30	66	4.5
Cyclohexanone	.42	108	3.8
Propionaldehyde	.26	67	3.8
Butyraldehyde	.42	84	5.0
2,3-Butanedione	.98	86	14.1
Formaldehyde	− .02	34	−0.6
Acetaldehyde	.14	50	2.8

[a] W. Rieman, III, *J. Chem. Educ.*, **38**, 338 (1961), unless noted. [b] Footnote 8. [c] Calculated by the method used in Table II.

now constant for a solute that is hydrogen bonded to solvent depends on the rate of change of ΔF_H with salt concentration, as well as the internal pressure changes. For some solutes, such as those shown in the upper part of Table IV, k_s/V is the same as for benzene, from which it is concluded that d $\Delta F_H/dc_s$ is zero.

For many solutes, d $\Delta F_H/dc_s$ is not zero. Presumably, direct interaction between solute and the ions of the added salt occurs. Long and Bergen have listed k_s values for a number of polar solutes, principally amines and carboxylic acids.[13] These data have been examined in detail.[14] In 41 out of 57 examples, the value of k_s/V was within 50% of the value for benzene so that even here the internal pressure effect accounts for the major part of the salt effect. The values of d $\Delta F_H/dc_s$ that were largest in magnitude were found for carboxylic acids (RCOOH) with salts of the alkali metal ions. The values were negative as expected for a significant interaction between RCOOH and the alkali metal ion. Other metal ions would presumably exhibit even more negative values, but data are not available. Significantly, d $\Delta F_H/dc_s$ for carboxylic acids was zero when tetraalkylammonium salts were added. No interaction between carboxylic acid and cation would be expected in these cases and this demonstrates that there is nothing abnormal about the carboxylic acids in general.

(13) F. A. Long and R. L. Bergen, *J. Phys. Chem.*, **60**, 1131 (1956).
(14) Ph. D. Thesis of Charles H. Spink, Pennsylvania State Univ., 1962

KINETICS OF COAL COMBUSTION: THE INFLUENCE OF OXYGEN CONCENTRATION ON THE BURNING-OUT TIMES OF SINGLE PARTICLES

BY GEOFFREY BEESTON

Department of Fuel Technology and Chemical Engineering, University of Sheffield, England

AND ROBERT H. ESSENHIGH

Department of Fuel Technology, College of Mineral Industries, The Pennsylvania State University, University Park, Pa.

Received November 24, 1962

The combustion behavior of captive particles from a single coal, in the size range 2 mm. down to 350 μ, has been studied as a function of oxygen vitiation and enrichment; this supplements previous work on a range of coals of volatile matter 5–40%, designed to study the influence of rank, but which were burned only in air. In these present studies, particles of 5 different diameters were burned in quiescent oxygen atmospheres (p_0) ranging from 3 to 70%, at an approximately constant temperature of about 1000°; and their burn-out times (t_b) were measured with a stopwatch. The results agreed very well with theory, which predicted that t_b was inversely proportional to $\ln(1 - p_0)$, thus implying that the reaction with respect to p at the solid surface is first order. The theory used was a modification of the Nusselt diffusion-film hypothesis of reaction control. The original theory was restricted to the condition that p_0 was small, in which case t_b is proportional to p_0, the first term of the logarithmic expansion; but with the wide range in oxygen concentration used in these experiments, the use of the full logarithmic expression was found to be necessary. From the theory, the value of the constant of proportionality could also be calculated from first principles, and this calculated value was found (fortuitously but acceptably) to be in exact agreement with the experimental value.

1. Introduction

Single particles of coal burn in two stages. The first is a volatile combustion stage and the second, with which this paper is primarily concerned, is burn-out of the solid carbon residue left after generation and combustion of the volatiles. Kinetically, this second, burn-out stage is a heterogeneous process in which oxygen reacts directly, at-and-with the solid surface. It has, therefore, been studied extensively, but as it were by proxy using relatively pure carbon in place of the coal; and the validity of extrapolating such results directly to coal residues has generally been then taken very much for granted. Direct work on coal has, of course, been done in the past but the results[1-3] have generally been too few, and the conditions too imprecise, for kinetic studies. Further experiments have, therefore, been carried out on single particles of coal under

(1) H. K. Griffin, J. R. Adams, and D. F. Smith, *Ind. Eng. Chem.*, **21**, 808 (1929).
(2) A. L. Godbert, *Fuel*, **9**, 57 (1930); A. L. Godbert and R. V. Wheeler, "Safety in Mines Research Board," Paper No. 73 H.M.S.O., London, 1932.
(3) A. A. Orning, *Trans. ASME*, **64**, 497 (1942); T. J. Omori and A. A. Orning, *ibid.*, **72**, 591 (1950).

more precisely specified conditions, to check proposed kinetic equations. The first results obtained, described elsewhere,[4,5] were concerned with the variation of burning time as a function of particle diameter and coal rank, with other parameters such as oxygen concentration, temperature, and ambient velocity, kept constant. This work has now been extended to study the influence of oxygen concentration, which is of particular interest as it also has direct bearing on the assumed but disputed[6] order of reaction at the solid surface. The object of this present paper is, therefore, to report the results of these further experiments on the influence of oxygen concentration on the burn-out times of the coal particle residues, together with a comparison between the experimental and predicted behavior.

2. Theory

As the general theory has been covered extensively in previous reviews and papers[4,5,7-9] only the salient points will be quoted in summary here to present the equations required for test by experiment.

The theory is based on the original analysis by Nusselt[10] in which he assumed that the rate controlling process in the reaction was the rate of diffusion of oxygen from the main stream to the solid particle surface, through a boundary diffusion layer. Reaction at the solid surface was assumed to be instantaneous, or effectively so, and it was also assumed to be first order with respect to the oxygen partial pressure adjacent to the solid surface. With these limiting conditions, Nusselts prediction was that the total burning time (t_b) of a solid carbon sphere would be proportional to the square of the initial particle diameter (d_0): thus

$$t_b = K_D d_0^2 \qquad (1)$$

where K_D is a predictable burning constant that is a function of temperature and oxygen partial pressure.

This equation was tested in the previous experiments; in the first instance[4] just as it stands using only a few coals, but subsequently[5] the number and rank range of coals was increased to determine the influence of coal rank. To do this, burning times (of both volatiles and residues) of particles in the size range 4000 to 300 μ were measured as a function of diameter. The particles were burned in air, between two small heating coils of resistance wire, under relatively quiescent ambient conditions, at an effectively constant temperature of about 1000°. In all, 10 coals were ultimately tested, ranging in volatile percentage from 5 to 40, and all were found to obey eq. 1. The value of the burning constant K_D had, of course, to be adjusted to allow for the effects of volatile loss and swelling, but the experimental values of the burning constant, K, were found[5] to be in good agreement with the following predicted relationship between K and K_D

$$K = [(C_f/100)/f]K_D \qquad (2)$$

where C_f is the fixed carbon percentage and f is a swelling factor whose values were found by measurement to be: unity for coals of V.M. less than 5%; and 1.5 for coals of V.M. greater than 10%. The basis of this prediction was the assumption that the coals first lost volatiles at constant diameter and then swelled by the linear factor f. This then provided a correction factor to the solid density σ that appears in the theoretical relation for K_D, given as

$$K_D = \sigma/3\rho_0 D_0 (T/T_0)^{0.75} \ln(1 - p_0) \qquad (3a)$$

$$= k/\ln(1 - p_0) \qquad (3b)$$

$$= k/p_0 \text{ (for small } p_0) \qquad (3c)$$

where ρ_0 is the STP density of air; D_0 is the STP diffusion coefficient of oxygen through nitrogen; T is the absolute temperature; and p_0 is the ambient fractional oxygen concentration (of value 0.21 for air).

This set of equations therefore provided us with relations between burning time, or burning constant, and the two additional variables: oxygen concentration and temperature, to be checked by comparison with measurement in further experiments. Our choice of variable for the experiments reported here was the first: that of oxygen concentration, for the reasons outlined in the Introduction. In doing this, we only used a single coal since, as the quantitative influence of rank is given by eq. 2, we assumed that validation on a single coal chosen at random should be satisfactory. The experiments were then carried out by measuring burning time as a function of oxygen partial pressure, using five different sizes of particle taken from the single coal, as described in the section following.

3. Experimental

To burn the particles in variable but controllable oxygen atmospheres, a small combustion unit was used inside a large perspex (plexiglass) box so that the ambient atmosphere could be controlled at will. The combustion unit was, in principle, that used in the previous experiments,[4,5] in which the coal particles were cemented to silica fibers and held by these cantilever-fashion, midway between two horizontal heating elements of electrical resistance wire.

The coal used was Winter (ex-Grimethorpe); a medium bituminous coal, no. 7 of the set prepared and used previously,[5] of analysis: ultimate—84.0% C, 5.5% H, 8.3% O, 1.8% N, 0.4% S (d.m.f. by Fereday and Flint[11] equation); proximate—36.0% V.M., 2.6% H_2O, 1.7% ash, 0.77% CO_2.

The perspex box used to house the combustion unit had dimensions: 1.5 by 1.5 ft. in plan section, by 3 ft. high (6.75 cu. ft.). The oxygen atmosphere inside could be adjusted as required over the range 3 to 70% O_2. To make up the required atmosphere, oxygen or nitrogen was metered in as required, and the analysis then checked by Orsat. The reason for making the box so large was that the oxygen depletion during combustion of a particle would not then be significant, and the atmosphere could, therefore, be taken as being effectively infinite, with the "main stream" or ambient oxygen concentration constant during the reaction, thus meeting the specified boundary conditions required by the theoretical analysis. In fact, the box was large enough for a number of particles to be burned without having to open and recharge the box for each particle, and without significant change in the box's atmosphere. To take advantage of this, a rail carrying 18 carriages was mounted in the box, and to each carriage could be attached one silica thread with its coal particle

(4) R. H. Essenhigh and M. W. Thring, Proc. Conf. "Science in the Use of Coal," Sheffield, 1958; Paper 29, p. D21: Institute of Fuel, London, 1958.

(5) R. H. Essenhigh, paper no. 62-WA-35, presented at A.S.M.E. Winter Annual Meeting, November, 1962, for publication in *Trans. ASME*.

(6) D. A. Frank-Kamenetskii, "Diffusion and Heat Exchange in Chemical Kinetics," Princeton University Press (Trans. 1955), Ch. II, pp. 64, 65.

(7) R. H. Essenhigh and M. G. Perry, Introductory Survey "Combustion and Gasification," Proc. Conf. "Science in the Use of Coal," Sheffield, 1958, p. D1: Institute of Fuel, London, 1958.

(8) R. H. Essenhigh and I. Fells, General Discussion on "The Physical Chemistry of Aerosols," Bristol, 1960; paper no. 24, p. 208: Faraday Society, London, 1961.

(9) R. H. Essenhigh, *J. Inst. Fuel* (London), **34**, 239 (1961).

(10) W. Nusselt, *V.D.I.*, **68**, 124 (1924).

(11) F. Fereday and D. Flint, *Fuel*, **29**, 283 (1950).

cemented on ready for burning. After burning, the oxygen concentration was checked by Orsat analysis.

The particles on the carriages were moved into position between the coils, as and when required, by means of a control rod extending outside the box. The heating coils were larger than those used previously. In place of the 2-cm. diameter flat spirals, wound from 18-gage nichrome resistance wire, the new heaters were square elements, of face area about 5 × 5 cm., made of nichrome strip. This strip was about 0.5 cm. wide, and was wound with 0.5-cm. spacing on a 0.5-cm. thick former; the gaps between the set of strips on one side of the former were, of course, substantially covered by the return strips on the other side so that the whole face area was radiant. The two heating units were then mounted horizontally with their faces about 1.5 cm. apart. The heating was electrical, as before, controlled by a variable transformer unit; with this, element temperatures of up to 1060°, as measured by an optical pyrometer, could be reached.

Burning times were measured with a stopwatch in place of the photocell and pen recorder units used previously. The photocell was abandoned because of light shielding and other difficulties experienced with the larger heating elements. This meant that very short volatile burning times could not be measured—those larger ones that were, were measured with a second stopwatch. However, the volatile measurements that were made were found to exhibit such considerable variability in the different oxygen atmospheres that their value was greatly reduced. Most measurements were therefore restricted to the residue burning times alone, using the stopwatch which was found to be perfectly satisfactory for these.

With this apparatus, the residue burning times were measured at different levels of oxygen concentration as the principal variable, for each of the following particle sizes: 1870, 1300, 928, 649, and 388 μ. The particles were derived from the single coal, and burned in effectively infinite atmosphere, at an approximately constant temperature of 1000°.

4. Results

4.1 Qualitative Behavior.—The general behavior of the particles was as before[4,5]: the particles burned in two stages, with the volatiles (when they burned at all) igniting first and burning with the characteristic luminous, flickering flame; and this was then followed in the burn-out stage by the much steadier glow of residue combustion. The particles did not ignite immediately; they required time to heat up to ignition, and this ignition time increased with decrease of oxygen concentration. This may indicate that preliminary, but significant oxidation may be occurring, with significant heat generation, before the volatiles ignited in flaming combustion. This requires closer investigation.

As in the previous experiments, the volatiles of the smaller particles often failed to ignite because of their small quantity and this failure increased, as was to be expected, as the oxygen was reduced. Where the volatiles did ignite in reduced oxygen, the usual fractional lag in time between finish of the volatile flame and start of the residue combustion was occasionally increased to a long delay ranging from two to thirty seconds. At the low oxygen concentrations, below 6%, the burning times also started to become very scattered, and at 3%, the particles failed to ignite at all.

At the other end of the scale, at high oxygen concentrations, the particles showed increasing tendency to decrepitate or explode. This happened whether the coils were already up to temperature before the particle was inserted (as was the case in general in these experiments), or whether the particle was already in position (as in the previous experiments) before switching on the heating current. If decrepitation is due to too rapid generation of volatiles before the coal becomes sufficiently plastic, this suggests that the volatiles generation must be influenced, contrary to previous expectation, by the ambient oxygen concentration. This would seem to imply that the oxygen causes some significant and rapid change in the constitution of the potential volatile material before generation, though how it should do this is by no means clear; this also requires further detailed study. In contrast, the general residue behavior is far better understood, and more predictable, as described in the sections following.

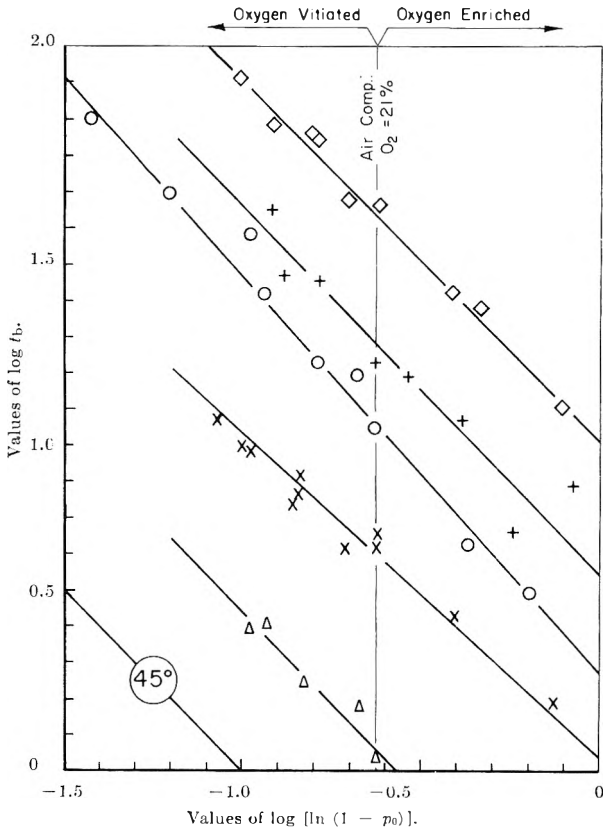

Fig. 1.—Double logarithmic plot of burning time, t_b, against the oxygen partial pressure function, ln (1 − p_0). d_0 values (μ): ◇, 1870; +, 1300; O, 928; ×, 649; △, 388.

4.2 Influence of Oxygen Concentration.—By combining eq. 1 and 3b we have for burn-out of the residues

$$t_b = [(C_f/100)/f]kd_0^2/\ln (1 - p_0) \qquad (4)$$

To test this equation, the experimental data obtained have, therefore, been presented in two graphs, Fig. 1 and 2. Figure 1 is a plot of log t_b against log [ln (1 − p_0)], to show that the slopes of the lines obtained are, within reason, close to 45°, or −1. Figure 2 is the alternative plot of t_b against the reciprocal of ln (1 − p_0), to show that the plots obtained are again acceptably linear and passing through the origin. Within the limits of accuracy of the measurements, these plots are, therefore, considered to substantiate eq. 4.

4.3 Influence of Particle Size.—From eq. 4 it is clear that the slopes of the lines in Fig. 2 (written as m) are related to particle size by

$$m = [(C_f/100)/f]kd_0^2 \qquad (5)$$

This equation has in turn been tested by plotting $(m)^{1/2}$ against d_0, as shown in Fig. 3. Here again the plot is reasonably linear, and also passes through the origin. Again within the limits of accuracy of this plot, it is considered to substantiate eq. 5.

4.4 Comparison with Prediction.—Now, the slope of Fig. 3 (written as M) is an experimental quantity

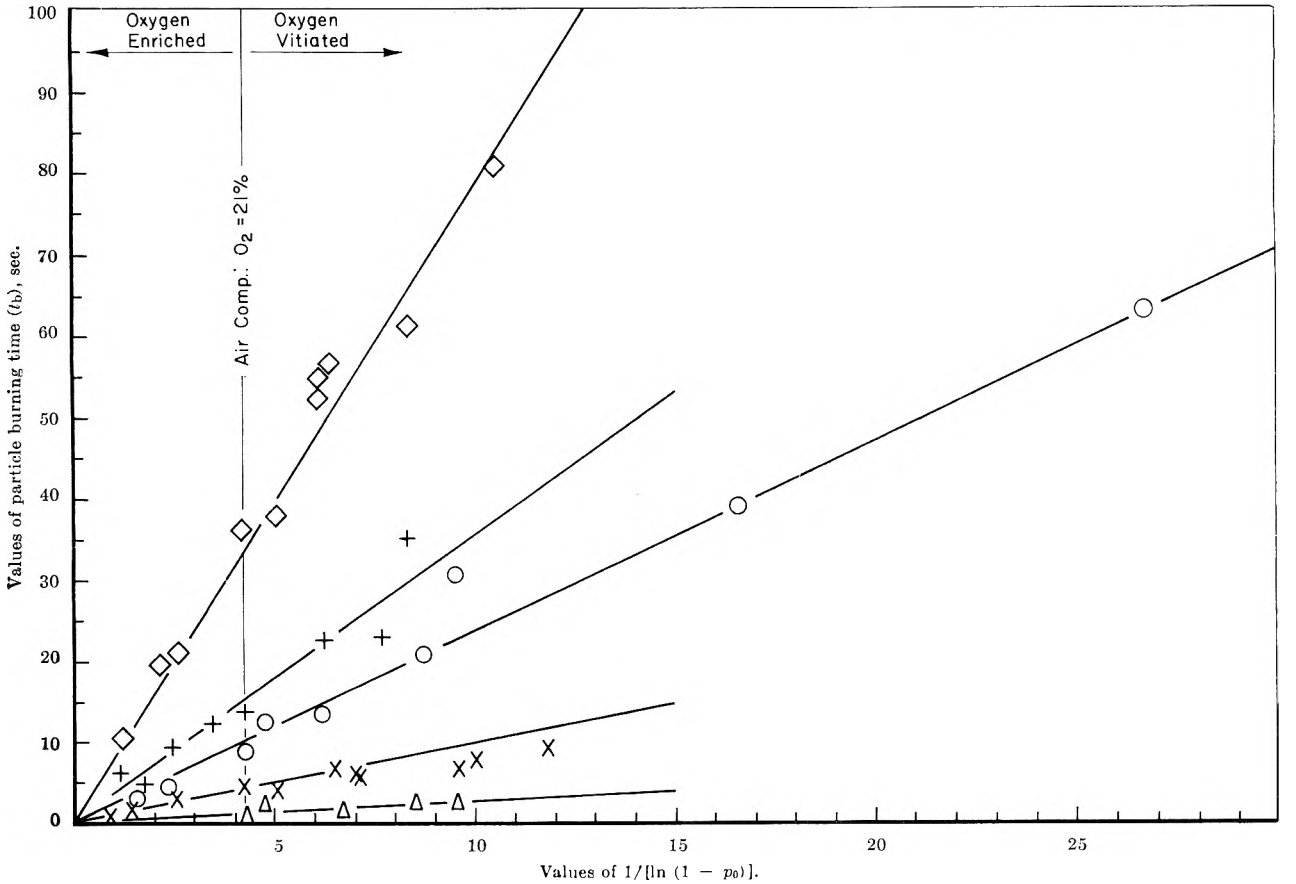

Fig. 2.—Linear plot of burning time, t_b, against the reciprocal of the oxygen partial pressure function ln $(1 - p_0)$. d_0 values (μ): ◇, 1870; +, 1300; O, 928; ×, 649; Δ, 388.

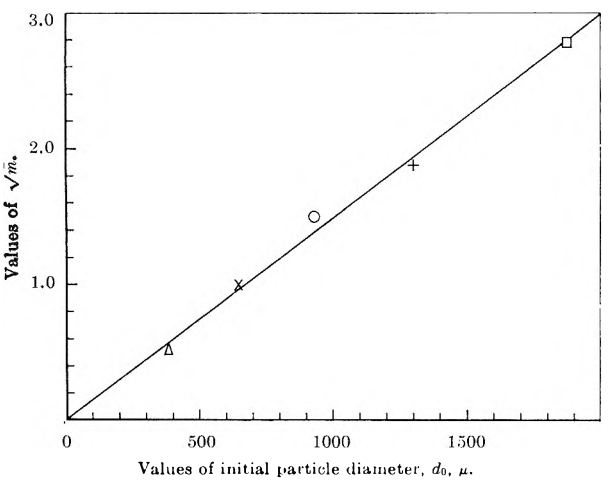

Fig. 3.—Variation of square root of Fig. 2 slopes (m) as a function of initial diameter of particle (d_0).

whose value is predicted from the appropriate terms in eq. 3a and 5, thus

$$M^2 = [(C_f/100)/f]\sigma/3\rho_0 D_0 (T/T_0)^{0.75} \qquad (6)$$

For the Winter coal, C_f is 60.7; f is 1.5; and σ is 1.25. For air, ρ_0 is 1.3×10^{-3} g./cc.; D_0 for oxygen diffusing through nitrogen at temperature T_0 (273°K.) is 0.181 cm.²/sec. The particle temperature is taken as 1000° (1273°K.), as in the previous experiments. With these values, the calculated value of M^2 is 225; we therefore have for M_{calcd} a value of 15, which is precisely the experimental value obtained from the slope of Fig. 3. This exact agreement is clearly fortuitous; but within an error of 5%, which is the estimate of the over-all error in both experimental and calculated values, it is clear that agreement is still satisfactory. Since this agreement was obtained by using the rank-influence equation 2, this also supports the assumption made that validation of the tested equations using a single coal, but chosen at random, would probably be satisfactory.

4.5 Burning Constant.—This is the constant K_D or K of eq. 1. It is calculated almost universally from measurements made in air, so tabulated values (as in reviews 7, 8) are given for $p_0 = 0.21$. From eq. 1, 2, 3, and 6, it is clear that

$$K = M^2/\ln(1 - p_0) \qquad (7)$$

Hence with values for M^2 of 225; and for ln $(1 - p_0)$ of 0.235 when p_0 is 0.21; this gives a value of K_{calcd} of 957 sec./cm.². This is lower than (though close to) the value obtained in the previous experiments[5] for this same coal (previous value: 1095 sec/cm.²) but this may be accounted for in part by the difference between the logarithmic term [ln $(1 - p_0)$] and the first term of its expansion [p_0] since the former has been used in this paper, but the latter was used in the previous paper[5]; the theoretical alternatives are compared in the two eq. 3b and 3c. Use of the first term expansion as in eq. 3c is very common, and is generally accepted as being valid for air or vitiated air. Just how widely the two terms differ at enriched concentrations is shown by Fig. 4 in which the logarithmic term is plotted against p_0. In vitiated air the two are clearly reasonably comparable, but even in air itself the difference amounts to nearly 12% (0.235 compared with 0.21). Use of the ln term in place of p_0 in the previous experiments would, therefore, reduce the value

of 1095 to 978. The further difference between this and the new value of 957 is well within 5% but can in any case be attributed to uncertainty in the precise temperature in the two cases. Agreement, however, is regarded as acceptable.

The significance of the logarithmic term also showed up in the graphs of Fig. 1, 2, and 3. To check their sensitivity to the first expansion term in place of the full expression, similar plots were prepared (not reproduced) with p_0 in place of $\ln (1 - p_0)$. The plots were found to vary significantly as follows: in equivalent Fig. 1, the plots showed slight but detectable curvature in spite of the fairly considerable scatter; in equivalent Fig. 2, convincingly straight lines could be run through the points, but the plots then showed marked intercepts on the oxygen-function axis, and the displacements from the origin were found to be statistically significant; finally, in equivalent Fig. 3, a straight line could again be run through the points, but again only with a statistically significant intercept. This agreement with the logarithmic term thus provides by far the best substantiation of the original Nusselt analysis in terms of the diffusion-film theory of reaction-rate control. What is yet undetermined, however, are the limits of applicability of the Nusselt equation and analysis; this is considered briefly in the next section.

5. Discussion

5.1 Reaction Order.—As stated in the Introduction, one of the principal reasons for carrying out the work described was to provide a more direct check on the assumed order of reaction at the solid surface. Now, because of the adjacent diffusion layer, that under these quiescent conditions is rate-controlling, it is only possible to check the surface order of reaction indirectly. To do this we assume some appropriate value for the surface order of reaction and then deduce what net, over-all, or "global" order of reaction should then follow. First of all, in choosing an order for the surface reaction, we have[7] two extreme limiting values: (1) zero when the temperature is low enough for the surface chemisorption sites to be fully saturated at all times; and (2) unity, when the temperature is high enough for the sequence of chemisorption, followed by desorption, to be effectively instantaneous. At intermediate temperatures the reaction approximates to a fractional order. If internal or pore reaction also takes place, the lower limiting order is then raised from zero to $^1/_2$.

Superimposed on this pattern is the oxygen supply by boundary layer diffusion. Now, in the first place, if the temperature is high enough for first-order reaction to prevail then we get the burning time equation that combines both the diffusional and adsorption resistance[9]

$$t_b = K_c d_0 + K_D d_0^2 \qquad (8)$$

where K_c is the high-temperature chemical burning constant and K_D is the diffusional burning constant. This clearly has limits, respectively, of a linear equation, or a square law equation, according to whether diffusion is unimportant or dominant. At the other extreme of low temperatures, when the reaction order is zero, the burning time equation is linear only[9]

$$t_b = K_c' d_0 \qquad (9)$$

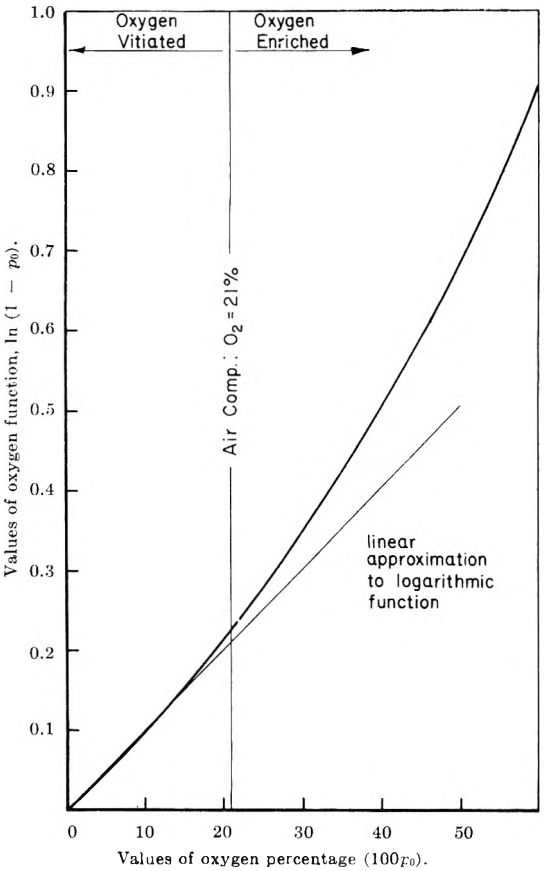

Fig. 4.—Variation of oxygen function ln $(1 - p_0)$ with oxygen partial pressure, p_0.

where K_c' is the low-temperature chemical burning constant. At intermediate temperatures the burning time is proportional to some intermediate power of the diameter, d_0^n, where n lies between 1 and 2. It is, therefore, obvious that determination of the power index n in any burning time experiments will give a clear guide to the relative importance of the three factors considered: (i) rate of diffusion; (ii) rate of chemisorption; and (iii) rate of oxide-film decomposition. In particular, a value of 2 for n is quite unambiguous in implying that the rate of boundary layer diffusion dominates the reaction control, and the significant corollary of this is that the surface rate-of-adsorption reaction must be first order.

In concluding that the reaction in our experiments was in the high temperature region, and diffusion controlled, we have altogether three confirmatory points provided by the experimental results. (1) The first is the "square-law" agreement illustrated by the square-root plot of Fig. 3; if the additional chemical term in eq. 8—$K_c d_0$—was also important, the line would be curved with a tendency to an intercept on the t axis. Other checks such as plotting (t_b/d_0) against d_0 confirmed that K_c was negligible under the conditions of experiment. (2) We also have the agreement between t_b and the oxygen function $\ln (1 - p_0)$. Since K_c is inversely proportional to p_0,[9] then if this was important the plot of t_b against $1/p_0$ would not have been so poor in comparison with the plot of Fig. 2 against $1/\ln (1 - p_0)$, as discussed in sec. 4.5. (3) There is, finally, the excellent agreement between the experimental and calculated values of the burning constant (written as K instead of K_D after correction for coal rank and swelling by eq. 2) as described in sec. 4.5.

Since the reaction is evidently diffusion controlled, it follows that the surface reaction must be first order.

5.2 Boundary Layer Thickness.—A secondary point of interest that also emerges from this is a reflection on the question of boundary layer thickness. In calculating heat and mass transfer to spheres it is almost universal to use Nusselts concept of the effective or "fictitious" boundary layer thickness. If the oxygen concentration at the solid surface of the particle of radius a is zero, its value at any other radius r from the center of the particle is given approximately by

$$p/p_0 = 1 - a/r \qquad (10)$$

Since p rises to the main-stream value p_0 only when r becomes infinite, the real, physical boundary layer must clearly be of infinite thickness if it is defined as the distance required for p to reach the main-stream value. If, however, (following Nusselt[10]) the real behavior indicated by eq. 10 is replaced by an equivalent behavior such that p is assumed to rise linearly to p_0 and then to remain constant with r, the main stream value is then reached at the Nusselt fictitious film thickness at $r = 2a$, or one radius out from the surface of the particle. It should be realized, however, that at $r = 2a$, $p = p_0/2$ (from eq. 10); in other words, the actual, physical rise in p is only half the fictitious value. This can be represented in another way by relating the fictitious film thickness to a definable real, or physical film thickness. This can be defined with physical realism as the distance within which p rises to, say, 99% of the main-stream value (this is a standard solution to continuum problems in which some relevant parameter reaches its limiting value only at infinity). We then have that, writing the boundary layer thickness as δ

$$\delta_{(\text{physical})} = 100a = 100\delta_{(\text{fictitious})}$$

The significance of this becomes immediately apparent when considering the behavior of dust flames since the interparticle distance at a stoichiometric concentration is generally of the order of only 30 particle diameters. This means that in real, physical terms, as opposed to fictitious film-thickness terms, most of the oxygen is already well inside the boundary layer of one particle or another in the flame. It is clear, therefore, that direct extrapolation of the results of this paper to particles in dust flames should be made with caution. Now, in addition to the points made above, a further complication that emerges is the additional inadequacy of the fictitious film concept, even for purposes of calculation, over the range of oxygen concentrations used in our experiments. Because our range was high, and the oxygen function $\ln (1 - p_0)$ could not be approximated by p_0 (as shown in Fig. 4), it means that eq. 10—which is also based on the same approximation of p_0 for $\ln (1 - p_0)$—is also inadequate to describe the behavior of the oxygen concentration over our full experimental range. An effective film thickness can still be defined, but the expression for it is so complex as to be valueless as it is then easier to solve the initial differential equation and not to bother about the "short cut" of using an effective or fictitious film thickness.

5.3 Range of Applicability.—The final point to be considered as a consequence of these results is their range of applicability: the temperature range of application is of particular importance.

Now, what we have established so far is that the solid surface reaction is first order at a temperature as low as 1000°. This, however, was unexpected, being about 200° lower than the expected value of the "higher critical temperature." This was estimated, by assessment[7] of the available literature, at 1200°. Below that, through the transition range down to 800°, the reaction order was expected to drop progressively from unity to zero. The explanation for this apparent contradiction would appear to be a consequence of the influence of the ambient gas velocity on the boundary layer thickness. The effect of ambient velocity is to promote such increased speed of mixing of the ambient gases that the thickness of the boundary layer, however defined, is progressively reduced. Initially, this must steepen the oxygen concentration gradient, with the result that both oxygen transfer, and therefore reaction rate, are increased. This increase can proceed just so far, up to the point that the rate of chemisorption exceeds the rate of reaction, and at that point the coverage of the solid surface by the chemisorbed film must increase; the surface reaction order then becomes fractional, and can drop progressively to zero as the ambient velocity also increases. This means that the transition range of temperature between the two extreme reaction conditions is velocity dependent. This dependence is shown very clearly by the single sphere experiments of Tu, Davis, and Hottel,[12] but the analytical function relating the two is still unknown.

It would therefore seem that previously published experiments that were assessed as showing a first-order reaction only down to 1200° cannot yet be directly correlated with the results of our experiments because the previous ones were carried out in flowing systems, while ours were in effectively quiescent systems. The increased film thickness that must have existed in our experiments can account qualitatively for the first-order reaction down as low as 1000°, but this interrelation between temperature and velocity is now, in our opinion, the most outstanding problem of the combustion system requiring to be resolved by future work.

6. Conclusions

For coal particles inside the size range 350 μ to 2 mm., burning in vitiated and enriched O_2 atmospheres (3 to 70%), at about 1000°, under quiescent ambient conditions, the combustion behavior was found to be as follows.

(1) Qualitative behavior was, in general, similar to that observed previously with coal particles burning in air; for particles large enough, combustion proceeded in two sequential states: (i) volatile evolution and combustion; followed by (ii) residue combustion.

(2) Particles below 1 mm. tended to produce too small a quantity of volatiles for their combustion, because of low limit requirements. The frequency of this combustion failure tended to increase as the oxygen concentration was reduced. At 3% oxygen, even the residues failed to ignite. At high oxygen concentrations the particles ignited and burned satisfactorily, but they showed increasing tendency to decrepitate or explode.

(3) Quantitatively, only the residue combustion was examined in detail. Burning times of the residues (t_b) were found experimentally to obey the relation pre-

(12) C. M. Tu, H. Davis, and H. C. Hottel, *Ind. Eng. Chem.*, **26**, 749 (1934).

dicted from the Nusselt diffusion theory of reaction control.

$$t_b = m/\ln (1 - p_0)$$

where p_0 is the ambient oxygen concentration and m is a predictable constant.

(4) The results also showed good agreement with the following predicted relation between the constant m and the initial particle diameter d_0

$$m = M^2 d_0^2$$

where M is another predictable constant.

(5) The experimental value of the second constant M was also found to be in good agreement with the predicted value, as calculated from the relation

$$M^2 = [(C_f/100)/f]\sigma/3\rho_0 D_0 (T/T_0)^{0.75}$$

where C_f is the fixed carbon of the coal; f is the swelling factor (of value 1.5 for bituminous coals); σ is the solid particle density; ρ_0 is the s.t.p. density of air; D_0 is the s.t.p. coefficient of oxygen diffusing through nitrogen; T is the absolute temperature and T_0 is the reference temperature of 273°K. The predicted and experimental values of M^2 were in fact identical, at 225; although this exact agreement was fortuitous it is still entirely satisfactory within the expected limits of error.

(6) The burning constant K in the Nusselt square-law equation

$$t_b = Kd_0^2$$

was also calculated, being given by

$$k = M^2/\ln (1 - p_0)$$

The value was 957 c.g.s. units, and this is in adequate agreement with values obtained previously for this same coal under similar (though not identical) experimental conditions.

(7) This general agreement with prediction therefore substantiates the primary assumption of the theoretical analysis: that the order of reaction at the solid particle surface with respect to oxygen concentration is unity. It also follows from the results that the rate of diffusion is the slow step that dominates the reaction rate, and that the importance of the chemisorption process is negligible under the conditions of experiment. There is background evidence from other previous experiments, however, indicating that this is true only for the fully quiescent system; and that, in a velocity field at these temperatures, the chemisorption process is likely to become significant, and increasingly so with increasing velocity. This is now the outstanding point requiring investigation in any subsequent work.

Acknowledgments.—The work described in this paper formed a part of a general program of research on Pulverized Fuel Firing, sponsored by the Electricity Supply Research Council of Great Britain. The work was carried out in the Department of Fuel Technology and Chemical Engineering, University of Sheffield, England. The authors are indebted to the ESRC for financial support of this work and for permission to publish this paper.

NOTES

THE DECARBOXYLATION OF OXALIC ACID IN CRESOLS AND GLYCOLS

By Louis Watts Clark

Department of Chemistry, Western Carolina College, Cullowhee, N. C.

Received October 19, 1962

Kinetic studies have been carried out in the past on the decarboxylation of oxalic acid in various solvents, including dioxane,[1] glycerol,[2] dimethyl sulfoxide, triethyl phosphate, aniline, methylaniline, dimethylaniline, quinoline,[3] 6-methylquinoline, and 8-methylquinoline.[4]

The present paper describes the results of kinetic studies carried out in this Laboratory on the decarboxylation of oxalic acid in five additional solvents, *o*-cresol, *m*-cresol, *p*-cresol, ethylene glycol, and 1,3-butanediol. A comparison is made of the reaction in these and in several other solvents previously studied.

Experimental

Reagents.—(1) Anhydrous oxalic acid, reagent grade, 100.0% assay, was used in this research. To ensure perfect dryness it was stored in a desiccator containing sulfuric acid. (2) The solvents were highest purity chemicals. Fresh samples of each liquid were distilled at atmospheric pressure directly into the dried reaction flask immediately before the beginning of each decarboxylation experiment.

Apparatus and Technique.—The details of the apparatus and technique used in this research have been described previously.[5] In these experiments a sample of oxalic acid weighing 0.1618 g. (corresponding to 40.0 ml. of CO_2 at STP on complete decarboxylation, based upon the actual molar volume of CO_2, 22,263 ml.) was weighed into a fragile glass capsule weighing approximately 0.1 g. and blown from 7 mm. soft glass tubing. The 100-ml. 3-neck flask was filled with approximately 50 ml. of solvent, saturated with dry CO_2 gas. The temperature of the oil bath was thermostatically controlled to within ±0.05°, a U. S. Bureau of Standards calibrated thermometer being used.

Results

It is a peculiar feature of the decarboxylation of oxalic acid that the resulting product, formic acid, tends to undergo decarbonylation readily.[6] This decarbonylation reaction is almost completely suppressed by the presence of minute traces of water.[6] The water molecule probably adds across the carbonyl double bond of the activated formic acid forming a stable hydrate, orthoformic acid. In studies on the decarboxylation of oxalic acid in dimethyl sulfoxide the secondary decarbonylation reaction was observed.[3] In the present investigation, in which only hydroxylic solvents were

(1) A. Dinglinger and E. Schöber, *Z. physik. Chem.*, **A178**, 401 (1937).
(2) L. W. Clark, *J. Am. Chem. Soc.*, **77**, 6191 (1955).
(3) L. W. Clark, *J. Phys. Chem.*, **61**, 699 (1957).
(4) L. W. Clark, *ibid.*, **62**, 633 (1958).
(5) L. W. Clark, *ibid.*, **60**, 1150 (1956).
(6) H. N. Barham and L. W. Clark, *J. Am. Chem. Soc.*, **73**, 4638 (1951).

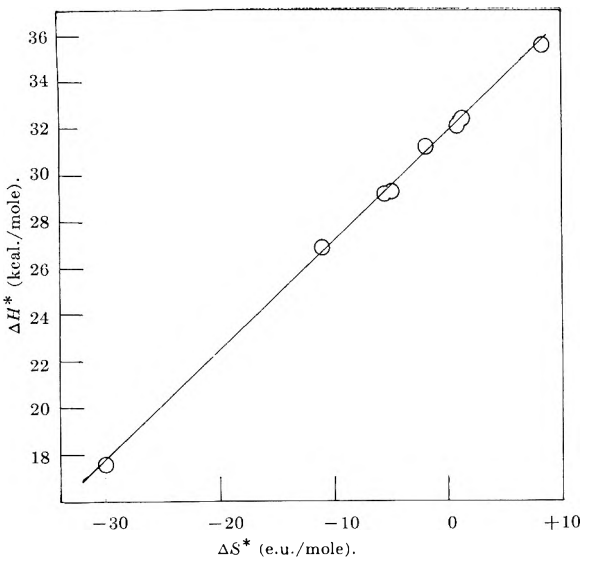

Fig. 1.—Enthalpy–entropy plot for the decarboxylation of oxalic acid in several solvents.

used, no secondary reaction occurred even at elevated temperatures. It is believed that the hydroxylic solvent molecule reacts with the carbonyl double bond of the formic acid in the same manner as does the water molecule, converting the acid into a stable orthoformic acid derivative.

Decarboxylation experiments were carried out in each solvent at three different temperatures over a 20° temperature range. The experiments were repeated two or three times at each temperature. In the case of each of the solvents used in this investigation the log $(V_\infty - V_t)$ was a linear function of time over about the first 80% of the reaction. The average rate constants, calculated in the usual manner from the slopes of the experimental logarithmic plots, are brought together in Table I. The parameters of the absolute reaction rate equation[7]

$$k = \frac{\kappa T}{h} e^{-\Delta H^*/RT} e^{\Delta S^*/R}$$

based upon the data in Table I, are shown in Table II, along with corresponding data for the reaction in several other solvents previously studied.

TABLE I

APPARENT FIRST-ORDER RATE CONSTANTS FOR THE DECARBOXYLATION OF OXALIC ACID IN THE CRESOLS AND SOME GLYCOLS

Solvent	Temp. (°C. cor.)	$k \times 10^4$ (sec.$^{-1}$)	Av. dev.
o-Cresol	140.63	1.62	±0.01
	149.63	3.80	.01
	160.50	10.2	.04
m-Cresol	139.38	1.98	.02
	149.63	4.47	.02
	161.21	10.8	.03
p-Cresol	150.47	2.79	.01
	160.50	6.69	.02
	169.32	14.0	.06
Ethylene glycol	131.41	7.47	.02
	141.24	11.7	.02
	151.65	22.3	.05
1,3-Butanediol	146.31	4.20	.02
	152.15	6.90	.03
	162.74	16.5	.05

(7) S. Glasstone, K. J. Laidler, and H. Eyring, "The Theory of Rate Processes," McGraw-Hill Book Co. Inc., New York, N. Y., 1941, p. 14.

TABLE II

ACTIVATION PARAMETERS FOR THE DECARBOXYLATION OF OXALIC ACID IN SEVERAL SOLVENTS

Solvent	ΔH^* (kcal./mole)	ΔS^* (e.u./mole)	$\Delta F^*_{194°}$ (kcal./mole)
Methylaniline[3]	35.5	+ 8.3	31.6
Dimethylaniline[3]	32.4	+ 1.3	31.8
o-Cresol	32.1	+ 0.9	31.7
p-Cresol	31.2	− 1.9	32.1
1,3-Butanediol	29.3	− 4.9	31.6
Dioxane[1]	29.2	− 5.5	31.8
m-Cresol	26.9	−11.0	32.0
Ethylene glycol	17.6	−30.0	31.6

Discussion of Results

It has been well established that the rate-determining step in the decarboxylation of malonic acid is the formation of a transition complex between solute and solvent species.[8] The results of studies on the decarboxylation of oxalic acid,[3] oxamic acid,[9] and oxanilic acid[10] in solution have indicated that these compounds likewise decompose according to a similar mechanism. Table II furnishes additional evidence in support of this postulated mechanism in the case of oxalic acid.

A plot of the values of ΔH^* *vs.* ΔS^* shown in Table II is a straight line of slope 467°K. This is the so-called isokinetic temperature, that is, the temperature at which the rate of reaction is the same regardless of the solvent (see Fig. 1).[11]

Petersen, *et al.*,[12] have discussed the effects of experimental error on the validity of the enthalpy–entropy relationship. They have shown that only if the range of ΔH^* values exceeds twice the maximum possible error in ΔH^* can any validity be assumed in the observed enthalpy–entropy relationship, and only if the range is much greater than this amount can any details of the relationship (*e.g.*, linearity) be inferred. Applying their analysis to the present reaction series it is found that the range of ΔH^* values is 17.9 kcal./mole (see Table II), whereas twice the maximum possible error in ΔH^* (assuming the maximum possible fractional error in the rate constant to be 0.05) is only 1.83 kcal./mole. The range of ΔH^* values is therefore much greater than twice the maximum possible error in ΔH^*, and therefore considerable confidence may be attached to the observed enthalpy–entropy relationship.

The isokinetic temperature for the decarboxylation of oxalic acid in the various solvents, 467°K., corresponds to a temperature of 194°. This is equal to, or very nearly equal to, the melting point of oxalic acid.[13]

The isokinetic temperature for the decarboxylation of oxanilic acid in a wide variety of solvents extending over a wide range of enthalpies and entropies of activation has been shown to be 423°K.—this is equal to 150°, the melting point of oxanilic acid.[14] Similarly,

(8) G. Fraenkel, R. L. Belford, and P. E. Yankwich, *J. Am. Chem. Soc.*, **76**, 15 (1954).

(9) L. W. Clark, *J. Phys. Chem.*, **65**, 180 (1961).

(10) L. W. Clark, *ibid.*, **65**, 572 (1961).

(11) J. E. Leffler, *J. Org. Chem.*, **20**, 1202 (1955).

(12) R. C. Petersen, J. H. Markgraf, and S. D. Ross, *J. Am. Chem. Soc.*, **83**, 3819 (1961).

(13) The melting point of oxalic acid reported in the literature (*cf.* "Handbook of Chemistry," N. A. Lange, Ed., Ninth Edition, Handbook Publishers, Inc., Sandusky, Ohio, 1956, p. 645)—186°—appears to be discrepant. Using reagent oxalic acid, anhydrous, which had been stored in a desiccator containing sulfuric acid, the melting point as determined by means of a thermometer which was checked against a thermometer calibrated by the U. S. Bureau of Standards turned out to be 194° (cor.). Eastman Organic Chemicals List No. 42, Distillation Products Industries, Rochester, New York 1960, 42nd Edition, p. 168, lists the melting point of their reagent oxalic acid, anhydrous, as 192°.

the isokinetic temperature for the decarboxylation of malonic acid in a large number of hydroxylic solvents has been shown to be 407°K.—this is equal to 134°, the melting point of malonic acid.[15]

In view of these results, the coincidence between the isokinetic temperature and the melting point of the acid may not be fortuitous but may represent a general kinetic relationship.

The intercept of the ΔH^*–ΔS^* plot on the zero axis (ΔH_0^*) is 31.8 kcal./mole. This is equal to ΔF_0^*, which is the free energy change of the reaction in each of the solvents at the isokinetic temperature, that is, at the melting point of oxalic acid.[11] Good agreement obtains between the theoretical and experimental values of ΔF_0^* as shown by the data in column 4 of Table II (see also Fig. 1).

A comparison of the activation parameters for the reaction in the two solvents 1,3-butanediol and ethylene glycol (lines 5 and 8 of Table II) indicates an unexpected difference in properties between these two liquids. The large negative entropy for the reaction in ethylene glycol points to extensive linear polymerization of the solvent. The small negative entropy of activation in the case of the 1,3-glycol indicates a much lower degree of association as compared with the 1,2-glycol. The reason for this profound difference in properties between these two glycols may be deduced by a comparison of the data for the reaction in these solvents and in dioxane (line 6 of Table II). The very close similarity in the parameters for the reaction in dioxane and in 1,3-butanediol suggests a close relationship in the structure and properties of these two liquids. As a matter of fact, if 1,3-butanediol is written in the chelated form, the molecule is seen to bear a striking resemblance to dioxane

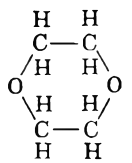

1,4-Dioxane

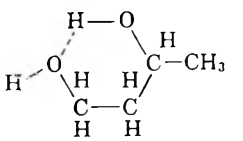

1,3-Butanediol

This kind of behavior is probably general for all 1,3-glycols. For other glycols which are incapable of chelating to form a six-membered ring type structure linear polymerization rather than cyclization would be the rule.

Acknowledgment.—The support of this research by the National Science Foundation, Washington, D. C., is gratefully acknowledged.

(14) L. W. Clark, *J. Phys. Chem.*, **66**, 1543 (1962).
(15) L. W. Clark, *ibid.*, **67**, 526 (1963).

CRYSTAL STRUCTURE OF ZIRCONYL PERCHLORATE DIHYDRATE BY X-RAY POWDER DIFFRACTION METHOD

BY P. RAMA MURTHY AND C. C. PATEL

Dept. of Inorganic and Physical Chemistry, Indian Institute of Science, Bangalore 12, India

Received October 19, 1962

Crystals of zirconyl perchlorate dihydrate, $ZrO(ClO_4)_2 \cdot 2H_2O$, prepared as reported by the authors,[1] were powered to about 300 mesh size and filled in a 0.5 mm. (i.d.) Lindemann glass capillary and sealed. The X-ray diffraction pattern of the substance was taken with a 143.2 mm. diameter G.E. camera, using nickel filtered CuKα radiation generated at 34 kv. and 18 ma. The specimen was rotated through 360° and exposed to the X-ray radiation for 16 hr. The d-spacings of the diffraction pattern were corrected for the film shrinkage. Since the crystals were found to be biaxial in nature,[1] the possibility of their being cubic, tetragonal, and hexagonal was ruled out. The lines of the diffraction pattern were indexed for orthorhombic system, using the Hesse–Lipson's method.[2,3] The observed and the calculated d-spacings, according to the orthorhombic system, together with the relative intensities, are given in Table I. The relative intensities were estimated visually.

TABLE I

X-RAY DATA OF ZIRCONYL PERCHLORATE DIHYDRATE[a]

Line no.	*hkl*	*d*-spacings obsd., Å.	*d*-spacings calcd., Å.	Relative intensities
1	011	11.89	11.89	50
2	002	8.066	8.066	60
3	030	5.852	5.861	20
4	023	4.570	4.591	20
5	040	4.393	4.400	100
6	100	4.180	4.178	30
7	102	3.723	3.731	30
8	112	3.642	3.651	20
9	051	3.435	3.442	20
10	060	2.936	2.936	25
11	114	2.864	2.871	25
12	124	2.794	2.769	25
13	151	2.662	2.662	25
14	070	2.520	2.516	25
15	125	2.471	2.460	30
16	153	2.415	2.412	30
17	106	2.262	2.267	30
18	154	2.237	2.244	30
19	126	2.191	2.193	20
20	155	2.074	2.070	25
21	107	2.021	2.021	25
22	127	1.971	1.970	30
23	232	1.924	1.923	30
24	182	1.894	1.894	30
25	233	1.861	1.859	20
26	128	1.781	1.781	20
27	192	1.732	1.733	20
28	119	1.641	1.642	20
29	129	1.618	1.621	20
30	139	1.590	1.588	20
	087		1.592	
31	234	1.562	1.570	15
32	273	1.546	1.546	15
33	159	1.493	1.493	15
34	079	1.458	1.460	15
35	228	1.436	1.436	15
36	198	1.332	1.332	15
37	315	1.286	1.282	15
38	362	1.251	1.249	15
39	366	1.143	1.144	15
40	393	1.116	1.115	15
41	404	1.037	1.035	15
42	453	1.006	1.007	15
43	407	0.9724	0.9716	15
44	580	.7854	.7857	25
45	582	.7825	.7825	20

[a] a = 4.20 Å., b = 17.59 Å. and c = 16.11 Å.

(1) P. R. Murthy and C. C. Patel, *Naturwissenschaften*, **22**, 693 (1961).
(2) R. Hesse, *Acta Cryst.*, **1**, 200 (1948).
(3) H. Lipson, *ibid.*, **2**, 43 (1949).

The results in Table I show that there is good agreement between the observed and the computed d-spacings for various reflections. The density of the crystals, as determined by specific gravity bottle using pure benzene as displacing liquid, was found to be 1.934 g./ml. at 25°, and the number of molecules of the dihydrate per unit cell was $4.05 \simeq 4$. From the systematic absence of the lines when l is odd in $00l$, the symmetry of the crystals corresponds to P_{222_1} (space group No. 17). The density of the crystals calculated from the X-ray data is 1.912 g./ml. Since the crystals are very hygroscopic, single crystal X-ray diffraction could not be carried out.

Acknowledgment.—The authors are thankful to Dr. Jagadish Shankar for helping in taking the powder pattern.

THE CHEMISTRY OF XYLYLENES. XIX. THE CO-PYROLYSIS OF *p*-XYLENE AND HEXACHLOROETHANE

BY L. A. ERREDE AND J. P. CASSIDY

Contribution No. 235 from the Central Research Laboratories of the Minnesota Mining and Manufacturing Company,[1] St. Paul, Minn.

Received October 25, 1962

Dainton and Ivin[2] studied the thermal decomposition of hexachloroethane in a closed system. They found that the rate of reaction is appreciable even at 300°. The products were tetrachloroethylene and carbon tetrachloride. Chlorine was isolated, however, when the reaction was terminated before complete conversion. They concluded that the formation of tetrachloroethylene involved a chain reaction.

$$Cl\cdot + CCl_3CCl_3 \longrightarrow Cl_2 + CCl_3CCl_2\cdot \quad (1)$$

$$CCl_3CCl_2\cdot \longrightarrow CCl_2{=}CCl_2 + Cl\cdot \quad (2)$$

They suggested that the chain reaction was initiated either by thermal rupture of the C–Cl bond or the C–C bond

$$CCl_3CCl_3 \longrightarrow CCl_3CCl_2\cdot + Cl\cdot \quad (3)$$

$$CCl_3CCl_3 \longrightarrow 2CCl_3\cdot \quad (4)$$

Calculation of bond dissociation energies based on molecular structure[3] gives 63 and 68 kcal. for the C–C and C–Cl bonds, respectively, in CCl_3CCl_3. This difference of 5 kcal. is quite significant and it suggests that C–C scission, not C–Cl, is the initiating process. The CCl_3 radicals thus produced abstract a chlorine atom from hexachloroethane, as shown in eq. 5, and thereby initiate the chain reaction exemplified by eq. 2 and 1.

$$CCl_3\cdot + CCl_3CCl_3 \longrightarrow CCl_4 + CCl_3CCl_2\cdot \quad (5)$$

If C–C bond rupture is indeed the initiating reaction, then it should be possible to trap CCl_3 radicals in large amounts, whereas if C–Cl is the initiating reaction then it should be possible to trap the radical fragments CCl_3CCl_2 and Cl in about equal amounts.

In previous publications[4–6] it was reported that the primary radical fragments generated by fast flow pyrolysis of CCl_4 and of CCl_3H at low pressure could be trapped by quenching with a second stream of pyrolyzed *p*-xylene. When confluence occurred at the exit of the pyrolysis zone, *p*-methylbenzyl chloride and β,β-dichloro-*p*-methylstyrene were produced in equal amounts by random coupling of the primary radical fragments as indicated by equations 6 and 7.

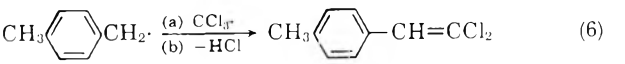

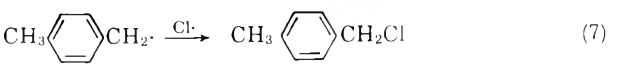

On the other hand, if confluence of the two fast flowing streams is delayed for only about 0.01 sec. after pyrolysis, the products are those produced by coupling of secondary radical fragments formed in the respective streams prior to mixing. Thus, coaxial pyrolysis of *p*-xylene and carbon tetrachloride gas streams, with confluence several inches beyond the furnace, gave α,α'-dichloro-*p*-xylene as a major product[5] (eq. 8), whereas the same experiment using *p*-xylene and chloroform gave α,α'-bis-trichloromethyl-*p*-xylene [also named *p*-bis-(β,β,β-trichloroethyl)-benzene] as a major product[6] (eq. 9).

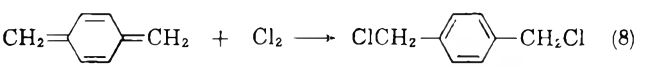

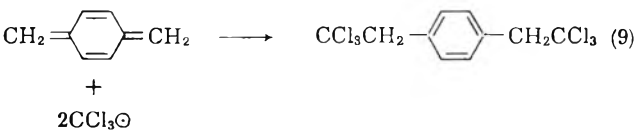

To ensure isolation of the primary fragments in the present work, a gas mixture of *p*-xylene and hexachloroethane (mole ratio 3.5/1) was pyrolyzed and the products were isolated as described in the Experimental section.

The pyrolysis conditions used in this experiment were known to afford about 0.43 mole of *p*-methylbenzyl radicals.[7] Twenty-five per cent of these radicals were isolated as β,β-dichloro-*p*-methylstyrene, 3% as *p*-methylbenzyl chloride, <1% as α,α'-bis-trichloromethyl-*p*-xylylene, 47% as a mixture of 1,2-di-*p*-tolylethane and diphenylmethanes, and 24% as an ill defined non-distillable residue,[4,5] which probably formed as a result of decomposition of chlorocarbons during the separation by vacuum distillation. Carbon tetrachloride and tetrachloroethylene were also produced in some amount, but these were only identified qualitatively by mass spectrometric analysis.

The fact that the amount of β,β-dichloro-*p*-methylstyrene isolated was eight times greater than the amount of *p*-methylbenzyl chloride isolated demonstrates that C–C bond rupture of hexachloroethane to give CCl_3 radicals is the initiating reaction.

The isolation of about two grams of α,α'-bis-trichloromethyl-*p*-xylene indicated that the C–C bond

(1) This work was done in the laboratories of the M. W. Kellogg Company. The data were acquired by the Minnesota Mining and Manufacturing Company with the purchase of the Chemical Manufacturing Division of the M. W. Kellogg Company in March, 1957.

(2) F. S. Dainton and K. J. Ivin, *Trans. Faraday Soc.*, **46**, 295 (1950).

(3) L. A. Errede, *J. Phys. Chem.*, **64**, 1031 (1960); **65**, 2262 (1961); *J. Org. Chem.*, **27**, 3425 (1962).

(4) Paper XVI: L. A. Errede and J. P. Cassidy, *J. Phys. Chem.*, **67**, 69 (1963).

(5) Paper XVII: L. A. Errede and J. P. Cassidy, *ibid.*, **67**, 73 (1963).

(6) Paper XVIII: L. A. Errede and J. P. Cassidy, *J. Org. Chem.*, **28**, 1059 (1963).

(7) L. A. Errede and F. DeMaria, *J. Phys. Chem.*, **66**, 2664 (1962).

of hexachloroethane must continue to rupture at an appreciable rate, even in the post-pyrolysis zone, since it was demonstrated that *p*-xylylene does not accumulate to any appreciable amount until the pyrolyzate has cooled to about 700° at a point 5 inches away from the pyrolysis zone of the furnace.[5]

Experimental

The pyrolysis system shown in Fig. 1 of ref. 8 was modified to include a flask containing a weighed amount of hexachloroethane (419 g.) which was located between manometer 11 and the furnace 10. The temperature of this flask was kept at 95°. The pyrolysis system was evacuated to 5 mm. pressure and *p*-xylene (672 g.) was metered to the system at the rate of 0.035 mole/min. as described previously.[8] The gas stream passed through the flask containing warm hexachloroethane into the pyrolysis furnace where co-pyrolysis occurred at 1000° for an average residence time of 0.006 sec. The pyrolysate was collected in toluene (3.1) kept at −78°. At the end of the pyrolysis the resultant solution was warmed to room temperature and volatile components were removed by rapid evaporation at 100° and 60 mm. pressure. A sample of the distillate was analyzed by means of a mass spectrometer and the presence of tetrachloroethylene and carbon tetrachloride in small amounts was detected. The residue (95 g.) was stored at room temperature for several days. A small amount (2.1 g.) of needle-like crystals precipitated from the dark oil. These were removed by filtration and washed with hexane. The product was purified by vacuum sublimation at 100° and subsequent recrystallization from methanol to give pure white needles of α,α'-bis-trichloromethyl-*p*-xylene (also named *p*-bis-(β,β,β-trichloroethyl)-benzene; m.p. 174–175°) showing no depression with an authentic sample prepared and identified as described in a previous publication.[6] The infrared spectrum of this product was identical with that reported earlier.[6]

The oily mother liquor was dissolved in hexane and the resultant solution was chilled to −78° to precipitate any additional α,α'-bis-trichloromethyl-*p*-xylene or *p*-xylylene dichloride. No precipitate formed, however, and the hexane was separated by distillation at atmospheric pressure and the residue was separated further by distillation at 2.4 mm. to afford 5 major fractions: (1) 2 g., b.p. 70–90°, (2) 20.2 g., b.p. 96–97°, (3) 10.0 g., b.p. 120–135°, (4) 11.8 g., b.p. 135–150°, and (5) 15 g., residue. Fraction 1 was mostly *p*-methylbenzyl chloride and fraction 2 was almost pure β,β-dichloro-*p*-methylstyrene[4] as indicated by infrared analysis. Fraction 2 was recrystallized from methanol to yield 15 g. of β,β-dichloro-*p*-methylstyrene in the form of white platelets (m.p. 32.5–33.5°). The third and fourth fractions were identified by infrared analysis as mixtures of 1,2-di-*p*-tolylethane and alkylated diphenylmethanes. These were combined and dissolved in methanol. The solution was chilled to −78° and 1,2-di-*p*-tolylethane (6 g.) crystallized from solution in the form of pearl-white platelets (m.p. 74–76°).[9] Fraction 5 was a complex mixture of decomposition products containing phenyl and olefinic groups as indicated by infrared analysis and chlorine as indicated by a qualitative test for halogen.

(8) L. A. Errede and B. F. Landrum, *J. Am. Chem. Soc.*, **79**, 4952 (1957).
(9) L. A. Errede and J. P. Cassidy, *ibid.*, **82**, 3653 (1960).

ON THE CALCULATION OF THERMAL TRANSPIRATION

By George A. Miller

School of Chemistry, Georgia Institute of Technology, Atlanta, Georgia

Received November 2, 1962

On the basis of the fundamental studies of a number of workers[1-6] Weber[7] developed his equation for the thermal transpiration of a gas along a closed cylindrical tube

$$\frac{dP}{dT} = \frac{P}{2T}\frac{1}{\alpha y^2 + \beta y + \mu}, \qquad y = d/\lambda \qquad (1)$$

where P is the pressure, T is the absolute temperature, d is the inside diameter of the tube, λ is the mean-free-path of the gas molecules, and the coefficients are given by the relations

$$\alpha \simeq \pi/128$$
$$\beta \simeq \pi/12$$
$$\mu = (1 + gy)/(1 + hy)$$
$$g - h + \beta = 1 \text{ or } {}^3/_4$$
$$g/h \simeq 1.25$$

Because thermal transpiration involves a transport phenomenon in a rarified gas, for which the usual methods of kinetic theory fail, the derivation of equation 1 contains a number of approximations. In particular a model is assumed in which the gas molecules are hard spheres of temperature dependent size, which undergo no specular reflection off the walls of the tube. Nevertheless, in view of the difficulty of determining pressures in the important submillimeter range, the existing body of thermal transpiration data should be considered with the same degree of reservation as the theory.

As pointed out by Weber, a useful approximate solution to equation 1 may be obtained by treating the left side as a quotient of finite differences. The solution may then be cast into one of several generalized forms in which a function of the temperature and pressure at the ends of the tube is obtained which is independent of the nature of the gas and the size of the tube. At present this approach is to be preferred not so much because the exact integration is tedious but because it permits data to be combined on a single, generalized plot. In this way it is indeed found difficult to reconcile sets of data from various sources with one another on the basis of any reasonable critique of the theory.

The solution suggested here is

$$\frac{dP}{dT}\frac{2T}{P} \simeq \frac{\Delta P}{\Delta T}\frac{2T}{P} \simeq \frac{1 - (P_1/P_2)}{1 - (T_1/T_2)^{1/2}} \equiv \Pi$$

$$\Pi = \frac{1}{\alpha y^2 + \beta y + \mu}, \quad T_2 > T_1 \qquad (2)$$

where y is some mean value between $y(P_1, T_1)$ and $y(P_2, T_2)$. This solution is exact in the limits where the theory is exact according to the relations

$$\lim_{y \to 0} (P_1/P_2) = (T_1/T_2)^{1/2}$$
$$\lim_{y \to \infty} (P_2 - P_1) = 0$$

The parameter y is calculated through the kinetic theory relation

$$\lambda P = kT/\pi(2)^{1/2}\sigma^2$$

where k is the Boltzmann constant and σ is the molecular hard sphere diameter. In the usual experimental arrangement P_2, T_2, and T_1, are known quantities and P_1 is to be calculated. The following convenient choice of y is made to avoid dependence on P_1

(1) J. C. Maxwell, *Phil. Trans. Roy. Soc.*, **170**, 231 (1879).
(2) M. Knudsen, *Ann. Physik*, **28**, 75 (1909); **31**, 205 (1910).
(3) G. Hettner, *Z. Physik*, **27**, 12 (1924).
(4) M. Czerny and G. Hettner, *ibid.*, **30**, 258 (1924).
(5) A. Sterntal, *ibid.*, **39**, 341 (1926).
(6) T. Sexl, *ibid.*, **52**, 249 (1928).
(7) S. Weber, *Commun. Phys. Lab. Univ. Leiden*, No. 246b (1937).

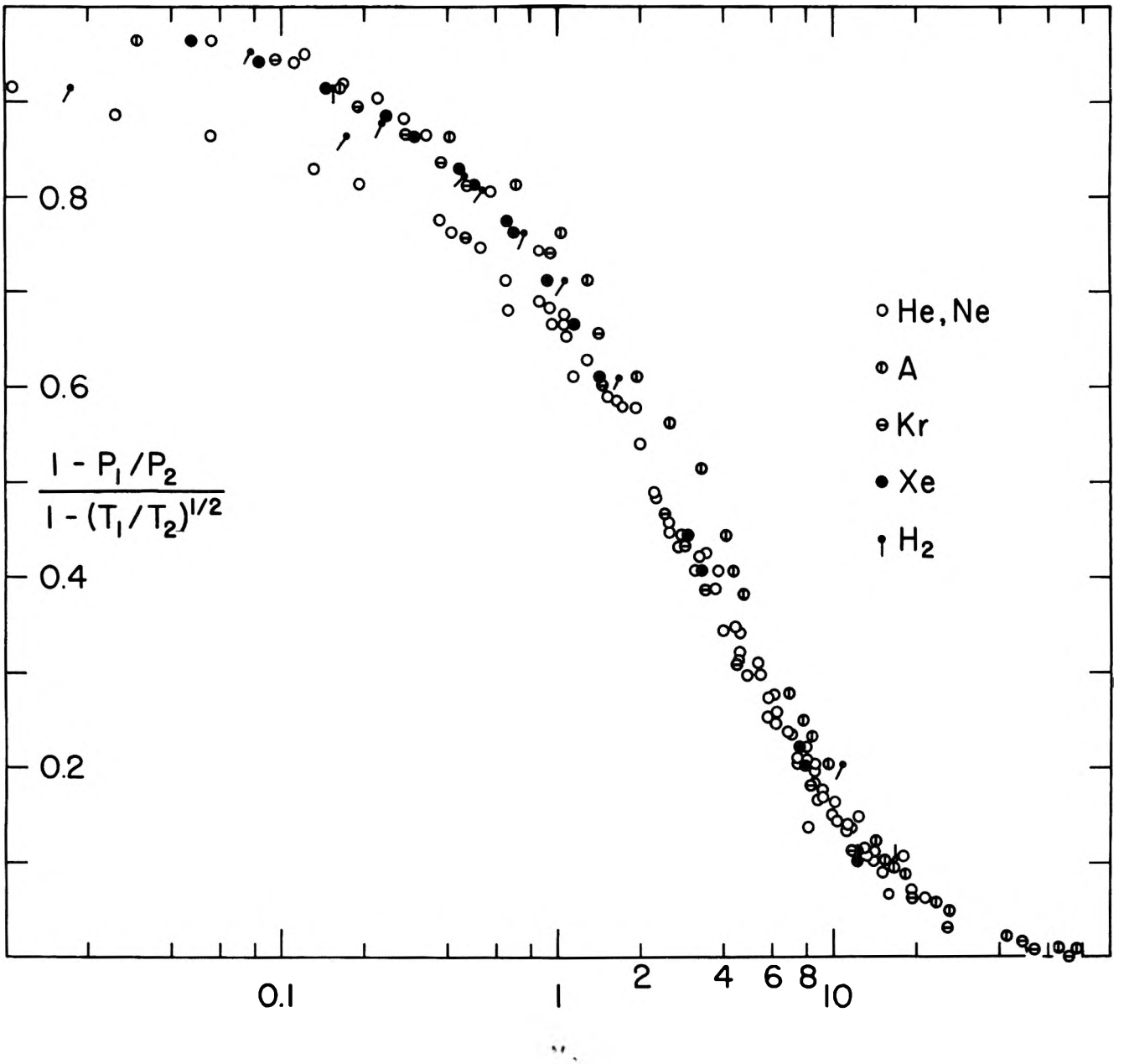

Fig. 1.—A generalized plot of thermal transpiration data from various sources: (gas, T_1/T_2) hydrogen and helium,[10] 90/273°K.; helium and neon,[11] 13.5, 20.4, 69, 90/297°K.: helium and argon,[12] 77, 195/297°K.; argon,[13] 77, 193/301°K.; krypton,[14] 78/299°K.: krypton,[15] 78/297°K.; neon, argon, xenon, and hydrogen,[16] 77, 90/299°K.

$$y = d/\lambda = P_2 d\pi(2)^{1/2}\sigma^2/kT = (P_2 d\sigma^2/2.33T) \times 10^3 \quad (3)$$

where P_2 is in mm., d is in mm., σ is in Å., and $T = (T_1 + T_2)/2$.

The hard sphere diameter is based on the experimental value of the coefficient of viscosity at the average temperature, T. Values of σ as a function of T have been tabulated for a number of gases.[8] Alternately, σ may be calculated from intermolecular force constants through the proper viscosity formulas. For the Lennard-Jones (12-6) potential the relation is

$$\sigma^2 = \sigma_{LJ}^2 \left(\frac{\Omega^{(2,2)*}(kT/\epsilon)}{0.984 f^{(3)}} \right)$$

where the symbols have the usual meaning.[9]

(8) Landolt-Börnstein, "Zahlenwerte und Funktionen," Sections 13 241 and 13 242, Springer-Verlag, Berlin, 1950–1951.

(9) J. O. Hirschfelder, C. F. Curtiss, and R. B. Bird, "Molecular Theory of Gases and Liquids," John Wiley and Sons, Inc., New York, N. Y., 1954.

Figure 1 is the generalized plot of data for the inert gases and hydrogen from a number of sources.[10–16] The scatter seems to lack any meaningful trends and, if anything, emphasizes the difficulty in measuring the thermal transpiration effect. However, certain sets of data points for hydrogen and helium (Weber and Schmidt), krypton (Rosenberg; Rosenberg and Martell), and xenon (Podgurski and Davis) fall consistently together. Another set for helium and neon (van Itterbeek and de Grande) deviate only at the lowest pressures. These four sets of data also agree reasonably well with equation 2 using Weber's approximate values for α and

(10) S. Weber and G. Schmidt, *Commun. Phys. Lab. Univ. Leiden*, No. 246c (1937).

(11) A. van Itterbeek and E. de Grande, *Physica*, **13**, 289 (1947).

(12) S. C. Liang, *J. Appl. Phys.*, **22**, 148 (1951).

(13) J. M. Los and R. R. Fergusson, *Trans. Faraday Soc.*, **48**, 730 (1952).

(14) A. J. Rosenberg, *J. Am. Chem. Soc.*, **78**, 2929 (1956).

(15) A. J. Rosenberg and C. S. Martell, Jr., *J. Phys. Chem.*, **62**, 457 (1958).

(16) H. H. Podgurski and F. N. Davis, *ibid.*, **65**, 1343 (1961).

β, and setting $g = 2.5$ and $h = 2$. The function Π is insensitive to g and h within the limits set by Weber for these two coefficients. Furthermore, these four sets of data represent a combination of techniques of pressure measurement, namely, the Pirani gage, an adsorption technique, the McLeod gage, and a vapor pressure technique. An adjustment of α and β has been made on the basis of these data alone. Values of β were first calculated with $\alpha = \pi/128$ for each data point in the region $y < 4$. The average value of β so obtained was used to calculate an average value of α for the data in the region $y > 4$. The calculation was repeated until consistent average values of the coefficients were obtained (Table I). The final form of equation 2 was

$$\Pi = \left(0.0300y^2 + 0.245y + \frac{1 + 2.5y}{1 + 2y}\right)^{-1} \quad (4)$$

TABLE I

THERMAL TRANSPIRATION CONSTANTS CALCULATED FROM DATA

Source	Gas		α ($\beta = 0.245$) ($g = 2.5$) ($h = 2$) ($y > 4$)	β ($\alpha = 0.0300$) ($g = 2.5$) ($h = 2$) ($y < 4$)
Ref. 10	H_2, He		...	0.181
Ref. 11	He, Ne		0.0271	.302
Ref. 14, 15	Kr		.0322	.262
Ref. 16	Xe		.0306	.234
		Av.	.0300	.245

It is seen from the selected values in Table II that there is little choice between the fitted coefficients in equation 4 and the approximate values listed under

TABLE II

SELECTED VALUES OF THE GENERALIZED COÖRDINATES FOR THERMAL TRANSPIRATION

	Π	
	$\alpha = \pi/128$ $\beta = \pi/12$ $g = 2.5$ $h = 2$	$\alpha = 0.0330$ $\beta = 0.245$ $g = 2.5$ $h = 2$
y		
0.01	0.993	0.993
.02	.985	.985
.04	.971	.972
.065	.956	.957
.1	.937	.938
.2	.889	.890
.4	.819	.823
.65	.757	.761
1.0	.687	.693
2.0	.549	.553
4.0	.375	.373
6.5	.252	.245
10	.158	.150
20	.061	.055
40	.0195	.0169
65	.0082	.0070
100	.0037	.0031

equation 1. For the four preferred sets of data the average deviation of Π from values calculated with equation 4 is 0.016; in the region $1 < y < 5$, the average deviation is 0.022. Equations 3 and 4 may be used to estimate the thermal transpiration ratio, P_1/P_2, for any gas for which the prerequisite viscosity data are available.

Over the entire pressure range the value of μ has the limits $1 < \mu < 1.25$. If μ is arbitrarily set at unity, one obtains what is essentially Liang's empirical equation,[17] along with the following relations for Liang's coefficients

$$\alpha_{He} = \alpha(\sigma_{He}^2 \times 10^3/2.33T)^2 \simeq 1.1 \times 10^5/T^2$$

$$\beta_{He} = \beta(\sigma_{He}^2 \times 10^3/2.33T) \simeq 5.6 \times 10^2/T$$

$$\varphi_g = \sigma^2/\sigma_{He}^2$$

$$T = (T_1 + T_2)/2$$

$$\alpha \simeq \pi/128,\ \beta \simeq \pi/12,\ \sigma_{He}^2 \simeq 5\ \text{Å}.^2$$

The rather different relations generally used with the Liang equation[17,18] are not of sufficient generality to apply if T_2 differs appreciably from room temperature. The small correction factor for the Liang equation at low pressures[15] may be accounted for by the fact that μ actually approaches unity only at very low pressures.

(17) S. C. Liang, *J. Phys. Chem.*, **57**, 910 (1953).

(18) M. J. Bennett and F. C. Tompkins, *Trans. Faraday Soc.*, **53**, 185 (1957).

THE COUPLING OF NUCLEAR SPINS OF PROTONS IN TWO ALLENES

BY R. K. KULLNIG AND F. C. NACHOD

Sterling-Winthrop Research Institute, Rensselaer, New York

Received October 17, 1962

We have observed the coupling of nuclear spins of the allenic protons in 2,2-dimethyl-3,4-octadienal (I)[1] and found the magnitude of the coupling constant ($J = 6.3$ c.p.s.) in good agreement with the findings of previous investigators of allenic compounds.[2-4] Unfortunately, experiments which are suitable to determine the sign of the coupling constant are beyond the scope of the Varian A-60 spectrometer. The

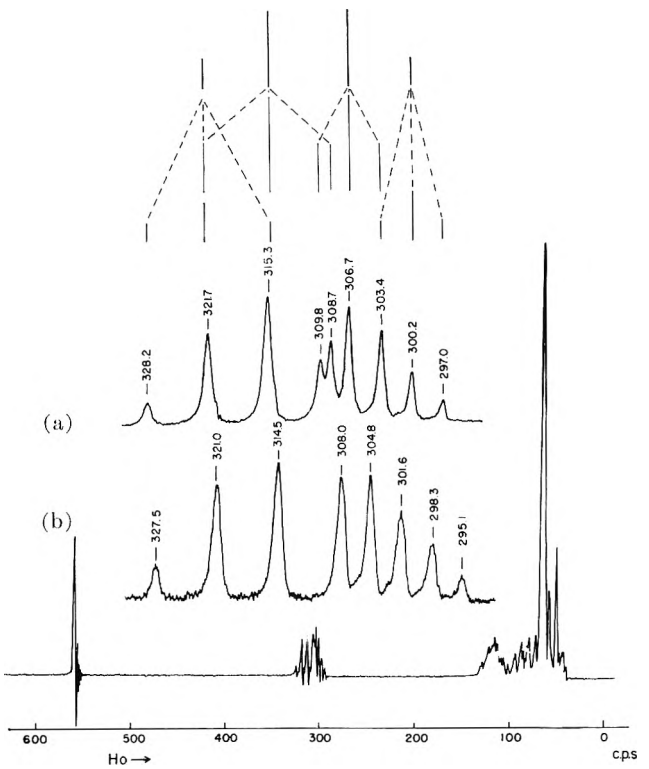

Fig. 1.—Proton resonance spectrum of 2,2-dimethyl-3,4-octadienal. Proton signal of C^5H and C^3H insert (a) neat; insert (b) 20% solution in CCl_4.

(1) The samples were obtained from Eastman Chemical Products, Inc., Kingsport, Tennessee.

(2) E. B. Whipple, J. H. Goldstein, and W. E. Stewart, *J. Am. Chem. Soc.*, **81**, 4761 (1959).

(3) S. L. Manatt and D. D. Elleman, *ibid.*, **84**, 1579 (1962).

(4) E. I. Snyder and J. D. Roberts, *ibid.*, **84**, 1582 (1962).

TABLE I

2,2-DIMETHYL-3,4-OCTADIENAL

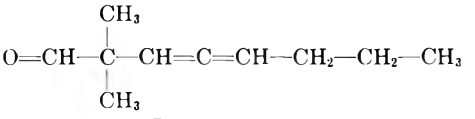

I

O=CH—	—C(CH3)2—	—CH=	C=CH	—CH2—CH2—CH3			
562	68	304.2	317.7	43–135	Neat	}	c.p.s. from TMS (internal standard)
560	67	302.2	317.0	45–137	20% in CCl_4	}	
1	6	1	1	7	Intensities		
Singlet sharp	Singlet sharp	See insert of Fig. 1		Complex of bands partially resolved			

TABLE II

2-BUTYL-2-ETHYL-5-METHYL-3,4-HEXADIENAL

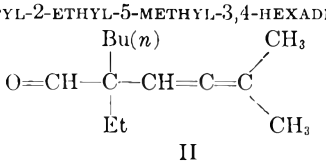

II

O=CH—	—C(Bu(n))(Et)—	CH=C=	C(CH3)2			
562	37–100	295	102	Neat	}	c.p.s. from TMS (internal standard)
558	37–100	292	102	20% in CCl_4	}	
1	14	1	6	Intensities		
Singlet sharp	Complex partially resolved	Septet resolved	Doublet resolved			

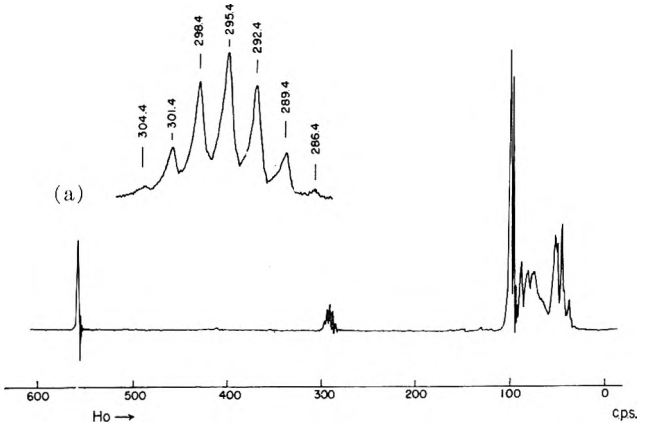

Fig. 2.—Proton resonance spectrum of 2-butyl-2-ethyl-5-methyl-3,4-hexadienal. Proton signal of C^3H: insert (a).

coupling between the spins of the C^6-methylene and the C^5-proton ($J_{5,6}$ = 6.5 c.p.s.) is the same as that of comparable protons in other olefins.[5] The coupling between the spins of the C^6-methylene and the C^3-proton ($J_{3,6}$ = 3.3 c.p.s.) compares well with a comparable parameter which was determined from the n.m.r. spectrum of 3-methyl-1,2-butadiene by Snyder and Roberts.[4] Similarly, the spin-coupling between the protons of the terminal methyl groups and the allenic proton in 2-butyl-2-ethyl-5-methyl-3,4-hexadienal (II)[1] was found to have about the same coupling constant (J = 3.0 c.p.s.).

No evidence of any spin-coupling between the allenic protons and the protons of the substituents on C_2 of either compound could be detected. The signal for the C^2-methyl groups of I was sharp, and the signal of the C^3 proton of II is a well resolved septet (*cf.* Tables I and II).

(5) J. A. Pople, W. G. Schneider, and H. J. Bernstein, "High-Resolution Nuclear Magnetic Resonance," McGraw-Hill Book Co., New York, N. Y., 1959, p. 238 (Table 11-2), p. 242 (Table 11-3).

MUTUAL DIFFUSION IN NON-IDEAL LIQUID MIXTURES. IV. METHANOL–CARBON TETRACHLORIDE AND DILUTE ETHANOL–CARBON TETRACHLORIDE SOLUTIONS

BY D. K. ANDERSON AND A. L. BABB

Department of Chemical Engineering, University of Washington, Seattle, Washington

Received August 20, 1962

In previous papers[1,2] the authors presented diffusion data for associated binary liquid systems. As part of this continuing program, diffusivities have been measured for dilute solutions of ethanol in carbon tetrachloride and the methanol–carbon tetrachloride system over the entire concentration range.

The mutual diffusion coefficients were measured using a Mach–Zehnder diffusiometer described fully elsewhere.[3] Temperatures were controlled at 25.0 ± 0.05°. The reagent grade solvents were obtained from Mallinckrodt Chemical Works and were used without further purification.

The diffusivities were obtained by measuring the interdiffusion of two solutions of very nearly equal concentration. The measured value was taken to be that of a solution with a concentration equal to the average of the two. The results are given in Tables I and II.

Although data were previously available[4] for the ethanol–carbon tetrachloride system, a series of deter-

(1) D. K. Anderson and A. L. Babb, *J. Phys. Chem.*, **65**, 1281 (1961).
(2) D. K. Anderson and A. L. Babb, *ibid.*, **66**, 899 (1962).
(3) C. S. Caldwell, J. R. Hall, and A. L. Babb, *Rev. Sci. Instr.*, **28**, 816 (1957).
(4) B. R. Hammond and R. H. Stokes, *Trans. Faraday Soc.*, **52**, 781 (1956).

TABLE I

SUMMARY OF EXPERIMENTAL DIFFUSIVITIES FOR DILUTE SOLUTIONS OF ETHANOL IN CARBON TETRACHLORIDE

Mole fraction ethanol in soln. A	0	0	0.0023	0.0035	0.0116	0.0231
Mole fraction ethanol in soln. B	0.0046	0.0100	.0114	.0143	.0205	.0326
Av. mole fraction	0.0023	0.0050	.0069	.0089	.0160	.0279
$D_{AB} \times 10^5$, cm.²/sec.	1.901	1.756	1.635	1.499	1.168	.993

TABLE II

SUMMARY OF EXPERIMENTAL DIFFUSIVITIES FOR METHANOL–CARBON TETRACHLORIDE

Mole fraction methanol in soln. A	0	0	0.0055	0.0132	0.0952	0.2020	0.393	0.596	0.793	0.900	0.996
Mole fraction methanol in soln. B	0.00513	0.0108	.0145	.0201	.1076	.2108	.405	.602	.801	.896	1.000
Av. mole fraction	0.00256	0.0054	.0100	.0167	.1014	.2064	.399	.599	.797	.898	0.998
$D_{AB} \times 10^5$, cm.²/sec.	2.446	2.173	1.769	1.363	.710	.556	.489	.799	1.264	1.723	2.248

minations was made for solutions dilute in alcohol so that the data could be extrapolated to pure carbon tetrachloride. This was necessary for calculations being made at the time.

Acknowledgment.—This work was supported by the U. S. Army Research Office (Durham).

THE VAPOR PRESSURE OF SOLID DECABORANE

BY GEORGE A. MILLER

School of Chemistry, Georgia Institute of Technology, Atlanta, Georgia

Received November 9, 1962

This paper presents results of the measurement of the vapor pressure of decaborane ($B_{10}H_{14}$) in the range of about 10^{-5} to 10^{-3} mm. These results have been combined with vapor pressure data in the vicinity of the triple point and the thermodynamic properties of the solid, liquid, and gas in a third law calculation. It is found that the internal consistency of these data is good enough to permit a reliable calculation of the heat of sublimation at 25°.

Experimental

The vapor pressure of solid decaborane was measured with a Knudsen gage and special procedure, described earlier in connection with the measurement of the vapor pressure of naphthalene.[1] From a maximum deflection measurement[2] the collision diameter of the $B_{10}H_{14}$ molecule was found to be about 9.6 Å. at room temperature. This value was used in an approximate form of the Weber equation[3] to calculate the thermal transpiration effect between sample and gage. It was found that the Knudsen limiting law was actually accurate enough for this purpose.

Decaborane was obtained from the Olin Mathesen Corporation and purified by a special procedure of slow sublimation *in vacuo*.[4] The purified sample was resublimed *in vacuo* into the sample bulb. During the period of measurement, which lasted three weeks, the sample decomposed very slowly, although it was kept at low temperatures. This was evidenced by a build-up of hydrogen above the sample to sub-micron pressures from one day to the next. The hydrogen could be detected by the fast rate at which it could be pumped off into the vacuum system proper. During measurement of the vapor pressure, the sample was pumped at least once every 30 min. No detectable amount of hydrogen could form in this period of time. The other products of decomposition were assumed to be boranes of negligible vapor pressure.[5] In fact, the vapor pressure was not found to change with time.

Smoothed values of the vapor pressure were obtained from the best straight line fit to a plot of log P *vs.* $1/T$ (Fig. 1). The estimated reliability is ±5% in the middle of the range and somewhat less (about ±10%) at either extreme. The four values used in the calculations below are

T, °K.	$1000/T$	log P, mm.
240	4.167	0.387–5
250	4.000	0.047–4
260	3.846	0.657–4
270	3.704	0.219–3

TABLE I

THERMODYNAMIC FUNCTIONS OF IDEAL GASEOUS DECABORANE IN CALORIES PER MOLE PER DEGREE

T, °K.	$\left(\frac{H^0 - H_0^0}{T}\right)$	$\left(\frac{H_0^0 - G^0}{T}\right)$
240		60.602
250		61.254
260		61.908
270		62.565
280		63.225
290	19.288	63.888
300	20.057	64.555
310		65.225
320		65.899
330		66.576
340		67.257
350		67.941
360		68.628
370	25.587	69.318
380	26.385	70.011

Results

The equations used to relate the vapor pressure (P) and the latent heat of vaporization (L) with the thermodynamic functions of solid, liquid, and vapor are

$$-RT \ln P = \Delta(G^0 - H_0^0) + \Delta H_0^0 \qquad (1)$$

$$L = \Delta H^0 = \Delta(H^0 - H_0^0) + \Delta H_0^0 \qquad (2)$$

They are valid if the vapor is ideal and if the standard state of the condensed phase is at the saturation pressure. The equation of state of decaborane vapor is not known; however, since the highest pressure under consideration is 25 mm., the lack of knowledge of the gas imperfection terms is not serious.

The thermodynamic functions for the condensed phase at saturation pressure and the vapor pressure near the triple point (371.93°K.) are given by Furukawa and Park.[6] Thermodynamic functions for the ideal gas at one atmosphere were calculated for the rigid-rotor harmonic-oscillator approximation, using molecular constants recommended by Evans[7] (Table I).

From the results of the calculation of ΔH_0^0 with equation 1 at ordinary and very low pressures (Table II), there appears to be no appreciable, long range drift in this quantity with temperature. The drift in ΔH_0^0

(1) G. A. Miller, *J. Chem. Eng. Data*, **8**, 69 (1963).
(2) G. A. Miller, *Rev. Sci. Instr.*, **33**, 8 (1962).
(3) G. A. Miller, *J. Phys. Chem.*, **67**, 1359 (1963).
(4) A. Haaland, Thesis, Georgia Institute of Technology, 1961.
(5) B. Siegel and J. L. Mack, *J. Phys. Chem.*, **62**, 373 (1958).
(6) G. T. Furukawa and R. P. Park, *J. Res. Natl. Bur. Std.*, **55**, 255 (1955).
(7) W. H. Evans, private communication.

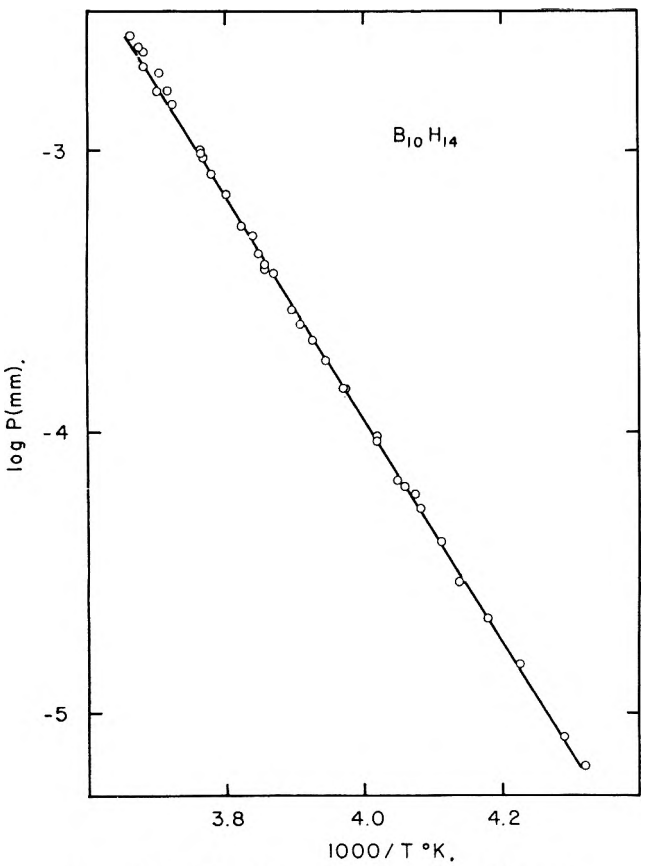

Fig. 1.—Decaborane vapor pressure data, this work.

between 240 and 270°K. (68 cal.) probably reflects the uncertainty in the vapor pressure data, since 68 cal. would correspond to an error in P of only 13%. From the calorimetric value of L at 378°K.,[6] one obtains, with eq. 2, ΔH_0^0 = 19171 cal./mole. Thus it appears that the vibrational frequency assignment used in these calculations[7] is essentially correct.

TABLE II

VALUES OF ΔH_0^0 OF SUBLIMATION OF DECABORANE FROM VAPOR PRESSURE DATA

T, °K.	$\Delta(H^{0} - G^{0})$	$-RT \ln P$	ΔH^{0}
240	10890	8230[a]	19120
250	11328	7818[a]	19146
260	11761	7405[a]	19166
270	12193	6995[a]	19188
345.45	15349	3662[b]	19011
355.12	15739	3411[b]	19150
361.81	16008	3108[b]	19116
371.53	16378	3049[b]	19427
		liquid	
371.93	16410	2754[c]	19164
380	16615	2546[c]	19161

[a] This work, from smoothed values of the vapor pressure. Reference 6, experimental values of the vapor pressure. [c] Reference 6, smoothed values of the vapor pressure as represented by the equation $\log P(\text{mm.}) = -4225.345/T - 0.0107975T + 6.63911$.

The above calculations would seem to indicate an over-all value, ΔH_0^0 = 19.16 ± 0.02 kcal./mole. This value may be used in eq. 1 and 2 to calculate the following quantities for decaborane at 25°: heat of sublimation, 18.33 kcal./mole; standard free energy of vaporization, 5.77 kcal./mole; vapor pressure, 4.48 × 10^{-2} mm. Alternately, the calorimetric value of L at 378°K. may be corrected to 25° by use of the enthalpy functions. The result is also 18.33 kcal./mole for the heat of sublimation at 25°.

THE POTENTIOMETRIC MEASUREMENT OF ION-PAIR DISSOCIATION CONSTANTS. THE ALKALI CHLORIDES AND $(CH_3)_4NCl$ IN 70% DIOXANE–30% WATER[1]

By E. LEE PURLEE[2] AND ERNEST GRUNWALD

Chemistry Department, Florida State University, Tallahassee, Fla.

Received November 16, 1962

Some years ago[3] we described a potentiometric method for measuring ion-pair dissociation constants, based on the cell represented in eq. 1.

Glass electrode/HCl(c_1), MCl(c_2), in

70.00 wt. % dioxane–30.00 wt. % water/AgCl–Ag (1)

We showed that this cell accurately measures the activity product, $a_H a_{Cl}$, of the ions of hydrochloric acid. Using a plausible and consistent method of allowing for long-range interionic effects,[3,4] we then could calculate the concentration product, $c_H c_{Cl}$, of the dissociated ions. Data for cells with $c_2 = 0$ thus enable us to obtain the ion-pair dissociation constant of hydrochloric acid (since $c_H = c_{Cl} < c_1$), the precision of fit to the data being excellent. Data for cells containing a mixed electrolyte, *e.g.*, HCl and NaCl, enabled us to evaluate not only c_H and c_{Cl}, but also the concentration of free sodium ions ($c_{Na} = c_{Cl} - c_H$) and of NaCl ions pairs ($c_{NaCl} = c_2 - c_{Na}$) in each solution. Although this method of studying the ion-pair dissociation of NaCl is rather indirect, the precision of the dissociation constants, K_d, was very satisfactory, the standard deviation for a long series of experiments being less than 2%.

We now report an extension of this work to other chloride salts. The experimental and computational methods are identical with those used previously[3] and need not be described again. A typical set of experiments, to illustrate the range of c_1 and c_2 and the precision of K_d, is shown for CsCl in Table I. All measurements were made at 25.00°. The consistency of our new results with those reported previously was checked by a new series of measurements for NaCl. The new value of $10^3 K_d$ is 5.32 ± 0.14; the previous value was 5.35 ± 0.07.

TABLE I

POTENTIOMETRIC MEASUREMENT OF K_d FOR CESIUM CHLORIDE IN 70.00 WT. % DIOXANE–30.00 WT. % WATER AT 25°

$10^4 c_1$	$10^4 c_2$	$10^3 K_d$
2.880	8.376	2.62
5.610	8.159	2.72
8.204	7.953	2.80
10.669	7.758	2.82
9.192	3.774	2.55
8.609	7.070	2.75
8.095	9.972	2.70
7.639	12.547	2.62

Our potentiometric values of K_d for chloride salts

(1) This work was supported by the National Science Foundation.

(2) E. L. P. Newport News Shipbuilding and Dry Dock Co., Newport News, Va.

(3) E. L. Purlee and E. Grunwald, *J. Am. Chem. Soc.*, **79**, 1366 (1957).

(4) H. P. Marshall and E. Grunwald, *J. Chem. Phys.*, **21**, 2143 (1953).

are summarized in Table II. These values, in common with all values of ion-pair dissociation constants, are subject to an unavoidable determinate error, since they depend on the particular model chosen for calculating the long-range interionic effects. Thus, for KCl in 70% dioxane–30% water at 25°, our potentiometric value of 10^3K_d is 2.35 ± 0.16, while the conductometric value reported recently by Lind and Fuoss[5] is 6.0 ± 0.2, or more than twice as large. A substantial part of this discrepancy results from a difference of models: Lind and Fuoss limit the concept of "ion pair" to a pair of ions at distance of closest approach, while the model used by us is more inclusive, allowing the interionic distance in the ion pair to extend to the Bjerrum distance $q = -z_1z_2e^2/2DkT$. We do not claim a fundamental superiority for the model on which the present values are based; nor do we profess a strong aesthetic preference, except that this model does fit the data better than other models we have tried.[3]

TABLE II

POTENTIOMETRIC K_d VALUES FOR CHLORIDE SALTS IN 70.00 WT. % DIOXANE–30.00 WT. % WATER AT 25°

Salt	10^3K_d	Salt	10^3K_d
HCl	6.67[3]	RbCl	2.57 ± 0.13
LiCl	2.87 ± 0.10	CsCl	2.70 ± .09
NaCl	5.32 ± .14	$(CH_3)_4NCl$	2.18 ± .08
KCl	2.35 ± .16[3]		

While the absolute values of K_d are thus uncertain, the relative values should be at least qualitatively correct. We may, therefore, infer from Table II that the dissociation constants for the various alkali halides are all quite similar in 70% dioxane–30% water, except for the markedly higher value obtained for NaCl. However, the relative tendency of alkali metal salts to dissociate depends markedly on the solvent. For example, the sequence of K_d values is Li > Na > K for iodides in methyl ethyl ketone,[6] K > Li > Na for picrates in pyridine, and K > Na >> Li for picrates in nitrobenzene.[7]

(5) J. E. Lind, Jr., and R. M. Fuoss, *J. Phys. Chem.*, **65**, 999 (1961).
(6) S. R. C. Hughes, *J. Chem. Soc.*, 634 (1947).
(7) C. A. Kraus, *J. Phys. Chem.*, **60**, 129 (1956).

N.M.R. SPIN-ECHO SELF-DIFFUSION MEASUREMENTS ON FLUIDS UNDERGOING RESTRICTED DIFFUSION

BY D. E. WOESSNER

Socony Mobil Oil Company, Inc., Field Research Laboratory, Dallas, Texas

Received December 10, 1962

The spin-echo technique for measuring self-diffusion coefficients in liquids[1-3] involves the attenuation of the spin-echo amplitude resulting from the diffusion of the molecules into regions having different values of applied magnetic field. For a two-pulse spin-echo from a liquid sample which experiences a uniform magnetic field gradient this attenuation is given by the relation

$$E/E_0 = \exp(-{}^2/_3\gamma^2G^2D\tau^3) \qquad (1)$$

in which γ is the nuclear gyromagnetic ratio, D is the bulk liquid self-diffusion coefficient, τ is the time interval between the two pulses, G is the magnetic field gradient along the direction of the applied magnetic field, E_0 is the echo amplitude when G is zero, and E is the spin-echo amplitude for the given G value. The derivation of this expression assumes that the diffusing molecules move in an infinite reservoir so that the Einstein relation $\langle(\Delta x)^2\rangle_{av} = 2D\tau$ holds.

Suppose, now, that the reservoir is not infinite so that the molecules experience physical barriers to their diffusive movements. The average displacement a molecule undergoes during a time interval τ should be less than that for an infinite reservoir. But as τ is decreased toward zero, the displacement of the average molecule should approach that for an infinite reservoir because fewer and fewer molecules move far enough to experience the barriers.

The size of the infinite reservoir to which eq. 1 applies is great enough so that the average distance between molecules and constrictive barriers is very large compared to $2(D\tau)^{1/2}$, the average distance a molecule moves in any direction during the time 2τ. For water at room temperature, this diffusion distance is 14 μ for $\tau = 0.02$ sec. The size which a reservoir must attain so that eq. 1 applies then, increases with increasing τ values.

Systems such as porous rocks and viscous colloidal suspensions should provide barriers so that eq. 1 no longer applies. This has been observed for water in a geological core and for water in aqueous suspensions of silica spheres. For τ values in the range of 0.01 to 0.03 sec., the values of E/E_0 were measured[4] as a function of G for fixed τ values. Plots of ln (E/E_0) *vs.* G^2 showed that ln (E/E_0) is directly proportional to G^2, as is the case for bulk liquids. These data can thus be interpreted by use of eq. 1 with the bulk liquid self-diffusion coefficient D replaced by a spin-echo diffusion coefficient D'.

For a qualitative discussion, one may use the relation $D' = \langle(\Delta x)^2\rangle_{av}/(4\tau)$, where $\langle(\Delta x)^2\rangle_{av}$ refers to the molecular displacement during 2τ. From the above considerations, one would expect D' to be a function of the diffusion distance $2(D\tau)^{1/2}$ and of the distance from molecules to barriers. In particular, D' should decrease as the ratio of diffusion distance to the molecule-to-barrier distance increases. Also, in the limit when $\tau = 0$, it is expected that $D' = D$; and with increasing values of τ, D' should decrease. These expectations are in agreement with the following data. When τ becomes long enough so that the diffusion distance is very large compared to the average molecule-to-barrier distance, D' should become independent of τ and be the diffusion coefficient obtainable by conventional means. This will occur when the relation $\langle(\Delta x)^2\rangle_{av} = 2D't$ holds for all $t > t_m$ such that $t_m << \tau$.

Since ln (E/E_0) is directly proportional to G^2, values of D' were determined by use of one non-zero G value. Figure 1 shows values of D'/D as a function of τ for two silica suspensions with water-to-silica weight ratios (X/m) of 3.65 and 7.50. The ultimate silica particles[5] are spheres of about 12 mμ diameter. They are aggregated into chain-like structures. The plots appear to be linear, D' decreases with increasing value, and the values extrapolated to $\tau = 0$ are only about 8% less than D. The average molecule-to-barrier distance

(1) H. Y. Carr and E. M. Purcell, *Phys. Rev.*, **94**, 630 (1954).
(2) D. C. Douglass and D. W. McCall, *J. Phys. Chem.*, **62**, 1102 (1958).
(3) D. E. Woessner, *J. Chem. Phys.*, **34**, 2057 (1961).
(4) D. E. Woessner, *Rev. Sci. Instr.*, **31**, 1146 (1960).
(5) A micro-fine precipitated silica, Quso F-20, Philadelphia Quartz Company, Philadelphia, Pennsylvania, was used.

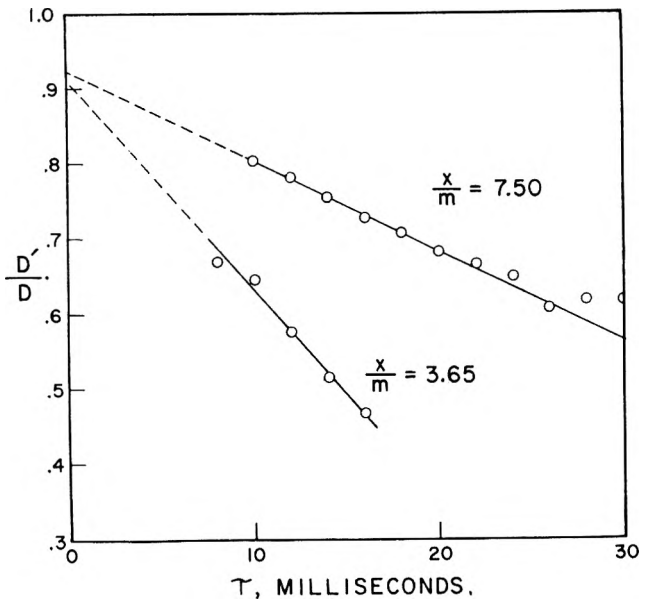

Fig. 1.—Relative spin-echo self-diffusion coefficients D'/D *vs.* τ for water in silica suspensions of water-to-silica weight ratios X/m.

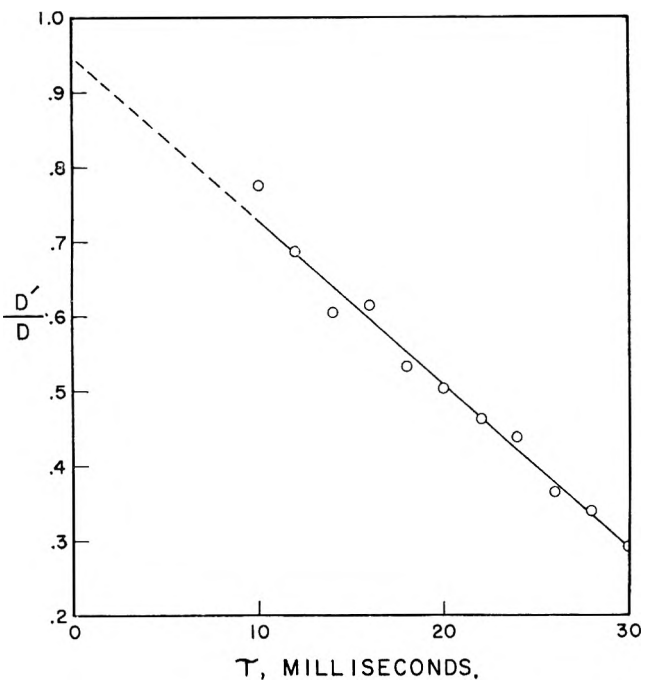

Fig. 2.—Relative spin-echo self-diffusion coefficients D'/D *vs.* τ for water in a saturated sandstone core (33% porosity, 22–28 μ median pore size).

for $X/m = 3.65$ is the smaller of the two values and D' is also smaller for this X/m value. The diffusion distance for water at room temperature for $\tau = 10$ msec. is $2(D\tau)^{1/2} = 9.7$ μ. If the water were uniformly distributed as spherical shells around the spheres, the median molecular distance to the nearest sphere would be 7 mμ for $X/m = 7.50$. Hence, even though the spheres are aggregated into chains, the average water molecule should have experienced the barrier during the 2τ values used in these measurements.

The data for water in a geological core (sandstone, 33% porosity, 22 to 28 μ median pore size) are given in Fig. 2. The plot is similar to that for the silica suspensions. If the pores were cylinders of 25 μ diameter, the median molecular distance to the pore wall would be 3.7 μ. This kind of geometry is evidently much

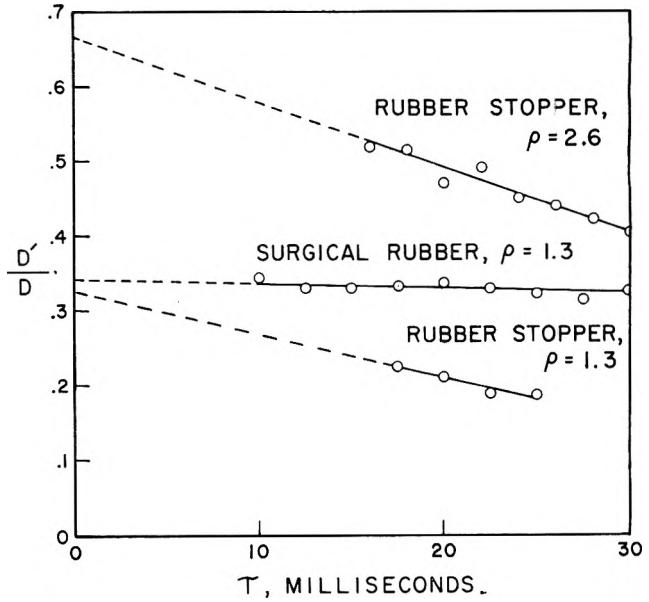

Fig. 3.—Relative spin-echo self-diffusion coefficients D'/D *vs.* τ for benzene in benzene–rubber systems of benzene-to-rubber volume ratios ρ.

more effective in reducing D' than that in the silica suspension.

Spin-echo diffusion measurements were made on benzene–rubber systems. The polymer chains presumably would present barriers on a more microscopic scale. The D' data for benzene absorbed into a sample of surgical rubber and a piece of a rubber stopper are given in Fig. 3. Again the plots are linear. However the D' values for the surgical rubber are independent of τ while those for the rubber stopper do decrease with increasing τ values as in the preceding examples. Furthermore, the D' values extrapolated to $\tau = 0$ are only a fraction of D. The small dependence of D' on τ for the rubber stopper apparently reflects a barrier effect as in the above examples. This sample is likely to be more cross-linked than is the surgical rubber. In making these measurements, it was necessary to know whether the rubber protons contributed significantly to the spin-echo. By measuring the T_2 of the rubber protons when the rubber was expanded by absorbing carbon tetrachloride, it was determined that the rubber protons did not interfere with benzene spin-echoes.

These experiments show that studies of the diffusive motions of small molecules in polymers can be done by the spin-echo technique. Measurements can be extended to smaller τ values without interference from the polymer signals by using diffusing molecules with a different nucleus, such as fluorine, whose spin-echo is detected. An advantage of the spin-echo technique is that no concentration gradient is used.

The results of these experiments suggest that spin-echo-diffusion measurements on fluids contained in a lattice can yield information on both the diffusion of the molecules and on the characteristics of the lattice. Diffusion values from conventional techniques represent averages over microscopic structures taken over a long time. The spin-echo technique commonly measures values over a much shorter time, of the order of 0.01 sec. The dependence of D' on τ may yield information on the mean size of the cavities in which the liquid molecules reside when the cavities are large com-

pared to the molecular size. For the rubber systems, the D' values at $\tau = 0$ may represent the mobility of the benzene molecules among the polymer chains. The present experiments suggest that the extrapolated D' values are close to the true D' values at $\tau = 0$. This idea as well as the others presented here should be investigated by further experimental and theoretical studies.

Recently, other workers[6] have studied the diffusion of water in a sodium carboxymethyl cellulose gel by a different spin-echo method and a conventional diffusion method involving about 24 hours diffusion time. The two methods yielded the same diffusion coefficient values. For this system, the diffusion distance may be large compared to the average molecule-to-barrier distance.

(6) W. T. Higdon and J. D. Robinson, *J. Chem. Phys.*, **37**, 1161 (1962).

MERCURY PHOTOSENSITIZED ISOMERIZATION OF 1,5-HEXADIENE[1]

By R. Srinivasan

International Business Machines Corporation, Thomas J. Watson Research Center, Yorktown Heights, New York

Received December 14, 1962

It has recently been shown[2] that the mercury photosensitized isomerization of 1-butene leads to methylcyclopropane as one of the products. The quantum yield of the isomer was found to change with the pressure of 1-butene, the value going through a maximum at about 65 mm.

Since the double bonds in 1,5-hexadiene are both terminal and isolated from each other, the mercury-sensitized isomerization of this compound may be expected to resemble that of 1-butene.

Experimental

1,5-Hexadiene from K and K Laboratories (Jamaica 33, N. Y.) was used as obtained. Vapor phase chromatography showed that it contained a small amount of another hydrocarbon as an impurity but the latter did not seem to undergo photosensitized reactions in the system, since it was recovered unchanged.

The light source was a bank of 12 germicidal lamps (General Electric G8T5) arranged in a circle with their long axes parallel to the narrow (10 mm. diameter) cylindrical quartz cell. The intensity of the 2537 Å. line at the center of the cell was 7.3×10^{15} quanta/cc./sec.

A conventional vacuum line in which stopcocks were not excluded was used to degas the sample, evacuate the cell, and fill it. Irradiation was carried to conversions which ranged from about 10% at the lowest pressure to less than 1% at the highest pressure.

Product analysis was carried out by gas chromatography on a 2-meter Ucon oil column (Perkin–Elmer Column R_x) at room temperature.

Results

Mercury-sensitized decomposition of 1,5-hexadiene gave two isomeric products as well as numerous other products which are believed to be of free radical origin. The isomers were identified to be allylcyclopropane (I) and bicyclo[2.1.1]hexane (II).

(1) This is part II of "Kinetics of the Photochemical Dimerization of Olefins to Cyclobutane Derivatives." For part I, see *J. Am. Chem. Soc.*, **84**, 4141 (1962).

(2) R. J. Cvetanovic and L. C. Doyle, *J. Chem. Phys.*, **37**, 543 (1962).

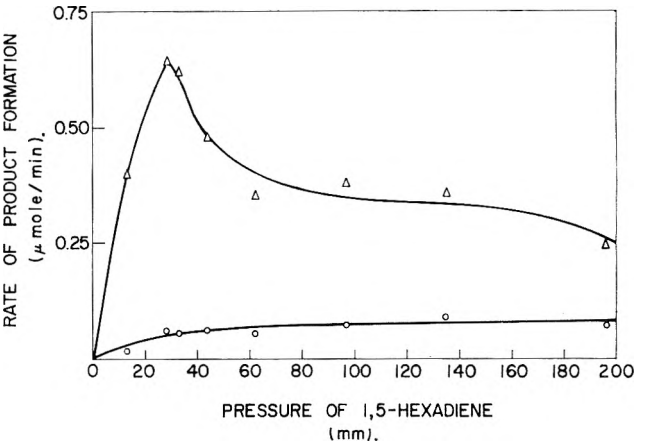

Fig. 1.—Rates of formation of isomeric products as a function of the pressure of 1,5-hexadiene: Δ, allylcyclopropane; ○, bicyclo[2.1.1]hexane. Room temperature; mercury resonance radiation (2537 Å.).

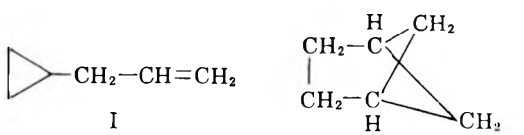

I

II

The infrared spectrum in each case agreed with that of an authentic sample prepared by the mercury-sensitized decomposition of norcamphor.[3] Quantitative analysis of these products was conducted by measuring the areas under their peaks in the chromatogram.

In Fig. 1, the rates of formation of allylcyclopropane and bicyclohexane are plotted as a function of the initial pressure of 1,5-hexadiene in the system. The rates may be taken as being proportional to the quantum yields. It also was observed that the products of free radical origin decreased steadily with an increase in pressure.

Discussion

The formation of allylcyclopropane from 1,5-hexadiene in this system is analogous to the formation of methylcyclopropane from 1-butene on mercury photosensitization.

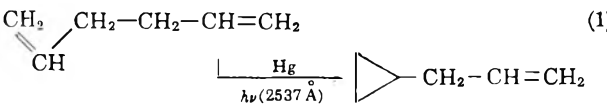

(1)

The fact that the yield of allylcyclopropane goes through a maximum at a pressure of 28 mm. of 1,5-hexadiene while the yield of free radical products decreases continuously with increasing pressure suggests that the details of the photochemical processes in the two systems may also be similar.[4]

Cvetanovic and Doyle[2] have proposed the following mechanism for the 1-butene–mercury system

$$B + Hg^* \longrightarrow B^*(+ Hg) \quad (2)$$

$$B^* \longrightarrow \text{decomposition} \quad (3)$$

$$B^* \longrightarrow C^* \quad (4)$$

(3) R. Srinivasan, *J. Am. Chem. Soc.*, **83**, 4923 (1961).

(4) It can be estimated that the quantum yield for allylcyclopropane at the maximum is about 0.10 which is of the same order of magnitude as the quantum yield reported for methylcyclopropane in the 1-butene–mercury system.[2]

$$B^* + M \longrightarrow B + M \quad (5)$$

$$C^* \longrightarrow \text{decomposition} \quad (6)$$

$$C^* + M \longrightarrow C + M \quad (7)$$

where B* and C* refer to excited molecules of 1-butene and methylcyclopropane, respectively. This mechanism will predict a maximum for the quantum yield of C.

On the assumption that a similar mechanism may be operative in the present study, equations 2 to 7 can be rewritten as (with *B* and *C* representing 1,5-hexadiene and allylcyclopropane, respectively)

$$B + Hg^* \longrightarrow B^* + Hg \quad (8)$$

and so on with equation 9 through 13 replacing equations 3 through 7. The following additional steps would account for the formation of bicyclo[2.1.1]-hexane (*H*).

$$B^* \longrightarrow H^* \quad (14)$$

$$H^* + M \longrightarrow H + M \quad (15)$$

$$H^* \longrightarrow \text{decomposition} \quad (16)$$

These equations will lead to an expression of the following nature for either *C* or *H*.

$$\Phi = \frac{[M]}{[a + (M)][b + c(M)]} \quad (17)$$

which is exactly similar to equation 1 that was derived by Cvetanovic and Doyle[2] in the case of 1-butene. It follows that the yields of *both* allylcyclopropane and bicyclo[2.1.1]hexane should show a maximum with pressure whereas in fact (Fig. 1) only the former shows such a maximum. The explanation for the disagreement may be one of two possibilities.

(i) In equation 17, the pressure at which Φ is a maximum will be a function of *a*, *b*, and *c* which in turn are ratios of the rate constants $k_8 \ldots . k_{16}$. Since the rate constants for the formation and decomposition of allylcyclopropane and bicyclohexane may differ considerably, the maximum for the latter will be different from that for the former.[5] Cvetanovic has pointed out[6] that a combination of a relatively high value for M_{max} and a relatively low value for Φ_{max} may make it *experimentally* difficult to locate the maximum in the case of bicyclo[2.1.1]hexane.

(ii) A second explanation is based on an alternative mechanism. The electronically excited triplet 1,5-hexadiene molecule that is formed in reaction 8 may contain up to 20 kcal./mole of vibrational energy which it may lose stepwise in several collisions. If the vibrational levels are designated by subscripts, the molecule of *B* that is formed in (8) will be B_n^*. The deactivation reactions may be represented by the general equation

$$M + B_n^* \longrightarrow M + B_m^* \quad (18)$$

From three of these levels (or sets of levels), n, m, and o, the three products, free radicals, *C*, and *H* may be formed

$$B_n^* \longrightarrow \text{free radicals} \quad (19)$$

$$B_m^* \longrightarrow C \quad (20)$$

$$B_0^* \longrightarrow H \quad (21)$$

With the addition of one more step to provide for the formation of excited 1,5-hexadiene molecules in the zeroth vibrational level

$$M + B_m^* \longrightarrow B_0^* + M \quad (22)$$

it can be derived that

$$\Phi_{\text{free radical}} = k_{19}/k_{19} + k_{18}M \quad (23)$$

$$\Phi_C = k_{18}k_{20}M/(k_{19} + k_{18}M)(k_{20} + k_{22}M) \quad (24)$$

$$\text{add } \Phi_H = k_{18}k_{22}M^2/(k_{19} + k_{18}M)(k_{20} + k_{22}M) \quad (25)$$

This mechanism is seen to predict the pressure dependence of all three of the products correctly.[7] In particular, the expression for Φ_C, is identical with eq. 17 and is capable of the same simplifications to give a linear dependence of $(M/\Phi_C)^{1/2}$ *vs.* M.

The present study admittedly does not resolve this conflict. However, it is clear that the experimental pressure dependence curves can be generated on the basis of more than one mechanism.

Acknowledgment.—The author wishes to thank Dr. R. J. Cvetanovic for his friendly criticism during the course of a lengthy correspondence. He is grateful to the members of the organic chemistry group at the Research Center for their advice and encouragement.

(5) It can be predicted that the maximum for bicyclo[2.1.1]hexane will occur at a higher pressure of 1,5-hexadiene than the maximum for allylcyclopropane.

(6) R. J. Cvetanovic, private communication.

(7) The prediction of the trends in the formation of bicyclohexane is only qualitatively correct. A comparison of the curve in Fig. 1 with eq. 25 clearly shows that other steps which involve *H* should be included in the mechanism.

A LANGMUIR DETERMINATION OF THE SUBLIMATION PRESSURE OF BORON[1]

BY ROBERT C. PAULE AND JOHN L. MARGRAVE

Department of Chemistry, University of Wisconsin, Madison, Wisconsin

Received January 9, 1963

Although several different groups of workers have reported Knudsen vapor pressure measurements on boron, no two sets of measurements agree and there is a difference of about 5×10^4 in vapor pressure values between the two extreme sets of measurements.

Searcy and Myers[2] have made B-vapor pressure measurements using an initial and final weighing technique with C, Ta, and ZrB_2 Knudsen crucibles. The lids and orifices of all three types of crucibles were made of Ta. Considerable reaction occurred between the B and the C or Ta crucibles and lids. After the experiments, some free B was found in the Knudsen cells. Since the borides of Ta and C are considerably less volatile than B, it was assumed that the vapor pressure of B was measured. Searcy and Myers gave a higher reliability to the vapor pressure measurements made in the ZrB_2 crucibles (with Ta lids and orifices), since these cells minimized boride formation.

Akishin, *et al.*,[3] made B-vapor pressure measurements

(1) Abstracted, in part, from the thesis of Robert C. Paule presented in partial fulfillment of the requirements for the Ph.D. degree of the University of Wisconsin, January, 1962.

(2) A. W. Searcy and C. E. Myers, *J. Phys. Chem.*, **61**, 957 (1957).

(3) P. A. Akishin, O. T. Mikitin, and L. N. Gorokhov, *Dokl. Akad. Nauk SSSR*, **129**, 1077 (1959).

TABLE I

LANGMUIR SUBLIMATION DATA FOR BORON

Expt. no.	ΔV,[b] volts	Δt, sec.	T, °K.	$-\log P_{atm}$	$\Delta\left[\frac{F - H^0_{298}}{T}\right]$, cal. deg.$^{-1}$ mole^{-1}	$\Delta F/T$, cal. deg.$^{-1}$ mole^{-1}	ΔH^0_{298}, kcal./mole^{-1}
2[a]	0.1014	3,660	1998[c]	7.159	35.68	32.76	136.7
	.0356	5,220	1918[c]	7.777	35.70	35.59	136.7
	.0590	53,640	1822[c]	8.580	35.73	39.26	136.6
	.1010	1,200	2071	6.669	35.65	30.56	137.0
	.1571	690	2152	6.228	35.62	28.50	138.0
3[a]	0.0069	51,660	1781	8.992	35.75	41.15	137.0
	.0237	15,000	1905	7.905	35.71	36.17	136.9
	.0462	7,320	1980	7.294	35.69	33.38	136.8
	.0503	87,060	1845	8.348	35.73	38.20	136.4
	.0319	8,160	1959	7.505	35.70	34.34	137.2
	.0247	28,080	1873	8.163	35.72	37.35	136.9

Av. 136.9 ± 0.3 kcal./mole

[a] Area of sample = 5.14 cm.^{2} for expt. no. 2 and 1.596 cm.^{2} for expt. no. 3. [b] Calibration showed $\Delta V/\Delta M$ = 23.8 mv./mg. [c] In addition to the normal pyrometer sighting window and mirror correction, a factor of 25° was added to correct for an initially undetected film on the mirror.

by observing with a mass spectrometer the vapors effusing from Ta and Mo Knudsen cells. Their data show a considerable scatter.

Priselkov, *et al.*,[4a] made B vapor pressure measurements by observing the rate of vapor condensation on cold plates placed in front of Mo and Ta Knudsen cells. Their data show a very strong dependence on the size of the orifice, with smaller orifices yielding higher measured vapor pressures. This dependence could indicate a very small evaporation coefficient for B. On the other hand, it could indicate that incorrect vapor pressure calculations were made since this same effect could arise from failure to correct for channeling in the orifice or from borides forming on the lid of the cell.

Verhaegen and Drowart[4b] have recently reported a heat of sublimation of 128.0 ± 2.5 kcal./mole from mass spectrometer studies of the effusate from B or B_4C contained in a graphite Knudsen cell, and cite agreement with other mass spectrometer studies,[5,6] while noting that weight-loss experiments seem to yield a higher heat, *i.e.*, a lower vapor pressure.[2,7] There have been no previous Langmuir studies on boron.

Experimental

Experimental Techniques and Apparatus.—In this work, the vapor pressure of B has been measured by the Langmuir technique, since this method allows one to minimize the problem of sample contamination or reaction at high temperatures. The experimental apparatus and general procedures have been described previously.[8] In addition to the previously described apparatus, a closed bottom Ta cylindrical sleeve was fitted into the graphite furnace and was used in two of the three boron experiments in order to reduce the possibility of a reaction between the boron sample and furnace vapors.

Polycrystalline B was deposited at Texaco Experiment, Incorporated, on a thin W filament by chemical vapor plating using H_2 and BBr_3. The B rod had a purity in excess of 99%. Emission spectrographic analysis revealed approximately 40 p.p.m. Fe, 20 p.p.m. Si, 3 p.p.m. Cu, and 1 p.p.m. Mg for similarly prepared rods. The sample was suspended from a W wire and no significant W–B interaction was observed.

Results

Visual inspection and X-ray diffraction spectra of the sample surfaces, made after the vapor pressure experiments, indicated varying degrees of B surface contamination, in the form of B_4C. At the temperature of the experiments, the vapor pressure of C, *per se*, is too low to contribute significantly to the formation of B_4C. It is more likely that vapors of the diffusion pump oil were absorbed onto the carbon of the cold furnace prior to the experiment and then desorbed and pyrolyzed at the higher temperatures of the experiment.

Experiment no. 1 was performed in the bare graphite furnace, which resulted in the formation of a considerable amount of B_4C, and the observed vapor pressure results were low, clearly indicating the formation of a surface film. Experiment no. 2 was run with the Ta sleeve inside the furnace and showed only a small amount of B_4C. Experiment no. 3 was also run with a Ta sleeve and special care was taken while heating the furnace in order to keep the ambient pressure as low as possible. As a result, sample no. 3 was only slightly contaminated with B_4C.

Because of the observed high degree of reactivity of B at high temperatures, and because the heat of formation of TaB_2 is < -45 kcal./mole,[9] it is assumed that complete reaction occurred between the B vapor atoms and the Ta sleeve (or the graphite furnace). The possible products, TaB_2 or B_4C, are considerably less volatile than B.

The appropriate equation relating the measured pressure, P, to the equilibrium pressure, P_{eq}, is

$$P = \alpha_{eo} P_{eq}$$

where α_{eo} is the evaporation coefficient *in vacuo*.

For the improbable case that the B vapor atoms did not react with the Ta sleeve or with the furnace walls, a multiplicative correction factor which could be as high as 2.56 might be necessary to correct for the channeling effect of the heating sleeve.

The vapor pressure of B was measured over the temperature range 1781–2152°K. and the data are given in Table I. Monatomic B(g) was considered to be the

(4) (a) Yu. A. Priselkov, Yu. A. Sapozhnikov, and A. V. Tsepyaeva, *Akad. Nauk SSSR, Izv. Otd. Tekhn. Nauk Metal I Toplivo*, **1**, 134 (1960); (b) G. Verhaegen and J. Drowart, *J. Chem. Phys.*, **37**, 1367 (1962).

(5) W. A. Chupka, Argonne National Laboratory Report ANL-5867, 1957, p. 75.

(6) P. Schissel and W. Williams, *Bull. Am. Phys. Soc.*, **4**, 139 (1959).

(7) H. Robson, Ph.D. Thesis, University of Kansas, 1959.

(8) L. Dreger and J. L. Margrave, *J. Phys. Chem.*, **66**, 1555 (1962), and earlier papers.

(9) L. Brewer and H. Haraldsen, *J. Electrochem. Soc.*, **102**, 399 (1955).

only important gaseous species and the evaporation coefficient was assumed to be unity. Akishin, *et al.*,[3] have mass spectrometrically observed only $B_1(g)$ at 2100°K., while Drowart and Verhaegen[4b] found some B_2 at 2330°K. Their detectability limit for a given vapor species was about 1%.

The second law ΔH^0_{298}(subl) was found to be 133.4 ± 5 kcal./mole while the third law calculation yielded ΔH^0_{298}(subl) = 136.9 ± 0.3 kcal./mole, in agreement with the second law value. The equation for the sublimation pressure of B is

$$\log P_{atm}(\text{solid}) = 7.239 - \frac{28{,}840}{T} \quad (1781\text{–}2152°\text{K.})$$

The boiling point is estimated to be 4050 ± 100°K. This estimate is obtained by use of the 136.9 kcal./mole for the third law heat of sublimation and extrapolated high temperature thermodynamic functions.[10]

The Langmuir sublimation pressure results are in close agreement with the results of Searcy and Myers, although their Knudsen data are slightly lower as might be expected if there was some reaction of the B samples with the Knudsen cells. The quantitative results of Akishin, *et al.*,[3] appear to have considerable scatter. Drowart and Verhaegen[4b] feel that uncertainties in relative ionization cross sections and multiplier yields cannot account for the difference observed. They suggest that interactions between the Knudsen cell and the sample occur in weight-loss experiments but do not explain how these same interactions are avoided in their work. Alcock and Grieveson[11] have also reported weight-loss data from graphite Knudsen cells in essential agreement with the work of Searcy and Myers.[2]

It appears that the mass spectrometer–Knudsen cell studies establish an upper limit for the sublimation pressure of boron and, further, that these Langmuir studies set a lower limit. The discrepancy could be explained if α_{en}, the Langmuir sublimation coefficient, is equal to 0.15 and if the ratios of hole size to sample area were somewhat larger in the work of Searcy and Myers[2] and of Robson.[7] The correction factor for channeling by the Ta-susceptor in the Langmuir experiments would also tend to lower the heat of sublimation, although it would appear that TaB_2 should form rapidly from the elements at 1780–2100°K. and eliminate the correction.

Acknowledgments.—The authors are pleased to acknowledge the financial support of this work by the United States Atomic Energy Commission and the Wisconsin Alumni Research Foundation. The samples of boron were generously provided by Dr. Claude P. Talley of Texaco Experiment, Inc.

(10) (a) S. Wise, R. Altman, and J. Margrave, *J. Phys. Chem.*, **64**, 915 (1960); (b) R. McDonald and D. Stull, *J. Chem. Eng. Data*, **7**, 84 (1962).

(11) C. Alcock and P. Grieveson, in "Thermodynamics of Nuclear Materials," Intern. Atomic Energy Agency, Vienna, Austria, pp. 571–572.

THE THERMAL DECOMPOSITION OF CYCLOBUTANE[1]

BY ROBERT W. CARR, JR.,[2] AND W. D. WALTERS

Department of Chemistry of the University of Rochester, Rochester, N. Y.

Received January 9, 1963

Previous publications[3–7] have reported studies of the thermal decomposition of cyclobutane in the vapor phase over the temperature range 410–500° mainly at pressures from 0.0005 to about 120 mm. At 449, 438, and 427° some work at initial pressures as high as 740 mm. and slightly higher has been performed. The first-order rate constants were found to decrease noticeably at pressures below about 20 mm. at 449°. Very few experiments have been done at pressures greater than 120 mm. where the first-order rate constants would be expected to be almost invariant with pressure if the decomposition is a quasi-unimolecular process. The present experiments at pressures up to 1500 mm. were performed in order to study more carefully the first-order region of the reaction and to obtain values for the Arrhenius parameters at pressures well above the onset of the fall-off. Moreover, if the rate constants should continue to increase as higher pressures are attained, the earlier conclusion that the decomposition is a simple unimolecular reaction (with no detectable free radical chain processes) would be open to question. On the other hand, if the rate constants should decrease with increasing pressure, a possibility which has been mentioned by Wilson,[8] the measurements might provide interesting information about intramolecular energy transfer.

Experimental

The cyclobutane had been prepared earlier in this Laboratory by Genaux through the photolysis of cyclopentanone and had been purified in a Podbielniak distillation apparatus. In the present work gas chromatographic analysis with a 3-meter column containing tetraisobutylene upon 60–80 mesh firebrick at 28° showed the purity to be at least 99.9%. The Phillips research grade ethylene used in this study was subjected to degassing, drying, trap-to-trap distillation, and a gas chromatographic check of purity.

Kinetic experiments were performed in two different thick-walled spherical Pyrex vessels. One had a capacity of 27.2 ml. and the other, which was filled with thin-walled Pyrex tubes to give a 9-fold increase in S/V ratio, had a volume of 21.2 ml. The reaction vessel was placed in a spherical cavity inside a cylindrical aluminum block (7.5 cm. diam.) which just fit the iron core of an electrically heated furnace. Capillary tubing (1 mm. i.d.) connected the vessel to the rest of the vacuum system. Temperature measurements were made by the use of two standardized platinum, platinum–13% rhodium thermocouples which lay tangent to the outside of the reaction vessel. The temperature was controlled automatically to about ±0.1°.

For experiments at pressures less than 1 atm. the initial pressure was measured with a mercury manometer. Initial pressures greater than 1 atm. were calculated from the measured amounts of reactant introduced. It was found that the undecomposed cyclobutane and the product ethylene could be separated satisfactorily on the basis of the difference in volatility at −130°. From the amounts of ethylene and unreacted cyclobutane measured in a gas buret, the percentages of decomposition were obtained and first-order rate constants calculated. In some experiments a portion of the reaction mixture was also analyzed mass spectrometrically and the results from the two methods of analysis were in good agreement.

Results

Products.—To ascertain whether other products are formed at the higher pressures, the reaction mixtures

(1) This work was supported by a grant from the National Science Foundation to the University of Rochester.

(2) National Science Foundation Summer Fellow, 1960.

(3) C. T. Genaux and W. D. Walters, *J. Am. Chem. Soc.*, **73**, 4497 (1951).

(4) F. Kern and W. D. Walters, *Proc. Natl. Acad. Sci. U. S.*, **38**, 937 (1952).

(5) C. T. Genaux, F. Kern, and W. D. Walters, *J. Am. Chem. Soc.*, **75**, 6196 (1953).

(6) H. O. Pritchard, R. G. Sowden, and A. F. Trotman-Dickenson, *Proc. Roy. Soc.* (London), **A218**, 416 (1953).

(7) D. F. Swinehart and R. W. Vreeland, Paper presented at the 138th National Meeting of the American Chemical Society, Division of Physical Chemistry, 1960; R. W. Vreeland, Ph.D. Thesis, University of Oregon, 1961.

(8) D. J. Wilson, *J. Phys. Chem.*, **64**, 323 (1960).

from several experiments at about 1500 mm. (25–35% decomposition, 427–460°) were separated into two portions, one of which was volatile at −130° and the other non-volatile at that temperature. Gas chromatographic analyses of the separated fractions showed the presence of only two substances, one with a retention time corresponding to ethylene and the other with the retention time of cyclobutane. The higher boiling fraction from a 1350 mm. experiment carried to 35% reaction at 460° was analyzed by mass spectrometry and infrared spectroscopy. The gas phase infrared spectrum was in good agreement with one found by Genaux[9] for pure cyclobutane. Comparison of the mass spectrum with that of pure cyclobutane showed that the cracking patterns were in good agreement, with all peaks accounted for except small ones at m/e = 42, 43, and 44, and two in the C_5 range. The substances contributing to these are probably no greater than 0.1 to 0.2% of the undecomposed cyclobutane.

The separated fractions from a 732 mm. experiment after 25% decomposition at 449° in the packed bulb were analyzed on the mass spectrometer. In the fraction non-volatile at −130° only cyclobutane was detected, but the fraction volatile at −130° showed small peaks at m/e = 40, 41, and 44. Although the substance giving the peaks was not identified, it probably did not exceed 0.1% of the ethylene. In other experiments near 1500 mm. (25% decomp., 420-449°) measurements in the gas buret showed that the initial amount of cyclobutane introduced into the vessel was equal, within experimental error, to the amount recovered plus one half of the amount of ethylene formed. All of the evidence indicates that the decomposition at two atmospheres proceeds essentially by the same reaction ($C_4H_8 \rightarrow 2C_2H_4$) as that observed earlier at lower pressures.

Kinetics.—The rate data for the decomposition of cyclobutane near 449° are presented in Table I. In the fourth column are the first-order rate constants corrected to 449°, the temperature dependence amounting to about 6% per °C. An inspection of the values from 100 to 1500 mm. reveals that there is no noticeable trend with pressure, and in fact, the average deviation over the 50-fold pressure range investigated is only 2.3%. The present values are in reasonable agreement with those obtained earlier in this Laboratory and when plotted against pressure, they join quite smoothly to the pressure-dependent values in the region below 30 mm. Since the decomposition of cyclobutane at 449° is somewhat endothermic,[5] it is conceivable that the temperature of the reacting gas at the center of the vessel might be appreciably lower than near the walls. By the use of an equation[10] taking into account only conduction of heat, it was calculated that for an initial pressure of 2 atm. at 449° the maximum temperature difference in the 27 ml. vessel might be ~2.8° (unless lowered by another heat transfer process), but for a pressure of 100 mm. it would not exceed 0.2°. As the data in Table I show, the rate constants from experiments in the packed vessel are in accord with those from the unpacked vessel. It was felt that the presence of packing would afford a test for the occurrence of heterogeneous processes and would provide for a greater temperature uniformity throughout the vessel since the thermal conductivity of glass is about 10^2 times that of cyclobutane. The fact that no observable effect on the rate was found in the packed vessel gives an indication that heterogeneous reactions and temperature gradients do not occur to a kinetically important extent under the conditions of this study.

The temperature dependence of the reaction was studied over the temperature range 419–460° at pres-

(9) C. T. Genaux, Master's Thesis, University of Rochester, 1953.

(10) S. W. Benson, "The Foundations of Chemical Kinetics," McGraw-Hill Book Co., New York, N. Y., 1960, pp. 426–431.

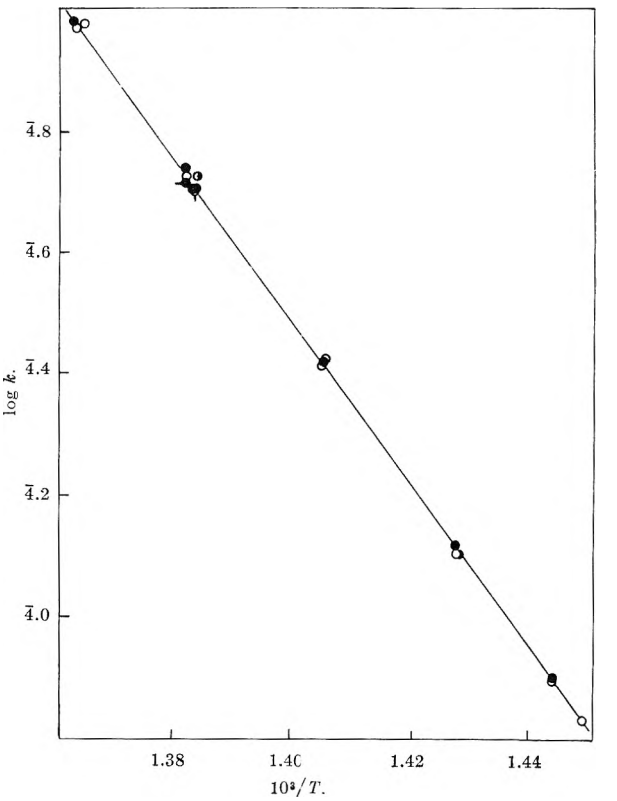

Fig. 1.—Temperature dependence of the first-order rate constant: ●, 650–790 mm.; ⊸●, 733 mm., packed vessel; ○, 1250–1500 mm.; ♀, 1490 mm., packed vessel; ◑, 1320 mm., analysis on mass spectrometer.

TABLE I

FIRST-ORDER RATE CONSTANTS FOR THE THERMAL DECOMPOSITION OF CYCLOBUTANE NEAR 449°

Init. press., mm.	Temp., °C.	$k \times 10^4$, sec.$^{-1}$	k (cor.) $\times 10^4$,[c] sec.$^{-1}$
33.8	449.1	5.20	5.17
69.9	449.0	5.38	5.38
71.9	448.9	5.09	5.14
102	449.2	5.37	5.31
123[a]	449.0	5.24	5.24
126	449.0	5.40	5.40
136	449.1	5.34	5.31
243[a]	449.0	5.08	5.09
245	449.1	5.01	5.00
245	449.1	5.27	5.25
305	450.4	5.56	5.10
660	450.1	5.17	4.85
673	449.4	5.09	4.97
733[b]	449.1	5.12	5.10
772	450.0	5.53	5.18
1260	450.0	5.35	5.04
1320[a]	449.1	5.32	5.29
1490[b]	449.2	5.07	5.01

[a] Percentage of decomposition determined by mass spectrometry. [b] Experiments in the packed vessel. [c] For the corrections, temperatures and rate constants with one more significant figure than those shown were used in the calculations and then rounded off.

sures near one atmosphere and near two atmospheres. Since there appeared to be no significant change in the value of the rate constant in the present work resulting either from an increase in pressure from 650 to 1500 mm. or from packing the vessel, the results from all experiments in the packed and unpacked vessels over the pressure region 650–1500 mm. were used for determination of the activation energy. The experimental data, plotted as log k *vs* $1/T$ in Fig. 1, give a straight line, from the slope of which an activation energy of 62.5 kcal./mole was calculated. In addition, the activation energy was calculated by the method of least squares on an IBM 650 computer and found to be 62.5 ± 0.4 kcal./mole. That the uncertainty in the value of the activation energy is probably in the neighborhood of 0.4–0.5 kcal./mole is indicated not only from the least squares deviation but also from the fact that when the experiments shown in Fig. 1 were divided into groups on the basis of essentially constant initial pressure, the values of the activation energy (determined from the smaller number of experiments) ranged from 62.1 to 62.9 kcal./mole. For each experiment in Fig. 1 the pre-exponential factor A was calculated from the relationship $k = A \exp(-62{,}500/RT)$. On the basis of the average value, which was 4.2×10^{15} sec.$^{-1}$ with an average deviation of 0.1×10^{15}, the rate expression

$$k = 4.2 \pm 0.1 \times 10^{15} \exp(-62{,}500R/T) \text{ sec.}^{-1} \quad (1)$$

will satisfactorily represent the data in the pressure region 650–1500 mm.

Discussion

Since the present study has shown that at pressures as high as 1500 mm. the pyrolysis of cyclobutane is a homogeneous reaction uncomplicated by side reactions and that the first-order constants at 449° have not changed detectably over the pressure range 240–1500 mm., the rate expression given in equation 1 for the pressure region 650–1500 mm. should correspond rather closely to the rate expression for the high pressure limit of the unimolecular decomposition of cyclobutane (k_∞).

The values for k_∞ and E_∞ have been estimated earlier by Vreeland and Swinehart[7] from their rate constants in the fall-off region (initial pressures, 20 mm. and below) by a sizable extrapolation of a $1/k$ *vs.* $1/P$ plot to a value of 0 for $1/P$. From experiments at 410–500° the relationship $k_\infty = 10^{15.35} \exp(-61{,}800/RT)$ sec.$^{-1}$ was obtained. They found, however, that a value $k_\infty = 10^{15.846} \exp(-63{,}200/RT)$ sec.$^{-1}$ would give Kassel fall-off curves in better agreement with their experimental data in the pressure dependent region. Either of these values of the activation energy could be regarded as in reasonable agreement with the value determined in this work. On the other hand it is noteworthy that for k_∞ at 449° the former expression gives a value of 4.45×10^{-4} sec.$^{-1}$, but the latter expression gives 5.25×10^{-4} sec.$^{-1}$ which is closer to the average value of k (5.12×10^{-4} sec.$^{-1}$) for the experiments in the pressure region 700–1500 mm. at 449° in Table I. The rate expression found earlier[5] for experiments at 120 mm. was $k = 4.0 \times 10^{15} \exp(-62{,}500/RT)$ sec.$^{-1}$ which is within 5% of that given by equation 1.

In the current investigation no evidence has been found that the first-order rate constants decrease with increasing initial pressure. It would be of interest to measure the rate of decomposition of cyclobutane at higher pressures, but more favorable conditions for testing the suggestion of Wilson[8] might be obtained by investigating the unimolecular reaction of a more complex molecule in which the bond undergoing scission had to receive the needed energy from degrees of freedom some distance from it and only weakly coupled to it. This question has been considered also by Flowers and Frey,[11] who studied the isomerization of 1,1-dimethylcyclopropane at pressures from 16 to 1596 mm. at 460°. The first-order rate constants were invariant with pressure over this one hundredfold range which extended upward from the region where the high pressure limit is first approached. They concluded that the high pressure rate constant for the unimolecular reaction of 1,1-dimethylcyclopropane does not go through a maximum.

Acknowledgment.—The authors wish to thank Mr. Carl Whiteman, Jr., for his assistance in making the infrared absorption measurements and the least squares calculations.

(11) M. C. Flowers and H. M. Frey, *J. Phys. Chem.*, **65**, 373 (1961).

FLUORINE N.M.R. SPECTROSCOPY. XIII. FURTHER COUPLING CONSTANTS FOR ISOTOPIC C_3F_8

BY GEORGE VAN DYKE TIERS

Contribution No. 259 from the Central Research Department, Minnesota Mining and Mfg. Company, St. Paul 19, Minnesota

Received January 14, 1963

In a previous paper[1] coupling constants were reported for the CF_3 group in perfluoropropane. At the time it was not possible to make analogous measurements upon the weaker and broader carbon-13 satellites of the CF_2 peak; however, subsequent improvements in resolution and sensitivity have made such studies feasible. With the present paper, all but two of the possible coupling constants for C_3F_8 are now reported, albeit no information on relative signs for the J-values is yet available.

Experimental

The sample, equipment and techniques have been described and shielding values have been reported.[1] Coupling constants and isotope shifts, measured on the weak, partially resolved C^{13} satellites to the CF_2 peak, have been obtained with acceptable precision by averaging the results of twelve separate determinations on each peak. The results are given in Table I; error values are standard deviations for the averaged values. First-order spin–spin analysis was used throughout.

TABLE I

FLUORINE N.M.R. COUPLING CONSTANTS AND ISOTOPE EFFECTS FOR THE CF_2 GROUP IN PERFLUOROPROPANE

Coupling system	J, c./sec.	Std. dev.[a]	$\Delta\phi$, p.p.m.[b]	Std. dev.[a]
$C^{13}F_2$	266.6	±0.2	+0.125	±0.002
$C^{13}CF_2$	32.6	±0.2	+0.024	±0.002

[a] Std. dev. of the average. [b] The isotope shift, $\Delta\phi$, is defined as $\phi(C^{13}$ isomer) − $\phi(C^{12}$ isomer). A typographical error is present in footnote *c*, Table II of ref. 1.

Discussion

The "direct" isotope shifts, $\Delta\phi(C^{13}F_2)$, are very similar to several previously reported for non-allylic CF_3 groups,[1,2] but are substantially smaller than those for allylic CF_3 groups,[3] for CF_2Cl groups,[4] and for $CFCl_2$

(1) G. V. D. Tiers, *J. Phys. Chem.*, **66**, 945 (1962).
(2) G. V. D. Tiers, *J. Phys. Soc. Japan*, **15**, 354 (1960).
(3) G. V. D. Tiers, *J. Chem. Phys.*, **35**, 2263 (1961).

groups.[5] When the C^{13} is not tetrahedral, much smaller "direct" shifts result,[2,6] but by Gutowsky's reasoning[7] one would not expect a simple relation between trigonal and tetrahedral C^{13} shifts. At present it is tentatively suggested that, for tetrahedral C^{13}, larger "direct" isotope shifts result when relatively more polarizable atoms are substituted upon C^{13}. One would expect to find some conformational effects in the case of CF_2 groups.

Quite different structural correlations have been suggested[8] for the variations found in the "direct" C^{13}–F coupling constant, and the present value for $J(C^{13}F_2)$ is far more appropriate in this regard than the value cited[8] which had been obtained from cyclo-C_4F_8 and consequently does not represent a tetrahedral bond structure about C^{13}.

As yet there does not seem to be sufficient information to permit even a tentative correlation of the "distant" isotope shifts or coupling constants; there are, of course, yet more structural variables to be taken into consideration.

Acknowledgment.—The author thanks R. B. Calkins and E. B. Aus for excellent maintenance and operation of the n.m.r. spectrometer.

(4) G. V. D. Tiers, unpublished results for $CF_2Cl—CCl=CCl_2$ and CF_2ClCO_2H.

(5) G. V. D. Tiers, *J. Phys. Chem.*, **67**, 928 (1963).

(6) G. V. D. Tiers and P. C. Lauterbur, *J. Chem. Phys.*, **36**, 1110 (1962).

(7) H. S. Gutowsky, V. D. Mochel, and B. G. Somers, *ibid.*, **36**, 1153 (1962).

(8) R. K. Harris, *J. Phys. Chem.*, **66**, 768 (1962).

FLUORINE N.M.R. SPECTROSCOPY. XIV. LIKE SIGNS FOR THE COUPLING CONSTANTS, $J(C^{13}H)$ AND $J(FH)$, IN DICHLOROFLUOROMETHANE

BY GEORGE VAN DYKE TIERS

Contribution No. 256 from the Central Research Laboratories, Minnesota Mining & Mfg. Co., St. Paul 19, Minn.

Received December 31, 1962

Recent theoretical[1] and experimental[2,3] work has been devoted to relating the signs of several common types of spin–spin coupling to that for the C^{13}–H bond. The absolute sign of the latter, commonly taken as positive,[1,4] provides a useful basis for the systematizing of all relative sign information. The present work concerns itself with the determination of the relative sign of a two-bond coupling constant, $J(FH)$, in dichlorofluoromethane.

Experimental

The $CHCl_2F$ sample and the n.m.r. equipment were the same as previously used,[3] except that the Model SD-60 spin decoupler[5] had been equipped with modules designed for strong irradiation of C^{13} nuclei at 10.70 Mc./sec. while observing fluorine at 40.000 Mc./sec. The field-sweep technique was used. The maximal attainable decoupling field, H_2, was measured as 318 ± 2 milligauss, by application of an analytical expression corresponding to Lauterbur's linear plot of applied decoupling frequency, ν_2, *vs.* $R/\gamma_2(1 - R^2)^{1/2}$, the slope of which is H_2 in milligauss.[6] γ_2 is the magnetogyric ratio for the nucleus decoupled and R is the ratio of apparent J, during irradiation, to the true J for the doublet undergoing varying degrees of collapse as γ_2 is changed. For this purpose a sample of CCl_3F was found especially convenient since its C^{13} satellite spectrum is a simple doublet. It is desirable that the maximal value of H_2 be large, as found here, in order that the proper region for ν_2 may be located without undue delay.

The decoupling observations, and the interpretation as to relative signs, are analogous to those of Lauterbur and Kurland[2]; *i.e.*, if the four satellite lines in the F^{19} spectrum be labeled *a*, *b*, *c*, and *d* in order of increasing field such that the spacings *ab* and *cd* correspond to $J(FH)$ while the spacings *ac* and *bd* represent $J(FC^{13})$, then irradiation of the C^{13} nuclei at one frequency, ν, will collapse lines *a* and *c* while causing little disturbance of *b* and *d*. At a slightly different frequency, ν'_2, lines *b* and *d* will move together while *a* and *c* are little affected. The frequency difference $(\nu_2 - \nu'_2)$ is equal to

$$|J(FH)|\left(\frac{J(C^{13}H)}{J(FH)} - \frac{\gamma_{C^{13}}}{\gamma_F}\right)$$

and if irradiation of the high-field (low-frequency) part of the C^{13} spectrum causes the collapse of the satellite lines *b* and *d* in the F^{19} spectrum, we must assign to $J(FH)$ the same sign as that of $J(C^{13}H)$. This is found to be the case, $(\nu_2 - \nu'_2)$ being +210 c./sec.; calculated values are +205.7 (like) and −234.3 (unlike).[7] We must remember that, if the four lines in the C^{13} spectrum be labeled A, B, C, and D in order of increasing field, with the spacings AB and CD yielding $J(C^{13}H)$ while AC and BD are equal to $J(FC^{13})$, then the "high-field part of the C^{13} spectrum" comprises lines B and D, not C and D as was true in Lauterbur and Kurland's work.[2] Especial care was taken, as before,[3] to establish that ν_2 was indeed higher in frequency than ν'_2; and Lauterbur's plot was also used to identify ν_2 and ν'_2 by locating the frequencies at which the lines extrapolate to $R/\gamma_2(1 - R^2)^{1/2} = 0$. This latter method is particularly suitable when spin decoupling must be used to measure J-values concealed by other spectral features.

The mean decoupling frequency for $C^{13}HCl_2F$, $(\nu_2 + \nu'_2)/2$, was found to be about 745 c./sec. above that for $C^{13}Cl_3F$, which would correspond, at 10.70 Mc./sec., to a 70 p.p.m. lower C^{13} shielding for $C^{13}HCl_2F$. However, it is necessary to correct for the difference in fluorine shielding values, which is about 81 p.p.m.[3] in the opposite direction. The net result is that, by this relatively crude technique, the C^{13} shielding of $C^{13}HCl_2F$ is estimated as roughly 11 p.p.m. *greater* than that of $C^{13}Cl_3F$.

Discussion

It has now been shown that the two-bond coupling constant, $J(FH)$, has the same sign as the one-bond constant, $J(C^{13}H)$, which is customarily considered positive. Elleman and Manatt[8] have found that, in CF_3-CH_2F, the two-bond and three-bond H–F coupling constants have the same sign, which we may now identify as positive relative to $J(C^{13}H)$. While certain two-bond couplings, notably $J(HCH')$ in olefins,[9] show reversal of signs as structure is altered, this is not surprising in view of the small magnitudes and considerable variability encountered. The saturated H–C–F system shows a fairly constant numerical value around 55 c./sec.[3,8,10] which may confidently be assumed not to vary in sign.

Spin-decoupling studies of this sort can be used to provide estimates of the shielding of the C^{13} nucleus responsible for the observed splitting. This is particu-

(1) M. Karplus, *J. Am. Chem. Soc.*, **84**, 2458 (1962).

(2) P. C. Lauterbur and R. J. Kurland, *ibid.*, **84**, 3405 (1962).

(3) G. V. D. Tiers, *ibid.*, **84**, 3972 (1962).

(4) See, however, E. M. Roberts, M. R. Foster, and F. F. Selig, *J. Chem. Phys.*, **37**, 485 (1962).

(5) Mfd. by the Nuclear Magnetic Resonance Specialties Co., Inc., Box 145, Greensburg Road, New Kensington, Pa.

(6) P. C. Lauterbur, private communication.

(7) In ref. 3 the analogous relation should be

$$\nu_2 - \nu'^2 = |J(FC^{13})|\left(\frac{J(C^{13}H)}{J(FC^{13})} - \frac{\gamma_H}{\gamma_F}\right)$$

if $J(FC^{13})$ were taken as positive; this yields $(\nu_2 - \nu'_2) = -91.5$ c./sec. (like sign) or −531.5 c./sec. (unlike).

(8) D. D. Elleman and S. L. Manatt, *J. Chem. Phys.*, **36**, 1945 (1962).

(9) C. D. Banwell, A. D. Cohen, N. Sheppard, and J. J. Turner, *Proc. Chem. Soc.*, 266 (1959).

(10) J. A. Pople, W. G. Schneider, and H. J. Bernstein, "High Resolution Nuclear Magnetic Resonance," McGraw-Hill, New York, N. Y., 1959, p. 196.

larly desirable, as the C^{13} spectra, which are often complex, weak and poorly-resolved, are difficult to analyze when accessory data cannot be gotten. In the present instance, the "chemical shift" for $C^{13}HCl_2F$ is about 11 p.p.m. on the high field side of that of $C^{13}Cl_3F$. Such a relative shift is certainly in harmony with the observations of Lauterbur,[11] according to which proton substitution in chloro- and ethoxy-substituted methanes produces a small upfield shift of the C^{13} resonance.

While the shielding value for $C^{13}Cl_3F$ has not been reported upon the accepted scale[11] for C^{13} spectra, it is here proposed that $C^{13}Cl_3F$ be adopted as a secondary C^{13} standard for use in $F\{C^{13}\}$ decoupling studies. It is readily available and gives good signals, and ultimately could be used as an internal standard, though such was not done in the present work. Even more important is the fact that fluorine shifts are increasingly being reported relative to CCl_3F; as shown in the Experimental section, it is necessary to correct the "apparent" C^{13} shifts for the large differences in fluorine shielding.

Acknowledgment.—The author thanks Charles A. Brown and Emmett B. Aus for this careful n.m.r. spectral work.

(11) P. C. Lauterbur, *Ann. N. Y. Acad. Sci.*, **70**, 841 (1958).

A SEMI-EMPIRICAL FORMULA FOR VISCOSITY OF A 12:6 LIQUID

By Dilip Kumar Majumdar

Faculty of Science, Department of Chemistry, University of Kalyani, West Bengal, India

Received July 3, 1962

In the present note, an attempt has been made to calculate the viscosity of a liquid of molecules which have a symmetrical field of force. For the purpose, we have taken the tunnel model of the liquid state as our starting point. On this model the molecules are imagined as moving in very long cells so narrow that the molecules in them move almost one-dimensionally. We imagine the volume V of the liquid divided into K hexagonal cylinders arranged in two-dimensional close packing, each of length l, and containing M molecules. The distance between the centers of neighboring cylinders being r, it follows that

$$\frac{V}{N} = \frac{1}{2}\sqrt{3}lr^2 \qquad (1)$$

where l is the space between the molecules in a given line and for our purpose we shall assume $l = r$. Barker[1] has given the partition function for a single molecule in a liquid on this model as

$$Z = \left(\frac{2\pi mkT}{h^2}\right)^{3/2} \exp(-F_1/kT) \exp\left(-\frac{1}{2}\frac{V(0)}{kT}\right) A_f \qquad (2)$$

where F_1 is the free energy per molecule of the one-dimensional system. The energy of the system when all the molecules are in their equilibrium positions is $V(0)$ and for a 12:6 fluid, $V(0)$ is given by

$$V(0) = N\epsilon\left\{11.8875\left(\frac{V_0}{V}\right)^2 - 5.2335\left(\frac{V_0}{V}\right)^4\right\} \qquad (3)$$

(1) J. A. Barker, *Proc. Roy. Soc.* (London), **A259**, 442 (1961).

where ϵ is the minimum energy for equilibrium separation of the molecules and $V_0 = N\sigma^3$, σ being the collision diameter. The free-cross-sectional area is $A_f = r^2S$. The integral S is a tabulated function of kT/ϵ and V/V_0, a table of which has been prepared by Barker, the required values of S being obtained by interpolation.

The values of ϵ/k and σ for argon, nitrogen, and benzene have been taken from Hirschfelder[2] and are given in Table I.

TABLE I

	Argon	Nitrogen	Benzene
σ (Å.)	3.465	3.681	5.270
ϵ/k °K.)	116	91.5	440
E_s (cal.)	2067.4	1660	1133
V_s, cm.^{3}	24.98	29.31	77.00
n	8.35	8.35	8.35

We have retained all the essentials of the above model of the liquid state, and following McLaughlin[3] we assume further that holes in the liquid are possible, in addition to the normally occupied lattice sites, the existence of holes being a necessary requirement for the flow of mass and momentum.

We now use Barker's partition function along with the rate theory equation[4] in order to evaluate the additional Gibbs' free energy of the activated state and following a procedure exactly analogous to McLaughlin's the coefficient of viscosity becomes

$$\eta = \frac{(2\pi mkT)^{1/2}}{2\pi\sigma a^2} A_f^{1/2} \exp(W'/kT) \exp(e_0/kT) \qquad (4)$$

Calculation of e^0.—The hole in the liquid may be supposed to correspond to a β site while a molecule may be supposed to occupy an α site of the Lennard-Jones model of the liquid state. Since, however, the flow of a liquid involved transfer of molecules from α to β-site (holes), the interaction energy or rather the height of the potential barrier e_0 is determined entirely by the repulsive part of the intermolecular forces. It is therefore possible to write[5]

$$e_0 = \omega_0\left(\frac{V_0}{V}\right)^4 = \epsilon\left(\frac{V_0}{V}\right)^4 \qquad (5)$$

Lennard-Jones has shown that ω_0 is approximately equal to the potential energy at the minimum of the potential energy curve for a pair of molecules.

Work of Formation of Hole W.—Eyring[6] has shown that the work W' required to form a hole of molecular size is a fraction of the average potential energy E_s of the molecules in their equilibrium positions in the solid state. Further the energy W' is itself a function of the volume.

For a normal liquid, at temperatures appreciably above the melting point, it is found that

$$W' = E_s\left\{\frac{V_s}{V} - \frac{1}{2n}\left(\frac{V_s}{V}\right)^3\right\} \qquad (6)$$

The values of E_s and n and the volume of the solid V_s at the melting points for argon, and C_6H_6 are given in Table I.

(2) J. Hirschfelder, C. F. Curtiss, and R. Bird, "The Molecular Theory of Gases and Liquids," John Wiley and Sons, Inc., New York, N. Y., 1954.
(3) E. McLaughlin, *Trans. Faraday Soc.*, **55**, 29 (1959).
(4) H. Eyring, "The Theory of Rate Processes," McGraw-Hill Book Co., New York, N. Y., 1941.
(5) J. Lennard-Jones, *Proc. Roy. Soc.* (London), **A169**, 317 (1939).
(6) H. Eyring, *J. Chem. Phys.*, **9**, 393 (1941).

TABLE II

	Temp., °K.	Molar volume, cm.³	η × 10³, poise			E_{active} (cal.)		
			Expt.	Eq. 11	McL.	Expt.	Eq. 11	McL.
Argon	84.2	28.28[10]	2.80[7]	2.58	3.17	450.4	707.68	732.68
	87.3	28.70	2.52	2.32	2.75		705.44	726.00
Nitrogen	69.1	33.09[10]	2.31[8]	2.35	2.01	471.4	628.12	628.92
	71.4	33.51	2.09	2.07	1.79		622.00	592.12
	77.3	34.61	1.58	1.60	1.40		606.78	580.38
Benzene	298.2	89.40[8]	6.01[9]	6.05	6.13	2438	3078.6	3200.6
	308.2	90.51	5.24	5.19	5.30		3067.0	3184.6
	318.2	91.67	4.62	4.66	4.60		3051.2	3162.0

From experimental studies on viscosity, it appears that a hole of molecular size is not required to be prepared for a molecule to move into it but a hole of much smaller size may be involved in viscous flow. So the actual work of formation (W) of a hole of size suitable for viscous flow is a fraction of W'. Therefore, we may write

$$W = \theta E_s \left\{ \frac{V_s}{V} - \frac{1}{2n} \left(\frac{V_s}{V} \right)^3 \right\} \qquad (7)$$

The value of θ has been empirically determined by equating known values of η, A_f, σ, etc., in equation 11 for nitrogen, argon, and benzene, at different temperatures. It is found that the values of θ range between 0.24 and 0.37 and increase with temperature. The plot of 12θ against T/T_c where T_c is the critical temperature for each of the compounds is linear and the best line through them is represented by

$$\text{For argon, } 12\theta = 1.663 + 3.921(T/T_c) \qquad (8)$$

$$\text{For nitrogen, } 12\theta = 2.826 + 2.642(T/T_c) \qquad (9)$$

$$\text{For benzene, } 12\theta = 0.878 + 3.737(T/T_c) \qquad (10)$$

Substituting the values of e_0 and W into equation 4 one obtains

$$\eta = \frac{(2\pi mkT)^{1/2}}{2\pi\sigma a^2} A_f^{1/2} \exp\left[\frac{\theta E_s}{kT} \left\{ \frac{V_s}{V} - \frac{1}{2n} \left(\frac{V_s}{V} \right)^3 \right\} \right] \exp\left[\frac{\epsilon}{kT} \left(\frac{V_0}{V} \right)^4 \right] \qquad (11)$$

The equation may be compared with that of McLaughlin[3] which is

$$\eta = \frac{(2\pi mkT)^{1/2}}{2\pi\sigma a^2} \vartheta_f^{1/3} \exp\left[\frac{\epsilon}{kT} \left(\frac{V_0}{V} \right)^4 \right] \exp\left[\frac{\omega z \epsilon}{kT} \times \left\{ 1.2045 \left(\frac{V_0}{V} \right)^2 - 0.5055 \left(\frac{V_0}{V} \right)^4 \right\} \right] \qquad (12)$$

z is the coördination number and usually taken equal to 12, ω is a fraction of the lattice energy and has been given an empirical estimate by McLaughlin, ϑ_f is the free volume per molecule.

In Table II, the values of η calculated according to equations 11 and 12 and the energies of activation are compared with the experimental data. The coefficient of viscosity calculated according to equation 11 is in better agreement with the experimental values, while the energies of activation for viscous flow do not seem to agree well.

It is seen from Table III that the ratio of the work of formation of a hole to the energy required by a molecule to move into the hole is between 3 and 5 which

TABLE III

	Temp., °K.	W/k	e_0/k	W/e_0
Argon	84.2	282.5	71.34	3.96
	87.3	284.5	67.20	4.23
Nitrogen	69.1	252.2	61.86	4.08
	71.4	252.1	58.86	4.28
	77.3	251.7	51.69	4.87
Benzene	298.2	1124	415.3	2.71
	308.2	1138	395.5	2.87
	318.2	1150	375.6	3.06

is in good agreement with the observation made by Eyring.[2] Since we are here comparing W and e_0 at constant pressure and not at constant volume, it is easy to understand the tendency of this ratio to slightly increase with temperature. Further it is seen that the activation energies for viscous flow as calculated from equation 11 are almost independent of temperature.

(7) Rudenko and Schubnikow, *Physik. Z. Sowjet*, **6**, 470 (1934).
(8) J. Timmermans, "Physico-Chemical Constants of Pure Organic Compounds," Elsevier, Amsterdam, 1950.
(9) Amer. Petroleum Inst. Project 44 (1948–1952).
(10) "International Critical Tables," McGraw-Hill Book Co., New York, N. Y., 1933.

RADIATION INDUCED REACTION OF NITRIC OXIDE WITH CYCLOHEXANE

BY STANISLAW CIBOROWSKI

Radiochemistry Department, Institute of General Chemistry, Warsaw, Poland

Received October 29, 1962

Nitric oxide is an efficient radical scavenger and is expected to react with the cyclohexyl radicals produced in irradiated cyclohexane, to give nitrosocyclohexane. $G_{(\text{nitrosocyclohexane})}$ should be a measure of the number of cyclohexyl radicals formed in the radiolysis. It is however known that nitrosocyclohexane reacts with NO, the products being nitrocyclohexane, cyclohexyl nitrate, and cyclohexyl nitrite. The formation of these products can best be explained by postulating the formation of an intermediate compound, N-nitroso-N-cyclohexylhydroxylamine nitrite.[1-3] It is therefore of interest to determine what is the net result of the two competitive reactions: (a) the radiation induced formation of nitrosocyclohexane and (b) its secondary reaction with nitric oxide.

Recently Burrell[4] has postulated that the reaction between nitrosocyclohexane and nitric oxide in irradiated solutions proceeds rapidly to give the products nitrocyclohexane and cyclohexyl nitrate. On the other

(1) J. F. Brown, *J. Am. Chem. Soc.*, **79**, 2480 (1957).
(2) L. G. Donaruma and D. J. Carmody, *J. Org. Chem.*, **22**, 635 (1957).
(3) L. Batt and B. G. Gowenlock, *Trans. Faraday Soc.*, **56**, 682 (1960).
(4) E. J. Burrell, Jr., *J. Phys. Chem.*, **66**, 401 (1962).

hand Müller and Schmid[5] found a rather high G-value ($G = 2.6$) for bis-nitrosocyclohexane formed in the system.

Experimental

Chemicals.—Chemically pure cyclohexane was used. Nitric oxide was prepared by treating C.P. sodium nitrite with dilute sulfuric acid. The gas evolved was purified by passing it through aqueous solutions of 90% sulfuric acid and 50% potassium hydroxide.

Irradiations.—Irradiations were made at 25° using Gammacell 220, a ^{60}Co source of activity about 4000 curies. The dose rate in cyclohexane was 3.2×10^{17} e.v./g. min. as determined by the Fricke dosimeter. The construction of Gammacell offered no possibility of changing this dose rate. The irradiations were carried out for 7–14 hours, the total dose being of the order of 10^{20} e.v./g. Nitric oxide was bubbled through cyclohexane at the rate 2000 ml. per hour per 800 ml. of cyclohexane. After the irradiation was finished pure nitrogen was bubbled through the reaction mixture.

Analysis.—Acids were extracted from the reaction mixture by shaking with excess sodium carbonate solution and determined by potentiometric titration with hydrochloric acid. Cyclohexanone was determined by means of hydroxylamine hydrochloride. Cyclohexanone oxime was determined colorimetrically as the yellow compound formed in the presence of ferric-ammonium sulfate and formaldehyde.

For infrared analysis Zeiss spectrophotometer UR-10 was used.

Results

In the reaction mixture colorless crystals were always found on the walls of the reaction vessel. Those crystals were purified by washing with diethyl ether and then recrystallized from water. The resulting product was identified as adipic acid by means of elementary analysis and determinations of the acid number and of the melting point. The acid number of the crystalline substance not recrystallized from water was 789 mg. of KOH/g. It was then higher than that of adipic acid (768 mg. of KOH). These results suggest the presence of some amounts of lower dicarbonic acids as glutaric or succinic.

No considerable amounts of cyclohexanone and cyclohexanone oxime were found. The concentration of cyclohexanone in the reaction mixture was below 0.005 wt. % what corresponded $G_{(\text{cyclohexanone})} < 0.1$. Cyclohexanone oxime concentration was below 0.002 wt. %, hence $G_{(\text{cyclohexanone oxime})} < 0.04$.

The infrared analysis showed the presence of both nitrocyclohexane (6.44 band) and cyclohexyl nitrate (6.10 μ band) in the reaction mixture. No nitrosocyclohexane (8.28 μ band) was found. No quantitative infrared determinations were made.

The G-value for adipic acid formation was determined as 0.8 ± 0.05 molecule per 100 e.v. absorbed. This value was the average from ten experiments, total dose in cyclohexane between 1.3×10^{20} and 2.6×10^{20} e.v./g. In this range no influence of total dose on adipic acid yield was observed.

Discussion

The primary step in the reaction investigated is the formation of cyclohexyl radicals. Nitric oxide molecules scavenge these radicals and nitrosocyclohexane is formed. It reacts with nitric oxide to give different secondary products.[2,4] This latter reaction probably requires much higher NO concentration than the reaction of cyclohexyl radicals scavenging. Then $G_{(\text{nitrosocyclohexane})}$ depends on the stationary NO concentration in the system. At lower NO concentration nitrosocyclohexane will be formed while at higher NO concentration nitrosocyclohexane will be transformed into secondary products. Since at a constant dissolution rate of nitric oxide in cyclohexane its stationary concentration in the irradiated system depends on the dose rate, it may be expected that the $G_{(\text{nitrosocyclohexane})}$ value is influenced by the dose rate.

On the basis of the above conclusions the difference between Müller and Schmid[5] results and the results given here can be explained. Müller and Schmid reported a considerably high $G_{(\text{nitrosocyclohexane})}$ value while in this work no nitrosocyclohexane was found. Burrell's[4] results are in accordance with those of this work. This difference can be explained by the different dose rates employed. In Müller and Schmid's work the dose rate was 50 Mrad. per hour, which corresponds to 5.2×10^{19} e.v./g. min., while in this work the dose rate was as low as 3.2×10^{17} e.v./g. min. The data concerning the dose rate used in Burrell's work are not available.

The formation of adipic acid was not reported by Burrell nor by Müller and Schmid. Adipic acid may be formed by oxidation of cyclohexane or secondary products as cyclohexanone, cyclohexanone oxime, or cyclohexene. The oxidizing agents can be oxides of nitrogen or radicals, as for example NO_3. Such compounds are formed in the secondary reaction of nitrosocyclohexane with nitric oxide.[1,2] On the basis of the data presented here it is however not possible to indicate the appropriate mechanism of adipic acid formation.

Acknowledgment.—The author is grateful to Mrs. K. Śledzinska for technical assistance and to Mr. Z. Gwiazda for infrared measurements.

(5) E. Müller and G. Schmid, *Chem. Ber.*, **94**, 1364 (1961).

ADSORBATE–ADSORBENT INTERACTIONS IN THE CHEMISORPTION OF CARBON MONOXIDE[1]

BY R. A. GARDNER[2] AND R. H. PETRUCCI

Morley Chemical Laboratory, Western Reserve University, Cleveland, Ohio

Received November 9, 1962

The vibration frequencies of gaseous ions are different from the vibration frequency of the parent molecule; so too are the numbers of valence or outershell electrons. It is proposed that a relationship exists between the vibration frequencies of gaseous molecules and ions and their numbers of valence electrons. For gaseous species the number of valence electrons should be integral, for example 8 for $(CO)^{++}$, 9 for $(CO)^{+}$, and 10 for the neutral molecule CO. Also the vibration frequencies of chemisorbed species have been shown by Eischens, Pliskin, and Francis,[3] by Gardner and Petrucci,[4] and by others to be different from those of the neutral molecule, in particular to be intermediate to those of the neutral molecule and its gaseous ions.

(1) Based on the doctoral dissertation of R. A. Gardner, Western Reserve University, June, 1959. First presented at the 136th National Meeting of American Chemical Society, Atlantic City, N. J., September 14–18, 1959; and then presented in part at the 18th Meeting of the IUPAC Congress, Montreal, Quebec, August 11, 1961.

(2) Chemical and Physical Research Department, Standard Oil Company (Ohio), Cleveland, Ohio.

(3) R. P. Eischens, W. A. Pliskin, and S. A. Francis, *J. Chem. Phys.*, **22**, 1786 (1959).

(4) R. A. Gardner and R. H. Petrucci, *J. Am. Chem. Soc.*, **82**, 5051 (1960).

In this investigation a particular relationship between the vibration frequency and number of valence electrons is proposed for gaseous carbon monoxide species and then applied to chemisorbed species to see if the chemisorbed species follow the same relationship as the gaseous species.

The results presented in a previous investigation of the chemisorption of carbon monoxide[4] suggest that the relationship between vibration frequency and number of valence electrons is that of a right hyperbola passing through the points[5,6]: $\nu(CO)^+ = 2183.90$ cm.$^{-1}$ (9 valence electrons); $\nu(CO) = 2143.27$ cm.$^{-1}$ (10 valence electrons); and $\nu(CO)^{2-} = 0$ cm.$^{-1}$ (12 valence electrons). The equation obtained by using these points is

$$[2269.96 - \nu(CO)][12.1182 - E(CO)] = 268.31 \text{ cm.}^{-1} \quad (1)$$

$\nu(CO)$ is the vibration frequency of the carbon–oxygen bond and $E(CO)$ is the number of valence electrons—a number which should be integral for gaseous species and non-integral for adsorbed species. In Table I this equation is applied to experimental data from the chemisorption of carbon monoxide on several adsorbents.

TABLE I

VIBRATION FREQUENCIES AND NUMBER OF VALENCE ELECTRONS (CALCULATED FROM EQ.1)

	"Intermedions"		"Carbonyls"	
Adsorbent	Infrared bands, cm.$^{-1}$	Number of electrons	Infrared bands, cm.$^{-1}$	Number of electrons
Copper metal[a]			2095	10.59
Copper(I) fluoride[b]			2143	9.95
Copper(II) oxide[c]	2173	9.35	2127	10.24
	2121[g]	10.32	2000	11.12
Cobalt[d]	2160	9.68	2179	9.17
	2091	10.62		
Iron oxide[e]	2127	10.24	2020	11.04
Iron	1960	11.25		
Silver[f]	2165	9.56	[h]	
	2165[g]	9.56		
	2099	10.55		

[a] A sample of copper nitrate supported on Cab-o-sil was decomposed at 450°. The oxide was reduced with hydrogen at this temperature for 12 hours. [b] Copper(I) fluoride was precipitated in a water slurry of Cab-o-sil from $CuCl_2$ and NH_4F. The precipitate was washed until free of chloride ions. The sample was heated *in situ* in the spectrometer cell to 400° and reduced with iron. [c] Cupric oxide supported on M-5 Cab-o-sil was produced by the decomposition of the nitrate at 400°, *in vacuo*. [d] The adsorbent was cobalt oxide produced by the decomposition of the nitrate supported on Cab-o-sil and reduced at 400° with purified hydrogen. [e] These data for iron and iron oxide were reported by Eischens and Pliskin.[7] [f] Supported silver nitrate was partially decomposed by heating at 250° for 15 minutes *in vacuo*. The addition of CO produced the band at 2165 cm.$^{-1}$. Hydrogen gas was next added to a total pressure of 0.5 atm. and the 2099 cm.$^{-1}$ band for chemisorbed CO then appeared. [g] These bands were determined with a grating spectrometer, others with a NaCl prism spectrometer. [h] Carbonyls may also exist on this surface but their presence was not detected.

The data in Table I seem to fall naturally into two groups which we have termed "intermedions" and "carbonyls." For both of these type structures the numbers of valence electrons as calculated from equation 1 are non-integral. With the carbonyl structures there seems to be no particular pattern to the non-integral numbers, but for the pairs of intermedions discovered on several adsorbent surfaces the differences in numbers of valence electrons correspond almost exactly to one electron and the fractional parts of the non-integral numbers are constant, *e.g.*, 0.56 for silver, 0.25 for iron, etc.

There appear to be still other differences between carbonyls and intermedions. Whereas it is probable that carbonyl structures can be present on most if not all adsorbent surfaces, it is much less certain that this is the case for intermedions. Of the adsorbent materials listed in Table I intermedions were found on all except copper metal and copper(I) fluoride, and of the various metal atoms present in these different adsorbents only copper and copper(I) atoms do not have d-orbital vacancies according to their normal electronic configurations; it is possible that d-orbital vacancies are a requirement for the formation of intermedions.

The effect of components added to metal adsorbents is to cause a shift in the absorption band of carbonyl structures in a manner that seems dependent on the electronegativity of the added component. For example, the band at 2095 cm.$^{-1}$ on copper film is shifted to 2146 cm.$^{-1}$ when fluorine is added to copper, *i.e.*, on copper(I) fluoride. Added components to metal adsorbents change the distribution of the various intermedions, but not their vibration frequencies. Again these changes seem dependent on the electronegativity of the added component. Eischens and Pliskin[7] report an infrared absorption band for carbon monoxide on iron at 1960 cm.$^{-1}$ (corresponding to an 11.25 intermedion) which was replaced by a band at 2127 cm.$^{-1}$ (corresponding to a 10.25 intermedion) upon the addition of oxygen to the system. A similar effect was noted on introducing hydrogen to the system silver–carbon monoxide (*cf.* footnote *f* in Table I).

The fractional part of the non-integral number of valence electrons associated with intermedions is thought to be a unique property of the particular metal adsorbent, *e.g.*, 0.56 for silver, 0.25 for iron, etc. It is proposed to refer to this fraction as the "polarization fraction" of the metal. Studies are now underway to relate these polarization fractions to more familiar metal properties, to provide a more theoretical interpretation of the concept of intermedions, and to apply the concepts of intermedions and polarization fractions to an interpretation of catalytic reactions.

(5) G. Herzberg, "Molecular Spectra and Molecular Structure. I. Spectra of Diatomic Molecules," D. Van Nostrand Co., Inc., Princeton, N. J., 1955, p. 522.

(6) E. K. Plyler, L. R. Blaine, and W. S. Connor, *J. Opt. Soc. Am.*, **45**, 102 (1955).

(7) R. P. Eischens and W. A. Pliskin, "Advances in Catalysis," Vol. X, Academic Press, Inc., New York, N. Y., 1958, p. 2.

MAGNETIC PROPERTIES OF $Ni_2O_3 \cdot H_2O$

BY JAMES T. RICHARDSON

Humble Oil & Refining Company, Baytown, Texas

Received November 12, 1962

The valence state of nickel in its higher oxides is in considerable doubt. When chlorine or bromine in alkaline solution is added to a solution of a nickel salt, the result is a black, hydrated oxide with a composition from $NiO_2 \cdot xH_2O$ to $Ni_2O_3 \cdot xH_2O$. Cairns and Ott[1] prepared and studied a compound $Ni_2O_3 \cdot 2H_2O$, which

(1) R. W. Cairns and E. Ott, *J. Am. Chem. Soc.*, **55**, 527 (1933); **55**, 534 (1933).

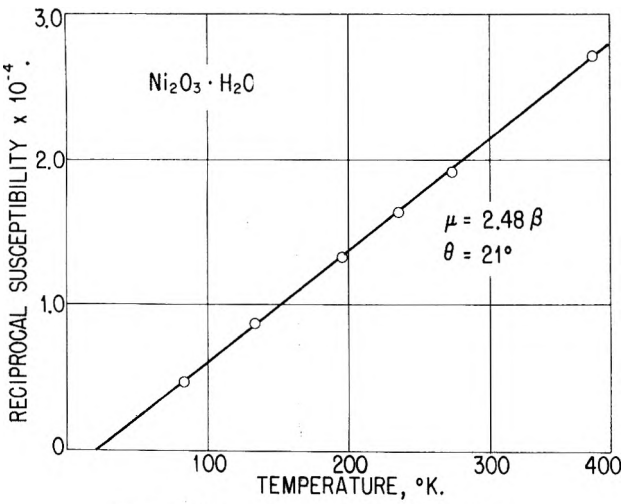

Fig. 1.—Curie–Weiss plot of $Ni_2O_3 \cdot H_2O$.

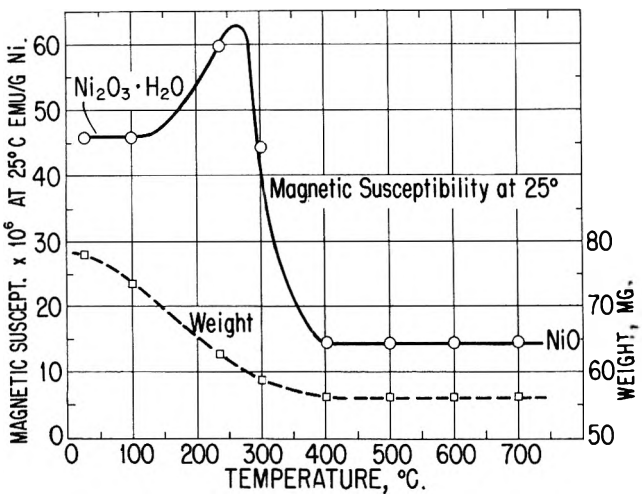

Fig. 2.—Magnetic susceptibility and weight changes for the decomposition of $Ni_2O_3 \cdot H_2O$.

decomposed on heating to $Ni_2O_3 \cdot H_2O$ and then to NiO. These authors[2] confirmed the presence of Ni^{3+} by X-ray absorption edge measurements, although Hanson and Milligan,[3] performing similar experiments, found no differences between these and NiO samples. Cairns and Ott also reported their failure to prepare anhydrous Ni_2O_3 by heating the hydrate. Recently, however, Aggarwal and Goswami[4] detected lines in electron diffraction patterns attributed to hexagonal Ni_2O_3 on the oxidized surface of nickel films. The existence of nickelic oxide is denied by Vainshtein,[5] who considers $Ni_2O_3 \cdot xH_2O$ to be a mixture of hydrated NiO and NiO_2.

In this investigation, three samples of $Ni_2O_3 \cdot xH_2O$ were prepared by adding bromine in KOH solution to solutions of nickelous chloride (a) with precipitation at 25° and air-drying, (b) with precipitation at 25° and drying at 100°, and (c) with precipitation at 100° and drying *in vacuo* at 25°. In each case chemical analyses were made for nickel (dimethylglyoxime method), "active" oxygen (Bunsen–Rupp test), and total oxygen (neutron activation analysis), with hydrogen obtained by difference. The results indicated the following compositions: (a) $Ni_2O_{3.02} \cdot 2.24H_2O$, (b) $Ni_2O_3 \cdot 1.50H_2O$, and (c) $Ni_2O_{3.05} \cdot 2.15H_2O$. X-Ray diffraction patterns of all three samples are identical and agree with sample A in ref. 1, designated by Cairns and Ott as "$Ni_2O_3 \cdot 2H_2O$." Magnetic susceptibility measurements were made from −196 to 100° on all samples, which demonstrated the same Curie–Weiss relationship shown in Fig. 1 for sample (b). The constants yield $\mu = 2.48\beta$ and $\theta = +21°$. Sample (a) was heat-treated for 24 hours at approximately 100° intervals up to 700°. Following each heat-treatment, the sample was cooled to room temperature and the magnetic susceptibility and weight measured. These data are plotted in Fig. 2. X-Ray absorption edge measurements revealed no differences between these samples and NiO. Conductivity and the Seebeck coefficient measurements show the material to be n-type, whereas NiO is p-type.

Both the room temperature susceptibility and the weight of the oxide reach a constant value when heat-treated above 400° with the susceptibility characteristic of NiO. Partial loss of H_2O occurs immediately upon heating to 100°, but with no change in the magnetic properties. Decomposition begins at about 130°, where the weight corresponds to $Ni_2O_3 \cdot 1.25H_2O$. The maximum in susceptibility between 100 and 400° is due to the presence of small particles of NiO, which exhibit enhanced superparamagnetic susceptibilities when prepared at lower temperatures.[6] This effect decreases with higher temperatures of heat-treatment and disappears above 400°.

The Curie–Weiss dependence of the susceptibility indicates the presence of one paramagnetic phase only. Chemical analysis identifies this phase as a hydrous oxide of trivalent nickel. Contrary to the findings of Cairns and Ott[1] but in agreement with Hüttig and Peter,[7] this oxide may be dehydrated below $Ni_2O_3 \cdot 2H_2O$ without changing either the structure or the magnetic properties. Decomposition to NiO occurs just before the monohydrate is reached. It, therefore, appears that, if this material is a true hydrate, it is $Ni_2O_3 \cdot H_2O$ with adsorbed water.

Trivalent nickel in a low spin state has a spin-only magnetic moment of 1.73β. The observed moment of 2.48β suggests, therefore, a low spin state with considerable unquenched orbital contribution. The positive sign of the Weiss constant is an indication of ferromagnetic coupling between the nickel atoms.

(2) R. W. Cairns and E. Ott, *J. Am. Chem. Soc.*, **56**, 1094 (1934).
(3) H. P. Hanson and W. O. Milligan, *J. Phys. Chem.*, **60**, 1144 (1956).
(4) P. S. Aggarwal and A. Goswami, *ibid.*, **65**, 2105 (1961).
(5) E. E. Vainshtein, *Zh. Eksperim i Teoret. Fiz.*, **20**, 442 (1950).
(6) J. T. Richardson and W. O. Milligan, *Phys. Rev.*, **102**, 1289 (1956).
(7) Hüttig and Peter, *Z. anorg. allgem. Chem.*, **189**, 190 (1930).

FREE RADICALS FORMED FROM *o*-SUBSTITUTED NITRO COMPOUNDS[1a]

BY A. J. TENCH[1b] AND P. COPPENS[1c]

Chemistry Department, Brookhaven National Laboratory, Upton, L. I., New York

Received November 10, 1962

The photochemical rearrangement of *o*-nitrobenzaldehyde to nitrobenzoic acid was discovered in 1901[2] and has been investigated by various workers (see for example ref. 3). The reaction is known to occur both in the solid state and in solution. It seemed possible that a paramagnetic species could be formed during the

(1) (a) Research performed under the auspices of the U. S. Atomic Energy Commission; (b) Chemistry Division, Atomic Research Establishment, Harwell, Didcot, Berks, England; (c) Crystallography Department, Weizmann Institute of Science, Rehovoth, Israel.
(2) G. Ciamician and P. Silber, *Ber.*, **34**, 2040 (1901).
(3) P. Leighton and F. A. Lucy, *J. Chem. Phys.*, **2**, 756 (1934).

photochemical process and that an electron spin resonance (e.s.r.) study would give useful information.

We have irradiated *o*-nitrobenzaldehyde within the microwave cavity of a Varian e.s.r. spectrometer with 100 kc. field modulation. The light source was a one kilowatt G.E. mercury lamp and light shorter than 3500 Å. was filtered out. Free radicals were observed in powdered *o*-nitrobenzaldehyde at liquid nitrogen temperature. The powder spectrum shows a distinct hyperfine structure, but anisotropic broadening of the peaks gives a large overlap and the spectrum is not easily analyzed; on warming to room temperature the signal largely disappeared. Free radical signals of comparable strength, but of a different nature, were obtained on the low temperature irradiation of *o*-nitrocinnamic acid and *o*-nitrobenzyl alcohol, which undergo reactions similar to that of *o*-nitrobenzaldehyde.[4,5] Negative results were obtained, however, on irradiation of nitrobenzene and *o*-nitrobenzoic acid. This is expected since these compounds do not undergo the above photochemical reactions. These results indicate that the photochemical reactions of *o*-nitrobenzaldehyde, *o*-nitrobenzyl alcohol, and *o*-nitrocinnamic acid may have a free radical intermediate. It may be noted that the ultraviolet spectra of nitrobenzene and *o*-nitrobenzoic acid are very similar to the ultraviolet spectrum of *o*-nitrobenzaldehyde.[6-8] Therefore the negative results obtained with the first two compounds cannot be due to insufficient absorption at wave lengths longer than 3500 Å.

We decided that it was preferable to study these compounds in solution since the anisotropic part of the coupling tensor is averaged out.[9] The spectra obtained during the irradiation of 0.1 to 1.0 molar solutions of *o*-nitrobenzaldehyde in deoxygenated ethyl alcohol and isopropyl alcohol show a well resolved fine structure (Fig. 1a), which can be readily interpreted in terms of nitrogen and proton hyperfine splitting constants (Table I). The solutions were contained in a flat cell, 1 mm. thick, similar to the Varian aqueous cell. The disappearance of the radicals after the lamp has been switched off is proportional to the square of the free radical concentration. The rate constant for this reaction was found to be 1.3 l. mole^{-1} sec.$^{-1}$ for an initially 1 molar solution of *o*-nitrobenzaldehyde in ethanol. The total number of radicals formed during the first 30 minutes was determined to be about 0.02% of the *o*-nitrobenzaldehyde concentration by comparison with a standard solution of DPPH in ethanol. In the same two samples the amount of conversion to *o*-nitrobenzaldehyde was determined by reacting the nitroso group with acidified KI and titrating the liberated iodine. About 4% of the *o*-nitrobenzaldehyde was converted in 30 minutes. The error in the measurement of the free radical concentration may be as high as a factor of 2 but the low concentration indicates that the free radical we observe is not an intermediate in the photochemical rearrangement to a nitroso compound.

The main feature of the spectrum of the radical produced on irradiation of *o*-nitrobenzaldehyde is the large interaction with one proton (see Table I). In order to aid the identification of this radical we have produced the negative ion of *o*-nitrobenzaldehyde by a method similar to that described by Geske and Maki.[10] The coupling constants of the negative ion $CHOC_6H_4NO_2^-$ in acetonitrile are listed in Table I. In this spectrum the large doublet splitting observed in the photochemically produced radical is absent, the highest proton coupling constant being about 3 gauss, while the nitrogen coupling constants are comparable in both radicals.

The comparison of these two spectra should be made in the same solvent since the solvent has been shown to influence the splitting constants.[11] When *o*-nitrobenzaldehyde was photolyzed in an acetonitrile solution only a very weak signal was observed; on the addition of 10% ethyl alcohol a well resolved spectra was obtained with essentially the same splitting constants as in 100% ethyl alcohol. Thus in this case the solvent effect on the radical is very small. On the other hand the negative ion of *o*-nitrobenzaldehyde shows a con-

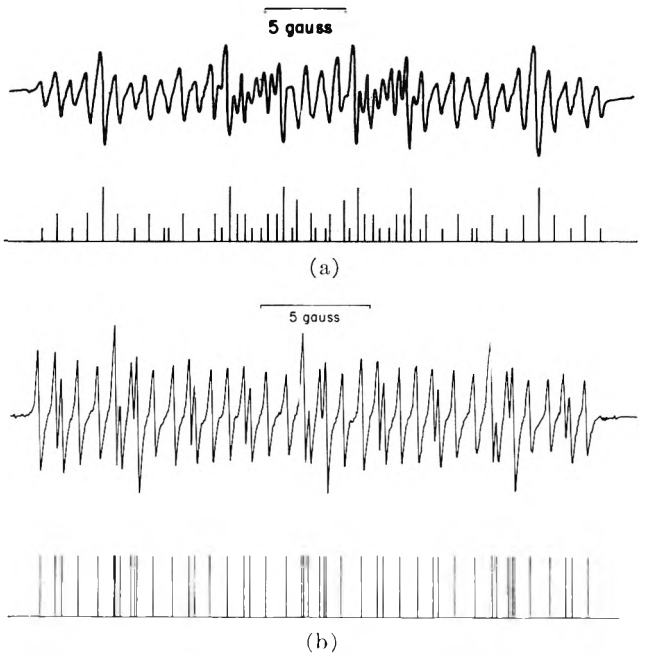

Fig. 1.—(a) E.s.r. spectrum of radical produced on ultraviolet irradiation of *o*-nitrobenzaldehyde; (b) e.s.r. spectrum of *o*-nitrobenzaldehyde negative ion in acetonitrile and 10% ethyl alcohol.

TABLE I

HYPERFINE COUPLING CONSTANTS (IN GAUSS)[a]

Photoradicals	a_N[c]	a_1	a_2	a_3	a_4	a_5
2-Nitrobenzaldehyde						
in 100% alcohol	8.1	11.2	2.90[d]	1.00[d]		
in 10% alcohol[b]	7.9	11.2	2.87[d]	0.95[d]		
5-Chloro-2-nitrobenzaldehyde						
in 100% alcohol	7.8	10.5	3.76	1.75	0.85	
Negative ions						
2-Nitrobenzaldehyde						
in acetonitrile	7.2	3.40	2.40	1.00	0.60	0.30
in 10% alcohol[b]	8.6	3.40	2.65	1.01	0.73	<0.15
5-Chloro-2-nitrobenzaldehyde						
in acetonitrile	6.55	3.02	1.67	0.50	<0.4	
6-Chloro-2-nitrobenzaldehyde						
in acetonitrile	8.55	4.03	3.00	1.88	0.93	

[a] All coupling constants quoted to ±0.05 gauss. [b] 10% ethyl alcohol–90% acetonitrile. [c] Nitrogen coupling constant. [d] Interaction with two equivalent spins of $I = 1/2$. All other data for a_1 to a_5 are for interaction with one spin of $I = 1/2$.

(4) F. Sachs and S. Hilpert, *Ber.*, **37**, 3425 (1904).
(5) I. Tanasescu, *Bull. soc. chim.*, **41**, 1074 (1927).
(6) A. E. Lutskii and V. T. Alekseeva, *J. Gen. Chem. USSR*, **29**, 3211 (1959).
(7) P. Grammaticakis, *Bull. soc. chim.*, [5], **18**, 224 (1951); [5], **20**, 825 (1953).
(8) H. Venner, *Chem. Ber.*, **89**, 1635 (1956).
(9) S. I. Weissman, *J. Chem. Phys.*, **22**, 1378 (1954).
(10) D. H. Geske and A. H. Maki, *J. Am. Chem. Soc.*, **82**, 2671 (1960).
(11) E. W. Stone and A. H. Maki, *J. Chem. Phys.*, **36**, 1944 (1962).

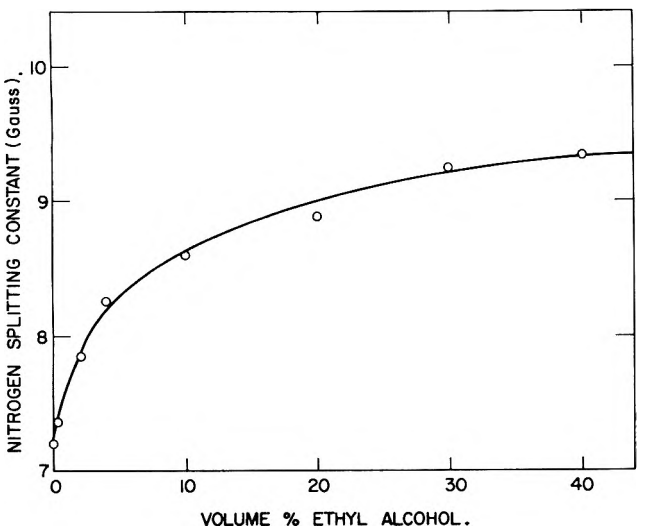

Fig. 2.—The effect on the nitrogen splitting constant of the negative ion of *o*-nitrobenzaldehyde of altering the solvent–composition by adding ethyl alcohol to the acetonitrile.

siderable solvent effect, the spectrum increasing in length as more ethyl alcohol is added, while at the same time the radical becomes less stable. The increase in length is caused mainly by a change in the nitrogen splitting constant the variation of which is given in Fig. 2. We attribute this change in the nitrogen splitting constant to a redistribution of the electron density in the nitro group due to increasing hydrogen bonding by the alcohol molecules.

Comparison of Fig. 1a and b indicates that even after the solvent effect is eliminated the photoradical spectrum is very different from that of the negative ion and since the spectrum of the positive ion should be similar to that of the negative ion,[12] we may say that the photoradical corresponds to neither of these ions.

The 5- and 6-chloro-substituted *o*-nitrobenzaldehydes are photosensitive and the comparison of the negative ions and photoradicals for 5-chloro compounds showed a large proton splitting of about 11 gauss in the photoradical but this is not present in the negative ion. Thus the 5-chloro compound behaves in the same way as *o*-nitrobenzaldehyde. The 6-chloro compound did not give a measurable photoradical, owing presumably to steric factors.

Very few examples of such a large proton splitting in aromatic compounds have been reported in the literature. Porter[13] has reported a proton splitting of 11.9 gauss attributed to the hydrogen on the nitrogen in a 2,4,6-tri-*t*-butylanilino radical (—N̈—H). Similar splitting constants for the proton attached to the nitrogen atom have been found by Stone and Waters[14] for the *p*-aminobenzoic acid radical (—N̈—H). Thus it would seem that the proton causing the large splitting in the photoradical is located directly on the nitrogen. We propose one of the following structures for the radical

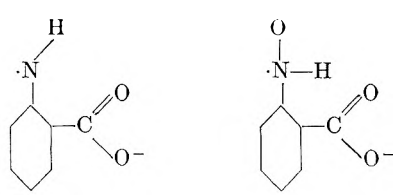

(12) R. Bersohn, "Determination of Organic Structures by Physical Methods," Vol. II, Academic Prses, New York, N. Y., 1962, p. 579.

A fraction of these radical ions would be protonated by the alcohol to give a neutral radical. The splitting of such a proton would probably be lost in the line width.[14] The photoradical probably arises from a side reaction to the conversion of the nitro group to a nitroso group since the low radical yield indicates conclusively that it is not an intermediate of the rearrangement to give nitrosobenzoic acid.

In the absence of single crystal studies it is not possible to say whether the photoradical in the solid state is the same as that seen in solution. The low temperatures necessary to stabilize the photoradical in the solid state indicate that the two radicals are probably different species.

(13) G. Porter, "The Fifth International Symposium on Free Radicals," Stockholm 1961.

(14) T. J. Stone and W. A. Waters, *Proc. Chem. Soc.*, 253 (1962).

THE THIRD VIRIAL COEFFICIENT OF POTASSIUM AS ESTIMATED FROM ITS VAPOR PRESSURE[1]

By J. F. Walling

Battelle Memorial Institute, Columbus, Ohio

Received November 15, 1962

The importance of dimers (or alternatively the second virial coefficient) has long been recognized in connection with all of the alkali metals. Simple thermodynamics predicts increasing complexity of saturated vapors of alkali metals with increasing temperature. The vapor pressure data discussed here are the first for potassium[2] that corroborate this prediction by displaying the effect of trimers.

The vapor pressure of carefully purified potassium was determined in a modified boiling point experiment. In brief, purified helium was maintained at constant pressure over a small sample of potassium contained in a test tube. Data were collected using a stainless steel test tube up to about 1100°K. At higher temperatures a container of 99% niobium–1% zirconium alloy was employed to avoid bothersome reactions. The imposed slow temperature rise of the metal, measured by means of a sheathed Pt *vs.* Pt–10% Rh thermocouple immersed in the liquid, was recorded as a function of time. It was possible, with the application of some corrections in the case of the stainless steel apparatus, to identify the estimated break in the curve with the onset of boiling. Pressures below two atmospheres were measured using a large (2.5-cm. diameter legs) mercury manometer back lighted and read with a cathetometer. A conventional barometer was used to determine atmospheric pressure in all measurements exceeding one atmosphere. Gravitational and mercury temperature corrections were applied. Pressures exceeding two atmospheres were measured using dead weight calibrated Bourdon-type gages. Data, in order of collection, are shown in Table I.

An apparent third law heat of sublimation to the monomer at absolute zero (ΔH_0^0) was calculated from each datum by using recently published free energy

(1) Based on research for the National Aeronautics and Space Administration under Contract NAS 5-584.

(2) The only other published potassium data which extend to sufficiently elevated temperatures seem to be in serious error. N. S. Grachev and P. L. Kirillov, *Inzhenerno-Fizicheskiy Zhurnal*, **3** [6], 62 (1960).

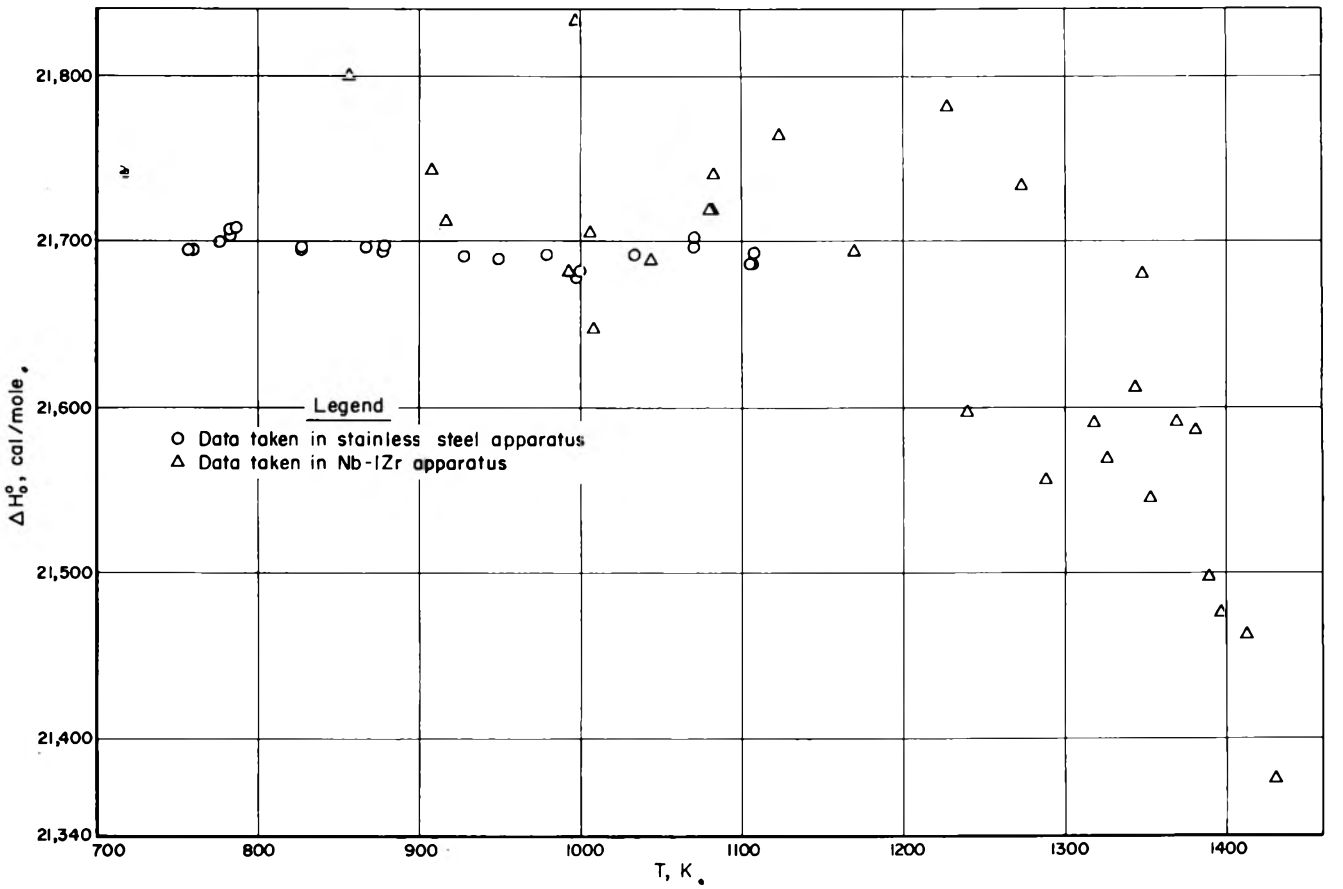

Fig. 1.—Apparent heat of sublimation to monomeric potassium at absolute zero.

TABLE I

POTASSIUM VAPOR PRESSURE

Pressure, atm.	Temp., °K.[a]	Pressure, atm.	Temp., °K.[a]
Stainless steel tube[b]		Nb–1Zr tube	
0.0450	783.0	0.2544	907.5
.0451	782.9	0.6535	997.3
.0473	786.0	13.63	1412.8
.1544	866.1	8.02	1318.5
.9798	1032.1	12.01	1389.3
1.3747	1070.1	5.080	1241.4
1.3761	1070.6	0.1268	856.0
0.0411	777.2	8.46	1326.3
.5776	978.2	11.18	1381.0
.0887	826.4	12.56	1396.3
.0887	826.4	9.82	1352.8
.3316	927.4	0.7836	1006.2
1.8730	1107.1	6.899	1289.5
		15.27	1430.5
Nb–1Zr tube		Stainless steel tube[b]	
0.2868	916.0	0.1851	879.9
0.7604	1006.1	.1850	879.9
1.0816	1042.6	.4207	948.4
1.4867	1080.5	.1803	877.8
1.4892	1081.9	.0306	759.6
1.4870	1080.6	.7165	999.0
5.852	1273.5	1.8489	1105.3
4.287	1226.8	1.8494	1105.3
10.52	1369.5	0.0296	757.7
9.14(−)	1344.0	0.7174	998.9
9.14(+)	1348.9		
0.6707	992.3		
3.024	1170.3		
2.068	1123.6		

[a] 0°K. was taken as −273.2°C. [b] In the stainless steel tube the thermocouple output when boiling began depended on depth of immersion. A correction has been applied. Observed temperatures for the first three points of the second stainless grouping were 1.6°K. lower than indicated in the table. For all other stainless points observations were 2.7°K. lower than indicated. Values for Nb–1Zr groupings contain no corrections.

functions and second virial coefficients.[3] The results are shown in Fig. 1. It is concluded that the data below about 1150°K. are consistent with the third law when the heat of sublimation at absolute zero is taken to be 21,710 ± 30 cal./mole. This agrees well with other determinations.

The behavior of the apparent ΔH_0^0 above about 1150°K. can be reasonably explained by assuming failure of the equation used for its calculation due to the inclusion of only second virial corrections. In view of experimental scatter in this region, the exponential $1915.4/T \exp[-4338.9/T]$ represents the product $BP/R'T$ well even at 1400°K.[4] Although it is necessary to extrapolate the free energy function of the liquid substantially above the upper limit of heat capacity measurements, the characteristically small temperature coefficient of such functions indicates that the error introduced is probably not serious for the present endeavor. Thus, if the equation is inadequate the fault lies mostly in an omission, not in the terms already present.

Therefore, a correction function ascribed solely to third virial effects was constructed. The correction is of the form $CP^2/2R'T$, where C is taken to be the third virial coefficient in the pressure expansion of the virial equation of state. Because of the small temperature interval involved, the approximately equivalent empirical form $(a/T)e^{B/T}$ was used. The equation which rep-

(3) R. J. Thorn and G. F. Winslow, *J. Phys. Chem.*, **65**, 1297 (1961).

(4) See ref. 3 for definition of symbols and meaning of exponential expression.

resents the data between 758 and 1430°K. with a standard deviation of log P of ±0.0097 is then

$$\log P = \frac{4794.3}{T} - 1.97108 \log T + 4.9800 \times 10^{-4}T - 1.0659 \times 10^{-7}T^2 + 10.1451 + \frac{1915.4}{T} \times \exp(-4338.9/T) + \frac{7.40 \times 10^4}{T} \exp[-1.056 \times 10^4/T]$$

The last term is the correction function determined by a least-squares analysis of the deviations of measured pressures from those calculated by means of all other terms in the equation.

The sensibility of this correction is suggested by the values of calculated thermodynamic functions for clusters of three atoms. The third virial coefficient used here is constituted of the formation constants (K_n) for clusters of n atoms by the relation[5] $C = [3K_2^2 - 2K_3]RT$, where $K_2 = -B/RT$. Thus, the empirical correction term was used to estimate crudely K_3 at three temperatures, the heat of formation of trimer at 1300°K., and the trimer entropy at 1300°K. Values appear in Table II. Uncertainties are approximate.

TABLE II

ESTIMATED PROPERTIES OF CLUSTERS OF THREE POTASSIUM ATOMS

T, °K.	C, atm.$^{-2}$	K_3, atm.$^{-2}$	ΔH_f, kcal./mole	S^0, e.u.
1200	-3.0×10^{-3}	2.5×10^{-3}		
1300	-1.5×10^{-3}	$(1.2 \pm 0.3) \times 10^{-3}$	-23 ± 12	106 ± 14
1400	-0.83×10^{-3}	6.1×10^{-4}		

The entropy value in Table II can be compared crudely with that calculated on the basis of ideal gas polymers. If one assumes arbitrarily that (1) the trimer is linear having internuclear distances equal to that in the dimer, (2) the four vibrations all appear at about 92 cm.$^{-1}$ as does the one in the dimer, (3) the ground electronic state is a doublet, and (4) the molecule is a rigid rotor and a harmonic oscillator, it is possible to estimate that the entropy of the ideal trimer at 1300°K. is about 24 e.u. greater than that of the ideal dimer, mostly because of vibrational contributions. The same difference based on the entropy value in Table II and a previous estimate for the dimer[6] is 33 e.u. Considering the crudity of the calculation the agreement is good. Certainly, it is improper to base any structural inferences on these data and calculations.

The suggested constant heat of polymerization (the dissociation energy of the dimer is 11.85 kcal./mole) is unlike the presumably analogous situation of H_2 and H_3 but not absurd.

The credibility of the vapor pressure data and interpretation of the correction is demonstrated. It is hoped that data from other kinds of measurements now in progress will lead to better values for the third virial coefficient.

Acknowledgment.—It is a pleasure to acknowledge the assistance of Mr. A. W. Lemmon, Jr., Dr. W. M. Goldberger, and Messrs. T. W. Culbertson, R. E. King, H. K. Nuzum, D. A. Peil, and L. A. Winkler in this investigation.

(5) H. W. Woolley, *J. Chem. Phys.*, **21**, 236 (1953).

(6) W. H. Evans, R. Jacobson, T. R. Munson, and D. J. Wagman, *J. Res. Natl. Bur. Std.*, **55**, 83 (1955).

THE REACTIONS OF METHYL RADICALS WITH AROMATIC COMPOUNDS. III. THE FLUOROTOLUENES

BY FRANCIS J. WUNDERLICH AND R. E. REBBERT[1]

Chemistry Department Georgetown University, Washington 7, D. C.

Received December 3, 1962

As in parts I[2] and II,[3] this investigation was undertaken so that a better representation of the rates of hydrogen atom abstraction by methyl radicals from aromatic compounds would be available. The fluorotoluenes were chosen so that a check could be obtained on the effect of the *para*, *ortho*, and *meta* substitutions. In the pyrolysis of the fluorotoluenes Szwarc and Roberts[4] found the dissociation energy of the C–H bond of the side chain to be the same (78 kcal.) within experimental error for all three isomers.

Experimental

The same apparatus and general procedure as described previously were used.[2] The *para*-, *ortho*-, and *meta*-fluorotoluenes were obtained from Eastman Organic Chemicals Co. Conversions were kept below 1%.

Results

The results are summarized in Table I.

The following equations give the best straight lines through the experimental points: for *p*-fluorotoluene

$$13 + \log \frac{k_3}{k_2^{1/2}} = 4.031 - \frac{1247}{T} \qquad (1a)$$

for *o*-fluorotoluene

$$13 + \log \frac{k_3}{k_2^{1/2}} = 4.209 - \frac{1315}{T} \qquad (1b)$$

for *m*-fluorotoluene

$$13 + \log \frac{k_3}{k_2^{1/2}} = 4.762 - \frac{1555}{T} \qquad (1c)$$

All the rate constants are in molecules, cc., and sec. k_3 and k_2 refer to the reactions

$$2CH_3 \longrightarrow C_2H_6 \qquad (2)$$

$$CH_3 + RH \longrightarrow CH_4 + R \qquad (3)$$

The activation energies for the hydrogen abstraction reactions are 5.7 ± 0.4, 6.0 ± 0.4, and 7.1 ± 0.2 kcal./mole, respectively, for *p*-, *o*-, and *m*-fluorotoluenes. The pre-exponential factors, $A_3/A_2^{1/2}$, for these three reactions are $1.1 \pm 0.6 \times 10^{-9}$, $1.6 \pm 1.0 \times 10^{-9}$, and $5.8 \pm 1.3 \times 10^{-9}$ molecule$^{-1/2}$ cc.$^{1/2}$ sec.$^{-1/2}$. The stated precisions in the activation energies and in the pre-exponential factors have been determined from the average deviation of the rate constants over the temperature interval used.

Discussion

As in the previous paper,[3] the results indicate that the C–H bond dissociation energies of the fluorotoluenes for the methyl group should follow the order: *para*, *ortho*, *meta*. The difference in activation energies and pre-exponential factors for the hydrogen abstraction reac-

(1) Division of Physical Chemistry, National Bureau of Standards, Washington 25, D. C.

(2) I. B. Burkley and R. E. Rebbert, *J. Phys. Chem.*, **67**, 168 (1963).

(3) W. A. Sanders and R. E. Rebbert, *ibid.*, **67**, 170 (1963).

(4) M. Szwarc and J. S. Roberts, *J. Chem. Phys.*, **16**, 609 (1948).

TABLE I

Temp., °C.	Acetone pressure (mm.)	RH (mm.)	Time (sec.)	Products (μmoles) CO	CH_4	C_2H_6	$\frac{k_3}{k_2^{1/2}} \times 10^{13}$ (cc.$^{1/2}$ molecules$^{-1/2}$ sec.$^{-1/2}$)
				p-Fluorotoluene			
333	52.9	61.4	2700	0.588	0.248	0.380	2.12
347	54.1	55.0	2700	1.29	0.387	0.651	2.67
352	54.1	52.0	1800	0.735	0.254	0.405	2.80
369	50.9	49.0	1800	0.725	0.388	0.408	4.49
405	25.3	25.6	1800	0.751	0.546	0.740	8.24
409	51.2	30.0	1800	1.57	0.995	0.690	11.1
437	52.8	52.1	1800	1.70	1.73	0.425	16.2
460	60.6	57.2	1800	3.06	3.26	0.591	20.7
				o-Fluorotoluene			
331	63.8	36.3	2700	1.08	0.233	0.855	1.95
343	39.9	40.8	2700	1.14	0.264	0.756	2.28
370	50.4	46.0	2700	2.25	0.776	1.43	3.89
391	43.3	42.4	1800	1.65	0.84	0.964	7.17
395	53.5	52.8	1800	2.19	1.16	1.24	6.42
417	42.9	43.3	1800	2.10	1.28	0.786	10.9
438	55.6	55.6	1800	2.44	2.54	0.970	17.9
461	60.6	57.3	1920	3.25	3.87	0.673	24.4
				m-Fluorotoluene			
340	55.8	62.5	1800	0.668	0.203	0.443	1.51
354	48.3	51.5	2040	0.991	0.304	0.677	2.36
381	49.9	53.1	1940	1.73	0.714	0.863	5.04
406	54.6	56.4	1860	2.31	1.44	1.035	8.02
432	59.2	61.6	900	1.68	1.26	0.437	14.3
448	59.2	23.4	900	1.86	1.25	0.466	20.2

tion for the *p*- and *o*-fluorotoluene is quite small and within the experimental error. However, there is a real and significant difference in these two factors between this pair and the *m*-fluorotoluene. It is interesting to note that the rate constants for all three are the same at 182°. Thus the difference in activation energy is partly off-set by a difference in the pre-exponential factor.

Szwarc and Roberts,[4] assuming a constant pre-exponential factor for all three fluorotoluenes, concluded in their pyrolysis experiments that the C–H bond dissociation energy was 78 ± 0.4 kcal./mole for all three isomers. However, a variation of five in the pre-exponential factor would increase this difference in dissociation energy to 3–4 kcal./mole. Our results would indicate that this is the case. Earlier results[5] have indicated that in various reactions, substitutions in the *para* or *meta* positions give similar pre-exponential factors. In these cases the reactions were carried out in solutions. Evidently this is not true in all cases.

The activation energy and the pre-exponential factor for the *m*-fluorotoluene hydrogen abstraction reaction are almost identical with those for toluene itself,[2] but when the fluorene atom is in the *ortho* or *para* position both are reduced. This is not too surprising since for both of these isomers one can write resonance structures as

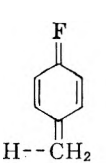

and

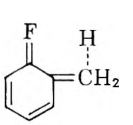

but this cannot be done for the *meta* isomer. Thus the fluorine atom in the *ortho* and *para* positions reduces both the activation energy and the steric factor while in the *meta* isomer it has very little effect on either of these.

One of the referees has suggested that methane could also be formed by the reaction

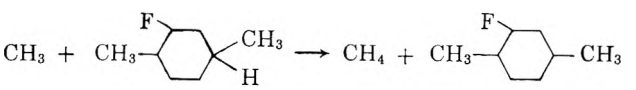

However, as mentioned in part I,[2] there is no evidence for the addition of methyl radicals to the benzene ring in this work, since the ratio $(CH_4 + C_2H_6)/CO$ is unity or slightly above under all conditions.

(5) E. G. Williams and C. N. Hinshelwood, *J. Chem. Soc.*, 1079 (1934); C. K. Ingold and W. S. Nathan, *ibid.*, 222 (1936); D. P. Evans, J. J. Gordon, and H. B. Watson, *ibid.*, 1430 (1937).

VISIBLE SPECTRA AND ACID ASSOCIATION CONSTANTS OF $[Re(en)_2O_2]^+$ TYPE COMPOUNDS[1]

BY R. KENT MURMANN AND D. R. FOERSTER

Department of Chemistry, University of Missouri, Columbia, Missouri

Received December 17, 1962

In the course of some studies of the rates of ligand exchange reactions with $[Re(en)_2O_2]^+$ type ions the visible spectra and acid association constants were measured. Three ions were studied: $[Re(en)_2O_2]^+$, $[Re(1,2\text{-pn})_2O_2]^+$, and $[Re(1,3\text{-pn})_2O_2]^+$.[2] The complexes are stable indefinitely in dilute acid media but slowly disproportionate in concentrated HCl and are slowly oxidized by dilute HNO_3 or $HClO_4$. In the range of acidities of 0 to 8 *M*, with all of the complexes studied,

(1) This work was supported by the Division of Grants, National Institute of Health (No. A-3006) and the University of Missouri Research Council.

(2) The abbreviations used are en = ethylenediamine, pn = propylenediamine.

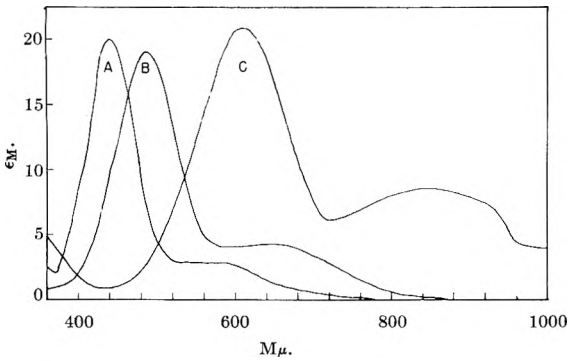

Fig. 1.—Absorption spectra: A, $[Re(en)_2O_2]^+$; B, $[Re(en)_2O(OH)]^{+2}$; C, $[Re(en)_2(OH)_2]^{+3}$. Maximum absorption of major peak at 440, 486, 610 mμ, respectively. For analogous complexes of 1,3-pn and 1,2-pn 441, 445; 490, 488; 610, 612, respectively. Spectral curves for the 1,2-pn and 1,3-pn complexes are essentially the same as shown for the en derivative.

three species were spectrally shown to exist corresponding to the solid compounds prepared by Lebedinsky and Ivanov-Emin.[3] They were $[Re(en)_2O_2]Cl$, $[Re(en)_2O(OH)]Cl_2$, and $[Re(en)_2(OH)_2]Cl_3$ and had a brown-green, violet, and blue color, respectively. We have confirmed their results on the solid species and since the spectral characteristics are nearly the same in the solid (KBr disks) and in solution, the ions in solution are probably the same as in the solid state. It is assumed that the H^+ adds to the oxygen of the complex since infrared spectra support this. Analogous complexes of 1,2-pn and 1,3-pn have shown the same spectral and chemical characteristics.

The acid association constants were evaluated by pH titration and by spectrophotometric means; both methods giving the same results. No difference in the acid association constants could be found between the en, 1,2-pn, and 1,3-pn complexes. For the first association corresponding to the reaction

$$[Re(en)_2O_2]^+ + H^+_{aq} \rightleftarrows [Re(en)_2O(OH)]^{+2}$$

$\log K_1 = 3.26 \pm 0.02$ at $\mu = 0.02$ and 25.3°.

The second association is extremely weak and can only be estimated. It was evaluated spectrophotometrically and because of the high ionic strength has only qualitative significance. Within experimental error the three complexes gave the same value for the reaction

$$[Re(en)_2O(OH)]^{+2} + H^+_{aq} \rightleftarrows [Re(en)_2(OH)_2]^{+3}$$

$\log K_2 = -0.9 \pm 0.1$ at $\mu = 5$ and 25.3°.

ΔH for the first association reaction (corresponding to K_1) was measured by the variation of K_1 with temperature and by calorimetric means. Although the reproducibility by the former method was poor, the two methods gave essentially the same values:

Complex	ΔH, kcal./mole
$[Re(en)_2O_2]^+$	-3.28 ± 0.15[a]
$[Re(en)_2O_2]^+$	$-3.50 \pm .05$[b]
$[Re(1,2\text{-pn})_2O_2]^+$	$-3.46 \pm .05$[b]
$[Re(1,3\text{-pn})_2O_2]^+$	$-3.44 \pm .05$[b]

[a] By temperature variation of K_1. [b] Calorimetrically.

The value of $\log (K_1/K_2)$ is about 4 which is in the normal range for di-acids where the oxygens are bound to the same atom. Compared to other ions of the same charge type, *i.e.*, $[Co(en)_2(NH_3)OH]^{+2}$ and $[Co(NH_3)_5OH]^{+2}$ these rhenium complexes are much more acidic. This is probably due to π-bonding of the oxygens by electron donation to the metal. This would be expected to occur with those metal ions having a small number of d-electrons such as Re(V).

The visible spectra of $[Re(en)_2O_2]^+$ type ions are shown in Fig. 1. Since the successive acid association constants differ greatly, solutions can be made which contain essentially one species. There is a gradual shift to lower energies of maximum absorbance with increasing protonation suggesting a decrease in ligand field stabilization energy. This agrees with the postulate that the complex is a distorted octahedron having the *trans*-oxygens more tightly bound than the planar nitrogen atoms. Further it suggests that the ground state contains two paired electrons in either the d_{xy} or $d_{z^2-y^2}$ orbital in agreement with the diamagnetism of the complex.

Experimental

Preparation of Compounds.—$[Re(en)_2O_2]Cl$ and $[Re(1,3\text{-pn})_2O_2]Cl$ were prepared by the method previously described for $[Re(en)_2O_2]Cl$.[3,4] They were twice recrystallized from a water–methanol mixture and dried under vacuum at 80° to give the anhydrous form. $[Re(1,2\text{-pn})_2O(OH)](ClO_4)_2$ was prepared by addition of the extremely soluble $[Re(1,2\text{-pn})_2O_2]Cl$ to 6 *N* $HClO_4$ and was precipitated with acetone. It was redissolved in 6 *N* $HClO_4$, reprecipitated with acetone, and dried under vacuum at room temperature. (The compound explodes violently with shock or heat.)

Anal. $[Re(en)_2O_2]Cl$; Calcd. for $ReC_4H_{16}N_4O_2Cl$: Re, 49.83; C, 12.84; H, 4.31; N, 14.96; Cl, 9.48; ox. change to ReO_4^-, 2.0 equiv./mole. Found: Re, 49.5; C, 12.95; H, 4.41; N, 14.86; Cl, 9.32; ox. change, 1.97. $[Re(1,3\text{-pn})_2O_2]Cl$; Calcd. for $ReC_6H_{20}N_4O_2Cl$: Re, 46.35; Cl, 8.82; ox. change, 2.0. Found: Re, 46.2; Cl, 8.71; ox. change, 2.01. $[Re(en)_2O(OH)](ClO_4)_2$; ox. change to ReO_4^-: Calcd. 2.00; Found: 2.02; titration with OH^-; Calcd., 1.00 equiv. OH^-/mole. Found: 0.98. $[Re(1,2\text{-pn})_2O(OH)](ClO_4)_2$; Calcd. for $ReC_6H_{21}N_4O_{10}Cl_2$: Re, 32.89; C, 12.72; H, 3.74; N, 9.89; titration with OH^-, 1.00 equiv./mole. Found: Re, 33.1; C, 12.79; H, 3.82; N, 9.73; titration with OH^-, 1.01 equiv./mole.

The visible spectra were taken with a Cary Model 12 and a Beckman DU spectrophotometer equipped with cell spacers through which water from a constant temperature bath was pumped. The temperature was controlled at 25.3° ± 0.05 and 1 cm. quartz matched cells were used. The complex concentration was between 2×10^{-2} and 2×10^{-3} mole/l., the lower value dictated by the low solubility in the strongly acidic region.

Acid Association Constants.—The first association constant, K_1, was determined by titration, at constant temperature (±0.02°), of a known amount of the complex $[Re(AA)_2O_2]Cl$ in water (5×10^{-2} molar) with a standard HCl solution (0.100 *M*) and following the pH with a Beckman Model GS pH meter. The pH meter was standardized at pH 7 and 9 at constant temperature with standard buffers before and after each titration. The pH was converted to $[H^+_{aq}]$ concentration using a calibration curve. The titration curves for $[Re(en)_2O_2]Cl$ and $[Re(1,3\text{-pn})_2O_2]Cl$ were identical. The association constants were evaluated from about ten points covering the middle 60% of the titration curve using the expression

$$K_1 = \frac{C_H - [H^+]}{(C_c - C_H + [H^+])[H^+]}$$

where C_c = total complex and C_H total acid concentration added. Log K_1 varied by less than 0.02 for each point in a single titration. Each complex was titrated twice ($[Re(en)_2O_2]Cl$ many more times) and log K_1 varied by less than ±0.02.

With $[Re(1,2\text{-pn})_2O(OH)](ClO_4)_2$ the titration was carried out using standard NaOH solution free of CO_2. The titration curve

(3) Lebedinsky and Ivanov-Emin, *J. Gen. Chem. USSR*, **13**, 253 (1943).

(4) R. K. Murmann, *J. Inorg. Nucl. Chem.*, **18**, 226 (1961); R. K. Murmann, "Inorganic Synthesis" to be published, 1963.

was identical with those of $[Re(en)_2O_2]Cl$ and $[Re(1,3\text{-}pn)_2O_2]Cl$ but reversed.

K_2 was evaluated using the large spectral differences in $[Re(AA)_2O(OH)]^{+2}$ and $[Re(AA)_2(OH)_2]^{+3}$. The absorbancy at the wave lengths of maximum absorbance for the two species was quickly measured on solutions containing a known amount of complex in 4–8 M standard HCl. Reduction or disproportionation slowly takes place in these concentrated acids necessitating rapid measurements. Using the expression

$$C_1 = \frac{A - \epsilon_2 l C_T}{l(\epsilon_1 - \epsilon_2)}, \quad C_1 + C_2 = C_T$$

(where C_1 and C_2 and C_T refer to the concentrations of the rhenium complexes), the concentration of each species was determined and converted to K_2. K_2 was constant at both wave lengths, within the experimental error stated, in the range 4–8 molar HCl and was not dependent on the total complex concentration.

Heats of Reaction.—The enthalpy of acid association was determined by the variation of K_1 with temperature. A graph of $\log K_1$ *vs.* T^{-1} for three temperatures, 2, 25.3, and 50.0°, gave a straight line with a slope corresponding to $\Delta H = -3.28$ kcal./mole. A more precise method utilized direct heat measurements.

A microcalorimeter was employed in the heat measurement wherein the concentrated rhenium complex solution was added to about 3 ml. of a 10^{-1} M HCl solution. The all glass microcontainer was suspended in a covered dewar flask which was immersed in a constant temperature bath. Mixing and stirring was accomplished by squeezing a rubber bulb located outside of the bath which was attached by a thin polyethylene tube to the small inlet. Temperature measurement was made with a stainless steel jacketed thermistor with a $^2/_3$ temperature change response of about 1 sec. The thermistor resistance was measured with an a.c. Wheatstone bridge and amplifier and was sensitive to 5×10^{-4}°. The apparatus was standardized using the 0.1 M KOH–HCl reaction. Corrections were made for the heat capacity of the cell, thermistor, etc., the heat capacity of the final solution, the heat capacity of the Hg, and the unreacted complex calculated from K_1. In the case of $[Re(1,3\text{-}pn)_2O_2]^+$ the protonated complex was first reacted with NaOH solution to the equivalence point before being added to the calorimeter. Each reaction was carried out three times after the apparatus was operating satisfactorily and ΔH agreed within ±0.05 kcal.

MASS SPECTROMETRIC STUDY OF THE VAPORS OVER BISMUTH–SULFUR MELTS[1]

BY DANIEL CUBICCIOTTI

Stanford Research Institute, Menlo Park, California

Received December 26, 1962

In a recent transpiration study of the vapor in equilibrium with Bi–S melts,[2] evidence was found for a gaseous species containing both Bi and S. Because evidence from transpiration data is indirect, confirmation by mass spectrometric methods is very desirable. In addition, species of secondary importance can be observed. An investigation of the species evaporating from liquid Bi containing small proportions of S seemed feasible because the total pressure of all species was sufficiently low, and thus the present study was undertaken.

Experimental

Weighed quantities of high purity Bi and S were melted in a quartz glass cup under nitrogen. The cup was fitted into a quartz glass sleeve which had a 0.5-mm. effusion hole in its top. The cup and sleeve were placed in a tungsten crucible and packed with quartz glass powder. The crucible was heated by radiation from a filament which surrounded it. The crucible and filament were enclosed by radiation shields; an opening was left in the assembly to allow a molecular beam uninterrupted passage from the quartz container to the mass spectrometer slit. The assembly was mounted in the source region of the Nuclide Analysis Associates mass spectrometer built for Professor Paul W. Gilles.

Temperatures were measured by a thermocouple in a hole in the bottom of the crucible; however, large temperature gradients were apparent along the height of the crucible, so the temperatures of the sample were not well known. The composition of the sample for which results are reported below was 0.11 in atom fraction S calculated from the weights of material used and 0.10 by chemical analysis for sulfur after the experiment was completed.

Results

Table I lists the ion masses observed, their probable neutral molecule origin, and the relative ion currents. No currents above background were observed for BiS_2^+, $Bi_2S_3^+$, BiO^+, $Bi_2O_3^+$, or S^+. (However background for mass 32 was high because of O_2^+.) The results show that BiS is by far the most important species containing Bi and S, but there is a small proportion of dimer. The order of importance of the ions observed is not unlike those observed for the Bi–Se and Bi–Te systems by Porter and Spencer[3] although they did not observe Bi–chalcogenide dimers.

TABLE I

MASS PEAKS OBSERVED IN VAPOR OVER LIQUID Bi WITH 10 ATOM % S AT ABOUT 700°

Ion	Probable neutral source molecule	Appearance potential, v.	Relative ion currents at 5 v. above appearance potential	Relative ion currents at 70 v.
S_2^-	S_2	11[a]	2.1	16
Bi^+	Bi	8[b]	0.2	2.0
BiS^+	BiS	8	0.62	3.8
Bi_2^+	Bi_2	8	0.34	1.3
Bi_2S^+	Bi_2S_2	14	0.003	0.03
$Bi_2S_2^+$	Bi_2S_2	...	...	~ 0.003

[a] This value was taken from F. H. Field and J. L. Franklin, "Electron Impact Phenomena," Academic Press, Inc., New York, N. Y., 1957, to establish the base to evaluate the other appearance potentials. [b] This is in good agreement with the ionization potential for Bi.

Thus, the mass spectrometer study confirmed the conclusions arrived at indirectly from the transpiration measurements: (1) the molecule BiS exists in the vapor over Bi–S melts and (2) it is the only important Bi–S species.

Acknowledgment.—The author is grateful to Professor Paul W. Gilles for many fruitful discussions, as well as for the use of his laboratory facilities at the University of Kansas.

(3) R. F. Porter and C. W. Spencer, *J. Chem. Phys.*, **32**, 943 (1960).

NUCLEAR MAGNETIC RESONANCE SPECTRAL CORRELATION OF SOME SYMMETRICALLY SUBSTITUTED EPOXIDES AND OLEFINS

BY M. H. GIANNI, E. L. STOGRYN, AND C. M. ORLANDO, JR.

Special Projects Unit, Esso Research and Engineering Company, Linden, N. J.

Received December 20, 1962

In an early communication Curtin, *et al.*[1], have shown the applicability of nuclear magnetic resonance spectroscopy to distinguish between *cis* and *trans* isomers of symmetrically substituted cyclic hydrocarbons. Thus

(1) This work was performed under the auspices of the U. S. Atomic Energy Commission.

(2) D. Cubicciotti, *J. Phys. Chem.*, **67**, 118 (1963).

(1) (a) D. Curtin, H. Gruen, and B. A. Shoulders, *Chem. Ind.* (London), 1205 (1958); (b) D. Curtin, H. Gruen, Y. G. Hendrickson, and H. E. Knipmeyer, *J. Am. Chem. Soc.*, **83**, 4838 (1961).

the n.m.r. spectra of *cis*- and *trans*-1,2-diphenylcyclopropane and 1,2-diphenylcyclopentane indicate that the τ-values for the aryl hydrogens are larger for the *cis* isomers than for the *trans* isomers (less shielding), while the τ values for the methine hydrogens (—C(H)—) are smaller for the *cis* isomers. It was also noted that the *cis* and *trans* stilbenes did not follow this pattern. The τ-values for the olefinic as well as the aryl hydrogens are both greater for the *cis* isomer than for the *trans* isomer.

In a recent publication, Anet[2] presented the n.m.r. data for some *cis* and *trans* symmetrically disubstituted cyclic derivatives of 2,3-butanediol. These compounds also fit the general pattern shown for the non-olefinic hydrocarbons. The τ-values of the methyl hydrogens for the *cis* isomers are larger than for the *trans* isomers while the τ-values for the methine hydrogens are smaller for the *cis* isomers than for the *trans* isomers. These data are listed in Table I.

TABLE I
PROTON CHEMICAL SHIFTS OF SOME SYMMETRICALLY SUBSTITUTED CYCLIC AND OLEFINIC COMPOUNDS

	τ CH_3	τ aryl	τ CH
cis-1,2-Diphenylcyclopropane[a]		2.49	6.99
trans-1,2-Diphenylcyclopropane[a]		2.32	7.32
cis-1,2-Diphenylcyclopentane[a]		2.62	6.71
trans-1,2-Diphenylcyclopentane[a]		2.44	7.11
cis-2,3-Butanediol cyclic carbonate	8.63		4.16
trans-2,3-Butanediol cyclic carbonate	8.59		4.34
cis-2,2,4,5-Tetramethyl dioxolane	8.95		5.83
trans-2,2,4,5-Tetramethyl dioxolane	8.85		6.62
cis-2-Butene oxide[b]	9.02		7.30
trans-2-Butene oxide[b]	8.85		7.43
cis-Stilbene oxide[c]		2.85	5.83
trans-Stilbene oxide[c]		2.73	6.33
cis-1,2-Divinylethylene oxide[d]			6.85
trans-1,2-Divinylethylene oxide[d]			7.15
cis-1,2-Di-(2-furyl) ethylene[d]			3.88
trans-1,2-Di-(2-furyl) ethylene[d]			3.24
cis-Stilbene		2.82	3.51
trans-Stilbene		2.60	3.01
Diethyl maleate[d]			3.72
Diethyl fumarate[d]			3.17
cis-1,2-Dibromoethylene			3.00
trans-1,2-Dibromoethylene			3.38

[a] Values converted from external methylene chloride. All spectra were run as approximately 10% solutions in carbon tetrachloride with tetramethylsilane as internal standard. [b] Prepared by the method of C. E. Wilson and H. J. Lucas, *J. Am. Chem. Soc.*, 58, 2396 (1936). [c] Prepared by the method of H. O. House, *ibid.*, 77, 3070 (1955). [d] The preparation and chemistry of these compounds will be discussed in a future paper.

We now report the chemical shifts (Table I, entries 9–16) for some symmetrically substituted epoxides and *cis*- and *trans*-1,2-di-(2-furyl)-ethylene. The chemical shifts for the epoxides correlate with the data for the non-olefinic compounds while the chemical shifts for the furylethylenes correlate with the stilbenes.

The n.m.r. spectra of *cis*- and *trans*-butene-2 oxide[3] give $\tau(CH_3)$ values of 9.02 and 8.85, respectively, while the τ(CH) values for the methine hydrogens are 7.30 and 7.43. The τ(CH) values for *cis* and *trans* stilbene oxide are 5.83 and 6.33, while τ(aryl) values are 2.85 and 2.78, respectively. The τ(CH) values for the *cis* and *trans*-1,2-divinylethylene oxide are 6.85 and 7.15, respectively. These values all fit the general pattern shown by the non-olefinic hydrocarbons.

The τ-values for the ethylenic hydrogens for *cis* and *trans*-1,2-di-(2-furyl)-ethylene follow the pattern set by the stilbenes. The olefinic hydrogens for the *cis* isomer have a τ-value of 3.88 while the τ-value for the *trans* isomer is 3.24.

It appears that the anisotropes[4] of the phenyl and furyl groups are responsible for the olefins not fitting the general pattern shown by the saturated symmetrically substituted compounds. Thus the olefinic hydrogens for the *trans* isomers are deshielded by the phenyl and furyl groups due to coplanarity.[5] A similar situation is found with diethyl maleate and diethyl fumarate[6] (entries 21 and 22, Table I), which follow the pattern set by the olefins due to the anisotropy of the carbonyl group.[5]

In contrast the τ-values for *cis*- and *trans*-1,2-dibromoethylene[6] are 3.00 and 3.38, respectively. In this instance the bromines in the *trans* isomer shift the vicinal hydrogen to higher fields. *cis*- and *trans*-butene-2[7] also follow the pattern shown by the non-olefinic compounds.

The spectra of the ethylenic compounds are of particular interest. The published[1,8] spectra of the *cis*- and *trans*-stilbenes show the aryl hydrogens of the *trans* isomer as a multiplet since the aromatic groups are coplanar[1,4] while the aryl hydrogens for the *cis* isomer give a singlet indicating that the rings are not coplanar.

Due to the lower order of symmetry of furyl as compared to the phenyl substituent, the suggestion for conformational preferences is even more definitive in the case of *cis*- and *trans*-1,2-di-(2-furyl)-ethylenes. Evidence for the preferred conformations is given by the rather large difference in chemical shift for the C_3 hydrogens of the furan ring. The C_3 hydrogen has a 3.75 τ value for the *trans* isomer and 3.24 τ for the *cis* isomer. Thus the C_3 hydrogen has different environments for the *cis* and *trans* isomers and the molecules must possess different geometries.

Acknowledgment.—This work was conducted under Army Contract DA-30-069-ORD-2487, supported by the Advanced Research Projects Agency.

(2) F. A. Anet, *J. Am. Chem. Soc.*, **84**, 747 (1962).

(3) It is interesting to note that the methine hydrogens in *trans*-butene-2 oxide give a quartet while the *cis* isomer spectrum shows a higher multiplicity indicating that the *cis* hydrogens are coupled while the *trans* hydrogens are either not coupled or the coupling is too small to observe. This is also the pattern found for the 1,2-divinylethylene oxides. The *trans* hydrogens give a doublet while the *cis* hydrogens give a more complicated pattern. In contrast, the methine hydrogens for both *cis* and *trans*-2,3-butanediol cyclic carbonate are coupled.[2] The difference is probably due to the existence of conformers in the case of the *trans*-2,3-butanediol cyclic carbonate.[2]

(4) L. M. Jackman, "Applications of Nuclear Magnetic Resonance Spectroscopy in Organic Chemistry," Pergamon Press, London, 1959.

(5) For a discussion of this effect, see ref. 4, Chapter 7.

(6) G. V. D. Tiers, "Tables of τ Values," Minnesota Mining and Manufacturing Company, St. Paul, Minnesota, 1958.

(7) J. H. Pople, W. G. Schneider, and H. J. Bernstein, "High-Resolution Nuclear Magnetic Resonance," McGraw-Hill Book Co., New York, N. Y., Chapter 11, 1959.

(8) "High Resolution NMR Spectra Catalogue," Varian Associates, Palo Alto, California, 1962.

A TRANSPIRATION STUDY OF LITHIUM HYDROXIDE[1]

BY JOAN B. BERKOWITZ-MATTUCK AND ALFRED BÜCHLER

Arthur D. Little, Inc., Cambridge 40, Massachusetts

Received January 21, 1963

The increased volatility of lithium oxide in the presence of water vapor was first reported by Brewer

and Margrave[2] and van Arkel, Spitsbergen, and Heyding.[3] The species LiOH(g) was identified mass-spectrometrically by Porter and Schoonmaker,[4] who worked at temperatures between 780 and 900° and with water vapor pressures of less than 10^{-2} mm. By analogy with their results on the higher alkali hydroxides, Porter and Schoonmaker suggested that the dimer $Li_2(OH)_2(g)$ should be an important species at lower temperatures and higher water vapor pressures.

In a more extensive mass-spectrometric investigation, Berkowitz, Meschi, and Chupka[5] studied the Li_2O(c)–H_2O(g) equilibrium in the range from 800 to 1100° at water vapor pressures of 0.04 and 0.16 mm. Under these conditions it was found that dimer accounted for a few per cent of the total lithium hydroxide pressure, and heats of formation of both monomer and dimer were obtained. In the only other quantitative investigation, Smith and Sugden[6a] and James and Sugden[6b] studied the formation of LiOH(g) in flames.

The present investigation was undertaken to extend the study of the Li_2O(c)–H_2O(g) system by use of the transpiration method to water vapor pressures beyond the range presently accessible to mass-spectrometric work. In this system, two competing equilibria must be considered

$$^1/_2H_2O(g) + {}^1/_2Li_2O(c) = LiOH(g) \qquad (1)$$

$$H_2O(g) + Li_2O(c) = Li_2(OH)_2(g) \qquad (2)$$

with equilibrium constants $K_1 = p_{LiOH}/p_{H_2O}^{1/2}$ and $K_2 = p_{Li_2(OH)_2}/p_{H_2O}$. The dimer–monomer ratio in the gas phase is therefore given by $p_{Li_2(OH)_2}/p_{LiOH} = (K_2/K_1)p_{H_2O}^{1/2}$, and the higher the water vapor pressure, the greater the importance of the dimeric species. The transpiration measurements to be described were made at temperatures of 1095 and 1145°K., and water vapor pressures of 4.58 and 19.5 mm. Under these conditions, one estimates from published data[5] that more than 90% of the lithium hydroxide in the equilibrium vapor is $Li_2(OH)_2$.

Experimental

A. Material.—The Li_2O(c) starting material was prepared by thermal decomposition of lithium peroxide.[7] The product showed the characteristic X-ray pattern for anhydrous lithium oxide.[8] Attempts to synthesize Li_2O(c) by degradation of Li_2CO_3(c) in a platinum boat at 1000°[2] always ended in failure; the product, gray in color, was shown by X-ray fluorescence to contain platinum.

B. Apparatus.—A transpiration apparatus of standard design[9] was constructed of Pyrex, with a reaction tube of fused quartz surrounded by an electrical resistance furnace. Dried, CO_2-free argon was used as a carrier gas. Water vapor was introduced into the gas stream by bubbling argon through water at a controlled temperature and then through a series of baffles to avoid mass transfer of liquid droplets. The water vapor–argon mixture was passed over a weighed sample of Li_2O(c) contained in a gold boat at the center of the furnace tube. Carrier gas flow rates were measured with a dibutyl phthalate capillary flowmeter,[10] calibrated *in situ* with argon by water displacement[11] from a Mariotte flask[12] to a precision of ±5%. A Richards bottling apparatus was incorporated at one side of the reaction tube to allow removal of unreacted Li_2O(c) for weighing without exposure to air.

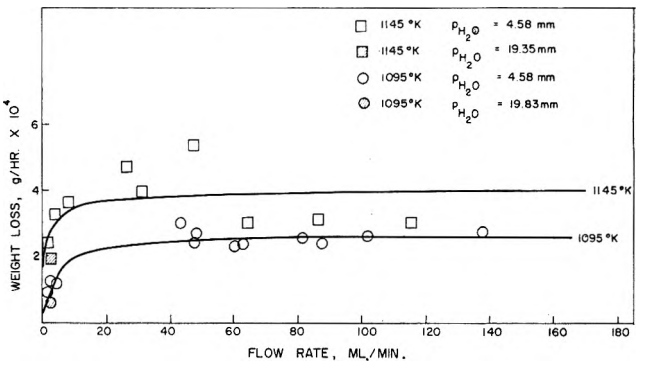

Fig. 1.—Lithium oxide weight loss *vs.* flow rate.

Results and Analysis

The experimental data obtained are plotted in Fig. 1 in terms of weight loss per unit time w *vs.* flow rate v for a water vapor pressure of 4.58 mm. Weight losses for runs made at higher water vapor pressures were reduced to the corresponding weight losses at 4.58 mm. by means of the mass-spectrometric monomer–dimer equilibrium constant[5] and are plotted as shaded points. It is clear from the figure that in these experiments, the range of flow rates for which diffusion is significant[13] overlaps the region where the vapor fails to reach saturation.[14] Therefore, the simple expression generally used to determine vapor pressures from transpiration experiments cannot be applied. If the principal reaction under study can be written as

$$Li_2O(c) + H_2O(g) \underset{k_b}{\overset{k_f}{\rightleftarrows}} Li_2(OH)_2(g), \quad K_2 = \frac{k_f}{k_b} = \frac{p_{Li_2(OH)_2}}{p_{H_2O}} \qquad (3)$$

the rate of formation of $Li_2(OH)_2$ per unit area of sample is given by

$$\frac{dc_{Li_2(OH)_2}}{dt} = k_f c_{H_2O} - k_b c_{Li_2(OH)_2} \qquad (4)$$

where k_f and k_b are the specific rate constants for the forward and reverse reaction, respectively, and c_i is the concentration of species i. If the lithium oxide sample extends from $x = 0$ to $x = l$ where x measures distance along the reaction tube, and if the concentration of $Li_2(OH)_2$(g) can be taken as zero at $x = 0$, one obtains at $x = l$

$$c_{Li_2(OH)_2} = c^0_{Li_2(OH)_2}(1 - e^{-\gamma/v}) \qquad (5)$$

for a constant partial pressure of water vapor. In (5),

(1) Supported by the United States Army Bureau of Research under the Advanced Research Projects Agency Program, and by the United States Air Force under a contract monitored by the Missile Development Center, Air Research and Development Command.

(2) L. Brewer and J. Margrave, *J. Phys. Chem.*, **59**, 421 (1955).

(3) A. E. van Arkel, U. Spitsbergen, and R. D. Heyding, *Can. J. Chem.*, **33**, 446 (1955).

(4) R. C. Schoonmaker and R. F. Porter, *J. Phys. Chem.*, **64**, 457 (1960).

(5) J. Berkowitz, D. J. Meschi, and W. A. Chupka, *J. Chem. Phys.*, **33**, 533 (1960).

(6) (a) H. Smith and T. M. Sugden, *Proc. Roy. Soc.* (London), **A219**, 204 (1953); (b) C. G. James and T. M. Sugden, *ibid.*, **A227**, 312 (1955).

(7) T. Moeller, "Inorganic Syntheses," Vol. V, McGraw-Hill Book Co., New York, N. Y., 1957, p. 1.

(8) ASTM X-Ray Power Data File, Baltimore, Md. (1957).

(9) N. W. Gregory and R. H. Mohr, *J. Am. Chem. Soc.*, **77**, 2142 (1955)

(10) A. Weissberger, "Technique of Organic Chemistry," Vol. III, Part II, "Laboratory Engineering," Interscience, New York, N. Y., 1957, p. 325 ff.

(11) G. W. Smith, *Ind. Eng. Chem., Anal. Ed.*, **4**, 244 (1932).

(12) Scientific Glass Co. Catalog (1959), Bloomfield, N. J., p. 690.

(13) U. Merten, *J. Phys. Chem.*, **63**, 443 (1959).

(14) W. E. Bell and U. Merten, "Kinetic Effects in the Transpiration Method of Vapor Pressure Measurements," General Atomics Report GA-1670, Sept. 9, 1960, San Diego 12, California.

$c^0_{Li_2(OH)_2}$ is the equilibrium concentration of $Li_2(OH)_2$(g) for a given partial pressure of water vapor and $\gamma = k_b l A$, where A is the cross-sectional area of the reaction tube. If both diffusion and saturation effects are taken into account and if the lithium hydroxide vapor is assumed to be dimeric, the weight loss measured in the transpiration equipment, the pressure of lithium hydroxide dimer formed, and the flow rate are related by the equation

$$w_{Li_2(OH)_2} = M_{Li_2O} \frac{p^0_{Li_2(OH)_2} v}{RT} \left(\frac{1 - e^{-\gamma/v}}{1 - e^{-\beta v}} \right) \quad (6)$$

where $T = 298°K.$ is the temperature at which the flow rate was measured, $p^0_{Li_2(OH)_2}$ is the equilibrium partial pressure of $Li_2(OH)_2$(g) for a given partial pressure of water vapor, and $\beta \equiv (l_2/A_2 + l_1/A) \cdot (1/D)$. In the latter expression, D is the interdiffusion coefficient for $Li_2(OH)_2$(g) and argon, l_2 and A_2 are length and cross-sectional area, respectively, of the isothermal constricted region of the apparatus, and l_1 is the length of tubing between the sample boat and the capillary.

Equation 6 has three parameters, $p^0_{Li_2(OH)_2}$, β, and γ, that may be evaluated from experiment. For $v \to 0$, $w \to w_0 = M_{Li_2O} p^0_{Li_2(OH)_2}/RT$, and for $v \to \infty$, $w \to w_\infty = M_{Li_2O} p^0_{Li_2(OH)_2} \gamma/RT\beta$. Over the range of flow rates studied a point (w^*, v^*) must exist for which $(1 - e^{-\gamma/v^*}) = (1 - e^{-\beta v^*})$, and hence $w^* = (w_0 w_\infty)^{1/2}$, while $w^*/v^* = M_{Li_2(OH)_2}/RT$. In order to draw the curves shown in Fig. 1, $w_{\infty,1095} = 2.6 \times 10^{-4}$ g. hr.$^{-1}$ and $w_{\infty,1145} = 4.0 \times 10^{-4}$ g. hr.$^{-1}$ (where the second subscript refers to the temperature in °K.) were estimated from the experimental data, since it is clear that in practice the asymptotic value of w is reached at finite flow rates. From the graph the values of 2×10^{-5} g. hr.$^{-1}$ and 1.4×10^{-4} g. hr.$^{-1}$ were chosen for $w_{0,1095}$ and $w_{0,1145}$ respectively. Values of w^* were computed and trial values of v^* selected until the curves shown in Fig. 1 were obtained. For both of these curves $v^* = 1.5$ ml./min. This procedure is expected to give values of $p^0_{Li_2(OH)_2}$ accurate to within a factor of two.

With the parameters given, equilibrium constants $K_{2,1095} = 0.105$ and $K_{2,1145} = 0.357$ were obtained for reaction 2.

Equation 6 permits an estimate of the efficiency with which gaseous water molecules react with Li_2O(c) to form $Li_2(OH)_2$(g). Unsaturation effects will become important at flow rates v such that

$$v = \gamma = \frac{k_f A l}{K} \quad (7)$$

For the present experiment one has approximately $l = 3$ cm., $A = 5$ cm.^{2}, and $K \approx K_{2,1100} \approx 1.3 \times 10^{-3}$, so that (7) becomes

$$v = 1.15 \times 10^4 k_f \text{ ml. sec.}^{-1} \quad (8)$$

If the rate of formation of $Li_2(OH)_2$(g) is written as the product of the number of collisions Z of water molecules per Li_2O unit and a collision efficiency α, then, for a surface density $\rho = 10^{15}$ sites cm.$^{-2}$ one obtains

$$k_f = \frac{\alpha Z}{\rho} = 2 \times 10^8 \quad (9)$$

Since unsaturation effects are apparent for flow rates greater than 5 ml. min.$^{-1}$, the collision efficiency α must be less than 10^{-13}.

Discussion

In the present experiments, the reaction rate becomes a limiting factor at moderate flow rates, and observed weight losses in the plateau region of Fig. 1 will depend on the surface area of the sample. This accounts for the poor reproducibility between experiments in that region. On the other hand, at low flow rates, weight losses are inconveniently small, and the flow rates are difficult to monitor and maintain. Therefore, the measured equilibrium constants are probably accurate to no better than a factor of two. Even so, they are an order of magnitude higher than those reported by Berkowitz, Meschi, and Chupka. In the present work the flow of water vapor is 0.29×10^{-6} v mole/min., where v is the volumetric flow rate in cc. min.$^{-1}$. The water vapor pressures and effusion orifice dimensions used in the mass-spectrometric experiments correspond to flow rates of 6×10^{-6} and 25×10^{-6} mole min.$^{-1}$. It is therefore just possible that the difference between the two sets of measurements is real, and that solid–gas equilibrium was not established in the earlier measurements.

It was not practicable to extend the transpiration measurements over a sufficiently wide temperature range to determine meaningful second-law enthalpies. No weight loss was observed in a 10 hour experiment at 1045°K. with a water vapor pressure of 4.58 mm. and a carrier gas flow rate of 4.0 ml. min.$^{-1}$. At 1170°K., on the other hand, extensive devitrification of the quartz reaction tube rendered the data suspect.

It is possible, however, to analyze the results at 1095 and 1145°K. by the third-law method,[15] to obtain an enthalpy of formation of $Li_2(OH)_2$(g). Thermal functions for Li_2O(c) and H_2O(g) have been reported in the literature.[16] For $Li_2(OH)_2$ free energy functions and absolute entropies were calculated using the vibrational frequencies and bond lengths estimated by Berkowitz, Meschi, and Chupka.[5] From the data at 1095 and 1145°K., respectively, one calculates the heat of formation of $Li_2(OH)_2$ at 0°K. as -183.6 and -186.1 kcal./mole. The heat of formation calculated from the paper of Berkowitz, Meschi, and Chupka is -180 kcal./mole, to be compared to an average value from this work of -185 kcal./mole.

(15) G. N. Lewis and M. Randall, "Thermodynamics," Second Edition, revised by L. Brewer and K. Pitzer, McGraw-Hill, New York, N. Y., 1961, p. 178.

(16) JANAF Thermochemical Tables, Quarterly Supplement No. 4, The Thermal Laboratory, Dow Chemical Co., Dec. 31, 1961.

THE EXCESS VOLUME OF BINARY MIXTURES OF NORMAL ALKANES

By José D. Gómez-Ibáñez and Chia-Tsun Liu

Hall Laboratory of Chemistry, Wesleyan University, Middletown, Connecticut

Received January 5, 1963

The so-called "principle of congruence" was formulated by Brønsted and Koefoed[1] in order to represent the excess free energies of binary mixtures of n-alkanes. At a given temperature and pressure, the excess thermody-

(1) J. N. Brønsted and J. Koefoed, *Kgl. Danske Videnskab. Selskab., Mat.-fys. Medd.*, **22**, No. 17, 1 (1946).

namic properties of a mixture of n-alkanes should be determined by the average length, or index, defined by the expression

$$n = \sum_i x_i n_i \qquad (1)$$

where x_i and n_i are, respectively, the mole fraction and the number of carbon atoms of component i in the mixture. Mixtures with the same index are said to be "congruent." The excess free energies of the three binary mixtures studied by Brønsted and Koefoed could be accurately represented by an expression of the form $G^E = A(n_1 - n_2)^2 x_2 x_2$, where $A = 2.69$ j./mole at 20°. Later, van der Waals and Hermans[2] were able to express the excess enthalpy of similar mixtures by means of the expression $H^E = B(n_1 - n_2)^2 x_1 x_2$, with $B = 5.11$ j./mole. Both equations represent symmetric parabolas in the composition.

Desmyter and van der Waals,[3] showed that the excess volume of mixtures of n-alkanes could not be represented by a similar equation, $V^E = C(n_1 - n_2)^2 \cdot x_1 x_2$, the experimental curve being skewed toward the region rich in the component of shorter chain length. The results are, nevertheless, consistent with the principle of congruence when expressed by means of eq. 1, and this has been shown to be the case, geometrically by Hijmans,[4] and analytically by McGlashan[5] and by Hijmans and Holleman.[6]

More recent measurements[7,8] have cast some doubts about the strictly symmetric form of the curves for G^E and for H^E indicated above. The problem is important when related to the required thermodynamic relationships between G^E, H^E, and V^E.[8]

The renewed interest in the principle of congruence prompts us to report some measurements of the excess volume of mixtures of n-alkanes carried out in our laboratory some time ago.[9] While the few results reported in the literature[3] were obtained by a dilatometric method, the present results were obtained by a pycnometric one.

Experimental

Procedure.—The procedure followed has been described in detail in a previous paper.[10] The results here reported are part of the same systematic program of study, and a discussion of the errors involved is to be found in the same reference.

Materials.—All materials used were Matheson Coleman and Bell reagents. The n-hexane and n-dodecane were the same materials previously described,[10] and the n-heptane was similarly purified. n-Hexadecane (m.p. 15–17°) was fractionally recrystallized until constant m.p. was obtained. The final fraction (m.p. 18.24–18.26°) was further recrystallized three times and the mother liquid still showed the same m.p. as the crystal. This was then vacuum distilled and the middle portion was used in our experiments. The density of this purified substance was 0.77002 g./cm.^{3} at 25°.

Results and Discussion

The values reported in Table I for the densities of n-heptane at 15, 25, and 35° and for n-hexadecane at 25 and 35° are each the average of several measurements and are accurate to within 0.0001 g./cm.^{3} or better. Comparison is made at 25° with the values reported in the Tables of the American Petroleum Institute,[11] and, in the case of n-heptane, values are included for dV/dT and α, the coefficient of thermal expansion, at 25°. They were obtained from a plot of the calculated molecular volumes *vs.* temperature. Similar data for n-hexane and n-dodecane have been previously reported.[10]

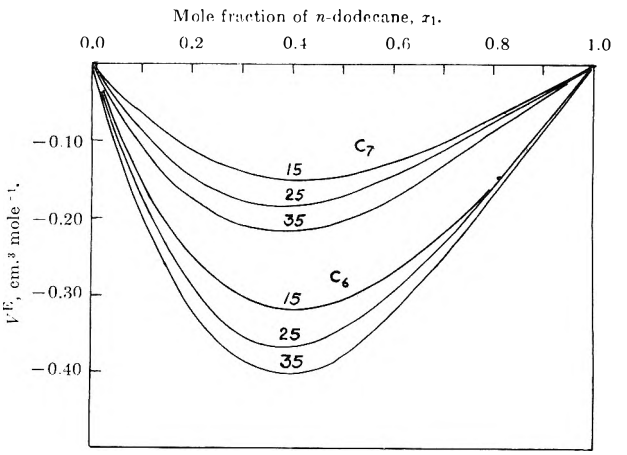

Fig. 1.—Excess volume of mixtures of n-hexane + n-dodecane and n-heptane + n-dodecane at 15, 25, and 35°.

TABLE I

DENSITIES OF n-HEPTANE AND n-HEXADECANE

Hydrocarbon	t, °C.	d, g./cm.^{3} (this work)	d (ref. 11)	dV/dT, cm.^{3}/deg. (25°)	$\alpha \times 10^3$, deg.$^{-1}$
n-Heptane	15	0.68817			
	25	.67972	0.67951	0.183	1.24
	35	.67133			
n-Hexadecane	25	.77002	.76996		
	35	.76320			

The values obtained for the excess volume of mixing for the systems $C_{12}H_{26}$–C_6H_{14}, $C_{12}H_{26}$–C_7H_{16}, and $C_{16}H_{34}$–C_6H_{14} are given in Table II. Using the data obtained, equations of the form

$$V^E = x_1 x_2 [A + B(x_1 - x_2) + C(x_1 - x_2)^2] \qquad (2)$$

(where x_1 refers always to the component of longer chain length) have been computed by the method of least squares. Table III summarizes the values of the coefficients for each case, and Fig. 1 represents the results for the systems $C_{12}H_{26}$–C_6H_{14} and $C_{12}H_{26}$–C_6H_{14}.

As can be seen, there is a negative excess volume on mixing, the contraction increasing in magnitude with increasing temperature, and such increase being practically linear over the range considered here. This is in agreement with the results reported by Desmyter and van der Waals[3] as is the fact that the excess volume of equimolar mixtures is proportional to the empirical expression

$$\left[\frac{1}{n_1 + 1} - \frac{1}{n_2 + 1}\right]^2$$

Only the results for the system n-hexadecane + n-hexane are commonly reported, and they are in substantial agreement, our values being somewhat smaller (by

(2) J. H. van der Waals and J. J. Hermans, *Rec. trav. chim.*, **69**, 971 (1950).
(3) A. Desmyter and J. H. van der Waals, *ibid.*, **77**, 53 (1958).
(4) J. Hijmans, *Mol. Phys.*, **1**, 307 (1958).
(5) M. L. McGlashan, *ibid.*, **4**, 87 (1961).
(6) J. Hijmans and Th. Holleman, *ibid.*, **4**, 91 (1961).
(7) M. L. McGlashan and A. G. Williamson, *Trans. Faraday Soc.*, **57**, 588 (1961).
(8) M. L. McGlashan and K. W. Morcum, *ibid.*, **57**, 907 (1961).
(9) The measurements reported here were carried out during the period 1957–1958.
(10) J. D. Gómez-Ibáñez and C.-T. Liu, *J. Phys. Chem.*, **65**, 2148 (1961).
(11) "Selected Values of Physical and Thermodynamic Properties of Hydrocarbons and Related Compounds," American Petroleum Research Project 44, Carnegie Press, Pittsburgh, Penna., 1953.

TABLE II

EXCESS VOLUME OF SOME MIXTURES OF NORMAL ALKANES

	$C_{12}H_{26}(x_1) + C_6H_{14}(x_2)$		$C_{12}H_{26}(x_1) + C_7H_{16}(x_2)$		$C_{16}H_{34}(x_1) + C_6H_{14}(x_2)$	
	Mole fraction x_1	$-V^E$, ml./mole	Mole fraction x_1	$-V^E$, ml./mole	Mole fraction x_1	$-V^E$, ml./mole
15°	0.08862	0.148	0.11897	0.068		
	.13376	.188	.14767	.085		
	.22309	.268	.20290	.116		
	.27143	.291	.27994	.149		
	.35476	.309	.39797	.148		
	.43864	.320	.44541	.143		
	.61901	.266	.55499	.135		
	.73655	.194	.62719	.124		
			.68996	.112		
25°	.10775	.182	.10786	.083	0.08736	0.322
	.16113	.257	.18538	.136	.15644	.45[illegible]
	.22244	.341	.25629	.179	.17030	.476
	.31712	.369	.32610	.183	.27230	.573
	.41233	.365	.43039	.176	.35064	.595
	.60421	.286	.54342	.156	.50327	.525
	.73255	.214	.70026	.103	.54760	.508
			.83964	.063	.67367	.398
35°	.10779	.207	.10789	.088	.08738	.378
	.16124	.281	.18541	.174	.15648	.536
	.22250	.337	.25634	.206	.27236	.642
	.31719	.391	.32614	.231	.35078	.665
	.41245	.409	.43045	.209	.50331	.63[illegible]
	.60438	.317	.54349	.187	.54769	.593
	.73272	.226	.70036	.115	.67392	.48[illegible]
			.83978	.085		

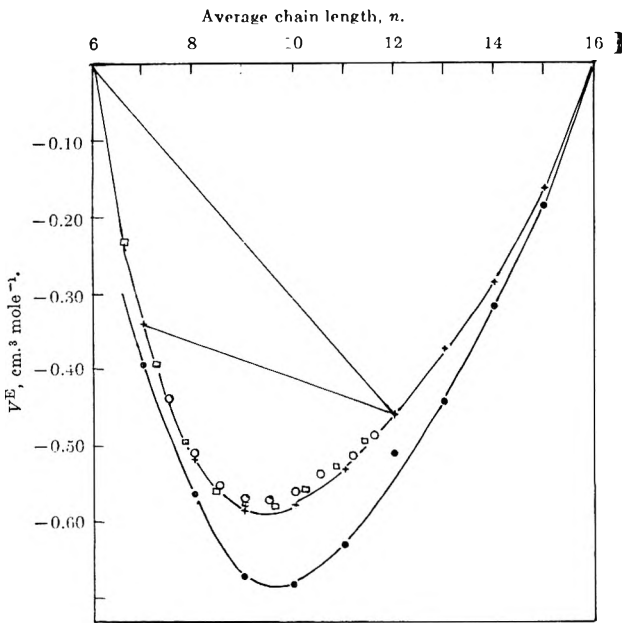

Fig. 2.—Excess volume of binary alkane mixtures as a function of the average chain length at 25°: ×, C_6H_{14}–$C_{16}H_{34}$; □, C_6H_{14}–$C_{12}H_{26}$; ○, C_7H_{16}–$C_{12}H_{26}$; ●, calculated from data for pure alkanes, C_7H_{16} – – – – – $C_{15}H_{32}$.

TABLE III

VALUE OF THE COEFFICIENTS IN EQUATION 2 FOR DIFFERENT MIXTURES OF *n*-ALKANES

System	t, °C.	A	B	C
$C_{12}H_{26}$–C_6H_{14}	15	−1.220	0.4962	−0.1446
	25	−1.389	.7692	− .1063
	35	−1.520	.8117	.0136
$C_{12}H_{26}$–C_7H_{16}	15	−0.5828	.2005	.0145
	25	− .6749	.3962	− .0088
	35	− .8085	.4714	− .0276
$C_{16}H_{34}$–C_6H_{14}	25	−2.1284	1.2404	−1.0320
	35	−2.4651	1.1948	−1.5658

0.03–0.04 cm.³/mole at $x = 0.5$) than those of Desmyter and van der Waals.

Remarkably, what both sets of data show in common is that, with respect to the principle of congruence, "the mutual agreement between different mixtures is better than the agreement between mixtures and pure substances."[4] According to Desmyter and van der Waals,[3] if the volume of the mixture depends only on the average number of carbon atoms per molecule, V^E should obey the relation

$$V^E = V_n^0 - (x_1 V_{n_1}^0 + x_2 V_{n_2}^0)$$

where $V_{n_1}^0$, $V_{n_2}^0$, and V_n^0 are the molar volumes of *n*-alkanes having n_1, n_2 and $n = x_1 n_1 + x_2 n_2$ carbon atoms per molecule, respectively. Using the method described in Hijmans,[4] we have chosen as our reference system the system $C_{16}H_{34}$–C_6H_{14} and have plotted in Fig. 2 our data at 25° as a function of the "index" or average chain length $n = 16x_{16} + 6x_6$. The "ideal" volume of mixing for a mixture of two alkanes having n_1 and n_2 carbon atoms, respectively, will be given by the straight line

$$V^{id} = \frac{n_2 - n}{n_2 - n_1} V(n_1) + \frac{n - n_1}{n_2 - n_1} V(n_2) \quad (3)$$

where $V(n_1)$ is the excess volume of a hexane–hexadecane mixture with an average chain length n_1; and similarly for $V(n_2)$. When the experimental values for V^E obtained for the systems $C_{12}H_{26}$–C_6H_{14} and $C_{12}H_{26}$–C_7H_{16} are added to equations of type 3, the results, as shown in Fig. 2, indicate a mutual agreement among the three systems which strengthens the principle of congruence, but which is also much better than that shown between the mixtures and the pure hydrocarbons.

Desmyter and van der Waals[3] attributed this situation to possible errors in the reported densities of the

pure hydrocarbons and to the fact that their dilatometric method permitted their measurements to be carried out under air-free conditions. The densities obtained by us for the pure substances are remarkably close to those reported in the literature and our method was a pycnometric one. The remarkable agreement between the two methods would seem to indicate that the explanation must lie somewhere else.

Acknowledgment.—The authors wish to thank the Wesleyan Computer Laboratory and Mr. David B. Brown, for help with some of the computations.

AN ELECTRODEPOSITION METHOD FOR FOLLOWING MODERATELY RAPID EXCHANGE REACTIONS

BY PER BERONIUS

Division of Physical Chemistry, Royal Institute of Technology, Stockholm 70, Sweden

Received December 11, 1962

The present note gives a short account of a new method, the so-called "integral method," for determining the rate of certain types of moderately rapid isotopic exchange reactions. The term "moderately rapid" refers to reactions with half-lives ranging between a few seconds and a few minutes. The method has been applied to the isotopic exchange between methyl iodide and sodium iodide in ethanol as solvent at such conditions that the half-life of the reaction was about 3 min.

Equations.—The principle of the integral method, for which a simplified rate equation has previously been deduced,[1] is suitably given by an example.

Consider the reaction which has been used in this work to make the first test of the method in practice

$$CH_3I + NaI^* \underset{k}{\overset{k}{\rightleftharpoons}} CH_3I^* + NaI$$

The asterisk indicates a radioactive atom (^{131}I) and k is the second-order velocity coefficient. One starts with a pure radioactive salt solution. A small amount (<1%) of its iodide content is deposited on a silver anode during t seconds at constant current strength i amperes. The electrode receives thereby an activity, which is denoted A_0. The exchange reaction is then started by rapidly adding the organic reactant. The electrolysis current is switched on at the moment of mixing, and a part of the iodide ions is deposited on a fresh anode during t seconds at unchanged current density. The electrolysis time is conveniently chosen[2] to correspond to a few half-lives of the reaction. The anode activity in this case is denoted A.

For a second-order reaction of the type studied, it can be shown that the rate equation of the integral method can be written

$$\frac{A}{A_0} = \frac{c_0}{a_0 + c_0}\left[1 + \frac{a_0}{c_0} \times \frac{1 - 2^{-n}}{n \ln 2}\right] \qquad (1)$$

where a_0 and c_0 are the concentrations of the organic and the inorganic species, respectively, and n is the number of half-lives of the reaction.

(1) P. Beronius, *Acta Chem. Scand.*, **15**, 1151 (1961).

(2) It is the intention of the author to discuss the choice of reaction time in a subsequent paper together with the complete deduction of the rate equation.

Denoting the reaction time (equal to the electrolysis time) by t and the half-life of the reaction by $t_{1/2}$ we have

$$n = t/t_{1/2} \qquad (2)$$

where $t_{1/2}$ is defined by the expression

$$t_{1/2} = \frac{\ln 2}{k(a_0 + c_0)} \qquad (3)$$

Equation 2 and eq. 3 give

$$k = \frac{n \ln 2}{t(a_0 + c_0)} \qquad (4)$$

The measured activities A_0 and A, together with the concentrations of the reactants, give the number of half-lives through the graphical solution of eq. 1. The specific rate constant is then calculated by eq. 4.

Experimental

The electrolytic cell, connected to a constant temperature bath at 25.0°, was the same as that previously[1] used for determining the rate of non-rapid reactions. Its effective volume was 50 ml. Stirring was provided by a stirring rod operated by a magnetic stirrer at a rate of 400 r.p.m. The anodes consisted of thin silver plates, the back of which had been coated with wax. Each had an area of 0.385 cm.^{2}.

Commercial "absolute" ethanol was refluxed with magnesium ethoxide[3] to remove water, and then distilled; b.p. 78.4° (760 mm.), d^{25}_4 0.78508. Methyl iodide was distilled in a column filled with copper turnings[4] to remove any traces of hydrogen iodide; b.p. 42.5–42.7° (760 mm.). Carrier-free $Na^{131}I$ was used as the radioactive indicator.

The electrolytic cell was filled with a radioactive sodium iodide solution of known concentration. Electrodeposition from this electrolyte gave A_0. A fresh anode was then put down and about 1 ml. of methyl iodide rapidly added by means of a syringe, through a very small hole in the lid of the cell. The current was switched on manually, as soon as the syringe had been emptied. The anode activity in this case is denoted A.

To avoid the necessity of determining the concentration of the organic constituent by subsequent chemical analysis, a third deposition, giving the equilibrium activity A_∞, was performed after a sufficiently long time for the system to come to equilibrium. The methyl iodide concentration could then be readily calculated. It can be shown that the quantities A_0 and A_∞ are related to the concentrations of the reactants by the expression

$$\frac{A_0}{A_\infty} = \left(1 + \frac{a_0}{c_0}\right) \qquad (5)$$

The electrolysis times were nearly 5 minutes in all cases. Table I summarizes the results of three kinetic runs.

The electrolysis time, the current strength, and the anode activity, measured by a proportional flow-counter, are given in columns 1–3. The methyl iodide concentration a_0 in the next column was calculated by eq. 5. The salt concentration c_0, in column 5, has been corrected for the amount of iodide deposited from the pure solution (1%). The number of half-lives, n, of the reaction, calculated by graphic solution of eq. 1, is given in column 6. The half-life of the reaction is given in the penultimate column and the specific rate constant, calculated by eq. 4, is given in the last. The mean k-value is 0.0103 l. mole^{-1} sec.$^{-1}$. The value previously reported in the literature[5] is 0.022 l. mole^{-1} sec.$^{-1}$.

Discussion

The data summarized in Table I reveal that the integral method is able to give reproducible results. As we have seen there is, however, a serious discrepancy be-

(3) H. Lund and J. Bjerrum, *Ber.*, **64**, 210 (1931).

(4) E. Cand, *Ann. fac. sci. Marseille*, **15**, 29 (1941).

(5) E. R. Swart and L. J. le Roux, *J. Chem. Soc.*, 406 (1957).

TABLE I

RESULTS OF EXCHANGE EXPERIMENTS IN ETHANOL AT 25.0° (INTEGRAL METHOD)

t, sec.	i, μa.	Activity, c.p.m.[a]	a_0, M	$c_0 \times 10^3$, M[b]	n half-lives	$t_{1/2}$, sec.	$k \times 10^4$, l. mole^{-1} sec.$^{-1}$	
293.82	384.0	41480 (A_0)						
294.03	384.5	24324 (A)	0.394	2.58	1.71	171.9	101.7	
294.07	384.3	270 (A_∞)						
294.04	384.0	48381 (A_0)						
294.15	383.5	29356 (A)	0.366	2.58	1.58	186.2	101.0	Mean: 103
294.09	383.8	339 (A_∞)						
294.09	383.8	58246 (A_0)						
294.07	384.0	34443 (A)	0.365	2.58	1.67	176.1	107.1	
294.12	383.8	409 (A_∞)						

[a] Corrected for dead-time losses, background counts, decay of the isotope and converted to equal amounts of current. [b] Corrected for the amount deposited in the pure solution (1%).

tween the mean k-value and the k-value previously reported.

To check the results obtained, the reaction was therefore also studied at such conditions that the half-life of the reaction was about half an hour ($t = 25°$, $a_0 = 0.0370\ M$, $c_0 = 0.00266\ M$). Thereby it was possible to follow the reaction, in the usual manner of the electrochemical method, by performing a number of depositions on different anodes at different reaction times. In this experiment the k-value 0.0101 l. mole^{-1} sec.$^{-1}$ was obtained, which is to be compared with the value 0.0103 l. mole^{-1} sec.$^{-1}$ obtained by the integral method. The agreement is thus very good.

The circumstance that the integral method is able to give accurate results, combined with the fact that the experimental technique is straightforward, suggests that this method might become a valuable tool in studying the kinetics of many isotopic exchange reactions, when the reaction time available is short.

In order to determine the possibilities as well as the limitations of the integral method, it will be the subject of further investigations in this Laboratory.

Acknowledgments.—The author is indebted to Professor Ole Lamm, Head of this Division, for his constant interest in this work. Mr. Stig Johansson has with skill assisted in the performance of the experiments. This work was financially supported by the Swedish Atomic Research Council.

THE ELECTRICAL CONDUCTIVITIES OF SOME IRON ISONITRILE COMPLEXES[1]

BY WALTER Z. HELDT AND CLAUS D. WEIS

E. I. du Pont de Nemours and Company, Explosives Department, Experimental Station Laboratory, Wilmington, Delaware

Received January 6, 1963

Szent-Györgyi's suggestion[2] that the transfer of π-electrons from molecule to molecule may play an important role in the fundamental processes of living organisms has stimulated numerous investigations into the conductivity of organic compounds.[3] Except for the phthalocyanines,[3c,4] little is known about the electrical properties of coördination complexes, although such complexes obviously play an important role *in vivo*. It was of interest, therefore, to determine whether there is any relationship between the conductivities of coördinated compounds and their chemical reactivities. In this communication we report on the conductivities of several iron(II) isonitrile complexes.

Experimental

The preparation of iron isonitrile complexes and their purification by chromatography on alumina and by repeated recrystallization was reported earlier.[5] All specimens used in this study were polycrystalline and chemically pure as determined by ultimate analysis. (No additional purity criteria were employed.[6]) The powdered polycrystalline specimens were compressed to cylindrical pellets of about 2.35 mm. in diameter and 2–4 mm. in length. The cross-sectional area and the length of each pellet were measured using a calibrated microscope. The applied pressure was 65–70 kg./cm.^{2}. The pellets were attached by means of a colloidal silver paste to brass electrodes mounted on an insulator and held in a jig. Thermocouples were attached to the electrodes at a distance of about 5 mm. from each specimen. The jig was then placed in a vacuum container and was heated by an electric heating coil controlled by a Variac. A pressure of 10^{-3} mm. was maintained during the measurements. The resistance measurements were made by means of a megohmmeter (General Radio Company, Type 1862 B) while applying a voltage of either 50 or 500 v. d.c. to the sample under test. The resistance and temperature for each sample were measured at the same time.

The measuring device was tested for accuracy with violanthrone and isoviolanthrone in the same temperature region as described by Inokuchi and his co-workers,[7] and we were able to reproduce to within 12% their reported values for σ_0 and ΔE for these two compounds.

Results and Discussion

The conductivity, σ, of the iron isonitrile complexes varied with temperature, T, in the following manner[3a]

$$\log \sigma = \log \sigma_0 - \frac{\Delta E}{2.303kT} \qquad (1)$$

(1) (a) Paper VIII in the series "Reactions of Coördinated Ligands"; (b) paper VII, W. Z. Heldt, *Inorg. Chem.*, in press. Presented in part at the Symposium for Homogeneous Catalysis and Reactions of Coordinated Ligands, American Chemical Society 141st National Meeting, Washington, D. C.; Advances in Chemistry Series No. 37, American Chemical Society, Washington, D. C., 1963, p. 95.

(2) A. Szent-Györgyi, *Science*, **93**, 609 (1941).

(3) (a) C. G. B. Garrett, "Organic Semiconductors," Chapter 15 in N. B. Hanney, "Semiconductors," Reinhold Publ. Corp., New York, N. Y., 1959, p. 634; (b) N. Riehl, *Naturwissenschaften*, **43**, 145 (1956); (c) D. D. Eley and G. D. Parfitt, *Trans. Faraday Soc.*, **51**, 1529 (1955); (d) D. R. Kearns and M. Calvin, *J. Am. Chem. Soc.*, **83**, 2110 (1961).

(4) (a) A. Epstein and B. S. Wildi, *J. Chem. Phys.*, **32**, 324 (1960); (b) W. Felmayer and I. Wolff, *J. Electrochem. Soc.*, **105**, 141 (1958); (c) A. T. Vartanyan, *J. Chem. Phys. USSR*, **22**, 769 (1948); (d) P. E. Fielding and F. Gutman, *J. Chem. Phys.*, **26**, 411 (1957).

(5) W. Z. Heldt, *J. Inorg. Nuclear Chem.*, **22**, 305 (1961).

(6) Only in the case of $(C_6H_5CH_2NC)_5FeCNBr$ did we succeed in growing single crystals. This was done from a chloroform–carbon tetrachloride solution by slow evaporation of the solvents. The crystals in this instance were up to 0.5 cm. long, needle-like, monoclinic, and had the following cell dimensions: $a = 8.22$ Å., $b = 14.7$ Å., $c = 32.6$ Å. (A. G. Scott unpublished results).

(7) (a) H. Akamatu and H. Inokuchi, *J. Chem. Phys.*, **18**, 810 (1950); (b) H. Inokuchi and H. Akamatu, "Electrical Conductivity of Organic Semiconductors, Solid State Physics," Vol. 12, F. Seitz and D. Turnbull, Editors, Academic Press, New York, N. Y., 1961, p. 93.

where k = Boltzmann's constant and σ_0 and ΔE are constants of the material. The values of ΔE were calculated from the experimental data by the least squares method. The data for one compound, cyanopentakis-(benzylisonitrile)-iron(II) bromide (compound 3 in Table I), are given in detail in Fig. 1. Results for the other compounds are summarized in Table I. The data reported for the isonitrile complexes were reproducible even after repeated heating and cooling cycles. Variations of less than 10% in ΔE for compound 3 were observed after 5–8 recrystallizations alternatively from methyl ethyl ketone and a chloroform–carbon tetrachloride mixture. Surface effects were minimized by conducting the measurements under 10^{-3} mm. pressure. The iron(II) complexes did not exhibit photoconductivity, in agreement with the results observed for potassium ferrocyanide.[8] At room temperature, all conductivities observed lie between 10^{-13} and 10^{-15} ohm^{-1} cm.$^{-1}$.

TABLE I

ELECTRICAL CONDUCTIVITIES OF IRON ISONITRILE COMPLEXES

	Complex	σ at 25°, ohm^{-1} cm.$^{-1}$	σ_0 at 25°, ohm^{-1} cm.$^{-1}$	ΔE, e.v.
1	$(C_6H_5CH_2NC)_4Fe^{II}(CN)_2$	2.95×10^{-14}	6.4×10^{-8}	0.36
2	$((C_6H_5)_2CHNC)_4Fe^{II}(CN)_2$	2.62×10^{-15}	2.4×10^{-7}	0.46
3	$(C_6H_5CH_2NC)_5Fe^{II}CNBr$	4.76×10^{-13}	5.2×10^{15}	1.62
4	$(C_6H_5CH_2NC)_5Fe^{II}CNHSO_4$	3.12×10^{-13}	1.9×10^{12}	1.53
5	$(C_6H_5CH_2NC)_5Fe^{II}CNClO_4$	1.65×10^{-14}	5.0×10^{9}	1.39
6	$(C_6H_5CH_2NC)_6Fe^{II}(ClO_4)_2$	2.78×10^{-14}	4.2×10^{4}	1.08
7	$((C_6H_5)_3NC)_4Fe^{III}(CN)_2Br$	1.11×10^{-14}	3.1×10^{-11}	0.20

The very large differences in both ΔE and σ_0 for tetrakis- (compounds 1 and 2, Table I), pentakis- (compounds 3–5), and hexakis-(benzylisonitrile) iron complexes (compound 6) and the good reproducibility of results suggest that the conductivity observed is intrinsic to the polycrystallites rather than due to impurities. The mechanism of conduction in these complexes is not understood. It is useful, however, to compare the activation energies, ΔE, (see Table I) for the conducting process with the relative reactivities of these compounds in solution toward the nitronium ion ($NO_2^{\oplus}$).[9] The relative reactivities of benzylisonitrile iron(II) complexes decrease in the following sequence: cyanopentakis-(benzylisonitrile)-iron(II) hydrogen sulfate (compound 4) > tetrakis-(benzylisonitrile)-iron(II) cyanide (compound 1) > hexakis-(benzylisonitrile)-iron(II) sulfate (equivalent to compound 6). The free energies of activation, ΔF^*, for this nitration process must be therefore: 6 > 1 > 4. The activation energies, ΔE, for the conducting process in solid state for the same compounds decrease in the sequence: 4 > 6 > 1.

The reactivity determination of various complexes in solution with electrophilic reagents such as the nitronium ion measures the donor capability of the most reactive aromatic ring in the complex or the cation localization energy L^+ of the aromatic system[10]; the electrophilicity or approximately the electron affinity of the attacking species remains constant. The change in the order of the conductivities in the above sequence may be understood in terms of the charge transfer model for the conducting process.[3c,11] The change transfer model

(8) H. Schindler, *Z. angew. Phys.*, **12**, 33 (1960).

(9) See ref. 1b.

(10) (a) G. W. Wheland, *J. Am. Chem. Soc.*, **64**, 900 (1942); (b) A. Streitwieser, Jr., "Molecular Orbital Theory," John Wiley and Sons, New York, N. Y., 1961, p. 338.

(11) (a) R. E. Mulliken, *J. Phys. Chem.*, **56**, 801 (1952); (b) R. P. Brown, *J. Chem. Soc.*, 2224 (1959).

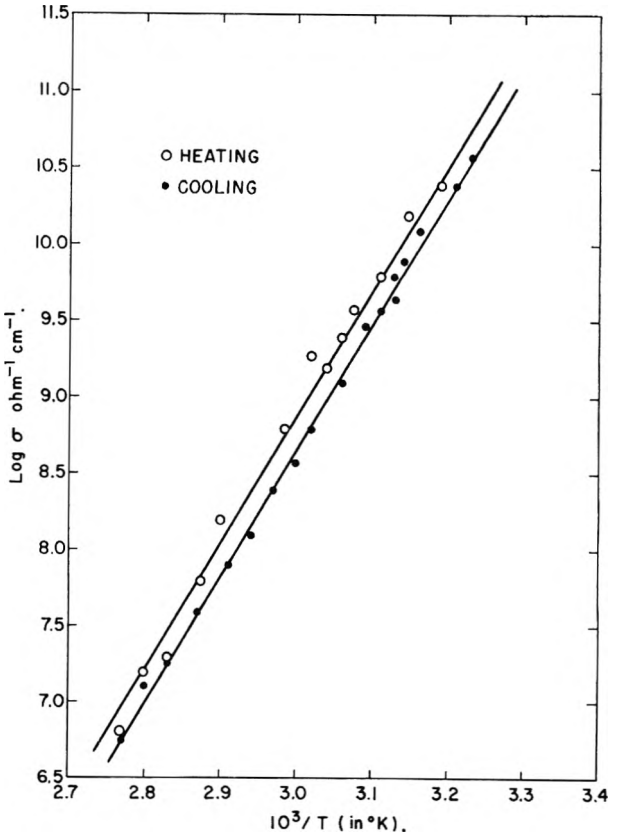

Fig. 1.—The effect of temperature on the conductivity of $(C_6H_5CH_2NC)_5FeCNBr$.

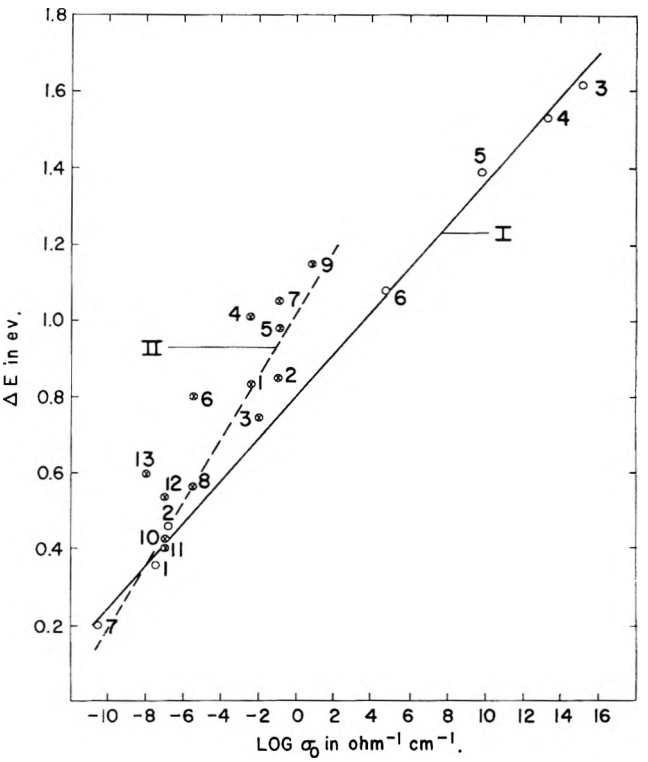

Fig. 2.—A linear relationship of ΔE *vs.* log σ_0 for iron isonitrile complexes (I) and of ΔE *vs.* log σ_0 for polyacenes (II). Numbers in Fig. 2 for iron isonitrile complexes refer to Table I. Numbers in Fig. 2 for polyacenes refer to the following: (1) anthracene,[a] (2) tetracene,[b] (3) pentacene,[b] (4) pyrene,[b] (5) perylene,[b] (6) anthranthrene,[b] (7) chrysene,[b] (8) ovalene,[c] (9) coroene,[a] (10) violanthrone,[c] (11) isoviolanthrone,[c] (12) pyranthrene,[c] (13) *m*-naphthodianthrene.[c] Ref.: [a] Eley, Parfitt, Perry, and Taysum, *Trans. Faraday Soc.*, **49**, 79 (1953)—powder samples. [b] Northrup and Simpson, *Proc. Roy. Soc.* (London), **A234**, 124 (1956)—film samples. [c] Inokuchi, *Bull. Chem. Soc.* (*Japan*), **24**, 222 (1951)—powder samples.

for a donor molecule A and an acceptor molecule B may be described by the equation[3a,12]

$$\Delta E = I_A - A_B + C \qquad (2)$$

where I_A is the ionization potential of A (equal to the energy of the highest occupied molecular orbital) and A_B is the electron affinity of B (equal to the energy of its lowest unoccupied orbital) and C is a constant relating to the distance the electron has to travel and the dielectric constant of the medium. The change in the order of conductivities of iron benzylisonitrile complexes as compared to their reactivities suggests that the conductivity of these solids will be determined by A_B, rather than by I_A.[13]

When σ_0 is plotted *vs.* ΔE, a linear relationship is obtained (Fig. 2). It is interesting that polyacenes show a similar linear relationship (Fig. 2). The larger deviations for polyacenes from a straight line are probably due to slight variations in experimental techniques employed by various workers and the various states under which the specimens were investigated. A comparison between the isonitrile complexes and polyacenes demonstrates most clearly the wide ranges of activation energies, ΔE, and in the constant σ_0 which may be achieved merely in one series of coördination complexes as compared to polyacenes.[14]

Acknowledgments.—The authors wish to thank Drs. C. Eugene Coffey, Glen R. Kepler, and Charles F. Wahlig for helpful discussions, and Mr. Charles G. Wortz for numerous measurements.

(12) M. J. S. Dewar and A. R. Leptey, *J. Am. Chem. Soc.*, **83**, 4560 (1961).

(13) An alternative explanation for the change in the order of reactivities and conductivities is that the former process proceeds in the transition state *via* a σ-complex and the latter process *via* a π-complex. (See ref. 1b for discussion.)

(14) A linear relationship between the frequency factor and the activation energy in the Arrhenius equation has been noted for conductivity,[15] diffusion,[15-17] viscosity,[15] electron emission,[16] equilibria of all types,[15] and numerous homogeneous[16] and heterogeneous reactions.[16] For discussions on the significance of this correlation the reader is referred to the literature.[15-17]

(15) P. Rüetschi, *Z. physik. Chem.*, **14**, 277 (1958).

(16) J. E. Leffler, *J. Org. Chem.*, **20**, 1202 (1955).

(17) R. F. Brown, *ibid.*, **27**, 3015 (1962).

RESONANCE TRANSFER OF EXCITATION ENERGY BETWEEN NUCLEOSIDES AND ACRIDINE ORANGE

BY SADHAN BASU AND JOHN GREIST

Chemical Laboratory, Indiana University, Bloomington, Indiana

Received January 21, 1963

In a previous communication[1] it has been shown that a fluorescence is excited in the region of 430–450 mμ in a solution of inosine, adenosine, thymidine, or uridine in water (0.02 M) on irradiation with light of wave length 350 mμ. This new fluorescence band of nucleosides partially overlaps with the absorption band of acridine orange in aqueous solution (Fig. 1). Thus the condition for resonance transfer of excitation energy by a Förster mechanism exists in these systems and it was surmised that the excitation transfer might be detected by measurements of fluorescence intensities of acridine orange in solutions of dye and nucleosides in water.

In the region 300–400 mμ where 0.02 M solutions of nucleosides show absorption shoulders, a solution of acridine orange (10^{-6} M) shows little absorption (Fig. 1). On exciting a solution of acridine orange with 350 mμ light, a weak fluorescence with a peak at 540 mμ is observed. In the presence of 0.02 M adenosine the fluorescence intensity of acridine orange at 540 mμ excited by 350 mμ light is increased by a factor of three over that observed in the absence of adenosine (Fig. 2). Evidently, the light energy at 350 mμ absorbed by adenosine is being transferred to the acridine orange from which it is being emitted as fluorescent light.

(1) S. Basu and J. Greist, *J. chim. phys.*, in press.

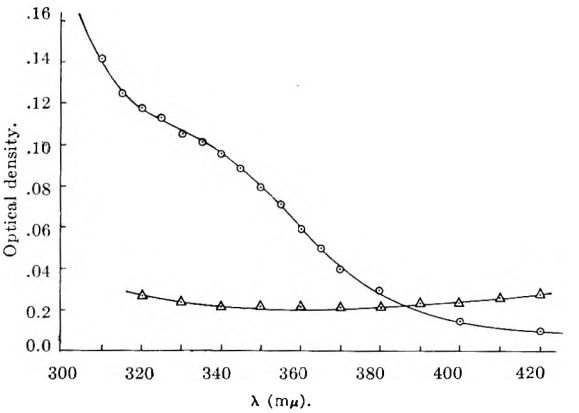

Fig. 1.—Absorption spectra: ⊙, adenosine (10^{-2} M); △, acridine orange (10^{-6} M).

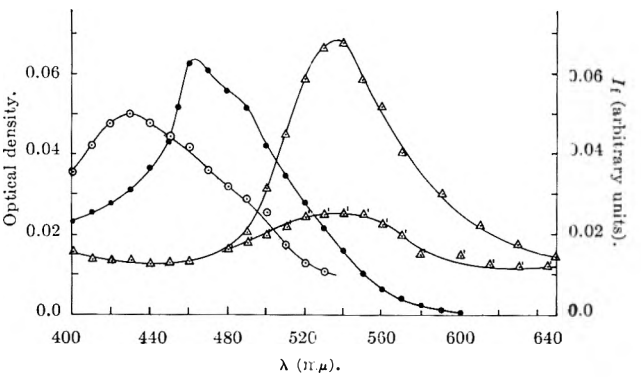

Fig. 2.—Absorption spectra: (a) acridine orange (10^{-6} M): ●, absorption: △′, fluorescence; (b) adenosine (10^{-2} M): ⊙, fluorescence with 350 mμ excitation; (c) acridine orange (10^{-6} M) + adenosine (10^{-2} M): △, fluorescence with 350 mμ excitation.

The efficiency of excitation-energy transfer from the donor M_1 (nucleoside) to the acceptor M_2 (acridine orange), *i.e.*, the number of M_2 molecules excited by transfer calculated for one excited M_1 molecule, was determined by comparison of the fluorescence intensity of M_2 on excitation by ultraviolet radiation in the absorption band of the donor (350 mμ) and in a band where the acceptor absorbs but the donor is transparent (450 mμ). If the fraction of 350 mμ light absorbed in M_1 equals α_{11} and that in M_2 equals α_{21}, then the transfer efficiency, T_{12}, is given by the relation

$$T_{12} = \frac{I_{21}/I_{22} - \alpha_{21}}{\alpha_{11}}$$

where I_{21} and I_{22} are the respective fluorescence intensities of M_2 under equal flux of exciting photons. The efficiencies T_{12} calculated for four different nucleoside–acridine orange systems are summarized as

Nucleoside	T_{12} (%)
Inosine	40
Adenosine	35
Uridine	31
Thymidine	28

According to Förster's theory there is a critical concentration for each system at which the transfer efficiency reaches a value of 100%. In the present study, the highest possible concentrations of nucleosides in water have been used. The efficiency values in the range of 30–40% as reported above, therefore, do not represent the most efficient situation. It may be asked if the efficiency could be increased by increasing the concentration of dye. When the dye concentration was increased from 10^{-6} to 10^{-3} M, some peculiar observations were made. There was no increase in the intensity of fluorescence of acridine orange (10^{-3} M) in the presence of nucleosides when excited with 350 mμ light compared to the intensity of the dye alone. The absorption intensity in the region of 300–400 mμ could be accounted for by the absorption of dye alone, *i.e.*, at higher dye concentration, nucleoside absorption in the region of 300–400 mμ disappears. Further, when the solution was excited with 450 mμ light, the fluorescence intensity of dye–nucleoside mixture was higher than that of dye alone, although optical density at 450 mμ was not different in the two cases. This suggests that there is some kind of association between dye and nucleoside at higher dye concentration. In fact acridine orange is known to undergo self-association at higher concentration and its association with nucleosides would not be surprising. This association, however, can bring about a degradation of the associated nucleoside molecules which are believed to be responsible[1] for the increased light absorption at 350 mμ. It is evident, therefore, that in order to study the energy transfer phenomenon between the associated nucleosides and the dye molecule, the dye concentration cannot be increased much without affecting the very nature of the associated species.

The low transfer efficiency for these systems may also be due to the operation of a cascade transfer mechanism; *i.e.*, instead of a resonance transfer of energy, the photon emitted by a nucleoside may be reabsorbed by a dye molecule which in turn will emit its own fluorescent light. Whereas the resonance transfer depends only on the distance between two molecules, *i.e.*, on the concentration, the cascade transfer depends on the distance over which the emitted photon can travel inside the solution before encountering one of the absorbing species, *i.e.*, on the geometric shape of the sample. Thus resonance transfer depends only on the concentration of the molecules and is independent of the shape of the sample; the cascade transfer depends on the thickness of the solution: the greater the thickness, the more efficient is the transfer.

Acknowledgment.—This work is part of a program supported by the Office of Naval Research.

COMMUNICATIONS TO THE EDITOR

REVERSIBLE PHOTOBINDING OF RIBOFLAVIN TO MACROMOLECULES IN AQUEOUS SOLUTION

Sir:

In the course of a study of the enhanced rate of photofading of riboflavin in the presence of polymers such as polyvinylpyrrolidone and the non-ionic surface active agent polyoxyethylene (20) sorbitan monoöleate, direct evidence was obtained for reversible photobinding of riboflavin to the macromolecules. Although there was no detectable binding of riboflavin by either polyvinylpyrrolidone or the surface active agent in absence of light, as determined by dialysis and solubility studies, reversible binding of riboflavin to the polymers was readily detected during illumination of the solutions with visible light. Oster and Wasserman[1] recently reported photo-induced binding of fluorescein dyes to solid substrates such as zinc oxide and alumina, but there has been no previous demonstration of photobinding in solution.

The photobinding was detected initially by comparing the quantity of riboflavin in the aqueous and polymer phases after heat precipitation of polyoxyethylene (20) sorbitan monoöleate at 95° in the presence and absence of light. The photobinding was demonstrated at room temperature by determining the effect of irradiation on the distribution of riboflavin between an ion-exchange resin, Amberlite 200[2] acid form, and an aqueous solution of either polyvinylpyrrolidone or polyoxyethylene (20) sorbitan monoöleate. Visible light had no effect on the distribution of riboflavin between the aqueous phase and the ion exchange resin in the absence of polymer. Table I presents data from a typical photobinding study.

Approximately 1.5–2.0 g. of resin was placed in a cuvette containing 50 ml. of polymer solution and sufficient riboflavin to provide a convenient absorbance in the aqueous phase after equilibration with the resin in the dark. The sample was illuminated with light from a 500-watt tungsten projection lamp, fitted with Corning filters 3-75 and 5–57 to eliminate light below 410 mμ and provide maximum transmission of wave lengths near the absorption maximum of riboflavin, 445 mμ. The sample was maintained at constant temperature during irradiation and samples of the aqueous polymer phase were removed for assay by means of a syringe fitted with a hypodermic needle.

The increased concentration of riboflavin detectable

(1) G. Oster and M. Wasserman, *J. Phys. Chem.*, **66**, 1536 (1962).

(2) Amberlite 200 is a sulfonated styrene-divinylbenzene copolymer Rohm & Haas Co., Philadelphia, Pa.

TABLE I

INFLUENCE OF VISIBLE LIGHT ON DISTRIBUTION OF RIBOFLAVIN BETWEEN AQUEOUS POLYMER SOLUTIONS AND AN ION-EXCHANGE RESIN (AMBERLITE 200)

Polyvinylpyrrolidone 2.0 g./100 ml.	Riboflavin in aqueous phase absorbance, 445 mμ
Before irradiation	0.584
Light on (3 min.)	.613
Light off	.562
Polyoxyethylene (20) sorbitan monoöleate 1.5 g./100 ml.	
Before irradiation	0.317
Light on (5 min.)	.329
Light off	.310

in the aqueous polymer phase during irradition is thought to result from interaction of a long-lived excited riboflavin species with the polymer. Evidence based on studies of polarization of fluorescence and the effects of additives such as potassium iodide indicates that the excited state involved is either a triplet or a reactive species arising from the triplet state.

Acknowledgment.—This investigation was supported by a PHS research grant, RG-9957, Division of General Medical Sciences, United States Public Health Service.

TEMPLE UNIVERSITY
SCHOOL OF PHARMACY
PHILADELPHIA 40, PA.

H. B. KOSTENBAUDER
PATRICK P. DELUCA

RECEIVED MARCH 4, 1963

STRESS-TEMPERATURE COEFFICIENTS FOR ISOTACTIC AND ATACTIC POLY-(BUTENE-1)

Sir:

The temperature coefficient of the unperturbed mean-square end-to-end distance $\langle r^2\rangle_0$ for a polymer chain can be evaluated, by recourse to the theory of rubber elasticity, from the stress-temperature coefficient for deformed networks comprising chains of the polymer. The relationship between the relevant quantities for simple elongation may be written

$$\left[\frac{\partial \ln (f/T)}{\partial T}\right]_{p,L} + \frac{\beta}{\alpha^3 - 1} = -\frac{f_e}{fT} = -\frac{\mathrm{d} \ln \langle r^2\rangle_0}{\mathrm{d}T}$$

where f is the tension, $f_e = (\partial E/\partial L)_{V,T}$ is the energy component of the tension, and β is the cubical thermal expansion coefficient. The strain is specified by α, the linear extension ratio, and is defined as L/L_i where L is the length of the sample at tension f and L_i is the length when $f = 0$. Studies of this nature have afforded essential information on the conformational energy associated with bond rotations in polyethylene, polyisobutylene, natural rubber,[1] and polydimethylsiloxane.[2] It is the purpose of this communication to present preliminary results of stress-temperature measurements on networks of isotactic and atactic poly-(butene-1), both in the amorphous state.

The isotactic and atactic polymers were obtained from the Avisun Corporation and the Petro-Tex Company, respectively. The isotactic sample was fractionally crystallized from a dilute solution in benzene. A high degree of isotacticity is indicated by the polymer density (d_{25} = 0.93 g./cc.), its melting point (~134°),[3] and the size and degree of perfection of its spherulitic growth as observed through a polarizing microscope. Both steric forms of the polymer were cross-linked by a variety of techniques: ultraviolet radiation, high-energy electrons, and γ-radiation. All irradiations were performed at room temperature under an inert atmosphere. Soluble constituents in the cross-linked samples were extracted with benzene at approximately 70°; their amounts varied between 17.3 and 1.1 weight %.

The apparatus and techniques employed in determining the stress-temperature coefficient have been described previously.[1] The stress was measured at 20° intervals in the range of 140 to 200°. Lower temperatures were avoided in order to exclude all possibility of crystallization in the isotactic samples. An inhibitor, N-phenyl β-naphthylamine, was incorporated in the samples in order to prevent oxidative degradation. The stress was recorded after it became sensibly constant at a given temperature, and each temperature cycle was checked for reversibility. A total of six isotactic and six atactic samples were examined, each at various values of α. The results are summarized in Table I.

TABLE I

	Isotactic poly-(butene-1)	Atactic poly-(butene-1)
Range of α	1.19 to 1.54	1.13 to 2.14
Number of determinations	13	10
f_e/f	0.04 ± 0.03	0.21 ± 0.02
$\frac{\mathrm{d} \ln \langle r^2\rangle_0}{\mathrm{d}T} \times 10^3$	0.10 ± 0.07	0.48 ± 0.05

The results for the isotactic polymer indicate that the unperturbed dimensions of the chain are nearly independent of temperature. Tobolsky, *et al.*, have indicated that $[\partial \ln (f/T)/\partial T]_{p,\alpha}$ is approximately zero for isotactic poly-(*n*-pentene-1).[4] This quantity cannot be identified exactly with $-\mathrm{d} \ln \langle r^2\rangle_0/\mathrm{d}T$,[5] but it may be presumed that the unperturbed dimensions are very nearly independent of temperature for this polymer also. These findings are at variance with the large *negative* temperature coefficient predicted for isotactic chains on the basis of the segmented helix model comprising short sequences of bonds alternating between *trans* and *gauche* states.[6,7] Rupture of this preferred helical sequence should be expected to involve an increase in energy; hence a negative temperature coefficient is predicted for $\langle r^2\rangle_0$.

The striking disagreement between theory and experiment indicated by our results might conceivably arise from imperfect stereoregularity in the polymer

(1) A. Ciferri, C. A. J. Hoeve, and P. J. Flory, *J. Am. Chem. Soc.*, **83**, 1015 (1961).

(2) A. Ciferri, *Trans. Faraday Soc.*, **57**, 846 (1961).

(3) Values of the density and melting point previously reported are d_{25} = 0.91 g./cc. and m.p. = 126–128° (G. Natta, P. Pino, P. Corradini, F. Danusso, E. Mantica, G. Mazzanti, and G. Moraglio, *J. Am. Chem. Soc.*, **77**, 1708 (1955)) and d_{25} = 0.92 g./cc. and m.p. 131° (W. R. Krigbaum, J. E. Kurz, and P. Smith, *J. Phys. Chem.*, **65**, 1984 (1961)). The comparison of densities of samples possibly having very different thermal histories is of limited significance. It is further obscured in the present instance by the possible occurrence of two different crystalline forms of isotactic poly-(butene-1).

(4) A. V. Tobolsky, D. W. Carlson, and N. Indictor, *J. Polymer Sci.*, **54**, 175 (1961).

(5) P. J. Flory, A. Ciferri, and C. A. J. Hoeve, *ibid.*, **45**, 235 (1960).

(6) T. M. Birshtein and O. B. Ptitsyn, *Zh. Tekhn. Fiz.*, **29**, 1075 (1959); O. B. Ptitsyn, *Vysokomolekul. Soedin.*, **4**, 1445 (1962).

(7) G. Allegra, P. Ganis, and P. Corradini, *Makromol. Chem.*, **61**, 225 (1963).

chains. The characteristics of our sample cited above cast doubt on this explanation, however. Alternatively, the results here reported may signify inadequacy of the underlying threefold bond rotational potential on which the theoretical treatment of the model is based. The profusion of interactions between non-bonded atoms in chains bearing fairly bulky substituents may tend to obliterate the ethane-like potential.

The temperature coefficient for the atactic chain differs markedly from that for the isotactic form. Current treatments of polymer chain configurations according to the methods developed for a one dimensional lattice require a regularly repeating sequence in the chain structure. Absence of such a pattern in the structure of atactic chains places their theoretical treatment out of reach at present.

Acknowledgment.—Support of the United States Air Force under grant AFOSR-62-131 is gratefully acknowledged.

DEPARTMENT OF CHEMISTRY J. E. MARK
STANFORD UNIVERSITY P. J. FLORY
STANFORD, CALIFORNIA

RECEIVED MARCH 15, 1963

THE CHROMATOGRAPHIC SEPARATION OF THE HYDROGEN ISOTOPES INCLUDING TRITIUM

Sir:

We have succeeded in separating on a single chromatographic column a gaseous mixture of hydrogen (H_2), deuterium (D_2), tritium(T_2), deuterium hydride (HD), and tritium hydride (HT). The column material, a mixture of 150–200 mesh alumina and ferric hydroxide, was prepared according to Moore and Ward,[1] care being taken to add an excess of ammonium hydroxide until the ammonia odor was quite perceptible. The column was constructed of 7-mm. Pyrex glass tubing 24 ft. long and coiled to fit into a dewar jar filled with liquid nitrogen. The material was packed into the column by applying compressed air at the inlet, a vacuum at the outlet, and vibrating the column by means of a drill motor.

Helium, flowing at 240 cc./min., was used as the carrier gas. The effluent gases were converted to their corresponding oxides with copper oxide in order to increase their sensitivity at the thermal conductivity detector which was maintained at 100°.

An electrometer, Nuclear-Chicago Dynacon, was used in series with the detector. The instrument was used qualitatively to aid in the identification of the tritium peaks.

A mixture containing 1.2×10^{-6} mole of carrier-free tritium gas and an equal amount of hydrogen gas, purified by passing through a palladium thimble, was allowed to reach equilibrium under the tritium beta radiation. A second equal molar mixture of 3.7×10^{-6} mole each of H_2, HD, and D_2 was also prepared. At the start of a run the two mixtures were combined and added to the chromatographic column.

The resulting chromatogram is shown in Fig. 1. The peaks were identified by their retention times

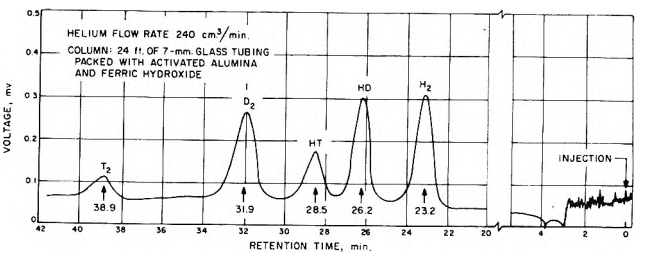

Fig. 1.—Chromatogram of 0.5 cc. sample containing the hydrogen isotopes.

which were independently obtained using the pure gases.

Several recent attempts have been made to explain the separation of the hydrogen isotopes on solid surfaces at low temperatures.[2-4] The fact that D_2 and HT are separable indicates that differences in total mass are not primarily responsible for the separations. We believe that the separations are caused by the electrostatic interaction between the polarized isotopes and the oxygen atoms of the Al_2O_3 lattice. This interaction converts two gas phase degrees of freedom, namely a translation and a rotation, into a vibration normal to the surface and hindered rotation or libration on the solid surface. A more detailed explanation of the separation will be submitted in the near future.

Acknowledgment.—The author wishes to express his appreciation to Dr. Sidney Benson for discussions and helpful suggestions.

(1) W. R. Moore and H. R. Ward, *J. Phys. Chem.*, **64**, 832 (1960).
(2) Y. L. Sandler, *ibid.*, **68**, 58 (1954).
(3) D. White and E. N. Lassettre, *J. Chem. Phys.*, **32**, 72 (1960).
(4) E. M. Mortensen and H. Eyring, *J. Phys. Chem.*, **64**, 433 (1960).

CHEMISTRY SECTION JAMES KING, JR.
SPACE SCIENCES DIVISION
JET PROPULSION LABORATORY
CALIFORNIA INSTITUTE OF TECHNOLOGY
PASADENA, CALIFORNIA

RECEIVED APRIL 23, 1963

DYNAMIC THEORY OF POLYMER SEGMENTAL MOTION

Sir:

A large number of mechanical and dielectric measurements on high polymers have been interpreted in terms of the (hindered) rotation of segments of the main chain with respect to each other, or of side chains with respect to the main chains.[1,2] A detailed analysis of the data, whenever possible, usually reveals the existence of a distribution of relaxation mechanisms, grouped around one preponderant or most probable type.[3] Rheological data likewise lead to distributions of relaxation or retardation times[4] which are descriptive of the various successful "jumps" or segmental reorientations, but up to now cannot, in general, be related to the details of the molecular structure.

The interplay of various quasi-independent degrees of freedom in a dissociating molecule has long been discussed in context with the theory of unimolecular

(1) J. A. Sauer and A. E. Woodward, *Rev. Mod. Phys.*, **32**, 88 (1960).
(2) H. A. Stuart, Ed., "Die Physik der Hochpolymeren," Vol. III, Springer Verlag, Berlin, 1955, p. 639; W. P. Slichter and E. R. Mandell, *J. Appl. Phys.*, **30**, 1473 (1959).
(3) D. J. Mead and R. M. Fuoss, *J. Am. Chem. Soc.*, **63**, 2832 (1941).
(4) A. C. Tobolsky, "Properties and Structure of Polymers," John Wiley and Sons, Inc., New York, N. Y., 1960, p. 98; see also Vol. IV of ref. 2.

reactions.[5] The starting point of this theory is an expression by Kac[6] for the average frequency of "upzeros," $\Gamma_n(q)$, of a function $f(t)$, defined as

$$f(t) = \sum_{i=1}^{n} \alpha_{i1}\epsilon_i^{1/2} \cos(\nu_i t + \psi_i)$$

with $\alpha_{i1}\epsilon_i^{1/2}$ as the weighted amplitude, ϵ_i the total energy, ν_i the frequency, and ψ_i the phase of the various harmonic motions contributing to the function $f(t)$. An "upzero" is defined as the point where $f(t)$ starts to exceed a certain crucial value, q. Upon identifying the components of $f(t)$ with the hindered rotational oscillations of polymer chain units relative to each other, one can compute $\Gamma_n(q)$ in terms of molecular parameters. $\Gamma_n(q)$ then is a measure for the "jump" frequency of a segment involving n degrees of freedom and requiring a critical total (angular) deflection q. One obtains

$$\Gamma_n(q) = \frac{F_{ot}^{n_t} F_{og}^{n_g}}{2\pi} \left\{\frac{M(n_t, n_g)}{B(n_t, n_g)}\right\} \exp\left\{\frac{-q^2}{nB^2(n_t, n_g)kT}\right\}$$

Here F_{ot}, F_{og}, B, and M are parameters descriptive of the details of the potential function used, and dependent on n_t and n_g, the average number of chain units in *trans* and *gauche* positions relative to their nearest neighbors.

If one takes into account the anharmonicity of the potential, and the finite height of the potential barriers, one has to use a high speed computer to obtain $\Gamma_n(q)$. This has been done for polyethylene and it is found that the concerted effect of relatively small rotational oscillations is very important to the over-all process. The potential shape near its minima consequently is a very crucial quantity, and the anharmonicity of the motion of very energetic chain unit plays a lesser part. This is particularly true at low temperatures. The findings offer a rather simple explanation for the so-called compensation law, that is the linear relationship found to exist between the activation energies and entropies of many physical rate processes.[7]

The function $\Gamma_n(q)$ shows a maximum for a certain value of n, indicative of the existence of an optimum segment length. Also $\Gamma_n(q)$ is strongly dependent on q, as is to be expected.

The detailed derivations and results will be published elsewhere in the near future.

Acknowledgments.—The author is indebted to Illinois Institute of Technology for a generous contribution of computer time to this work. This work was sponsored by a grant from the National Science Foundation.

(5) N. B. Slater, "The Theory of Unimolecular Reactions," Cornell University Press, Ithaca, N. Y., 1959.

(6) M. Kac, *Am. J. Math.*, **65**, 609 (1943).

(7) P. Ruetschi, *Z. physik. Chem.* (Frankfurt), **14**, 277 (1958); see also R. M. Barrer, *J. Phys. Chem.*, **61**, 178 (1957), and references cited therein.

CHEMISTRY DEPARTMENT W. W. BRANDT
ILLINOIS INSTITUTE OF TECHNOLOGY
CHICAGO 16, ILLINOIS

RECEIVED APRIL 22, 1963

THE NEUTRON IRRADIATION OF A GRAPHITIZED CARBON BLACK

Sir:

The predictions of Halsey,[1] with regard to the formation of stepwise isotherms on highly homogeneous surfaces, have been realized on a number of materials.[2-4] The development of such homogeneity during the heat treatment of a non-graphitized black is indicated by the appearance of steps in the isotherms[5] as opposed to the more usual sigmoidal shape. In view of the known effects on the bulk properties of graphite it would seem reasonable to suppose that the homogeneous character of the surface might be destroyed by extensive neutron irradiation. In order to test this hypothesis it was decided to carry out sorption studies on samples of unirradiated and neutron irradiated graphitized carbon black. Argon isotherms were determined at 77.4°K. on an unirradiated sample (sample A) and two irradiated samples (samples B and C) of a graphitized carbon black (S6-D3).[6]

The carbon black samples were evacuated at 400° prior to sorption measurements and/or irradiation. Samples B and C were then sealed in quartz ampoules and placed in a low temperature (approximately 50°) neutron irradiation facility at the Oak Ridge National Laboratory, Oak Ridge, Tenn. Both the fast and thermal neutron integrated flux values for the two samples irradiated were 2.6×10^{19} n./cm.^{2} (sample B), and 4.7×10^{20} n./cm.^{2} (sample C). The quartz ampoules were reopened *in vacuo* in the sorption apparatus and the isotherms determined without further high temperature evacuation. It was found that even for sample C, the stepwise isotherm form was retained. Within experimental error, the surface area of sample B remained unchanged. However, that for sample C showed a small but significant decrease from 85.3 m.^{2}/g. to 82.5 m.^{2}/g. taking the sorbed area of the argon molecule to be 13.7 Å.^{2}.[7]

The results indicate that the surface remains essentially homogeneous as far as physical adsorption is concerned, but that a small decrease occurs in surface area. In view of the known displacement of carbon atoms to interstitial positions, the results appear somewhat surprising. That an increase in the number of surface vacancies should occur appears likely.[8] But whether the increase would be sufficient to significantly change the homogeneous surface is uncertain. Presumably an equilibrium number of vacancies are produced, displaced atoms tending to fill previously formed vacancies or to add on to the edge of a crystallite. This hypothesis could explain the experimental observations. Indeed it may even be that the over-all effect is a smoothing of the surface as predicted for copper surfaces by Smoluchowski[9] and verified by Riehl, *et al.*[10]

(1) G. D. Halsey, *Advan. Catalysis*, **4**, 259 (1952).

(2) W. B. Spencer, C. H. Amberg, and R. A. Beebe, *J. Phys. Chem.*, **62**, 719 (1958).

(3) D. C. Fox and M. J. Katz, *ibid.*, **65**, 1045 (1961).

(4) R. A. Pierotti, *ibid.*, **66**, 1810 (1962).

(5) M. H. Polley, W. D. Schaeffer, and W. R. Smith, *ibid.*, **57**, 469 (1953).

(6) This material was kindly supplied by the Godfrey L. Cabot Corp., Cambridge, Mass.

(7) P. H. Emmett and M. Cines, *J. Phys. Colloid Chem.*, **51**, 1248 (1947).

(8) G. R. Hennig, G. J. Dienes, and W. Kosiba, International Conference on the Peaceful Uses of Atomic Energy, P/1778, Vol. 17, United Nations, New York, N.Y. 1958, p. 301.

(9) R. Smoluchowski and A. Spilners, "Reactivity of Solids," Elsevier Publishing Co., Amsterdam, 1961, p. 475.

(10) N. Riehl, W. March, and R. Sizmann, ref. 9, p. 446.

STATE UNIVERSITY OF NEW YORK AT BUFFALO
BUFFALO, NEW YORK DAVID ALLAN CADENHEAD

RECEIVED APRIL 6, 1963